

Konferenzbeiträge / Atti / Proceedings

Building Simulation Applications BSA 2013

1st IBPSA Italy conference

Bozen-Bolzano, 30th January – 1st February 2013

Edited by

**Marco Baratieri, Vincenzo Corrado,
Andrea Gasparella, Francesco Patuzzi**

bu,press

bozen
bolzano
university
press



FREIE UNIVERSITÄT BOZEN
LIBERA UNIVERSITÀ DI BOLZANO
FREE UNIVERSITY OF BOZEN · BOLZANO

Konferenzbeiträge / Atti / Proceedings

Building Simulation Applications BSA 2013

1st IBPSA Italy conference

Bozen-Bolzano, 30th January – 1st February 2013

Edited by

**Marco Baratieri, Vincenzo Corrado,
Andrea Gasparella, Francesco Patuzzi**

bu,press

bozen
bolzano
university
press

Scientific committee

Jan Hensen – Technische Universiteit Eindhoven
Ardeshir Mahdavi – TU Wien Austria
Natale Arcuri – Università della Calabria
Paolo Baggio – Università di Trento
Vincenzo Corrado – Politecnico di Torino
Andrea Gasparella – Free University of Bozen-Bolzano

Organizing committee

Paolo Baggio – Università degli Studi di Trento
Marco Baratieri – Free University of Bozen-Bolzano
Francesca Cappelletti – IUAV University of Venice
Alfonso Capozzoli – Politecnico di Torino
Vincenzo Corrado – Politecnico di Torino
Enrico Fabrizio – Politecnico di Torino
Andrea Gasparella – Free University of Bozen-Bolzano
Norbert Klammsteiner – Energytech G.m.b.H./S.r.l. - Bozen-Bolzano
Francesco Patuzzi – Free University of Bozen-Bolzano
Paola Penna – Free University of Bozen-Bolzano
Piercarlo Romagnoni – IUAV University of Venice

Other reviewers and chairmen

Marco Manzan – University of Trieste
Luigi Marletta – University of Catania
Livio Mazzaella – Politecnico di Milano
Marco Noro – University of Padova
Giovanni Pernigotto – Free University of Bozen-Bolzano
Alessandro Prada – Free University of Bozen-Bolzano
Fabio Sicurella – Professional Engineer, Catania

Design: DOC.bz

Printing: Dipdruck, Bruneck-Brunico

© 2013 by Bozen-Bolzano University Press

Free University of Bozen-Bolzano

All rights reserved

1st edition

www.unibz.it/universitypress

ISSN 2531-6702

ISBN 978-88-6046-058-5

E-ISBN 978-88-6046-105-6



This work—excluding the cover and the quotations—is licensed under the Creative Commons Attribution-ShareAlike 4.0 International License.

Table of contents

Introduction <i>Andrea Gasparella</i>	1
Predictive building systems control logic with embedded simulation capability <i>Ardeshir Mahdavi</i>	3
The air energy balance equation paradox <i>Livio Mazzarella</i>	15
BENIMPACT Suite: a tool for ZEB whole life cycle analysis <i>Silvia Demattè, Maria Cristina Grillo, Angelo Messina, Antonio Frattari</i>	29
Daylight harvesting: a multivariate regression linear model for predicting the impact on lighting, cooling and heating <i>Stefano Moret, Marco Noro, Konstantinos Papamichael</i>	39
Derivation of meteorological reference year with hourly interval for Italy <i>Gianluca Antonacci, Ilaria Todeschini</i>	49
The admittance method for calculating the internal temperature swings in free running buildings <i>Luigi Marletta, Gianpiero Evola, Maria Giuga, Fabio Sicurella</i>	59
Interoperability between building information models and software for lighting analysis <i>Chiara Aghemo, Laura Blaso, Daniele Dalmaso, David Erba, Matteo Del Giudice, Anna Osello, Giovanni Fracastoro, Anna Pellegrino, Pablo Ruffino</i>	69
Active slab design by lab tests and modelling <i>Stefano Avesani, Daniel Neyer, Paolo Baldracchi, Ulrich Filippi Oberegger, Roberto Lollini</i>	79
Investigation of different simulation tools for solar photovoltaic modules <i>Francesco Frontini, Matteo Marzoli, Narghes Doust</i>	89
Social and energy redevelopment of an old building <i>Stefano Fortuna, Paolo Neri, Fabio Peron</i>	95
Extending the use of parametric simulation in practice through a cloud based online service <i>Emanuele Naboni, Yi Zhang, Alessandro Maccarini, Elian Hirsch, Daniele Lezzi</i>	105
Dynamic modelisation of interaction between wall and indoor air <i>Lorenzo Moro, Piercarlo Romagnoni, Paolo Baggio</i>	113
Toward an EnergyPlus decision tool for evaluation of energy performances during early-stage building design <i>Marco Picco, Marco Marengo</i>	121
Lighting control system: energy efficiency and users' behaviour in office buildings <i>Michela Chiogna, Antonio Frattari</i>	131
Quasi-steady state calculation method for energy contribution of sunspaces: a proposal for the European standard improvement <i>Francesco Passerini, Rossano Albatici, Antonio Frattari</i>	141

Thermal performance of the building walls <i>Balaji N.C., Monto Mani, Venkatarama Reddy B.V.</i>	151
Simulation of wind-driven ventilation in an urban underground station <i>Roberta Ansuini, Alberto Giretti, Roberto Larghetti, Costanzo Di Perna</i>	161
Comfort and energy performance of a HVAC system under real conditions for an office block <i>Paolo Valdiserri, Cosimo Marinosci, Laura Pedretti</i>	171
Integrated BIPV performance assessment for tropical regions: a case study for Bangalore <i>Gayathri Aaditya, Rohitkumar Pillai, Monto Mani</i>	181
Multi-objective optimisation of external shading devices for energy efficiency and visual comfort <i>Gianluca Rapone, Onorio Saro, Giovanni Zemella</i>	191
Procedure for buildings' energy modelling suited for integrated control simulation <i>Chiara Dipasquale, Matteo D'Antoni, Roberto Fedrizzi, Michaël Kummert, Luigi Marletta</i>	199
Influence of the boundary conditions on the definition of a reference residential building for the Italian context <i>Davide Bettoni, Matteo D'Antoni, Roberto Fedrizzi</i>	209
Optimisation of an HVAC system for energy saving and thermal comfort in a university classroom <i>Giovanni Semprini, Cosimo Marinosci, Alessandro Gober</i>	217
An open access tool for building energy audits harmonizing European standards <i>Daniele Testi, Elena Menchetti, Eva Schito, Walter Grassi</i>	225
Energy performance of shading devices for thermal and lighting comfort in offices <i>Anna Maria Atzeri, Giovanni Pernigotto, Francesca Cappelletti, Andrea Gasparella, Athanasios Tzempelikos</i>	233
Parametrical analysis for the evaluation of the technical and economic effectiveness of different refurbishment measures <i>Francesca Cappelletti, Paola Penna, Piercarlo Romagnoni, Andrea Gasparella</i>	243
Buildings and biomass cogeneration systems: integrated simulation approach <i>Dario Prando, Francesco Patuzzi, Giovanni Pernigotto, Andrea Gasparella, Marco Baratieri</i>	253
On the influence of several parameters in energy model calibration: the case of a historical building <i>Roberta Pernetti, Alessandro Prada, Paolo Baggio</i>	263
Energy simulation and design of a hot box suitable for dynamic tests of building envelope opaque components <i>Alessandro Prada, Davide S. Gigli, Andrea Gasparella, Marco Baratieri</i>	275
The effect of material uncertainties on envelope heat transfer simulations <i>Alessandro Prada, Paolo Baggio, Marco Baratieri, Andrea Gasparella</i>	285
Quasi-steady state and dynamic simulation approaches for the calculation of building energy needs: Part 1 thermal losses <i>Giovanni Pernigotto, Andrea Gasparella</i>	295
Quasi-steady state and dynamic simulation approaches for the calculation of building energy needs: Part 2 thermal gains <i>Giovanni Pernigotto, Andrea Gasparella</i>	305
Improving summer energy performance of highly insulated buildings through the application of a thermal analysis by numerical simulation <i>Ilaria Ballarini, Vincenzo Corrado</i>	313

Energy performance characterisation of vented opaque envelope through simplified methodologies <i>Vincenzo Corrado, Alice Gorrino, Simona Paduos</i>	323
Impact of using cool paints on energy demand and thermal comfort of a residential building <i>Diana Dias, João Machado, Vítor Leal, Adélio Mendes</i>	333
Long term evaluation of building energy performance: comparison of the test reference year and historical data series in the North Italian climates <i>Giovanni Pernigotto, Gianluca Antonacci, Paolo Baggio, Andrea Gasparella, Jan Hensen</i>	343
Analysis of the impact of ventilated cavities on the performance of opaque components <i>Alessandro Prada, Marco Baratieri, Andrea Gasparella</i>	353
GA-optimisation of a curtain wall façade for different orientations and climates <i>Debora Bogar, Gianluca Rapone, Ardeshir Mahdavi, Onorio Saro</i>	363
Use of PCM materials for the reduction of thermal energy requirements in buildings <i>Francesco Reda, Domenico Mazzeo, Natale Arcuri, Roberto Bruno</i>	373
Energy and daylighting interaction in offices with shading devices <i>Francesca Mazzichi, Marco Manzan</i>	385
Evaluating the nature and significance of ambient wind regimes on solar photovoltaic system performance <i>Abhishek Rao, Monto Mani</i>	395
Thermo-fluid dynamics of woody biomass flue gas in the heat accumulation stoves <i>Paolo Scotton, Daniele Rossi, Mauro Barberi, Stefano De Toni</i>	407
List of authors	I F Í Á

Introduction

Andrea Gasparella – Free University of Bozen-Bolzano, Italy

Building simulation has been in constant development for several decades. Taking advantage of the benefits of the increased computational power of personal computers, building simulations have become one of a number of common productivity tools available to practitioners and designers in the building physics and building energy systems sectors. As in similar cases, the increasing popularity of an instrument that was originally “just for insiders”, raises some concerns over the proper use of building simulations, their correct application field and how to interpret accurately the increasingly detailed results being produced. More precise detail in hypotheses and input is required to perform a solid building simulation and this leads to a process of greater complexity, a lengthier time span and higher costs. Thus a sensible balance between effort and benefit and is required.

Therefore, it is not surprising that common topics of debate in the wider “building simulation” community are uncertainty and sensitivity analysis, simulation codes validation, input data measurement and analysis. The question is: how uncertain and reliable are the results due to the uncertainty of inputs and to the approximations introduced by some simplified algorithms?

A second trend, which has been consolidating with the enhancement of computation capabilities, is the development of more detailed and complex simulation approaches which integrate the different aspects that interact, such as thermal, humidity lighting, acoustics and the related comfort considerations. Building simulations are extending the possibilities to go into even more detail in the analysis of the complex phenomena that can lead to a building performing well. Moreover, the simulation scale of the considered subjects is widening from the human to the urban,

ranging from physiology and psychology to meteorology.

Further, yet more in general: what are building simulations useful for? And in particular, what are the novel applications of building simulations? Calibrated simulations for energy diagnosis, model predictive control, simulation predictive control, multi-objective optimization, and so on, are just a part of the answer. It is likely much more will be invented in the future.

All the above, combined with the catalytic effect of the current sensitivity to energy and environmental issues, especially in the building sector, would make it indubitably worthwhile to have a further building simulation conference. The first was in Italy, where the broad range of widely variable climatic conditions put the performance of more simplified approaches and design criteria to the test. This was the first of a series of occasions to be developed in Bolzano, the region that has brought us CasaClima/KlimaHaus and was the first attempt to effect changes in the design and building approach for higher performance buildings.

This was the context in which the first IBPSA-Italy conference took place at the Free University of Bozen/Bolzano from January 30 to February 1, 2013, and which enjoyed positive outcomes. The event comprised more than 70 delegates, 118 authors, 44 presentations and two keynote speeches.

The event was much more than just a national meeting, thanks to the special presence of Jan Hensen and Ardeshir Mahdavi who captured the audience with their keynote speeches on “Computational building energy simulation for design of high-performance buildings” and on “Predictive building systems control logic with embedded simulation capability: experiences, challenges, and opportunities” respectively. The event also provided a valuable opportunity to

discuss with an international audience, thanks to the participation of delegates from several countries abroad.

It was also something more than a scientific conference due to its explicit focus on the application potential of building simulations and on the strategies for the diffusion of the use of building simulations outside of research institutions and this was proved by the final round table open to the public. A hundred delegates, the participation of local professional associations of

engineers and architects, of the AICARR (the Italian Association of Air conditioning, heating and refrigeration) and the CTI (the National Thermo-technical Committee, in charge of the development of technical standards), of the IBPSA-Italy and the IBPSA-Germany/Austria and the presence of the ANDIL (the Association of Italian Clay Brick and Roof Tile producers) mean that there is every confidence of an even brighter future for Building Simulation applications in Italy.

Predictive building systems control logic with embedded simulation capability: experiences, challenges, and opportunities

Ardeshir Mahdavi – Department of Building Physics and Building Ecology, Vienna University of Technology, Vienna, Austria

Abstract

In predictive simulation-based building systems control, candidate control options (i.e., various combinations of the control device states) for future time instances are proactively simulated and evaluated with regard to control objectives. Thus, preferable control actions are identified and instantiated. A number of virtual and prototypical implementations of this concept have been introduced in the past, especially in the field of lighting and shading controls. Further studies augmented the simulation-based predictive building systems strategy with agent-based technologies and machine-learning methods. More recently, we have explored applications in natural ventilation and passive cooling. Using content from previous publications, this keynote addresses simulation-supported predictive building systems control, focusing on its application toward passive cooling in buildings.

outdoor day-night temperature amplitudes and buildings' inherent thermal inertia. The intelligent use of passive control methods combined with innovative building systems as well as advanced sensory and actuating components have the potential to significantly decrease the energy use for space cooling (Lomas 2006, Garça et al. 2003, Krausse et al. 2007, Salmeron et al. 2009, Mahdavi and Pröglhöf 2004, 2005, 2006, Mahdavi et al. 2009). This possibility was explored within the framework of a number of recent research projects. Thereby, the primary ingredients of passive cooling (thermal mass and amplitudinal variation of outdoor temperature) were harnessed via a sensor-supported simulation-assisted predictive system control strategy. To evaluate this method, it was implemented and tested in five offices in two office buildings in Vienna and Stalhofen, Austria.

1. Introduction

Deployment of simulation-assisted control approach toward ventilation-supported passive cooling represents an interesting and important case in point. The cooling energy demand in central Europe is rapidly increasing, due in part to developments regarding climate change and urban heat islands. Conventional cooling systems are energy-intensive and problematic from the environmental point of view. Development of alternative energy-efficient alternatives for space cooling in new and existing buildings is thus of importance both environmentally and economically. One innovative possibility to address this challenge is to explore the potential of technologically revisited and updated passive cooling techniques, which are primarily based on

2. Predictive simulation-based control

2.1 General structure

The application of simulation-assisted control method in the building performance domain was introduced in Mahdavi 1997 and further elaborated, amongst others, in Mahdavi, 2001. This concept, which should not be confused with model-predictive control (García et al. 1989), involves the incorporation of explicit numeric performance simulation in the control core of buildings' environmental systems (e.g., for window ventilation and shading controls). Thereby, candidate control options (i.e., alternative combinations of the possible states of different control devices) for a future time instance are proactively accessed via performance simulation.

The simulation results for these alternative control constellations are compared with regard to the control objective. Thus, better performing control actions are identified and instantiated, either directly by the building's control unit, or through informed occupants' actions. A number of virtual and prototypical implementations of this concept have been introduced in the past, especially in the field of lighting and shading controls (see, for example, Mahdavi et al. 2000; Mahdavi 2008). Further studies augmented the simulation-based predictive building systems strategy with agent-based technologies and machine-learning methods (Chang and Mahdavi 2002, Mo and Mahdavi 2003). More recently, we have explored the application of simulation-powered control systems to the natural ventilation and passive cooling domains (Mahdavi et al. 2009, Schuss et al. 2010).

In the present implementation, the control method generates and evaluates alternative operation possibilities using genetic algorithms and the multi-domain simulation results. Figure 1 illustrates the basic sequence involved in the approach, which is typically instantiated on a regular basis (e.g., once every hour). The control procedure was implemented in the matlab environment (Matlab 2010) and uses HAMbase (van Schijndel 2007) and (Radiance 2010) as embedded simulation tools. Services for data monitoring, communication, and weather forecast were programmed in C and run independently. Monitoring data (internal and external sensors) together with the web-based weather forecasts data were stored in a SQLite database.

2.2 Performance indicators

To guide the operation of the control system, a number of performance functions and indicators were defined and applied to evaluate the multi-domain simulation results. The overall performance indicator i (Equation 1) is the weighted sum of all individual indicators i_x . The value of each indicator and the sum of the weighting factors w_x is in the range of 0 to 1. Hence i must be in the same range. The ranking of the alternative control possibilities is done by maximum to minimum sorting.

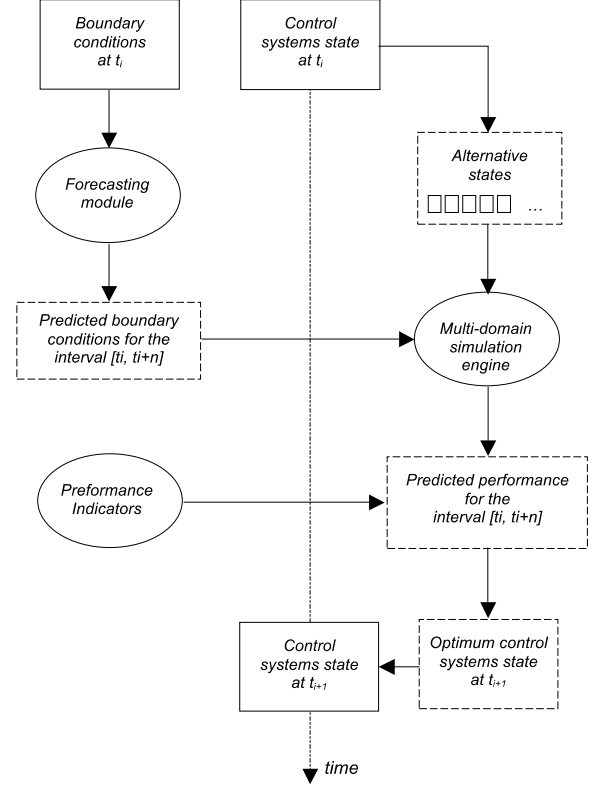


Fig. 1 – Illustration of the simulation-assisted control process

$$i = \sum_x i_x \cdot w_x$$

$$i, i_x, w_x \in [0, 1] \quad \text{and} \quad \sum_x w_x = 1 \quad (1)$$

The calculation of each indicator is based on the simulated predictive trend of the related system parameter (e.g., room air temperature). For each parameter, the sum of deviations d_{period} is calculated for the future n time steps shown in Equation 2.

$$d_{period} = \sum_{k=t_i}^{t_i+n} d(k) \quad (2)$$

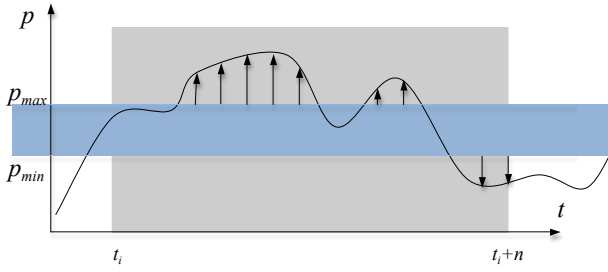
The calculation of each deviation depends on a fixed set point (Equation 3) or an acceptable parameter range as shown in Equation 4 and Figure 2. The general indicator i_x could be derived either linearly (Equation 5) or exponentially (Equation 6).

$$d(t) = |p(t) - p_{sp}(t)| \quad (3)$$

$$d(t) = \begin{cases} p_{\min} - p(t) & \text{if } p(t) < p_{\min} \\ 0 & \text{if } p_{\min} \leq p(t) \leq p_{\max} \\ p(t) - p_{\max} & \text{if } p(t) > p_{\max} \end{cases} \quad (4)$$

$$i_x = \begin{cases} 1 - \frac{d_{\text{period}}}{d_{\text{period max}}} & \text{if } d_{\text{period}} < d_{\text{period max}} \\ 0 & \text{if } d_{\text{period}} \geq d_{\text{period max}} \end{cases} \quad (5)$$

$$i_x = 1 - e^{-C \cdot d_{\text{period}}} \quad (6)$$


 Fig. 2 – Deviation calculation for a general system parameter p

The principle calculation procedure for HVAC and lighting power use are expressed in equations 7 and 8 respectively.

$$i_{PHVAC} = \frac{1}{n} \sum_{t=t_i}^{t_i+n} 1 - \frac{P_{HVAC}(t)}{P_{HVAC_{\max}}} \quad (7)$$

$$i_{PL} = \frac{1}{n} \sum_{t=t_i}^{t_i+n} 1 - \frac{P_{Lighting}(t)}{P_{Lighting_{\max}}} \quad (8)$$

2.3 Generation of alternative control schedules

The predictive control method needs a set of alternative operation states in terms of the relevant device control schedules. Using all possible combinations over the whole forecast interval would lead to an unmanageable number of possibilities. An approach using genetic algorithms (see Figure 3) provides a possibility to handle this challenge.

Thereby, a number of default operation schedules

were used together with randomized schedules as the initial setup. Needed state definitions and device attributes were stored in a predefined data structure to generate the schedules automatically. Based on the first generation simulation, the best-ranked schedules were selected to generate new child schedules in a random multipoint crossover reproduction process. For this purpose, the high-ranked schedules were crossed with themselves as well as with additional randomly selected schedules as parent elements. The selection of the fittest alternative (schedule) was done via the previously mentioned performance indicators.

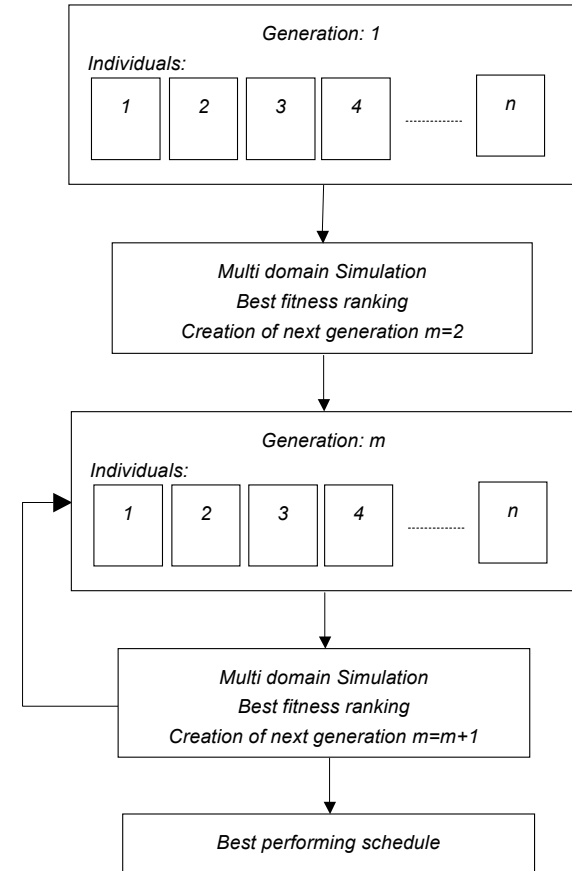


Fig. 3 – Illustration of the genetic generation of the desired operation schedules

3. Implementation

Two office buildings in Austria were selected to implement and systematically test and evaluate the approach. The first object (VUT) consists of three adjacent office rooms in an old office building of Vienna University of Technology. The second test

facility (FIBAG) consists of two rooms (identical in layout but located on two adjacent floors) in an office building in Stallhofen, Styria. Note that the offices in VUT were actively used during the test period. This provided the opportunity to test the method's operation under realistic conditions. The corollary was, however, a few instances of user interference with the system's operation. In contrast, tests in FIBAG were conducted under unoccupied conditions.

3.1 VUT

Three occupied nearly identical south-oriented office spaces (R1, R2, and R3) were specifically targeted for our study (see Figure 4). The office R1, which has manually operated windows and internal venetian blinds, was kept as is and used as a reference. The other two offices were equipped with window actuators (for automated operation), as well as internal (R2) and external (R3) window shades. Additionally, PCM elements as well as a ceiling fan were installed in R3.

An overview of the deployed hardware equipment is provided in Table 1 and the hardware system schema is illustrated in Figure 5. All rooms were equipped with sensors to measure indoor parameters such as air, surface, and globe temperatures, relative humidity, occupancy, illuminance at the ceiling and in the workplace, air velocity, and carbon dioxide concentration (Figure 6). In addition, outdoor environmental data was collected (Figure 7) in front of the offices (air temperature, relative humidity, wind speed, and precipitation) and on the rooftop (global horizontal radiation, and diffuse horizontal radiation). Shade position and door/window status were also monitored.

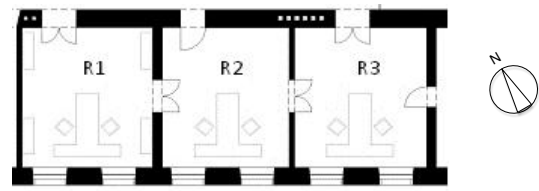


Fig. 4 – VUT - office layout

3.2 FIBAG

The predictive control approach was also implemented in two rooms in a new office building in Styria, Austria (see Figure 8). The building structure with a concrete skeleton (ceilings and staircases) and the lightweight internal and external walls is typical for new office buildings in Austria. This circumstance, combined with the glass and aluminium façade, results in a reduced useable thermal storage mass and thus aggravates the impact of solar gains.

The two rooms are identical in terms of layout (Figure 9 and 10) and are located in the first and second floor on the northwest corner of the building. The offices were equipped with actuators for lighting, shading, and window operation. Indoor conditions in both rooms as well as the external climate were monitored with sensors for thermal and lighting parameters. One room was controlled with the proposed predictive simulation-based control method. The second room was used as a reference.

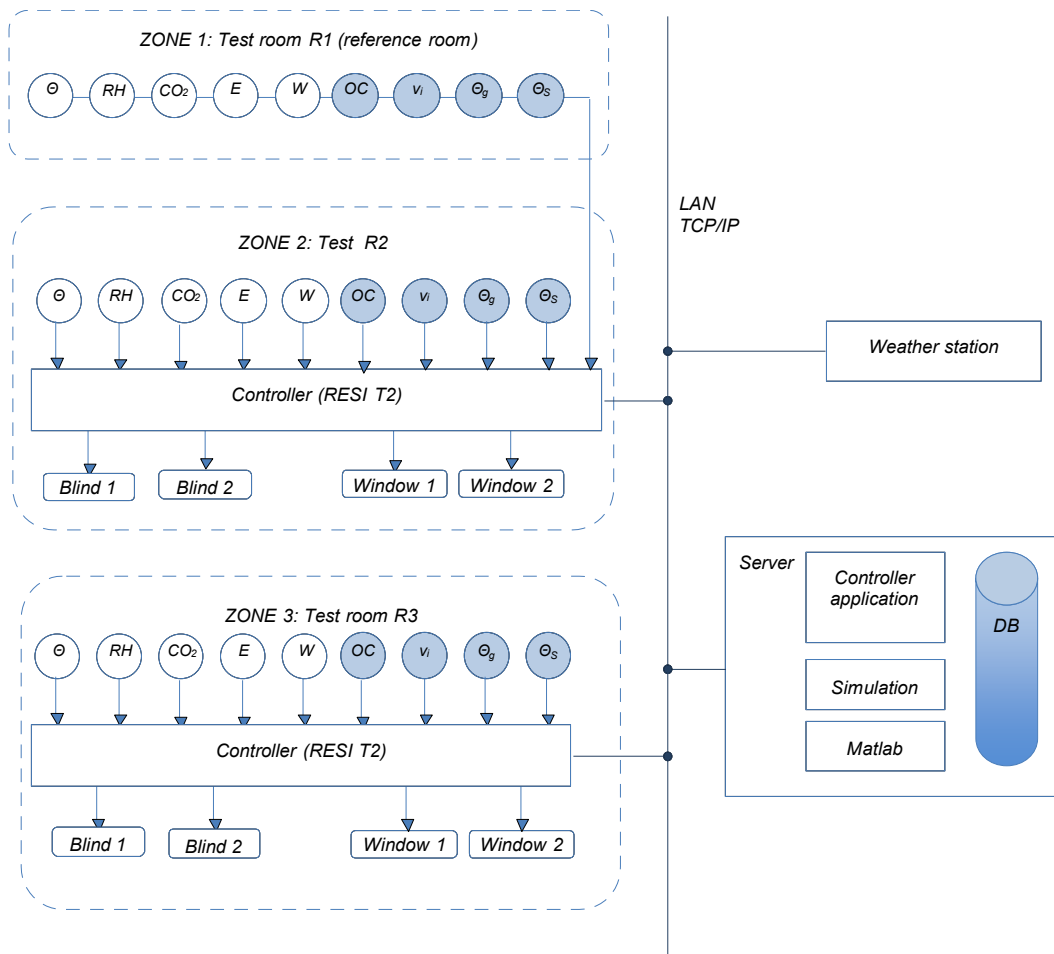


Fig. 5 – VUT - Hardware systems schema

HARDWARE	DESCRIPTION
Indoor climate sensors	Compact indoor climate stations to measure air temperature, relative humidity, and velocity as well as carbon dioxide and illuminance in the workplace.
Outdoor climate sensors	Weather station for air temperature, relative humidity, precipitation, global irradiance, wind speed, and wind direction.
User action and presence sensor	Presence: PIR - Sensor with adjustable threshold time; Door opening: magnetic contact sensors
Window automation	Two synchronized adjustable drives for each window to control the window opening position continuous.
Shading automation	Single drives with a special gear unit for height and angle positioning
Lighting control	The room controller can adjust dimming levels between 10 to 100% of the total lighting power
Backbone and communication network	IP base communication with access to building data points and data history

Table 1 – Summary of deployed hardware components



Fig. 6 – VUT – Internal climate sensors

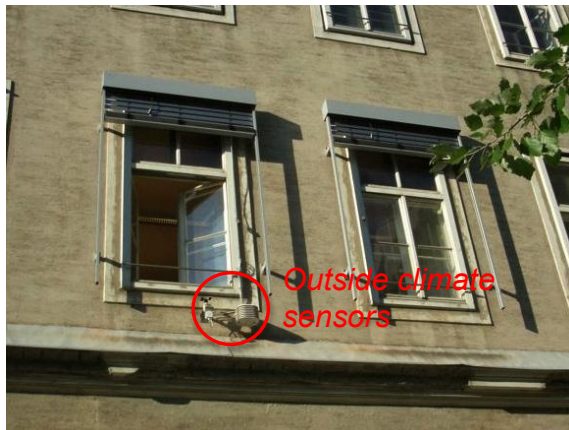


Fig. 7 – VUT – Façade with climate sensors



Fig. 8 - FIBAG – Office building with two test rooms (marked)

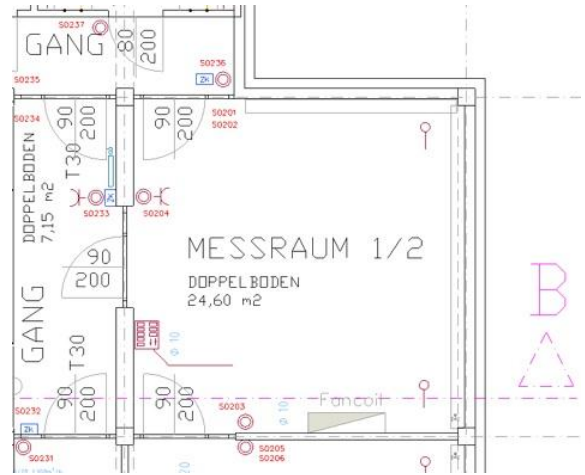


Fig. 9 – FIBAG - Test room layout



Fig. 10 – FIBAG - internal view of test room

3.3 Evaluation period

The control method was deployed in the operation of two test facilities during two months in summer 2010. However, parts of July were used for initial testing of the control setup. In August the system operated continuously. Hence, the present treatment focuses (with the exception of Figure 9), on August data. The control cycle was executed once every hour. Figure 11 illustrates a typical outcome of such a cycle. The left side of the plot represents the history trends of the room air temperature (grey) and the outdoor air temperature (red). The predicted outside temperature is plotted on the right sight together with multiple simulation-based predictions of air temperature trends due to the virtual enactment of candidate control options. The best performing option is marked in black.

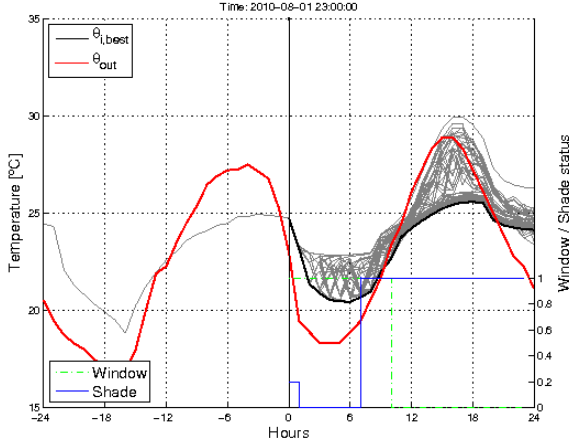


Fig. 11 – Indoor and outdoor (red) temperature history (left) and multiple predictions (right) with the best performing course (thick black) in the test room for a day in August 2010

To identify the preferable control option, two performance indicators (i) were used. One was related to the air temperature (θ_{air}) and the second related to mean interior surface temperatures of the room (θ_s). These two indicators were weighted equally (w_{air} , w_s).

$$i = i_{\theta_{air}} \cdot w_{\theta_{air}} + i_{\theta_s} \cdot w_{\theta_s} = \frac{1}{2} \cdot i_{\theta_{air}} + \frac{1}{2} \cdot i_{\theta_s} \quad (9)$$

To derive the indicator values, a negative exponential formulation was used based on corresponding time-dependent aggregate deviations (Equation 10 and 11). In these equations, c represents a calibration factor.

$$i_{\theta_{air}} = 1 - e^{-c \cdot d_{\theta_{air}}} \quad (10)$$

$$i_{\theta_s} = 1 - e^{-c \cdot d_{\theta_s}} \quad (11)$$

In case of the storage temperature indicator, aggregated deviations are calculated as a sum of all discrete time deviations $m(t)$ in the forecast interval (Equation 12). In case of air temperature (Equation 13), only the occupancy hours (8:00-17:00) are considered, as represented by $g(t)$. Figures 12 and 13 illustrate this circumstance.

$$d_{\theta_s} = \sum_{t=t_i}^{t_i+n} m_{\theta_s}(t) \quad (12)$$

$$d_{\theta_{air}} = \sum_{t=t_i}^{t_i+n} m_{\theta_{air}}(t) \cdot g(t) \quad (13)$$

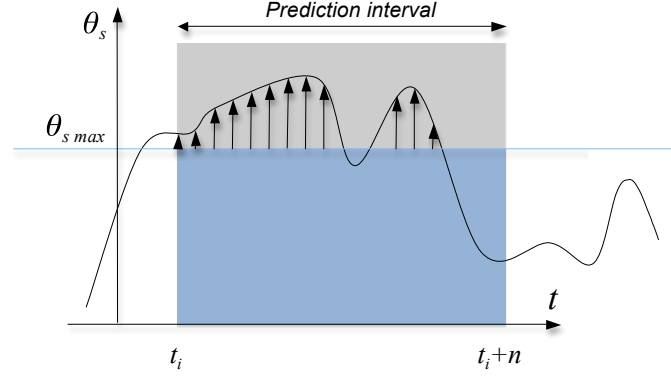


Fig. 12 – Deviation calculation for the surface temperature performance indicator

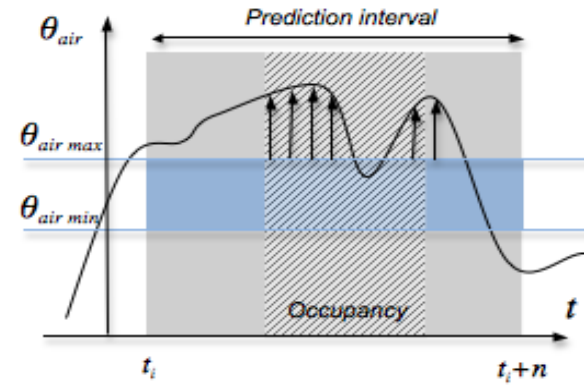


Fig. 13 – Deviation calculation for the air temperature performance indicator

4. Results

The test results point to the potential of the proposed predictive control: As compared to the reference rooms, the rooms with the predictive control systems demonstrated preferable indoor climate conditions.

4.1 VUT

To illustrate the performance of the method, Figure 14 shows the indoor and outdoor air temperature trends for three successive days in July 2010. The better thermal performance of the controlled rooms is obvious. The peak temperature readings in R3 and R2 were 4 K and 2 K lower respectively compared to the reference room R1.

To evaluate the system's performance in more detail, Predicted Mean Vote values (PMV) as well

as mean overheating was calculated for August (working hours, 8:00 to 17:00). PMV-based comfort assessment in the context of free-running buildings has been questioned. Nonetheless, given its familiarity, it is used here to document the relative differences between the reference and controlled rooms. Figure 15 depicts the monthly mean PMVs and the mean overheating (computed for a reference overheating temperature of 26°C) for R1 (reference room), R2, and R3. As compared to the reference room, rooms R2 and R3 show better results. The collected data was also processed in terms of psychometric charts (Figures 16 to 18). The (red) dots represent mean hourly values during working hours (08:00-17:00). The (green) polygons show the applicable thermal comfort zone according to the adaptive thermal comfort theory (Szokolay 2004). The psychometric charts display a similar trend. R3, as the best-equipped room, was 38% less outside the thermal comfort zone compared to R1. Likewise, R2 was about 24% less outside the thermal zone than R1.

In addition to such numeric comparisons, a user feedback was collected via questionnaires. In general, users in R2 and R3 generally had a better view of the thermal environment than in the reference room. Nighttime ventilation regime, added shading devices, and the possibility to control the devices with the system's GUI was explicitly rated positive. The noise generated by the motorized actuators while opening or closing windows and blinds was commented on negatively. Moreover, users expressed the need for a more fine-tuned glare control.

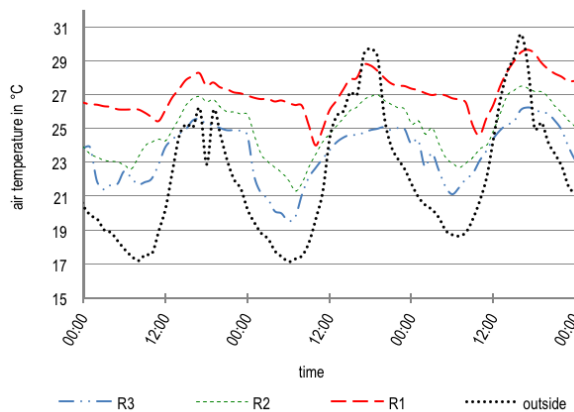


Fig. 14 – Typical air temperature trends in July 2010

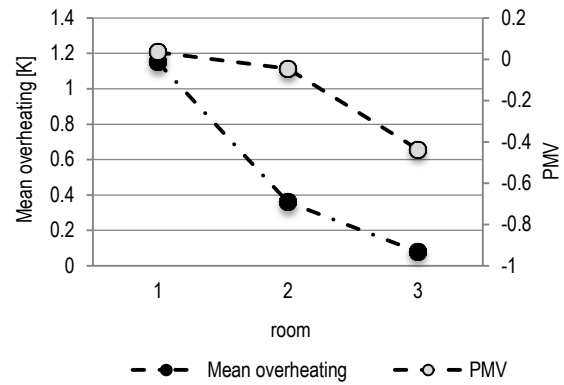


Fig. 15 – Mean overheating of indoor air and mean PMV values (VUT, August 2010)

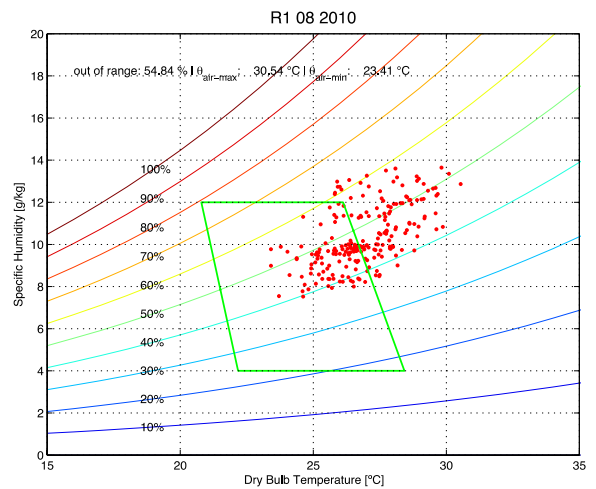


Fig. 16 – Measured temperature and humidity in R1 (VUT) during working hours, August 2010

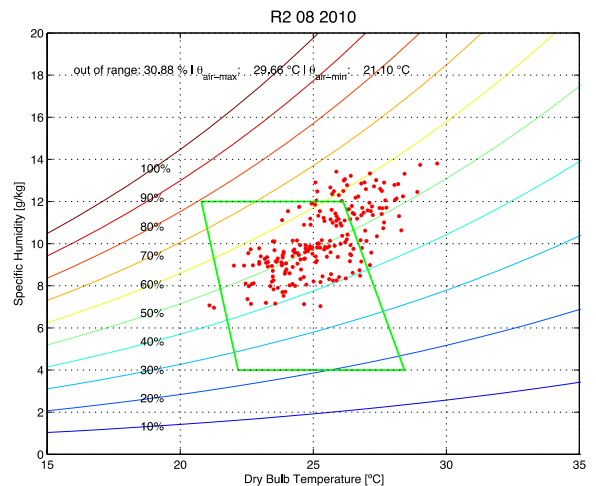


Fig. 17 – Measured temperature and humidity in R2 (VUT) during working hours, August 2010

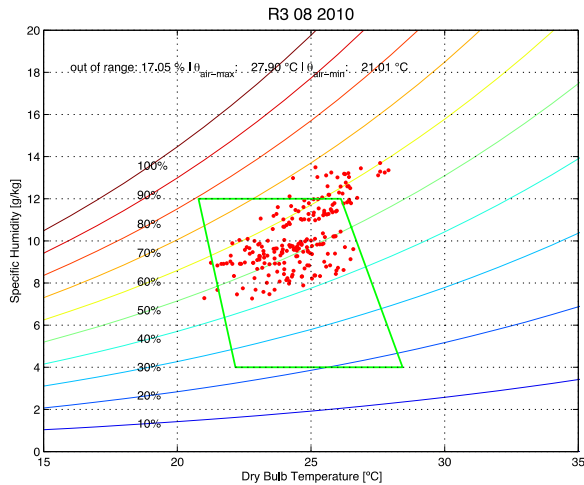


Fig. 18 – Measured temperature and humidity in R3 (VUT) during working hours, August 2010

4.2 FIBAG

Monthly mean PMV and overheating values for test spaces in FIBAG are shown in Figure 19. As compared to the reference room 2, room 1, which was operated via the simulation-based control method, provided better thermal conditions.

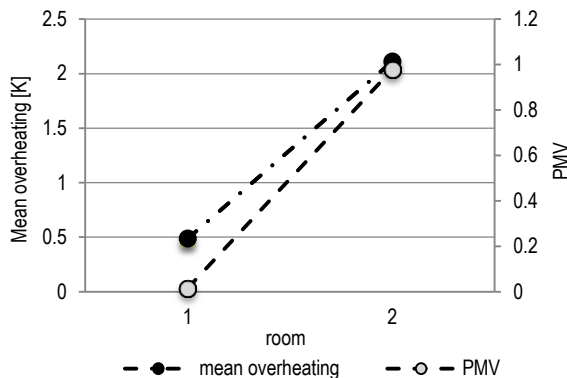


Fig. 19 – Mean overheating of indoor air temperature and mean PMV values (FIBAG, August 2010)

Psychrometric charts (August 2010) display a similar trend (see Figures 20 and 21). As compared to the reference room 2, thermal conditions in room 1 were 35% longer in the thermal comfort zone (working hours).

4.3 Weather prediction quality

The quality of the integrated online weather forecasts was analyzed in terms of differences to the stored local monitored weather data. Generally speaking, forecast for air temperatures showed

quite acceptable deviations in an overall one-degree range with some outliers around 2 to 4 degrees (Figure 22).

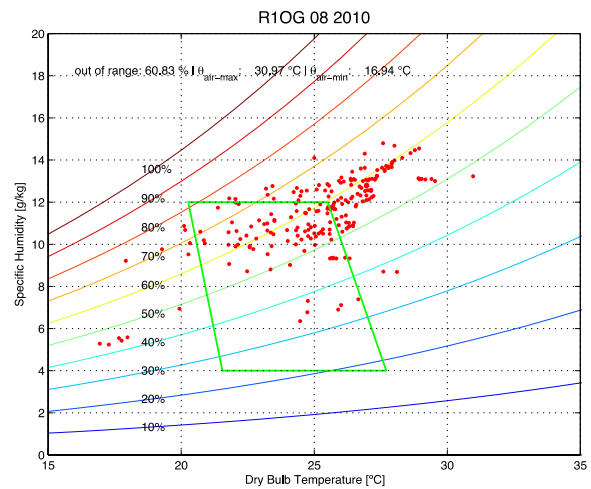


Fig. 20 – Measured temperature and humidity in room 1 during working hours (FIBAG, August 2010)

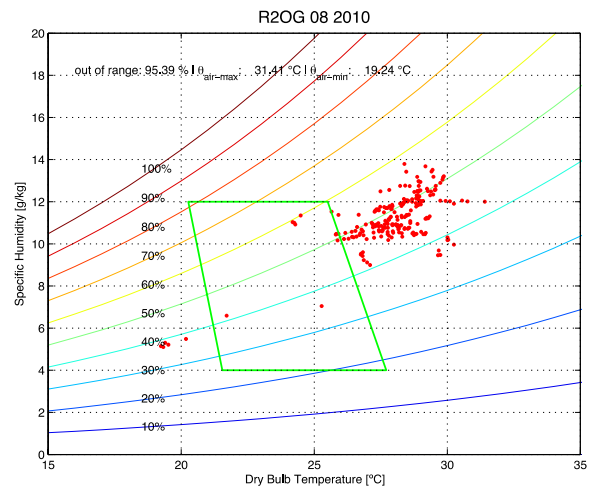


Fig. 21 – Measured temperature and humidity in room 2 during working hours (FIBAG, August 2010)

5. Conclusions

The research results illustrate the potential of the predictive simulation-assisted approach to offer low-cost and energy-efficient indoor environmental control (ventilation-supported passive cooling). Compared to the reference rooms, the rooms with the predictive control systems clearly demonstrated preferable indoor climate

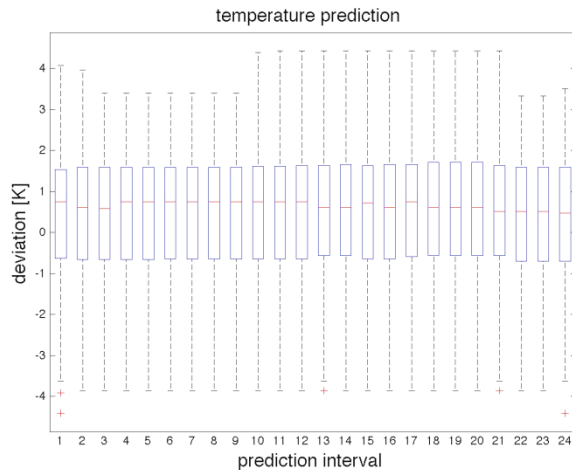


Fig. 22 – Temperature forecast deviation of 2010 data for 1 to 24 hour prediction

conditions. A number of measures could further improve the performance of the system in the passive cooling deployment case:

- Minimization of internal loads: The installed power of the electric devices (computers, artificial lights, etc.) should be minimized. Devices should be switched off (or set to hibernate) when not in use.
- Importance of informing the users: Users should be instructed regarding the proper operation of building systems. Moreover, the users should be given proper feedback about the implications of their actions and behavior.
- Accuracy of input parameters for the predictions: The quality of the weather forecast is critical. Especially the prediction of solar radiation needs improvement.
- Calibration of the simulation tool: The performance of the simulation-based control obviously depends decisively on the reliability of the predictions. Careful calibration of the initial simulation model via measurement data is thus the single most important precondition for the successful implementation of simulation-based predictive building systems control.

The results and the experiences with the implementation suggest that the proposed approach has considerable potential. Specifically, it can be realized in existing structures with a reasonable degree of investment.

6. Acknowledgement

The author acknowledges Dr. Matthias Schuß and his instrumental role in the implementation of the research project presented in this keynote paper. This research was supported in part by a fund from FFG "Naturally Cool" (Project-Nr: 817575). Additional support was provided via the K-Project "Multifunctional Plug & Play Façade" (Project-Nr: 815075) and the "Hans Höllwart Forschungszentrum für integrales Bauwesen AG".

References

- Chang, S., Mahdavi, A. 2002. A hybrid system for daylight responsive lighting control. *Journal of the Illuminating Engineering Society*, Volume 31, Number 1, Winter 2002, pp. 147-157.
- Garça, G.C., Linden, P.F., McConahey, E., Haves, P. 2003. Design and testing of a control strategy for a large, naturally ventilated office building. *Proceedings of the 8th International IBPSA Conference, Building Simulation 2003*, pp. 399-406, Augenbroe, G., Hensen, J. (eds.), Volume 1, Eindhoven, Netherlands.
- García, C. E., David M. Prett, D. M., Manfred Morari, M. 1989. Model predictive control: Theory and practice—A survey. *Automatica*, Volume 25, Issue 3, May 1989, Pages 335-348, Elsevier Science Ltd.
- Krausse, B., Cook, M.J., Lomas, K.J. 2007. Environmental performance of a naturally ventilated city centre library. *Energy and Buildings* 39, Issue 7, pp. 792-801, Todorovic B., Meier A.K. (eds.), Elsevier.
- Lomas, K. J. 2006. Architectural design of an advanced naturally ventilated building form. *Energy and Buildings*, Volume 39, Issue 2, pp. 166-181, Elsevier.
- Mahdavi, A. 1997. Toward a Simulation-assisted Dynamic Building Control Strategy. *Proceedings of the Fifth International IBPSA (International Building Performance Simulation Association) Conference*, Vol. I, pp. 291-294.
- Mahdavi, A. 2001. Simulation-based control of building systems operation. *Building and*

- Environment, Volume 36, Issue 6, ISSN: 0360-1323. pp. 789-796.
- Mahdavi, A. 2008. Predictive simulation-based lighting and shading systems control in buildings. Building Simulation, an International Journal, Springer, Volume 1, Number 1, ISSN 1996-3599, pp. 25-35.
- Mahdavi, A., Chang, S., Pal, V. 2000. Exploring Model-Based Reasoning in Lighting Systems Control. Journal of the Illuminating Engineering Society, Volume 29. Number 1. Winter 2000. pp. 34-40.
- Mahdavi, A., Orehounig, K., Pröglhöf, C. 2009. A simulation-supported control scheme for natural ventilation in buildings. Proceedings of the 11th IBPSA Conference, Building Simulation 2009, pp. 783-788, Glasgow, Scotland.
- Mahdavi, A., Pröglhöf, C. 2004. Natural ventilation in buildings – Toward an integrated control approach. Proceedings of the 35th Congress on Heating, Refrigerating and Air-Conditioning, pp. 93 – 102, Belgrade, Serbia.
- Mahdavi, A., Pröglhöf, C. 2005. A model-based method for the integration of natural ventilation in indoor climate systems operation. Proceedings of the 9th International IBPSA Conference, Building Simulation 2005, pp. 685–692, Montreal, Canada.
- Mahdavi, A., Pröglhöf, C. 2006. A model-based approach to natural ventilation. Building and Environment, Volume 43(4), pp. 620–627, Elsevier.
- Matlab, 2010. MATLAB Release 2010a, The MathWorks, Inc., <http://www.mathworks.com>.
- Mo, Z., Mahdavi, A. 2003. An agent-based simulation-assisted approach to bi-lateral building systems control. Proceedings of the Eight International IBPSA Conference (Eindhoven, Netherlands), Vol. 2. pp. 887-894, Augenbroe, G., Hensen, J. (eds). ISBN 90 386 1566 3.
- Radiance, 2010. Radiance Synthetic imaging system Version 4, University of California, <http://radsite.lbl.gov/radiance/>.
- Salmeron, J.M., Sanchez, J., Ford, B., van Steenberghe, T., Alvarez, S. 2009. Passive and hybrid draught cooling in buildings and software for design. Rehva Journal. Volume 46, Issue 6, pp. 34–39, ISSN 1307-3729.
- Schuss, M., Pröglhöf, C., Orehounig, K., Dervishi, S., Müller, M., Wascher, H., Mahdavi, A. 2010. Predictive model-based control of ventilation, lighting, and shading systems in a building. BauSIM 2010, Martens B., Mahdavi A. (eds.), Vienna, Austria.
- Szokolay, S.V., 2004. Introduction to architectural science: the basis of sustainable design. Elsevier Science, Oxford, pp. 16–22, ISBN 0 7506 58495.
- van Schijndel, A.W.M. 2007. Integrated heat air and moisture modeling and simulation. PhD thesis, Eindhoven University of Technology, available at: <http://alexandria.tue.nl/extra2/200612401.pdf> or <http://sts.bwk.tue.nl/hamlab> [accessed June 2010]

The air energy balance equation paradox

Livio Mazzarella – Department of Energy, Politecnico di Milano, Italy

Abstract

In building physics applications, mainly related to the building energy performance simulations, the master equation is the inner air energy balance equation. Historically the followed approach in writing down such master equation was to adopt the simplifying hypothesis of incompressible fluid for the air assumed dry. This hypothesis, among others, reduces the general integral energy balance equation to the usual formulation which is reported in textbooks and manuals and has been used in available energy simulation programs, such as Energy Plus, Esp-r, TRNSYS, etc. Later the moist air problem, the indoor air humidity control, has been faced just by adding a new integral balance equation: the water vapour mass balance equation. In this work it is pointed out how this "layered" historical approach leads to a paradox: an incompressible fluid is used to describe an ideal gas in an ideal gas mixture. Herewith the general integral energy balance equation is directly written in terms of moist air under ideal gas hypothesis and it is shown how, under acceptable specific hypothesis, it is possible to obtain a similar but conceptually different final formulation, which mainly differs in the transient storage term.

1. Introduction

In almost all textbooks and guides dealing with building physics, thermal loads calculations for HVAC design, buildings thermal performances and energy requirements, the generalised (i.e. unsteady) energy balance equation for the building zone is not commonly reported, meaning the indoor air integral energy conservation equation. For instance, guides like CIBSE Guide [CIBSE, 2006], the ASHRAE Handbook [ASHRAE, 2009], the Carrier Handbook [Carrier, 1965] do not report any energy balance equation, as they are focused on heating and cooling load calculations. Also

building physics textbooks do not give any detailed information on such basic equations, like [Hagentofl, 2001], [Hens, 2010], and just a few lines are normally present in buildings' heating and cooling textbooks without any explanation, like [Kreider, 2002], [Balaras, 1996]. Surprisingly also books devoted to energy performance modelling and simulation appear to be insufficient in analysing and describing that item, like [Underwood, 2004] and [Clarke, 2001]. Almost all those texts and the scientific literature dealing with energy transfer and performances in building (just as an example (Abuku, 2009)) use as an "energy" balance equation or "heat balance" or "sensible energy" balance equation for a building zone the following equation:

$$\begin{aligned} \rho_a c_p V_a \frac{dT_a}{dt} = & \sum_{j=1}^{N_{Surfaces}} A_j h_{cv_j} (T_{S_j} - T_a) + \\ & + \sum_{j=1}^{N_{zone}} \dot{m}_j c_p \cdot (T_{a_j} - T_a) + \dot{m}_{inf} c_p \cdot (T_{a,ext} - T_a) + \\ & + \dot{Q}_I^{(CV)} + \dot{Q}_{SYS}^{(CV)} \end{aligned} \quad (1)$$

where the first term represents the indoor air thermal energy increase or decrease due to zone surfaces-to-fluid convective heat flows, inter-zone air mixing, heat transfer due to infiltration of outside air, convective internal load and air H&C system input to the zone.

Few of them then add the "latent energy" balance equation, which is always written as humidity ratio balance equation (i.e. water vapour mass balance equation), as follows:

$$\begin{aligned} \rho_a V_a \frac{dx_a}{dt} = & \sum_{j=1}^{N_{Surfaces}} A_j h_{m_j} (x_{s_j} - x_a) + \sum_{j=1}^{N_{zone}} \dot{m}_j \cdot (x_{a_j} - x_a) + \\ & + \dot{m}_{inf} \cdot (x_{a,ext} - x_a) + \dot{M}_I^{(x)} + \dot{m}_{SYS} \cdot (x_{SYS} - x_a) \end{aligned} \quad (2)$$

where the first term represents the indoor air humidity increase or decrease due to zone

surfaces-to-fluid convective moisture flows, inter-zone air flows, humidity transfer due to infiltration of outside air, humidity internal load and air H&C system humidity net contribution to the zone.

Finally the three most known and used computer simulation tools for building energy performance assessment, Energy Plus (Energy Plus, 2012), ESP-r (Clarke, 2001; Aissan, 2005) and TRNSYS (TRNSYS, 2007), are just employing equation (1) and equation (2) for each zone air node without any reference to a deep explanation on their consistency with the simulated problem: moist air.

Analysing equations (1) and (2) it is evident that the following hypotheses are recalled:

- dry air as incompressible inviscid fluid in equation (1);
- moist air as ideal gas mixture in equation (2) as usually assumed to allow the writing of the water vapour mass balance in terms of humidity ratio and dry air mass flow rate.

Are they consistent with each other? It seems not. This contradiction may be, apparently, solved just observing that equation (1) can also be valid for an ideal gas which undergoes an isobaric process. Then what about the dry air mass conservation equation, which is embedded into equation (1) and (2) and implicitly assumes again dry air as incompressible fluid?

To solve this contradiction, the energy balance equation for a moist air volume (zone) will be directly derived in terms of moist air enthalpy and internal energy together with the mass conservation equation for both components, dry air and water vapour.

2. Basic Conservation Principles

To state clearly all necessary hypotheses to obtain a reliable energy balance equation for the zone indoor moist air, the best procedure is to start from the basic conservation principles:

- mass conservation principle;
- momentum conservation principle;
- energy conservation principle;

adding the necessary phenomenological or constitutive laws and the state equations for the considered phenomena and system.

Following the Eulerian approach (i.e. control volume approach), the integral form of the aforementioned conservation principles are given by:

$$\frac{dm^{(\alpha)}}{dt} = \sum_{j=1}^{N_\phi} \Phi_{cv_j}^{(m^{(\alpha)})} + \sum_{k=1}^{N_\sigma} \dot{M}_k^{(\alpha)} = \sum_{j=1}^{N_{\phi+\sigma}} \Phi_{cv_j}^{(m^{(\alpha)})} \quad (3)$$

$$\frac{d\mathbf{P}}{dt} = \sum_{j=1}^{N_{\phi+\sigma}} \Phi_{cv_j}^{(\mathbf{P})} + \mathbf{F}_s + \mathbf{F}_b \quad (4)$$

$$\frac{dE}{dt} = \sum_{j=1}^{N_{\phi+\sigma}} \Phi_{cv_j}^{(E)} + \Phi_T + \dot{W}_s + \dot{W}_b \quad (5)$$

where equation (3) has been written for a generic phase α of a material component, and thus the source term $\dot{M}_k^{(\alpha)}$ is just representing mass exchange between different phases. Because the source terms we deal with, $\dot{M}_k^{(\alpha)}$ is not a point source distributed inside the whole control volume, these source terms are included into extra advective flows $\Phi_{cv_j}^{(m^{(\alpha)})}$. This is possible because in our cases we usually have a clear separation surface between the source and the fluid; thus the mass “produced” by the sources can be simply represented through a flow that crosses the source-bounding surface (internal CV boundaries). Herewith the advective term is used instead of convective to stress the mass transfer due to bulk flow only (i.e. without mass diffusion). In the vectorial equation (4) \mathbf{P} is the momentum vector and \mathbf{F}_s and \mathbf{F}_b are respectively the superficial forces resultant vector and the body forces resultant vector, while the $\Phi_{cv_j}^{(\mathbf{P})}$ terms represent the momentum advection through the CV boundaries. In equation (5) E is the CV total energy, Φ_T is the conductive heat transfer from the bounding material surfaces to the fluid and fluid-to-fluid through the inlet/outlet mass flow surfaces, \dot{W}_s and \dot{W}_b respectively the power of surface forces and body forces, while the $\Phi_{cv_j}^{(E)}$ terms are the advective energy flows through the CV boundaries.

These integral principles can also be expressed in terms of local quantities as:

$$\frac{d}{dt} \int_{CV} \rho^{(\alpha)} dV = - \sum_{j=1}^{N_{\phi+\sigma}} \int_{S_{CV,j}} \rho^{(\alpha)} \mathbf{v} \cdot \mathbf{n} dS \quad (6)$$

$$\begin{aligned} \frac{d}{dt} \int_{CV} \rho \mathbf{v} dV = & - \sum_{j=1}^{N_{\phi+\sigma}} \int_{S_{CV,j}} (\rho \mathbf{v}) \mathbf{v} \cdot \mathbf{n} dS + \\ & + \int_{CV} \mathbf{f}_s dV + \int_{CV} \rho \mathbf{f}_b dV \end{aligned} \quad (7)$$

$$\begin{aligned} \frac{d}{dt} \int_{CV} \rho e dV = & - \sum_{j=1}^{N_{\phi+\sigma}} \int_{S_{CV,j}} (\rho e) \mathbf{v} \cdot \mathbf{n} dS + \\ & - \sum_{i=1}^{N_s} \int_{S_{CV,i}} \boldsymbol{\phi}_T \cdot \mathbf{n} dS + \\ & + \int_{CV} \mathbf{f}_s \cdot \mathbf{v} dV + \int_{CV} \rho \mathbf{f}_b \cdot \mathbf{v} dV \end{aligned} \quad (8)$$

where the local quantities are the volumetric mass ρ , the velocity vector \mathbf{v} , the specific force vectors by unit of surface \mathbf{f}_s and by unit of mass \mathbf{f}_b , the specific total energy e , the heat flow density vector $\boldsymbol{\phi}_T$.

To derive the local conservation principles the structure of the specific force vectors by unit of surface has to be consider, i.e.:

$$\mathbf{f}_s = \mathbf{T} \cdot \mathbf{n} \quad (9)$$

where \mathbf{T} is the symmetric stress tensor, obtaining:

$$\frac{\partial \rho^{(\alpha)}}{\partial t} + \text{div}(\rho^{(\alpha)} \mathbf{v}) = 0 \quad (10)$$

$$\frac{\partial}{\partial t} (\rho \mathbf{v}) + \text{div}(\rho \mathbf{v} \mathbf{v}) - \text{div}(\mathbf{T}) - \rho \mathbf{f}_b = 0 \quad (11)$$

$$\frac{\partial}{\partial t} (\rho e) + \text{div}(\rho e \mathbf{v}) + \text{div}(\boldsymbol{\phi}_T) - \text{div}(\mathbf{T} \cdot \mathbf{v}) - \rho \mathbf{f}_b \cdot \mathbf{v} = 0 \quad (12)$$

where $\mathbf{v} \mathbf{v}$ is the dyadic product¹ of vector \mathbf{v} with itself.

In equations (5), (8) and (12), assessing the energy conservation, the total and the specific total energy is used, defined as the sum of internal and kinetic energy:

$$E = U + E_k \quad ; \quad e = u + \frac{1}{2} v^2 \quad (13)$$

Substituting equation (13), second term, into equation (12) we obtain:

$$\begin{aligned} \frac{\partial}{\partial t} (\rho u) + \frac{\partial}{\partial t} \left(\rho \frac{v^2}{2} \right) + \text{div}(\rho u \mathbf{v}) + \text{div} \left(\rho \frac{v^2}{2} \mathbf{v} \right) + \\ + \text{div}(\boldsymbol{\phi}_T) - \text{div}(\mathbf{T} \cdot \mathbf{v}) - \rho \mathbf{f}_b \cdot \mathbf{v} = 0 \end{aligned} \quad (14)$$

which suggests the possibility to split the energy conservation principle into two balance equations, one related to the internal energy, the other to the kinetic energy.

2.1 Local Balance Equations

To achieve such a result allows us to have the dot product of the velocity vector \mathbf{v} and the local momentum conservation equation (11); this will result in the following balance equation (no longer conservation principle):

$$\frac{\partial}{\partial t} \left(\rho \frac{v^2}{2} \right) + \text{div} \left(\rho \frac{v^2}{2} \mathbf{v} \right) - \mathbf{v} \cdot \text{div}(\mathbf{T}) - \rho \mathbf{v} \cdot \mathbf{f}_b = 0 \quad (15)$$

which is the *local Mechanic Energy Balance Equation*. Subtracting equation (15) from equation (14) the *local Internal Energy Balance Equation* is derived:

$$\frac{\partial}{\partial t} (\rho u) + \text{div}(\rho u \mathbf{v}) + \text{div}(\boldsymbol{\phi}_T) - \text{tr}(\mathbf{T} \cdot \nabla \mathbf{v}) = 0 \quad (16)$$

where $\text{tr}()$ is the trace operator² as defined in linear algebra, and it comes out from the following differentiation rule:

$$\text{div}(\mathbf{T} \cdot \mathbf{v}) = \mathbf{v} \cdot \text{div}(\mathbf{T}) + \text{tr}(\mathbf{T} \cdot \nabla \mathbf{v}) \quad (17)$$

Using such a rule an alternative writing of equation (15) is possible as:

$$\begin{aligned} \frac{\partial}{\partial t} \left(\rho \frac{v^2}{2} \right) + \text{div} \left(\rho \frac{v^2}{2} \mathbf{v} \right) + \text{tr}(\mathbf{T} \cdot \nabla \mathbf{v}) + \\ - \text{div}(\mathbf{T} \cdot \mathbf{v}) - \rho \mathbf{v} \cdot \mathbf{f}_b = 0 \end{aligned} \quad (18)$$

which evidences, when compared with equation (16), the coupling term between mechanic energy and internal energy.

¹ the dyadic product of two vectors \mathbf{a} and \mathbf{b} is denoted by the juxtaposition $\mathbf{a} \mathbf{b}$, and its result, called dyad, is a second order tensor.

² the trace of an n-by-n square matrix A is defined to be the sum of the elements on the main diagonal, and the dot product between the two second order tensors, the stress tensor and the dyad constituted of the nabla operator and the velocity vector, is equivalent to a 3-by-3 square matrix and is a scalar quantity.

To clarify the meaning of such a coupling term it is convenient to introduce the usual splitting of the stress tensor in isotropic and anisotropic components,

$$\mathbf{T} = -P\mathbf{I} + \mathbf{D} \quad (19)$$

where P is the thermodynamic pressure and \mathbf{D} the deviatoric stress tensor.

Substituting equation (19) into equation (18) and (16) it follows:

$$\begin{aligned} \frac{\partial}{\partial t} \left(\rho \frac{v^2}{2} \right) + \text{div} \left(\rho \frac{v^2}{2} \mathbf{v} \right) - P \text{div}(\mathbf{v}) + \text{tr}(\mathbf{D} \cdot \nabla \mathbf{v}) + \\ + \text{div}(P\mathbf{v}) - \text{div}(\mathbf{D} \cdot \mathbf{v}) - \rho \mathbf{v} \cdot \mathbf{f}_b = 0 \end{aligned} \quad (20)$$

$$\begin{aligned} \frac{\partial}{\partial t}(\rho u) + \text{div}(\rho u \mathbf{v}) + \text{div}(\boldsymbol{\phi}_T) + P \text{div}(\mathbf{v}) + \\ - \text{tr}(\mathbf{D} \cdot \nabla \mathbf{v}) = 0 \end{aligned} \quad (21)$$

Defining

$$\phi_D \equiv \text{tr}(\mathbf{D} \cdot \nabla \mathbf{v}) \geq 0 \quad (22)$$

$$\dot{w}_{R,c/e} \equiv -P \text{div}(\mathbf{v}) \quad (23)$$

to be respectively the *local dissipation function* and the *local reversible compression/expansion power*, equations (20) and (21) can be more significantly rewritten as:

$$\begin{aligned} \frac{\partial}{\partial t} \left(\rho \frac{v^2}{2} \right) + \text{div} \left(\rho \frac{v^2}{2} \mathbf{v} \right) + \dot{w}_{R,c/e} + \phi_D + \\ - \dot{w}_s - \dot{w}_b = 0 \end{aligned} \quad (24)$$

$$\frac{\partial}{\partial t}(\rho u) + \text{div}(\rho u \mathbf{v}) + \text{div}(\boldsymbol{\phi}_T) - \dot{w}_{R,c/e} - \phi_D = 0 \quad (25)$$

that clearly shows reversible and irreversible conversion of local mechanic energy into internal energy.

The local reversible compression/expansion power, using the local mass conservation equation (10), can then be rewritten as:

$$\dot{w}_{R,c/e} \equiv \frac{P}{\rho} \left(\frac{\partial \rho}{\partial t} + \mathbf{v} \cdot \nabla \rho \right) = \frac{P}{\rho} \cdot \frac{D\rho}{Dt} \quad (26)$$

where the last term is the material derivative³ of the mass by volume.

³ Material derivative is defined as $\frac{D}{Dt} \equiv \frac{\partial}{\partial t} + \mathbf{v} \cdot \nabla$

2.2 Enthalpy Local Balance Equations

It is useful at this stage to introduce a new thermodynamic quantity, the specific enthalpy:

$$h = u + P/\rho \quad (27)$$

Substituting that into equation (25) and using equation (22) and (23) leads to a new useful equation, the *local enthalpy balance equation*:

$$\begin{aligned} \frac{\partial}{\partial t}(\rho h) + \text{div}(\rho h \mathbf{v}) + \text{div}(\boldsymbol{\phi}_T) + \\ - \frac{\partial}{\partial t}(P) - \mathbf{v} \cdot \nabla P - \text{tr}(\mathbf{D} \cdot \nabla \mathbf{v}) = 0 \end{aligned} \quad (28)$$

which, recalling the definition of material derivative and using the definition given through equation (22), can be rewritten as:

$$\frac{\partial}{\partial t}(\rho h) + \text{div}(\rho h \mathbf{v}) + \text{div}(\boldsymbol{\phi}_T) - \frac{DP}{Dt} - \phi_D = 0 \quad (29)$$

Integral balance equations

From the local balance equations, the following integral balance equations can be finally derived:

$$\frac{dE_k}{dt} = \sum_{j=1}^{N_{\phi+\sigma}} \Phi_{cv_j}^{(E_k)} - \dot{W}_{R,c/e} - \Phi_D + \dot{W}_s + \dot{W}_b \quad (30)$$

$$\frac{dU}{dt} = \sum_{j=1}^{N_{\phi+\sigma}} \Phi_{cv_j}^{(U)} + \Phi_T + \dot{W}_{R,c/e} + \Phi_D \quad (31)$$

$$\frac{dH}{dt} = \sum_{j=1}^{N_{\phi+\sigma}} \Phi_{cv_j}^{(H)} + \Phi_T + \int_{CV} \frac{DP}{Dt} dV + \Phi_D \quad (32)$$

3. Constitutive Laws

The conservation principles alone do not allow us to solve any problem, and the specific nature of the problem and of the matter constituting the system have to be introduced via constitutive laws.

3.1 Newtonian Stokes Compressible Fluid

The constitutive equation for the deviatoric stress tensor of a Newtonian compressible fluid, applying the Stokes' relation, is the following:

$$\mathbf{D} = \mu (\nabla \mathbf{v} + \nabla \mathbf{v}^T) - \frac{2}{3} \mu \text{div}(\mathbf{v}) \mathbf{I} \quad (33)$$

Equation (33) shows that the deviatoric stress tensor is a function of the dynamic viscosity and of

the gradient and the divergence of the velocity vector.

3.2 Fourier Heat Flux Density

The conductive heat transfer inside a fluid can be described using the Fourier postulate:

$$\Phi_T = -\lambda \cdot \nabla T \quad (34)$$

and for an isotropic medium:

$$\Phi_T = -\lambda \nabla T \quad (35)$$

3.3 Ideal Gas Laws

The constitutive equations for an ideal gas are:

$$u = u_0 + c_v(T - T_0) \quad ; \quad c_v = \text{const} \quad (36)$$

$$h = h_0 + c_p(T - T_0) \quad ; \quad c_p = \text{const} \quad (37)$$

$$\frac{P}{\rho} = \frac{R}{M_m} T \quad (38)$$

3.4 Moist Air Constitutive Equations

Almost all psychrometric quantities are based on the Ideal Gas Laws applied to an ideal gas mixture constituted of dry air and water vapour, both considered ideal gasses (i.e. compressible fluids). There are three main relationships based on this constitutive hypotheses, the humidity by mass definition, the moist air specific internal energy and enthalpy:

$$x \equiv \frac{dm^{(wv)}}{dm^{(da)}} = \frac{dm^{(wv)}}{dV} \cdot \frac{dV}{dm^{(da)}} = \frac{\rho^{(wv)}}{\rho^{(da)}} \quad (39)$$

$$u^{(ma)} = u^{(da)} + x \cdot u^{(wv)} \quad (40)$$

$$h^{(ma)} = h^{(da)} + x \cdot h^{(wv)} \quad (41)$$

all relatives to the unit of mass of dry air.

It is very common to fix the reference point 0 for the dry air specific enthalpy and the water vapour specific enthalpy as follows:

$$h_0^{(da)} \equiv 0 \quad \text{at} \quad T = 273.15 \text{ K} \quad (42)$$

$$h_0^{(w)} \equiv h_{TP}^{(hw)} \equiv 0 \quad \text{i.e. at} \quad T = 273.16 \text{ K}$$

i.e. zero degree Celsius for the first and the water triple point for the second (0.01 °C)

The water vapour specific enthalpy is usually expressed (ASHRAE, 2009; Kreider, 2002) in terms of temperature considering the phase change process from saturated liquid to saturated vapour along the triple point isothermobaric evaporation path and then the superheated vapour performing

as an ideal gas. This approach results in the following constitutive equation for the water vapour specific enthalpy:

$$h^{(wv)}(T) = h_{TP}^{(hw)} + \Delta h_{l \rightarrow w}^{(w_{TP})} + c_p^{(w)}(T - T_{TP}) \quad (43)$$

where $\Delta h_{l \rightarrow w}^{(w_{TP})}$ is the phase change enthalpy.

Combining equation (37) for dry air with equations (42) and (43) into equation (41), the constitutive law for moist air specific enthalpy is obtained as:

$$h^{(ma)}(T) = c_p^{(da)}(T - 373.15) + x \cdot [\Delta h_{l \rightarrow w}^{(w_{TP})} + c_p^{(w)}(T - 373.16)] \quad (44)$$

which can be rewritten, with a negligible approximation, using the Celsius temperature, ϑ , as:

$$h^{(ma)}(T) = c_p^{(da)} \vartheta + x \cdot [\Delta h_{l \rightarrow w}^{(w_{TP})} + c_p^{(w)} \vartheta] \quad (45)$$

Similarly, analogous expression can be derived for the specific internal energy of moist air:

$$u^{(ma)}(T) = c_v^{(da)} \vartheta + x \cdot [\Delta u_{l \rightarrow w}^{(w_{TP})} + c_v^{(w)} \vartheta] \quad (46)$$

4. Additional Relationships

4.1 Newton's Law of Cooling

The convective heat transfer between a solid surface and a moving fluid, conductive at the interface, can be described at the integral level as:

$$\Phi_T = \sum_{i=1}^{N_s} h_{cv,i} (T_{s_i} - T_{fr}) \quad (47)$$

5. Moist Air Balance Equations

The control volume (i.e. indoor air of the building zone) is filled with moist air; thus in the following the conservation principles in terms of integral equations and the integral balance equations will be used together with the moist air constitutive equations.

5.1 Dry Air Mass Conservation

The integral mass conservation principle for dry air is, from equation (3),:

$$\frac{dm^{(da)}}{dt} = \sum_{j=1}^{N_b} \Phi_{cv_j}^{(m^{(da)})} \quad (48)$$

or, from equation (6):

$$\frac{d}{dt} \int_{CV} \rho^{(da)} dV = - \sum_{j=1}^{N_\phi} \int_{S_{CV,j}} \rho^{(da)} \mathbf{v} \cdot \mathbf{n} dS \quad (49)$$

Applying the Integral Mean Value Theorem on both sides of equation (49), keeping constant the CV, we get:

$$V_{CV} \frac{d}{dt} \langle \rho^{(da)} \rangle_{CV} = \pm \sum_{j=1}^{N_\phi} A_{S_{CV,j}} \langle \rho^{(da)} v_n \rangle_{S_{CV,j}} \quad (50)$$

where the terms on the right side are usually expressed in terms of mass flow rate (always positive quantities) splitting the sum in inlet and outlet flows:

$$\pm \sum_{j=1}^{N_\phi} A_{S_{CV,j}} \langle \rho^{(da)} v_n \rangle_{S_{CV,j}} = \sum_{j=1}^{N_{\phi,in}} \dot{m}_{in_j}^{(da)} - \sum_{j=1}^{N_{\phi,out}} \dot{m}_{out_j}^{(da)} \quad (51)$$

Thus equation (50) can be written as:

$$V_{CV} \frac{d}{dt} \langle \rho^{(da)} \rangle_{CV} = \sum_{j=1}^{N_{\phi,in}} \dot{m}_{in_j}^{(da)} - \sum_{j=1}^{N_{\phi,out}} \dot{m}_{out_j}^{(da)} \quad (52)$$

5.2 Water Vapour Mass Balance

From equation (3), with the source term made explicit, the integral mass conservation principle applied only to the vapour phase of water is:

$$\frac{dm^{(wv)}}{dt} = \sum_{j=1}^{N_\phi} \Phi_{cv_j}^{(m^{(wv)})} + \sum_{k=1}^{N_\sigma} \dot{M}_k^{(wv)} \quad (53)$$

or, from equation (6):

$$\frac{d}{dt} \int_{CV} \rho^{(wv)} dV = - \sum_{j=1}^{N_\phi} \int_{S_{CV,j}} \rho^{(wv)} \mathbf{v} \cdot \mathbf{n} dS + \sum_{k=1}^{N_\sigma} \dot{M}_k^{(wv)} \quad (54)$$

Applying the Integral Mean Value Theorem on both sides of equation (54), keeping constant the CV, we obtain:

$$V_{CV} \frac{d}{dt} \langle \rho^{(wv)} \rangle_{CV} = \pm \sum_{j=1}^{N_\phi} A_{S_{CV,j}} \langle \rho^{(wv)} v_n \rangle_{S_{CV,j}} + \sum_{k=1}^{N_\sigma} \dot{M}_k^{(wv)} \quad (55)$$

which can be rewritten as

$$V_{CV} \frac{d}{dt} \langle \rho^{(wv)} \rangle_{CV} = \sum_{j=1}^{N_{\phi,in}} \dot{m}_{in_j}^{(wv)} - \sum_{j=1}^{N_{\phi,out}} \dot{m}_{out_j}^{(wv)} + \sum_{k=1}^{N_\sigma} \dot{M}_k^{(wv)} \quad (56)$$

Applying the constitutive equation (39) to equation (55) it follows:

$$V_{CV} \frac{d}{dt} \langle x \cdot \rho^{(da)} \rangle_{CV} = \pm \sum_{j=1}^{N_\phi} A_{S_{CV,j}} \langle x \cdot \rho^{(da)} v_n \rangle_{S_{CV,j}} + \sum_{k=1}^{N_\sigma} \dot{M}_k^{(wv)} \quad (57)$$

which can be written as

$$V_{CV} \frac{d}{dt} \langle x \cdot \rho^{(da)} \rangle_{CV} = \sum_{j=1}^{N_{\phi,in}} \dot{m}_{in_j}^{(da)} \langle x \rangle_{S_{in_j}} - \sum_{j=1}^{N_{\phi,out}} \dot{m}_{out_j}^{(da)} \langle x \rangle_{S_{out_j}} + \sum_{k=1}^{N_\sigma} \dot{M}_k^{(wv)} \quad (58)$$

only under the following hypothesis:

$$[H.0] \langle a \cdot b \rangle = \langle a \rangle \cdot \langle b \rangle + \text{cov}(a, b) ; \quad \text{cov}(a, b) \cong 0$$

i.e. there is no or a weak cross correlation between a and b over the average operator field (covariance ≈ 0), in this case between the dry air mass flow rate and the air humidity over the inlet/outlet cross section.

5.3 Moist Air Enthalpy Balance

The integral enthalpy balance expressed by equation (32) can be written, in terms of specific quantities and splitting the enthalpy flows due to pure advection from those related to vapour sources, as:

$$\begin{aligned} \frac{d}{dt} \int_{CV} \rho^{(da)} h^{(ma)} dV = & - \sum_{j=1}^{N_\phi} \int_{S_{CV,j}} \rho^{(da)} h^{(ma)} \mathbf{v} \cdot \mathbf{n} dS + \\ & + \sum_{k=1}^{N_\sigma} \dot{M}_k^{(wv)} h_k^{(wv)} + \Phi_T + \int_{CV} \frac{DP}{Dt} dV + \Phi_D \end{aligned} \quad (59)$$

and introducing the constitutive law for moist air specific enthalpy given by equation (45), it turns out in:

$$\begin{aligned} \frac{d}{dt} \int_{CV} \rho^{(da)} \{ c_p^{(da)} \mathcal{G} + x \cdot [\Delta h_{l \rightarrow w}^{(w_{TP})} + c_p^{(w)} \mathcal{G}] \} dV = \\ = - \sum_{j=1}^{N_\phi} \int_{S_{CV,j}} \rho^{(da)} \{ c_p^{(da)} \mathcal{G} + x \cdot [\Delta h_{l \rightarrow w}^{(w_{TP})} + c_p^{(w)} \mathcal{G}] \} \mathbf{v} \cdot \mathbf{n} dS + \\ + \sum_{k=1}^{N_\sigma} \dot{M}_k^{(wv)} h_k^{(wv)} + \Phi_T + \int_{CV} \frac{DP}{Dt} dV + \Phi_D \end{aligned} \quad (60)$$

Applying the Integral Mean Value Theorem on the left side of equation (60), keeping constant the CV, we obtain:

$$\begin{aligned} \frac{d}{dt} \int_{CV} \rho^{(da)} \{c_p^{(da)} \mathcal{G} + x \cdot [\Delta h_{l \rightarrow w}^{(w_{TP})} + c_p^{(w)} \mathcal{G}]\} dV = \\ = V_{CV} \frac{d}{dt} \left\{ c_p^{(da)} \langle \rho^{(da)} \mathcal{G} \rangle_{CV} + \Delta h_{l \rightarrow w}^{(w_{TP})} \langle \rho^{(da)} x \rangle_{CV} + \right. \\ \left. + c_p^{(w)} \langle \rho^{(da)} x \cdot \mathcal{G} \rangle_{CV} \right\} \end{aligned} \quad (61)$$

and applying hypothesis [H.0] it becomes:

$$\begin{aligned} \frac{d}{dt} \int_{CV} \rho^{(da)} \{c_p^{(da)} \mathcal{G} + x \cdot [\Delta h_{l \rightarrow w}^{(w_{TP})} + c_p^{(w)} \mathcal{G}]\} dV = \\ \equiv V_{CV} \left[c_p^{(da)} + \langle x \rangle_{CV} c_p^{(w)} \right] \frac{d}{dt} \langle \rho^{(da)} \mathcal{G} \rangle_{CV} + \\ + V_{CV} \left[\Delta h_{l \rightarrow w}^{(w_{TP})} \frac{d}{dt} \langle \rho^{(da)} x \rangle_{CV} + \right. \\ \left. + c_p^{(w)} \langle \rho^{(da)} \mathcal{G} \rangle_{CV} \frac{d}{dt} \langle x \rangle_{CV} \right] \end{aligned} \quad (62)$$

where

$$c_p^{(ma)} \{ \langle x \rangle_{CV} \} \equiv [c_p^{(da)} + \langle x \rangle_{CV} c_p^{(w)}] \quad (63)$$

is the moist air constant pressure specific thermal capacity.

Applying the Integral Mean Value Theorem on the convective enthalpy flow terms of the right side of equation (60), keeping constant the CV, we obtain:

$$\begin{aligned} - \sum_{j=1}^{N_\phi} \int_{S_{CV,j}} \rho^{(da)} \{c_p^{(da)} \mathcal{G} + x \cdot [\Delta h_{l \rightarrow w}^{(w_{TP})} + c_p^{(w)} \mathcal{G}]\} \mathbf{v} \cdot \mathbf{n} dS = \\ \pm \sum_{j=1}^{N_\phi} A_{S_{CV,j}} \left\{ c_p^{(da)} \langle \rho^{(da)} v_n \mathcal{G} \rangle_{S_{CV,j}} + \right. \\ \left. + \Delta h_{l \rightarrow w}^{(w_{TP})} \langle \rho^{(da)} v_n x \rangle_{S_{CV,j}} + c_p^{(w)} \langle \rho^{(da)} v_n x \mathcal{G} \rangle_{S_{CV,j}} \right\} \end{aligned} \quad (64)$$

Applying hypothesis [H.0], i.e. assuming that:

$$\begin{aligned} \langle \rho^{(da)} v_n \mathcal{G} \rangle_{S_{CV,j}} &\equiv \langle \rho^{(da)} v_n \rangle_{S_{CV,j}} \langle \mathcal{G} \rangle_{S_{CV,j}} \\ \langle \rho^{(da)} v_n x \rangle_{S_{CV,j}} &\equiv \langle \rho^{(da)} v_n \rangle_{S_{CV,j}} \langle x \rangle_{S_{CV,j}} \\ \langle \rho^{(da)} v_n x \mathcal{G} \rangle_{S_{CV,j}} &\equiv \langle \rho^{(da)} v_n \rangle_{S_{CV,j}} \langle x \rangle_{S_{CV,j}} \langle \mathcal{G} \rangle_{S_{CV,j}} \end{aligned} \quad (65)$$

the enthalpy flow terms can be rewritten as:

$$\begin{aligned} - \sum_{j=1}^{N_\phi} \int_{S_{CV,j}} \rho^{(da)} \{c_p^{(da)} \mathcal{G} + x \cdot [\Delta h_{l \rightarrow w}^{(w_{TP})} + c_p^{(w)} \mathcal{G}]\} \mathbf{v} \cdot \mathbf{n} dS = \\ \equiv \sum_{j=1}^{N_{\phi, in}} \dot{m}_{in_j}^{(da)} \left\{ c_p^{(da)} \langle \mathcal{G} \rangle_{S_{CV,j}} + \langle x \rangle_{S_{CV,j}} [\Delta h_{l \rightarrow w}^{(w_{TP})} + \right. \\ \left. + c_p^{(w)} \langle \mathcal{G} \rangle_{S_{CV,j}}] \right\} - \sum_{j=1}^{N_{\phi, out}} \dot{m}_{in_j}^{(da)} \left\{ c_p^{(da)} \langle \mathcal{G} \rangle_{S_{CV,j}} + \right. \\ \left. + \langle x \rangle_{S_{CV,j}} [\Delta h_{l \rightarrow w}^{(w_{TP})} + c_p^{(w)} \langle \mathcal{G} \rangle_{S_{CV,j}}] \right\} \end{aligned} \quad (66)$$

Substituting the equalities given by equations (62), (63) and (66) into equation (60) the integral enthalpy balance becomes:

$$\begin{aligned} V_{CV} c_p^{(ma)} \{ \langle x \rangle_{CV} \} \frac{d}{dt} \langle \rho^{(da)} \mathcal{G} \rangle_{CV} + \\ + V_{CV} \left[\Delta h_{l \rightarrow w}^{(w_{TP})} \frac{d}{dt} \langle \rho^{(da)} x \rangle_{CV} + \right. \\ \left. + c_p^{(w)} \langle \rho^{(da)} \mathcal{G} \rangle_{CV} \frac{d}{dt} \langle x \rangle_{CV} \right] = \\ = \sum_{j=1}^{N_{\phi, in}} \dot{m}_{in_j}^{(da)} \left\{ c_p^{(ma)} \{ \langle x \rangle_{S_{CV,j}} \} \langle \mathcal{G} \rangle_{S_{CV,j}} + \langle x \rangle_{S_{CV,j}} \Delta h_{l \rightarrow w}^{(w_{TP})} \right\} + \\ - \sum_{j=1}^{N_{\phi, out}} \dot{m}_{in_j}^{(da)} \left\{ c_p^{(ma)} \{ \langle x \rangle_{S_{CV,j}} \} \langle \mathcal{G} \rangle_{S_{CV,j}} + \langle x \rangle_{S_{CV,j}} \Delta h_{l \rightarrow w}^{(w_{TP})} \right\} + \\ + \sum_k^{N_\sigma} \dot{M}_k^{(wv)} h_k^{(wv)} + \Phi_T + \int_{CV} \frac{DP}{Dt} dV + \Phi_D \end{aligned} \quad (67)$$

which is a very complex expression.

5.4 Moist Air Internal Energy Balance

The same procedure used for enthalpy can be used for internal energy starting from equation (31) obtaining:

$$\begin{aligned}
 & V_{CV} c_v^{(ma)} \left\{ \langle x \rangle_{CV} \right\} \frac{d}{dt} \langle \rho^{(da)} g \rangle_{CV} + \\
 & + V_{CV} \left[\Delta u_{l \rightarrow w}^{(wTP)} \frac{d}{dt} \langle \rho^{(da)} x \rangle_{CV} + \right. \\
 & \left. + c_v^{(w)} \langle \rho^{(da)} g \rangle_{CV} \frac{d}{dt} \langle x \rangle_{CV} \right] = \\
 & = \sum_{j=1}^{N_{\phi, in}} \dot{m}_{in_j}^{(da)} \left\{ c_v^{(ma)} \left\{ \langle x \rangle_{S_{CV,j}} \right\} \langle g \rangle_{S_{CV,j}} + \langle x \rangle_{S_{CV,j}} \Delta h_{l \rightarrow w}^{(wTP)} \right\} + \\
 & - \sum_{j=1}^{N_{\phi, out}} \dot{m}_{out_j}^{(da)} \left\{ c_v^{(ma)} \left\{ \langle x \rangle_{S_{CV,j}} \right\} \langle g \rangle_{S_{CV,j}} + \langle x \rangle_{S_{CV,j}} \Delta u_{l \rightarrow w}^{(wTP)} \right\} + \\
 & + \sum_k^{N_{\sigma}} \dot{M}_k^{(wv)} u_k^{(wv)} + \Phi_T + \dot{W}_{E,c/e} + \Phi_D
 \end{aligned} \tag{68}$$

where

$$c_v^{(ma)} \left\{ \langle x \rangle_{CV} \right\} \equiv \left[c_v^{(da)} + \langle x \rangle_{CV} c_v^{(w)} \right] \tag{69}$$

is the moist air constant volume specific thermal capacity.

6. Simplified Moist Air Balance Equations

The moist air balance equations derived in the previous paragraph are quite complex and different from the normally used balance equations (1) and (2). To achieve similar formulas, simplifying hypotheses will be employed, which also give more insight into the possible application field of such equations.

The first important simplifying hypothesis is that assessing a **very small average mass by volume change** with respect to the time for the dry air still remaining a compressible fluid; i.e.:

[H.1]

$$\begin{aligned}
 \langle \rho(\mathbf{r}, t) \rangle &= \langle \rho_a + \Delta \rho(\mathbf{r}, t) \rangle = \rho_a \left[1 + \frac{\langle \Delta \rho(\mathbf{r}, t) \rangle}{\rho_a} \right] \\
 \frac{\langle \Delta \rho(\mathbf{r}, t) \rangle}{\rho_a} &\ll 1 \quad \Rightarrow \quad \langle \rho(\mathbf{r}, t) \rangle \cong \rho_a
 \end{aligned}$$

where ρ_a is a constant reference value for the dry air mass by volume, \mathbf{r} is the position vector.

The second important simplifying hypothesis is the **full mix hypothesis**; i.e.:

$$[H.2] \quad \langle a \rangle_{S_{out}} \equiv \langle a \rangle_V$$

i.e. each surface averaged quantity advected out of the control volume has the same value of the volume averaged related quantity.

The third simplifying hypothesis is the **negligible dissipation function** hypothesis,

$$[H.3] \quad \Phi_D \cong 0$$

The integral dissipation function is null for inviscid fluid (null dynamic viscosity), but is also vanishing for non-null viscosity when the velocity vector gradient is very small and/or is affecting a very small part of the control volume (see equations (22) and (33)). The surface-to-volume ratio of the zone volume is an index of such condition: high values of S/V as in air ducts do not allow to neglect the dissipation function as instead allow low values of S/V as in rooms.

6.1 Unsteady Dry Air Mass Balance

Under hypothesis [H.1] the unsteady dry air mass balance equation (52) for compressible fluid becomes:

$$\sum_{j=1}^{N_{\phi, in}} \dot{m}_{in_j}^{(da)}(t) \cong \sum_{j=1}^{N_{\phi, out}} \dot{m}_{out_j}^{(da)}(t) \tag{70}$$

which looks like the steady state mass balance, but is not. This because:

$$\begin{aligned}
 V_{CV} \frac{d}{dt} \langle \rho(\mathbf{r}, t) \rangle_{CV} &= \rho_a V_{CV} \frac{d}{dt} \left[1 + \frac{\langle \Delta \rho(\mathbf{r}, t) \rangle_{CV}}{\rho_a} \right] \cong \\
 &\cong \rho_a V_{CV} \frac{d}{dt} [1] = 0
 \end{aligned} \tag{71}$$

6.2 Water Vapour Mass Balance

Under hypothesis [H.1] the unsteady water vapour mass balance equation (58) becomes:

$$\begin{aligned}
 V_{CV} \cdot \rho_a \frac{d}{dt} \langle x \rangle_{CV} &= \sum_{j=1}^{N_{\phi, in}} \dot{m}_{in_j}^{(da)} \langle x \rangle_{S_{in_j}} - \\
 &- \sum_{j=1}^{N_{\phi, out}} \dot{m}_{out_j}^{(da)} \langle x \rangle_{S_{out_j}} + \sum_{k=1}^{N_{\sigma}} \dot{M}_k^{(wv)}
 \end{aligned} \tag{72}$$

and, under hypothesis [H.2], after substitution of equation (70) into (72), it turns out in:

$$V_{CV} \cdot \rho_a \frac{d}{dt} \langle x \rangle_{CV} = \sum_{j=1}^{N_{\phi, in}} \dot{m}_{in_j}^{(da)} \left(\langle x \rangle_{S_{in_j}} - \langle x \rangle_{CV} \right) + \sum_{k=1}^{N_{\sigma}} \dot{M}_k^{(wv)} \quad (73)$$

6.3 Moist Air Enthalpy Balance

Under hypothesis [H.1], [H.2] and [H.3] and using the dry air mass balance equation (70), the moist air enthalpy balance equation (67) becomes:

$$\begin{aligned} V_{CV} \rho_a c_p^{(ma)} \left\{ \langle x \rangle_{CV} \right\} \frac{d}{dt} \langle \mathcal{G} \rangle_{CV} + \\ + V_{CV} \rho_a h^{(wv)} \left\{ \langle \mathcal{G} \rangle_{CV} \right\} \frac{d}{dt} \langle x \rangle_{CV} = \\ = \sum_{j=1}^{N_{\phi, in}} \dot{m}_{in_j}^{(da)} \left\{ c_p^{(ma)} \left\{ \langle x \rangle_{S_{CV,j}} \right\} \langle \mathcal{G} \rangle_{S_{CV,j}} + \langle x \rangle_{S_{CV,j}} \Delta h_{l \rightarrow w}^{(w_{TP})} \right. \\ \left. - c_p^{(ma)} \left\{ \langle x \rangle_{CV} \right\} \langle \mathcal{G} \rangle_{CV} + \langle x \rangle_{CV} \Delta h_{l \rightarrow w}^{(w_{TP})} \right\} + \\ + \sum_{k=1}^{N_{\sigma}} \dot{M}_k^{(wv)} h_k^{(wv)} + \Phi_T + \int_{CV} \frac{DP}{Dt} dV \end{aligned} \quad (74)$$

where

$$h^{(wv)} \left\{ \langle \mathcal{G} \rangle_{CV} \right\} = \left[\Delta h_{l \rightarrow w}^{(w_{TP})} + c_p^{(w)} \langle \mathcal{G} \rangle_{CV} \right] \quad (75)$$

is the water vapour specific enthalpy at the volume averaged air temperature.

If in the advective enthalpy flows we add and subtract the term:

$$c_p^{(ma)} \left\{ \langle \mathcal{G} \rangle_{S_{CV,j}} \right\} \langle \mathcal{G} \rangle_{CV} - c_p^{(ma)} \left\{ \langle \mathcal{G} \rangle_{S_{CV,j}} \right\} \langle \mathcal{G} \rangle_{CV} = 0 \quad (76)$$

and split the source terms as it follows:

$$h_k^{(wv)} \left\{ \mathcal{G}_k \right\} = h^{(wv)} \left\{ \langle \mathcal{G} \rangle_{CV} \right\} + c_p^{(w)} \left(\mathcal{G}_k - \langle \mathcal{G} \rangle_{CV} \right) \quad (77)$$

equation (74) can be rewritten as:

$$\begin{aligned} V_{CV} \rho_a c_p^{(ma)} \left\{ \langle x \rangle_{CV} \right\} \frac{d}{dt} \langle \mathcal{G} \rangle_{CV} + \\ + h^{(wv)} \left\{ \langle \mathcal{G} \rangle_{CV} \right\} \cdot \left\{ V_{CV} \rho_a \frac{d}{dt} \langle x \rangle_{CV} \right\} = \\ = \sum_{j=1}^{N_{\phi, in}} \dot{m}_{in_j}^{(da)} c_p^{(ma)} \left\{ \langle x \rangle_{S_{CV,j}} \right\} \left(\langle \mathcal{G} \rangle_{S_{CV,j}} - \langle \mathcal{G} \rangle_{CV} \right) + \\ + h^{(wv)} \left\{ \langle \mathcal{G} \rangle_{CV} \right\} \cdot \left\{ \sum_{j=1}^{N_{\phi, in}} \dot{m}_{in_j}^{(da)} \left(\langle x \rangle_{S_{CV,j}} - \langle x \rangle_{CV} \right) \right\} + \\ + \sum_{k=1}^{N_{\sigma}} \dot{M}_k^{(wv)} \left\{ \right\} + \sum_{k=1}^{N_{\sigma}} \dot{M}_k^{(wv)} c_p^{(w)} \left\{ \mathcal{G}_k - \langle \mathcal{G} \rangle_{CV} \right\} + \\ + \Phi_T + \int_{CV} \frac{DP}{Dt} dV \end{aligned} \quad (78)$$

6.4 Moist Air Internal Energy Balance

Using the same hypothesis, [H.1], [H.2] and [H.3] and the dry air mass balance equation (70), and following the procedure undertaken for the enthalpy balance, the internal energy balance equation (69) becomes:

$$\begin{aligned} V_{CV} \rho_a c_v^{(ma)} \left\{ \langle x \rangle_{CV} \right\} \frac{d}{dt} \langle \mathcal{G} \rangle_{CV} + \\ + u^{(wv)} \left\{ \langle \mathcal{G} \rangle_{CV} \right\} \cdot \left\{ V_{CV} \rho_a \frac{d}{dt} \langle x \rangle_{CV} \right\} = \\ = \sum_{j=1}^{N_{\phi, in}} \dot{m}_{in_j}^{(da)} c_v^{(ma)} \left\{ \langle x \rangle_{S_{CV,j}} \right\} \left(\langle \mathcal{G} \rangle_{S_{CV,j}} - \langle \mathcal{G} \rangle_{CV} \right) + \\ + u^{(wv)} \left\{ \langle \mathcal{G} \rangle_{CV} \right\} \cdot \left\{ \sum_{j=1}^{N_{\phi, in}} \dot{m}_{in_j}^{(da)} \left(\langle x \rangle_{S_{CV,j}} - \langle x \rangle_{CV} \right) \right\} + \\ + \sum_{k=1}^{N_{\sigma}} \dot{M}_k^{(wv)} \left\{ \right\} + \sum_{k=1}^{N_{\sigma}} \dot{M}_k^{(wv)} c_v^{(w)} \left\{ \mathcal{G}_k - \langle \mathcal{G} \rangle_{CV} \right\} + \\ + \Phi_T + \dot{W}_{R,c/e} \end{aligned} \quad (79)$$

6.5 Discussion

We can see, both from the enthalpy and the internal energy balance equations, how the moist air energy balance is constituted of two different contributions: one, “thermal”, due to an increase/decrease of the volume averaged air temperature, the other just due to an increase of the water vapour mass content of the moist air (this

because of the hypothesis of ideal gas mixture). These two contributions can be split into two separated balance equations as we show in the next paragraph.

7. “Sensible” and “Latent” Energy Balance Equations

In the field of Heating, Ventilating, Air Conditioning (HVAC), it is common to use terms like “sensible heat” and “latent heat”, which are moist air enthalpy changes that are referring to psychrometric processes driven respectively by only temperature difference and only humidity difference. In the first case we refer to the thermal energy balance, in the second just to the humidity balance equation, as we show later. Looking at the Moist Air Enthalpy Balance, given by equation (78), and comparing it with the Water Vapour Mass Balance, given by equation (73), it is evident that we can delete the second terms (between braces) on the left and right side of equation (78). In fact, those terms are just the left and the right side of the water vapour mass balance equation times an identical quantity, the water vapour specific enthalpy at volume-averaged temperature. The same concerns the Moist Air Internal Energy Balance. Thus, we have available two alternative **thermal energy balance** equations (or **sensible energy**):

- **enthalpy based:**

$$\begin{aligned} V_{CV} \rho_a c_p^{(ma)} \{ \langle x \rangle_{CV} \} \frac{d}{dt} \langle g \rangle_{CV} = \\ = \sum_{j=1}^{N_{\phi, in}} \dot{m}_{in_j}^{(da)} c_p^{(ma)} \{ \langle x \rangle_{S_{CV,j}} \} \left(\langle g \rangle_{S_{CV,j}} - \langle g \rangle_{CV} \right) + \\ + \sum_k^{N_{\sigma}} \dot{M}_k^{(wv)} c_p^{(w)} \{ g_k - \langle g \rangle_{CV} \} + \Phi_T + \int_{CV} \frac{DP}{Dt} dV \end{aligned} \quad (80)$$

- **internal energy based:**

$$\begin{aligned} V_{CV} \rho_a c_v^{(ma)} \{ \langle x \rangle_{CV} \} \frac{d}{dt} \langle g \rangle_{CV} = \\ = \sum_{j=1}^{N_{\phi, in}} \dot{m}_{in_j}^{(da)} c_v^{(ma)} \{ \langle x \rangle_{S_{CV,j}} \} \left(\langle g \rangle_{S_{CV,j}} - \langle g \rangle_{CV} \right) + \\ + \sum_k^{N_{\sigma}} \dot{M}_k^{(wv)} c_v^{(w)} \{ g_k - \langle g \rangle_{CV} \} + \Phi_T + \dot{W}_{R,c/e} \end{aligned} \quad (81)$$

and **one water vapour mass balance equation**, equation (73), which can be seen as a “latent energy” balance equation if multiplied for the water vapour specific enthalpy or internal energy at volume-averaged temperature. Thus, we can have also two “latent energy” balance equation:

- **enthalpy based:**

$$\begin{aligned} h^{(wv)} \{ \langle g \rangle_{CV} \} \cdot V_{CV} \rho_a \frac{d}{dt} \langle x \rangle_{CV} = \\ = h^{(wv)} \{ \langle g \rangle_{CV} \} \cdot \left\{ \sum_{j=1}^{N_{\phi, in}} \dot{m}_{in_j}^{(da)} \left(\langle x \rangle_{S_{in_j}} - \langle x \rangle_{CV} \right) + \sum_{k=1}^{N_{\sigma}} \dot{M}_k^{(wv)} \right\} \end{aligned} \quad (82)$$

- **internal energy based:**

$$\begin{aligned} u^{(wv)} \{ \langle g \rangle_{CV} \} \cdot V_{CV} \rho_a \frac{d}{dt} \langle x \rangle_{CV} = \\ = u^{(wv)} \{ \langle g \rangle_{CV} \} \cdot \left\{ \sum_{j=1}^{N_{\phi, in}} \dot{m}_{in_j}^{(da)} \left(\langle x \rangle_{S_{in_j}} - \langle x \rangle_{CV} \right) + \sum_{k=1}^{N_{\sigma}} \dot{M}_k^{(wv)} \right\} \end{aligned} \quad (83)$$

which eventually have to be used together with their “sensible” counterpart.

7.1 Discussion

What equations are then more suitable for a building zone energy balance?

In the HCAV calculation enthalpy based equations are preferred because enthalpy incorporate the flow work, which is an important quantity for thermodynamic open systems as almost all HVAC systems and the building itself are.

The second point in favour of enthalpy based equations is the consideration that the reversible compression/expansion power:

$$\dot{W}_{R,c/e} \equiv - \int_{CV} P \operatorname{div}(\mathbf{v}) dV = \int_{CV} \left(\frac{P}{\rho} \cdot \frac{D\rho}{Dt} \right) dV \quad (84)$$

is something not so simple to calculate: the velocity and pressure field over the control volume have to be known. The only hypothesis that makes this term disappear is that of incompressible fluid, but, dealing with an ideal gas mixture, we cannot apply it.

The “latent energy” balance is not a problem, because it is only conventional and can be taken back to the unique water vapour mass balance

equation (73). This equation can be then rewritten in the same way as equation (2), just specialising the advective and the source terms.

For the thermal energy balance, despite the choice of using the enthalpy based equation, it is not so simple to recover an expression like equation (1).

In the enthalpy based thermal energy balance there is an extra term due to compressibility: the volume integral of the pressure material derivative:

$$\int_{CV} \frac{DP}{Dt} dV = \int_{CV} \left[\frac{\partial P}{\partial t} + \mathbf{v} \cdot \nabla P \right] dV \quad (85)$$

Also this integral is not a simple calculation and needs to know the velocity and pressure field over the control volume. Nevertheless, the difference with the reversible compression/expansion power is that the condition under which it vanishes is simple to state and can be achieved on a practical level.

If in space and time isobaric processes occur inside the control volume, the integral is null.

8. The Isobaric Thermal Balance Equation

Starting from the enthalpy based thermal energy balance defined by equation (79), by the use of the following hypotheses:

$$[\text{H.4}] \quad \sum_k^{N_a} \dot{M}_k^{(wv)} c_p^{(w)} \{ \mathcal{G}_k - \langle \mathcal{G} \rangle_{CV} \} \cong 0$$

The overheating of the sources water vapour respect to the volume averaged air temperature is small enough.

$$[\text{H.5}] \quad \text{Isobaric processes} \Rightarrow \int_{CV} \frac{DP}{Dt} dV = 0$$

introducing the following positions:

$$\begin{aligned} V_{CV} &= V_a \\ c_p^{(ma)} \{ \langle x \rangle_{CV} \} &= c_p^{(ma)} \\ \langle \mathcal{G} \rangle_{CV} &= \mathcal{G}_a \\ \langle \mathcal{G} \rangle_{S_{CV,j}} &= \mathcal{G}_{a,in_j} \\ N_{\phi,in} &= N_{zone} + N_{infiltration} + N_{internal} + N_{system} \\ N_s &= N_{en,s} + N_{internal} + N_{system} \end{aligned} \quad (86)$$

and the Newton's Law of Cooling equation (47), the isobaric thermal balance equation has the following aspect:

$$\begin{aligned} V_a \rho_a c_p^{(ma)} \frac{d\mathcal{G}_a}{dt} &= \sum_{i=1}^{N_{en,s}} A_i h_{cv_i} (\mathcal{G}_{s_i} - \mathcal{G}_a) + \\ &+ \sum_{j=1}^{N_{zone}} \dot{m}_{in_j}^{(da)} c_p^{(ma)} (\mathcal{G}_{a,in_j} - \mathcal{G}_a) + \sum_{j=1}^{N_{infiltr}} \dot{m}_{in_j}^{(da)} c_p^{(ma)} (\mathcal{G}_{a,in_j} - \mathcal{G}_a) + \\ &+ \sum_{i=1}^{N_{int,s}} A_i h_{cv_i} (\mathcal{G}_{s_i} - \mathcal{G}_a) + \sum_{j=1}^{N_{int}} \dot{m}_{in_j}^{(da)} c_p^{(ma)} (\mathcal{G}_{a,in_j} - \mathcal{G}_a) + \\ &+ \sum_{j=1}^{N_{system}} \dot{m}_{in_j}^{(da)} c_p^{(ma)} (\mathcal{G}_{a,in_j} - \mathcal{G}_a) + \sum_{i=1}^{N_{sys,s}} A_i h_{cv_i} (\mathcal{G}_{s_i} - \mathcal{G}_a) \end{aligned} \quad (87)$$

or, placing

$$\begin{aligned} \dot{Q}_I^{(CV)} &= \sum_{i=1}^{N_{int,s}} A_i h_{cv_i} (\mathcal{G}_{s_i} - \mathcal{G}_a) + \sum_{j=1}^{N_{int}} \dot{m}_{in_j}^{(da)} c_p^{(ma)} (\mathcal{G}_{a,in_j} - \mathcal{G}_a) \\ \dot{Q}_{SYS}^{(CV)} &= \sum_{i=1}^{N_{sys,s}} A_i h_{cv_i} (\mathcal{G}_{s_i} - \mathcal{G}_a) + \sum_{j=1}^{N_{system}} \dot{m}_{in_j}^{(da)} c_p^{(ma)} (\mathcal{G}_{a,in_j} - \mathcal{G}_a) \end{aligned} \quad (88)$$

it can be written as

$$\begin{aligned} V_a \rho_a c_p^{(ma)} \frac{d\mathcal{G}_a}{dt} &= \sum_{i=1}^{N_{en,s}} A_i h_{cv_i} (\mathcal{G}_{s_i} - \mathcal{G}_a) + \\ &+ \sum_{j=1}^{N_{zone}} \dot{m}_{in_j}^{(da)} c_p^{(ma)} (\mathcal{G}_{a,in_j} - \mathcal{G}_a) + \sum_{j=1}^{N_{infiltr}} \dot{m}_{in_j}^{(da)} c_p^{(ma)} (\mathcal{G}_{a,in_j} - \mathcal{G}_a) + \\ &+ \dot{Q}_I^{(CV)} + \dot{Q}_{SYS}^{(CV)} \end{aligned} \quad (89)$$

an equation which is quite identical to the usual equation (1). The main difference is in the use of the moist air constant pressure thermal capacity instead of the dry air one, which is also in principle a function of the air humidity by mass. However, it is important to note that such a correspondence is possible only by the application of hypotheses [H.4] and [H.5]

8.1 Surprise

The developed equation is based on the Ideal Gas Law; thus from the constitutive equation (3) we can derive the differential equality:

$$d(\rho^{(da)} \mathcal{G}) = d(\rho^{(da)} T) = \frac{M_m^{(da)}}{R} dP \quad (90)$$

Applying to equation (90) the same decomposition used in [H.1], it follows:

$$\rho_a d\mathcal{G} + \rho_a d\left(\frac{\Delta\rho^{(da)}}{\rho_a} \mathcal{G}\right) = \frac{M_m^{(da)}}{R} dP \quad (91)$$

and thus for such a hypothesis (very small mass by volume changes) it turns out in:

$$\rho_a d\mathcal{G} \cong \frac{M_m^{(da)}}{R} dP \quad (92)$$

Applying the volume average operator and dividing for dt, we finally obtain:

$$\rho_a \frac{d\langle\mathcal{G}\rangle_{CV}}{dt} \cong \frac{M_m^{(da)}}{R} \frac{d\langle P \rangle_{CV}}{dt} \quad (93)$$

Equation (93) states that if an isobaric process occurs the left side, i.e. the temperature time derivative, it is null.

That means that the left side term of the isobaric thermal balance equation (89) is approximately zero, and thus the balance equation should be:

$$\begin{aligned} & \sum_{i=1}^{N_{m,s}} A_i h_{cv_i} (\mathcal{G}_{s_i} - \mathcal{G}_a) + \sum_{j=1}^{N_{zone}} \dot{m}_{in_j}^{(da)} c_p^{(ma)} (\mathcal{G}_{a,in_j} - \mathcal{G}_a) + \\ & + \sum_{j=1}^{N_{in}} \dot{m}_{in_j}^{(da)} c_p^{(ma)} (\mathcal{G}_{a,in_j} - \mathcal{G}_a) + \dot{Q}_I^{(CV)} + \dot{Q}_{SYS}^{(CV)} \cong 0 \end{aligned} \quad (94)$$

instead of equation (1).

The “sensible energy” storage term (i.e. the temperature driven part of the moist air enthalpy storage term) is vanishing when applying the ideal gas hypothesis because, under the isobaric process assumption, the thermal expansion due to temperature increase results into an air displacement out of the control volume. The enthalpy increase due to temperature increase is balanced by the enthalpy decrease due to control volume mass reduction.

9. Conclusion

In the present work a consistent analytical derivation of the energy balance equation for building zone internal moist air is presented based on the following hypotheses:

compressible fluid with very small average mass by volume changes during the occurring processes; full mix of all properties inside the control volume; negligible dissipation function, i.e. negligible effects of shear stresses on the energy balance;

negligible overheating of the sources water vapour respect to the volume averaged air temperature; isobaric processes.

Under such hypotheses, the resulting “sensible energy” equation looks like the usual employed thermal energy balance equation in the most used building simulation programs. Small marginal differences are located in the constant pressure specific thermal capacities, which are, in the first case, the moist air ones (slightly depending on the humidity content), while in the second the dry air ones.

But, if the ideal gas hypothesis is consistently applied to the first term (i.e. the storage term) of such equation, this vanishes. Thus, the resulting thermal energy balance equation for the air node in a building zone is not anymore a first order differential equation in the air node temperature, but just an algebraic equation.

This is an important result not only for the correctness of the solution, but also because it eliminates stability problems related to its numerical time integration.

10. Nomenclature

Symbols

A	surface area [m ²]
c_p	constant pressure specific thermal capacity [J/(kg K)]
c_v	constant volume specific thermal capacity [J/(kg K)]
D	Deviatoric stress tensor [N/m ²]
e	specific total energy [J/kg]
E	total energy [J]
f	specific force vector by unit of surface (s) or by unit of mass (b)
F	force vector [N]
h	superficial heat transfer coefficient [W/(m ² K)], (cv) subscript, or superficial mass transfer coefficient, [kg _(DA) /(s m ²)], (m) subscript
h⁽ⁱ⁾	specific enthalpy [J/kg]
H	enthalpy [J]
I	unit second order tensor
m	mass [kg]

\dot{m}	mass flow rate [kg/s]
M_m	molar mass [kg/kmol]
$\dot{M}^{(\alpha)}$	source of α phase or humidity [kg/s]
\mathbf{n}	surface normal unitary vector (positive outward)
p	partial pressure [Pa]
P	thermodynamic pressure [Pa]
\mathbf{P}	momentum vector [N·s]
R	universal gas constant [J/(kg K)]
u	specific internal energy [J/kg]
U	internal energy [J]
\mathbf{v}	velocity vector [m/s]
V	zone volume [m ³]
t	time [s]
T	temperature [K]
\mathbf{T}	stress tensor [N/m ²]
x	air humidity by mass [kg _{wv} /kg _{da}]
\dot{w}	specific mechanical power [W/m ³]
\dot{W}	mechanical power [W]
Δh	phase change specific enthalpy [J/kg]
Δu	phase change specific internal energy [J/kg]
ϑ	temperature [°C]
μ	dynamic viscosity [Pa·s]
λ	thermal conductivity [W/(m K)]
$\boldsymbol{\lambda}$	thermal conductivity tensor [W/(m K)]
ρ	volumetric mass [kg/m ³]
Φ_T	heat flow density vector [W/m ²]
$\Phi^{(x)}$	flow through a surface of quantity x
$\Phi^{(P)}$	momentum flow [N]
$\langle \rangle$	integral average operator
∇	nabla [m ⁻¹]

Subscripts/Superscripts

a	zone indoor air
b	body
c/e	compression/expansion
cv	convective
CV	control volume
D	dissipative
en	envelope
ext	External
da	dry air
fr	fluid reference
I	internal gains
in	inlet

inf	infiltration
k	kinetic
l	liquid
lw	liquid water
m	moisture
ma	moist air
n	normal
N	number
out	outlet
R	reversible
s, S	surface
SYS	heating and/or cooling system
T	thermal
TP	triple point
v	vapour
w	water
wv	water vapour
σ	water vapour mass source
ϕ	advective flows

References

- Abuku, M., Janssen, H., Roels, S.. 2009. An Onset To whole Building Hygrothermal Modelling under Wind-Driven Rain Loads. Eleventh International IBPSA Conference, Glasgow, Scotland.
- Aissah, P.K. 2005. Indoor air quality - Combining air humidity with construction moisture. Ph.D. Thesis. ESRU. Univ. Strathclyde, Glasgow, UK
- ASHRAE. 2009. ASHRAE Handbook - Fundamentals
- Carrier. 1965. Handbook of Air Conditioning System Design. McGraw-Hill
- CIBSE. 2006. CIBSE Guide A - Environmental design
- Balaras, C. 1996. In "Passive Cooling of Buildings", Santamouris, M., Asimakopoulos D. Ed.. James&James
- Clarke JA. 2001. Energy simulation in building design. Second Edition, Butterworth-Heinemann, Oxford, UK.
- Energy Plus. 2012. Energy Plus Engineering Reference.
- Hagentofl C.-H. 2001. Introduction to Building Physics. Studentlitteratur AB, Sweden
- Hens, H.S.L.C.. 2010. Applied Building Physics. Wiley

Kreider J.F., Curtis, P.S., Rabl A. 2002. Heating and Cooling of Buildings. Design for Efficiency. 2nd Edition, McGraw-Hill

TRNSYS. 2007. TRNSYS 16 – Volume 6 -Multizone Building modeling. Solar Energy Laboratory, Univ. of Wisconsin-Madison

Underwood, C.P., Yik, F.W.K. 2004. Modeling Methods for Energy in Building. Blackwell Science

BENIMPACT Suite: a tool for ZEB whole life cycle analysis

Silvia Demattè – EnginSoft, Trento, Italy

Maria Cristina Grillo – Department of Civil and Environmental Engineering, University of Trento, Italy

Angelo Messina – EnginSoft, Trento, Italy

Antonio Frattari – Department of Civil and Environmental Engineering, University of Trento, Italy

Abstract

The building sector is predominantly responsible for energy consumption and environmental impact in the European Union. For this reason the European legal framework related to this sector has had a huge evolution over recent years. The “nearly Zero Energy Building” (nZEB) concept was introduced in 2010 with the Energy Performance Building Directive (recast) 2010/31/EC which stated “...zero consumption as a long-term goal for our buildings...”. By 2020 all new buildings will have to be “nearly Zero Energy” (nZEB) and the majority of their energy consumption has to be covered by renewable sources. It is important to underline that the definition nZEB does not concern only the energy efficiency of a house, but also the environmental impact and the life-cycle cost of the adopted solutions. Designing and realizing such buildings is a very ambitious task, which needs to be supported by appropriate tools and software. This paper presents BENIMPACT Suite (Building’s ENvironmental IMPACT evaluator & optimizer): a new tool for assessing buildings’ performance, developed by EnginSoft (Italy). The suite is organized in different core modules which allow to verify how the building performance is influenced by different design choices, such as envelope shape and materials, plant systems, renewable sources use, etc. One of the test cases used to validate BENIMPACT Suite is CasaZeroEnergy, a ZEB concluded in 2010 and located in Felettano (UD), in north-eastern Italy. This building is an experimental house designed and monitored by the Laboratory of Building Design of the University of Trento (Italy) and built by Polo Le Ville Plus Group (Cassacco-Italy). Energy performance, renewable energy production and Life Cycle Assessment of this building were modelled and evaluated using the BENIMPACT Suite and simulation results were compared to monitored and literature data.

1. Introduction

We want the buildings in which we live to be safe, healthy, functional, comfortable, and also aesthetically integrated into the urban context. They also need to be properly designed to be energy efficient and environmentally friendly to contribute in minimizing environmental loads, according to the international framework on building sustainability.

1.1 European regulation: an overview

Ten years ago, in 2002, the first Energy Performance of Buildings Directive (EPBD) 2002/91/EC was released in order “to promote the improvement of the energy performance of buildings within the Community, taking into account outdoor climatic and local conditions, as well as indoor climate requirements and cost-effectiveness”. Minimum energy performance was required for new buildings and existing buildings which were subjected to major renovations.

Since then, sustainable design and green strategies applied to the building sector have become more and more popular among governments, designers and researchers. Solar passive design and energy performance, insulation thickness increment, plant equipment improvement, renewable resources on site systems have become a trend. Adopting a benchmark energy performance level made it possible to drastically reduce energy consumption in buildings.

With the aim to reduce negative impacts from the building sector, and to help a faster diffusion of “smart” design strategies, the European Union has introduced several policies and regulations. Some examples are the following directives: the

2005/32/EC on Energy using Products (EuP), the 2006/32/EC Energy Saved Directive (ESD) on energy end-use efficiency and energy services, and its new version, the 2009/125/CE on Energy related Products (ErP). The Directive 2009/28/EC promotes the use of energy from renewable sources and requires that Member States should fix, by 2015, a minimum level of energy from renewable sources for new buildings and existing buildings subjected to major renovation.

The most important release of this general framework is the revision of the 2002 EPBD, the 2010/31/EC, known as Energy Performance of Buildings Directive (recast), which requires zero consumption as a long-term goal for European buildings. The recast fixes 2020 as the deadline for all new buildings to be “nearly Zero Energy” (for public buildings the deadline is the end of 2018): very high energy performance, and very low or almost zero energy demand, mostly covered by energy from renewable sources produced on-site or nearby. Nevertheless, the current system’s boundaries only consider the energy consumed for building management. Energy and environmental impacts from the other phases of its life cycle (material production, construction, maintenance, dismissing) are totally omitted, although it has been demonstrated that this amount of energy and sources gives an average contribution of 30% of the overall impact (Sartori and Hestnes, 2007). This value can rise up to 50% for low energy buildings.

1.2 Barriers in achieving the nZEB target

ZEB could strongly help to reduce energy consumption, environmental loads and operational costs. Even if the development of energy efficient constructions is strongly stimulated by legislative requirements, there is still a wide range of non-technological barriers that must be overcome in order to reach a wide diffusion of the zero energy building standard.

First of all, extra initial costs are far from the construction business’s mind. Usually, both contractors and clients are mainly driven by short-term profit-making and focus on the lowest price bidding and not on the added value that can be achieved implementing environmentally friendly

measures. Furthermore ZEB are not usual constructions. They need a high level of knowledge and skills that are not always available in design and construction teams. Several professionals are involved in the design process, and this might lead to problems if there are lapses in the communication among the different project team members. All actors must fully understand the issues and concerns of other parties and interact closely throughout all phases of the project. This is why an integrated design approach is needed to achieve multiple benefits such as higher efficiency and cost effective buildings. One of the main problems is the lack of tools needed by project teams to coordinate their work and to consider and evaluate different design alternatives.

In most mechanical industrial fields, ranging from aerospace to bio-mechanics, sophisticated 3D computer simulation tools have been used to predict responses to specific forcing actions in specific environments in order to integrate all the opportunities offered by different materials and technologies. The same kind of tools should be used in the construction sector. Although many are trying to develop a standard Building Information Modelling (BIM), there is currently no software able to take into account all the features that a ZEB shall have. Thus, there is an evident need to develop software for buildings design that can help to predict how the building will perform and enable them to model economic and environmental consequences of different design choices.

2. BENIMPACT Suite

2.1 Short overview on BENIMPACT Suite

BENIMPACT Suite wants to be a way to promote integrated design Computer-Aided Engineering (CAE) and intelligent Digital Prototyping (iDP) in the housing field.

BENIMPACT Suite is composed by different modules (Energy, LCA, Cost) that can work both as a standalone or as an integrated system (Global evaluation and Optimization). It should turn into a complete suite, whose aim is to help designers

check the quality of their solutions and find the “optimal” set of choices between different alternatives of building envelopes and energetic systems. It analyzes the whole life cycle of a building and searches for the “optimal” trade-off between opposed goals: energy consumption, environmental impact and cost. Indeed, in order to achieve the highest level of independence from traditional fossil fuel sources and the lowest environmental impact (materials use, energy consumption and pollutant emissions into the atmosphere), every new building must be designed straight from the preliminary phase so as to maximize all the chances given by the natural environment and by current technologies..

If the final aim is to spread awareness of sustainable design in a spontaneous way, the necessity to design “environmentally friendly” constructions must be compatible also with the amount of investment. We believe that the opportunity to find “smart” solutions will lead to an increment of sustainable buildings (new or renewed ones), less natural source depletion and a reduction in greenhouse gas emissions.

BENIMPACT Suite is connected to databases that can be updated by developers, companies and final users in order to keep up with innovation.

Each type of evaluation belongs to a specific functional unit that can run as a stand-alone. For each design, the energetic unit performs an annual energetic dynamic simulation with hourly steps, and calculates annual energy consumption. Other functional units then calculate global energy consumption, environmental impact (Life Cycle Assessment) and costs (Life Cycle Costing) for the entire life cycle of the building.

Thermodynamic performances are verified using a package composed of “Energy Plus” and some features implemented by EnginSoft

. Environmental impact and costs are calculated using specific routines implemented by EnginSoft. The calculation of the whole environmental impacts is performed by using the IBO database (IBO - Austrian Institute for Healthy and Ecological Building) according to the “IBO-Guidelines to calculate the OI3 indicators for buildings”, but without limiting the maximum value of this parameter to 100. The OI3 indicator is

calculated also for heating and cooling energy and not only for building construction elements, in order to perform a more comprehensive calculation.

A routine is available to evaluate cost performance, but since prices are strongly influenced by the local market and the amount of purchased goods, the cost database has to be supplied by the user.

The multi-objective optimization is based on a genetic algorithm which searches for the “Pareto Frontier”, which collects the best solutions and represents the ideal limit beyond which every further implementation compromises the system. It is currently running on modeFRONTIER, a multidisciplinary and multi-objective software, which is also used to integrate the different functional units.

2.2 Validation of BENIMPACT Suite: case study selection

In order to test the project validity, BENIMPACT Suite was applied to different case studies, both new buildings and energy retrofitting. The validation test was made on two buildings where the monitoring data was available. Due to the fact that the use of monitored data is the most accurate way of testing strength and weakness of a software/tool, the availability of such data was the main criterion used for the selection of case studies.

The first case study was Palazzo Kofler (BZ, Italy), built at the beginning of the 20th century, retrofitted with the ClimateHouse standard and subjected to monitoring for two years. The second case study was a new building, CasaZeroEnergy in Felettano (UD, Italy), monitored in the last 12 months.

Following, the validation of the model performed on CasaZeroEnergy will be explained.

This methodology was divided into several steps:

1. Analysis of the local climate,
2. Analysis of the main building features,
3. Decision on which monitored data are important for the analysis and validation of thermal behaviour prediction,
4. Analysis of the energetic behaviour of the real building through chosen monitored data,

5. Building model construction,
6. Dynamic energy simulation,
7. Comparison of energy simulation results and monitored values,
8. LCA using BENIMPACT Suite,
9. Comparison of LCA results and values calculated by using SimaPro.

3. CasaZeroEnergy

“CasaZeroEnergy” is a detached house, concluded in 2010. It was designed according to the principles of bio-climatic architecture (Fig. 1). This means that every building element was designed in order to minimize environmental impacts, using eco-friendly materials, reducing losses and maximizing free gains from the context, using passive design strategies, both for heating and cooling.



Fig. 1 – View of “CasaZeroEnergy” in Felettano, Udine – Italy.

3.1 Local climate

The house site is characterized by a mild and humid continental climate with an average annual temperature of 13°C. There is no dry season, and summer months are quite hot. Prevalent wind runs from north to south and is useful for passive cooling (Fig. 2).

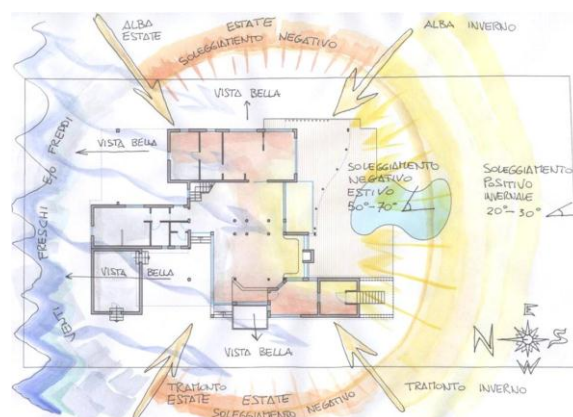


Fig. 2 – Bioclimatic concept of “CasaZeroEnergy” in Felettano, Udine – Italy.

3.2 Building shape

The building has a compact shape, with a reduced Surface/Volume ratio of 0.78, in order to minimize winter heat losses. The main facade of the building is south - south-west oriented to benefit from the apparent sun path in winter (Fig. 2). On the south facade a great sunspace is, with a glazed surface of 3.60 x 6.30 m². Openings on the east and west sides are protected from the summer sunshine with a system of shading achieved by moving louvers.

The building has two roofs. The biggest one, sloping, north facing, protects the house from cold winds in winter. The second one, on the south, is flat, lower than the other one, and arranged to bring photovoltaic panels. The windows on the south facade, above the flat roof, have the function to allow air movement for summer passive cooling, letting out the air entered from the opposite northern side.

3.3 Building envelope and structure materials

The building was built with renewable, recycled and recyclable materials with low embodied energy content and carbon dioxide emissions during the construction phase. For example, the hardscapes are realized with bricks and stone slabs from the demolition of old buildings within 50 km, to contain pollution from transport.

Also the structure is very low impacting, thanks to the choice of using wood as the main structural material. The walls are light-weight structures, made by a timber-frame system with wooden posts and beams. The gap insulation between the pillars

is in wood fibre, while the external insulation layer, aimed to reduce thermal bridges, is in cork. In this way the walls U-value was reduced to 0.218 W/m²K. Also the roof U-value is very low and equal to 0.205 W/m²K. Inner walls are made with wood studs and plasterboard finishing. Windows and glazed parts have a U-value of 1.3 W/m²K and 1.1 W/m²K respectively.

3.4 Passive systems and renewable energy

One of the main features of this building is that it is not connected to the gas network and it works only by using electricity, totally produced by a photovoltaic plant of 108.9 m², 13.4% efficiency and 14.6 kW of pick. Other alternative energy systems are installed in the building. The first one is the sunspace on the south facade, which allows the incoming solar radiation to be conveniently stored. The external glazes of this system are fully openable to regulate the temperature both in summer and winter.

In CasaZeroEnergy, exhausted air is naturally replaced through the openings on the north and south facades. In this way it is possible to ensure a good indoor environmental quality, the day-time cooling of the living space and the night-time cooling of the building elements. Shading systems are very important to avoid overheating during summer. For this reason these systems were properly sized and selected, in order to control and adjust the incoming heating and lighting solar radiation. Furthermore, on the building roof there is a solar collector plant of 20.91 m², 72% efficiency for DHW production.

An under-floor heating and cooling system is connected to a geothermal heat-pump that exploits the constant temperature of the earth at the deep of 2.5 m under the garden surface. The resulting nominal energy efficiency performance for heating and cooling mode are respectively a COP of 3 and an EER of 2.6.

3.5 Monitoring data

During the monitoring period, temperatures and electricity were measured respectively by sensors and multi-meters in twelve different rooms of the

house. These spaces were selected because of their different exposition and final use (bedrooms, living room, kitchen, bathrooms, laundry, etc.).

The main scope of the monitoring has been to understand how CasaZeroEnergy behaves and to validate the quality of this ZEB project.

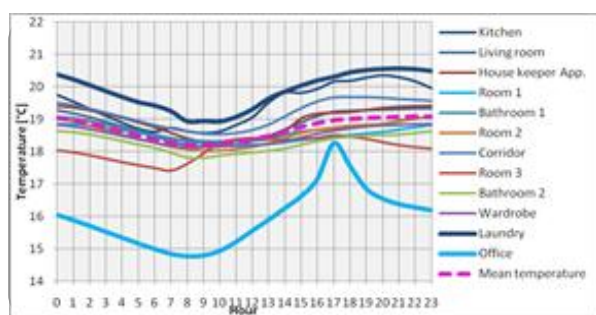
Starting from monitored data, the typical (average) day was defined both for the summer and winter period. The first one was calculated in the period between June 1st to July 31st 2011 and the second one was calculated considering the whole winter season 2011-2012 (December 21st to March 21st). Typical summer and winter days for the twelve rooms consist in 24 temperatures which are the hourly averages of the two monitored periods.

The typical winter day (Graph 1) shows that ten of the twelve monitored rooms display similar temperatures, within less than a 1.5°C difference from the average temperature. The two exceptions are the laundry and the office. Generally these rooms have a constant set-point temperature of 18°C and warmer hours depend on internal gains and solar heat gains. Causes of the different behaviour of the laundry are higher internal gains due to the presence of several pieces of equipment, which release sensible and latent heat contributions, and the windows opening during the first hours in the morning, which reduces the room temperature. The different temperature evolution in the office, however, is caused by a different set point and heating system. This space has a set point of 15°C and is heated during the day by an electric heater.

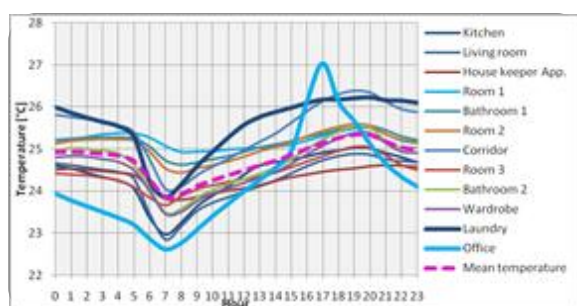
There is another important space which has not been monitored yet: the sunspace. It is very important for the passive heating of the building, because of its capacity to preheat the air and store the heat. Properly managed, the green house can be used to maximize passive solar gains from October to March, reducing the energy demand.

Also in the typical summer day (Graph 2), the same two rooms, the laundry and the office, have an inhomogeneous behaviour. The laundry is still warmer due to its higher internal gains except in the morning, when the windows are usually opened to allow the entire house to benefit from the passive cooling down effect of fresh winds from north. As in winter, the office curve presents

an odd behaviour, different from every other room. This is due to the fact that this space is not cooled. In particular it becomes overheated during the afternoon because of its west window, which has no sun protection. From the comparison of the two graphs (Graph 1 and Graph 2), it is possible to appreciate that the summer and winter behaviour of the office is similar: the two curves have an identical shape and they are just shifted along the temperature axis. This difference of temperature depends on the higher amount of solar radiation entering the room in summer.



Graph 1 – Monitored temperatures: typical winter day



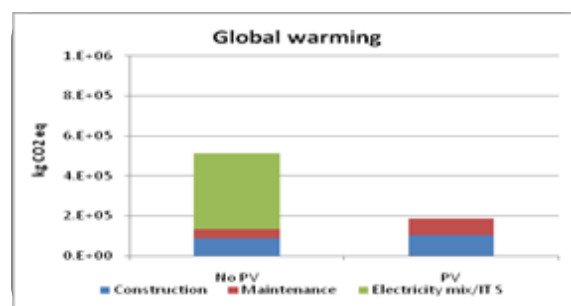
Graph 2 – Monitored temperatures: typical summer day

3.6 LCA with SimaPro

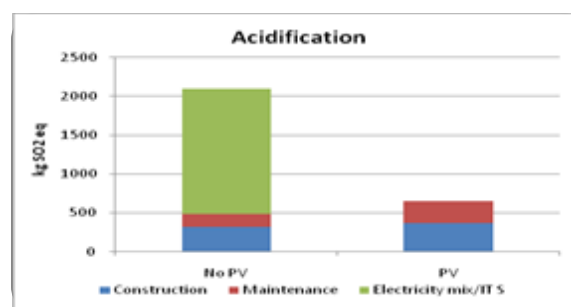
LCA of CasaZeroEnergy was performed by using SimaPro, one of the most complete software packages at an international level for developing environmental performance analysis. For this work the EPD (Environmental Product Declaration) method was selected as the calculation method for LCA. Because of the lack of an Italian database of materials, the assessment has been performed with EcoInvent database (CH). This database is mainly composed of European average data, and it does not consider the biotic contribution in storing carbon dioxide of wood.

In order to perform this simulation, the life of the

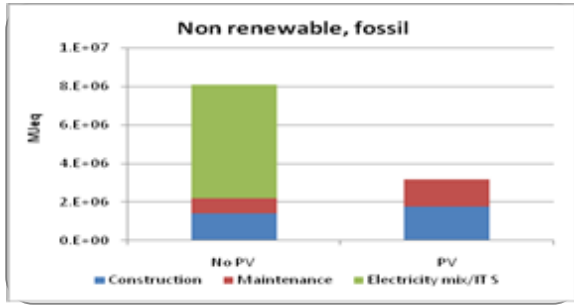
building was divided into three phases: construction, maintenance and use. For the construction phase every building component (external walls, floors, roofs, partitions) was modelled, omitting to consider transportation impact. Maintenance and use contributions were evaluated basing on the assumption of a building life span of 75 years. Maintenance operations were modelled taking into account the number of intervention of renovation of every single construction material. It has been estimated that the environmental impact produced by maintenance operations accounts for nearly 45% of the total. Also the contribution of the PV plant was taken into account and its convenience was evaluated through comparison with another model which works using electricity. As explained above, CasaZeroEnergy works only with electricity and that the PV plant is able to produce enough energy to cover all needs, so that no electrical energy has come from the grid. This means that, with PV panels, the usage phase does not have any further environmental impact as shown in Graph 3, Graph 4 and Graph 5.



Graph 3 – SimaPro: Global warming potential



Graph 4 – SimaPro: Acidification potential



Graph 5 – SimaPro: Non renewable energy

From the graphs it is possible to observe that the PV plant increases impacts for construction and maintenance, but at the same time it strongly reduces the global life cycle impact. Comparing the total impact of the house during its life cycle, it resulted that environmental loads produced by the building without PV plant are nearly the triple of the house with PV. This means that there is an effective convenience in producing energy with a PV plant.

4. BENIMPACT Suite Validation

4.1 Energy performance

The first step required to prepare an energy analysis model for a building is dividing it into thermal zones. A higher number of thermal zones affects the time required to run an energy simulation. Thus, it is important to identify the lowest number of zones able to correctly reproduce the building behaviour. Basing on the previous analysis, the model was divided into four thermal zones: sunspace, laundry, office and the rest of the house (Fig. 3).

Some hypotheses on set point temperatures, air change rates and internal heat gains were made. Set point temperature values were deduced from monitored data, while for internal gains the starting point were values given by Italian directives.

In the summer, the sunspace is open and without a heating system it is possible to better appreciate the influence of internal gains. For this reason, a model without the sunspace was prepared and verified using summer monitored data. Summer

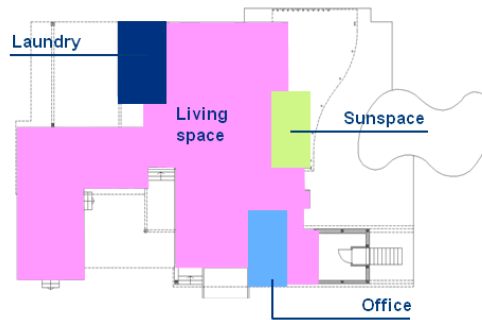
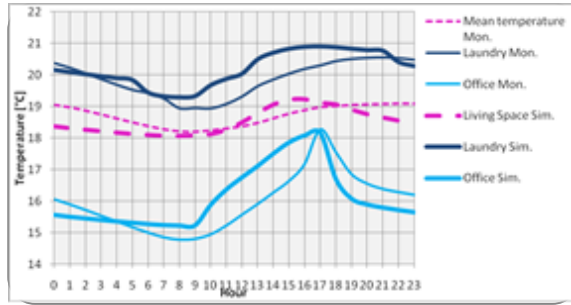


Fig. 3 – Thermal zones of the building model.

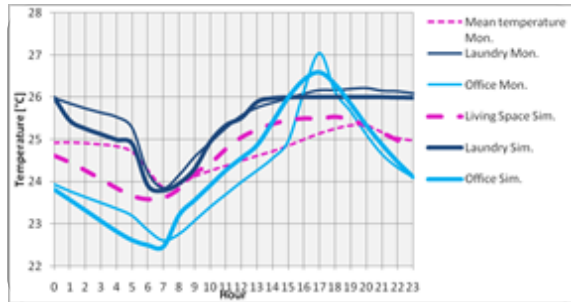
thermal simulations were run and the behaviour of the building was checked varying inputs until the model and the real building converged. At first, we also ran simulations without turning on the cooling. The living space was the easiest to adjust because it is used as a standard living space. For the laundry, increasing internal heat gains were simulated to meet the real behaviour of the room, strictly related to the presence of equipment. Windows opening, scheduled as resulted from monitoring, was then added. The introduction of this ventilation ratio was necessary for the overlapping of the model to the real building.

After that, the sunspace was added. In modelling this element the most difficult part was defining the air exchange rates between the living space and the sunspace and between the sunspace and the external environment. Furthermore an appropriate schedule for the sunspace opening management had to be defined, because of the lack of real data. When the whole building model with all the four thermal zones was ready, the winter thermal simulation was verified. In order to perform this analysis, it was necessary to complete the office thermal zone definition by the introduction of a standard electric heater. The schedule of the heater was supposed looking at the monitored data.

As shown in Graph 6 and in Graph 7, the building model with four thermal zones well simulates the real temperature evolution of the building. Small differences are due to the faster response of the model, which has less internal mass, since most internal walls and the furniture are not simulated.



Graph 6 – Monitored vs. simulated temperatures: typical winter day



Graph 7 – Monitored vs. simulated temperatures: typical summer day

Thus it is possible to affirm that the required useful energy to cover the heating and cooling needs of the building, which are respectively 20 kWh/m²/year and 12 kWh/m²/year, can be reasonable. Moreover, those needs could be even lower than expected thanks to the higher thermal mass contribution. It is important to underline that this building is not provided with a mechanical ventilation plant with heat recovery. Therefore, the calculated energy demand is very low and the possibility to implement such a system would give greater energy results, but affecting the concept of bioclimatic architecture of the building.

As shown in Table 1, the installed PV plant covers the geothermal heat pump needs, for both heating and cooling seasons, and it also furnishes enough electric energy for home appliances and indoor lighting (Other). Moreover, 10 MWh are sold to the grid.

Another analysis was made to check the effective contribute of the sunspace to reduce the heating energy consumption. For this reason, average day useful heating power required by the living space with and without sunspace were compared and the green house contribution could be truly appreciated, reducing the useful heating energy requirements of the building by 4 kWh/m²/year.

Electric Energy	Heat	Cool	Other	TOT
Consumed [kWh]	2650	1160	5000	8811
From PV plant [MWh]	-	-	-	19
To be sold [MWh]	-	-	-	10

Table 1 – Annual Electric Energy Balance by final use

4.2 LCA with BENIMPACT Suite

The LCA routine of BENIMPACT Suite can be used to easily assess the ecological impact of a building throughout its life cycle of building components and buildings: construction, maintenance and disposal.

The implemented method is based on the IBO database, using values that do not consider the biotic contribution in storing carbon dioxide of wood. Three impact index are calculated basing on the following ecological indicators:

- Global Warming Potential (GWP),
- Acidification potential (AP),
- Primary Energy Content, renewable and non-renewable (PEI_e, PEI_{ne}).

A global Eco-index for the entire life of a building is also calculated. Such an index is of great importance for BENIMPACT Suite because it is used to specify the environmental impact performance when driving optimizations. This index is based on the OI₃ index and IBO formulas, but we decided to consider only positive values of the three partial eco-indicators (OI_{GWP}, OI_{AP}, OI_{PEI_{ne}}), and not to limit their upper value to 100. In this way we are able to easily identify environmental impacting constructions, and to take into account the primary energy contribution.

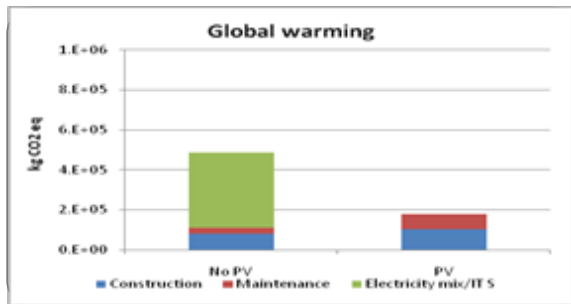
As a first step, we compared the LCA results obtained using BENIMPACT Suite to those calculated using SimaPro. We obtained smaller values using the IBO database, due to the fact that the IBO database is based on local data instead of European average values. For this reason we added new materials to our database, characterized by SimaPro impacts, replaced them in the model and re-run the LCA analysis. Results are reported in Graph 8, Graph 9, and Graph 10, which show the same behaviour as Graph 3, Graph 4 and Graph 5. Small differences depend on the

fact that in the LCA analysis ran with BENIMPACT Suite we considered only the thermal envelope of the house, without taking into account structural components. In this way the LCA routine was also validated.

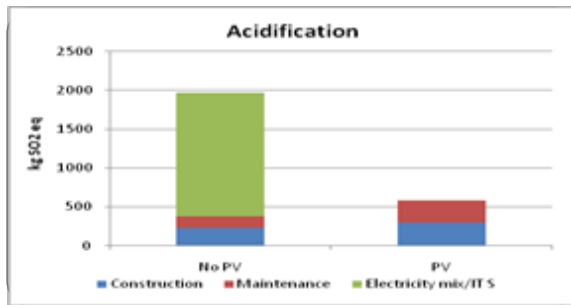
Finally, the global eco-indicator index was calculated, and results are reported in Table 2.

Global Eco-indicator	OI_3 [-]	
	No PV	PV
Construction	30	45
Maintenance	13	46
Electricity mix/IT S	302	0
Total	345	91

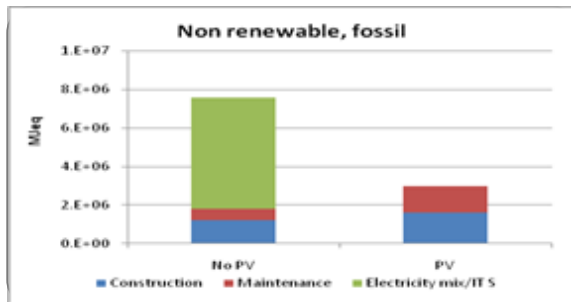
Table 2 – Global Eco-indicator with BENIMPACT Suite. PV plant effect on CasaZeroEnergy



Graph 8 – BENIMPACT: Global warming potential



Graph 9 – BENIMPACT: Acidification potential



Graph 10 – BENIMPACT: Non renewable energy

5. Conclusions

In order to spread awareness of sustainable design, “environmentally friendly” constructions must be characterized by “smart” investment, which need scientific evidence.

The test case of CasaZeroEnergy proves that BENIMPACT Suite is an effective tool to assess the energy needs and the environmental impact of a whole building, for heating/cooling plant sizing, and to verify the thermal behaviour of different rooms.

Thermodynamic and environmental performances were analyzed, hour by hour and for the entire life of the building, using the software package “Energy Plus” and some prototypes implemented by EnginSoft, showing that the specific micro-climatic condition and users habits can really affect the behave of the building or some of its rooms (see Graph 1 and Graph 2).

The validation also showed the robustness of the LCA routine implemented in BENIMPACT Suite: it works with more than one database even if results strongly depend on the input database.

6. Nomenclature

Symbols

AP	Acidification Potential [kg SO ₄ ⁻]
BIM	Building Information Modeling
CAE	Computer-Aided Engineering
DHW	Domestic Hot Water
EPBD	Energy Performance of Buildings Directive
EPD	Environmental Product Declaration
ErP	Energy related Products
ESD	Energy Saved Directive
EuP	Energy using Products
GWP	Global Warming Potential [kg CO ₂ eq.]
IBO	Austrian Institute for Healthy and Ecological Building
iDP	intelligent Digital Prototyping
LCA	Life Cycle Assessment
LCC	Life Cycle Costing
nZEB	nearly Zero Energy Building

OI_AP	Acidification Potential Eco – Indicator [-]
OI_GWP	Global Warming Potential Eco – Indicator [-]
OI_PElne	Primary non-renewable Energy Eco – Indicator [-]
OI_3	Global Eco – Indicator [-]
PEIe	Primary renewable Energy Content [MJ]
PEIne	Primary non-renewable Energy Content [MJ]

References

- Abdalla G., Maas G., Huyghe J. 2009. Barriers to Zero Energy Construction (ZEC) – Technically possible; why not succeed yet?, Conference Proceedings of PLEA 2009, Quebec City (Canada).
- Charron R., Athienitis A. 2008. The Use of Genetic Algorithms for a Net-Zero Energy Solar Home Design Optimisation Tool, Conference Proceedings of PLEA 2006, Geneve (Switzerland).
- Demattè S., Grillo M. C., Messina A., Frattari A. 2012. Benim pact Suite: A Tool For Zeb Performance Assessment, Conference Proceedings of ZEMCH 2012, Glasgow (UK).
- European Community 2002. 2002/31/EC directive – Energy performance of Buildings.
- European Community 2010. 2010/31/EC directive – Energy performance of Buildings II.
- Frattari A., Messina A. 2011. CasaZeroEnergy: an Italian example of a Low Carbon Building, Conference proceedings of Low Carbon Earth Summit (LCES) 2011, Dalian (Cina).
- Frattari A., Albatici R., Chiogna M., Passerini F. 2010. An intelligent sustainable building to save energy, Conference proceedings of Renewable Energy 2010: Advanced Technology Paths to Global Sustainability, Yokohama (Japan).
- Frattari A. 2011. Utilizzo di metodologie di simulazione energetica dinamica e di ottimizzazione nel progetto di un edificio “near zero energy”, Conference proceedings of EnginSoft International Conference – CAE Technologies for Industry and ANSYS Italian Conference 2011, Verona (Italy).
- Gatti L., Laner A., Margonari M., Messina A., Trabucco D., Viannei V., Zanato M. 2010. Multi-objective optimization in the design of sustainable buildings, Conference proceedings of EnginSoft International Conference – CAE Technologies for Industry and ANSYS Italian Conference 2010, Montichiari - BS (Italy).
- IBO Institute Of Austria 2011. IBO-Guidelines to calculating the OI3 indicators for buildings.
- Messina A., Laner A., Trabucco D. 2009. BENIMPACT* - Building’s Environmental Impact Evaluator & Optimizer, Conference proceedings of EnginSoft International Conference – CAE Technologies for Industry and ANSYS Italian Conference 2009, Bergamo (Italy).
- Messina A. 2011. ‘ECO-BUILDING e Tecnologie CAE, la necessità di un incontro’, Conference proceedings of EnginSoft International Conference – CAE Technologies for Industry and ANSYS Italian Conference 2011, Verona (Italy).
- Sartori, I. and A. Hestnes, 2007. Energy use in the life cycle of conventional and low-energy buildings: A review article. Energy and Buildings, 39, 249 – 257.
- Thièbat F. 2011, ‘Integrazione tra LCA e LCC: sviluppo di un modello di valutazione economico-ambientale’. Progetto Sostenibile, 27, 62-69.
- Zanato M., Demattè S., Messina A. 2011. ‘BENIMPACT SUITE - Piattaforma software per la progettazione integrata di edifici ecosostenibili’, Conference proceedings of EnginSoft International Conference – CAE Technologies for Industry and ANSYS Italian Conference 2011, Verona (Italy).

Daylight harvesting: a multivariate regression linear model for predicting the impact on lighting, cooling and heating

Stefano Moret – Università degli Studi di Padova, Engineering and Management Dept., Vicenza, Italy

Marco Noro – Università degli Studi di Padova, Engineering and Management Dept., Vicenza, Italy

Konstantinos Papamichael – University of California Davis, Department of Design, Davis (CA), USA

Abstract

On a worldwide scale lighting accounts for 20% to 50% of buildings' energy use [1] and 19% of the global electricity consumption [2], and therefore represents a key opportunity for energy efficiency efforts in different countries due to its relevant impact and often short payback periods of investments. Among the various strategies developed to foster efficient lighting, daylight harvesting (i.e. the deployment of controls to reduce electric lighting based on available daylight in interior spaces) in combination with dynamic daylighting devices (i.e. windows and skylights able to modify their Visible Light Transmittance and Solar Heat Gain Coefficient) has shown dramatic potential for energy savings, peak electricity demand reduction and occupant visual comfort improvement.

This paper is focused on daylight harvesting implementations utilizing fenestration systems that incorporate dynamic components, such as electrochromic glazing and operable louvers, assessing their impact on building energy performance and occupant visual comfort through advanced modeling techniques based on the EnergyPlus simulation engine. EnergyPlus is used in combination with the Building Controls Virtual Test Bed (BCVTB), which supports simulation of multiple fenestration and electric lighting control strategies, based on occupancy/vacancy and daylight availability. Results show dramatic savings potential on electric lighting (35-41%) and cooling (16-29%) loads, but also potential for significant increase in heating loads, especially in heating-dominated climates.

Since case-by-case simulation is often not affordable for real buildings, parametric simulations are performed varying the values of key design and context parameters in JEPlus and the results are used to develop a linear multivariate regression model for predicting the impact of daylight harvesting strategies on electric lighting, cooling and heating loads as functions of a limited set of input parameters. This approach proves to be very useful for

order-of-magnitude estimation of building energy requirements during the early, schematic phases of building design, as well as high-level analyses for investment and policy making goals. The approach is very suitable for the development of a quick and easy-to-use tool for such purposes.

1. Introduction

1.1 Literature review

Daylight harvesting and electrochromic technologies have been widely studied by the "Windows and Daylighting" group at Lawrence Berkeley National Laboratory since their first appearance in the 1980s. In an extensive simulation work published in 2004, DOE-2.1E [3] is used to simulate the effect of lighting and fenestration controls on the annual energy balance of a three-story commercial building in five different US climates [4]: results show 10-24% savings in all climates compared to a baseline case with ASHRAE 90.1-1999 compliant windows with no daylighting controls and 0.30 WWR (Window-to-Wall Ratio). Electrochromic glazing generate 5-9% additional savings in South perimeter zones over lighting controls compared to low-E spectrally selective glazing, and 5% in the other zones in most climates.

The Pacific Northwest National Laboratory performed a similar study using EnergyPlus v3.0, evaluating the addition of electric lighting controls and electrochromic glazing to an ASHRAE 90.1 baseline case for small and medium office buildings [5]. Results, averaged for Northern and Southern climates, show total savings of 3-6% for the small office case, and 4-5% for the medium office case.

1.2 Motivation and method

The aim of the present study is to assess the potential impact of electric lighting and fenestration controls on commercial buildings energy consumption (lighting, cooling and heating) and to develop a linear regression model able to predict this impact quickly and easily through a limited set of input values for key design and context parameters, thus avoiding the need for time-consuming case-by-case detailed simulations that are not attractive during initial, schematic design decisions on fenestration and electric lighting.

The first part of the paper is focused on simulations performed with EnergyPlus at different levels of complexity to assess the impact of daylight harvesting strategies in different climates. Initial simulations are focused on a very small space with a single skylight, aiming at exploring the complexity and effectiveness of the simulation approach. After successfully configuring the approach itself, further simulations are performed using US Department of Energy (DOE) validated building models and realistic control algorithms implemented in the Building Controls Virtual Test Bed (BCVTB).

The second part of the paper is focused on the development of a multivariate linear regression model based on multiple JEPlus parametric simulations for key design (fenestration and lighting controls) and context (US locations) variables to characterize the model at its partial derivatives, i.e. to understand how each variable defining initial building conditions influences the impact of energy efficiency strategies on annual building energy performance.

1.3 Simulation toolkit

Annual energy simulations of the dynamic fenestration and electric lighting systems are performed using the EnergyPlus v7.1 software environment [6].

Custom control algorithms for electrochromic glazing management are implemented using the EnergyPlus external interface and the Building Controls Virtual Test Bed v1.1 software [7].

Parametric simulations in EnergyPlus are automated using the JAVA shell JEPlus v1.3 [8].

This state-of-the-art toolkit allows a more innovative

and reliable simulating approach in comparison to what can be found in the literature studies dealing with the topic.

2. Simulation

2.1 Simple office space with skylight

The first goal of this effort is to assess the complexity and effectiveness of simulating the impact of dynamic glazing and electric lighting controls on building energy consumption in different climates, considering a simple 25 m² small office space with a single skylight (Skylight-to-Roof Ratio = 0.04), and the following features (Fig. 4):

- ASHRAE 90.1-2004 construction and skylight for three US climates: Phoenix, AZ (US climate zone 2), Baltimore, MD (US climate zone 4) and Minneapolis, MN (US climate zone 6).
- Fluorescent lighting at 10.8 W/m², dimmable in power from 20% to 100%.
- Two illuminance control points at the centre of space: one at 0.8 m from floor and one right under the skylight.
- Ideal loads simplification for HVAC system: a COP of 4 is used to translate cooling into electricity load.
- Skylight simulated as a double-glazing window, with very thin translucent internal layer to diffuse the transmitted daylight.
- The electrochromic glazing effect is simulated as “switchable glazing” using the EnergyPlus “MeetDaylightIlluminanceSetPoint” function. When dynamic glazing is simulated, the ASHRAE compliant external layer is replaced by a theoretical glazing switching between a clear state (VLT=SHGC=1) and a fully tinted state (VLT=SHGC=0) in a continuous mode. For simplicity, it is assumed that the values of Visible Light Transmittance (VLT) and Solar Heat Gain Coefficient (SHGC) are equal for baseline glazing, based on the experimentally assessed linear relation between the two coefficients [9]. The switchable glazing state is automatically selected by the EnergyPlus function to maintain 500 lux horizontal illuminance at the reference point at 0.8 m height from the floor.

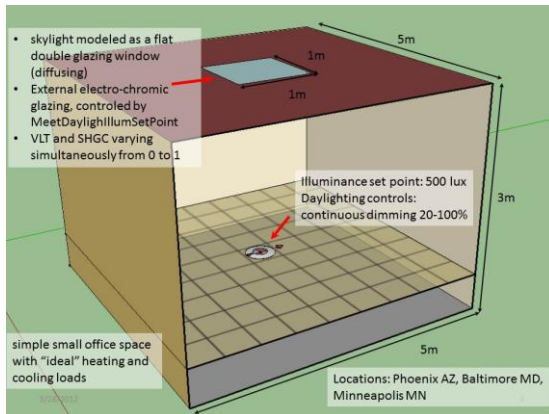


Fig. 4 – The simple office space with skylight

Five simulation runs are performed for each of the three weather files:

- 1) Without skylight
- 2) Skylight with ASHRAE 90.1 compliant properties
- 3) Same as #2 with addition of lighting controls
- 4) Same as #3 with electrochromic glazing instead of the baseline skylight
- 5) Same as #4 with electrochromic glazing disabled during the heating season

The results of the 15 simulations are reported in Table 3 with a breakdown of lighting and HVAC consumption. Percentage values for energy savings in cases #3, #4 and #5 are relative to case #2, because case #1 does not present any fenestration.

Due to the simplifications introduced in the modeling phase the results should be considered in relative terms, i.e. to determine how lighting and fenestration controls affect electric lighting and HVAC energy requirements in different locations relative to the ASHRAE 90.1 compliant non-dynamic case. Occupant comfort is not taken into consideration at this stage beyond maintenance of 500 lux minimum illuminance at the work plane. The most critical observations are as follows:

- **Lighting:** Lighting controls produce relative energy savings on lighting energy of 58-60%, with consequent positive effect on cooling loads and negative effect on heating loads, due to reduction of heat contribution from the electric lighting system.
- **Cooling:** Positive impact of switchable glazing on cooling consumption providing additional energy savings over those from the lighting controls. Savings are higher than values found in literature.

- **Heating:** Negative impact of switchable glazing on heating energy requirements, in addition to the negative effect of lighting controls.
- Positive overall effect of using switchable glazing only during summer, i.e. disabling them during the heating season, resulting in reduction of cooling savings but, on average, giving a larger positive contribution to heating loads.

As previously stated, comparison between absolute values and, therefore, total savings might be highly influenced by the modeling simplifications. Particular attention should be given, though, to the increased loads in heating-dominated climates, like Minneapolis, MN, where the negative effects of switchable glazing on heating loads balanced the positive effects on lighting and cooling reduction bringing the overall performance back to the baseline of the ASHRAE-compliant fenestration case.

2.2 DOE validated models with custom control algorithms using the BCVTB

After the small office space simulations, the same approach is adopted with DOE standardized building models with realistic control algorithms and taking into account occupant visual comfort, seeking validation in comparison to real buildings.

The US Department of Energy (DOE), within the framework of the so-called “Commercial Building Initiative” [10], published a set of “standard or “reference energy models for the most common commercial buildings to serve as a starting point for energy efficiency research. The models represent reasonably realistic building characteristics and construction practices” [11] and are optimized for different US climates.

From the various available standard models in EnergyPlus v5.0, a small office prototype building is chosen, with the following characteristics (Fig. 5):

- One core zone and four daylit perimeter zones
- WWR = 0.212
- Windows and constructions optimized for the three US climates of Phoenix (AZ), Baltimore (MD) and Minneapolis (MN) according to ASHRAE 90.1-2004 standard
- Detailed design for HVAC system: natural gas for heating loads, electricity for cooling loads

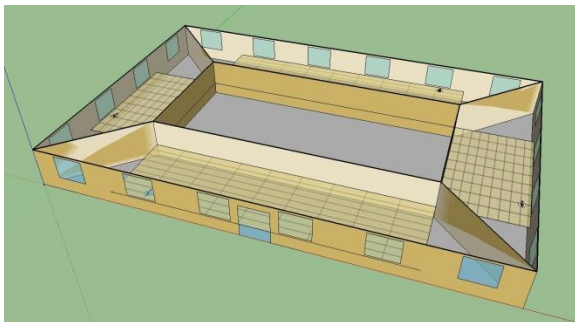


Fig. 5 – DOE standard small office building model

Workplane illuminance maps and daylighting control points are placed in each of the four daylight perimeter zones.

Five simulations runs are performed for each of the three US locations:

- 1) Baseline: no controls, ASHRAE 90.1 glazing
- 2) Same as #1 with addition of lighting controls
- 3) Same as #2 but with switchable glazing, using the “MeetDaylightIlluminanceSetPoint” control function of EnergyPlus
- 4) Same as #3 with switchable glazing disabled during the heating season
- 5) Switchable glazing is managed using a custom control algorithm implemented in the BCVTB

The BCVTB supports implementation of custom control algorithms in EnergyPlus through its external interface. Newly released actuators support glazing switching at every timestep at one of four discrete states ($VLT = SHGC = \{65\%, 10\%, 2.5\%, 0\%\}$). The control algorithm takes into account daylight workplane illuminance and glare index values at each reference point, the zones’ occupancy level, mean air temperature and thermostat setpoint. In case #5 the control algorithm selects at every simulation timestep the switchable glazing state that minimizes energy consumption without negative effects on occupant visual comfort.

The main difference with the small office space with the single skylight is that the performance results of the base case for the 5-zone small office are validated, thus allowing comparison of absolute values. Table 4 summarizes the simulations output. For cases #1 through #4:

- **Lighting:** savings are similar in the three locations, ranging between 35% and 41%, with positive contributions of electrochromics. Savings are lower than in the previous

simulation runs because only perimeter zones benefit from daylight harvesting. HVAC loads are consequently influenced by the reduction of heat gain from reduced lighting.

- **Cooling:** Switchable glazing have a positive effect on cooling loads, quite regular in absolute values, from 10% savings in Phoenix to 21% in Minneapolis in addition to the savings from the lighting controls.
- **Heating:** Switchable glazing have a negative effect on heating loads, fairly constant in percentage values, between 11% and 14%. This highlights once more the negative effects in heating-dominated climates. Deploying switchable glazing only during the cooling season helps reduce heating season penalties.

The control strategy does not take into account occupant luminous comfort, i.e. disabling glass switching in winter can produce discomfort glare, while fully tinted windows can be highly unpleasant for vision.

In case #5 where occupant luminous comfort is also considered for the control of the switchable glazing, the positive effects on both cooling and heating loads are reduced in comparison to the values achieved in case #4, resulting in a slight increase of the total building energy consumption compared to the cases where luminous comfort is not considered. However the energy reduction is still very significant: compared to the baseline case #1, total annual savings for case #5 are 28.9 GJ (23%) in Phoenix, AZ, 17.2 GJ (10%) in Minneapolis, MN, and 17.9 GJ (15%) in Baltimore, MD.

In general, the estimated savings from lighting and fenestration controls are again equal or higher than those of previous studies found in the literature.

3. Linear model development

As shown in the previous section, electric lighting and fenestration controls for daylight harvesting have significant energy efficiency potential. However, performing such simulations for actual building projects requires significant effort. Moreover, it requires detailed input, which is not usually available during the early, schematic phases of building design. As a result, consideration of

potential benefits from advanced lighting and fenestration controls becomes prohibitively expensive. To resolve this issue, a simplified energy savings predictive model is developed, utilizing a small number of key variables that are most critical in the consideration of energy savings from advanced lighting and fenestration controls for daylight harvesting. Parametric simulations are then performed bracketing the value range of each parameter with low, medium and high values. The results of the simulations are then used to determine regression coefficients in logical expressions that link the identified key variables to lighting, cooling and heating energy requirements.

3.1 Simplified Energy Savings Predictive Model Identification

The first step towards the development of a simplified predictive model is the identification of key variables that have the most effect on the energy savings potential of electric lighting and fenestration controls for daylight harvesting. The following variables are identified as the most appropriate:

- LES [lm/W]: luminous efficacy of electric light sources
- E [lm/m²]: average illuminance levels, taking into account over and under-illuminated areas
- Occupant behaviour, in terms of lighting system management (dimming, on/off switching,...)
- h_{OP} [h]: occupancy, annual hours of operation
- WWR [-]: Window-to-Wall ratio
- LSG [-]: light to solar gain ratio (VLT/SHGC) for the glazing. This variable reflects the heating contribution given by daylight, i.e. the luminous efficacy of the daylight radiation (LER). The higher the LSG value the higher the performance of the glazing, i.e. less solar heat gain for the same amount of transmitted visible light
- Location, in terms of Cooling Degree Days (CDD) and Heating Degree Days (HDD).

The floor surface area of the building isn't included in the list since specific energy consumption [J/m²] is ultimately relevant: extrapolation of results for buildings much larger than the simulated models shall be carefully evaluated.

The following assumptions can be made:

- “E” (illuminance value) is constant for a specific commercial building type, as it is generally set by regulations worldwide
- Lights are switched on and off according to occupancy schedules, which in turn are constant for specific commercial building types
- All spaces are day-lit, i.e. the model is valid to the extent that all areas taken into account have daylight availability
- The model is linear to the above listed variables or their reciprocals

According to these assumptions, three of the above listed variables (E, h_{OP}, occupants' behaviour), can be considered constant for a specific building type, i.e. not impacting its energy balance. As these factors are left out, only four variables (WWR, LES, LSG and Location) remain as initial conditions strongly affecting the impact of electric lighting and fenestration controls on building energy use.

The total energy consumption of a building is simplified in this study as the sum of lighting, heating and cooling loads. Therefore, three different functions are needed to predict each component:

- L: impact on lighting energy savings
- H: impact on heating energy increase
- C: impact on cooling energy savings

A negative effect of daylight harvesting on heating loads is assumed, as a consequence of the previous simulations' output.

A thorough theoretical analysis follows, with the aim of assessing whether the four identified independent variables impact each of the three aforementioned functions, the strength of this relationship and if the dependence is direct or inverse. The following pattern is obtained for the three functions:

$$L = \alpha_L * \frac{1}{LES} + \beta_L * WWR \quad [1]$$

$$H = \alpha_H * \frac{1}{LES} + \beta_H * \frac{1}{WWR} + \gamma_H * \frac{1}{LSG} + \delta_H * HDD \quad [2]$$

$$C = \alpha_C * \frac{1}{LES} + \beta_C * WWR + \gamma_C * \frac{1}{LSG} + \delta_C * CDD \quad [3]$$

Where α_i , β_i , γ_i , δ_i ($i = \{L, H, C\}$) are real constants to be determined by simulations and multivariate linear regression techniques, and “ad hoc” normalization is introduced to constrain each

function in the interval [0,1]. Since all the components are positive, H represents heating losses in absolute value.

L, H, C will predict respectively lighting savings, heating losses and cooling savings by the means of the linear functions $f_L(L)$, $f_H(H)$, $f_C(C)$. In the same way, $f_{LC}(L, C)$ can be used to predict aggregated savings in lighting and cooling, while $f(L, H, C)$ can predict total savings, considering heating as well:

$$f_i(i) = a_i * i + b_i \quad [4]$$

With $i = \{L, H, C\}$

$$f_{LC}(L, C) = a_{LC} * (L + C) + b_{LC} \quad [5]$$

$$f(L, H, C) = a * (L - H + C) + b \quad [6]$$

3.2 Parametric simulations in JEPlus

Since the patterns in Equations [1] to [6] are theoretically determined, batches of parametric simulations are needed as litmus paper of the developed model validity. JEplus, a JAVA shell allowing users to define parameter trees and run customized simulation batches on a single building model, is adopted for the purpose.

The goal of these parametric runs being to evaluate the impact of the four previously identified variables on a building model energy consumption, 81 simulations are performed by permutation of the following values of the key parameters:

- LSG = {1, 1.5, 2} for the windows. LSG=1 baseline case has ASHRAE 90.1-2004 compliant properties for each location
- LES = {15 lm/W, 80 lm/W, 150 lm/W}, corresponding respectively to incandescent, fluorescent and LED light sources
- WWR = {0.15, 0.30, 0.60} with windows evenly distributed and centered on the four lateral facades of the building
- Location: HDD = {1131, 3782, 6315} and CDD = {5150, 1655, 1163} values calculated for the three locations of Phoenix (AZ), Baltimore (MD), Minneapolis (MN)

Building constructions are optimized for each location according to ASHRAE 90.1-2004.

Simulations are performed combining all possible 3^4

= 81 permutations of the above listed values. Each simulation is performed twice in order to compare the initial “baseline” case with a “best practice” daylight harvesting system installed in the space, the latter being simulated by the addition of lighting and fenestration controls in EnergyPlus.

Fig. 6 depicts the 100 m² office model used for the simulations, in its configuration with WWR = 0.15 and with the predisposition for daylighting controls to monitor daylight illuminance values in the space.

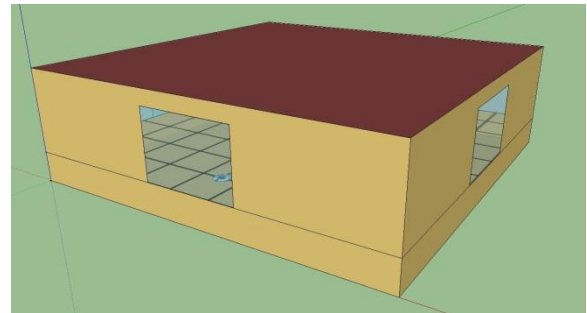


Fig. 6 – The small office model used for the parametric runs (WWR = 0.15)

The output variables for the 162 resulting simulations are:

- Lighting load
- District cooling load
- District heating load

For the HVAC system, simplified “ideal loads” are considered instead of a customized HVAC apparatus which adds unnecessary simulation time and complexity for the high-level perspective of the study. In order to reflect the impact of cooling loads on electricity consumption, a COP value of 4 is again assumed for the cooling system. Relative and absolute values of lighting and HVAC loads are checked for consistency by comparison with the DOE commercial buildings reference models.

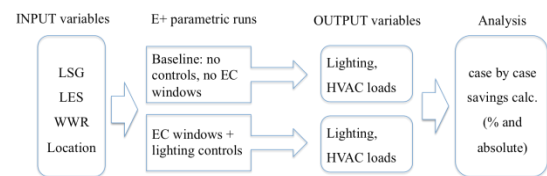


Fig. 7 – The parametric simulations approach

Since the model aims at predicting savings generated by daylighting solutions in different conditions, an analysis is performed in Microsoft Excel in order to assess savings generated by the

addition of lighting and fenestration controls compared to the baseline cases for each set of LES, LER, WWR and location as input variables. The analysis approach is illustrated by the diagram in Fig. 7: for every set of input variables combination, two runs are performed - with and without fenestration and lighting controls - and savings are calculated in absolute and percentage values.

With the energy saving data obtained from the parametric runs, an extensive analysis is performed in Microsoft Excel in order to examine the impact of each single variable, with a sensitivity analysis evaluating the model at its “partial derivatives”.

3.3 Multivariate linear regression coefficients

The output of the parametric simulations gives fundamental indications to correct the previously identified equations. After the adjustments, least squares multivariate linear regression is used to determine the coefficients in Equations [1], [2], [3]. The modifications and final results are here shown for the three components L, H and C:

- Lighting savings: WWR impact is negligible ($\alpha_L = 1, \beta_L = 0$). Lighting savings in GJ are predicted with $R^2 = 0.993$. New equations are:

$$L = \frac{1}{LES} \quad [7]$$

$$f_L(L) = 38.46 * L - 0.1788 \quad [8]$$

- Heating increase: not impacted by LES and proportional to WWR, not to its reciprocal. Heating losses in GJ are predicted with $R^2 = 0.807$. New equations are:

$$H = \beta_H * WWR + \gamma_H * \frac{1}{LSG} + \delta_H * HDD \quad [9]$$

$$\{\beta_H, \gamma_H, \delta_H\} = \{6.326, 1.127, 7.395\}$$

$$f_H(H) = -15.97 * H + 5.518 \quad [10]$$

- Cooling savings: fairly constant in absolute values, not impacted by location ($\delta_C = 0$). Cooling savings in GJ are predicted with $R^2 = 0.962$. New equations are:

$$C = \alpha_C * \frac{1}{LES} + \beta_C * WWR + \gamma_C * \frac{1}{LSG} \quad [11]$$

$$\{\alpha_C, \beta_C, \gamma_C\} = \{0.979, 3.749, 2.012\}$$

$$f_C(C) = 17.576 * C - 3.792 \quad [12]$$

4. Discussion and result analysis

The least squares regression analysis shows good effectiveness of the model at predicting the three components of energy consumption. Lighting and cooling savings can be estimated with a high degree of confidence, while heating increase is the most difficult to forecast. This suggests comparing the validity of the model for the aggregated functions $f_{LC}(L, C)$ and $f(L, H, C)$, accounting respectively for electricity savings (lighting and cooling) and total savings.

Results in Fig. 8 and Fig. 9 show very good prediction capabilities for aggregated savings: heating losses can therefore be also accurately estimated as the difference between total savings and savings on lighting and cooling loads.

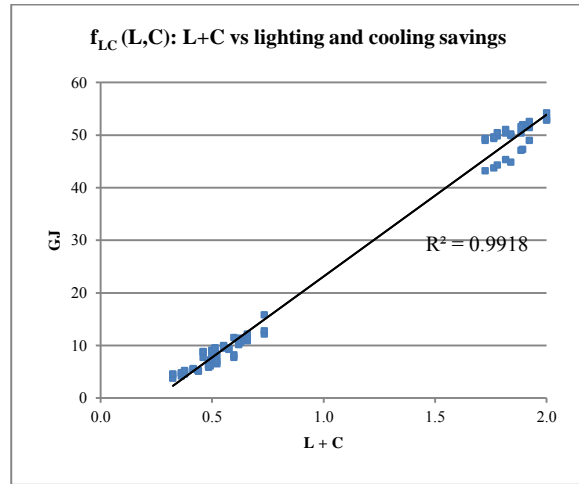


Fig. 8 – f_{LC} : (L+C) vs lighting and cooling savings

5. Conclusions

The developed multivariate regression linear model can predict with a satisfactory degree of confidence savings in lighting, cooling and heating which can be obtained by electric lighting and fenestration controls for daylight harvesting. The prediction can be made starting from a handful of simple and easy-to-determine variables, thus eliminating the need for extensive simulations and detailed building descriptions. Results shown in the paper are obtained for a 100 m² office building, thus extrapolation to other types and size of buildings should be carefully evaluated.

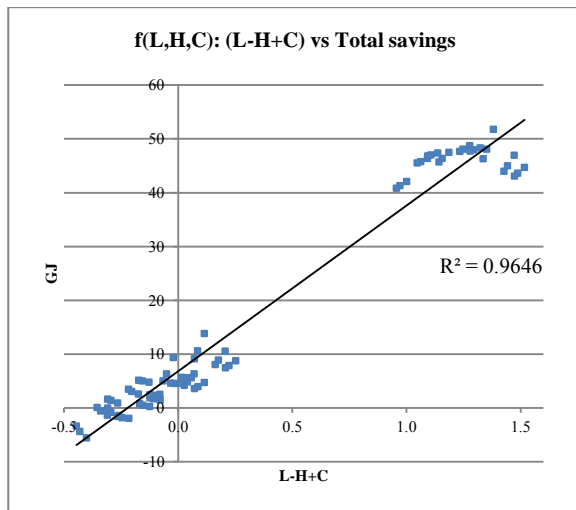


Fig. 9 – f : $(L-H+C)$ vs total savings

Further developments are foreseen to be the inclusion of economic factors in order to assess the value of lighting and fenestration control systems in building design, and compare them to the investment costs of energy efficiency measures. Future developments could also include the realization of a quick energy analysis tool to provide order-of-magnitude energy savings indications to be implemented in early, schematic phases of building design, policy making and investment analyses. Building simulation shall have two paths in the future: on one hand, extremely powerful and dynamic tools (e.g. EnergyPlus) are needed to increase precision in detailed single buildings simulations, while quick and easy-to-use high-level tools should be adopted for decision-making support in consideration of energy strategies, where order-of-magnitude indications are sought. It is the authors' belief that the parametric simulations approach used for model development as presented in this paper is very promising for further formalization and adoption in energy efficiency practice.

References

- [1] P. Hawken, A. Lovins und L. H. Lovins, *Natural Capitalism*, Back Bay Press, Time Warner Book Group, 2000.
- [2] IEA - International Energy Agency, „Light's Labour's lost - Policies for Energy-efficient Lighting,” 2006.
- [3] Lawrence Berkeley National Laboratory, „DOE-2,” 2012. [Online]. Available: <http://gundog.lbl.gov/dirsoft/d2whatis.html> . [Zugriff am 2012].
- [4] E. Lee, M. Yazdanian und S. Selkowitz, „The energy-savings potential of electrochromic windows in the US commercial building sector,” 2004.
- [5] D. Belzer, „An exploratory Energy Analysis of Electrochromic Windows in Small and Medium Office Buildings - Simulated Results Using EnergyPlus,” 2010.
- [6] US Department of Energy - EERE, „EnergyPlus Energy Simulation Software,” 2012. [Online]. Available: <http://apps1.eere.energy.gov/buildings/energyplus/>.
- [7] Lawrence Berkeley National Laboratory, „Building Controls Virtual Test Bed,” 2012. [Online]. Available: <http://simulationresearch.lbl.gov/bcvtb>.
- [8] De Montfort University - IESD, 2012. [Online]. Available: <http://www.iesd.dmu.ac.uk/~jeplus/wiki/doku.php>.
- [9] Florida Solar Energy Center, „Window Selection Guidelines for South Florida Residences,” 1992. [Online]. Available: <http://www.fsec.ucf.edu/en/publications/html/FSEC-cr-562-92/appendixD.htm>.
- [10] US DOE, „Commercial Building Initiative,” 2012. [Online]. Available: http://www1.eere.energy.gov/buildings/commercial_initiative/.
- [11] National Renewable Energy Laboratory, „U.S. Department of Energy Commercial Reference Building Models of the National Building Stock,” 2011.

Phoenix, AZ

#	Skylight?	Lighting Controls?	Fenestration Controls?	Lighting [GJ]		Cooling [GJ]		Heating [GJ]		Total [GJ]	
1	no	no	no	2.86		4.97		1.18		9.01	
2	yes	no	no	2.86		5.15		1.16		9.17	
3	yes	yes	no	1.16	-59%	4.82	-6%	1.37	18%	7.35	-20%
4	yes	yes	yes	1.14	-60%	4.54	-12%	1.56	34%	7.24	-21%
5	yes	yes	yes, only summer	1.14	-60%	4.64	-10%	1.37	18%	7.15	-22%

Baltimore, MD

#	Skylight?	Lighting Controls?	Fenestration Controls?	Lighting [GJ]		Cooling [GJ]		Heating [GJ]		Total [GJ]	
1	no	no	no	2.86		0.76		5.76		9.38	
2	yes	no	no	2.86		0.90		5.77		9.53	
3	yes	yes	no	1.17	-59%	0.69	-23%	6.40	11%	8.26	-13%
4	yes	yes	yes	1.17	-59%	0.54	-40%	7.32	27%	9.03	-5%
5	yes	yes	yes, only summer	1.17	-59%	0.55	-39%	6.52	13%	8.24	-14%

Minneapolis, MN

#	Skylight?	Lighting Controls?	Fenestration Controls?	Lighting [GJ]		Cooling [GJ]		Heating [GJ]		Total [GJ]	
1	no	no	no	2.86		0.48		9.35		12.69	
2	yes	no	no	2.86		0.61		9.52		12.99	
3	yes	yes	no	1.18	-59%	0.43	-30%	10.24	8%	11.85	-9%
4	yes	yes	yes	1.17	-59%	0.28	-54%	11.53	21%	12.98	0%
5	yes	yes	yes, only summer	1.17	-59%	0.29	-52%	10.66	12%	12.12	-7%

Table 3 – Simulations for the simple office with skylight case (end uses loads)

Phoenix, AZ

#	Lighting Controls?	Fenestration Controls?	Lighting [GJ]		Cooling [GJ]		Heating [GJ]		Total [GJ]	
1	no	no	56.69		59.82		9.04		125.55	
2	yes	no	36.84	-35%	55.79	-7%	10.39	15%	103.02	-18%
3	yes	yes	33.34	-41%	49.98	-16%	11.88	31%	95.20	-24%
4	yes	yes, only summer	33.34	-41%	51.08	-15%	9.27	3%	93.69	-25%
5	yes	yes, 4 states (BCVTB)	33.34	-41%	52.89	-12%	10.72	19%	96.95	-23%

Baltimore, MD

#	Lighting Controls?	Fenestration Controls?	Lighting [GJ]		Cooling [GJ]		Heating [GJ]		Total [GJ]	
1	no	no	56.69		19.79		44.40		120.88	
2	yes	no	35.29	-38%	17.40	-12%	50.90	15%	103.59	-14%
3	yes	yes	33.85	-40%	14.74	-26%	58.16	31%	106.75	-12%
4	yes	yes, only summer	33.85	-40%	15.25	-23%	46.59	5%	95.69	-21%
5	yes	yes, 4 states (BCVTB)	34.32	-39%	15.45	-22%	53.23	20%	103.00	-15%

Minneapolis, MN

#	Lighting Controls?	Fenestration Controls?	Lighting [GJ]		Cooling [GJ]		Heating [GJ]		Total [GJ]	
1	no	no	56.69		12.28		97.07		166.04	
2	yes	no	35.59	-37%	11.03	-10%	106.59	10%	153.21	-8%
3	yes	yes	34.04	-40%	8.71	-29%	117.82	21%	160.57	-3%
4	yes	yes, only summer	34.04	-40%	9.65	-21%	100.14	3%	143.83	-13%
5	yes	yes, 4 states (BCVTB)	37.32	-34%	9.54	-22%	102.02	5%	148.88	-10%

Table 4 – Simulations for the DOE standard, validated small office model (end uses loads)

Derivation of meteorological reference year with hourly interval for Italy

Gianluca Antonacci – CISMA Srl, Bolzano, Italy

Ilaria Todeschini – CISMA Srl, Bolzano, Italy

Abstract

The present paper describes the work which has led to the creation of the meteorological reference year for the whole of Italy, according to the algorithm contained in the UNI EN ISO 15927-4 technical standard. The work was done on behalf of CTI (Comitato Termotecnico Italiano). The above standard specifies a method to derive the hourly values of weather data needed to assess the annual energy needs for building heating and cooling. The obtained time series is built up by 8760 hourly records extracted from longer time series (theoretically at least 10 years).

In meteorological data processing particular attention was paid to the quality check of collected data. The reference year thus contains records for the following parameters: temperature, solar radiation, relative humidity, wind speed. The first three are the key values for calculation of the energy budget needed for heating and cooling.

This approach enables the development of calculation methodologies towards the direction of a dynamic thermal design in which the external forcing is given with hourly interval, instead of through monthly averages as currently contemplated in the current version of UNI 10349 standard.

The reconstruction procedure of the meteorological reference year is based on the extraction of hourly data from multi-year records and subsequent statistical analysis; the algorithm is discussed in detail in the paper. For each Italian administrative Province, weather stations operated by local agencies were taken into account where at least ten years of data were available. Besides the implementation of the algorithm, we discuss the practical problems encountered in managing these meteorological data, caused by strong heterogeneity resulting from different types of networks, sensors, data acquisition methods and standards. The uncertainty about the result caused by these issues is also qualitatively assessed and the advantages and disadvantages of the adoption of

hourly varying time series with respect to averaged values for the thermal design of buildings is discussed.

1. Introduction

The aim of this work is to construct a reference year of hourly values of appropriate meteorological data suitable for assessing the average annual energy consumption for heating and cooling, according to the UNI EN ISO 15927-4 standard. In fact, to correctly simulate the building behaviour, not only the mean values of meteorological parameters are important, but also the frequency distribution of the individual parameters and the cross correlation between them. In this way, a dynamic project of building plants can be done.

Therefore, the aim of the present work is to provide the tools and the data to update the UNI 10349 with a new and more detailed set of values.

The reason for taking into account almost ten years (but indeed preferably more) can be explained by considering that unusual periods of warm or cold weather can in this way be excluded from the computation of the reference meteorological year.

The present paper basically copes with the methodological aspect of the work, description of the algorithm and encountered difficulties. On the other hand, detailed numerical results will be distributed to end users from CTI.

Already in the early phase of data collection some issues about the data quality became quite evident, making it clear that it would not be possible to obtain completely homogeneous results. Therefore, as explained and discussed further in the article, some inconsistencies have remained in the downstream process. While the initial idea was to “manipulate” the data as little as possible, during

the work we were forced to introduce corrections and compensations in order to achieve results which could be treated as valid for the whole of Italy.

2. Description of the algorithm

The procedure allows to identify a series of hourly data in which the mean value of individual variables, their frequency distribution and correlations between the different variables within each month are as close as possible to the corresponding calendar month of the long term data set.

The procedure is characterized by two main steps: firstly the selection from the multi-year record of the “best” (i.e. statistically most representative) month is made for each calendar month. Secondly the hourly values in the selected month are adjusted so as to provide a smooth transition between months deriving from different years.

The meteorological reference year must contain 8760 values of hourly dry-bulb temperature, solar radiation, relative humidity and wind speed. Whilst the first three parameters are crucial for the energy requirements computation for heating and cooling, the wind speed can be considered as a secondary parameter.

For each meteorological parameter, p , the procedure consists in:

calculation of the daily means, p , from at least ten years (but preferably more) of hourly data of p ;

calculation, for each calendar month, of the cumulative distribution function of the daily means over all years in the data set, $\Phi(p,m,i)$, by sorting all the values in increasing order and then using Equation (1):

$$\Phi(p,m,i) = \frac{K(i)}{N+1} \quad (1)$$

where $K(i)$ is the rank order of the i -th value of the daily means within that calendar month in the whole data set;

calculation, for each year of the data set, of the cumulative distribution function of the daily means within each calendar month, $F(p,y,m,i)$, by sorting all the values for that month and that year in increasing order and then using Equation (2):

$$F(p,y,m,i) = \frac{J(i)}{(n+1)} \quad (2)$$

where $J(i)$ is the rank order of the i -th value of the daily means within that month and that year; calculation, for each calendar month, of the Finkelstein-Schafer statistic, $FS(p,y,m)$, for each year of the data set using Equation (3):

$$F_s(p,y,m) = \sum_{i=1}^n (F(p,y,m,i) - \Phi(p,m,i)) \quad (3)$$

ranking, for each calendar month, of the individual months from the multiyear record in order of increasing size of $FS(p,y,m)$;

for each calendar month and each year, add the separate ranks for the three climate primary parameters (temperature, solar radiation and relative humidity);

for each calendar month, for the three months with the lowest total ranking, calculate the deviation of the monthly mean wind speed from the corresponding multi-year calendar-month mean; the month with the lowest deviation in wind speed is selected as the “best” month to be included in the reference year.

When each calendar month is selected, the last eight values of the month and the first eight values of the next month for each meteorological parameter should be adjusted in order to avoid a sharp transition between months that derive from different years. This smoothing procedure should be done by means of interpolation. In this work a smoothing procedure with running medians of five hours windows has been performed. This adjustment also includes the last eight hours of December and the first eight hours of January so that the reference year can be used repeatedly in simulations lasting more than 12 months.

This statistical computation has been carried out by means of the statistical software R, whereby a semi-automatic implementation has been made possible.

Once the reference meteorological year has been selected according to this procedure, the hourly values of diffuse and direct radiation, along with the vapour pressure, were derived.

Most weather meteorological stations measure only the global solar radiation. For many applications, however, the knowledge of the amount of diffuse and direct radiation is

important. In this work the diffuse fraction of the solar radiation was obtained by adopting the function proposed by Boland et al. (2008). The major advantage of this kind of formulation is that this function is logistic and not piecewise-defined as other commonly used formulations (e.g. Erbst). The diffuse fraction of the solar radiation on the horizontal, k , can be evaluated by means of Equation (4):

$$k = \frac{1}{1 + e^{-5.0 + 8.6K_T}} \quad (1)$$

where K_T is the hourly clearness index is defined as the fraction between the global solar radiation I_{global} and the extraterrestrial radiation H_0 :

$$K_T = \frac{I_{\text{global}}}{H_0} \quad (2)$$

The orbit of the Earth is not a circle, but an ellipse, hence the distance between Earth and Sun varies over the year, so an eccentricity correction factor can be defined as:

$$E_0 = (a_0 + a_1 \cos(\Gamma) + a_2 \sin(\Gamma) + a_3 \cos(2\Gamma) + a_4 \sin(2\Gamma)) \quad (3)$$

where Γ , the angle of the Sun for the N th day of the year, can be evaluated as:

$$\Gamma = 2\pi \frac{N-1}{365} \quad (4)$$

and the coefficient proposed by Spencer (1971) are summarized in Table 1.

$a_0=1.000110$	$a_1=0.034221$	$a_2=0.001280$
$a_3=0.000719$	$a_4=0.000077$	

Table 1 – Coefficients for the evaluation of the eccentricity correction factor, as proposed by Spencer (1971)

As a consequence, the direct normal radiation is defined as:

$$I_0 = 1367 \cdot I_{\text{global}}$$

The solar declination δ can be calculated using equation proposed by Spencer (1971):

$$\delta = b_0 + b_1 \cos(\Gamma) + b_2 \sin(\Gamma) + b_3 \cos(2\Gamma) + b_4 \sin(2\Gamma) + b_5 \cos(3\Gamma) + b_6 \sin(3\Gamma) \quad (5)$$

where the coefficients are summarized in Table 2.

$b_0=0.006918$	$b_1=-0.399912$	$b_2=0.070257$
$b_3=-0.006758$	$b_4=0.000907$	$b_5=-0.002697$
$b_6=0.00148$		

Table 2 – Coefficients for the evaluation of the solar declination, as proposed by Spencer (1971)

Thus, the equation of time adjustment (in hours) proposed by Spencer is:

$$E_0 = \frac{24}{2\pi} (c_0 + c_1 \cos(\Gamma) + c_2 \sin(\Gamma) + c_3 \cos(2\Gamma) + c_4 \sin(2\Gamma)) \quad (6)$$

where the coefficients are summarized in Table 3.

$c_0=0.000075$	$c_1=0.001868$	$c_2=-0.032077$
$c_3=-0.014615$	$c_4=-0.040849$	

Table 3 – Coefficients for the equation of time, as proposed by Spencer (1971)

The local solar time $LSoT$ can be then estimated as:

$$LSoT = GMT + E_0 + \frac{1}{15} (\lambda - LSTM) \quad (7)$$

where λ is the local longitude (positive for East) and $LSTM$ the local standard time meridian.

Finally the sun height can be defined as:

$$H_s = \frac{\pi}{2} - \arccos[\cos(\phi) \cos(\delta) \cos(\omega) + \sin(\phi) \sin(\omega)] \quad (8)$$

with ϕ is the latitude and ω the hour angle can be defined as:

$$\omega = 15 (LSoT - 12) \frac{\pi}{180} \quad (9)$$

Now the extraterrestrial radiation can be calculated by means of equation (13):

$$H_0 = E_0 [\cos(\text{lat}) \cos(\delta) \cos(\omega) + \sin(\text{lat}) \sin(\omega)] \quad (10)$$

Once the diffuse radiation is evaluated by means of equation (4), the direct radiation is automatically defined as:

$$I_{\text{direct}} = I_{\text{global}} - I_{\text{diffuse}} \quad (11)$$

Besides, the saturation pressure can be estimated by means of the formulation contained in the ASHRAE handbook, depending on the temperature range. For the temperature range of -100°C to 0°C is given by:

$$\ln(p_{\text{ws}}) = d_1 T^{-1} + d_2 + d_3 T + d_4 T^2 + d_5 T^3 + d_6 T^4 + d_7 \ln(T) \quad (12)$$

while for the temperature range of 0°C to 200°C is given by:

$$\ln(p_{\text{ws}}) = d_8 T^{-1} + d_9 + d_{10} T + d_{11} T^2 + d_{12} T^3 + d_{13} \ln(T) \quad (13)$$

where the temperature T is the absolute temperature and the coefficients are summarized in Table 4.

d ₁ =-5.6745359E+03	d ₂ =6.3925247E+00
d ₃ =-9.6778430E-03	d ₄ =6.2215701E-07
d ₅ =2.0747825E-09	d ₆ =-9.4840240E-13
d ₇ =4.1635019E+00	d ₈ =-5.8002206E+03
d ₉ =1.3914993E+00	d ₁₀ =-4.8640239E-02
d ₁₁ =4.1764768E-05	d ₁₂ =-1.4452093E-08
d ₁₃ =6.5459673E+00	

Table 4 – Coefficients for the evaluation of the vapour saturation pressure (ASHRAE handbook)

Thus, the vapour pressure p_w can be calculated starting from the hourly values of relative humidity RH:

$$p_w = \frac{RH}{100} p_{ws} \quad (17)$$

3. Choice of the meteorological station

For each Italian province, weather stations operated by local agencies were taken into account where at least ten years of data were available, even if in some cases the effectively usable record length turned out to be shorter. Only the stations where all the four meteorological parameters were measured were considered.

For each reference station, one of the most important criteria for the choice of the representative meteorological station was the length of the record. Also the amount of non-valid data has played a significant role in the selection process. If more than one weather station was available, the more suitable station for the entire territory of the province was selected.

In the lower layers of the atmosphere, average temperature approximately decreases with the altitude at a fairly uniform rate. For this reason, measured temperature values depend on the weather station altitude. It is therefore necessary to correct the hourly values of temperature and consequently vapour pressure when referring to another location characterized by a different altitude value with respect to the monitoring station.

The vertical temperature gradient depends on the geographical area. In Italy five different areas have been identified in the present UNI 10349 standard, whose corresponding values are reported in Figure 1. We adopted the same classification, and

although it is quite rough, revisiting this classification is out of the scope of present work.

The corrected temperature T_{corr} at the altitude z can be calculated:

$$T_{corr} = T_{station} - (z - z_{station}) \delta_t \quad (18)$$

where $z_{station}$ and $T_{station}$ are respectively altitude and measured temperature at the selected weather station.

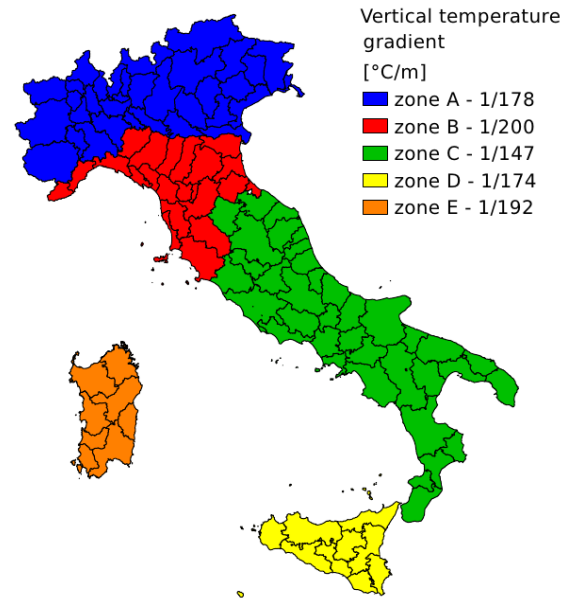


Fig. 1 – Geographical zone with different values of the vertical temperature gradient δ_t , according to UNI 10349 technical standard

4. Example of reference meteorological year

Following is an example of the result of the meteorological reference year building procedure (Fig. 2). For each month, it is possible to compare the hourly temperature values with the corresponding monthly average (black line) provided by the present UNI 10349. Please note that this average value does not correspond to the monthly average of the selected reference month but it refers to average values of three decades of meteorological data. A further discussion regarding the differences between the present method (UNI 10349) and the reference meteorological year as described in this work is presented in the following paragraph.

5. A synthesis of results

After the described elaboration, which clearly adopts a local approach, the obtained hourly meteorological data were also extrapolated, although in quite an approximate way, in order to obtain a synthetic result for the whole of Italy and to compare the meteorological reference years obtained in the different provinces.

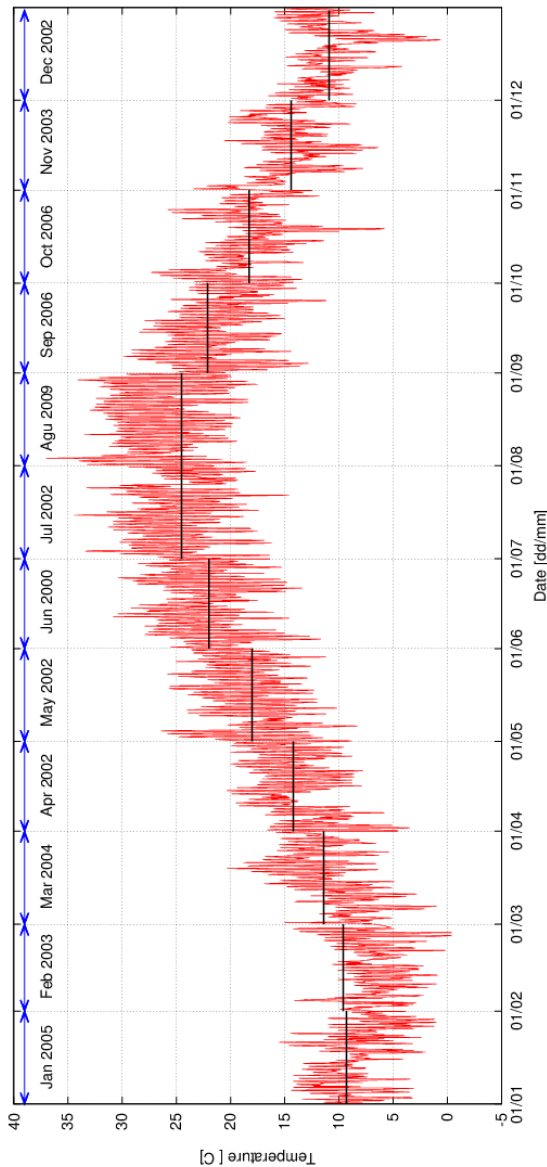


Fig. 2 – Example of the hourly temperature values identified by means (the figure is referred to the city of Brindisi) of the algorithm proposed by UNI EN ISO 15927-4 and monthly averages according to current version of UNI 10349 standard

Annual average values of temperature, global radiation, relative humidity and vapour pressure were calculated for each Italian municipality; the

correction for different values of altitude were applied to temperature and consequently vapour pressure. For this reason their values vary within the same province, while relative humidity and global radiation, which were not corrected with the altitude, show a unique value within each province. This is obviously a rough approximation, and should therefore be used only as a first indication. The approach was used only in order to maintain consistency with the current version of the UNI 10349 standard, but simply extrapolating meteorological values to a whole territory would not make much sense, as the statistical approach contained in the UNI EN ISO 15927-4 cannot take into account the spatial variability of orography and land use, both strongly influencing wind speed, relative humidity and solar radiation. Therefore the only extrapolation on temperature, along the vertical coordinate, could be considered as acceptable from the climatological point of view.

6. Description of the encountered problems

Beside the implementation of the algorithm, a strong effort has been directed towards the solution of several practical problems encountered in managing meteorological data. The problems were principally caused by strong heterogeneity resulting from different types of networks, sensors, data acquisition methods and standards.

In fact, nowadays a major problem in managing Italian meteorological data is the heterogeneity of the observational network. It should also be considered that the current version of UNI 10349 is based on an analysis that might have been less accurate, but certainly more homogeneous, as at the time it was issued the observational network was managed by the National Weather Service before it was dismantled. Currently we have 20 different regional services with different stations, different sensor types, different criteria for installation, different placement (ranging from urban to rural), different procedures for data management and different ranges of available periods. As consequences, the mean monthly values of some stations as derived with the present

work deviate from those of the current standard (UNI 10349). With reference to this, it should also be considered that the adopted method is in any case different from the older one which led to the current version of the UNI 10349 standard. The latter is in fact built up of the monthly values of parameters, simply averaged over three decades, while the depicted algorithm gives a “characteristic” monthly value, namely the

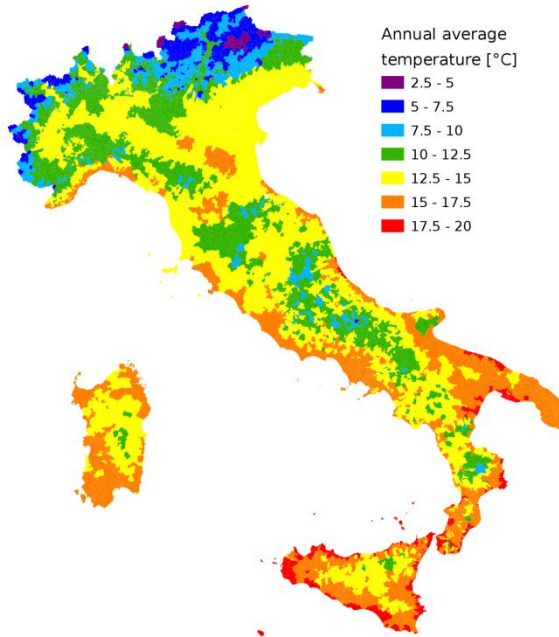


Fig. 3 – Map of the annual average temperature

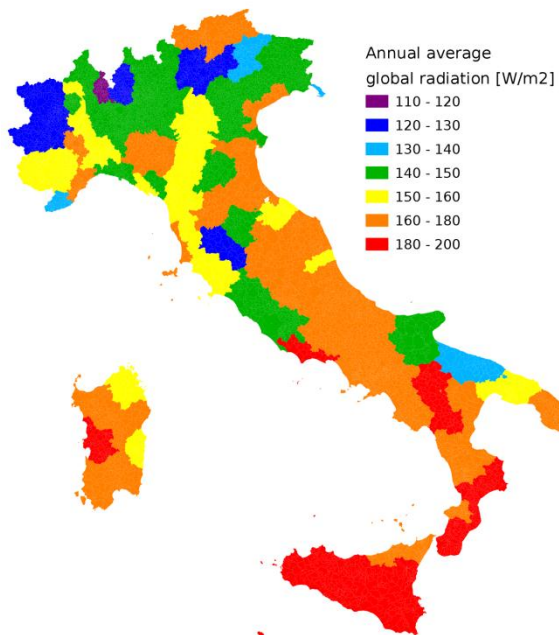


Fig. 4 – Map of the annual average global solar radiation

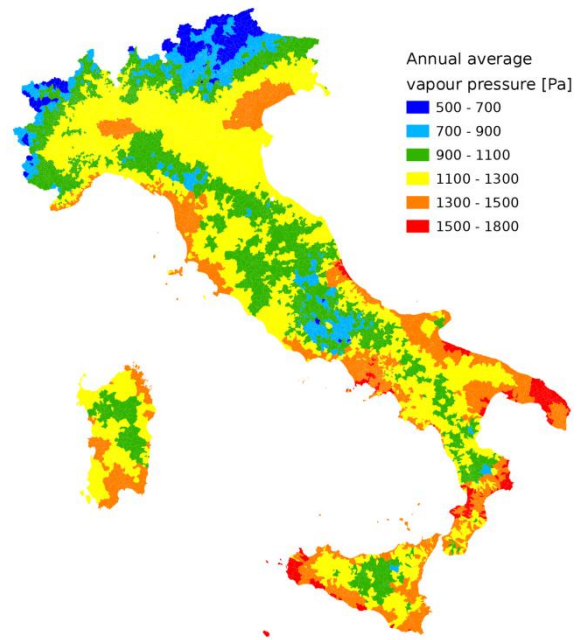


Fig. 5 – Map of the annual average vapour pressure

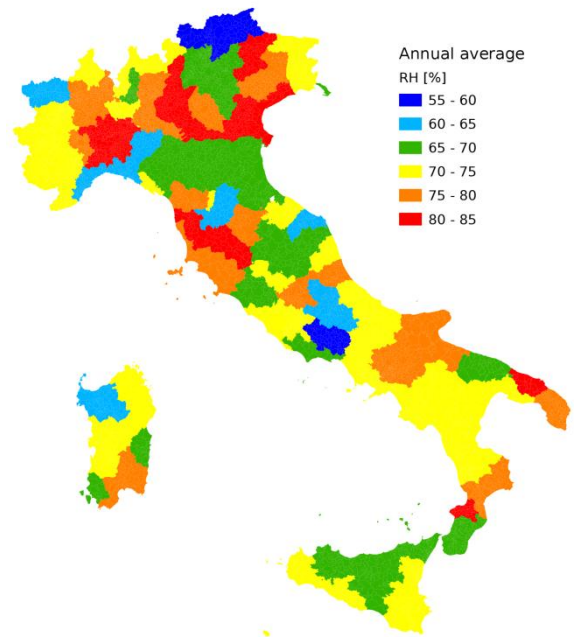


Fig. 6 – Map of the annual average relative humidity

value less deviating from the average. The two values can be practically considered as coinciding only for very long time series (several decades), which indeed is not the case for the present analysis.

These difficulties are so relevant because it is not possible to define a unique procedure to overcome them, given the heterogeneity of the data and of

their corresponding problems. Data quality is in fact strongly inhomogeneous and most of the times it is not evident.

A short overview of the main problems is presented in the following paragraphs, along with a brief description of the adopted solutions.

6.1 Lack of data

The problem of a lack of data could not be ignored, since periods without any valid data were present in almost every time series that has been analyzed. The UNI EN ISO 15927-4 suggests much care should be exercised in the quality control of the raw data. In accordance with the regulation, missing values shall be generated by linear interpolation or by an estimate, and sudden, unnatural jumps or singular values shall be examined and corrected. This approach is cannot be adopted for long periods of time without any valid data, since the basic principle of the regulation is to use real measured data as much as possible instead of theoretical and interpolated values.

For this reason, to avoid non-valid data in the meteorological reference year, all the months with significant amounts of non-valid data, even of just one parameter, were not considered and not used by the algorithm.

The selection process of the “best” (i.e. statistically most significant) month to be included in the reference meteorological year is certainly influenced and modified by this choice. Nevertheless, this approach was preferred in order to preserve the original data.

6.2 Homogenization

Homogenization was necessary in order to make comparable data that derive from different sources. In fact, the analysed data were collected by the different local agencies, whose standards are not unique. Also the criterion adopted in the choice of the localization is strictly influenced by the aim of the station and it is different for example for agro-meteorological, air quality or hydrographic stations.

One example of this homogenization process is the adjustment of the time axis to the standard local time (UTC+1 for Italy).

Moreover, the theoretical hour of sunrise and sunset was calculated and compared with the corresponding measured ones in each weather station. In some cases, the length of the day was systematically shorter than the theoretical one, probably due to a bad positioning of the radiometer. Global radiation values at sunrise and sunset were therefore obtained by means of interpolation.

Relative humidity data larger than 100%, measured in case of oversaturation in some weather stations, were fixed to 100%.

Usually the lowest value of the measured wind speed coincides with the cut-in threshold value typical of the installed anemometer. A common value of 0.1 m/s was chosen as arbitrary threshold value for wind speed.

Although the homogenization process, the heterogeneity was not completely eliminated, as it can be seen for example in the annual average solar radiation map in Figure 4. Some provinces in the south of Italy are characterized by smaller values of solar radiation if compared with the contiguous ones. This behaviour is due to the fact that the considered meteorological stations are very different. The only option was to modify collected data before adopting the described procedure, but that was not the purpose of the UNI EN ISO 15927-4 technical standard.

6.3 Validation

The most part of the analysed meteorological data were supposed to be validated by the local agencies that manage the weather stations. Validation is a crucial process that consists in examination of data in order to detect possible errors, but also in the standard procedures that include periodical calibration of the instruments, data screening and also preventive maintenance. Nevertheless, although theoretically validated, a large amount of data showed clearly unnatural values that had to be compensated or eliminated where corrections were not feasible.

The main corrections that were made are reported below:

- values exceeding 50% of the 99th percentile (both maximum and minimum values) were eliminated;
- values repeated for more than 5 hours were eliminated;
- global radiation values higher than the solar constant were eliminated;
- offset of the entire time series due, for example, to the existence of an urban heat island or to a change in the position of the sensor was eliminated;
- linear detrending was applied where the drift of temperature and solar radiation sensors was clear and identifiable.

6.4 Length of the temporal series

The UNI EN ISO 15927-4 standard provides the correct procedure to evaluate the reference meteorological year. Before applying the suggested algorithm it is therefore necessary to identify for each province the most representative weather station. As already explained, the most important criterion for the choice of the weather station was the length of the available temporal series. Significant differences exist between different regions. In fact, some regions have collected more than 20 years of meteorological data, in other regions less than 10 years were available (notice that a minimum 10 years length is the one recommended by the UNI EN ISO 15927-4). In some cases, the meteorological reference year was forcibly evaluated on the basis of shorter temporal series due to lack of data covering continuously a longer period.

7. Conclusions

A reference meteorological year is a data set of hourly values of temperature, solar radiation, relative humidity and wind speed throughout a year. The months have been selected from individual years and concatenated to form a complete year. This work describes the procedure

adopted to build it for each Italian province, according to the UNI EN ISO 15927-4 standard.

The most important characteristic of this approach is that it enables the development of calculation methodologies towards the direction of a dynamic thermal design in which the external forcing is given with hourly interval, instead of through monthly averages as currently contemplated in the UNI 10349 standard. In fact, a more accurate evaluation of heating and cooling loads in buildings and the performance of solar thermal and photovoltaic systems requires accurate and reliable meteorological data series as input. For this reason a reference meteorological year is a more appropriate data source when evaluating the thermal performance of buildings through numerical simulations.

Unfortunately a great heterogeneity characterizes meteorological data provided by the local agencies all over Italy. A stronger effort should therefore be directed to enhance a homogenization procedure in order to obtain more comparable data sets. In fact, a major issue with the data management was that we were forced in some cases to do (or redo) the data validation process. Strictly speaking, this action would need to gather also all the information about the sensors, their calibration and data filtering algorithms. This was out of the scope of the present work, but according to the authors, it should be reconsidered for the future, at least for the most critical cases. As a consequence, the initial intention of barely modify original data, has been clearly and forcibly reconsidered.

As a conclusion, we believe that the obtained results, which will be distributed by CTI in the future, should be intended as a first valuable step that overcomes the limitation of the monthly mean climatological values, allowing dynamic simulations with higher time resolution. Results should, however, certainly be improved in the future, at least through the timely extension of the time series as they become available, but also through finer discrimination of reliable data. It should, in fact, be underlined once more that the whole procedure as foreseen by the UNI EN ISO 15927-4 standard is implicitly based on the assumption that quality checked, long enough and continuous data series are available.

A further reflection should also be reserved for the purpose for which these climatological series will be used. When using them to analyse meteorological parameters which are strictly referred to the measurement location (or the surrounding area for which the station can be considered as representative), the adoption of the presented time series can be considered as suitable. In fact, extending the results over a larger area is conceptually more questionable, as it introduces a strong hypothesis on spatial variation. In this case a more comprehensive (in space) approach should be taken into consideration, thus overcoming the limitation of punctual (always intended as spatially) statistics.

8. Acknowledgement

This work was carried out on behalf of the CTI (Comitato Termotecnico Italiano) as part of the research coordinated and carried out by ENEA. The authors would like to thank Prof. Baggio (University of Trento) for the valuable suggestions and Dr. Murano (Comitato Termotecnico Italiano) for the accurate checking of the results.

9. Nomenclature

Symbols

E_0	Eccentricity factor [-]
F	Cumulative distribution function of the daily means within each month
FS	Finkelstein-Schafer statistic
GMT	Greenwich Mean Time
H_0	Extraterrestrial radiation [W/m ²]
H	Sun height [rad]
I_{global}	Global solar radiation [W/m ²]
$I_{diffuse}$	Diffuse solar radiation [W/m ²]
I_{direct}	Direct solar radiation [W/m ²]
k	Diffuse fraction of the global solar radiation in the horizontal [-]
KT	Hourly clearness index [-]
$LSTM$	Local Standard Time Meridian
$LsoT$	Local Solar Time
p_{ws}	Saturated vapour pressure [kPa]

p_w	Vapour pressure [kPa]
RH	Relative humidity [%]
T	Temperature [°C]
z	Altitude [m]
Γ	Angle of the sun for the Nth day of the year [rad]
λ	Longitude [°]
δ	Solar declination [rad]
δ_t	Vertical temperature gradient [°C/m]
Φ	Cumulative distribution function of the daily means over all years
ω	Hour angle [rad]
ϕ	Latitude [°]

References

- ASHRAE Fundamentals Handbook, 2005. Psychrometrics, Chapter 6, 6.2.
- Crawley M. J., The R Book, Wiley 2007, ISBN 978-0-470-51024-7.
- Boland J., Ridley B. and Brown B. 2008. Models of diffuse solar radiation, Renewable Energy, Vol. 33, 575-584.
- Spencer J.W., 1971. Fourier series representation of the position of the Sun, Search 2 (5), 172.
- UNI EN ISO 15927-4 2005. Hygrothermal performance of buildings, calculation and presentation of climatic data. Part 4: Hourly data for assessing the annual energy use for heating and cooling.
- UNI 10349 1994. Riscaldamento e raffrescamento degli edifici. Dati climatici, CTI.

The admittance method for calculating the internal temperature swings in free running buildings

Luigi Marletta – Department of Industrial Engineering, University of Catania, Catania, Italy

Gianpiero Evola – Department of Industrial Engineering, University of Catania, Catania, Italy

Maria Giuga – Department of Industrial Engineering, University of Catania, Catania, Italy

Fabio Sicurella – Professional Engineer, Catania, Italy

Abstract

In order to describe the dynamic thermal response of buildings, the dynamic transfer properties, such as the thermal admittance and the decrement factor, can be used. These parameters, firstly introduced in the Seventies by some British researchers, allow us to quantify the response of the building fabric to sinusoidal temperature variations occurring on both sides of the fabric. Their use has been recently suggested in some international standards, such as the EN ISO 13786:2007.

However, little reference is made in the scientific literature to a further dynamic transfer property, the surface factor, that describes the response of the opaque components of a building to sinusoidal radiant heat fluxes occurring on their internal surface. The surface factor is worth being exploited, since the effect of wall inertia on the radiant heat gains is relevant in the study of the thermal behaviour of a building, especially in summer.

In this paper, an operational formulation of the surface factor is firstly provided starting from its conceptual definition. Afterwards, based on all the previously mentioned dynamic transfer properties, a comprehensive procedure for the assessment of the cyclic temperature swings in an enclosed space is introduced. Thanks to the use of the Fourier analysis, this procedure allows tackling any periodic driving force, and not only sinusoidal ones. The reliability of the procedure is validated against the test cases proposed in the Standards EN ISO 13791:2012 and EN ISO 13792:2012.

Finally, the results shown in the paper enable us to realize the size of the approximation introduced by calculating the dynamic transfer properties only with the first harmonic, i.e. based on sinusoidal driving forces with a period $P = 24$ hours, as suggested by the simplified approach proposed in the EN ISO 13792:2012 standard.

1. Introduction

The *thermal admittance* and the *decrement factor* are suitable concepts to describe the thermal response of the building opaque components in dynamic conditions. Such parameters were firstly introduced by Loudon at the Building Research Station, UK (Loudon, 1970), and further developed by (Millbank et al., 1974), (Davies, 1973) and (Davies, 1994). Thanks to this pioneering work, the foundations of the *Admittance Procedure* (AP) were laid: it is a technique for estimating energy transfers through the building envelope, which balances simplicity and accuracy and is mainly used for calculating temperature swings inside buildings. More details about the Admittance Procedure can be found in the CIBSE guide on the thermal response of buildings (CIBSE, 2006).

As far as the *thermal admittance* is concerned, it measures the heat flow rate entering the internal surface of a wall as a response to a unit cyclic temperature fluctuation of the air occurring at the same side (Millbank et al., 1974). The *decrement factor*, on the other hand, relates the amplitude of the cyclic external temperature swing acting on the wall to the periodic heat flux released to the indoor air. The decrement factor is normally cited together with the *time lag*, i.e. the time shift between the cyclic energy input and the corresponding response of the wall. Thus, the decrement factor provides information about the dampening of the periodic thermal signal passing from outside to inside, whereas the time lag gives the delay between a peak in the outdoor temperature profile and the corresponding peak in the heat flux released to the indoor air.

It should be remembered that, even if they only

apply to sinusoidal heat fluxes, the dynamic thermal properties can be used to characterize the response of the envelope to any real forcing condition. As a rule, any periodic function can be decomposed, by means of the Fourier analysis, in a series of sinusoidal functions, called *harmonics*, whose frequency is a multiple of the first one, the so-called *fundamental harmonic*. By summing up the response to each harmonic it is possible to obtain the response to the original periodic excitation. When studying the energy performance of buildings, a daily variation occurs for the main forcing conditions, thus the period of the fundamental harmonic is set to $P_1 = 24$ hours.

The interest in the dynamic thermal properties is also testified by some recent international Standards: the ISO Standard 13786:2007 recommends their adoption for the characterization of the thermal behaviour of the envelope, whereas the ISO Standard 13792:2012 proposes a simplified procedure for the determination of the internal temperature in summer, based on the use of the dynamic properties.

2. Methodology

2.1 Decrement factor and thermal admittance

Let us consider an homogeneous slab of finite thickness, subject to sinusoidal temperature variations θ_{si} and θ_{so} on its internal and external surface, respectively. Let $\bar{\theta}_{si}$ and $\bar{\theta}_{so}$ be the mean values, whereas $\tilde{\theta}_{si}$ and $\tilde{\theta}_{so}$ are the respective cyclic fluctuations around the mean value.

Under the hypothesis of unidirectional conductive heat transfer through the slab thickness in the direction normal to its surfaces, the cyclic heat fluxes \tilde{q}_i and \tilde{q}_o occurring at the two surfaces of the slab can be written as a function of the surface temperature in the following form:

$$\begin{bmatrix} \tilde{\theta}_{si} \\ \tilde{q}_i \end{bmatrix} = \begin{bmatrix} z_1 & z_2 \\ z_3 & z_4 \end{bmatrix} \begin{bmatrix} \tilde{\theta}_{so} \\ \tilde{q}_o \end{bmatrix} \quad (1)$$

Here, the elements of the transmission matrix can be calculated as follows (Davies, 1994):

$$z_1 = z_4 = \cosh(t + it) \quad (2)$$

$$z_2 = \frac{\sinh(t + it)}{\xi \cdot (1 + i)} \quad (3)$$

$$z_3 = \xi \cdot (1 + i) \cdot \sinh(t + it) \quad (4)$$

In Equations (2) to (4), i is the imaginary unit ($i^2 = -1$). Only two parameters appear in the definition of the matrix, namely the cyclic thickness t and the thermal effusivity ξ , defined in Eqs. (5) and (6), that collect all the data concerning the thermal properties of the material, the slab thickness L and the period P of the cyclic energy transfer:

$$t = \left[\frac{\omega}{2 \cdot \lambda / (\rho c)} \right]^{1/2} \cdot L = \left[\frac{\pi}{P \cdot 3600} \cdot \frac{\rho c}{\lambda} \cdot L^2 \right]^{1/2} \quad (5)$$

$$\xi = \left[\frac{2\pi \cdot \lambda \cdot \rho \cdot c}{P \cdot 3600} \right]^{1/2} \quad (6)$$

In practice, it is more useful to obtain an equation which involves the air temperatures $\tilde{\theta}_i$ and $\tilde{\theta}_o$ instead of the temperatures on the wall surface. In this case, the film thermal resistances R_{si} and R_{so} must be introduced, and the final expression for a multi-layered construction made up of n different homogenous layers becomes:

$$\begin{bmatrix} \tilde{\theta}_i \\ \tilde{q}_i \end{bmatrix} = \begin{bmatrix} Z_1 & Z_2 \\ Z_3 & Z_4 \end{bmatrix} \begin{bmatrix} \tilde{\theta}_o \\ \tilde{q}_o \end{bmatrix} \quad (7)$$

The transmission matrix Z of the multi-layered wall is obtained through the product of the matrices related to the each layer, including the transmission matrix containing the film resistance:

$$\begin{bmatrix} Z_1 & Z_2 \\ Z_3 & Z_4 \end{bmatrix} = \begin{bmatrix} 1 & R_{si} \\ 0 & 1 \end{bmatrix} \prod_{k=1}^n \begin{bmatrix} z_{1k} & z_{2k} \\ z_{3k} & z_{4k} \end{bmatrix} \begin{bmatrix} 1 & R_{so} \\ 0 & 1 \end{bmatrix} \quad (8)$$

In Eq. (7), the sol-air temperature can be used in place of the outdoor temperature if the effect of the solar radiation absorbed on the outer surface of the wall has to be taken into account.

According to the presented methodology, one can introduce the so-called periodic thermal transmittance X , defined as the ratio of the cyclic heat flux released on the internal surface of the wall to the cyclic temperature excitation on the other side of the wall, while holding a constant indoor temperature ($\tilde{\theta}_i = 0$, see Eq. 9). The decrement factor f is defined as the amplitude of the periodic thermal transmittance, normalized with respect to the steady thermal transmittance U ; moreover, the time lag ϕ is the phase of the complex number X , measured in hours and referred to a solicitation having a period P (see Eq. 10).

Finally, the admittance Y is conceptually similar to the periodic thermal transmittance, but in this case the temperature excitation $\tilde{\theta}_i$ and the wall response \tilde{q}_i are measured by the same side (see Eq. 11).

$$X = \left. \frac{\tilde{q}_i}{\tilde{\theta}_o} \right|_{\tilde{\theta}_i=0} = -\frac{1}{Z_2} \quad (9)$$

$$f = \left| \frac{X}{U} \right| \quad \varphi = \frac{P}{2\pi} \cdot \arctan \left(\frac{\text{Im}(X)}{\text{Re}(X)} \right) \quad (10)$$

$$Y = \left. \frac{\tilde{q}_i}{\tilde{\theta}_i} \right|_{\tilde{\theta}_o=0} = -\frac{Z_4}{Z_2} \quad (11)$$

According to the ISO Standard 13786:2007, the behaviour of the building envelope is fully described by the values of the dynamic transfer properties for $P = P_1 = 24$ h. However, all the relations previously introduced can be applied to any harmonic of order n , i.e. having a period $P_n = P_1/n$.

2.2 The surface factor

Despite the interest shown in the scientific literature towards the dynamic transfer properties, little reference is made to the thermal response of the opaque components to the radiant heat fluxes occurring on their internal surface, such as those associated to solar heat gains through the windows or to internal radiant loads.

Some attempts were made in the past in this sense. For instance, worth mentioning is the *thermal storage factor* defined in the Carrier method (Carrier, 1962) as the ratio of the rate of instantaneous cooling load to the rate of solar heat gain. This factor has to be determined through appropriate tables depending on the weight per unit floor area of the opaque components and the running time. Therefore, its use requires interpolation among table data, it is rather rough because it does not account for the actual sequence of the wall layers, and it lacks any theoretical basis, as it comes from numerical simulations.

A substantially different approach can be found in the framework of the Admittance Procedure, laid down in the early Seventies (Millbank et al, 1974), where these contributions are taken into account by means of the so called *surface factor*. Nonetheless, the surface factor has been deserved little attention: to the authors' knowledge, little reference is made to

this parameter in the whole scientific literature (Beattie and Ward, 1999) (Rees et al., 2000), while its definition has been only recently recovered in the CIBSE guide (CIBSE, 2006) and in the international Standard ISO 13792:2012.

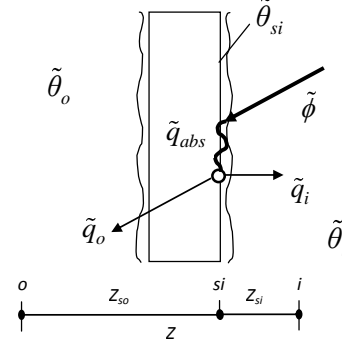


Fig. 1 – Energy balance on the internal surface for the definition of the surface factor

According to the definition provided by (Millbank et al., 1974), the *surface factor* F quantifies the thermal flux released by a wall to the environmental point per unit heat gain impinging on its internal surface, when the air temperatures on both sides of the wall are held constant and equal. With reference to Fig. 1, let us call $\tilde{\phi}$ the cyclic radiant thermal flux acting on the internal surface of the wall, as a result of the radiant energy released by internal sources or transmitted through the glazing; the following definition holds:

$$F = \left. \frac{\tilde{q}_i}{\tilde{q}_{abs}} \right|_{\tilde{\theta}_i = \tilde{\theta}_o = 0} = \frac{\tilde{q}_i}{\alpha \cdot \tilde{\phi}} \quad (12)$$

Here, α is the fraction of the radiant thermal flux that is absorbed by the wall. This amount of thermal energy will be then re-emitted to the internal (q_i) and to the external environment (q_o): the ratio between such contributions equals the inverse ratio of the corresponding thermal impedances. This leads to the following expression:

$$\tilde{q}_i = \alpha \cdot \tilde{\phi} \cdot \left(\frac{Z - Z_{si}}{Z} \right) = \tilde{q}_{abs} \cdot \left(1 - \frac{Z_{si}}{Z} \right) \quad (13)$$

At this stage, one must consider that the thermal impedance Z_{si} between the surface of the wall and the indoor air is purely resistive: thus, $Z_{si} = R_{sF}$, being R_{sF} the inner side thermal resistance. Moreover, the inverse of the wall thermal impedance Z corresponds to the thermal admittance Y . Such positions imply the following expression for the surface factor:

$$F = \frac{\tilde{q}_i}{\tilde{q}_{abs}} = 1 - Y \cdot R_{sf} \quad (14)$$

The previous definition corresponds to the one provided in the CIBSE guide and in the ISO 13792:2012 international standard. The value calculated according to Eq. (14) is a complex number, to quantify in terms of amplitude and argument. The latter can be assessed through Eq. (15), and will always result negative, which means that it describes a delay of the wall response to the radiant heat flux acting on it. For this reason, since now on this term will be named *time shift* and will be assigned a positive sign.

$$\varphi_F = \frac{P}{2\pi} \cdot \arctan\left(\frac{\text{Im}(F)}{\text{Re}(F)}\right) \quad (15)$$

However, it is important to underline that the internal surface resistance R_{sf} is not necessarily the same as that used for in Eq. (8), i.e. for the definition of X and Y , since the definition framework of such parameters is not the same. The Standard ISO 13792:2012 suggests to use $R_{sf} = 0.22 \text{ m}^2 \cdot \text{K} \cdot \text{W}^{-1}$.

2.3 The energy balance for a room

According to the definition of the previously mentioned dynamic transfer properties, the response of an opaque component subject to external periodic forcing conditions can be written as follows.

Equation (16) describes the density of heat flux released by a wall to the indoor environment as a response to the n -th harmonic component of the forcing conditions. Here, θ_o is the sol-air temperature, which accounts for both the outdoor temperature and the solar irradiation absorbed on the outer surface. On the other hand, Eq. (17) is the stationary term, obtained by considering the average value of each forcing condition. The periodic response of the wall is obtained by recombining such contributions as in Eq. (18); the summation of the harmonics is truncated to the harmonic of order N_H .

$$\tilde{q}_{i,n} = X_n \cdot \tilde{\theta}_{o,n} - Y_n \cdot \tilde{\theta}_{i,n} + F_n \cdot \tilde{\phi}_n \quad (16)$$

$$\bar{q}_i = U \cdot (\bar{\theta}_o - \bar{\theta}_i) + F \cdot \bar{\phi} \quad (17)$$

$$q_i(\tau) = \bar{q}_i + \sum_{n=1}^{N_H} \tilde{q}_{i,n} \quad (18)$$

Finally, the energy balance on the indoor environment can be written as in Eq. (19). Here, one can recognize the contributions due to:

- heat transfer through the windows;
- infiltration of outdoor air (n_a is the number of air changes per hour);
- convective part of the internal loads, Q_{int} (people, lighting, appliances)

The thermal balance reported in Eq. (19) does not contain any contribution due to heating or cooling plants, since it refers to free-running buildings. It can be repeated at each time step τ (here, $\tau = 1 \text{ h}$); due to the negligible thermal capacity of the indoor air, the thermal balance assumes the same form as for steady state conditions.

$$\sum_{k=1}^6 q_{i,k,\tau} + (U_w A_w + 0.34 \cdot n_a V) [\theta_{o,\tau} - \theta_{i,\tau}] + Q_{int,\tau} = 0 \quad (19)$$

Equation (19) can be used to calculate the time profile of the indoor air temperature θ_i . Starting from such information, one can also calculate the temperature of the inner surface of the k -th wall as:

$$\theta_{si,k}(\tau) = \theta_i(\tau) + q_{i,k}(\tau) \cdot R_{si} \quad (20)$$

The last point to address is the determination of the radiant thermal flux ϕ coming from external agents and acting on the inner surface of each wall. This term appears in Eq. 17 (mean value) and Eq. 16 (cyclic variation around the mean value), and is basically due to the solar radiation transmitted through the glazing and to the radiant component of the internal loads. However, its evaluation is not easy, as it implies the knowledge of the distribution of such radiant flows in the indoor environment.

In this study, the authors chose to adopt a simplified approach, based on the Ulbricht hypothesis, i.e. the uniform distribution of the radiant heat gains ψ over all the surfaces that form the boundary of the enclosure. According to this model, the radiant flux acting on the generic surface can be calculated as:

$$\phi = \frac{\psi}{(1 - r_m) \cdot A_{tot}} \quad (21)$$

Here, r_m is the mean reflectivity of the enclosing surface. In its evaluation, it is suitable to split short-wave (sw) and long-wave (lw) radiant fluxes, as the reflectivity of walls and glazing to such contributions is not the same. Thus, Eq. (21) can be written as:

$$\phi = \frac{1}{A_{tot}} \cdot \left[\frac{\psi_{lw}}{(1 - r_{m,lw})} + \frac{\psi_{sw}}{(1 - r_{m,sw})} \right] \quad (22)$$

Here, ψ_{sw} relates to the solar radiation transmitted through the glazing, whereas ψ_{lw} is mainly related to

internal radiant sources and to the fraction of solar energy absorbed by the glazing and re-emitted towards the indoor environment. All of the data needed in Eq. (22) are usually known.

In the following, the validation of the formulation presented so far is discussed, by using the test cases reported in the EN ISO 13791 and EN ISO 13792 standards, which concern the calculation of the internal temperature of a room in summer without mechanical cooling. It should be remembered that, despite the admittance procedure being well established in the literature, some novel features are introduced in the present study:

- the use of the surface factor for describing the response of the walls to internal radiant fluxes;
- the adoption of the Ulbricht hypothesis for evaluating the distribution of such radiant fluxes in the indoor environment.

The validation procedure will evaluate the reliability of this approach. It will also be helpful in identifying the most appropriate value to be used for the term R_{sF} (see Eq. 14). Furthermore, the approximation introduced by truncating the sum in Eq. (19) to the first harmonic ($P = 24$ h), as suggested by the simplified approach proposed in the Standard EN ISO 13792:2012, will be also discussed.

3. The Validation Procedure

The validation of new mathematical codes for the dynamic simulation of buildings can be performed by comparing the simulated results to appropriate reference values, obtained through experimental measurements or by means of well established codes.

The EN ISO 13791 and EN ISO 13792 international standards propose a procedure that allows the validation of mathematical models for the calculation of the summer internal temperature in enclosures without mechanical cooling. In both standards, the procedure consists in the calculation of the hourly profile of the operative temperature for a test room; the minimum, average and maximum values shall then be compared to the reference values indicated in the standard. Actually, the two documents use the same validation procedure and the same test cases; the difference lies in the

reference values and in the range of allowed acceptable discrepancy for the calculated results. Indeed, according to ISO 13791, a difference of less than 0.5 K between reference values and simulated values can be accepted. On the other hand, ISO 13792 introduces three classes on the basis of the difference Δ between the calculated values and the reference values:

Class 1: $-1 \text{ K} < \Delta < 1 \text{ K}$

Class 2: $-1 \text{ K} < \Delta < 2 \text{ K}$

Class 3: $-1 \text{ K} < \Delta < 3 \text{ K}$

The model is classified according to the worst result.

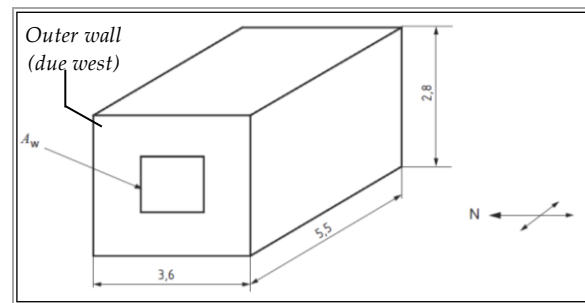


Fig. 2 – Geometry proposed by the ISO Standards

	Y	X	ϕ	F	ϕF	U
Wall (all)	4.66	0.08	-11.7	0.35	-2.0	0.49
Partition (all)	0.77	0.34	-1.1	0.91	-0.6	0.35
Ceiling (2)	5.14	0.12	-9.6	0.20	-3.1	0.71
Floor (2)	5.41	0.12	-9.6	0.45	-3.1	0.71
Ceiling (1)	0.61	0.01	-11.5	0.92	-0.4	0.24
Floor (1-3)	5.40	0.01	-11.5	0.45	-3.1	0.24
Roof (3)	5.10	0.08	-7.4	0.20	-2.9	0.43

Table 1 – Dynamic transfer properties (in brackets, the ISO test cases)

Figure 2 shows the geometry of the test room. Two different cases are available, which differ in the size A_w of the window (3.5 m² for case A, 7.0 m² for case B). Furthermore, in Case A there is a single pane window provided with an external shading device, whereas Case B implies a double pane glazing. The climatic conditions are also different: case A applies to warm climates (latitude 40°N), whereas case B applies to temperate climates (latitude 52°N)

For each room geometry, different sub-cases are possible, distinguished by a test number (from 1 to 3, according to the type of floor/ceiling) and by a second letter, associated to ventilation rate ($a = 1$ ACH, $c = 10$ ACH). Case *b* applies a variable ventilation rate, but it is not considered in the

framework of this study, since the proposed model only allows constant parameters. All the surfaces, except the outer wall and the roof in the test number 3, are bounded by similar rooms.

Table 1 collects the dynamic transfer properties for the vertical and horizontal envelope components, calculated for the fundamental harmonic ($P = 24$ h) with the relations introduced in the previous sections, as required by the standards. Concerning the glazed element and the shading device, the external, internal and cavity thermal resistances are assigned, as well as the short-wave reflectance and transmittance. The standards also prescribe the time profile of the internal sources to be used in the simulations, and an equal proportion of the heat flow transferred to the room by convection and radiation (50% each).

Thus, all the input values needed for the simulations are assigned, and they can be easily implemented in the calculation procedure shown in the previous section. The calculation was carried out by using $N_H = 6$ harmonics, since a preliminary analysis showed that no significant variation of the results would be introduced by the addition of further harmonics.

The calculation provides the time profile for the indoor temperature and for each surface temperature; these results can be finally used for the determination of both the mean radiant temperature and the room operative temperature according to Eq. (23) and (24).

$$\theta_{mr}(\tau) = \frac{\sum_{k=1}^6 A_k \cdot \theta_{si,k}(\tau)}{\sum_{k=1}^6 A_k} \quad (23)$$

$$\theta_{op}(\tau) = 0.5 \cdot [\theta_{mr}(\tau) + \theta_i(\tau)] \quad (24)$$

4. Results and discussion

Before discussing the validation outcomes, it is convenient to clarify something about the surface resistance R_{sf} . The values of this parameter to be used for the calculation of F (see Eq. 14) should not be the same as for the calculation of X and Y (see Eq. 8). In fact, while F rests on the hypothesis of constant air temperature on both sides of the wall, for X and Y this constraint does not hold, and any suitable value of the surface thermal resistance can be adopted.

The ISO Standard 13792 prescribes $R_s = 0.22 \text{ m}^2 \cdot \text{K} \cdot \text{W}^{-1}$ (i.e. $h = R_s^{-1} = 4.5 \text{ W} \cdot \text{m}^{-2} \cdot \text{K}^{-1}$) for all the dynamic properties (X , Y , F) and for any wall. However, due to the relevance of this point, the authors conducted a parametric analysis aimed at assessing the influence of the coefficient h on the outcomes of the validation procedure. In the following two values will be considered: $h = 4.5 \text{ W} \cdot \text{m}^{-2} \cdot \text{K}^{-1}$ (default value) and $h = 2.5 \text{ W} \cdot \text{m}^{-2} \cdot \text{K}^{-1}$.

It is also important to outline that, although the approach to the validation procedure is common in ISO 13791 and ISO 13792, some differences still stand. For instance, there are some discrepancies between the values of the solar radiation impinging on the west wall, and - above all - different reference values are assigned for the room operative temperature.

Figure 3 shows the discrepancy Δ between the results of the simulations and the reference values provided in the ISO Standards, for each test case considered in this study. The compliance of the calculation procedure to the standards has to be assessed by looking at the minimum, the average and the maximum room operative temperature; thus, the diagrams report the discrepancy Δ for each one of these parameters. Two ranges are highlighted: the narrow one ($-0.5 \text{ K} < \Delta < 0.5 \text{ K}$) is the range that assures the compliance to ISO 13791, whereas the largest one ($-1 \text{ K} < \Delta < 1 \text{ K}$) must be respected in order for the calculation procedure to be classified in Class 1 according to ISO 13792.

However, in most of the unfavourable cases, Δ keeps within the range $0.5 - 1 \text{ K}$, and only in very few cases Δ is higher than 1 K . On the whole, $h = 4.5 \text{ W} \cdot \text{m}^{-2} \cdot \text{K}^{-1}$ (hollow triangles) seems to introduce a lower discrepancy than $h = 2.5 \text{ W} \cdot \text{m}^{-2} \cdot \text{K}^{-1}$ (filled triangles). On the contrary, when looking at the comparison between simulations and reference values provided in ISO 13792, the discrepancy Δ is very often negative. However, this standard is less strict than ISO 13791, as it allows a higher discrepancy ($-1 \text{ K} < \Delta < 1 \text{ K}$). Thus, almost all cases comply to the Standard: if $h = 4.5 \text{ W} \cdot \text{m}^{-2} \cdot \text{K}^{-1}$ (hollow squares), only case B.1.a shows a discrepancy higher than 1 K . However, this is sufficient to classify the calculation procedure in Class 2. When $h = 2.5 \text{ W} \cdot \text{m}^{-2} \cdot \text{K}^{-1}$ (filled squares) the condition required for Class 1 is always met.

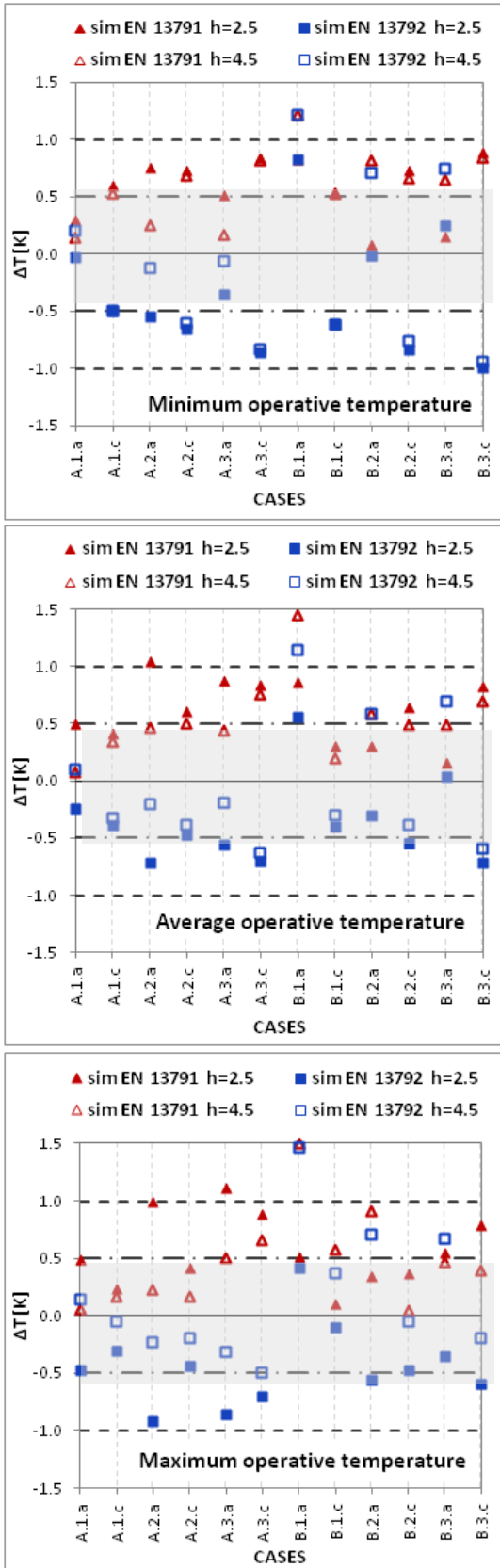


Fig. 3 – Verification of the compliance to the ISO Standards: discrepancy with the reference values (a: min Top, b: average Top, c: max Top)

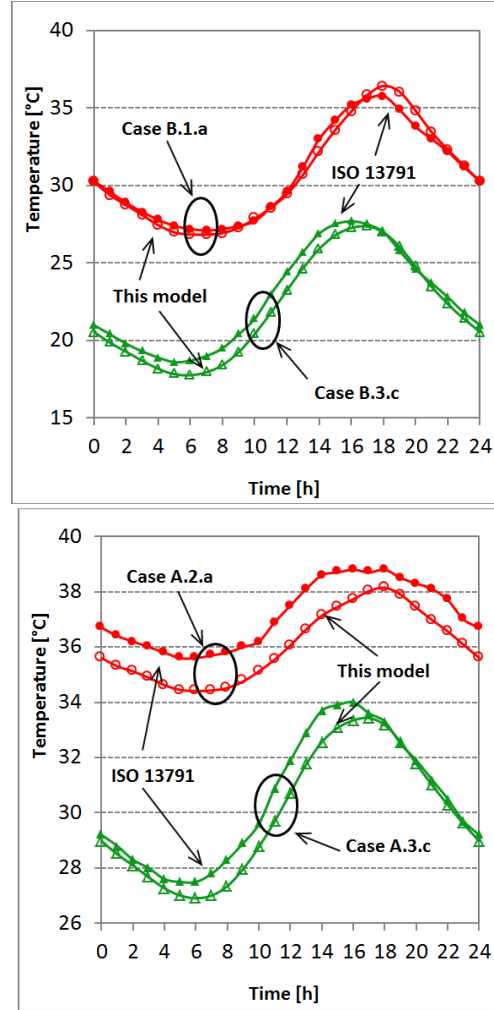


Fig. 4 – Comparison between simulated results and reference values for the operative temperature

Figure 4 shows the comparison between simulated and reference daily profile of the operative temperature for the most unsatisfactory cases emerging from Fig. 3. The comparison is based on ISO 13791, since ISO 13792 does not provide any reference daily profile.

4.1 The influence of the number of harmonics on the building response

In the previous section, it was shown that the mathematical model discussed so far proves sufficiently reliable if adopting $N_H = 6$ harmonics in the Fourier analysis. However, one must remark that, both in the scientific literature and in the international standards, the dynamic transfer properties are normally used by looking only at the fundamental harmonic ($N_H = 1$).

With reference to the case B.1.c of ISO 13792, Fig. 5 shows that, if comparing the room operative temperature calculated by truncating the sum of Eq. (18) to $N_H = 1$ and $N_H = 6$, the results are quite different. Indeed, the difference between the two profiles can also be higher than 1 K during some hours of the simulated day.

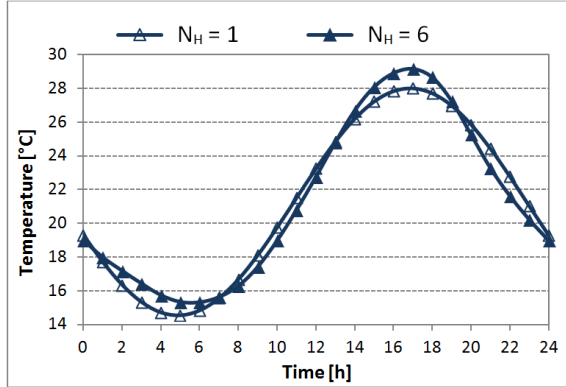


Fig. 5 – Simulated results for $N_H = 1$ and $N_H = 6$ (test case B.1.c)

Test cases	Discrepancy with EN 13792 ($N_H = 1$)			Class for $N_H = 1$	Class for $N_H = 6$
	ΔT_{min}	ΔT_{avg}	ΔT_{max}		
A.1.a	0.1	0.1	0.7	1	1
A.1.c	0.8	0.4	0.8	1	1
A.2.a	0.6	0.7	<u>1.1</u>	<u>2</u>	1
A.2.c	0.9	0.5	0.8	1	1
A.3.a	0.3	0.5	<u>1.0</u>	<u>2</u>	1
A.3.c	<u>1.1</u>	0.8	<u>1.0</u>	<u>2</u>	1
B.1.a	0.6	0.8	0.4	1	1
B.1.c	1.2	0.5	<u>1.1</u>	<u>2</u>	1
B.2.a	0.2	0.2	<u>1.1</u>	<u>2</u>	1
B.2.c	<u>1.2</u>	0.6	<u>1.1</u>	<u>2</u>	1
B.3.a	0.1	0.2	0.8	1	1
B.3.c	<u>1.3</u>	0.8	<u>1.2</u>	<u>2</u>	1

Table 2 – Effect of the number of harmonics on the classification of the mathematical procedure

It is then interesting to evaluate such a difference for some other representative cases. The results of this calculation are reported in Fig. 6, where the curves refer to the most unfavourable cases addressed during the validation procedure. Here:

$$\Delta\theta_N = \theta_{op}|_{N_H=1} - \theta_{op}|_{N_H=6} \quad (25)$$

If the validation procedure were carried out by using $N_H = 1$, the discrepancy highlighted in Fig. 6 would lead the model to be downgraded to Class 2, as shown in Table 2, whereas for $N_H = 6$ it deserves

Class 1. The misleading effect of considering only the first harmonic in the evaluation of X and Y was already observed by (Gasparella et al., 2011).

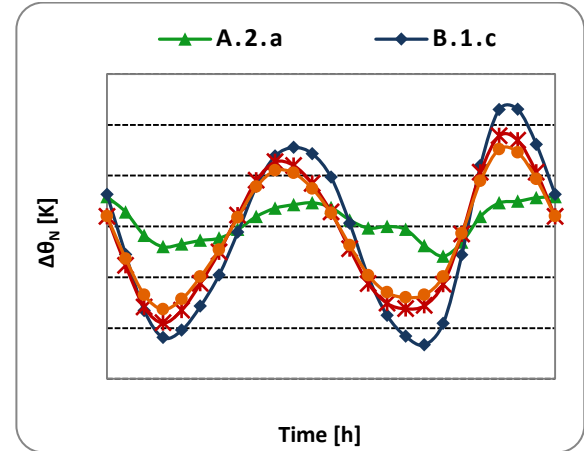


Fig. 6 – Difference between the simulations with $N_H = 1$ and those with $N_H = 6$

5. Conclusion

In this study, the validation of an original calculation code for the evaluation of the dynamic thermal response of buildings was addressed. This code is based on the Admittance Method and is supported by the use of the *surface factor*, a concept rarely exploited so far in the literature, that allows the explicit consideration of the radiant heat gains acting on the surfaces of the enclosure. These effects are normally accounted for through numerical methods or by means of *thermal storage factors* determined through appropriate tables, like in the Carrier method. On the contrary, the use of the *surface factor* allows a rigorous analytical approach having general validity.

The overall mathematical model discussed so far resulted sufficiently reliable on the basis of the validation procedure proposed in the ISO Standards 13791 and 13792. The results also showed that, in order to obtain more satisfactory results, an appropriate value must be used for the inner surface resistance R_{sf} in the calculation of the surface factor. Even if the Standard EN 13792 suggests to use $R_{sf} = 1/4.5$, the paper underlines that in some cases $R_{sf} = 1/2.5$ provides better results, leading to the achievement of Class 1.

Finally, it was also shown that, when using methods based on the harmonic analysis, the adoption of the only fundamental harmonic may be inadequate for a reliable prediction of the building thermal response. As an example, according to the ISO 13792, the proposed model, if based on the first harmonic ($N_H = 1$), would be classified in Class 2, whereas it deserves Class 1 if $N_H = 6$.

6. Nomenclature

Symbols

A	area (m^2)
c	specific heat capacity ($J\ kg^{-1}\ K^{-1}$)
f	decrement factor (-)
F	surface factor ($W\ m^{-2}\ K^{-1}$)
h	heat transfer coefficient ($W\ m^{-2}\ K^{-1}$)
L	thickness (m)
n	order of the harmonic (-)
N	total number of harmonics (-)
P	time period (h)
q	density of heat flux ($W\ m^{-2}$)
\tilde{q}	cyclic density of heat flux ($W\ m^{-2}$)
Q	thermal power (W)
r	reflectivity (-)
R	thermal resistance ($m^2\ K\ W^{-1}$)
t	cyclic thickness (-)
U	thermal transmittance ($W\ m^{-2}\ K^{-1}$)
V	volume (m^3)
X	periodic transmittance ($W\ m^{-2}\ K^{-1}$)
Y	thermal admittance ($W\ m^{-2}\ K^{-1}$)
Z	thermal impedance ($m^2\ K\ W^{-1}$)

Greek letters

α	absorption coefficient (-)
ϕ	time shift (h)
ϕ	radiant heat flux ($W\ m^{-2}$)
λ	thermal conductivity ($W\ m^{-2}\ K^{-1}$)
ψ	radiant thermal power of a source (W)
ρ	density ($kg\ m^{-3}$)
θ	temperature (K)
$\tilde{\theta}$	cyclic temperature variation (K)
ω	angular frequency ($rad\ h^{-1}$)
ξ	thermal effusivity ($W\ m^{-2}\ K^{-1}$)

Subscripts

a	air
c	convective
H	harmonic
i	indoor
lw	long wave
m	mean
mr	mean radiant
o	outdoor
op	operative
si	inner surface
so	outer surface
sw	short wave

References

- Beattie, K.H., Ward, I.C., 1999. The advantages of building simulation for building design engineers, Proceedings of IBPSA International Conference, Kyoto, Japan.
- Carrier Air Conditioning Company, 1962. System Design Manual, Syracuse, New York.
- CIBSE, 2006. Guide A: Environmental Design, 7th ed., Chartered Institute of Building Services Engineers, London.
- Davies, M.G., 1973. The thermal Admittance of layered walls, Building Science, vol. 8, pp. 207-220.
- Davies, M.G., 1994. The thermal response of an enclosure to periodic excitation: the CIBSE approach, Building and Environment, vol. 29-2, pp. 217-235.
- Gasparella, A., Pernigotto, G., Barattieri, B., Baggio, P., 2011. Thermal dynamic transfer properties of the opaque envelope: analytical and numerical tools for the assessment of the response to summer outdoor conditions, Energy and Buildings, vol. 43, pp. 2509-2517.
- ISO 13786:2007. Thermal performance of building components - Dynamic thermal characteristics - Calculation methods.
- ISO 13791:2012. Thermal performance of buildings - Calculation of internal temperatures of a room in summer without mechanical cooling - General criteria and validation procedures.
- ISO 13792:2012. Thermal performance of buildings - Calculation of internal temperatures of a room in

- summer without mechanical cooling – Simplified methods.
- Loudon, A.G., 1970. Summertime temperatures in buildings without air conditioning, *Journal of The Institution of Heating and Ventilation Engineers*, vol. 37, pp. 280 - 292.
- Millbank, N.O., Harrington-Lynn, J., 1974. Thermal response and the admittance procedure, *Building Service Engineering*, vol. 42, pp. 38-51.
- Rees, S.J., Spitler, J.D., Davies M.G., Haves, P., 2000. Qualitative comparison of North American and U.K. cooling load calculation methods, *International Journal of HVAC&R Research*, vol. 6, no. 1, pp. 75-99.

Interoperability between building information models and software for lighting analysis

Chiara Aghemo – Politecnico di Torino - DENERG, Turin, Italy

Laura Blaso – Politecnico di Torino - DENERG, Turin, Italy

Daniele Dalmaso – Politecnico, di Torino - DISEG, Turin, Italy

David Erba Politecnico – Politecnico, di Torino - DISEG, Turin, Italy

Matteo Del Giudice – Politecnico, di Torino - DISEG, Turin, Italy

Anna Osello – Politecnico, di Torino - DISEG, Turin, Italy

Giovanni Fracastoro – Politecnico di Torino - DENERG, Turin, Italy

Anna Pellegrino – Politecnico di Torino - DENERG, Turin, Italy

Pablo Ruffino – Politecnico, di Torino - DISEG, Turin, Italy

Abstract

Lighting analysis models are being integrated into building information models (BIM) quickly. The BIM of the Politecnico di Torino (Polito) campus used in the Smart Energy Efficient Middleware for Public Spaces (SEEMPubS) project is an integrated representation of each building to merge architectural, structural, electrical and HVAC elements and components. In the Polito campus there are three types of buildings: historical, modern and contemporary. A special approach has been adopted to model and to exchange data between software about historical buildings because they are characterized by paints, stuccos, etc.

The aim of this research was to set a parametric model able to share information without data loss, testing the interoperability between architectural software like Revit Architecture and lighting analysis software like Daysim and Radiance. As the process of exchanging data from Revit to Daysim and Radiance is not direct, Ecotect Analysis was used as an “interoperable bridge” with good results. Three different formats were tested: IFC, gbXML and FBX and for each one problems and possible solutions were analysed. Up to now, Ecotect was used in two different ways: to define material parameters before the export phase and to visualize analytical data obtained from Daysim and Radiance. In our tests some errors have occurred referring to data retention like material properties, but at present the main problems have been solved. Indications about performance of daylighting and energy consumption have been obtained, although a lot of work should still be done. The correct data exchange that we obtained enabled the optimization of the building

simulation process by avoiding the need to remodel the same building in the lighting applications.

1. Introduction

Building information modelling (BIM) has received much attention in recent years due to its possibility of developing a new methodology of design, construction and facility management based on information exchange. This process is achieved through the interoperability of software that is defined as “the need to pass data between applications, and for multiple applications to jointly contribute to the work at hand” (Eastman C. et al., 2008). In this way a single building model can be used to perform all the simulations needed for its design and operation like lighting and thermal analysis, without the necessity to remodel it in any applications. On the other hand, this process is still not easy on account of the shortage of complete technical standards.

“Detailed technical standards are required to unambiguously define the requirements of specific information exchanges as user of the exchange standards will do so with various types of software.”

“At present, data exchanges between two application are typically carried out in four ways: direct; proprietary links between specific BIM tools; proprietary file exchange formats, primarily dealing with geometry; public product data model exchange

formats like IFC, or XML – based exchange format” (Osello A., 2012). However, although the possibilities of exchange may appear numerous, there are cases which still require the use of an “interoperable bridge” to complete the procedure.

The present paper presents a set of criteria for the creation of a suitable parametric model. On the basis of these criteria, it describes the related tests aimed at data exchange between architectural and lighting analysis software carried out during the Smart Energy Efficient Middleware for Public Spaces (SEEMPubS) project. The project in fact is aimed at implementing a Building Management System based on the integration of both building information modelling and advanced ICT based control and monitoring system to increase the energy efficiency of public buildings. Actually, energy efficiency was, in the design phase of the project, mainly assessed through lighting and HVAC dynamic simulations.

The tests on data exchange between architectural and energy software have come to the definition of a procedure that allows interoperability by avoiding the need for external input from users for the exchange of information related to the model.

2. Simulation

All tests were conducted on six couples of rooms, selected for the SEEMPubS project, on the campus of the Polito. In these rooms, the new control and monitoring solutions for lighting, heating/cooling and electrical appliances were deployed to demonstrate the efficacy of the planned BMS. For these rooms lighting and thermal simulations were needed to assess the effectiveness, in terms of comfort and energy savings, of possible different control strategies. The choice of the rooms was conducted according to the following criteria: representativeness with respect to the campus and other public buildings; energy saving potential, estimated according to their architecture, orientation, system and occupancy characteristics. The selected spaces are divided as follows:

- Four offices at the Valentino Castle, premises of the School of Architecture
- Two offices and two classrooms at the Main Campus in Corso Duca degli Abruzzi

- Four offices at Cittadella Politecnica, recently built next to the Main Campus, Politecnico’s research centre

Building information model of each room was realized through Autodesk Revit, merging the architectural model with structural, mechanical, electrical and HVAC models. Methodologically, the model setup followed five phases which were functional to the type of activity for which the model itself is built.

The first phase provided for the definition of standards necessary to enable the collaborative work. The model was organized by dividing the various elements, according to their specific function, thanks to the use of WORKSETS in order to facilitate the sharing of work.

The second phase, related to a preliminary site inspection and starting from achieved documents, concerned modelling quickly the existing structure in an urban scale. This model includes building location, typology, size, volume, construction period and is used to analyze the main aspects of the building’s performance, with a particular emphasis on energy efficient and sustainable design and management.

The third phase enabled the realization of a preliminary model that, at any time, can be enriched with all the specific information such as doors and windows, materials and walls stratigraphy. A survey was carried out in two different and complementary ways:

- Using a total station and a GPS receiver in order to establish precise GPS coordinates of the essential exterior and interior building elements

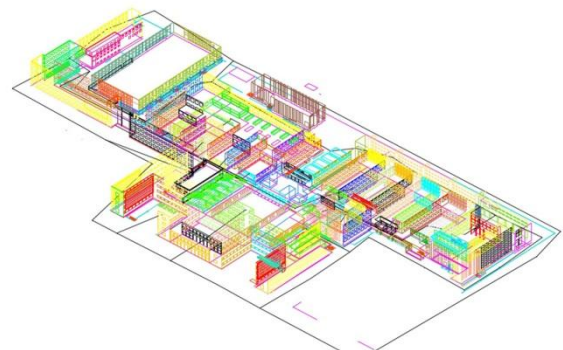


Fig. 1 – Survey of the Main Campus realized through a total station

- Using Electronic Distance Meter (EDM laser) to take quickly the measurements of the rooms

The fourth phase concerned the choice of the software tools that may be used in an interoperable way like Revit Architecture, Revit MEP, 3dStudioMax, Ecotect Analysis, Daysim, Radiance, Sketch Up and AutoCAD.

With the fifth phase began the setting of a method of continuous cross-checking and updating of data, with the intention to create an integrated model which is as correct as possible for each use. This phase was closely related to the previous one and it is continuously evolving. In fact, the exact knowledge of what type of data and from which software they can be successfully exchanged requires interesting considerations on the standards to be used in the integrated model to optimize the BIM process.



Fig. 2 – Example of final model of the Main Campus

Subsequently to the setting of the model, in the SEEMPubS project, thermal and daylighting simulations were required to estimate the rooms' energy performance.

In this paper the tests and procedures adopted to exchange data between architectural model and software for daylighting analysis are described. In the project lighting simulation was necessary to estimate the availability of daylight in the rooms, in order to define the control strategy of electric lighting based on daylight availability and on the rooms' utilization schedules. Furthermore, after the definition of the possible electric lighting control rules, the lighting simulation was used to estimate the consequent energy performance of the lighting systems (Fracastoro G.V. et al., 2012).

To proceed with the lighting analysis it was

necessary to correctly characterize all construction components of the model (walls, floors, false ceiling, windows, window's frame, doors, internal obstruction and furniture etc.). This process occurred utilizing the Revit embedded logical division, thus reaching the Typology detail level (Family type). Therefore, in each family of homogeneous elements different types have been created for each object according to the materials that constitute them. As far as the modeling of the external environment surrounding the study object is concerned, which might influence the daylighting calculation, it has also been modeled with different typologies of building elements. To speed up the analysis process, the spaces were modelled using simplified furniture and external obstruction. Then, to obtain a correct lighting analysis, it was necessary to proceed with the optical characterization of all surfaces that may be involved in terms of interaction with light inside the room.

The characterization of materials' optical properties is an essential phase of 3D model preparation for the subsequent lighting simulation. Therefore, the reflection and/or transmission properties of each material and its mode of reflection (specular, diffused, mixed, etc.) must be defined. In this project the optical properties of the room and furniture surfaces were defined measuring, with a spectrophotometer, the chromatic characteristics and the visible reflectance. Transparent materials were characterized measuring the visible transmittance with a luminance meter. Moreover, by using software that in addition to numerical results also provides a rendering of the lighting environment, it is also necessary to define the materials' chromatic characteristics. The general rule consists therefore in diversifying volumes in relation to material, so that it is possible to associate their light reflection, light transmission and the chosen material's rugosity.

Several applications are available to perform daylighting analysis, characterized by different calculation approaches, accuracy and type of achievable results (Pellegrino A., 2012). Some of them are based on the concept of daylight factor, which assesses a room's daylight availability through the calculation of the ratio between indoor and outdoor illuminance under a reference sky condition (Dialux, Ecotect Analysis, etc.), others

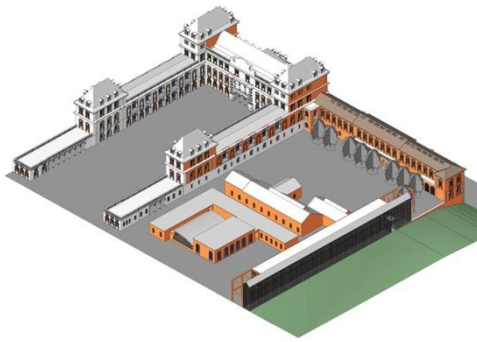


Fig. 3 – Final model of the Valentino castle Campus

calculate the illuminances within a room taking into account more detailed sky luminance distribution, which could vary from clear to intermediate to overcast, depending on the designer's input or on the climate of the considered site (Radiance, Daysim, Lightsolve, etc.). The two groups of software usually differ also for the accuracy of the algorithms used to calculate both direct and reflected components of daylight. Among the second group of applications some can be used to calculate time varying illuminances profile, for instance to assess Dynamic Daylighting Performance Metrics such as Daylight Availability or Useful Daylight Illuminances. This analysis, based on climate data and, usually, on a yearly basis, is the premise for a more detailed calculation of the electric energy consumption of the lighting systems, in particular when automatic control systems are used.

For the SEEMPubS project, daylighting simulations and consequent electric lighting energy calculations were performed using the climate-based dynamic application called Daysim (Reinhardt C.F., 2001). From the operating point of view, to start the simulations it was necessary to import a 3D model of the room under study and its external obstructions. The 3D model, in this case, was realized with the Revit applications, which allow a complete modeling from the architectural and systems point of view, compared to other software such as SketchUp, AutoCAD, Ecotect Analysis. Hence, Ecotect Analysis has been used for the following three purposes:

- Like an "interoperable bridge", because, unlike Revit, one of Ecotect Analysis' functions allows model exportation to lighting application such as Daysim or Radiance, automatically creating the files required for the subsequent lighting

calculation. These contain the geometric characterization and material assignment (.rad extension), viewport definition (.vf extension), coordinates and orientation of points in the calculation grid (.pts extension), climatic file (.wea) and finally the complete Daysim file (.hea)

- In order to define materials' optical properties and the calculation plan to be used in Radiance or Daysim simulation
- In order to graphically process the numerical data obtained with Daysim / Radiance, which are imported in the .dat format (coming from Radiance) and .da (coming from Daysim) and therefore their 3D visualization.

It must be specified that, despite Ecotect being developed as a simulation program aimed at evaluating buildings' performance, with particular attention to energy aspects from the point of view of sustainable design, in this case it was not used directly to perform the lighting analysis because higher accuracy and more detailed results were required. Moreover, this software does not directly allow a dynamic climate-based simulation.

In order to proceed with model exportation from Revit into Ecotect Analysis, and later to Daysim, three different procedures are defined and tested. Different results are analyzed and the most appropriate procedure from the point of view of lighting simulation is chosen.

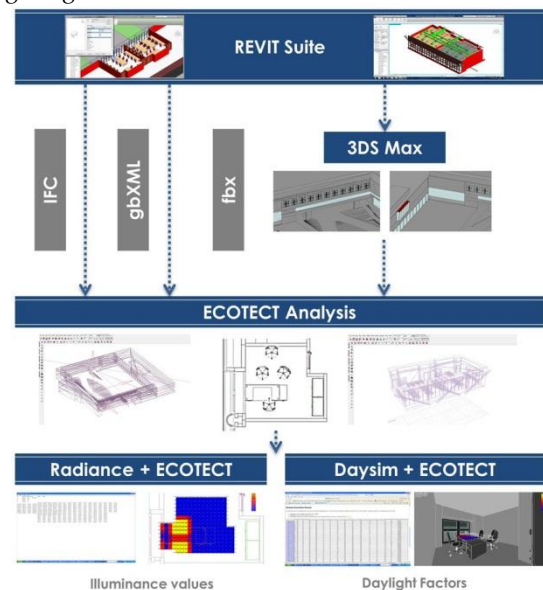


Fig. 4 – Layout of the procedures followed

The first export procedure consisted in following the traditional approach suggested by literature: exporting the file in Industry Foundation Classes (IFC) format. IFC is the main buildingSMART data model standard and it is an open format; therefore it can be used to exchange and share BIM data between applications developed by different software vendors without having to support numerous native formats. IFC is registered by ISO as ISO/PAS 16739 and is in the process of becoming official International Standard ISO/IS 16739. File importation occurs through the MODEL/ANALYSIS DATA modality because is the only one of the two available importation modes to be compatible with .ifc files, and it can directly import the .ifc files in the Ecotect Analysis application. During the procedure, the imported elements are listed in the importation window, including surface and single elements, as well as elements realized in Revit that are being imported in Ecotect Analysis.

The second procedure analyzed consists in exporting the 3D model through the creation of a Green Building schema XML file (gbXML). gbXML is an open scheme which facilitates data exchange of building properties stored in 3D building information models (BIM) to engineering analysis tools. In order to correctly export the data in the gbXML format it is essential to include in Revit model the ROOM entity. This consists in assigning to every closed space (delimited by a floor, walls, and ceiling) a label, precisely ROOM, identifying the room's volume; this operation allows thus to identify in advance the THERMAL ZONE used by Ecotect Analysis to the lighting simulations. If this operation is not performed, the gbXML file is not created. The gbXML standard enables the export of various types of information, in addition to ROOMS. In fact, it is possible to export the building's geographical location, its construction type, shading surfaces and any other architectural element that makes up the building. Trying to import the file in Ecotect Analysis, it is possible to verify that the ROOMS are imported as well as the building elements modeled with Revit.

Both the first two procedures presented problems during the importation phase in Ecotect Analysis. Therefore the third methodology was studied and tested.

The third procedure concerns exporting the model from Revit in the .fbx format. In this case exportation only occurs correctly in an elevation or axonometric view of the model, otherwise the command is not available. This operation has no control setting, because the command is closed and the operator cannot interact. Since Ecotect do not accept .fbx files, a third intermediate application has been introduced. This additional tool is 3dStudioMax. The use of this application has been necessary because it was not possible to export from Revit a file format compatible with Ecotect Analysis maintaining the model unaltered. Through 3dStudioMax, it is possible to export the file in a .3ds format fully compatible with the lighting simulation application used for the SEEMPubS project.

In the 3dStudioMax environment, the .fbx files are not directly imported, but a linkage operation must be performed through the command FILE LINK MANAGER. This instrument also allows the user to select among different link options, the one most appropriate for the creation modality of the Revit files. Among the available options, the importation of the elements composing the model was chosen grouping them based on the element TYPOLOGY. In this way, the parametric model realization logic in Revit was respected completely. In this phase, measurement unit setup operations are very important, in fact the right setting must be verified before linking the Revit file; in particular it is necessary that the 3dStudioMax units are consistent with those in which the parametric model has been realized.

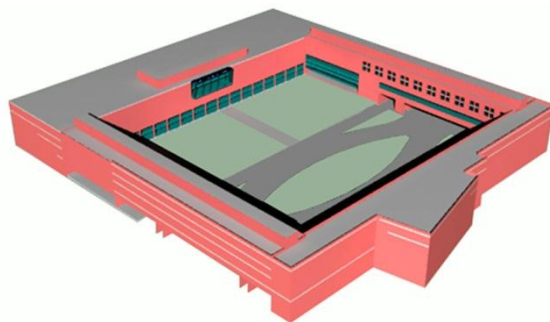


Fig. 5 – Model optimized in 3dStudioMax

Within the 3dStudioMax environment it is possible, as opposed to the previous procedures, to make changes to the model both from the architectural

point of view and on the denomination of the element typologies in order to obtain a better uniformity. Another operation, recommended, though not essential, is to eliminate the camera and the light spot that the 3dStudioMax application automatically imports from .fbx file. This last operation is feasible reloading the .fbx file and unchecking the relative options in the dialog box. Moreover, these two specific objects are not useful for modelling and for subsequent simulation. At this point it is possible to export the file in the .3ds format and subsequently to import in Ecotect Analysis.

The import mode, with respect to the previous procedures, is not MODEL/ANALYSIS DATA but the command denominated 3D CAD GEOMETRY, which allows for the listing of all model elements grouped by TYPOLOGY and to assign them the correct ZONE.

The materials, after importing the model in Ecotect Analysis, were characterized. Particular attention was paid to analysing each surface, consequently, reflection and/or transmission properties were defined. For the SEEMPubS models, field measurements of luminous reflectances and transmittances of the different room and furniture surfaces were carried out and the data used to characterize the materials' optical properties of the models.

Finally, through the specific command the model can be exported to Daysim for the final lighting and energy simulations.

Before starting lighting simulations with Daysim, the models, built in Revit and exported in Ecotect, were validated using the Radiance application.

Radiance is an open-source, highly accurate, ray-tracing software system for UNIX computers and it predicts the light levels and appearance of a space (Larson G.W. et al.,1998). Its algorithms (Monte Carlo backwards raytracing) allow an accurate simulation of the phenomenon of interaction between light and surfaces; furthermore Radiance does not have any limitation on the geometry or the spaces that can be simulated. As for daylight sources, Radiance can take into account different sky luminance distributions, considering both direct and diffuse solar radiation.

From Ecotect, the model was then imported into

Radiance and its validation was carried out by comparing the illuminances calculated with Radiance to the illuminance measured in the corresponding real room with same sun position and sky condition (Mardaljevic J., 1995).

As an example, table 1 presents some first results obtained for a clear and an overcast sky condition. The measurements were done in a single office (DAUIN office) in correspondence of two points on a horizontal plane: one near the window (point 1), one far from the window (point 2). The relative differences between calculated and measured values range from -12% to 29.4%, therefore confirming a good accuracy of the model used for the lighting simulation.

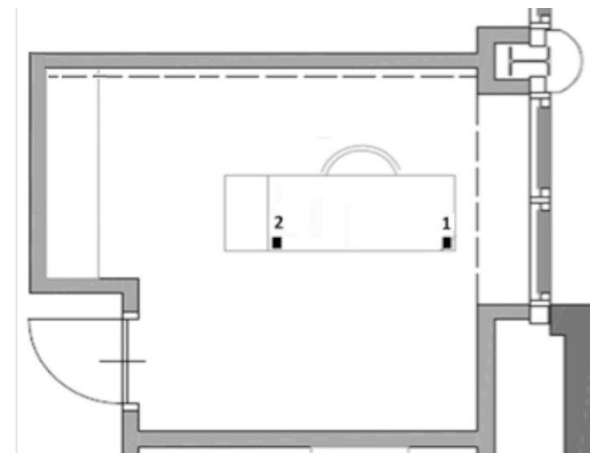


Fig. 6 – Detection point in DAUIN office

Sky condition	Point	Measured Illuminance (lx)	Calculated Illuminance (lx)	Relative difference (%)
Clear Sky	1	26618	31840	19.6
	2	1088	958	-12.0
Overcast sky	1	246	276	11.9
	2	74	96	29.4

Table 1 – Comparison between measured and calculated illuminances.

After validation, the models were used for lighting analysis with Daysim. Daysim in fact, calculates the annual daylight availability in arbitrary buildings based on the Radiance backward ray tracer, using external daylighting conditions derived from standard meteorological local datasets. It includes specific occupant behaviour model algorithms to mimic occupant use of personal controls such as

light switches and venetian blinds and to predict the electric lighting use due to automated lighting controls such as occupancy sensors and photocell controlled dimming systems. In addition to daylighting metrics, among its outputs, the total annual energy demand for lighting [kWh] and the LENI value [kWh/m²year] are included (EN 15193, 2007).

Within the SEEMPubS project, Daysim was used to calculate the rooms' electric lighting energy demand for different proposed control strategies and to estimate the corresponding energy saving with respect to the manual lighting control usually adopted in the Politecnico rooms (Acquaviva A., et al., 2012).

In this paper an example of the achieved results is presented (figure 7; table 2). Results are referred to the DAUIN office, which is a single office, with an internal movable shading device, southwest oriented. Inputs for simulation are:

Occupancy profile: from 9:00 a.m. to 6:00 p.m., with lunch and intermediate breaks

User requirements and behaviour: target illuminance of 500 lx, mix of active and passive user's behaviour and active user behaviour for lighting; active behaviour depending on the user's need to avoid direct sunlight on work plan for blinds

Lighting control systems: different lighting control strategies were simulated to compare their effectiveness with respect to the manual control

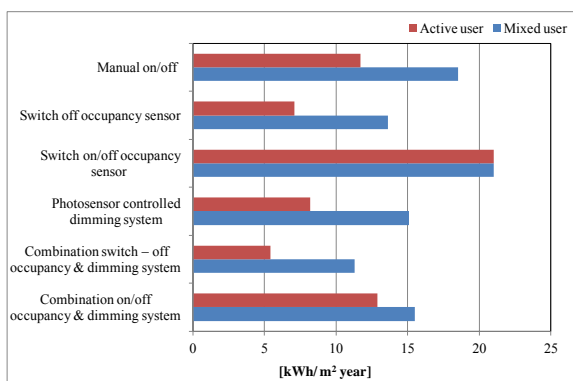


Fig. 7 – Energy demand for different control strategies

Control strategies	Energy savings with respect to manual control (%)
	Mixed user behaviour
Switch off occupancy sensor	-26%
Switch on/off occupancy sensor	+14%
Photosensor controlled dimming system	-18%
Combination switch off occupancy and dimming system	-39%
Combination on/off occupancy and dimming system	-16%

Table 2 – Calculated percentage of energy saving with different control strategies, respect to manual control

3. Discussion And Result Analysis

As outlined in the introduction, interoperability of software is the basic instrument for a successful Building Information Model process. In order to realize a complete parametric model, suitable for data exchange between architectural software and energy analysis software, three different procedures were investigated.

Each procedure has presented difficulties or errors. In the first two cases, data exchange was realized through open formats like IFC and gbXML that have proven not fully adaptable to the cases under study. Among the errors encountered with the first procedure, which used the IFC standard, it is of particular importance the fact that window frames, which are fundamental for lighting analysis, are not imported. Besides, model representation turns out incomplete because it is imported with the constructive elements misaligned with respect to the original model. This suggests that the first procedure is not the best one and for these reasons a second way was analyzed.

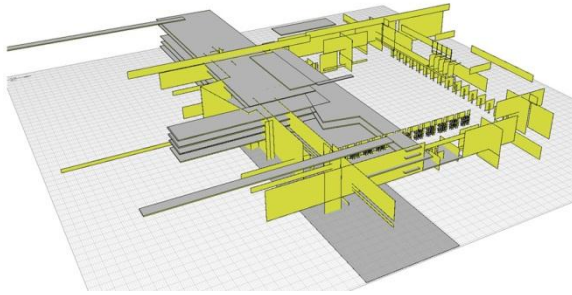


Fig. 8 – Errors encountered during the importation of IFC file in Ecotect Analysis

The second procedure consisted in the use of gbXML exchange format, which required that each space is defined by a ROOM. Even in this case several issues arose when opening the file in Ecotect Analysis.

Through this kind of exportation, the model is correctly regenerated and all elements maintain their reciprocal position, nevertheless the elements' volumetric characteristic is not maintained. Solids lose their connotation because they are transformed into surface, placed side by side but not exactly matching. The same problem occurred for the ROOMS that are represented by their surfaces. For instance, in the case of the window frames, they are broken down in two orthogonal planes composing the structure of the frame itself. A similar problem concerns vertical and horizontal surfaces, like walls, floor, ceiling, etc.

These transformations make lighting simulation unfeasible because, due to the excessive model simplification, there is a risk of destroying the real glass surface obstruction and of identifying daylight penetration points where surfaces do not perfectly match. Consequently, the model becomes unusable for lighting calculations.

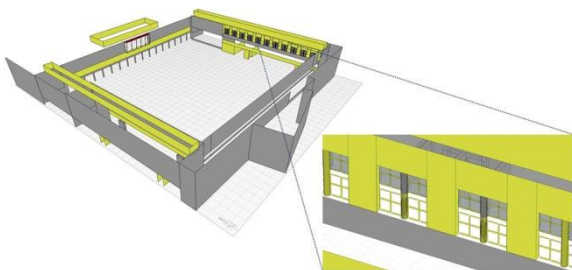


Fig. 9 – Elements exported by gbXML which do not maintain their volumetric characteristic

The third procedure, that concerns the use of an intermediate application (3dStudioMax), appears to be the most appropriate both for what concerns

modeling in the Revit applications and for the analyses in Ecotect Analysis. However, it is necessary to highlight some basic steps for successful data exchange.

Firstly, the elements used for modelling in Revit environment (FAMILY TYPE) must be created in a suitable way in order to facilitate the subsequent operations of ZONE assignment in Ecotect Analysis. Besides, particular attention must be paid to the materials, which will concretely conform to their belonging ZONE. At the same time, the nomenclature of these elements (TYPE) must not exceed twelve characters, in fact, a longer denomination would be cut in the Ecotect Analysis environment with the risk of losing information useful for identification. For example, glass component modeling is very important because with Revit, it was not possible to export the component as 3DFACE. 3DFACE is the best typology of elements to import in Daysim and Radiance for the units characteristics association, like insulated glass or triple glazed, in order to avoid simulation errors due to the calculation complexity in terms of refraction of the light beam hitting the entire glass component. In this way, during the importation phase in Ecotect Analysis glass, being a solid, it is divided in its components' faces. However, materials' characteristic must be associated to one face only and other faces must be deleted. The following simulations could be influenced by the choice of characterizing inner or outer face and some errors can occur in the results (not very significant).

Afterwards, linking and file opening times are slightly longer than the two previous procedures. Obviously, the higher the simplification of the 3D model, the shorter the time is. Longer file opening times were found when the Revit model contained particularly elaborate windows and when the model included several objects. Moreover, particularly complex parametric elements (higher than 64K) are not automatically exported by 3dStudioMax. This implies that a MERGE operation on the model must be performed before the exportation in order to include these elements.

Particular problems arise while modeling a glass curtain wall, in a Revit environment. This family type differs from the importation rules in 3dStudioMax seen above; in fact, assigning two

different names to two different curtain walls is not influential. In the importation into Ecotect Analysis they were recognized as one single element: the problem was solved temporarily by replacing the glass curtain walls with a WALL object to which transparency characteristic was assigned.

Finally, whereas Daysim and Radiance require a reference surface against which lighting simulations perform, it is possible to define this surface directly in Revit through the creation of a specific solid exportable into Ecotect Analysis and employable without problems.

Unlike the two first procedures, also in this case solids are converted into surface, but these are well aligned with each other and are perfectly matched. The same happens for the window frames that guarantee the correct obstruction compared to the incoming daylight.

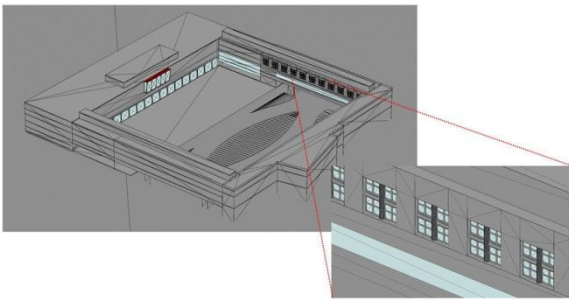


Fig. 10 – Ecotect Analysis view of the correct 3ds file exported through FBX

It could be concluded that this type of exportation allows to import the model in Ecotect Analysis correctly and appropriately with regard to the technical needs for lighting simulation.

The results of the validation phase of the model, carried out with Radiance, showed a difference between measured and simulated illuminances ranging from -12% to +30%, depending on the considered sky conditions (clear or overcast sky) and on the position of the verification point within the room. This discrepancy might be attributed to the interaction of the different aspects which are involved in the simulation process: 1) the correspondence of the sky model generated by Radiance starting from the measured outdoor illuminances (direct and diffuse horizontal illuminances) with the real sky condition; 2) the optical characterization of room with opaque and

transparent surfaces; 3) the accuracy of the instruments which were used for the indoor and outdoor illuminance measures; 4) the accuracy of the geometrical model, with particular attention to the modeling of the glass surfaces.

As for the buildings' energy performance, simulations carried out with Daysim for the SEEMPubS project were very useful in defining the most effective control strategy to reduce energy consumption for lighting, based on both the annual daylighting conditions and the use of the space (type of activity, user behavior, etc.). From the data presented in the paper a combination of manual and automatic control turned out to be the most effective solution (39% of saving with respect to totally manual on/off control). The control strategy provides for turning on lights manually, and for automatic dimming and switching off. The control strategy based on switching on/off light through the occupancy sensor was more expensive than the others, manual control included. This result can be explained by the presence of daylight in the room during the year. When daylight is sufficient for the occupants' needs, users, with not a completely passive behavior, can switch lights off, while occupancy sensors, detecting the users' presence, always keeps them on. Furthermore, occupancy sensors have a stand-by power consumption during the year which increases the overall energy demand for lighting.

4. Conclusion

In the last few years, interoperability has become a crucial topic to develop Building Information Modeling. Our study focused on interoperability between architectural software and lighting analysis software. Three different procedures were studied and tested many times to guarantee correct data exchange that allowed lighting simulations.

Firstly, a Building Information Model was realized for each couple of rooms in order to enable correct energy analysis, then the exportation phase started. In all procedures difficulties or errors related to the definition of the elements' geometry and their mutual spatial arrangement were found; only in the third procedure this did not happen, due to the

introduction of additional software like 3dStudioMax.

Ecotect Analysis has played a key role in our tests, becoming an “interoperable bridge” that allowed us to exchange the information required from Revit to Daysim or Radiance and vice versa. At the end, the goal of interoperability is clear, but many unsolved issues still exist to turn this idea into reality. However, with this study we have tried to overcome the difficulties explained above allowing for a better sharing of information between the different subjects involved in the design process.

This interoperable bridge allowed the lighting simulation to run, both with Radiance and Daysim, thanks to the development of 3D models complete with all the information needed.

References

- Acquaviva A., Blaso L., Dalmasso D., Lo Verso Valerio R.M., Osello A., Patti E., Pellegrino A., Piumatti P. (2012). Increasing energy efficiency in existing public buildings through the implementation of a Building Management System based on interoperable networks. In: The 2nd International Conference on Building Energy and Environment (COBEE), Topic 10 - Intelligent buildings and advanced control techniques, Boulder, Colorado, August 1-4, 2012, pp. 929 – 936, ISBN 9780981688190.
- Eastman C., Teicholz P., Sacks R., Liston K., (2008). BIM Handbook. A guide to Building Information Modeling for Owners, Managers, Designers, Engineers, and Contractors, John Wiley & Sons, Hoboken, New Jersey, p. 66.
- Fracastoro G.V., Virgone J., Aghemo C., Pellegrino A., Blaso L., Savoyat J., Johannes K. (2012). Energy efficiency in public buildings through ICT based control and monitoring systems, In: Proceedings of the 5th International Building Physics Conference (IBPC), Kyoto, 28-31 May 2012, pp. 825-832.
- Larson G. W., Shakespeare R. A. (1998). Rendering with Radiance. The Art and Science of Lighting Visualization, Morgan Kaufmann Publishers, ISBN 1-55860-499-5.
- Mardaljevic, J., (1995). Validation of a lighting simulation program under real sky conditions. In: Lighting Research and Technology, December 1995, Vol. 27 no. 4, pp. 181-188.
- Osello A. (2012). The Future of Drawing with BIM for Engineers and Architects, Dario Flaccovio Editore, Palermo, pp.41, ISBN 9788857901459.
- Pellegrino A. (2012). Drawbacks and perspectives of the use of computer simulations in lighting design, in: Atti e Rassegna Tecnica – Società degli ingegneri e Architetti di Torino, vol. LXVI n. 1-2-3, pp. 281-289.
- Reinhart C.F., (2001). Daylight Availability and Manual Lighting Control in Office Buildings “Simulation Studies and Analysis of Measurements, Ph.D. thesis, Technical University of Karlsruhe, Faculty of Architecture, October 2001.
- <http://seempubs.polito.it/>
- <http://buildingsmart.com/standards/buildingsmart-standards/ifc>
- <http://www.gbxml.org/aboutgbxml.php>

Active slab design by lab tests and modelling

Stefano Avesani – Eurac Research, Bolzano, Italy

Daniel Neyer – University of Innsbruck, Innsbruck, Austria

Paolo Baldracchi – Eurac Research, Bolzano, Italy

Ulrich Filippi Oberegger – Eurac Research, Bolzano, Italy

Roberto Lollini – Eurac Research, Bolzano, Italy

The design of a prefabricated active slab for heating and cooling has been supported by lab tests and simulations. The aim was to find performance indicators of an active concrete slab for different reference office rooms and climate conditions. Control strategies in terms of radiant circuit mass flow, inlet temperature, room set point, and temperature deadband have been assessed regarding indoor thermal comfort and energy demand of the investigated thermal zones. The work has given the possibility to test and simulate the behaviour of the slab and to assess the approaches. The methodology consisted of the following steps: (i) design with one-dimensional finite difference models of a pipe heat exchanger, lumped parameter models in TRNSYS and a three-dimensional finite element (FE) model, (ii) first prototype realization and lab test, (iii) refinement and validation of the models according to lab test results, and (iv) parametric studies on reference rooms. Tests have been performed with a double climatic chamber (ISO 8990) connected to an external hydraulic circuit simulating the energy generation system. The models have been used to calculate transient and steady-state temperature and heat flux fields. The FE model consists of the slab with the inlet fluid temperature as step forcing function. Parametric studies of the hygrothermal behaviour of two adjacent rooms have been performed in TRNSYS using reference weather files of three climates, four room geometries and four thermal loads. For each boundary condition, several temperature deadbands and inlet temperatures have been considered. A performance database has been created supporting companies and engineers in components sizing for integration in HVAC systems and optimization of control strategies depending on internal and external loads.

1. Introduction

Low temperature radiant slab technologies match the challenge of energy demand reduction and exploitation of renewable energy in terms of performance and costs (Koschenz M., 2000). Low temperature and buffering of peak loads advance the usage and efficiency of renewable technologies such as solar thermal systems and heat pumps. The use of radiant systems has been spreading since their first commercial installations in the 80's, so that today many products are on the market. The possibility of integrating the radiant circuit already during the prefabrication phase enhances working precision and ease of installation. On the other hand, some structural constraints do not offer much flexibility in the radiant system design such as the position of the coil within the prefabricated slab. In the literature, many studies deal with improvements in modelling and testing of radiant systems (Sattari S., 2006; Karlsson H., 2006; Ferkl L., 2010; Okamoto S., 2010; Al-Othmani M., 2009; Tian Z., Love J.A., 2009). The suitability of simplified models depends mainly on geometry and operation parameters of the system, such as the mass flow rate. On the other hand, detailed models involve strongly coupled space and time dependent physics and are therefore complex to develop and computationally expensive.

Goals of the work have been: the support of a company in the design and optimization of a prefabricated radiant slab, the provision of standard performance figures for the built product, and the development and assessment of control strategies. In this paper, a critical overview of methodology and results is given.

2. Methods

The methodology has been based on simulations and lab tests. First, the slab's thermal behaviour was tested in the lab. Next, numerical models were calibrated according to test results and known parameters. Finally, the models were run to predict the slab's thermal performance under the design boundary conditions.

Several models have been built depending on the design goals. Preliminary design was based on a simplified one-dimensional (1D) finite difference model (FDM). 3D Finite Element Models (FEM) were used for the calculation of the temperature field and heat fluxes fields under steady state standard boundary conditions as described in the UNI EN 1264 (UNI EN 1264, 2009); the slab operation modes were computed and evaluated with TRNSYS for four reference offices (single, double, open office and meeting room) in three different climates (Bolzano, Brunico and Venice). Lab measurements provided both steady-state and transient values, FEM models were run only in steady-state and TRNSYS simulations gave the transient behaviour of the slab.

2.1 Description of the radiant slab

The radiant system proposed by the company is a concrete prefabricated slab with a hydraulic circuit embedded close to the ceiling. Pipes have an external diameter of 0.02 m and a spacing of 0.15 m. In Fig. and Table , a typical construction is specified.

2.2 Lab test

The active slab was tested within the guarded hot box at EURAC (Giovanardi A., 2010). The lab is equipped with two fully instrumented climatic chambers, one external hydraulic circuit (providing water at desired temperature and mass flow), and a solar simulator (not used in this case). The testing concept consisted in maintaining constant boundary conditions on the surfaces of the sample and in feeding the hydraulic circuit with a controlled water temperature and flow, considering both winter (heating) and summer (cooling) conditions. The aim of the tests was to

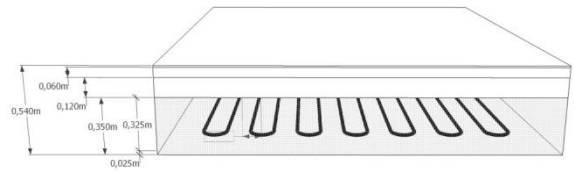


Fig. 1 – Active slab with coil close to the ceiling.

MATERIAL	LAMBDA/RHO/CP	THICKNESS
Name	[W/mK]/[kg/m³]/[J/kgK]	[m]
Concrete	2.1 / 2500 / 840	0.025
Pipeline PEX	0.35 / 938 / 1000	0.02
Concrete	2.1 / 2500 / 840	0.025 + 0.28
Lightweight concrete	0.08 / 350 / 400	0.12
Screed	1.4 / 2150 / 840	0.06
Floor	1.5 / 2300 / 1000	0.01

Table 1 – Slab construction from bottom (ceiling) to top (floor).

measure the surfaces' heat fluxes through the ceiling and floor and their temperatures. Measurements both of the initial and final steady-states and of the transient period between these two were performed. Tests with step function boundary condition were carried out according to the following procedure: (i) keeping constant boundary conditions at the slab surfaces (air velocity and temperature) and constant fluid flow rate and temperature; (ii) step variation of fluid flow and temperature; (iii) achievement of steady-state after a step variation of the fluid inlet temperature.

Table 2 summarizes the tests carried out and the imposed boundary conditions. During all tests, the variables reported in Table 3 were measured.

	T air [°C]	T inlet fluid [°C]	Mass flow [l/h]
H	20	From 20 to 25	113
H	20	From 25 to 35	113
C	26	From 26 to 22	113
C	26	From 22 to 17	113
H	20	23 (first 6 hours) and 25 (second 6 hours)	113 on/off
H	20	25	113 ± 20%

Table 2 – Test conditions of the slab (H: heating conditions; C: cooling conditions).

Although the active slab is a horizontal building element, it was tested in a vertical position, the only one allowed by the setup of the guarded hot box. However, both climatic chambers, hot and cold, were set up in order to reproduce reliable boundary conditions controlling the temperature and keeping the velocity of the airstreams directed on the target surfaces constant.

Variable	Sensor type	Position
Slab surface temperatures	Thermo couples	16 points on the ceiling, 9 points on the floor
Internal chamber surface temperatures	Thermo couples	9 per chamber
Heat fluxes	Heat plate (0.49 m x 0.49 m)	1 for the ceiling and 1 for the floor
Chamber air temperatures	Pt100	9 sensors per chamber
Mass flow	Electromagnetic meter	1 in the hydraulic circuit
Water temperatures	Pt100	1 at the inlet and 1 at the outlet of the hydraulic circuit

Table 3 – Lab measurements' points and sensor typology.

The heat flux through the floor surface was directly measured with the heat plate as measured temperatures on the floor surface differ by less than 0.3 K - therefore also the heat flux through it can be considered homogeneous. The same procedure could not be applied for the ceiling due to the inhomogeneity of the heat flux near the coil. Hence, the ceiling heat flux at steady state conditions was calculated as the difference between the total heat flux transferred from the fluid to the slab and the heat flux measured at the floor. Radiant and convective surface heat transfer coefficients were estimated for both floor and ceiling using surface (floor, ceiling, and chamber wall) and air temperatures, air velocity, and heat plate measurements.

2.3 FEM model

The aim of developing a FEM model was to evaluate the slab thermal performances (i) under steady-state reference boundary conditions (as stated in the norms), (ii) both for the tested specimen and for the maximum slab dimensions (respectively 2.4 m times 2.4 m and 6 m times 2.4 m), and (iii) for different mass flow rates. A 3D FEM model was set up in COMSOL, coupling heat transfer in solids and fluids with fluid dynamics. The model was validated with lab data as explained afterward.

The FEM model consists of two steady-state decoupled submodels with Dirichlet boundary conditions at the internal surface of the pipe determined iteratively. In Submodel A, the 3D heat transfer in solids was solved on the material layers (one cuboid for each material) and on the pipeline (linear extrusion of an annulus). In Submodel B, the pipe was considered stretched, without curves. Hence, a 2D rectangle was set as the domain to which the equations of fluid dynamics and fluid heat transfer were applied. The hypothesis of axial symmetry at the pipe centre was used. Moreover, the pipe thickness was modelled just in 2D as a rectangle as well. The link between Submodel A and Submodel B was performed imposing the temperature calculated in the other Submodel at the common interface (cylindrical pipe surface for the 3D Submodel A and line 7 for the 2D Submodel B - Fig. 2).

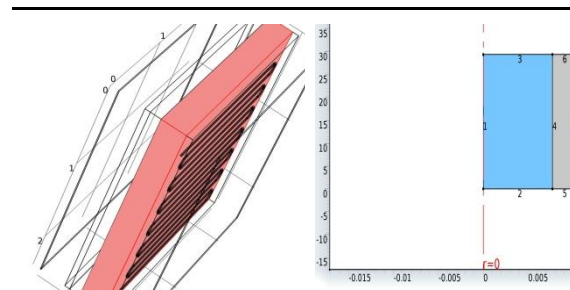


Fig. 2 – 3D slab model without pipe (left). 2D pipe model symmetric on the pipe centre axis (x axis = radius, y axis = length): highlighted the boundary condition on line 7 interface between the 2D and 3D models (right).

Steady-state 3D heat transfer in solids (Submodel A) is governed by Equation 1:

$$\nabla \cdot (\lambda \nabla T) + \dot{Q} = 0 \quad (1)$$

Steady-state 2D fluid dynamics and heat transfer in fluids (Submodel B) is described by Equations 2 and 3:

$$\rho(\mathbf{u} \cdot \nabla)\mathbf{u} = \nabla \cdot [-p\mathbf{I} + \mu(\nabla\mathbf{u} + (\nabla\mathbf{u})^T)] \quad (2)$$

$$\rho c_p \mathbf{u} \cdot \nabla T = \nabla \cdot (\lambda \nabla T) + Q \quad (3)$$

Model boundary conditions were set as follows. For Submodel A, the surface heat transfer coefficients, surface emissivity and ambient and boundary surfaces' temperatures were kept constant at the slab's bottom (ceiling) and top (floor) surface, while adiabatic conditions were assumed along the slab's lateral surfaces. For Submodel B, inlet fluid velocity and temperature as well as outlet pressure were kept constant.

The mesh was generated featuring a fine grid in the most critical regions (especially at the fluid-solid interfaces and in the volume of the pipeline) and a coarser one where large gradients of temperatures were not expected - due to the high thermal resistance from the pipe plane to the floor. Boundary conditions were: the fluid inlet temperature and mass flow, the reference pressure at the fluid outlet (2D model), the temperature at the solid interface between pipe and concrete (2D and 3D model), the convective heat exchange coefficient on the ceiling and floor surfaces, the reference ambient air temperature, the infrared emissivity of the ceiling, the floor and the two reference boundary surfaces parallel to them (3D model). For these two planes the surface temperature was also set. All other boundary surfaces have been set adiabatic.

The FEM model was validated by comparing steady-state surface heat fluxes and temperatures and outlet fluid temperatures with the respective test outputs. Hence, lab boundary conditions were set in the FEM simulations and the surface emissivity and convective heat transfer coefficient of the surfaces tuned until an agreement between the two was reached. Outputs of the model are 3D fields of surface temperatures and heat fluxes and outlet fluid temperature.

2.4 TRNSYS Model

TRNSYS 17.1 was used to estimate the yearly performance of the activated slab for different usage profiles, control strategies, and climates. The

model of thermo-active building element (Koschenz et al., 2000) avoids the complex and computationally expensive FE calculations, nevertheless allowing yearly performance estimates. The 2D solution of the heat conduction differential equation can be represented by a network of resistances. This model has strong geometric limitations (TRNSYS 17.1, 2012). Therefore, a workaround was devised and tested in order to overcome these restrictions. Construction properties were manipulated so that all geometric and resistance criteria were fulfilled and the resulting heat fluxes and surface temperatures match the lab test results. To find these properties (density, heat capacity, conductivity, and the thickness) a two-thermal zones model simulating the hot box setup (vertical slab separating left and right chambers) was created. Lab boundary conditions (air temperature inside the chamber, the chamber internal surfaces' temperatures, and the air speed along the slab) were used. By tuning the radiative and convective heat transfer coefficients and entering measured fluid inlet temperatures into the model, the deviation between measured and simulated fluid outlet and slab surface temperatures was minimized. The properties used in the following simulations are a tube wall thickness of 0.045 m, a conductivity of 4.2 W/(mK), a capacity of 420 J/(kgK) and a density of 1250 kg/m³. Infrared radiation was modelled with the TRNSYS detailed model based on view factor. Heating and cooling demand were calculated based on the fluid temperatures. The parametric study performed in TRNSYS considered different thermal zone geometry, ventilation rates, and internal loads. For the yearly simulations, four different profiles were defined based on the Swiss standard SIA 2024 (SIA 2024, 2006). They were applied to each of the following reference rooms: single office, double office, meeting room, and open space office. The lighting schedule is further multiplied by an on/off control signal. In the following, the relevant boundary conditions are exemplified for the double office room.

The arrangement of the reference rooms was chosen such that the influence of up- and downward directed energy fluxes could be studied. Both rooms were treated in the same way (internal loads and temperature setpoint), leading to a two thermal zone

one over the other, with only one external wall and one window per zone. Some other important boundary conditions are explained in Table 4.

As a control strategy, a simple on/off controller was chosen. The effect of different deadbands and temperature setpoints were studied. A graphical explanation of the working of the controller can be found in Fig. 3 with heating and cooling setpoints equal to 21°C and 26°C, respectively, and a deadband of 1 K for heating and cooling.

The operative temperature (simplified as the average of radiation and air temperature) was used as an input variable to the controller.

3. Results

3.1 Standard steady state and dynamic performance figures

The lab test and FEM simulations gave steady state performances at lab and normed boundary conditions (UNI EN 1264), respectively. Energy performances were assessed in terms of surfaces'

Name	Specification
Climate/ weather	Bolzano, Brunico, Venice (IT) Source (METEONORM 7)
Constructions / orientation	South surface "external", all inner walls "adiabatic", radiant slabs with "active layer" (Table) between zones
Windows	U-value 0.61 W/m ² K, g-value 0.402, TRNSYS window ID 13004, area 60% of total wall surface
Shading	External, $f_c = 0.4$; on if $I > 140$ W/m ² and off if $I < 120$ W/m ² on the receiver
Ventilation	$n = 36\text{m}^3/(\text{h p})$, T_{supply} min 18°C, max 26°C
Infiltration	$n_{50} = 1.5$ air changes per hour
Internal gains	According to SIA 2024
Persons	According to SIA 2024
Light	According to SIA 2024, plus: off if I >140 W/m ² , on if $I < 120$ W/m ²
Supply temp. heating/cooling	Parametrically changed, but constant during each simulation; 30°C, 28 °C, 26 °C for heating / 15°C, 17°C, 19°C for cooling
Active layer geometry	Geometry shown in Figure 1

Table 4 – Table of TRNSYS boundary conditions used

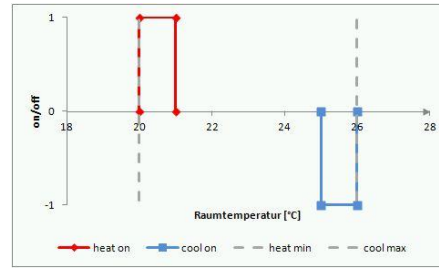


Fig. 3 – On/off controller with deadbands and temperature setpoints

heat fluxes against logarithmic temperature differences between water and ambient temperatures. Heat flows mainly through the bottom surface, as the thermal resistance of the layer delimited by coil and top surface is much higher ($R_{\text{ceiling}} = 0.011$ m²K/W, $R_{\text{floor}} = 1.7$ m²K/W). In fact, the rate between ceiling and floor specific heat flux is more than 15. In Figure 4 both lab test and FEM simulations results are reported. Ratios between heat flux and logarithmic difference of temperature are 6.5 and 4.6 in heating, 5.7 and 6.2 in cooling for lab and FEM respectively.

Surface temperatures were also measured and evaluated from the point of view of radiant discomfort. Ceiling and floor temperature differences were compared with the comfort classes' limits suggested by (EN ISO 7730). For a fluid inlet temperature of 35°C, the average surface temperature difference between ceiling and floor at the steady-state condition goes up to 5 K (Fig. 5).

In FEM simulations, after validation, standard boundary conditions according to EN 1264 were set in order to provide the slab thermal performances as required by that norm. Results are reported in Fig. 4, Fig. 6 and Fig. 7. The ceiling surface has the higher temperature gradients all over the surface. The maximum temperature difference reaches 7 K and is between the inlet corresponding point (the warmest) and the lower right corner (Fig. 4).

FEM models were used to evaluate the impact of a bigger slab with different mass flow rate on the slab thermal performance. The role of the mass flow rate is to assure adequate heat fluxes through

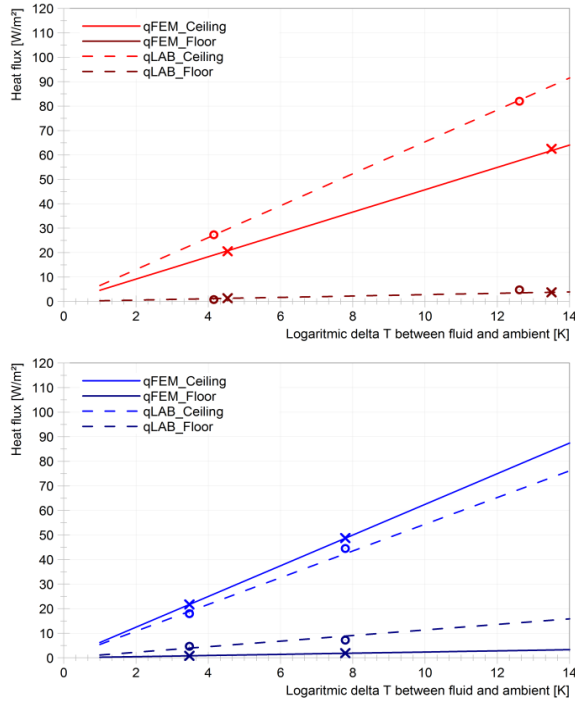


Fig. 4 – Lab test and 3D FEM simulations results in heating (above) and cooling (below).

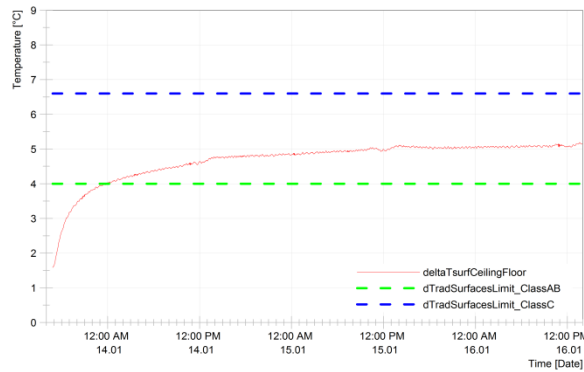


Fig. 5 – Measured temperature difference between ceiling and floor in heating mode in time. Temperatures averaged over the sample surface.

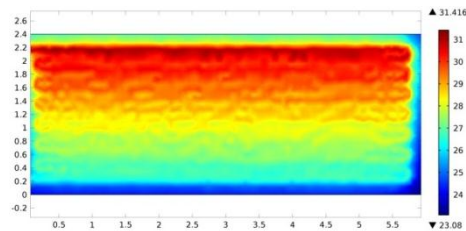


Fig. 6 – FEM steady-state ceiling surface temperatures: inlet fluid temperature 35°C; mass flow rate 113 kg/h; slab dimensions 2.4 m times 6 m.

the surfaces and fluid inlet-outlet temperature differences of at most 5 K (as recommended by design). Hence, a comparative assessment of the heat fluxes has been performed (Fig. 7). For a

bigger slab, differences are not relevant ($< 2 \text{ W/m}^2$). Nevertheless, for a bigger slab the inlet mass flow plays a role impacting with $\pm 15 \text{ W/m}^2$ for a mass flow rate doubling/halving.

The time-dependent thermal response of the slab was measured in the lab. Fig. 5 shows the time range between two steady-states - the initial condition at 20°C and the final conditions with fluid inlet temperature of 35°C and surface heat fluxes constant in time. Nevertheless, steady-state conditions will never be realized in a system installed in an actual building as the normally employed control strategies are based on thermal charging and discharging of the concrete depending on the setpoints and on the real (dynamic) boundary conditions. Therefore, heat fluxes through the slab surfaces were also evaluated in an on-off test, in which the circulating pump was periodically switched on and off every three hours representing a possible control strategy. After three hours, more than 50% of the steady-state power had been reached (Fig. 8).

Even if the slab thermal response is quite slow (time constant of 6 h with driving temperature difference between fluid inlet temperature and environment of 5°C), the high thermal inertia of the system delivers a satisfactory amount of energy to the ambient also when the pumps are off (90 Wh/m² for fluid inlet temperature of 25°C).

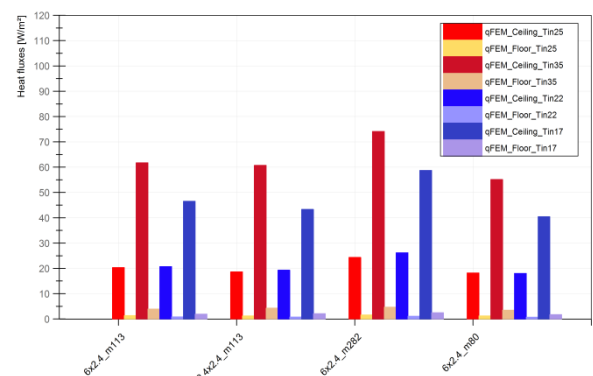


Fig. 7 – Parametric analysis of active slab: slab dimensions and inlet fluid mass flow vary.

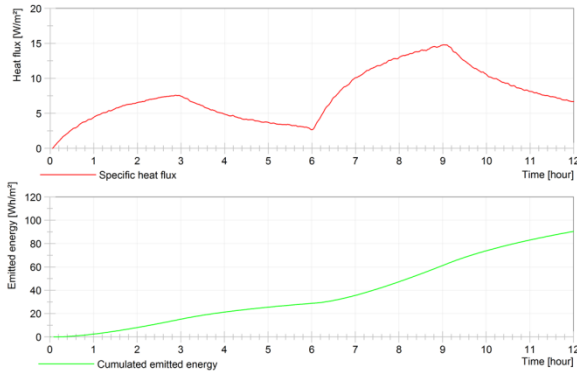


Fig. 8 – Radiant heat and energy at the ceiling surface obtained in a 12 hours lab test (heating mode) using an on-off based control strategy.

3.2 Energy demand and thermal comfort

Concerning the model accuracy, between lab and TRNSYS results, referring to steady state and dynamic lab tests' and TRNSYS's results in heating and cooling modes, a maximum average deviation of <5% for the fluid outlet temperature, <10% for surface temperatures and <15% for the heat flux directed up- and downwards could be achieved.

The TRNSYS simulation results have been analysed in terms of energy demand for heating and cooling, on-off control cycles, running hours of the pump, and thermal comfort. Results for the Bolzano case are only reported in detail: the Brunico and Venice results are summarized at the end. Hysteresis deadband for the on-off regulation of the slab pumps, fluid inlet temperatures, air setpoints were parametrically changed. The heating and cooling demand increases slightly with an increase of the deadband Fig. 9.

Considering ideal load calculation (no plant) ventilation losses for supplying to the indoor environment with neutral air (20°C in heating and 26°C in cooling) are 24 kWh/m²y and 1.2 kWh/m²y in winter and summer respectively. Transmission losses account for 13.5 and 6 kWh/m²y in winter and summer respectively. Adding the active slab, energy demand varies between 15.3 and 23.8 kWh/m²y depending on the deadbands.

Furthermore, results show that differences in annual energy demands using other supply temperatures (15/30, 17/28, 19/26, and ideal) are less than 1 kWh/(m²y). This is not true for the number of on/off cycles or the running hours. With increasing deadband, the number of on/off cycles

decreases. The minimum is at about 20 cycles per year for a deadband of 5 K. The running hours react the other way round but with another trend. A large deadband implies long pump operation until the tripping point is reached.

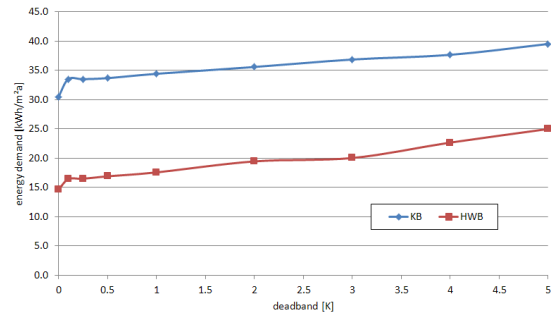


Fig. 9 – Evaluation of the heating (HWB) and cooling (KB) demand for the Bolzano case and different deadbands.

An analysis of the air temperature distribution over a year shows that the output power of the slab, for constant mass flow and temperature of the fluid, is high enough to reach the minimum and maximum required temperatures – also for other fluid inlet temperatures. Minimum and maximum allowed temperatures (20°C and 26°C) are actually always respected (Fig. 11).

The thermal comfort analysis was done based on the Predicted Mean Vote (PMV) as defined in the ISO 7730 (EN ISO 7730, 2006) and in (Fanger P.O, 1982). One representation is shown in Fig. 12, which reports the time distribution of the PMV over the year for different control deadbands (with constant parameters $c_{lo}=1$, $m_{et}=1.2$, $v=0.2$ m/s).

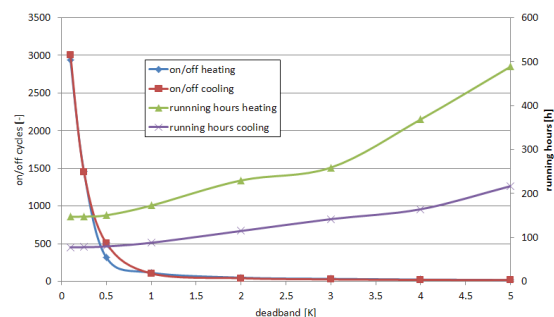


Fig. 10 – Evaluation of pump running hours and on/off cycles for heating and cooling for the Bolzano case and different deadbands.

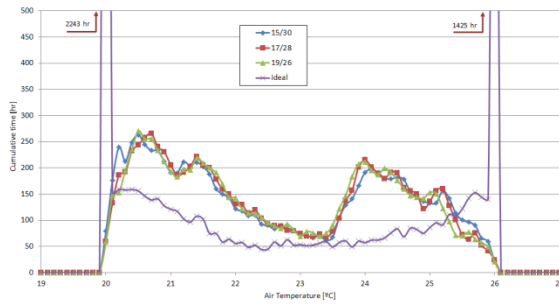


Fig. 11 – Evaluation of the temperature distribution over a year for the Bolzano case and different supply temperatures.

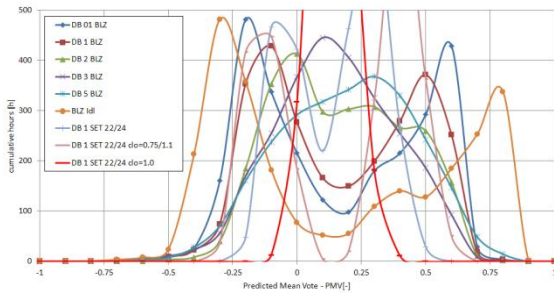


Fig. 12 – Evaluation of the thermal comfort in terms of cumulated number of hours of use of the system in a year for different deadbands and setpoints during which the PMV has the indicated value.

Only the right hand PMV peaks for ideal system (no deadband), 0.1 K and 1 K deadband are outside the allowed class B (maximum of 10% thermally dissatisfied people and $PMV \pm 0.5$ (EN ISO 7730)).

Analogous simulations have been performed for other climates (Venice and Bruneck in Italy) as well. Moreover, extremes like sudden temperature drops or bad architectural solutions (excessive glazing) have been analysed.

Concerning Venice's humid climate, simulations have been done both with and without humidity control systems. Without any strategy against condensation apart from standard on-off pump control, in the Venetian climate, for defined ventilation rates and internal loads, condensation occurred after 7.5 hours equivalent to 30 simulation time steps. Increasing the supply temperature from standard 15°C up to 19°C reduce the number of condensing hours, but not eliminate it.

In the extreme conditions mentioned above, no problems with the heating and cooling power supply occurred. Neither for the extreme glazing (80% of the external wall surface) in combination with an extreme profile for a meeting room (internal and external loads, simultaneously), nor

for an outdoor temperature drop of ± 10 K (leading to outdoor air temperatures around $-20^{\circ}\text{C}/+40^{\circ}\text{C}$), the maximum power limits have been reached.

4. Conclusions and discussion

In this paper the methodology used to model and test a radiant prefabricated slab are shown together with the achieved results. The following issues have been faced and resolved.

Methodology: Key parameters for the modelling and testing have been the convective heat exchange coefficients, the emissivity and the active surfaces' view factors. If convection and radiation measurements and calculation are not accurate enough, neither the energy demand (heating and cooling), nor the thermal comfort can be predicted reliably. Lab and FEM results have had different purposes: lab tests have been used just to validate the models - as the lab convective heat exchange coefficients could not be changed. FEM simulations have aimed at evaluating the performance at norm boundary conditions, for different slab dimensions, fluid inlet temperatures and flow rates.

Differences in the lab and FEM steady-state performance reported in Fig. 4 are discussed here: firstly values of the surface heat exchange coefficients in lab and in simulations have been different (as reported in Table 5). Secondly, the lab chambers' ambient conditions could not be kept exactly at 20 (and 26) °C in heating (and cooling) mode: the chamber air temperature differed from the set point by a maximum of 0.7 K. The chamber surfaces reached a maximum of 2 K difference with the air setpoint.

Lab: A radiant device was tested in the guarded hot box with the support of a hydraulic circuit with variable fluid inlet temperatures and mass flow rates. Steady-state performances have been measured. Other dynamic tests, such as the on-off control of the circulation pump, were performed and showed interesting results for the evaluation of the slab reaction time. Besides the time constant, the dynamic variation of the heat flux and the released energy based on a three hours on-off

	Laboratory	FEM (EN1264)
	[W/m ² K]	[W/m ² K]
h radiant ⁴	4.8	4.9
h convective	~ 10 - 12 (ceiling heating and cooling) ~16 (floor heating and cooling)	5.5 (heating floor, cooling ceiling) 1.5 (cooling floor, heating ceiling)

Table 5 – Surface heat exchange coefficients for lab tests (air velocity flowing on the floor surface is higher than the ceiling) and FEM simulations (convective coefficients from the UN EN 1264)

pump control strategy were measured, offering more useful information for the designers.

Measurements and calculation of the heat fluxes have been performed with different methods. Direct measurements of the heat fluxes (with a 0.4 m times 0.4 m heat plate) and of the temperatures are very sensitive to the positioning of the measuring device on the slab surface, especially for inhomogeneous temperature fields (as caused by the thermoactive coil close to the slab bottom surface). Indirect measurements, based on the energy delivered to / absorbed by the slab, show more robustness.

FEM: FEM models' results were very useful for detailed evaluation of the space temperature fields which have deep implication in the thermal indoor comfort assessment (Fig. 6). Nevertheless, simplifications in the modelling approach and in the mesh choice have to be carefully considered balancing between model reliability and usability. As an example, surface temperatures fluctuations of Fig. 6 are mainly due to a too coarse 3D mesh. These steady-state calculations needed a simulating time in the order of 0.5 hours with a 4 core 16 Gb RAM calculator. Time-dependent 3D FEM models were not used because of the unaffordable calculation time without further model simplification.

TRNSYS: Simplified models - such as the TRNSYS model - have some strong limitations, but work well within clearly defined ranges if tuned with measurement data.

The radiant slab: The studied thermo active slab shows a good performance in terms of power, energy and thermal comfort if it is combined with a mechanical ventilation system that can supply neutral air to the indoor environment. In fact, the active slab can cover the transmission losses and the part of the ventilation losses not covered by the heat recovery system, resulting in an heating energy demand of circa 18 kWh/m²y for a deadband of 0.5 K. The increase of the energy demand with the deadband Fig. 9 can be explained by an overheating or overcooling up to a certain level before the system is switched off.

Power peaks covering was verified simulating unfavourable climate conditions and building features. Nevertheless, setpoint temperatures could have been kept because the simulated air conditioning system had enough power to supply air at adequate temperature. The slab provides the base load and the air conditioning system the peak load (like the sudden temperature drop).

Considering global indoor comfort, PMV time frequency over the year changes with the increasing deadband, from two peaks (corresponding to the two setpoint – heating and cooling) on both sides to a single peak (Fig. 12). This is mainly because the heating and cooling setpoints have not been optimised – just fixed at 20°C and 26°C. If the setpoints and the clothing factors were optimised, an ideal distribution could be reached with a setpoint of 22/24°C and a clothing factor of one.

As is clear in Fig. 5, floor-ceiling temperature difference could have an impact on the radiant asymmetry local discomfort switching from comfort class A-B and to C in case of high fluid inlet temperature (35°C) and standard mass flows (19 kg/m²h).

Dynamic tests show that the slab reaction time is low in terms of time constant; nevertheless, simulations have allowed to verify the low risk of overheating and overcooling with a correct on-off control strategy.

Considering the active slab key parameters, the main differences in heat fluxes and surface temperatures are caused by varying the mass flow rate (just for a bigger slab), while slab dimensions have less influence on the results for a well-

⁴ Linearized radiant coefficient

designed mass flow. On the one hand, a bigger slab means a longer coil and more heat losses along it. A bigger slab means less influence of boundary effects on pipe heat transfer. The mass flow rate plays an important role in controlling the fluid inlet-outlet temperature difference and the resulting surface temperatures that in turn determine the heat fluxes.

To avoid condensation in humid climates, either the supplied air can be dehumidified, or the slab surface temperature has to be kept above a certain level. This can be done using a higher supply temperature or a control strategy that switches the cooling off before the surface is getting too cold. With condensation occurring only during few hours, and keeping hydrothermal comfort conditions throughout the year in a reasonable range, a shutdown of the cooling system could be sufficient.

5. Nomenclature

T	Temperature [K]
u	Velocity [m s^{-1}]
p	Pressure [Pa]
Q	Heat flux [W]
F	Volume forces [N m^{-3}]
C _p	Specific heat [$\text{J kg}^{-1} \text{K}^{-1}$]
μ	Dynamic viscosity [Pa s]
ρ	Density [kg m^{-3}]
λ	Conductivity [$\text{W m}^{-1} \text{K}^{-1}$]

References

- Koschenz M., Lehmann, B., 2000, Handbuch Thermoaktive Bauteilsysteme TABS, EMPA Energiesysteme / Haustechnik, Dübendorf Schweiz.
- METEONORM 7, www.meteotest.ch, (last accessed November 2nd 2012).
- TRNSYS 17.1, The Transient Energy System Simulation Tool, www.trnsys.com, (last accessed November 2nd 2012).
- SIA 2024, Merkblatt 2024: Standard-Nutzungsbedingungen für die Energie- und Gebäudetechnik, schweizerischer Ingenieur- und architektenverein, Zürich, 2006
- Fanger P.O., 1982, Thermal comfort, analysis and applications in environmental engineering, Reprint. - Malabar, Fla.: Krieger
- EN ISO 7730, 2006, Ergonomics of the thermal environment
- UNI EN 1264, 2009, Water based surface embedded heating and cooling systems
- Sattari S., 2006, A parametric study on radiant floor heating system performance, Renewable Energy 31 (10) (2006) 1617–1626
- Karlsson H., 2006, Thermal system analysis of embedded building integrated heating: numerical model and validation of hydronic floor heating systems, Chalmers Reproservice, Sweden
- Okamoto S. et al., 2010, A simplified calculation method for estimating heat flux from ceiling radiant panels, Energy and Buildings 42 (1) (2010) 29–33
- Ferkl L., Sirok J., 2010, Ceiling radiant cooling: comparison of ARMAX and subspace identification modelling methods, Building and Environment 45 (1) (2010) 205–212
- Al-Othmani M. et al., 2009, Experimental and Theoretical study of transient human thermal comfort response in convective and radiative environments, HVAC&R Research 15 (5) (2009) 855–873.
- Tian Z., Love J.A., 2009, Energy performance optimization of radiant slab cooling using building simulation and field measurements, Energy and Buildings 41 (3) (2009) 320–330
- A. Giovanardi, P. Baldracchi, R. Lollini, 2010. A new test rig for the assessment of building envelope components integrating solar active systems. Eurosun - International Conference on Solar Heating, Cooling and Buildings, Graz

Investigation of different simulation tools for solar photovoltaic modules

Francesco Frontini – University of applied Science and Arts (SUPSI), Canobbio, Switzerland

Matteo Marzoli – University of applied Science and Arts (SUPSI), Canobbio, Switzerland

Narghes Doust – Politecnico di Milano, Milano, Italy

Abstract

Renewable energy resources will be an increasingly important part of power generation in the new millennium. Besides assisting in the reduction of the emission of greenhouse gases, they add the much-needed flexibility to the energy resource mix by decreasing the dependence on fossil fuels. Furthermore, as many international studies have already demonstrated, the use of photovoltaic is a crucial point to achieve the Net Zero Energy Building (nZEB) standard. In order to allow the designers to count on the renewable energy resources to compensate the energy needed, an easy and reliable tool is necessary, besides the building energy simulation tools. This paper aims to present a comparison between different simulation tools, in order to underline differences and similarities rather besides comparing the numerical responses.

Several parameters related to the PV panels will be discussed in order to compute their influence on each numerical model. Further investigations of this preliminary study will be done in order to analyse the PV models in order to find the best way to simulate and to model building integrate photovoltaic element (BIPV).

1. Introduction

Simulation modelling has become an important part of our world and it is used very often to predict different energy scenarios and to evaluate the cost-effectiveness of a particular solution. Simulation is also widely used to optimize new technologies and to investigate their behaviour in different context and configuration. Recent advances in simulation methodologies, availability of software, and technical developments have made simulation one of the most widely used and

accepted tools in system analysis and operation research.

Simulation tools are also used in the design phase of Photovoltaic systems. They are very important because this is the phase where the client decides if the Photovoltaic system is cost-effective and economically attractive or not.

For this reason in the last decade different tools have been developed both by PV industries and by Research institutes in order to help planners work. Mitchel et al 2009, identified 13 different types of software (RETScreen, NREL Solar Advisor, ESP-r, SolarGIS, INSEL, SolarDesign, PV F-Chart, PVSYST, TRNSYS, SolarPro, PV DesignPro-G, PV Sol, PV Sol Expert) but many others are available such as DDS-CAD, Polysun, Valentin Software, SolarNexus.

Within this work, the authors investigate the capability of three simulation tool for the modelling of photovoltaic (PV) system and how they can be improved to simulate building integrated photovoltaic elements: PVSYST as the worldwide known software for PV-system simulation, TRNSYS and ESP-r as worldwide used software for Building energy simulations.

2. Method

In order to compare the capabilities of the three software packages to simulate the PV-system production and its interaction with the building envelope, a simulation analysis was done for a building integrated photovoltaic (BIPV) system installed on a tilted roof of a low energy house in Bergamo. The city lies 249 m above sea level, with a latitude of 45.70°N and a longitude of 9.67°E. The annual total solar radiation in Bergamo is

1,398 kWh/m² with approximately 1,900 hours of sunshine.

Table 1 summarizes the technical specification of the considered PV panel. In all the performed simulations the model proposed by Perez was used (Perez 1988) to model the sky conditions and the radiation distribution of the tilted surface.

ELECTRICAL DATA		
Measured at Standard Test Conditions (STC): Irradiance 1000W/m², AM 1.5, and cell temperature 25° C		
Nominal Power (+5/-0%)	P _{nom}	333 W
Cell Efficiency	η	22.9 %
Panel Efficiency	η	20.4 %
Rated Voltage	V _{mpp}	54.7 V
Rated Current	I _{mpp}	6.09 A
Open-Circuit Voltage	V _{oc}	65.3 V
Short-Circuit Current	I _{sc}	6.46 A
Maximum System Voltage	IEC	1000 V
Temperature Coefficients	Power (P)	− 0.38 %/K
	Voltage (V _{oc})	− 176.6 mV/K
	Current (I _{sc})	3.5 mA /K
NOCT	45° C +/- 2° C	
Measured at Nominal Operating Cell Temperature (NOCT): Irradiance 800W/m2, 20° C, wind 1 m/s		
Nominal Power	P _{nom}	247 W
Rated Voltage	V _{mpp}	50.4 V
Rated Current	I _{mpp}	4.91 A
Open-Circuit Voltage	V _{oc}	61.2 V
Short-Circuit Voltage	I _{sc}	5.22 A
Number of cells connected in series in module		96
Individual module area (A)		1.63 m2

Table 1 – Technical specification of the PV panel

3. Description of the three tools

3.1 TRaNsient SYstems Simulation (TRNSYS)

TRNSYS is a commercially available simulation program, evolved in 1975. This software is the outcome of an international collaboration between the United States, France, and Germany. TRNSYS alleviates the accession of mathematical models, the potentialities of the multi-zone building model, the usable add-on components, able to port with other simulation programs. It is one of the most pliable energy simulation software packages. The main components used in the TRNSYS numerical simulation are based on mathematical models written in FORTRAN and are:

- type 56b: This component models the thermal behaviour of a building divided into different thermal zones; it is useful to include thermal behaviour of BiPV modules;
- type 194: Photovoltaic array. This component determines the electrical performance of a photovoltaic array. The model is based on the calculation method presented by DeSoto et al 2005 . Type 194 has been used in simulations involving utility grid connections. The model determines the current and power of the array at a specified voltage. Other outputs include current and voltage at the maximum power point.
- type 15: Weather Data Processor. This component reads and interprets weather data available in a series of standardized formats. In particular in the model implemented was used a Typical Meteorological Year version 2 (TMY2) format created with Meteonorm.

The model used in type 194 is based on the five-parameter equivalent circuit model that is presented in Duffie and Beckman 1999. The main thrust of this model is to reliably extrapolate performance information provided by the manufacturer at standard rating conditions (1000 W/m², 25 °C, 1.5 AM) to other operating conditions. The model, as described by De Soto et al. 2005, is based on the equivalent circuit diagram shown in Figure 2.

In particular the five parameters used to model the PV cell were calculated by an engineering equation-solver application which calculates the 5 parameters required to characterize the energy conversion from PV modules, according to the model developed by DeSoto et al 2005.

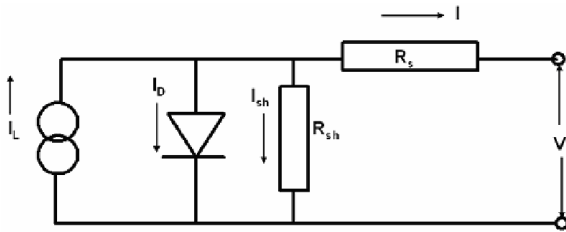


Fig. 1 – Equivalent electrical circuit

3.2 PVSYST

PVSYST (Mermoud, 1995) is a photovoltaic system analysis software program developed by the Energy Group at the University of Geneva in Switzerland and can be used at any location that has meteorological and solar insolation data. It is widely used due to the many parameters available for the user to modify. It is a PC software for the study, sizing, simulation and data analysis of complete PV systems. It is suitable for grid-connected, stand-alone, pumping and DC-grid (public transport) systems, and offers an extensive meteorological and PV-components database.

For POA (plan of array) radiation, the default is the model described in Hay 1979, however the user can also specify the Perez model (Perez et al. 1987). PVSYST uses the one-diode equivalent circuit model for calculating performance in cSi (crystalline silicon) and HIT (hetero-junction intrinsic thin layer) modules, and a modified version for what they consider “stabilized” thin film modules, such as aSi (amorphous silicon), CiS

(copper-indium (di)selenide or copper-indium gallium (di)selenide technologies) and CdTe (cadmium telluride).

The five parameters required by the model are defined, also in this case, from the engineering equations that govern the electrical process starting from standard conditions. Since this procedure may lead to solutions without physical meaning, just three of the equations are considered and an explicit choice of the resistance (R_s) parameter is directly performed by the user by means of a graphical interface. In the cases in which an experimental measurement of the complete I/V characteristic is available, the definition of the R_s parameter is defined minimizing the error between experimental data and model results (PVSYST User Guide 2012).

3.3 ESP-R

ESP-r is an integrated modelling tool for the simulation of the thermal, visual and acoustic performance of buildings and the assessment of the energy use and gaseous emissions associated with the environmental control systems and constructional materials. In undertaking its assessments, the system is equipped to model heat, air, moisture and electrical power flows at user determined resolutions.

The model in ESP-r actually comprises two models: a simple one based on a constant efficiency, and a more elaborate one based on an equivalent one-diode model.

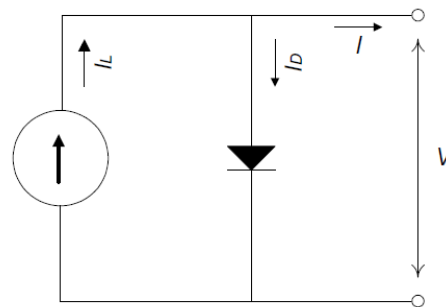


Fig. 2 – One diode model implemented in ESP-r

The current-voltage (I-V) characteristic of a solar cell can be obtained by considering an equivalent circuit of cell (Markvart 2000). This is known as the equivalent one-diode circuit and is illustrated in Fig. 2. The output current, I , is equal to the difference between light-generated current and the

diode current.

The data input requirements for the model are:

1. Open circuit voltage at reference conditions (V).
2. Short circuit current at reference conditions (Amps).
3. Voltage at maximum power point at reference.
4. Conditions (V).
5. Current at maximum power point at reference conditions (Amps).
6. Reference insolation (W/m²).
7. Reference temperature (K).
8. Number of series connected cells (not panels) (-).
9. Number of parallel connected branches (-).
10. Number of panels in surface (-).

To support PV-integrated building simulation and enable heat and power utilisation studies, the PV model has been implemented within the ESP-r system as active material. This guarantees a special behaviour to multi-layered construction nodes in order that they can transform some part of their absorbed solar energy to electricity according to the previously described mathematical model and the use of an electrical power flow network to allow the modelling of local electricity use and co-operative switching with the grid.

4. Simulation results

The aim of this paper is to compare the results of the three simulations. The power of the system and as a consequence the energy output is investigated. Further analysis has to be done to check the thermal characteristic of the BiPV modules.

The 10kWp BiPV system is installed on a tilted roof. The 30 high efficiency modules lie on the roof plane which it is tilted of 15° and with an Azimuth of 45° West (see Fig. 3).

The thermal characteristics of the building are reported in Table 2.

In order to understand the results of the three simulations, only two characteristic weeks' results are plotted (Fig. 4, Fig. 5): typical summer week and typical winter week.

Fig. 6 shows the predicted power generation of the BiPV array, respectively for a typical summer and winter week.

Looking at the results a good fit is observable between the three solutions. Some small differences (smaller than 11%) can be seen just near to the peak values (this is due to the predominance of the direct irradiance). This consideration may lead to conclude that the differences, even though small, in energy production are also influenced by

Model: comparison of BiPV model with TRNSYS and PVSYST

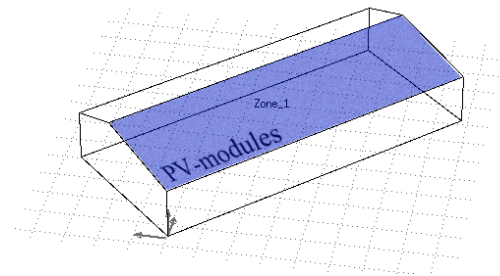


Fig. 3 – The picture shows the simulated model. It is one Zone model with a tilted roof.

	U-VALUE [W/m ² K]	Boundary
Roof	0.33	External
BiPV Roof	0.33	External
External wall	0.2	External
Partition	1.3	Adiabatic

Table 2 – Construction specifications

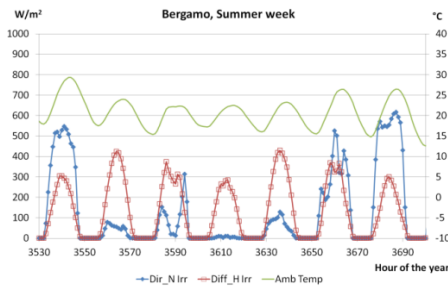


Fig. 4 – Typical Summer Week in Bergamo (ITA).

thermal models of the PV panel and not only from the definition of electrical parameters. Considering the whole year the total energy yield differences is about 5% between ESP-r and PVSYST and -11% between TRNSYS and PVSYST.

5. Conclusion

The simulation results using the one diode models implemented in TRNSYS, PVSYST and ESP-r are comparable. The three resulting energy curves have similar shapes both in winter and in summer. However, if we consider the PVSYST result as a benchmark, the TRNSYS model seems to underestimate the energy production during the seasons and the ESP-r model over-predict the amount of power generated at midday, especially on sunny days.

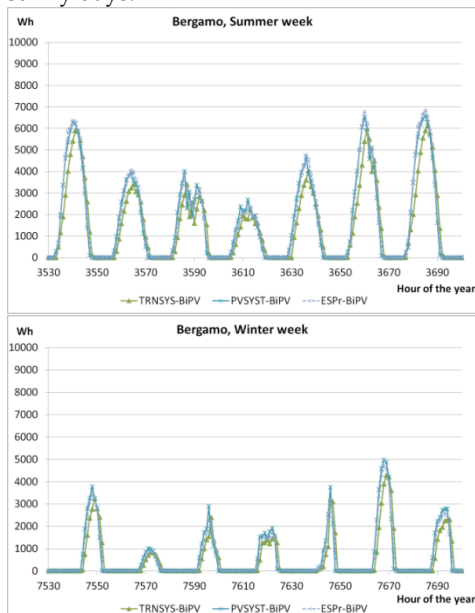


Fig. 6 – Left picture: power generation of the array predicted by the three simulation tools in a typical summer week. Right picture: power generation of the array predicted by the three simulation tools in a typical winter week.

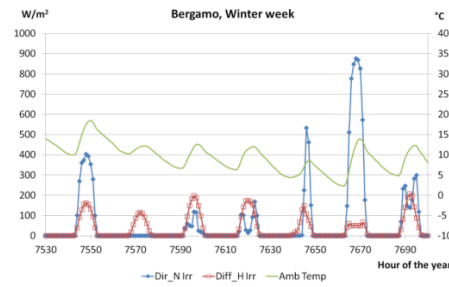


Fig. 5 – Typical Winter Week in Bergamo (ITA).

6. Discussion

Modelling building-integrated photovoltaics (PV) in building energy simulation tools presents many challenges. For example, photovoltaics respond to many environmental influences, such as irradiance, temperature, wind speed, angle of incidence of solar rays, and spectral distribution of irradiance. Furthermore, PV modules are susceptible to shading from one part of the building onto the module.

In addition, parameters characterizing PV modules are often hard to obtain. Manufacturer's data often provide relatively easy access to parameters such as open circuit voltage, short circuit current, and nominal efficiency under standard test conditions (1000 W/m², 25 °C, air mass 1.5). But representing accurately the electrical characteristics of the modules from such a small set of parameters, and under a wide range of environmental conditions, is challenging.



Fig. 7: Roofs and facade installation monitoring campaign is now ongoing at ISAAC-SUPSI to validate the tools prediction.

Finally, most PV simulations programs are chiefly interested in the power output of the module. By contrast, tools for energy simulation in buildings require additional outputs such as light reflected

by the modules and transmitted through it, and radiative, convective and conductive heat transfer at the front and the back of the PV array.

The author of this paper started to analyse the differences between the state of the art tools in order to identify a possible amelioration of the model.

A monitoring campaign is also needed in order to validate the present tools and to improve them. This is what is currently ongoing at the Institute for Applied Sustainability to the Built Environment (ISAAC-SUPSI). Different roof integrated BiPV modules and facade integrated PV systems are currently under investigation and the achieved result will be presented in a further research paper.

7. Nomenclature

Symbols

Amb	Ambient
BiPV	Building Integrated Photovoltaic
Diff_H	Horizontal Diffuse irradiation [W/m ²]
Dir_N	Normal Direct irradiation [W/m ²]
PV	Photovoltaics
Temp	Temperature [°C]

References

Klise G. T., Stein J.S. 2009. Models Used to Assess the Performance of Photovoltaic Systems, SANDIA REPORT (SAND2009-8258)

PVSYST documentation is available online at: <http://www.pvsyst.com/index.php>

TRNSYS documentation is available online at: <http://sel.me.wisc.edu/trnsys/>

ESP-R documentation is available online at: <http://www.esru.strath.ac.uk/Programs/ESP-r.htm>

Mermoud, A. 1995. Use and Validation of PVSYST, A User-Friendly Software for PV-system Design. 13th European Photovoltaic Solar Energy Conference, Nice, France.

DeSoto W., Klein S.A., Beckman W.A. 2005. Improvement and Validation of a Model for PV Array Performance, Solar Energy Journal.

Duffie J.A., Beckman W.A. 1999. Solar Engineering of Thermal Processes, second ed. Wiley Interscience, New York.

Hay J.E. 1979. Calculating of Monthly Mean Solar Radiation for Horizontal and Inclined Surfaces, Solar Energy, Vol. 23,1979, pp. 301–307.

Perez R., Stewart R., Arbogast C., Seals R., Menicucci D. 1987. A New Simplified Version of the Perez Diffuse Irradiance Model for Tilted Surfaces. Solar Energy, Vol. 39, 1987, pp. 221–231.

Perez, R., Stewart, R., Seals, R., and Guertin, T. 1988. The Development and Verification of the Perez Diffuse Radiation Model, Sandia Report SAND88-7030.

PVSYST User's Guide. 2012, PVsyst Contextual Help. <http://files.pvsyst.com/pvsyst5.pdf>

Social and energy redevelopment of an old building

Stefano Fortuna – University IUAV of Venice, Venice, Italy

Paolo Neri – LCA-lab, Bologna, Italy

Fabio Peron – University IUAV of Venice, Venice

Abstract

The experiment wants to show how a projection exploiting the knowledge of the life cycle analysis of materials has less impact than the same project without the use of this kind of analysis.

Recently, the life cycle analysis (LCA) has been commonly used as a check instrument in the design of new buildings, but it is not yet used regularly in existing redevelopments, most of all if they concern a very old building as the example below.

The life cycle assessment was introduced in 1993 by the SETAC (Society of Environmental Toxicology And Chemistry) and it is a method of systematic analysis that values the environmental impacts of a product, the process of production and its activities throughout the life cycle. The life cycle of products surrounds all the phases of the production and also the use and the end of the components of the process itself. The analysis starts from the extraction of the natural resources and the production of energy for the productive process; material and energy are parts of the phases of production, transport and use, as they are part of the phase of recycling, reuse and disposal.

We have decided to use a life cycle approach, because we can obtain knowledge of the damage and the environmental potentials, due to what happens in each single operative phase. Our goal is to use solid notions about the environmental impacts of a production choice like the renovation of a building from 1836.

1. Introduction

1.1 The fortress of Sant'Andrea in Venice

The fortress of Sant'Andrea was constructed in the 15th century on the stones of a previous fortress and was built there to protect the "Bocca di Lido"

from attack by the Turks who had just broken the peace treaty and had occupied Cyprus. The architect Michele Sanmicheli from Verona drew up the project, he knew the defence works very well because of his curiosity and the knowledge of other kinds of defences near Treviso, and because of this interest he was put in prison accused of being a spy.

The fortress situated at the entrance of the "Bocca di Lido" went through several restyling interventions in order to follow the different military functions based on changes in defence strategies. Because of their very static and tough shape, the redevelopments have never kept up with the real need (Marchesi P., 1978).

We do not have much historical information about this because of military classified information which has only recently been lifted. The most important interventions can be summarized in some historical ages: the birth of the Sanmicheli fortress in the 15th century, the addition of the officers' house during the 17th century, the building of two sleeping barracks in the 1830s, the addition of the stores at the end of the 19th century.

We are interested in the sleeping barracks, because after a structural renovation they will be used for a cultural centre with the following facilities: library, newspaper library, managing area, offices, multifunctional room, bar, a small bookshop, exposition area and a room for building up the expositions. The nearby areas will be reused, but we are not interested in them for the moment.

The main intervention to be undertaken in order to redevelop the barracks and change the use is the rebuilding of a definite volume. The external walls are in a good state: they just need to be cleaned and to have a sufficient insulating layer inside while

the roof is mostly collapsed, so it is going to be destroyed and rebuilt in the same shape but with a strong energy performance improvement, thanks to the use of an insulating layer. The floor is quite damaged and largely absent due to tree growth. It is going to be completely destroyed and rebuilt at the same level but with the insert of better thermal and hygrometric materials.

1.2 LCA methodology

The elaboration of a LCA, following the SETAC procedure, is divided in 4 steps:

- Goal and scope definition
- Life cycle inventory (LCI) in which we make an inventory of incomes (materials, energy, natural resources) and outgoings (air, emissions, water, soil) relevant in the system
- Life cycle impact assessment (LCIA) of environmental potentials, related to these input and output
- Analysis of the results and the evaluation of the improvements (life cycle interpretation) of the two previous steps

The description of the structure of the life cycle evaluation can be found in the UNI ISO 14040 standard (EN/ISO 14040, 2000).

The richer the database of the substances taken and released in the environment by the industrial process to obtain the product, the more accurate is the LCA. The evaluation of the results of LCA depends on the choice of methods used to connect the substances emitted in the environment, to the impact categories and on the importance that we gave to those substances. Those choices are very important and difficult, because they involve several technical, social and economic problems, like the environment impact and the link between costs and benefits.

1.3 The IMPACT 2002+ method

This was developed by the Swiss Federal Institute of Technology of Lausanne. As shown in Figure 1, the damage categories are:

- Human health, compared in DALY and coming from the 5 following impact categories Human toxicity, Respiratory (inorganics), Ionizing

radiations, Ozone layer depletion, Photochemical oxidation;

- Ecosystem quality, expressed in PDF*m²*yr, coming from impact categories Aquatic ecotoxicity, Terrestrial ecotoxicity, Terrestrial acidification/nutrication, Aquatic acidification, Aquatic eutrophication and Land occupation;
- Climate change, expressed in kgCO₂eq to air, come from the only impact category Global warming;
- Resources, in MJ, built from midpoint categories, Non renewable energy and Mineral extraction.

1.3.1 The characterization

In Impact 2002+ the results are first connected to the 14 impact categories, and then to the damage categories. Characterizations factors of the different substances are based on the principle of equivalence. This means that each category has its own referent substance and the points given to the different substances are given in Kgeq related to the referent point established for each category. The main goal for all impact categories is the determination of the long term effects obtained by the use of an infinite temporary horizon.

The process of the impact characterization finds the link between the midpoint categories and the damage categories. The factors of midpoint characterization "Respiratory Effects", "Photochemical oxidation", "Ionizing radiation", "Ozone layer depletion", "Terrestrial acidification/nutrication", "Land use occupation" and "Mineral extraction" are obtained by Eco-Indicator 99, adopting the equalitarian cultural perspective.

For climate change, the most recent global warming potentials are employed with a temporary horizon of 500 years to consider the long-term effect of changing climate gas emissions. The characterization factors for "Aquatic acidification" and "Aquatic eutrophication" are adapted from Hauschild and Wenzel's research (Wenzel 2001).

The characterization factors for the consumption of renewable resources are calculated with the superior warming power. The calculation for

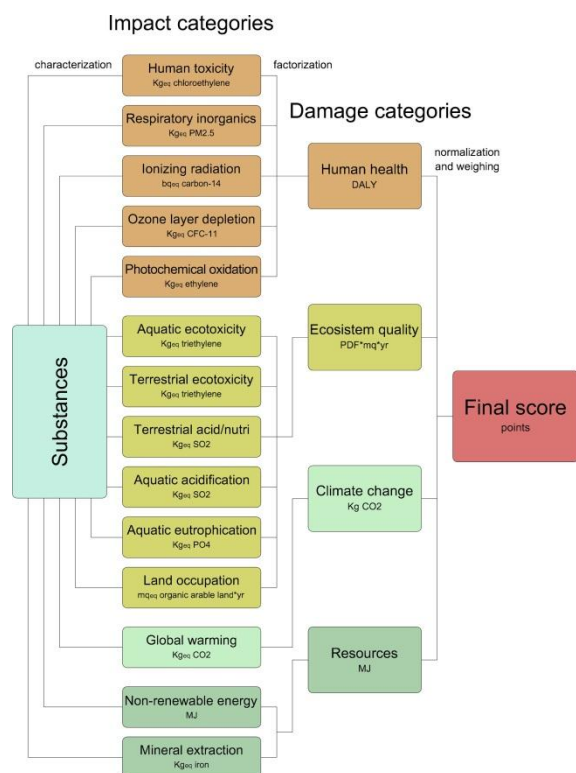


Fig. 1 – Scheme of IMPACT 2002+ method

"carcinogens" and "non carcinogens" impact categories is more difficult. The link between the substance and the effect is calculated by a code. It is almost the same for the aquatic ecosystem impact.

1.3.2 The normalization

The normalization aims to analyze the relative weight of each class of impact related to the total damage adding a normalization factor to the impact categories and to the damage categories in order to easily understand the results. The normalizations come comparing the specific impact per unit of global impact emission determined by the whole substances of each category.

The normalization factors are found in the following ways:

- In Human Health the normalization factor is calculated in agreement with Eco-Indicator 99 with two exceptions: the impacts caused by climatic changes are not considered, but the toxicity of the polluting substances for humans is calculated like a sum of carcinogenic and non carcinogenic effects.

- Even in the Ecosystem Quality, the normalization factor is calculated in the same way as in Eco-Indicator 99 with two differences: the damage to the quality of the ecosystem caused by the transformation of the soil and by the photo chemical oxidation is not considered and the damage to the quality of the ecosystem is divided among the damage categories for the water and the earth's ecosystem
- In Climate Change the valuation of the normalization is based on the total annual emissions of CO₂ produced in Europe, multiplied by the potentials of global warming in a horizon of 500 years.
- In Resources the valuation of normalization is calculated as the total consumption of non renewable energy in Europe, including nuclear energy consumption.

1.3.3 The evaluation

Each of the four damage categories are considered separately without further evaluation. The weight factor is simply equal to 1.

1.4 The choice of a method

All the analyses are made in several ways -Eco-Indicator (Eco-Indicator 99, 2000), IMPACT 2002+ (Frischknecht R., 2007), EPS 2000 (Steen B., 1999) EDIP 2003 (Frischknecht R., 2007), IPCC (Frischknecht R., 2003), ReCiPe (Goedkoop M., 2008)-, but we have chosen the IMPACT method, because (Neri, 2008; Neri, 2009):

- it measures the impact categories comparing the quantities of equivalent emissions which represents the most accepted standards, because it is surely measureable;
- it measures the damage categories comparing the effects they produce on the people (life years lost), on the environment (number of vegetarian species influenced), on the resources available (non renewable used energy). Those effects are measurable with difficulty, but easily understood by the community;
- it holds all the most important impact categories;
- the weights given to the emissions and to the impact categories reduce the damage due to the use of the territory of Eco-Indicator 99 even if it

makes the ecotoxicity of the Earth to come out, especially if this is due to heavy metals;

- it measures the energy consumption by non renewable combustibles (fossils and uranium), it is one of the best ways to value the environmental damage of a product;
- it considers the European basin to measure the effects of emissions.

1.5 The LCA applied to the restructuring of the buildings.

In this process we have adopted a different way of thinking (Neri, 2008), because the roofs of the barracks have already collapsed. We have split the building life in two parts: the first part with its own LCA analysis for everything which is no longer there because it has been destroyed, and the second part with its own LCA analysis with the impact of all the new materials added and with the resources needed to ensure the restored building remains standing for at least 100 years. All the ancient parts not substituted, for example the walls made by bricks, weigh on the LCA for their life part, as $100/(2011+100-1836)$. 2011 is the date of the renovation project, 100 is the life time used for the LCA, 1836 is the date of the building construction.

2. Simulation

2.1 The LCA of the building

The building was built over several periods: between 1554 and 1559 the external walls were constructed with stones from Istria and bricks; after 1750 the 3 storey house on the north-west corner; in the 1830s the 2 sleeping barracks behind the fortress and in the 1900s the store houses (Fortuna, 2011; giabon). The LCA concerns:

- the structural components which are unchanged adding an allocation equivalent $100/275$ for the sleeping barracks for the production and for their end life
- the structural components which are dismissed (the roof and the floor) adding an allocation equivalent to $100/100$
- the building of the new roof, the insulation of the external wall, the maintenance and the life

end with an allocation equivalent to $100/100$

- the air-conditioning and heating systems
- the photovoltaic plant made of special bent tiles designed to hold the panel and able to satisfy almost the whole electrical power need
- the power consumption for 100 years of air-conditioning and lightning of the cultural centre situated in the barracks.

2.1.1 Life end of the several existing packages

We are using the database of SimaPro (the software used for the LCA analysis, Goedkoop M., 2008) for all the materials we are going to add to the barracks.

What remains of the ancient roof is probably 30%, but it will be dismantled because it has not been well preserved: wooden parts will be used to build some panels of MDF; the roofing flat bricks, still perfect, will be re-used to make the new roof, the bent tiles still existing will be re-used with some others. We are using the broken bent tiles, after crushing, for the preparation of the foundations.

The renovation includes for the floor a layer of insulation, but this material would create some problems (a new step) for handicapped people, so we have decided to destroy completely the floor using the remains after crushing.

2.1.2 The materials for the renovation

Material	Quantity	Unit	Eco points
Bricks	201446	kg	$5,4E^{-5}$
Concrete	121	m ³	0,0475
Cork slabs	23572	kg	$2,53E^{-7}$
Fiber wood	236	m ³	0,131
Plaster	41544	kg	$4,02E^{-5}$
Plasterboard	12983	kg	0,00011
Steel	15747	kg	0,000543
Wood (fir)	67	m ³	0,056

Table 1 – Database of the main materials and related damage expressed in Eco points

The materials needed to renovate are mostly some insulating materials useful for the energy system of the building and elements to make the new floor. On the roof we have to use new trusses, some virgin wood, while on the wall we will use

plasterboard everywhere.

For the insulation we have compared a chemical material, the XPS, with a natural material, cork. The first one can be thinner and lighter than the second, but cork is stronger against wet and salty water, and it probably will only need to be substituted in 50 years. Therefore, we preferred to use cork.

3. Discussion and result analysis

In order to choose the less impacting materials, several packages of the same termohygrometric and thermal qualities have been compared through the LCA. The less impacting ones have been chosen and then the impact factors based on the different phases of the life of the whole building have been compared.

3.1 Comparison between technological packages

The solution of the ventilated roof with roof tiles in "cotto" is less impacting than the non ventilated one: 0.22427 vs. 0.24477 Pt (each square metre, - 8,38%). This is due to a smaller damage of the impact categories: Carcinogens, Respiratory inorganics, Global warming and Non renewable Energy.

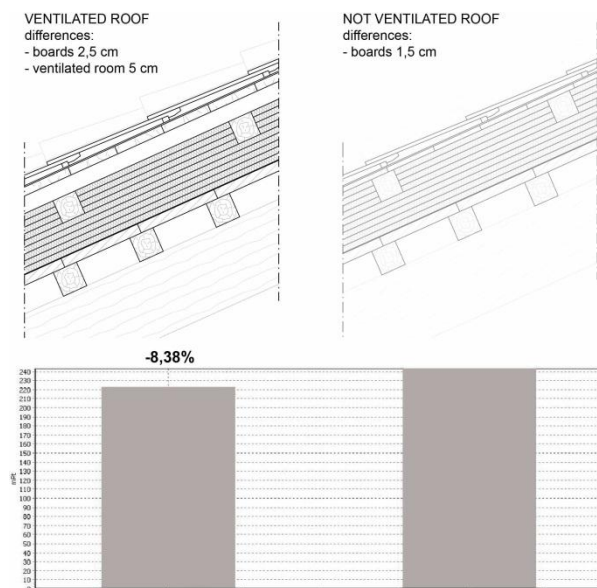


Fig. 2 – Comparison between roofs expressed in Eco points

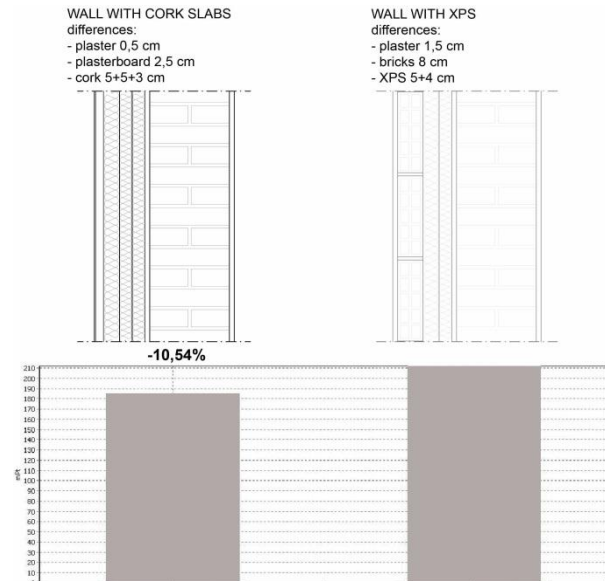


Fig. 3 – Comparison between external walls expressed in Eco points

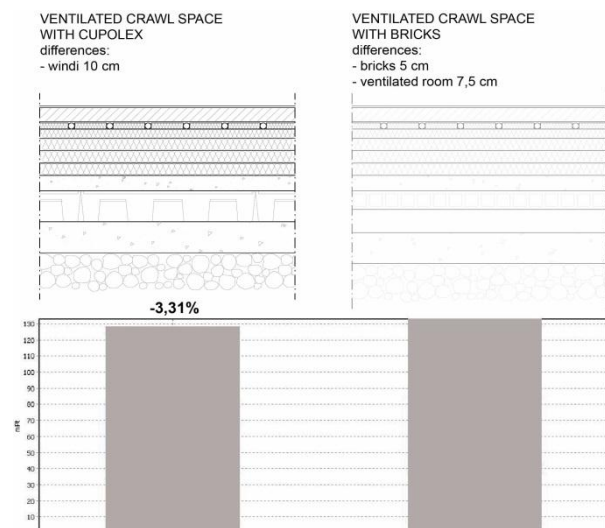


Fig. 4 – Comparison between ventilated crawl spaces expressed in Eco points

The cork solution is less impacting: 0.23781 vs. 0.26584 Pt (each square metre, -10,54%), which is due to a smaller damage of the impact categories: Respiratory inorganics, Global warming and Non-renewable energy.

The solution with cupolex is less impacting: 0.12953 vs. 0.13396 Pt (each square metre, -3,31%), due to a smaller damage of the impact categories: Respiratory inorganics, Global warming.

From the analysis of the results of the evaluation we noticed that:

- the total damage is worth 1.19E3 Pt due to the lightening electricity at 30%, to the electricity for instruments at 17.48% and to the auxiliary systems electricity at 16.64%.
- the damage is also due to the Human Health at 22.94%, to the Ecosystem Quality at 9.66% and to the Resources at 67.73%.

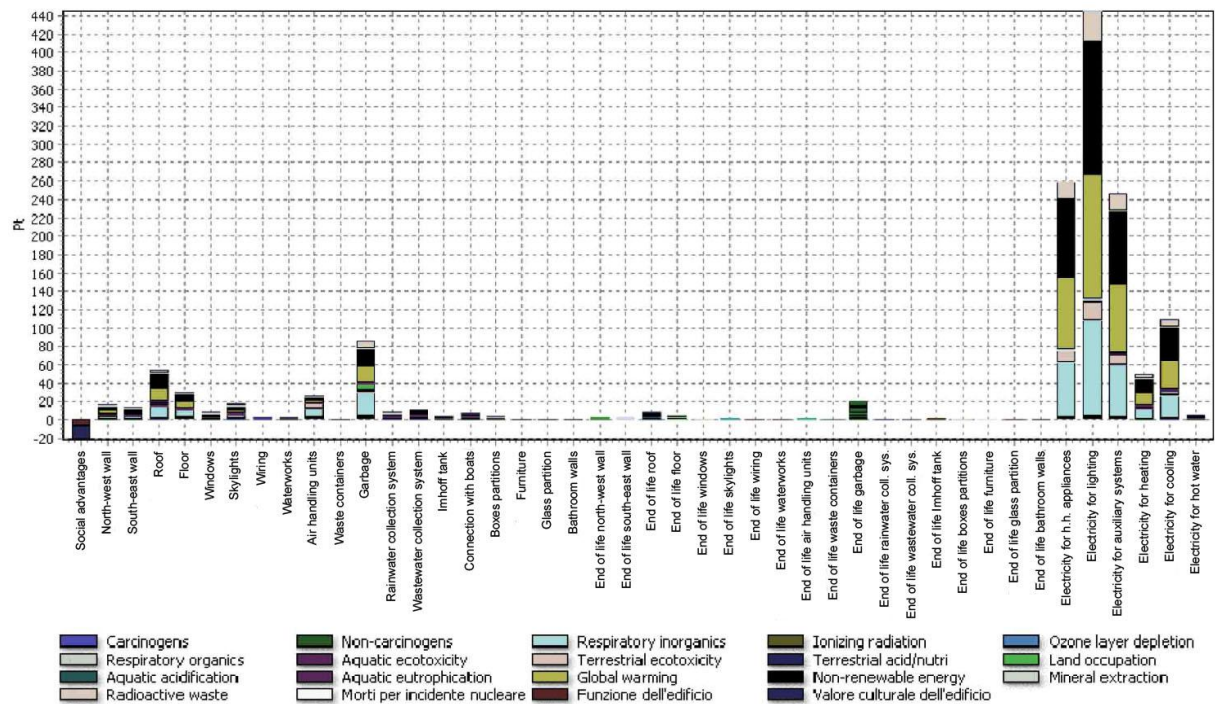


Fig. 5 – Analysis of all single elements

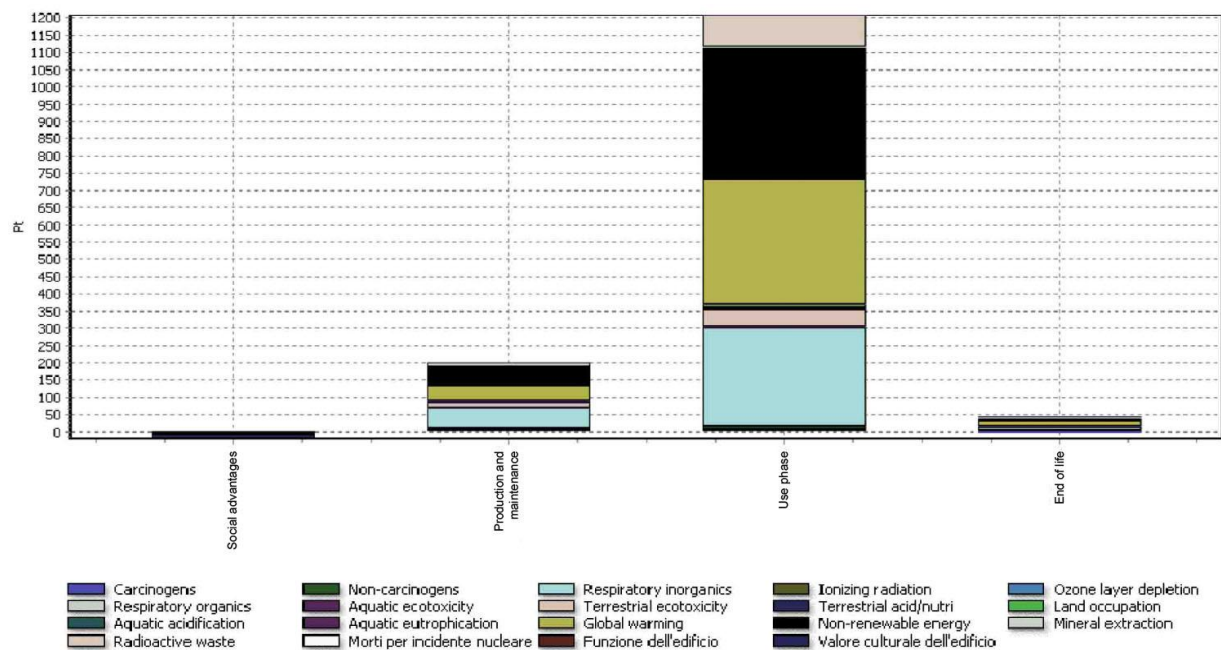


Fig. 6 – Analysis divided for phases of life: (social advantages) construction, use, end of life

From the analysis of the results we notice that:
 the total damage is worth 1.19E3 Pt
 the production and keeping phases need the 14.1%,
 the use phase needs 83.3% and the life end the 2.6%
 the first column is negative because of social advantages

3.2 The sensitiveness analysis

3.2.1 The photovoltaic roof

The architectural constraints do not allow the installation of photovoltaic panels in cities' historic centres, and this also has an effect on the fortress. We decided to analyze the photovoltaic roof made with PV roof tiles, which are almost like traditional tiles, but they can give us a part of the electricity we need for the cultural centre. The information about these tiles given to us by the firm indicates an area of 18 square metres to produce 1 kWp, with an inclination of 30 degrees and the south direction. So we used the free program Simulare and, with a comparison of all this information, we found a result of 20000 kWh year at the beginning of the life cycle of the PV roof and 17000 kWh year after 30 years.

So we did a LCA to control the impact of the roof if using photovoltaic roof tiles and traditional terracotta tiles, and we found that the photovoltaic roof has more impact compared to traditional roof tiles fitted, although the photovoltaic energy has about 9 times less impact related to the same Wh from the electricity grid in Italy. This big difference is due to the use of plastic materials (polymer PMMA for the realization of the covering and techno polymer ASA for the remaining part of the roof tile) in the construction of the photovoltaic tile. These materials are able to cancel the visual difference that exists between terracotta roof tiles

and solar roof tiles, but the solution of the problem of the vision creates a disadvantage for PV tiles.

3.2.2 Determination of the minimum wall damage

At the end we decided to define the meeting point of minimum environmental damage is between the thickness of insulation and the fuel consumption for air conditioning. In fact, with an increase in the thickness of the insulating material, the consumption of energy for heating and cooling decreases. After this point the damage caused by the extra material used for the insulation is not covered by lower consumption.

We chose the north-west wall for this study because the surface mass is so huge that we have to use the maximum expected value for the summer equivalent temperature, which corresponds to a wall weight of 700 kg per square metre. So on this wall all the values were kept constant, except for the amount of insulating material and the transmittance.

3.3 Analysis of the whole building

From the analysis of the results of the evaluation we noticed that:

- the total damage is worth 1.19E3 Pt due to the lightning electricity at 30%, to the electricity for instruments at 17.48% and to the auxiliary systems electricity at 16.64%.
- the damage is also due to the Human Health at 22.94%, to the Ecosystem Quality at 9.66% and to the Resources at 67.73%.

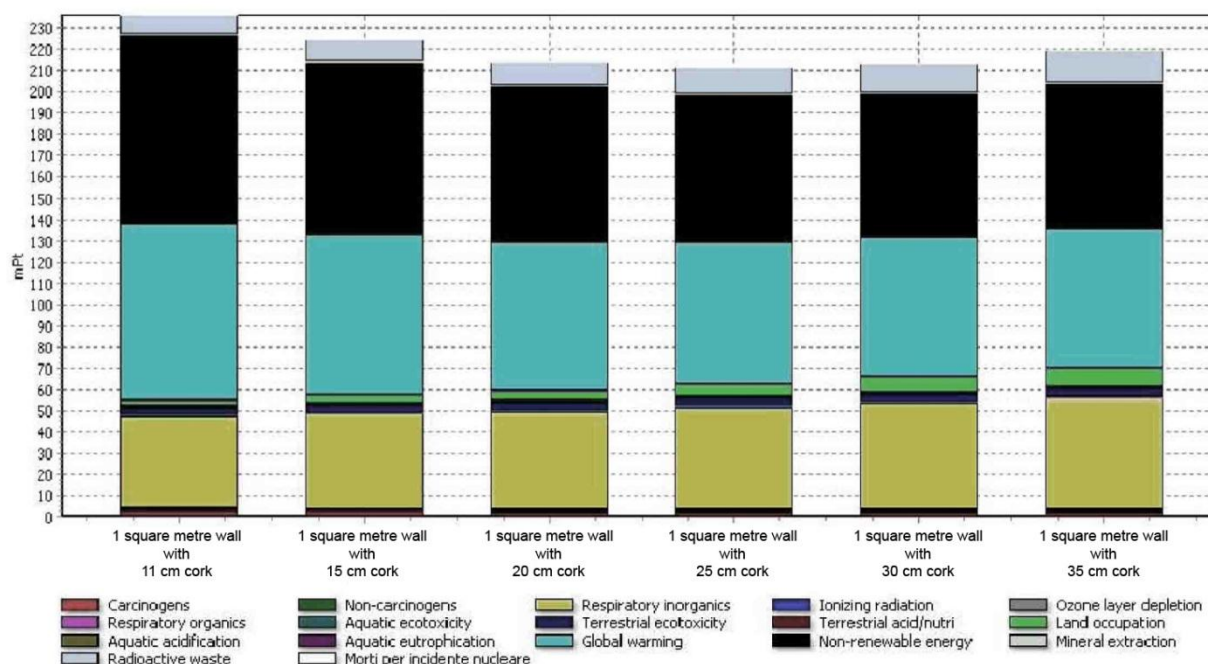


Fig. 7 – Minimum damage for the wall

4. Conclusion

Summarizing this study we can obtain the following conclusions:

- The best roof is the one which is ventilated because you can save a lot of energy for cooling in the summer
- It is better not to use a PV roof with PV roof tiles because of the PMMA which has a lot of environmental impact
- We used the less impacting end of life for all components, i.e. the one which requires the reuse of a material when it is possible. We also used for the new concrete the old one in situ after a crush treatment.
- For this LCA we keep in consideration existing materials only for the years we are going to use them.
- The most important part of the damage comes from the consumption of the electrical energy during the life of the building.
- The maximum damage comes from the depletion of the resources.
- The XPS has a better environmental impact related to cork
- For the use of insulation, it is better to have a lower transmittance than the one given us

by the law. With the LCA we can define the better bend which describes the damage in relation to the depth of the insulation. For the external wall of this case study the optimum is with 25 cm of insulation.

References

- Fortuna Stefano, 2011. L'uso dell'analisi sul ciclo di vita dei materiali come strumento di riduzione dell'impatto ambientale nel processo di riqualificazione di un edificio storico, degree thesis, Università IUAV di Venezia
- Fortuna Stefano, 2011. Riqualificazione dai punti di vista sociale ed energetico del dormitorio nord est del forte di Sant'Andrea a Venezia, technical report ENEA UTVALAMB-P795-020, Bologna Arcoveggio
- Eco-Indicator 99, 2000. Manual for Design, Ministry of Housing, Spatial Planning and the Environment, The Hague, Netherlands
- EN/ISO 14040, 2000. Environmental management - life cycle assessment - principles and framework (ISO 14040:2000), CEN European Bureau for Standardisation
- Frischknecht R., Jungbluth N., et.al., 2003. Implementation of Life Cycle Impact Assessment Methods, Final report ecoinvent 2000, Swiss Centre for LCI. Dübendorf, Switzerland

- Frischknecht R., Jungbluth N., Althaus H.J., Doka G., Dones R., Hischier R., Hellweg S., Humbert S., Margni M., Nemecek T., Spielmann M., 2007. Implementation of Life Cycle Impact Assessment Methods: Data v2.0.ecoinvent report No. 3, Swiss centre for Lyfe Cycle Inventories, Duebendorf, Switzerland
- Goedkoop M., Oele M., de Schryver a., Vieira M., 2008. SimaPro Data Base Manual, PRé Consultants, The Netherlands
- Goedkoop M., et al., 2008. ReCiPe 2008: A life cycle impact assessment method which comprises harmonised category indicators at the midpoint and the endpoint level, Ministry of Housing, Spatial Planning and the Environment, The Hague, Netherlands
- <http://digilander.libero.it/giabon/>
- Marchesi Pietro, 1978. Il forte di Sant'Andrea a Venezia, Castella
- Neri Paolo et al., 2008. Verso la valutazione ambientale degli edifici: Life Cycle Assessment a supporto della progettazione eco-sostenibile, Alinea Firenze
- Neri Paolo et al., 2009. Analisi ambientale della gestione dei rifiuti con il metodo LCA, CNR Area Ricerca Bologna, <http://lcarifiuti.net>
- Neri Paolo et al., 2011. L'analisi ambientale dei prodotti agroalimentari con il metodo del Life Cycle Assessment, ARPA Sicilia
- Steen B., 1999. A systematic approach to environmental strategies in product development (EPS). Version 2000 - General system characteristic, Centre for Environmental Assessment of Products and Material Systems, Chalmers University of Technology, Technical Environmental Planning. CPM report
- Wenzel H., Hauschild M., 2001. Environmental Assessment of Products: Methodology, Tools and Case Studies in Product Development, Kluwer Academic Publisher

Extending the use of parametric simulation in practice through a cloud based online service

Emanuele Naboni – Institute of Architectural Technology - Royal Danish Academy of Fine Arts, School of Architecture, Copenhagen, Denmark

Yi Zhang – Institute of Energy and Sustainable Development, De Montfort University, Leicester, United Kingdom

Alessandro Maccarini – Institute of Architectural Technology - Royal Danish Academy of Fine Arts, School of Architecture, Copenhagen, Denmark

Elia Hirsch – Institute of Architectural Technology - Royal Danish Academy of Fine Arts, School of Architecture, Copenhagen, Denmark

Daniele Lezzi – Barcelona Supercomputer Center, Barcelona, Spain

Abstract

The aim of the present research is to facilitate the implementation of parametric energy studies among the Architecture, Engineering & Construction (AEC) industry by creating an online service to execute parametric energy simulations using cloud computing.

A web-based service was developed to submit parametric simulations based on the open-source energy simulation program EnergyPlus. An adapted version of jEPlus (parametric shell for EnergyPlus) was created to handle the jobs execution on the VENUS-C [1] cloud infrastructure. In addition, a web client called HUB-Engineering (HUB-E) was developed. The latter allows submissions of parametric simulations and results retrieval from any device connected to the internet. The results can be visualized and explored with a freeware interactive Parallel Coordinates Plot (PCP).

Finally, a workflow is proposed to integrate the online cloud-based service within design processes of architectural and engineering practices. The workflow is tested with the parametric simulation of the energy performance of a building simulating 221,184 design options. By developing the first version of the service, which will be accessible to the AEC community, and by testing it successfully, the research shows the potential impact of cloud computing when coupled with parametric energy simulation.

1. Introduction

1.1 Background

On a global average, building-related activities consume more than 40% of a country's energy. The reduction of new and existing buildings' energy consumption is an issue that the AEC industry is facing. The effective use of parametric building performance simulation can contribute by optimizing building energy design, as it allows in-depth analysis.

In general, there are two strategies (Fig. 1) for thinking about the generation and evaluation of design alternatives: the conventional way is to generate a model, evaluate it, change design variables, re-evaluate the model, change design variables again, and so forth, until the final design is satisfactory. Conversely, a parametric strategy consists of generating several design solutions at the same time, evaluating them by the desired criteria and choosing the most "performative" one.

Thus, parametric studies show a wider range of solutions and contribute to maximum energy savings (Paoletti et al., 2011; Pratt et al., 2011). Despite this potential, parametric energy studies are rarely used because they require a long time to run the computations as well as powerful hardware. Complex and detailed parametric analysis models require simulation to a scale that is nowadays only available to large private, academic and government research laboratories.

There are two ways to extend the use of parametric simulation to a large group of users: either reduce the number of computations by using optimization algorithms (e.g., Coley and Schukat 2002; Nielsen 2002; Wetter and Wright 2004) or increase the computational power by using parallel executions of EnergyPlus using local computer clusters (Zhang 2010; Garg et al., 2010; Zhang et al., 2010; Hopkins et al., 2011; Pratt 2011).

However, the use of cloud infrastructures is still a novel approach (Hopkins et al 2011; Li et al 2011; Burton et al., 2012). Therefore, the present research focuses on developing a fast and user-friendly online service to run parametric studies on the cloud, allowing a quick evaluation of many design alternatives. The service is based on the parametric shell jEPlus v1.3. In a future research, a more recent version named jEplus+EA, which uses an optimization algorithm (GenOpt [2]), can be implemented to evaluate the potential of coupling cloud computing with optimization techniques.

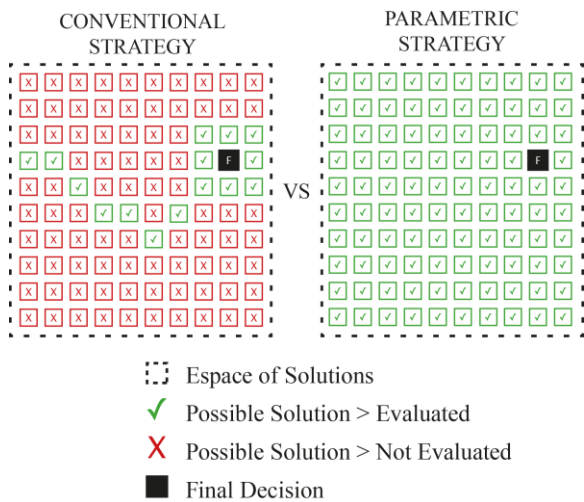


Fig. 1 – Conventional strategy vs. parametric strategy

1.2 The research project

One of the aims of this research project is to use an industry-quality, highly scalable, and flexible Cloud Computing infrastructure to empower parametric energy simulations through the easy deployment of an end-user service for architects and engineers.

This was done by creating a structure that allows the running of EnergyPlus [3], a whole building energy

simulation program, on the Venus-C Cloud infrastructure through the adaptation of jEplus [4] and the development of the web client HUB-E [5].

One of the objectives of this paper is to structure the general workflow (Fig. 2) of the developed online service that allows its incorporation into building design practice. The description of reduced computational time and the possibilities of energy savings achieved by the service is introduced.

2. Online Service

The architecture of the proposed service includes four layers:

- The VENUS-C infrastructure provides the virtualization layer where to execute the simulations;
- The platform level includes the COMPSs programming framework (Lezzi et al., 2011), onto which jEplus is ported;
- The HUB-E website implements the client interface for submitting and managing jobs on the cloud;
- The Protovis-based, high-dimensional visualization tool allows for the analysis and presentation of results.

2.1 VENUS-C infrastructure and COMPSs

Venus C (Virtual Multidisciplinary Environmets USING Cloud Infrastructures) is funded under the European Commission's 7th Framework Programme. Developed in the Barcelona Supercomputing Center (BSC), the COMP Superscalar (COMPSs) is a programming framework to provide users with interoperability and dynamic scalability of computational resources in the context of the VENUS-C platform.

Multi-threaded processes can be migrated to the Venus-C platform by implementing a Java wrapper that incorporates the COMPSs workflow (Lezzi et al., 2011). This approach significantly simplifies the process of implementing multiple EnergyPlus executions into the cloud.

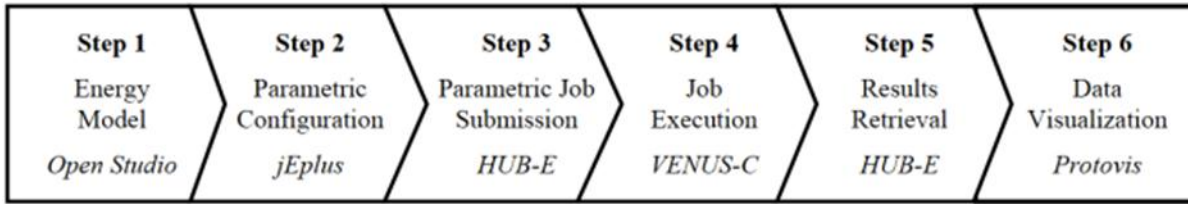


Fig. 2 – Proposed workflow

2.2 jEplus-VenusC

jEplus is an EnergyPlus simulation manager designed especially for parametric studies (Zhang, 2009).

It can carry out parallel executions of EnergyPlus models on various platforms, including multi-core computers, computer networks, and clusters.

The porting of jEplus to the Venus-C platform further expands its capability. jEplus-VenusC is the developed execution agent that implements COMPs' workflow using APIs. Users can now submit jEplus-VenusC, EnergyPlus executables, and jEplus project files to the Venus-C platform in order to run simulations on the cloud.

2.3 HUB-E client interface

Engineering HUB (HUB-E) is a web-based platform that provides cloud-powered services for architects and civil engineers. HUB-E is adapted to the VENUS-C Infrastructure and it is the component that allows users to interact with the cloud, submit the energy parametric package files and retrieve results with a user-friendly graphical interface.

HUB-E is connected to the Barcelona Supercomputing Center (BSC), where the simulations are run. The available hardware infrastructure consists of 80 cores:

- Nodes with 12 Intel Xeon X5650 Six Core at 2.6GHz processors, 24GB of memory and 2TB of storage each;
- Nodes with 16 AMD Opteron 6140 Eight Core at 2.6GHz processors, 32GB of memory and 2TB of storage each.

2.4 PROTOVIS visualization tool

Protovis.js [6] is an open-source script that allows users to create Parallel Coordinate Plot (PCP) graphs. PCP is interactive and manages high-dimensional data sets, allowing a quick

interpretation of the results. This way architects are able to determine the most efficient design option among several of them.

3. Proposed Workflow

For the purpose of making parametric energy studies accessible to architects and engineers beyond the research community, special attention was paid to inter-operability, user-friendliness and usage of open-source services. An architectural design-oriented workflow (Fig. 2) was designed. The first step of a six-step workflow (see below) is based on any of the third-party EnergyPlus interfaces. The second step uses jEplus and steps three to six are implemented using the developed online service. The actual version of the online service has integrated the third to fifth steps, while the sixth and final step has been partially implemented and this step will be subject to further refinements.

3.1 Step 1: Energy model

The designer creates the energy model with a tool that is able to generate *EnergyPlus input files* (.IDF, .RVI), such as OpenStudio [7] or DesignBuilder [8]. Other user-friendly EnergyPlus GUIs can be used, such as Ecotect [9] or Vasari [10] (Fig. 3).

3.2 Step 2: Parametric configuration

The parametric study is defined by jEplus, which allows the user to set different options to be tested (i.e. types of windows). Once the parameters are configured, the project is saved and packed in a ZIP file together with the files described in step 1 and the weather file(s) (EPW) (Fig. 4).

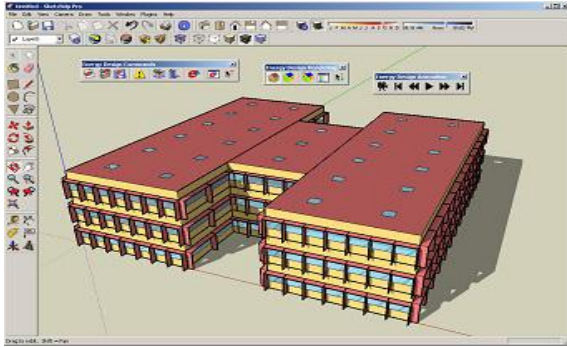


Fig. 3 – Step 1, Energy model (OpenStudio)

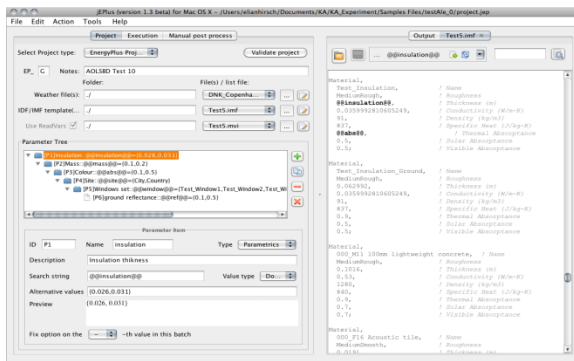


Fig. 4 – Step 2, Parametric Configuration

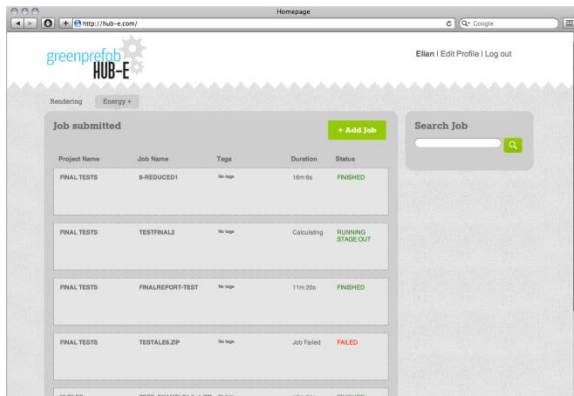


Fig. 5 – Step 4, Job submission, execution and retrieval results (HUB-E)

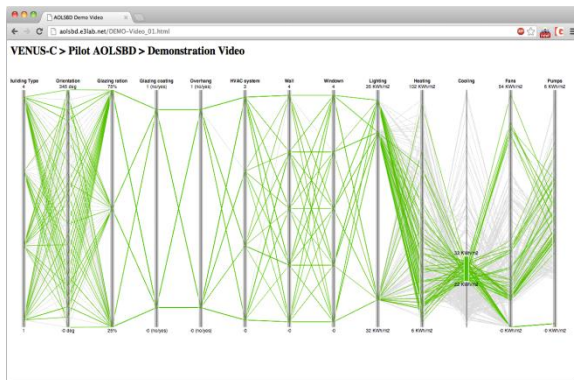


Fig. 6 – Step 6, Data visualization (PCP)

3.3 Step 3: Parametric job submission

The user logs into www.hub-e.com and creates a new “Parametric Job”, assigns tags to it, uploads the ZIP file, and executes it.

3.4 Step 4: Job Execution

Once the parametric job is submitted, the user is redirected to a “Jobs List” where jEplus jobs are ordered by submission dates and displayed with their corresponding statuses as well as the duration of the simulations (Fig. 5).

3.5 Step 5: Results retrieval

When the execution is finalized, the job status will read “Finished” after which the user can download the results in a zipped file (three CSV files). The SimResult.csv file shows a raw data output.

3.6 Step 6: Data visualization

Finally, the user is able to post-process results by using any spreadsheet application and high-dimensional visualizing tool such as Parallel Coordinates Plot (PCP) (Fig. 6).

4. Test case

The beta version of the online service was tested by a selected architect with basic skills of energy modeling and a good understanding of building energy design. He created a large parametric experiment of architectural optimization with 221,184 variable combinations. The objective is to show how, by using the proposed workflow, an architect could address an energy design problem with methods that are usually only accessible to a few research centers equipped with computation clusters.

A “shoe box” energy model was designed using OpenStudio. The test building has a total floor area of 1600 m² and four thermal zones (Fig. 7) and it is located in Copenhagen. Occupancy, internal gains and thermostat-schedule settings are those of a standard office.

4.1 Variables

The test case model was parametrized as followed:

- Ground reflectance: 3 steps, from white to black;
- Orientation: 16 discrete 22,5 degrees increments of rotation;
- Façade color: 3 different solar absorption coefficients of the external walls;
- Insulation thickness of external walls: 8 steps that progressively increase from 0.12 m to 0.4 m.
- Glass type: 6 different window sets within the following ranges: U-value (0.6-1.4 W/m²K), SHGC factor (0.4-0.7) and VT (0.55-0.8);
- Thermal mass: 4 different concrete thicknesses (external walls) ranging from 0.1 m to 0.4 m;
- Overhangs depth: 4 steps that progressively increase from 0 m to 1.2 m;
- Ground floor assembly: 2 different floor assemblies, heavy and light, of 0.4 m and 0.1 m of concrete thickness, respectively.

All of the above constructive solutions comply with the Danish standard BR10 [11]. “Ideal air loads heating energy” and “ideal air loads cooling energy” (annual) are the output variables added in the .rvi file.

In order to understand the applicability and the advantages of the proposed service in comparison to conventional ways of utilizing simulations, a parallel experiment was conducted. Starting from the same “shoe box” model, the same architect was asked to optimize the building performance in accordance with his typical design routine. He tested 50 design options (according to his intuition, expertise and experience) with a standard dual-core pc.

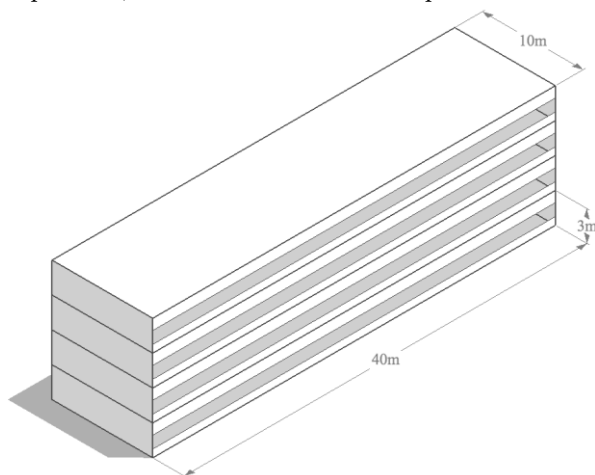


Fig. 7 – Building energy model

5. Discussion and results

There are two main factors of interest to be compared between a conventional workflow and the one proposed here: the time it takes to run the computations and the level of energy saving potential.

Figure 8 shows the time comparison between the conventional design and our cloud-based workflow. Even though the proposed cloud-based design requires approximately double the time, the clear advantage is related to the larger number of design alternatives (221,184 vs. 50). It is worth mentioning that the computational time for running the parametric simulation in the cloud was 71 hours and 20 minutes (1.17 seconds per job) and that such a large experiment, if run on a standard dual-core pc, would take 122 days.

Despite the fact that the analysis of the test case results is not the scope of this paper, a brief description is given.

This description is presented to highlight the “energy saving potential” of the proposed workflow. Figure 9 compares energy consumptions (heating and cooling) obtainable by a conventional design approach to parametric simulation processes performed on a desktop computer, a cluster and on the proposed cloud service, respectively. According to the available cpu power and the time of computation, a number of variables deemed relevant by the authors were selected and investigated.

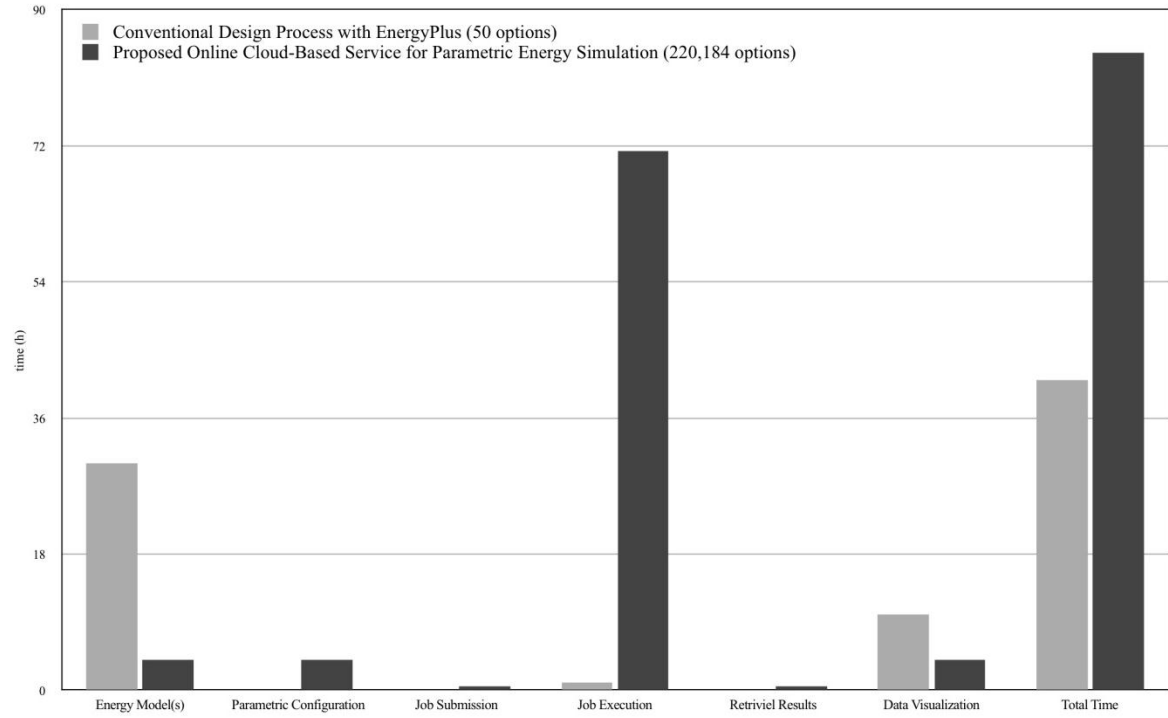


Fig. 8 – Time comparison: conventional design vs. proposed workflow

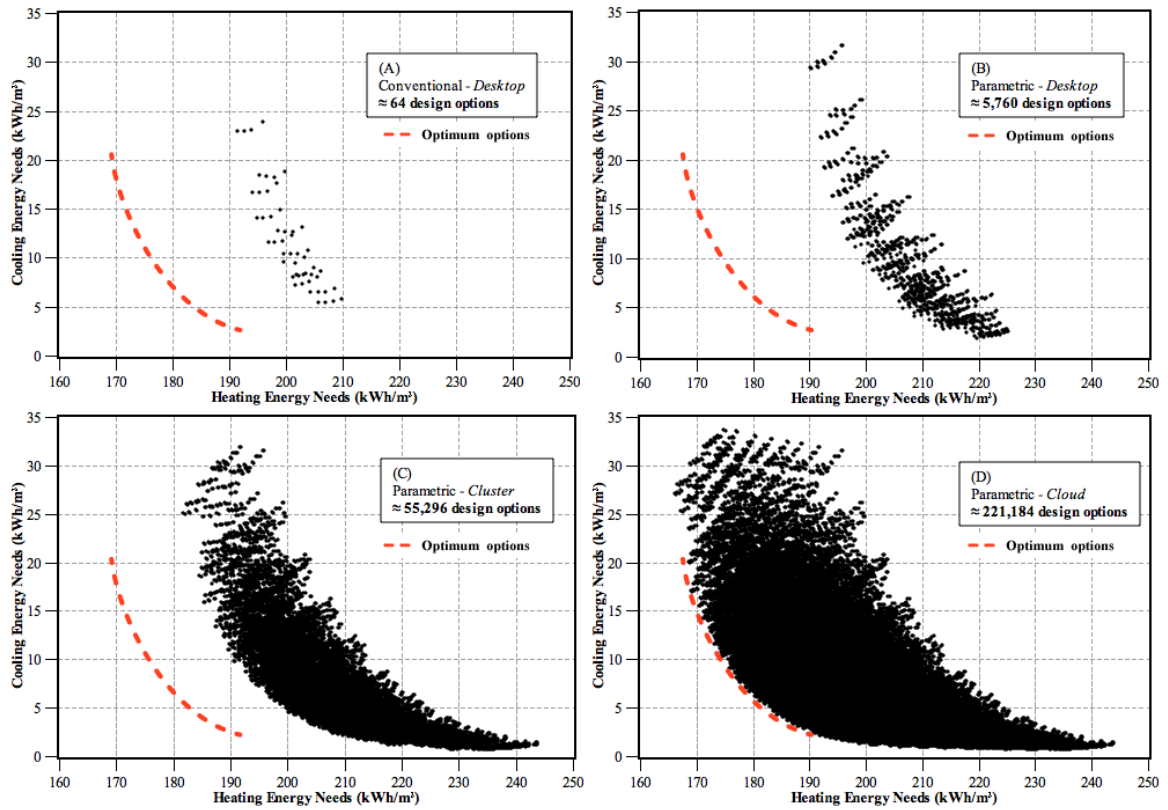


Fig. 9 – Energy comparison: conventional workflow vs. proposed workflow

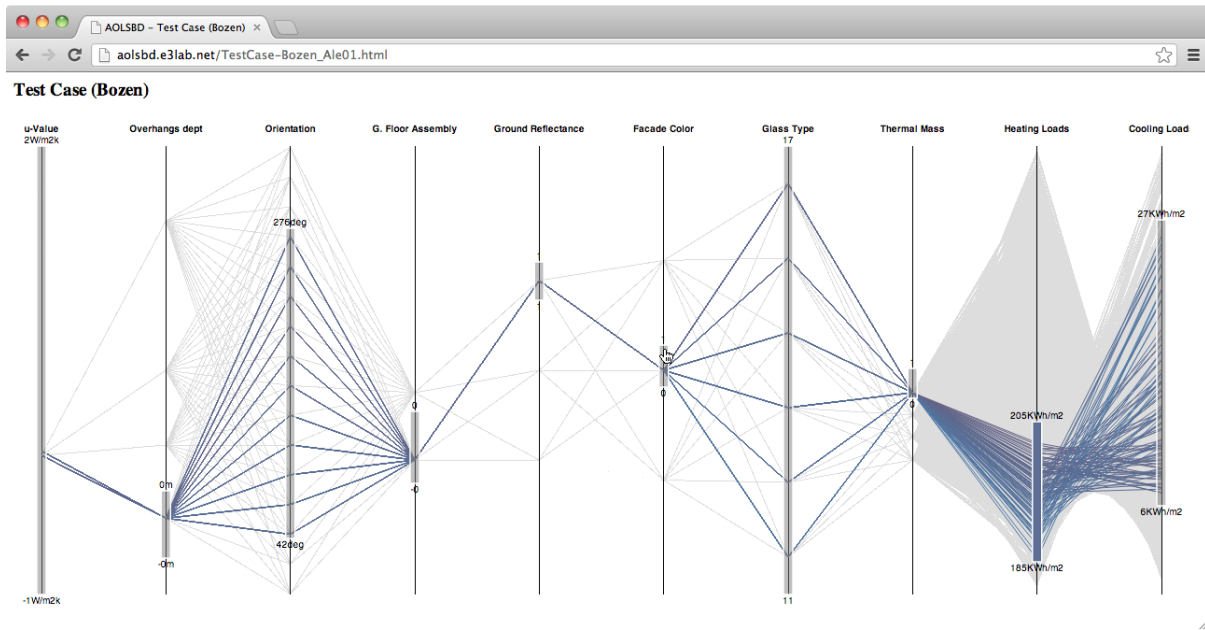


Fig. 10 – Parallel Coordinate Plot representing the results of the experiment

71.3 Hours (time used by the Cloud) was taken as a reference point to analyze how many jobs could run on a desktop computer and on a standard cluster (Table 1).

	Cores	Time	Design options
Desktop PC	2	71.3 h	5,760
Cluster	20	71.3 h	55,296
Cloud	80	71.3 h	221,184

Table 1 – Design options according to computational time

The graph, which illustrates the comparison of heating and cooling shows how the increasing number of variables lead to a range of simulations closer to the optimum set of solution (red curve). For instance, the cloud-based parametric study allows to reach the design option with the lowest heating energy need (166,09 kWh/m²). When comparing such a value with the best performance obtained with a conventional design process using a desktop PC, the energy saving is increased by 33%. Finally, in order to understand the relationship between design variables and energy consumption, an interactive PCP was created (Fig. 10).

This allows architects to quickly visualize the most “performative” solutions filtering the results through selected variables.

6. Conclusion

The authors have identified and developed an open-source and cloud-based service that can be applied in architectural and engineering practices, spreading the use of parametric energy simulation beyond the confinements of research centers.

The developed cloud-based workflow is user-friendly and suitable for architects familiar with energy simulation. It has been shown that it significantly reduces computational time for parametric simulations and that it could reduce buildings energy consumption to a higher degree than in a conventional design process.

The online service needs some further development, particularly with respect to completing the incorporation of the interactive Parallel Coordinate Plot into the online service and conducting a pilot study for architectural and engineering practices. In addition, further developments should include the implementation of optimization algorithms into the proposed workflow.

7. Acknowledgements

This work is partly funded and realized within the AOLSBD pilot project of the VENUS-C project. VENUS-C (Virtual multidisciplinary Environments Using Cloud infrastructures) is co-founded by the e-Infrastructure Unit, DG Connect, European Commission. Special thanks are given to F. Barzon and A. Sheferaw (GreenPrefab), I. Korolija (De Montfort University) and I. Blanquer (VENUS-C) for their contribution during the project.

References

- Burton, C. and M. Shaxted (2012). Development and implementation of a parametric energy tool for building owners, eSim 2012 IBSPA-Canada Conference.
- Coley, D.A. and S. Schukat (2002). Low-energy design: combining computer-based optimization and human judgment. *Building and Environment*, 37, 1241-1247
- Garg, V., K. Chandrasen, S. Tetali and J. Mathur (2010). EnergyPlus simulation speedup using data parallelization concept. AMSE 2010 4th International Conference on Energy Sustainability (pp. 1-6)
- Hopkins Asa S., A. Lekov, J. Lutz and G. Rosenquist (2011). Simulating a nationally representative housing sample using EnergyPlus. LBNL
- Lezzi D., R. Rafanell, F. Lordan, E. Tejedor, R.M. Badia (2011). Proceedings of 4th Iberian Grid Infrastructure Conference, Santander, Spain (pp. 73-84)
- Lezzi D., R. Rafanell, A. Carrion, I. Blanquer, V. Hernandez, R.M. Badia (2011). Enabling e-Science applications on the Cloud with COMPSs. Euro-Par 2011: Parallel Processing Workshops 7155, (pp. 25-34)
- Li H., P. de Wilde, Y. Rafiq (2011). A methodology for building performance simulation using high power computing. 2011 eg-ice workshop
- Nielsen T.R. (2002). Optimization of Buildings with Respect to Energy and Indoor Environment. Ph.D. Thesis. Department of Civil Engineering, Technical University of Denmark.
- Paoletti G., S. Avesani, D. Exner, R. Lollini (2011). Designing low energy buildings: application of a parametric tool and case studies. PLEA 2011 – 27th International Conference on Passive and Low Energy Architecture.
- Pratt, K. and David E. Bosworth (2011). A method for the design and analysis of parametric building energy models. Proceedings of Building Simulation 2011: 12th Conference of International Building Performance Association, Sydney, Australia
- Wetter, M. and J.A. Wright (2004). A comparison of deterministic and probabilistic optimization algorithms for nonsmooth simulation-based optimization. *Building and Environment*, 39, 989-999.
- Zhang Y. (2009). “Parallel” EnergyPlus and development of a parametric analysis tool. 11th Conference of International Building Performance Association IBPSA, Glasgow, UK
- Zhang Y. and I. Korolija (2010). Performing complex parametric simulations with jEplus. SET 2010 – 9th International Conference on Sustainable Energy Technologies, Shanghai, China
- [1] VENUS-C, www.venus-c.eu
- [2] GenOpt, <http://simulationresearch.lbl.gov/GO/>
- [3] EnergyPlus, <http://apps1.eere.energy.gov/buildings/energyplus/>
- [4] jEplus, <http://www.iesd.dmu.ac.uk/~jeplus/wiki/doku.php>
- [5] HUB-E, www.hub-e.com
- [6] Protovis.js, <http://mbostock.github.com/protovis/>
- [7] OpenStudio, <http://openstudio.nrel.gov/>
- [8] Design Builder, <http://www.designbuilder.co.uk/>
- [9] Ecotect, <http://usa.autodesk.com/ecotect-analysis/>
- [10] Vasari, <http://autodeskvasari.com/>
- [11] BR10, <http://www.bygningsreglementet.dk/>

Dynamic modelisation of interaction between wall and indoor air

Lorenzo Moro – Dipartimento di Ingegneria Industriale, Università degli Studi di Padova, Padova, Italy

Piercarlo Romagnoni – Dipartimento di Progettazione e Pianificazione in Ambienti Complessi,

Università IUAV di Venezia, Venezia, Italy

Paolo Baggio – Dipartimento di Ingegneria Civile e Ambientale, Università degli Studi di Trento, Trento, Italy

Abstract

The current methodology used for testing the thermohygroscopic behaviour of building structures is proposed by the standard UNI EN ISO 13788.

This Standard evaluates the risk of hygroscopic damages due to:

- 1) critical moisture conditions of the inner surfaces of the building;
- 2) interstitial condensation within the structures

The proposed procedures are valid in the case of steady state and are applied on a monthly basis. However, the steady state calculation is not completely correct mainly because the vapour production is not constant neither in time nor in space. For example, residential buildings are not occupied during most of the day. Therefore, in the case of a residential building, there is an intense generation of moisture mainly during a certain period of the day. Then, for a better control of the indoor values of relative humidity (and of partial vapour pressure) inside a given room, the indoor moisture production should be not considered constant and it may be appropriate to assess the importance of the hygroscopic properties the walls and furniture, able to act as a moisture buffer.

In this paper, using a simplified model taking into account the interactions between the vapour concentration of the indoor air and the interior walls and furniture, the role played by the hygroscopic capacity of the indoor walls and furniture for the evaluation of indoor relative humidity is analyzed.

1. Introduction

Moisture is produced inside a building by human activity (respiration, perspiration, washing clothes and cleaning, baths and showers), from

houseplants, humid basements and other sources [Tenwolde, A. et alii, 2001; Tenwolde, A., 1994]. The modern lifestyle forces people to work or go to school during the day and only during the evening and night are residential buildings fully occupied. The consequence can be a cycle of falling relative humidity RH during the day and rising RH in the evening, also related to air temperature control. The standard EN ISO 13788 aims to avoid both interstitial condensation and condensation on the internal surfaces that could promote the mould growth [Fang L. et alii, 1998; Grant C. et alii, 1989; Viitanen, H., 1996]. The basic assumption for the calculations required by this standard is that the walls and house itself do not appreciably affect the internal moisture level. This is a realistic assumption if the materials used have a poor moisture sorption capacity and furthermore if the interior surfaces are coated with paint impermeable to moisture. In this paper, it is shown how it is possible to obtain a notable effect on the dampening of the indoor relative humidity variations using moisture adsorbent materials and permeable paint in the interior surfaces of the house.

2. Theoretical model

The most popular models for the evaluation of humidity inside the indoor environment provide a simple steady state balance, between the production of moisture due to the activities of people and ventilation, neglecting the moisture buffering effects of materials in contact with indoor air.

The absorption properties of the walls can play an important role to moderate the variation of indoor relative humidity.

The model presented here is not appropriate for detailed building simulations, but it can be used as a basis to take into account the hygroscopic interaction between the indoor air and different materials of walls and furniture.

The model assumes that the moisture production has a sinusoidal variation along the day around a mean value \bar{G}_w . This is an approximation of a day night cycle of moisture production in the ambient. The hygroscopic surface is assumed to behave as a semi-infinite solid.

2.1 Heat transfer model

The heat flux in an isotropic medium is governed by Fourier's law:

$$\mathbf{q} = -\lambda \nabla T \quad (1)$$

where λ [$\text{W} \cdot \text{m}^{-1} \cdot \text{K}^{-1}$] is the thermal conductivity and T [K] the temperature.

The general differential equation of heat conduction is:

$$\rho c \frac{\partial T}{\partial \tau} = \nabla \cdot (\lambda \nabla T) \quad (2)$$

with ρ [$\text{kg} \cdot \text{m}^{-3}$] and c [$\text{J} \cdot \text{kg}^{-1} \cdot \text{K}^{-1}$], respectively, the density and specific heat of the material.

Consider the heat transfer in semi-infinite solid which is exposed at the surface $x = 0$ to a sinusoidal temperature variation of amplitude ΔT around \bar{T} and period τ_0

$$T_s = \bar{T} + \tilde{T} = \bar{T} + \Delta T e^{i(\omega \tau - \phi)} \quad (3)$$

The temperature solution is:

$$T_s = T_m + \Delta T e^{i(\omega \tau - \phi) - (1+i)x/d^*} \quad (4)$$

where x [m] is the spatial coordinate, d^* [m] is the penetration depth:

$$d^* = \sqrt{\frac{a \tau_0}{\pi}} \quad (5)$$

where $a = \lambda / \rho c$ the thermal diffusivity [$\text{m}^2 \cdot \text{s}^{-1}$]

The heat flux q [$\text{W} \cdot \text{m}^{-2}$] at the surface $x = 0$ can be determined by Fourier's law as follows:

$$\begin{aligned} q &= -\lambda \left. \frac{\partial T}{\partial x} \right|_{x=0} = (1+i) \frac{\lambda}{d^*} \Delta T e^{i(\omega \tau - \phi)} = \\ &= (1+i) b \sqrt{\frac{\pi}{\tau_0}} \Delta T e^{i(\omega \tau - \phi)} = \frac{\tilde{T}}{Z} \end{aligned} \quad (6)$$

$b = \sqrt{\lambda \rho c}$ is the thermal effusivity [$\text{J} \cdot \text{m}^{-2} \cdot \text{K}^{-1} \cdot \text{s}^{-0.5}$]

that indicates the ability of a material to absorb and release heat and Z is the thermal impedance:

$$Z = \frac{d^*}{2\lambda} + \frac{1}{i\omega \rho c d^*} = R + \frac{1}{i\omega C} \quad (7)$$

If the considered thermal process takes place at a node (the environment) that is coupled to the surface of a building component by means of a thermal surface resistance $R_{si} = 1/h_i$ it is possible rewrite the equation (7) as:

$$Z = \frac{1}{h_i} + \frac{d^*}{2\lambda} + \frac{1}{i\omega \rho c d^*} = R + \frac{1}{i\omega C} \quad (7')$$

Where h_i [$\text{W} \cdot \text{m}^{-2} \cdot \text{K}^{-1}$] is the surface heat transfer coefficient.

Hence we can conclude that heat flux exchange at surface of semi-infinite slab can be represented by a resistance and a capacitance in series.

2.2 Moisture transfer

In a similar way for the vapour transfer the moisture flux is given by Fick's law:

$$\mathbf{g} = -\delta \frac{\partial p_v}{\partial x} \quad (8)$$

where δ is the water vapour permeability [$\text{kg} \cdot \text{m}^{-1} \cdot \text{s}^{-1} \cdot \text{Pa}^{-1}$] and p_v [Pa] the water vapour pressure.

The general differential equation of diffusion of moisture is :

$$\frac{\partial w}{\partial \tau} = \nabla \cdot (\delta \nabla p_v) \quad (9)$$

with w the moisture content [$\text{kg} \cdot \text{m}^{-3}$]

Further derivation gives:

$$\frac{\partial w}{\partial RH} \frac{\partial RH}{\partial \tau} = \frac{\xi}{p_{vs}} \frac{\partial p_v}{\partial \tau} = \nabla \cdot (\delta \nabla p_v) \quad (10)$$

Where ξ is the moisture capacity [$\text{kg} \cdot \text{m}^{-3}$], RH the relative humidity [-]. The function describing $w(RH)$ is the sorption isotherm (Figure 1).

Notice the similarity with the heat transfer equations (2). Hence, the moisture transfer solutions can be obtained from heat transfer solutions exchanging thermal conductivity λ with the water vapour permeability δ and the volumetric thermal capacity ρc with ξ/p_{vs} .

In the case of sinusoidal moisture variation at the surface with amplitude Δp_v the moisture flux at the surface $x = 0$ is then given by:

$$\begin{aligned} g &= (1+i) \frac{\delta}{d_v^*} \Delta p_{vi} e^{i(\omega\tau - \phi)} = \\ &= (1+i) b_v \sqrt{\frac{\pi}{\tau_0}} \Delta p_{vi} e^{i(\omega\tau - \phi)} = \frac{\tilde{p}_{vi}}{Z} \end{aligned} \quad (11)$$

where d_v^* is called moisture penetration depth [m]:

$$d_v^* = \sqrt{\frac{\delta_v p_{vs}}{\xi}} \sqrt{\frac{\tau_0}{\pi}} \quad (12)$$

The moisture penetration depth corresponds to the depth of the wall that participates to the dynamic moisture exchange between the component and the indoor environment, τ_0 [s] is the period of fluctuation, $\omega = 2\pi/\tau_0$ [s^{-1}] is the pulsation and p_{vs} [Pa] the saturation vapour pressure.

ξ is the so called *moisture sorption capacity* [$\text{kg} \cdot \text{m}^{-3}$] and it is the slope of sorption curve ($\xi = \partial u / \partial RH$, see Figure 1): it shows how much moisture content w (in mass by volume [kg/m^3]) must be absorbed/desorbed by the material per unit change in ambient RH before a new equilibrium has been attained after the ambient relative humidity has changed to a new value. In the following model the hysteresis phenomena

have been neglected.

b_v is the moisture effusivity [$\text{kg} \cdot \text{m}^{-2} \cdot \text{s}^{-0.5} \cdot \text{Pa}^{-1}$]:

$$b_v = \sqrt{\delta_v \frac{\xi}{p_{vs}}} \quad (13)$$

It measures the ability of a material to exchange moisture across its surface, when the humidity value changes at its surface and Z is the moisture impedance of the wall [$\text{m}^2 \cdot \text{s} \cdot \text{Pa}/\text{kg}$] defined as follows:

$$Z = \frac{d_v^*}{2\delta_v} + \frac{1}{i\omega \xi \frac{d_v^*}{p_{vs}}} = R_v + \frac{1}{i\omega C_v} \quad (14)$$

with the specific water vapour resistance R_v [$\text{m}^2 \cdot \text{s} \cdot \text{Pa} \cdot \text{kg}^{-1}$] and the surface hygroscopic capacity C_v [$\text{kg} \cdot \text{m}^{-2} \cdot \text{Pa}^{-1}$]

$$R_v = \frac{d_v^*}{2\delta_v} \quad (15)$$

$$C_v = \frac{\xi d_v^*}{p_{vs}} \quad (16)$$

It is possible to conclude that the water vapour flow rate exchange at surface of semi-infinite slab can be represented by a resistance and a capacitance in series.

If a moisture superficial resistance $R_{vs} = 1/\beta_i$ is considered, the RC circuit of moisture transfer at the surface can be represented by an impedance Z due to a specific water vapour resistance R_v and a surface capacitance C_v in series as showed in Figure 2.

Where β_i [$\text{kg} \cdot \text{m}^{-2} \cdot \text{s}^{-1} \cdot \text{Pa}^{-1}$] is the surface water vapour transport coefficient.

Indoor air humidity value is the result of a mass balance among moisture gain, moisture loss and moisture storage. According to the conservation of water mass, water vapour which enters in a room with supply air plus the water vapour produced in that room G_w should equal the water vapour removed with the exhaust air plus the water absorbed by the surfaces of materials in contact

with indoor air plus the water vapour stored in the room air (Figure 3).

The balance can be illustrated by the following equation (17) :

$$\begin{aligned} \rho_{ve} \frac{nV}{3600} + G_w = \\ = \rho_{vi} \frac{nV}{3600} + \sum_n A_n g_n + V \frac{\partial \rho_{vi}}{\partial \tau} \end{aligned} \quad (17)$$

where τ [s] is the time, ρ_{vi} [kg·m⁻³] the water vapour concentration inside, ρ_{ve} [kg·m⁻³] the water vapour concentration outside, n [h⁻¹] the ventilation rate (i.e. the number of room exchanges per unit time), V [m³] the volume of the room, G_w [kg·s⁻¹] the moisture production rate, A [m²] the surfaces available for hygroscopic buffering and g [kg·m⁻²·s⁻¹] the specific water vapour flow rate exchange with absorbing surfaces.

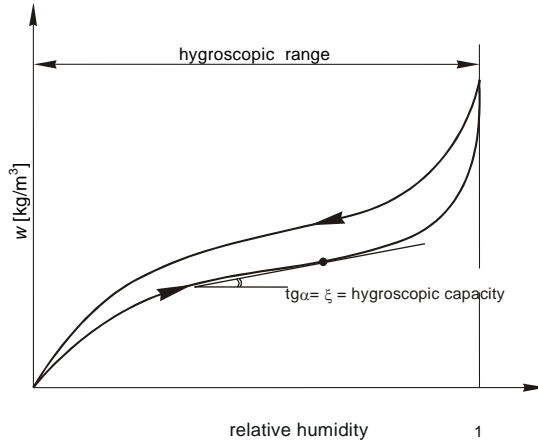


Fig. 1 – Sorption curve. The slope of the curve indicates the moisture capacity ξ .

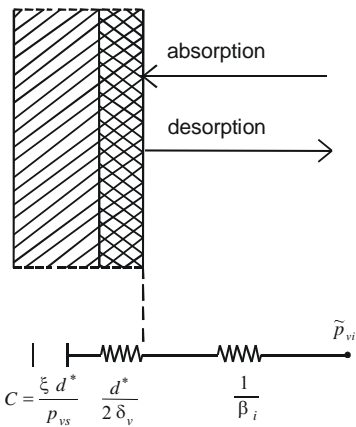


Fig. 2 – The RC configuration simplified model

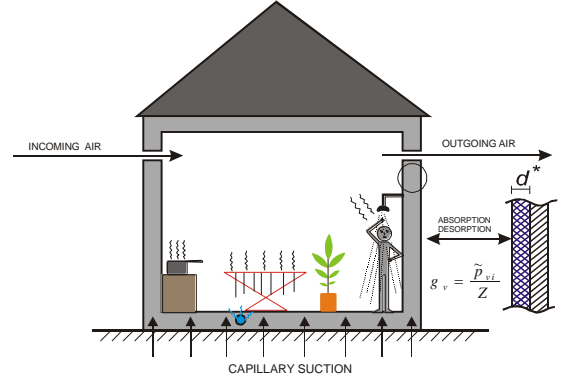


Fig. 3 – Moisture balance of the room

Assuming that the temperature dependency of the vapour concentration is negligible, the moisture balance equation (17) can be rewritten with inside vapour pressure as dependent variable:

$$\begin{aligned} p_{vi} = p_{ve} + \frac{G_w R_w T_i \cdot 3600}{nV} + \\ - \frac{R_w T_i \cdot 3600}{nV} \sum_n A_n g_n - \frac{\partial p_{vi}}{\partial \tau} \cdot \frac{3600}{n} \end{aligned} \quad (18)$$

where p_{vi} [Pa] is the inside vapour pressure, p_{ve} [Pa] is the vapour pressure outside and R_w [J·kg⁻¹·K⁻¹] is the gas constant for water.

The moisture production G_w term includes vapour from people, animals and plants, and released because of housekeeping activities (cooking, washing, cleaning, etc.) [Tenwolde A. et alii, 2001; Viitanen H., 1996].

The moisture production is assumed to have a sinusoidal variation around a mean value $\overline{G_w}$:

$$\tilde{G}_w = G_w - \overline{G_w} = \Delta G_w e^{i(\omega \tau - \phi)} \quad (19)$$

In the simplified model, the water vapour flux exchanged per unit area with the absorbing surfaces can be evaluated by the relation:

$$g_n \cong \frac{\tilde{p}_{vi}}{Z_n} \quad (20)$$

The equation (18) assuming that p_{ve} has a sinusoidal variations around a daily average value with the same frequency then becomes:

$$\tilde{p}_{vi} = \frac{\tilde{p}_{ve} + \frac{\tilde{G}_w R_w T_i \cdot 3600}{nV}}{1 + \frac{R_w T_i \cdot 3600}{nV} \sum_n \frac{A_n}{Z_n} + i \frac{\omega \cdot 3600}{n}} \quad (21)$$

If the computation is performed in a steady state the equation (18) becomes (UNI EN ISO 13788):

$$p_{vi} = p_{ve} + \frac{G_w R_w T_i \cdot 3600}{nV} \quad (22)$$

The difference between inside and outside vapour pressure increases proportionally to moisture production, and inversely to ventilation rate.

The equations of the model above described have been implemented in a Matlab m-file. This file has been used for the numerical simulations of the next section.

3. Numerical examples

We suppose to analyze the hygric response of a room of 65 m³ with a total absorbing area of 100 m². The occupancy and activities lead to a daily sinusoidal moisture variation of amplitude $\Delta G_w = 200$ g/h (i.e. the presence of 4 people). The inside air temperature is 20°C and the starting average relative humidity is $RH = 0.5$.

The surface water vapour transport coefficient is assumed equal to $\beta_i = 1.4 \times 10^{-8}$ [kg · m⁻² · s⁻¹ · Pa⁻¹].

We consider two different cases with different moisture buffering properties of the materials in contact with indoor air. The first case (Table 1): with high sorption capacity of the walls' surfaces and interior surfaces covered with highly permeable paints. The materials adopted in the second case (Table 2) are characterized by low sorption capacity and interior surfaces coated with impermeable paints.

The proposed case study can provide some indications about the hygric capacity of material. Table 1 and Table 2 show the daily indoor water vapour pressure variations Δp_{vi} , the peaks of vapour pressure p_{vi} and relative humidity RH , and the amplitude of relative humidity ΔRH inside the room as a function of ventilation rate n .

The results obtained show how the daily indoor variations of relative humidity can be reduced

starting from around 48% for a room with poor water vapour absorbing surfaces to 17% for a room with high vapour absorbing surfaces and permeable painting. Looking at the evolution of the RH amplitude inside the room, it appears how the moisture buffering properties of the materials can play an important role in the case of lower ventilation rate. Figure 4 shows the values of RH amplitude inside the room as a function of the room ventilation rate n . In order to take into account the effect of surface water vapour transport coefficient the simulations were performed also with $\beta_i = 0.45 \cdot 10^{-8}$ kg·m⁻²·s⁻¹·Pa⁻¹ (low β_i dashed line) and $\beta_i = 4.35 \times 10^{-8}$ kg·m⁻²·s⁻¹·Pa⁻¹ (high β_i dot-dash line). The graphs of Figure 6 show the weak influence of the coefficient and particularly there is no appreciable effect for the low buffering materials case (dashed line and dot dash line are superposed).

n	Δp_{vi}	p_{vi}	RH	ΔRH
h^{-1}	Pa	Pa	%	%
0.	396.40	1564.9	67.0	17.0
0.3	372.06	1540.56	65.9	15.9
0.4	348.31	1516.81	64.9	14.9
0.5	326.56	1495.06	64.0	14.0
0.6	306.76	1475.26	63.1	13.1
0.7	288.78	1457.28	62.4	12.4
0.8	272.45	1440.95	61.7	11.7
0.9	257.63	1426.13	61.0	11.0
1	244.14	1412.64	60.4	10.4

Table 1 – Amplitude of the RH in the room in the case of walls finished with moisture buffer materials ($d^* = 0.0154$ m, $b_v = 11.88 \cdot 10^{-8}$ kg m⁻² s^{-0.5} Pa⁻¹)

n	Δp_{vi}	p_{vi}	RH	ΔRH
h^{-1}	Pa	Pa	%	%
0.2	1122.90	2292.01	98.1	48.1
0.3	947.35	2115.85	90.5	40.5
0.4	802.81	1971.31	84.4	34.4
0.5	689.38	1857.88	79.5	29.5
0.6	600.63	1769.13	75.7	25.7
0.7	530.37	1698.87	72.7	22.7
0.8	473.88	1642.38	70.3	20.3
0.9	427.70	1596.2	68.3	18.3
1	389.39	1557.89	66.7	16.7

Table 2 – Amplitude of the RH in the room in the case of walls finished with low moisture buffer materials ($d^* = 0.0254$ m, $b_v = 65.4 \cdot 10^{-9}$ kg m⁻² s^{-0.5} Pa⁻¹)

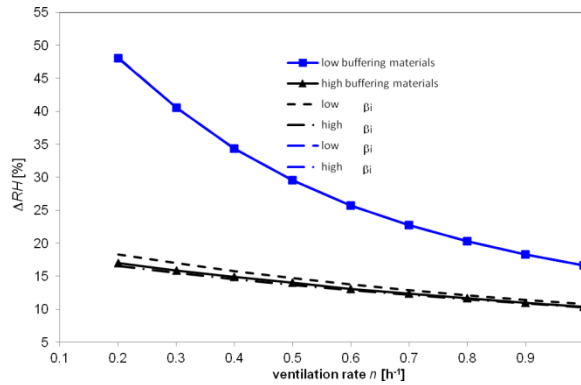


Fig. 4 – Relative humidity amplitude ΔRH inside the room as a function of ventilation rate n .

4. Conclusions

Building materials (i.e. plaster) and material used as furnishings (i.e. carpets,...) and other objects are able to adsorb moisture directly from the indoor air. Using the proposed simplified model, it has been possible to simulate a notable dampening effect on indoor relative humidity variations when moisture buffering materials are used.

The simplified model used in this paper can simulate the dynamic indoor conditions of a room. Moreover, such models can show the order of magnitude of the impact on the indoor humidity variations of the moisture buffering capacity of materials used in the walls, floors, ceiling and furniture.

The obtained data underlines the importance of a correct ventilation rate n in order to avoid indoor RH values that could favour mould growth.

It may be concluded that the use of absorbent plasters on the internal surfaces of the walls and the use of paints of high permeability contribute to dampen the indoor humidity fluctuations.

However, due to the complexity of the transient heat and moisture transfer process these results should be considered preliminary and further analyses should be carried out using more sophisticated heat and mass transfer models.

5. Nomenclature

$\overline{G_w}$ = average moisture production [$\text{kg}\cdot\text{s}^{-1}$];

R_v = specific water vapour resistance [$\text{m}^2 \text{ s Pa kg}^{-1}$];

C_v = surface hygroscopic capacity [$\text{kg}\cdot\text{m}^{-2} \cdot \text{Pa}^{-1}$];

Z = vapour impedance [$\text{m}^2 \cdot \text{s} \cdot \text{Pa}\cdot\text{kg}^{-1}$];

V = volume [m^3];

d^* = penetration depth [m];

τ_0 = the period of fluctuation [s];

b_v = moisture effusivity [$\text{kg} \cdot \text{s}^{-0.5} \cdot \text{Pa}^{-1} \cdot \text{m}^{-2}$];

ξ = moisture sorption capacity [$\text{kg}\cdot\text{m}^{-3}$];

δ_v = water vapour permeability [$\text{kg} \cdot \text{m}^{-1}\cdot\text{s}^{-1} \cdot \text{Pa}^{-1}$];

p_v = vapour pressure [Pa];

n = ventilation rate [h^{-1}];

RH = relative humidity [-];

ρ = concentration [$\text{kg}\cdot\text{m}^{-3}$];

t = time [s]

References

- Carmeliet J., Roels S. "Determination of the Moisture Capacity of Porous Building Materials", *Journal of Thermal Envelope and Building Science*, 24, 209-237, (2002).
- Fang L., Clausen G., Fanger P.O. "Impact of Temperature and Humidity on the perception of Indoor Air Quality", *Indoor air*, 8, 80-90, (1998).
- Grant C., Hunter C. A., Flanningam B., Bravery A. F. "The moisture requirements of moulds isolated from domestic dwellings". *International Biodeterioration*. 25, 259-284 (1989).
- Peuhkuri R., Rode C., Hansen K. K. "Moisture buffer capacity of different Insulating Materials", In: *Proceedings of Performance of Exterior Envelopes of Whole Building XI*, Clearwater Beach, Florida (2004).
- Tenwolde, Anton, S. Walker. "Interior moisture design loads for residences." In: *Buildings VIII: Performance of exterior envelopes of whole buildings VIII; integration of building envelopes*, December 7th, 2001, Clearwater Beach, Florida. Atlanta, GA: American Society of Heating, Refrigerating and Air - Conditioning Engineers, Inc. 2001.

Tenwolde, Anton, "Ventilation, humidity and condensation in manufactured houses during winter", ASHRAE Transaction, 100 (1), 1994.

UNI EN ISO 13788, "Hygrothermal performance of building components and building elements. Internal surface temperature to avoid critical surface humidity and interstitial condensation. Calculation methods", (2003).

Viitanen, H. 1996, "Factors affecting the development of mould and brown rot decay in wooden material and wooden structures. Effect of humidity, temperature and exposure time. Dissertation." Uppsala, SLU, For. Prod. 58 p.

Toward an EnergyPlus decision tool for evaluation of energy performances during early-stage building design

Marco Picco – Dept. of Engineering, University of Bergamo, Dalmine, Italy

Marco Marengo – Dept. of Engineering, University of Bergamo Dalmine, Italy

Abstract

The paper analyses the benefits of energy analysis application in early-stage design. The research highlights the barriers that prevent this early integration and finally proposes the development of a simplified software tool tailored around the optimization of energy efficiency during early-stage design. Generally, the research aims to identify (a) the accuracy in results obtainable through progressive simplifications of the building model, (b) the most significant building parameters with respect to the output accuracy and (c) the maximum level of simplifications able to ensure the respect of time requirements dictated by early-stage building design and to maintain an acceptable level of accuracy.

Here, a single case study of a large multi-storey office building is modelled starting with a detailed simulation performed through EnergyPlus and Openstudio software. The detailed model is then analysed and progressively simplified. At each progressive simplification step, a comparison with the detailed model is given in terms of building energy loads and power curves of the system.

Total differences between detailed and simplified models are analysed to determine the quality of the results of the simplified model.

1. Introduction

The daily operation of commercial and residential buildings comprises roughly one-third of the world's primary energy consumption. Because buildings are typically operated for many years, there is great potential for reducing global energy needs through improved building design (Urban et al., 2006).

Most of the energy consumed in buildings is the result of fossil fuel combustion, either directly or in the generation of electricity. One major path to reduce human impact on global warming is to

design buildings and building renovations that have minimal energy demands and meet those demands with renewable energy rather than fossil fuels (Uttinger et al., 2009).

Computer modelling and simulation is a powerful technology for addressing interacting architectural, mechanical, and civil engineering issues in buildings. Building performance simulations can help in reducing emission of greenhouse gasses and in providing substantial improvements in fuel consumption and comfort levels, by treating buildings and their thermal systems as complete optimized entities and not as the sum of a number of separately designed and optimized sub-systems or components (Hensen, 2004).

Many existing energy simulation tools for buildings are very sophisticated and promise a high level of accuracy. Popular tools such as Energy Plus and DOE-2 are quite effective at simulating final building designs and are typically used for demonstrating compliance with performance standards such as LEED.

However, despite the proliferation of many building energy analysis tools in the last ten years, architects and designers are still finding it difficult to use even basic tools (Punjabi et al., 2005). Findings confirm that most BPS tools are not compatible with architects' working methods and needs (Attia et al., 2009; Gratia et al., 2002).

Although building energy simulation is a useful tool for predicting performance and comparing design options, most energy simulations occur too late in the design process (Ellis et al., 2008). In the traditional design process, the energy engineer uses simulation, if at all, as a tool for equipment sizing and code compliance only after the architect has completed the architectural design. Part of the problem is that existing simulation tools are not

practical for the design process. Experience with real buildings has shown that low-energy design is not intuitive and that simulation should therefore be an integral part of the design process (Torcellini et al., 1999; Hayter et al. 2001).

In conceptual design it is important to be able to evaluate multiple concepts, and to quantify, rank-order, and even to be able to semi-automatically generate design alternatives. Qualification and quantification of variant solutions is here more important than detailed assessment of a single case. Therefore, in this approach the level of resolution can be generally low.

These initial concept decisions are critical as they can determine the majority of a building's energy use profile. Unfortunately, energy modelling is rarely leveraged in the concept phase to provide information that could drive these critical decisions. This is a missed opportunity, since energy modelling in the concept phase can be a very powerful tool for the entire design team (Tupper et al., 2010).

Needs related to the design process can be easily identified as time and accuracy. Accuracy is an essential prerequisite for every analysis used for decision making, in every field. If the analysis is not accurate the results could be misleading and the decisions made based on those results could be non-optimal or even completely wrong. The problem becomes significantly more relevant during the design process of buildings, where decisions taken can concern a large amount of energy and can affect the building for many years. To worsen this issue is the difficulty to modify wrong decisions made early in subsequent design phases or even during the management of the building.

Accurate energy analysis requires time, up to several weeks in more complex cases, and the more accurate the analysis must be the more time it will require. This is in contrast with the necessity to minimize the time requirements to make it compatible with design times, but to do so simplifications to the building model and simulation tool are needed, with the drawback of a loss in accuracy. Another way to reduce time requirements could be the introduction of default values and databases for inputs, with the possible risk of reducing the model detail level and degree of freedom, themselves influencing the accuracy or relevance of the final result.

2. Strategy for the decision tool

The present study is part of a research framework for the development of a tool that targets the early-stages of the design process: a time when design details are often sparse and uncertain, simulation time is limited, and major decisions are not yet finalized. Most tools are overly complicated for this task and do not provide an easy way to compare the trade-offs between design options (Urban et al., 2006). The aim of this project is to provide a fast way to assist designers in the decision making process during the first hours of design.

By restricting the input space to the most critical design parameters a tool could rapidly predict a design's performance. The primary objective is not an exact performance prediction of the final building design. What is important is that the user is able to identify which design factors have the highest impact on energy use and thermal comfort relative to the others.

Although restricting the detail in the inputs, the computational model is still quite sophisticated, being based on the energyPlus simulation engine.

It is also interesting to note that, by using a complete simulation engine like energyPlus, it is possible to generate an IDF file of the simplified model, which can then be integrated and expanded in the subsequent design phases.

In particular the research concentrates on the analysis of large commercial buildings in Italy. The main field of application of building performance simulation during design should be on large buildings as total costs better justify the inclusion of this kind of studies. Commercial buildings are also generally more energy intensive, leaving more room for the implementation of energy saving solutions, and less suited to standard energy saving solutions compared to residential structures.

As previously mentioned, the proposed tool will not directly perform any energy calculation, instead, based on the data inputs required, it will generate an energyPlus input file leaving energy calculations to the standard EnergyPlus simulation engine.

It is crucial to identify the adequate level of accuracy needed at each design phase and develop a corresponding model/tool of the building sufficiently simplified not to require data not yet

available, to be run and evaluated compatibly with the corresponding design phase times and meanwhile complex enough to guarantee an adequate level of accuracy so that obtained results can still be relevant.

Exactly this relation of accuracy and time needed is the basis of this study, analysing the gradual simplification of a complex building model evaluating changes in time and input needed to build the model and run the simulation and the gradual loss in accuracy in relation to the complete model, to find the optimum level of simplification of the model needed to apply energy analysis at each design phases with adequate time and accuracy, particularly focusing on the conceptual phase.

The research is developed in three main phases, first a simulation protocol is written, able to create an energy model of the building starting from general inputs available during conceptual design, in the second step the protocol is tested and improved through its application to an adequate number of case studies and lastly the protocol is to be implemented into a design tool able to generate the building model and run simulations with a limited number of input data.

All the case studies will be developed following the same pattern as seen in figure 1: a complete building model will be implemented in EnergyPlus and assumed as the “base case model”; from there a given number of simplification steps will be applied, each analysing one major aspect of the simplification protocol as detailed in the next section. For each

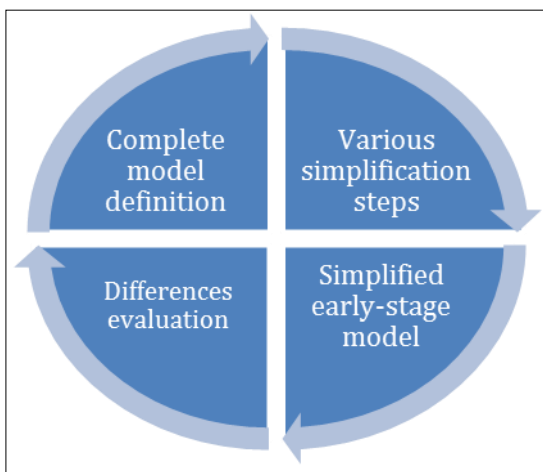


Fig. 1 – Simplification process

step, output differences from the base case in term of energy and power loads are analysed to identify the total difference generated by the simplified model.

In the following section the first of those case studies is implemented and analysed also describing the major aspects of the simplification protocol.

3. Case study simulation

The case study in exam is an office building built in 1954, fully renovated in 2007, situated in Bolzano, Italy, and certified as Klimahaus Gold with a calculated energy demand of 7 kWh/m²y according to Klimahaus calculation. The heated surface amounts to 2,841 m² for an inner volume of 12,817 m³ (Troi et al., 2008).

The building shell is designed as an ETIC system with 35 cm of EPS insulation, reaching a U-value of 0.08 W/m²K. The facade arrangement mirrors that of the existing structure, with a 16 % window-to-wall fraction. The windows are of the 3-pane type with plastic frame, insulated in the sunscreen plane with polyurethane. The result is passive-house suitable windows with a U-value of 0.79 W/(m²K).

On the system side, the building is provided with mechanical ventilation handled by a central AHU which provides refrigeration and dehumidification of the intake air. The AHU is also equipped with an high efficiency enthalpic heat recovery system with a 90% sensible effectiveness and 75% latent effectiveness. The refrigerant circuit is powered by an air-to-air electric chiller with a 3.5 nominal COP and 87.5 kW capacity.

Air heating is handled by re-heater coils in the air system and additional fan-coils, all connected to a water circuit powered by one central condensing boiler with 60 kW capacity and estimated 100% efficiency.

3.1 Detailed model

As a first step in the analysis a complete and exhaustive building model (figure 2) is created using energyPlus and its interface plugin Openstudio.

The model consists in thirty-five homogenous thermal zones, fully describing all conditioned rooms, underground semi-conditioned spaces and

all accessory non-conditioned volumes like deposits and interspaces. The vertical effect of staircases is also taken into account, modelling the two existing stairwells as an unique thermal zone each.

Twenty-three construction types are identified to characterize the construction in its entirety, of which two are transparent, triple glazed Krypton windows for above ground and double glazed air windows for underground spaces. To do so twenty-five different “material” objects are modelled.

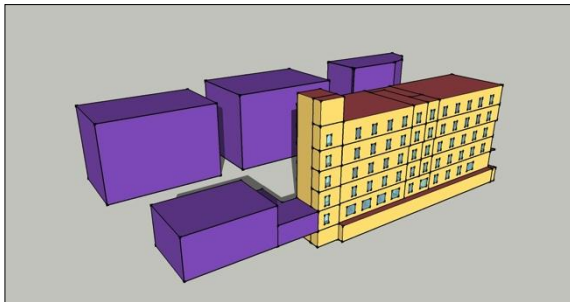


Fig. 2 – Overall view of the complete model

Each window is modelled individually for a total of 198 fenestration surfaces, of which forty-five are inter-zone surfaces modelled in the underground interspaces. All the relevant shadowing objects have been modelled comprising all the adjacent structures, in this case situated to the north-west of the building, and the building specific solar obstructions, consisting only in canopies above the two main entrances of the building as there is no individual shadowing for the various fenestrations. Four zone archetypes are defined to characterize the various zones, each one defined in terms of occupancy, lights, electrical equipment and air infiltration, each defined by a design value function of the zone area and an appropriately written time schedule. Temperature and humidity set-points and set-backs are also defined for each archetype following the real behaviour of the building thanks to monitored data.

The system has been modelled as a VAV system with humidity control comprised of a central AHU with cooling and heating coils and reheat coils for each zone. Additional fan-coils are not modelled limiting the conditioning system to the coils in the airstream. Nonetheless obtained results are in accordance with available monitored data. All coils are connected to hot and cooled water circuits

respectively powered by a central gas boiler and an electric centrifugal chiller. Heat recovery is also modelled as previously described.

Standard monthly mean ground temperature reported in the weather file have been modified to better represent actual conditions of the case study.

The simulation is performed for the duration of one solar year, starting January 1st and ending December 31st, under conditions provided by weather file “Bolzano 160200 (IGDG)” of the energyPlus database, identified as being the closest to the real building location.

Results of the simulation are then calibrated based on actual measured data available for the building mainly in terms of internal set-points to better represent the behaviour of the real building.

Six points of comparison are identified in simulation results to evaluate the accuracy of subsequent model simplifications. Those reference data are identified based on the concept of evaluating the accuracy of the model in reference to the most useful data typically used during early design stage.

The six points of comparison are defined as the annual building energy loads for heating and cooling, the peak power requirement for both heating and cooling systems and the power-time curves for heating and cooling.

The first two reference points are deemed the most relevant for comparison of different building design, therefore extremely useful during concept design. The last four points are more useful in system sizing so to know the required equipment size and use of the system over time.

Following, the simplification process is analysed defining each step singularly on a general standpoint and detailing its application to the case study in exam.

3.2 STEP 01. Simplified Constructions

The first step in the simplification process concerns the building constructions. The simplification is based on the identification of a single construction type for each kind of surface present in the model. The simplified constructions scheme is based on the identification of six construction types: exterior walls, exterior roof, exterior floor, fenestrations, interior walls and interior floors. Of those, in the

suggested tool, only the first four will be required to the user as input data, the last two will be derived by the software based on the input data provided for the other constructions.

In more detail the first three constructions, regarding opaque surfaces, are to be characterized by a single thermal conductivity value, in $\text{W/m}^2\text{K}$, of the complete construction package for each surface type and one global information regarding the construction mass for the entire building, by which the two interior constructions will also be deduced. Starting by those values a fictitious construction is to be reconstructed by the tool in the form of material and construction objects required by energyPlus resulting in construction packages with the characteristics inputted in the data. A construction mass information, in the form of database selection, is required to properly account for thermal inertia of the building. The fourth kind of construction references transparent surfaces, windows and fenestration in general, and is believed not to be properly represented by a limited amount of data, therefore this construction will be selected by a provided database for which energyPlus itself already provide various entries.

This simplification step constitutes a relevant reduction in the input data required by the model, going from a complete description of each construction present and all the materials that compose it to a total of three input data for conductivity and two database selections.

In the case study here analysed, for each construction type previously mentioned, a weighted mean, function of the total surface area, of the conductivity of all construction present is done and an average conductivity is identified. Based on the known structural type of the building the six reference constructions are identified. For fenestrations the construction is identified by the only relevant type of windows present, triple glazed windows with insulated plastic frame.

3.3 STEP 02. Removal of external obstructions

The second simplification step is identified in the removal of all external obstructions modelled, like external buildings or other external elements,

consisting in the removal of any shadowing surface implemented in the complete model but not specifically planned as an obstruction for the single fenestrations. Shadowing surfaces for fenestrations can be simplified requiring the vertical distance by the window and the horizontal length of the overhang.

This step is not dictated by the unavailability of needed information, as the position of the building and its surroundings are one of the first information known, but by the observation that the modelling of external obstruction would be a too cumbersome and detailed work for this stage and is in fact one of the most common simplifications applied in practice without noticing; conversely shadowing of fenestrations can be a specific design choice with significant impact on energy needs and so needs to be modelled but exact dimensions of each shadowing element are probably not yet known.

3.4 STEP 03. Zones Lumping

Lumping of zones for each floor consists in the characterization of each floor of the building with one single thermal zone. This, with the simplification of constructions, permits to define an entire building floor with a really limited number of building surfaces and therefore a limited number of input needed. Also limiting the number of zones on floor to one impacts on the need for defining zone archetypes, eliminating all accessory zones and characterizing each floor, and therefore the building itself, by its dominant intended use. This is a relevant simplification hypothesis and is expected to greatly impact the model behaviour.

This simplification is greatly in accordance with the available data during the initial design phases as zone distribution and characteristics are typically not known, or only generally assumed, during early-stage design.

In the case study each floor is represented by a new single zone, losing the modelling of staircases, and each zone-floor is characterized by the zone archetype considered dominant in the complete model. The result is the selection of the office archetype for each floor with the exception of underground and top ones, consisting of a small

storage room, characterized by the deposit archetype.

3.5 STEP 04. Simplified transparent surfaces

This simplification step is meant to reduce the data input to fully model transparent surfaces of the entire building. It requires the previous simplification step, namely the lumping of zones for floor to be performed. The idea underlying this step is to model the sum of all transparent surfaces on each floor with only four transparent surfaces, one for each relative cardinal direction. For each building floor and for each direction only one transparent surface is identified with the purpose to model all the surfaces oriented in that direction.

Two solutions have been identified as the most adequate for the purpose: the modelling of one single surface with total area equal to the summed area of all surfaces in the complete model and generated based on a reference fenestration height for a total of two data inputs for each surface and a total of eight for each floor, and the modelling of one reference surface representative of one single fenestration of the complete model then multiplied through a surface multiplier to obtain the total area of the fenestration, thus requiring three input data for each direction.

Different simulations have been performed based on those two modelling hypothesis and no relevant differences can be noticed in term of result accuracy, with differences of ~0.1% in respect to each other and not significantly favouring one of the two solutions. Based on those considerations the first of the two solutions is preferred, presenting comparable accuracy results but a much simpler data input structure requiring less information with a simpler building model.

Like the previous ones, this simplification is greatly in accordance with information available during early design process.

3.6 STEP 05. Single floor standardization

The intention of this simplification step is to be able to geometrically describe one single floor element to represent the entire building, greatly reducing the number of input required for the model especially in

the case of multiple storey buildings. This is attempted through the cancellation of all accessory spaces and by standardizing the different floor plans to a reference one.

In the case study this simplification step is performed by cancelling all the accessory zones, the deposit zones on the roof and the underground cavity interspaces, still considered in the model through the application of appropriate outside boundary conditions to the underground floor, this will be replicated in the final tool with the addition of one data input in reference to underground boundary conditions.

3.7 STEP 06. Zone squaring

In conjunction with the previous step this simplification is meant to allow the full geometrical description of the building with a really limited number of inputs. In particular this step intent is to describe the geometry of a single zone with a simple rectangular box.

The major geometrical aspect which impacts the thermal behaviour of a building can be identified in the area of the vertical dispersant surfaces, so maintaining them as near as possible to the detailed model is the first priority of the simplified model. The simplified zone box is therefore modelled equalling the relative south-north and relative east-west exposed surfaces area to the ones of the complete model.

The second major aspect which influences thermal behaviour is the zone floor area, which is a dispersant surface for the terminal zones and characterizes all internal gains and air changes. Modelling the zone as a simple box can lead to very large errors in the estimation of floor area, so an additional input is required for the medium floor area of the building.

The final simplified model is characterized by four data inputs: South-north face length, east-west face length, medium floor height and total floor area.

Like for the previous simplification, this one is also associated with the idea that an accurate geometrical model of the building is not needed during the first design stages due to continuous changes in building shape, therefore favouring an easier and faster

modelling process to better suite integrated design process.

In the case study this simplification step has been applied, in a first stage, with three different floor area estimation methodologies to evaluate their effect. Floor area equal to the area of the box generated by vertical surfaces, floor area equal to the mean floor area of the building and floor area specified for each floor.

As expected, the first solution presents a relevant difference in results due to the significant errors in modelled floor area compared to actual floor area, in this case being the building quite regular in shape the output difference corresponds to 2.5%, which is considered relevant and can become a lot larger with different and more complex building shapes; the difference between the last two cases is instead considered marginal (<1%) and not influenced by building shape. The third option is the more accurate but the second one requires significantly less input data and is more suited for early design phases so it is favoured over the alternatives. The complete analysis is performed based on the second floor area estimation method.

3.8 STEP 07. Standardization of transparent surfaces

During step 04 the calculation of total area of transparent surfaces for each cardinal direction has been made singularly for each floor. In this simplification step this calculation is carried out for the entire building and then divided for the number of floors, obtaining the same surface area for each floor and therefore significantly reducing the number of inputs required by the model.

The simplification is also in accordance with the design process itself as, generally, the detailed dimension of the single windows are not fixed until the later design phases and therefore an accurate calculation of fenestration area different for each floor is not possible and easily subject to changes. It is therefore more useful to refer to a mean fenestration area for each direction.

3.9 STEP 08. Number of floors modelled

The last simplification step is meant to model a building through a fixed number of floors, and

therefore thermal zones, regardless of the actual number of floors of the real building, reproducing them through the use of zone multipliers applied to the modelled zones.

This step does not have any relation with the design process in any of its phases as the number of floors is already known and is essential information which cannot be overlooked. Moreover the actual number is taken into account by this simplification, just not directly by modelling each floor with a zone. This also does not change the input scheme or reduce the number of inputs required for the creation of the model as the only input concerned by this step is the number of building floors, which is essential as previously mentioned.

The intention of this simplification step is for a more standardized model that the tool needs to recreate. If the number of floors is fixed, the model needed to describe it has the same structure independent from the building itself, allowing for an easier development of the tool. Also, in the case of high-rise buildings or buildings with a great number of floors in general, this step is useful to avoid the generation of a too complex model from which long simulation times would originates.

In the case study this simplification is implemented by modelling a total of three zones, or floors, as seen in figure 3: one for the underground deposit, one for the top floor and one for the middle floors to which a multiplier of four is applied to fully model all the building floors. The zones are linked differently from the complete model to guarantee an appropriate behaviour of the model.

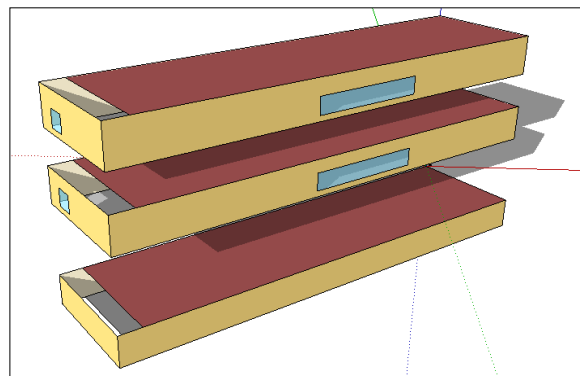


Fig. 3 – Overall view of the fully simplified model

4. Result analysis

A full year simulation has been performed for each simplification step previously detailed. For each simulation the results have been obtained and subsequently compared to those of the complete model in term of total annual loads, peak power loads and power curves shape for both cooling and heating in order to evaluate differences generated by simplification.

Table 1 reports the obtained results from the VAV model for total heating loads, results reported are, in order, the total estimated heating loads for the building, the percentage difference from the previous step, the total percentage difference from the complete model and lastly the cumulative absolute percentage difference between the complete model and all the previous simplification steps.

It can be seen that major difference generation occurs during simplification steps 03 and 08, which are respectively the zone lumping simplification step and the number of floor simplification step, with a 5.79% and a 4.81% difference increase from the previous steps. For step 03 this was expected as the simplification requires major changes in the model and a strong approximation in the operation of the building, also merging zones tend to mitigate extreme conditions. Differences in step 08 can be attributed to the humidity control implemented in the VAV system.

Relevant differences are also generated by floor standardization simplification step, due to the removal of semi-external unconditioned zones, and interestingly a difference of 3.0% is generated by the remove of external shadowing surface, which in this case study consist in the nearby buildings.

Total generated difference for heating loads for the whole simulation period equals to 15.55%.

In figure 4 a representation of the various heating power curves can be seen from which it is possible to notice that differences in terms of total peak power for heating are relatively small and only add to a total of less than 4% for all the simplifications. Also no major differences can be identified in the resulting curves, this is also confirmed by running statistic likelihood tests with the complete model results as the null hypothesis, for which the result is that there is no relevant difference in the two curves.

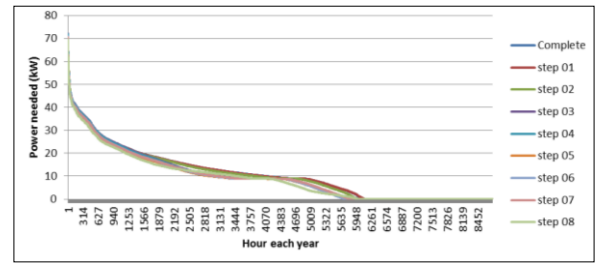


Fig. 4 – Heating power curves comparison for each simplification step

Similar analyses can be carried out for the cooling loads of the building (table 2 and figure 5) from which it is possible to notice that differences in step 03 and 08 becomes larger, due to the mixing of various zone conditions, and are still the most relevant for the same reasons mentioned above. Also difference in the shadow simplification step increases for the cooling period as differences for the other steps tends to decrease, reaching a total of 14.56% for all the steps.

In terms of cooling power curves no major differences can be identified as confirmed by statistical likelihood tests but this time the differences in power peaks become more relevant starting from the 141kW power peak of the complete model and decreasing at 129kW for the final simplification, for a total difference of nearly 9%, still below the total difference registered for total cooling loads.

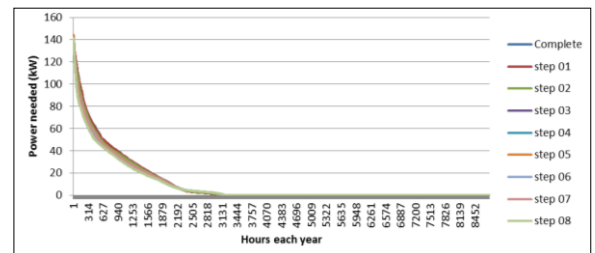


Fig. 5 – Cooling power curves comparison for each simplification step

Applying the simplification protocol on this particular case study for the “external obstruction” step, all the external buildings and canopies at the entrances have been removed. The building does not present any particular shadowing technology for single fenestrations, so this aspect of the simplification cannot be considered in the analysis as irrelevant in this case.

	FULL MODEL	SIMPLIFICATIONS							
		STEP 01	STEP 02	STEP 03	STEP 04	STEP 05	STEP 06	STEP 07	STEP 08
	kWh	kWh	kWh	kWh	kWh	kWh	kWh	kWh	kWh
Total	94566	94387	91556	86255	85023	81911	83015	83903	79864
Diff %	0.00	-0.19	-3.00	-5.79	-1.43	-3.66	1.35	1.07	-4.81
Diff % tot	0.00	-0.19	-3.18	-8.79	-10.09	-13.38	-12.21	-11.28	-15.55
Diff% cum	0.00	0.19	3.19	8.98	10.41	14.07	15.42	16.49	21.30

Table 1 – Percentage differences on heating loads for each simplification step

	FULL MODEL	SIMPLIFICATIONS							
		STEP 01	STEP 02	STEP 03	STEP 04	STEP 05	STEP 06	STEP 07	STEP 08
	kWh	kWh	kWh	kWh	kWh	kWh	kWh	kWh	kWh
Total	94022	94170	90365	85288	85130	85057	85397	87184	80331
Diff %	0.00	0.16	-4.04	-5.62	-0.18	-0.09	0.40	2.09	-7.86
Diff % tot	0.00	0.16	-3.89	-9.29	-9.46	-9.53	-9.17	-7.27	-14.56
Diff% cum	0.00	0.16	4.20	9.82	10.00	10.09	10.49	12.58	20.44

Table 2 – Percentage differences on cooling loads for each simplification step

5. Conclusions

Buildings are responsible for a tremendous amount of energy consumption also due to their long lifetimes and continuous operation. Efficient design is critical, especially at the early stages as poor decisions made early become difficult or impossible to correct later. Existing energy simulation tools fail to meet the needs of architects and building designers at the early stages of design due to the excessive complexity of the tools and amount of required information.

The proposed simplification protocol seeks to meet this need by providing a fast and simple way to perform building energy simulations and assist with the selection of appropriate building components and systems during early design stages.

It is believed that a difference of 20% between the detailed and simplified models is an acceptable result to provide useful information for the design process, taking into account the lack and uncertainty in information provided during early design phases. Differences found between the simplified model implemented and a detailed model for this specific case study, are in the worst case equal to 15.6% for heating loads and 14.6% for cooling loads, in line with expectations. Even better results are achieved in term of heating and cooling peak loads, with the

respective differences of -4% and -9% with respect to the complete model.

Although based on only one case study the presented results, featuring differences within the margin of 20% compared to a detailed model, bodes well that the simplification protocol and the expected tool can provide useful information for the design process, driving the research toward the implementation of new case studies able to improve the simplification protocol and generalize the obtained results, culminating in the creation of the proposed simplified design tool.

The application of the case study also allowed to evaluate various possible simplification techniques for specific problems like transparent surfaces and building floor area identifying the best solution in term of differences generated and inputs required.

It can also be noticed that many of the differences observed are concentrated on the lower tail of the two power curves when the loads become lower and discontinuous, typical of mid seasons and, for the heating power curve, humidity control during summer.

It can be concluded that the application of the described protocol can help reduce the time requirements for a dynamic simulation from up to

several days to only 2-4 hours at the cost of an acceptable increase in result uncertainty. The expected simulation tool should increasingly reduce time requirements through automation of model creation to under one hour.

6. Acknowledgements

We acknowledge the EURAC research group, Institute for Renewable Energy, and particularly Eng. Roberto Lollini and Eng. Annamaria Belleri, for the help in the identification of the proposed case study building and in retrieving all the building information needed. We also thanks Dr. Arch. Michael Tribus, designer of the building renovation, for providing design plans.

References

- Attia, S., et al., 2009. Architect friendly: a comparison of ten different building performance simulation tools. Building simulation 2009, Eleventh International IBPSA Conference Glasgow, Scotland July 27-30, 2009
- Ellis, P.G., et al., 2008. Energy design plugin: An EnergyPlus plugin for SketchUp. SimBuild2008, Third National Conference of IBPSA-USA Berkeley, California, July 30 – August 1, 2008
- Gratia, E., De Herde, A. 2002. A simple design tool for the thermal study of an office building. Energy and Buildings, 34: p. 279-289.
- Hayter, S.J., Torcellini, P.A., Hayter, R.B., Judkoff, R. 2001. The Energy Design Process for Designing and Constructing High-Performance Buildings. Clima 2000/Napoli 2001 World Congress - Napoli (I), 15-18 September 2001
- Hensen, J. 2004. Towards more effective use of building performance simulation in design. 7th International Conference on Design & Decision Support Systems in Architecture and Urban Planning, Eindhoven, 2-5 July 2004
- Punjabi, S., Miranda, V. 2005. Development of an integrated building design information interface. in IBPSA. Building Simulation 2005, Ninth International IBPSA Conference, Montréal, Canada, August 15-18, 2005
- Torcellini, P.A., Hayter, S.J., Judkoff, R. 1999. Low-Energy Building Design - The Process and a Case Study. ASHRAE Transactions, V 105, Part 2, pp. 802-810. Atlanta, GA: American Society of Heating Refrigerating and Air-Conditioning Engineers.
- Troi, A., et al., 2008. Towards Zero Energy Renovation: Ex-Post Building in Bolzano/Italy. PLEA 2008 - 25th International Conference on Passive and Low Energy Architecture, Dublin, 22nd - 24th October 2008
- Tupper, K., Fluhrer, C. 2010. Energy modelling at each design phase: Strategies to minimize design energy use. Simbuild 2010. Fourth National Conference of IBPSA-USA New York City, New York August 11 – 13, 2010
- Urban, B., Glicksman, L. 2006. The MIT Design Advisor – A fast, simple tool for energy efficient building design. Simbuild 2006 Second National IBPSA-USA Conference Cambridge, MA August 2-4, 2006
- Uttinger, D.M., Bradley, D.E. 2009. Integrating energy simulation in the design process of high performance building: a case study of the Aldo Leopold Legacy center. Building simulation 2009, Eleventh International IBPSA Conference Glasgow, Scotland July 27-30, 2009

Lighting control system: energy efficiency and users' behaviour in office buildings

Michela Chiogna – University of Trento, Trento, Italy

Antonio Frattari – University of Trento, Trento, Italy

Abstract

Due to new European standards and requirements regarding energy performance in non-residential buildings, it is strategic to explore and quantify the benefits of typical energy saving design measures (automatic systems) compared with traditional operation systems (manual system) considering appropriate reference case studies so to benchmark the performance of automatic control systems. In order to set up design and intervention strategies towards energy saving and environmental protection, efficient daylight-responsive systems for illumination of buildings, including installation of automatic lighting control systems, can provide a significant contribution. Moreover, it is becoming increasingly important to establish a realistic baseline of the actual lighting energy consumption in buildings for the different scenarios nowadays used (both manually and automatically operated), which incorporates occupants' behaviour. The analysis of the energy-saving potential of automated lighting scenarios have been monitored in real use conditions and not in controlled laboratory environments, in order to prove the automation systems efficiency in operating time. The building analyzed is an office block of 6 floors, each with 35 units. Different automation scenarios (in number, typology and location of devices installed) were implemented during the renovation activity carried out in 2007. The building configuration, characterized by the same number and offices distribution for each floor, allows for the simultaneous comparison of the operation systems implemented. The monitoring activity was carried out for two years, starting from February 2008. Using standardisation techniques that consider differences in occupancy duration, as well as indoor and outdoor illuminance levels, it is possible to define the quantitative difference between energy performance of conventional and automatic control scenarios.

1. Introduction

As far as the importance of environmental issues is concerned, the built environment plays an important role: the residential and commercial sectors account for more than 40% of end energy consumption in the European Union and are thus responsible for an important part of carbon dioxide emissions systems (UNEP, 2007). According to an IEA (International Energy Agency) estimation, the lighting electricity use ranges from 5% to 15% of the total electrical energy use in industrialized countries. Approximately 50% of lighting energy (531 TWh) in IEA member countries evaluated is used within the service sector (Mills, 2002).

Considerable savings could be achieved even by application of intelligent control technologies in existing buildings, with acceptable economical parameters (Zalesk, 2006). New European regulations refer specifically to the use of occupancy and light sensors to control the artificial light and to improve the systems' efficiency (UNIEN 15913-2008).

Design software tools are intended to help designers with the elements of daylighting design (IEA, 2000) in order to preview the energy saving obtainable using automation lighting systems: specifically the dimming regulation of artificial light as a function of the natural light level detected in discrete points (Erhorn et al., 1994; Reinhart et al., 2001; Reinhart et al., 2001). These simulation tools require lengthy input processes and are too time consuming to be used by architects and designers. Therefore, simplified methods to estimate energy saving of artificial lighting use from daylighting have been developed. Among them the most important operate giving geometrical factor (windows area, windows type, perimeter area) and do not include automation

control systems (Krarti et al., 2005).

Moreover, energy simulation tools for existing buildings do not adequately model the actual performance of daylighting systems: indeed it is possible to overestimate electrical lighting energy saving by 20.7% annually (Seo et al., 2011). The main causes are temporal problems, outdoor illuminance and sky luminance distribution simulation, fenestration features operation, indoor illuminance level expected, human factors and lighting control results.

The last two factors express a high variability and influence significantly the final result of the energy saving amount expected using automation systems. For this reason the international scientific community carried out several studies in order to monitor and analyze users' interactions with building control systems and devices (Hunt, 1979; Reinhart et al. 2002, Mahdavi et al., 2008).

The computational modelling of occupants' control-oriented actions in building performance simulation applications can be significantly improved based on such empirical information on user behaviour (Mahdavi et al., 2007) and on data monitored in real use condition. In this way, it is possible to collect data about both building users' interactions with building control systems and devices' efficiency in order to develop a stochastic model for predicting lighting energy consumption.

For this reason it is strategic to explore and quantify the benefits of typical energy-saving design measures (automated systems) compared with a traditional operation system (manual system), defining suitable reference cases for benchmarking the performance of automated lighting control. The analysis of the energy-saving potential of automated lighting scenarios should be monitored in real use conditions and not in controlled laboratory environment, in order to prove the automation systems efficiency in operating time (Mahdavi et al., 2008).

2. Case study

A specific case study has been analyzed: an office building in Trento (northern Italy) in which a total refurbishment of the electrical system and

informatics net have been carried out recently. The building has 6 floors, each of 1200 m², with a similar indoor distribution. The two main expositions are north and south. The building is characterized by four different and modular office typologies, each with the same power density installed and with the same natural light condition, even if with different surface and occupant number (Table 1).

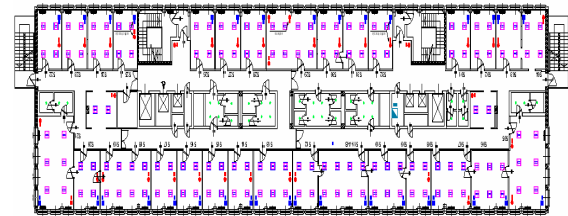


Fig. 1 – Floor type

There is the same windows typology (dimension 1.15m x 1.20m) with a constant inter-axis along both the façades. The same shading system is present: internal venetian blind, manually operated. The artificial light is provided by lamps (1/55 W each, tubes T5). They have been designed in order to maintain 500 lux at the end of the luminaires life, by night. In the first utilization period they produce an over-density of luminous flux.

In the central part of the building service spaces are positioned: corridors, bathrooms, stairs and elevators.

OFFICE TYPOLOGY	DEPTH (m)	WIDTH (m)	SURFACE (m ²)	WINDOW SURFACE (m ²)	ELECTRICAL POWER (W / m ²)
A	5	3,5	17,5	2,76	12,57
B	5	5,25	26,25	4,14	12,57
C	5	7	35	5,52	12,57
D			40-56	6,9	11,00-9,82

Table 1 – Office typology

The D type office represents a peculiar situation regarding:

- *utilisation modality*: not office but meeting room , with different occupancy level;
- *exposition*: not only one but two façade with South East/ South West windows;
- *surface*: the meeting rooms can be different floor by floor;
- *power density*: could be different in relation with the surface area.

Excepted from D type, the other office types can be homogeneously compared, distinguished only by

façade expositions. In this paper we will refer about S_xyy or N_xyy office where:

S = south façade

N = north façade

x = floor

yy = office progressive number

If there is no office number the code refers to the average data for a specific floor (e.g. S_1, N_1; etc.).

2.1 Technology applied

As reported in the introduction, it is strategic to prove the effectiveness of the automation system in real use condition in order to obtain a benchmarking of the correction factor to introduce in the software tool calculation. Simulation tools (Relux 2009, Adeline 3) have been used in this research just to estimate the indoor illuminance level available in the building monitored and the relative energy saving obtainable using dimming technology.

The research focus is not the simulation result but the real energy-saving data derived by the monitoring campaign.

The lighting system on the fifth floor is still manually operated, as required in the previous installation system (switching on/off the office luminaires by two channels: right table zone, left bookshelves zones).

In each of the other five floors a specific scenario has been applied using automation systems with different type and number of controlled parameters and increasing complexity level, as described in the following. With scenario is intended in this paper a real setting of controls, not a simulation result.

Scenario 1 (6th FLOOR): requires that the IR occupancy sensor installed (Figure2) switches off the light if nobody is detected in the office for more than 15 minutes.

The used devices also have the light level detection function, in order to turn off the light if unnecessary, but their sensitivity is not high enough (the illuminance threshold is manually selected) and it can suddenly and improperly control the lighting operation.

With this technology is not possible to monitor and record the value read by the devices; thus it is difficult to give a functionality diagnosis of these

sensors. Asking the users, they have complained of errors in the presence detection.

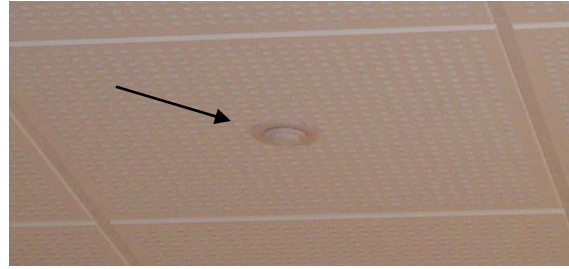


Fig. 2 – Presence sensor

Scenario 2 (4th FLOOR): implies in addition that lights are switched off, if the daylight-based task illuminance level exceeds 500 lx.

It is also possible to manually dim the luminaires. Technology by KNX (www.knx.org) has been used; digitally sends on the bus the communication telegrams, enabling the monitoring action.

These devices (Figure 3) give more accurate measures (higher number of switching segments), and moreover their application program allows the maintenance of a constant illuminance level, even not enabled in this application, in order to investigate this specific activation modality. In this application the user decision ability is higher, using a dimming regulation modality: the light intensity is manually selected and maintained until the absence is detected. Defects in brightness reading depend on the surface colour corresponding to the detection direction (vertical line) that could describe a different condition compared to that one on the working surface.

Because the KNX installation flexibility, in the future this configuration could be changed just downloading a new device parameterization.



Fig. 3 – Brightness and presence sensor

Scenario 3 (3rd FLOOR): the luminaires are switched on when occupancy is detected and dimmed (by two separately controlled circuits, depending on the windows distance) so as to provide predefined minimum illuminance levels (500 lux). It is moreover possible to force the automated regulation in compliance with users' preferences, maintaining this value until the absence is detected.

The smart devices applied in order to detect the presence are the same used for scenario 1. Two luminance sensors have been installed for each façade in order to detect the natural light level incoming from the windows. The two reference rooms have been chosen in order to avoid the use of shading system for the detected windows, and in this way to obtain the higher level of natural light contribution for the two expositions façades.

Obviously it is possible to have lower inside illuminance level and probably lower dimming value in offices where the venetian blinds are partially closed.

The installation position and direction of these devices is a crucial point in order to manage a correct measure. It is strictly related to its internal position in correspondence with the window. For the specific case study there is a homogeneous distribution in the façade of the transparent surfaces. The dimming percentage required is selected by the electrical engineer during the commissioning process, operated directly by manual regulation, using the manual calibration of each dimming channel.

The installation in each office of both this specific light sensor and the presence detector was evaluated as being too expensive a solution. It is not possible to record the illuminance level detected by these sensors because it is an internal variable to the system's functionality.

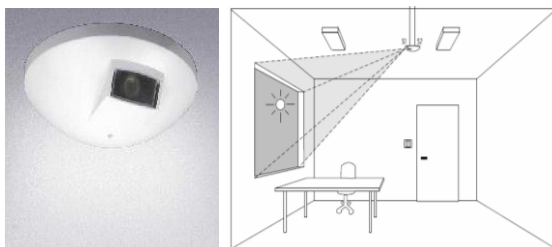


Fig. 4 – Light sensor and its installation modality

The communication protocol, applied to control this lighting control system, is the DSI. In the installed configuration it is not possible to record the dimming percentage as a digital value.

Scenario 4 (2nd FLOOR): the activation modalities are the same as scenario 3 (possibility to switch between the automatic and manual control of the artificial light). The procedure and the number of the inside illuminance measures are different. In this case there is one light/occupancy sensor for each office, with a specific artificial light level required. The detection point is positioned in the middle of the room, on the working desk.

The communication protocol is KNX, as for scenario 2. The regulation actions of the devices for this scenario can be recorded (occupancy, inside illuminance, dimming percentage, manually forced command).

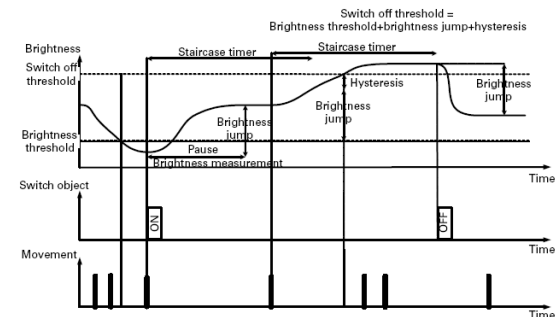


Fig. 5 – Functionality system for the presence/light sensor: constant illuminance level maintenance

Scenario 5 (1st FLOOR): requires the unlocking function of the occupancy sensors by switching in each office. This allows that when the occupancy detector is enabled, the light is automatically dimmed in order to maintain a minimum illuminance level of 500 lux.

The user can autonomously decide to have only the light turn on or off but with the dimming level directly calculated by the system, with any possibility to be manually changed.

The used technology is still the KNX protocol (gateway DALI), and all the parameters controlled by the bus system are simultaneously recorded. This was the last floor to be built, so an additional function for the installed devices was available, concerning the occupancy detection: the detection area can be divided in four sectors. With this

application B sector could be excluded, preventing switching on the light in one office with the open door even if somebody walks in the corridor closed to the detected area.

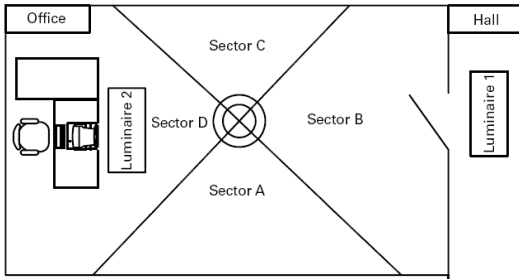


Fig. 6 – Detection area subdivision

3. Method

The research activity has the aim of setting up a new approach for the design of lighting systems in office buildings using smart devices in order to achieve:

- higher energy saving,
- better visual comfort conditions,
- user satisfaction for smart technology utilization modality.

The analysis of these three topics has been developed in real use conditions and not in controlled laboratory environments. In this way it is possible to test the potentialities and limits of technological solutions currently available on the market, the comfort perceived by humans and performed by the system, the interaction between users and partially/completely automated systems.

In order to quantify the difference between energy performance of conventional lighting systems and each automated control scenarios, the energy demand of each case has been considered separately and a pair wise comparison has been performed.

In this research the manual lighting system is assumed as operated by an on/off switch; the automated scenarios are defined above.

In order to test scenarios so as to reduce the energy demand and guarantee at the same time visual comfort improvement, the following factors have been considered:

- control of the user's presence in the office, as a necessary condition to turn on the light;

- regulation of the artificial light, in relation to the natural light level;
- possibility of a manual regulation of the light, forcing the automatic regulation, in order to better meet the user's needs.

The balance between manual and automatic regulation is a crucial point in order to evaluate the realistic usability to the analyzed technology.

To carry out this analysis it is necessary to compare homogeneous or normalized environments (by specific factors) simulating the same boundary conditions.

In order to understand and model users' behaviour in offices operated manually and to quantify the energy saving potentials of automation systems for lighting control, a typical day data analysis was carried out. In this way it is possible to perform an hourly data analysis, depicting typical patterns of presence, actions, and energy use over time instead of mere daily overviews (Mahdavi et al., 2006). All collected data are temporally expressed in terms of a sequence of three-minute intervals. In this way the data collection results are synchronized and it is possible to relate different events occurring at the same time interval in a specific room.

We compare the lighting energy use in the offices for the implemented scenarios using standardisation techniques. In particular the following normalisation factors have been considered:

- *Occupancy level*: energy consumption (Wh/m^2) is related to actual presence time in the classrooms resulting in occupancy-normalised values (W/m^2);
- *Outside illuminance*: For the scenarios implemented, the occupancy periods could differ from classroom to classroom. Thus, the corresponding outdoor illuminance levels (and thus the effectively available daylight) were compared to see if the boundary conditions could be assumed to be identical for the scenarios;
- *Indoor illuminance factor*: To compare manual and automated operation scenarios in terms of energy consumption, one should consider the visual performance requirements (in this case illuminance levels). The automated scenario guarantees that minimum illuminance levels are maintained, unlike in the manual operation. To

take this effect into consideration, a specific illuminance factors were formulated in relation with the indoor illuminance level requirements defined in compliance with the UNI EN 12464-2/2004 regulations.

The analytical definition of the normalisation factors expressed above are detailed, presented and justified in (Chiogna et al., 2011).

In order to quantify the difference between energy performance of conventional versus each automated control scenarios, we isolated the energy demand of each case and performed a pair-wise comparison.

4. Results and discussion

Monitoring results are stored in a databank and structured by the supervision software Gefasoft 7.1. For each day, a file is generated with temporally ordered data. Each single message is labelled with a distinctive number by means and the different data points have been synchronized using the Visual Basic program.

Figure 7 compares the mean presence value in the traditional floor with the presence levels for the 5 automated control scenarios.

As Figures 7 and 8 demonstrate, there is a difference between the monitored occupancy levels in each different floor of the building not only during typical day analysis (Figure 7) but also considering the monthly occupancy hours (Figure 8). Thus, it was necessary to normalise the energy use values based on the occupancy data so as to make a comparison between various scenarios possible.

A normalisation was also performed regarding the available outdoor illuminance levels, even though in this case the variations of illuminance levels for various scenarios was not so relevant throughout the observation period (Figure 9).

In winter months (Figure 10) as in summer months the correspondence between low illuminance level and high-energy demand is respected considering the mean value in the whole observation period.

The major consumption in winter months confirms the correlation between outside illuminance level and energy demand.

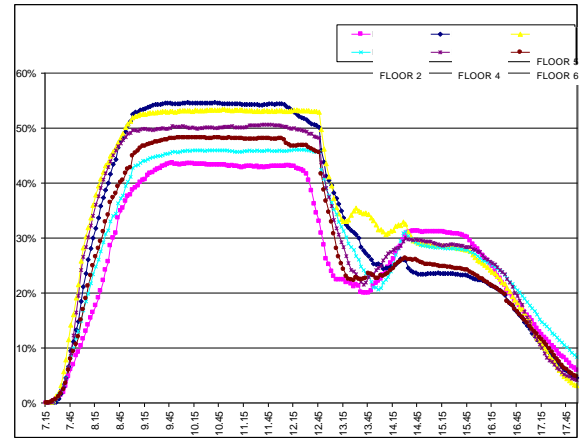


Fig. 7 – Presence levels in percentage each floor of the building in April

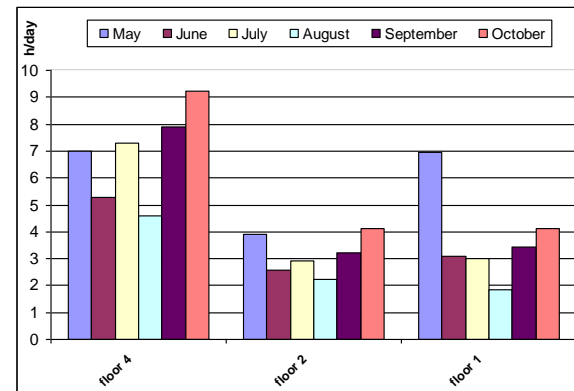


Fig. 8 – Mean presence daily hours from May to October level in floor 1,2 and 4

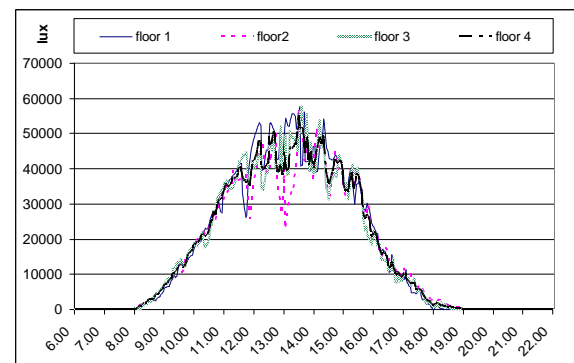


Fig. 9 – Outdoor illuminance levels for occupancy hours: floor 1,2,3,4 in September

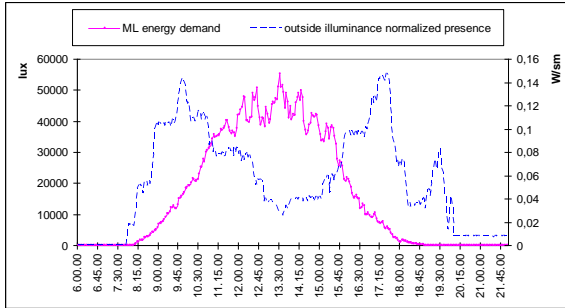


Fig. 10 – Correlation between outdoor illuminance and energy demand for floor 2 in winter time

Figures 11-14 show the energy saving respectively in summer and winter months for each floor calculated not just as absolute value but as value additionally normalized for the following factors: presence, outdoor illuminance and inside illuminance. Moreover, the percentage of energy saving has been converted in two values correlated to environmental and economic factors: CO₂/m² and €/m² (Fig 14 -16). The conversion factor in order to express kWh in grams of CO₂ equivalent is 580 (ISPRA, 2011); the price of electricity used for the calculation is 0,14588 €/kWh (mean price in 2009 for the private use of the electricity). The effect of normalisation factors is significant in the energy saving calculation.

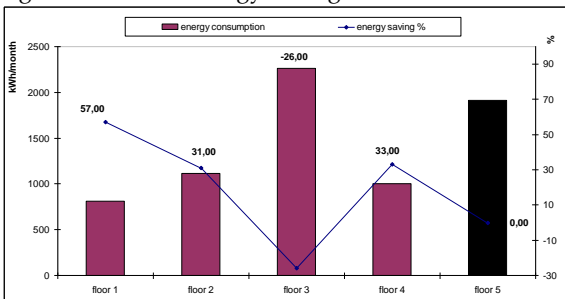


Fig. 11 – Energy saving of each scenario (normalized by presence, indoor and outdoor factor) in the summer months

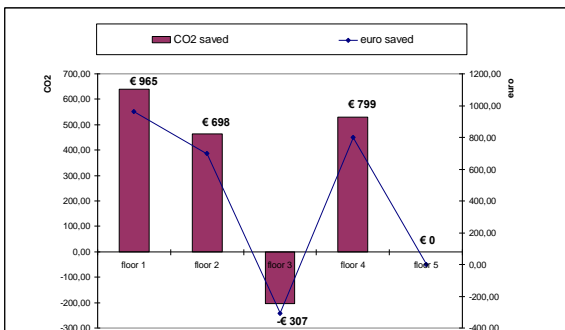


Fig. 12 – Energy saving of each scenario, in terms of CO₂/month and €/month, in the summer months

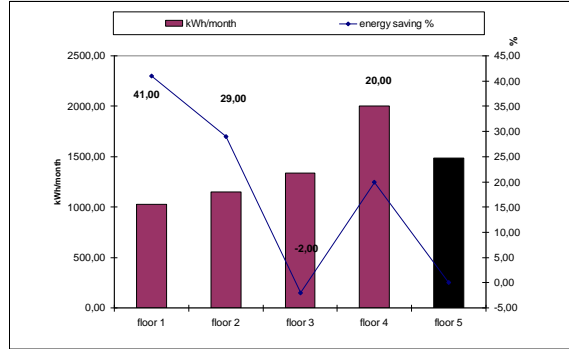


Fig. 13 – Energy saving of each scenario (normalized by presence, indoor and outdoor factor) in the winter months

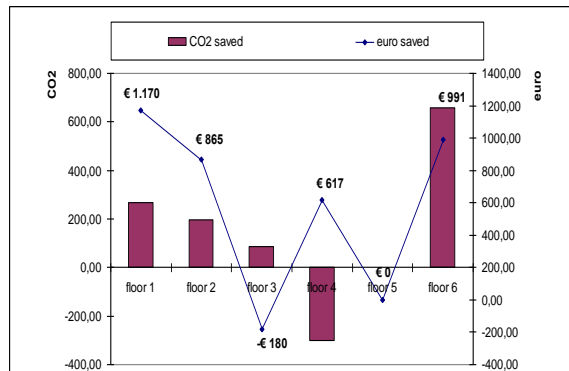


Fig. 14 – Energy saving of each scenario, in terms of CO₂/month and €/month in the winter months

The use of automation techniques allows to reach a significant energy saving amount (Figure 11-14). The overall energy use comparison between traditional and automated classrooms shows that, depending on the observation month,

- floor 1 requires 41% to 51% less energy for electrical lighting;
- floor 2 consumes monthly 30% to 31% less electrical energy for lighting;
- floor 3 needs 2% to 26% more electrical energy for lighting;
- floor 4 needs 20% to 33% less electrical energy for lighting;

For the scenario 1, applied at the sixth floor, it was not possible to normalize the energy consumption using the data monitored by the KNX systems. Using the presence schedule data of the worker, only a monthly presence normalisation factor has been calculated. In this case, it was not possible to evaluate the effective presence in the office or just in the building of the worker. For this reason, the results about this floor have been not included in this analysis. Only the qualitative impression of the

users was investigated: the general impression was that the system does not perform because of the improper turning off of the lights even if people were in the office.

For the data detailed above, it is clear that an automated scenario not correctly implemented, such as the scenario 3 applied on the third floor, can produce increasing energy consumption also in comparison with offices operated manually.

Considering the trend of energy demand considering the use of the dimming regulation (floor 1 and 2) or not (floor 4) it is clear the different lighting energy use in relation with the outside illuminance level.

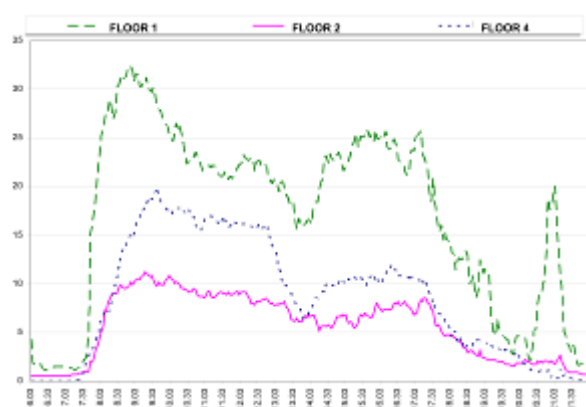


Fig. 15 – Lighting energy use percentage in June: typical day representation for the floors 1, 2 and 4

5. Conclusion

The research results demonstrate that the use of automated systems for the artificial light control can yield considerable energy savings (between 30% and 60% in the observed winter semester), depending on the complexity of the parameters controlled and on the number and of the devices installed.

The tested automated systems could be further improved using a shading control system.

The next research steps involve further data analysis of additional data (correlation between orientation and energy demand) and documentation of control-oriented user behaviour.

The behaviour model extracted from this data analysis could be incorporated in software tools for lighting performance simulation in buildings.

6. Acknowledgements

The research activity was carried out by the CUnEdI (University Center for Intelligent Buildings – Centro Universitario Edifici Intelligenti) at the University of Trento (Italy), in collaboration with the APE (Provincial Energy Agency - Azienda Provinciale per l'Energia).

References

- Erhorn H, Szerman M. Documentation of the Software Package. Stuttgart, Germany: ADELIN; 1994.
- Chiogna M, Mahdavi M, Albatici R, Frattari A, Energy efficiency of alternative lighting control systems, *Lighting research and technology*, 2011, DOI: 10.1177/1477153511427427
- Hunt D. The use of artificial lighting in relation to daylight levels and occupancy, *Building and Environment*, 1979; 14: 21-33.
- IEA, Daylight in Building –Solar Heating and Cooling Programme Task 21, section 6 Design Tolls, 2000.
- ISPRA, produzione termoelettrica e produzione CO2 – Fonti rinnovabili e progetti sottoposti ad ETS, 135/2011; 32 (in Italian). Istituto superiore per la Protezione e la ricerca Ambiente (ISPRA). Retrieved 10 September 2011, from http://isprambiente.gov.it/site/_contentfiles/00009400/94_86_Rapporto_135_2011.pdf.
- Krarti M, Erickson PM, Hillman TC. A simplified method to estimate energy savings of artificial lighting use from daylighting, *Building and Environment* 2005; 40: 747–754.
- LBL, DOE-2. Supplement version 2.1E, LBL-34947. Berkeley, CA: Lawrence Berkeley National Laboratory, 1993.
- Mahdavi A, Lambeva L, Mohammadi A, Kabir E, Pröglhöf C. Two case studies on user interactions with buildings' environmental systems, *Bauphysik* 2007, 29 Heft 1: 72-75.
- Mahdavi A, Mohammadi A, Kabir E, Lambeva L. Occupants' operation of lighting and shading systems in office buildings. *Journal of Building Performance Simulation*, 2008; 1 (1): 57-65
- Mahdavi A, Mohammadi A, Kabir E, Lambeva L. Shading and Lighting in Office Buildings in

- Austria: a study of user control behaviour, *Building simulation* 2008; 1: 111-117
- Mills E. The \$230-billion Global Lighting Energy Bill, 2002, http://evanmills.lbl.gov/pubs/pdf/global_lighting_energy.pdf [1/3/2011], expanded from version published in the Proceedings of the 5th International Conference on energy-Efficient Lighting, May 2002, Nice, France, Evan Mills, Ph.D. International Association for Energy-Efficient Lighting and Lawrence Berkeley National Laboratory.
- Reinhart CF, Herkel S. The simulation of annual daylight illuminance distributionse a state-of-the-art comparison of six RADIANCE-based methods. *Energy and Buildings* 2000; 32:167-187.
- Reinhart CF, Walkenhorst O. Dynamic RADIANCE-based daylight simulations for a full scale test office with outer Venetian blinds. *Energy and Buildings* 2001; 33(7):683-697.
- Reinhart CF. Lightswitch 2002: a model for manual control of electric lighting and blinds, *Solar Energy* 2004; 77 (1): 15-28.
- Seo D, Ihm P, Krarti M. Development of an optimal daylighting controller, *Building and Environment* 2011; 46: 1011-1022.
- UNEP, Building and Climate Change, ISBN 978-92-807-2795-1, 2007.
- UNI EN 15193-2008, Energy performance of buildings — Energy requirements for lighting.
- Zalesak M. Possible impacts of intelligent technologies application in residential buildings on energy efficiency proceeding on CD of KNX scientific Conference Vienna 2006.

Quasi-steady state calculation method for energy contribution of sunspaces: a proposal for the European standard improvement

Francesco Passerini – University of Trento, Trento, Italy

Rossano Albatici – University of Trento, Trento, Italy

Antonio Frattari – University of Trento, Trento, Italy

Abstract

Problems concerning global warming have been faced in the building sector by diminishing energy consumption in buildings by means of three main modes of action: the use of highly efficient systems powered preferably by renewable energy sources, the improvement of the energy characteristics of the envelope and the design of passive devices both for heating and for cooling. The latter are also encouraged by the recent Directive 2009/28/EC. In particular, sunspaces have been and are still nowadays widely used because they meet two different requirements: the heating of adjacent rooms and/or of supply air with the creation of comfortable spaces to live in especially in the cold season. Although an extensive literature is present on the subject, calculation methods for appropriate dimensioning of sunspaces still suffer from a lot of uncertainties concerning both the real management of the users, the correct characteristics of the materials and the environmental boundary conditions (solar radiation and wind velocity above all) that strongly influence the performance of passive devices. Dynamic simulation tools are not largely used in this field especially because they are not yet user friendly. Moreover, problems are experienced when facing multiple reflections, precise estimation of convective coefficients, two and three-dimensional heat transmission. So, quasi-steady state calculation methods are generally preferred especially in the pre-design phase. Method 5000 and the Standard EN ISO 13790:2008 are the most common ones. Concerning the latter, research has been carried out in order to identify problems and propose solutions so to improve the results maintaining the simplified and easy approach. Calculations based on the technical standard and on the new proposal have been compared among them and with dynamic simulations concerning some particular features of sunspaces. The difference in results are pointed out and a critical analysis is presented.

1. Introduction

According to Annex I of the European Directive 2010/31/EU, even “passive solar systems” can be taken in consideration in the calculation of the energy performance of a building. The 32th preamble of the European Directive 2009/28/EC on the promotion of the use of energy from renewable sources states that “Passive energy systems use building design to harness energy”, meaning that concepts concerning energy efficiency and renewable energy exploitation are integrated in the architectural design. Sunspaces (also known as “bioclimatic greenhouses” or “conservatories”) are a particular kind of passive solar system. It is self-evident that they are not only energetic elements but they are overall architectonic spaces.

Generally speaking, the calculation methods for the energy performance of buildings and of their parts can be divided into two main categories (see the European technical standard EN ISO 13790:2008, pp. 15-16): quasi-steady state methods and dynamic methods. Obviously, the dynamic methods can model in a more realistic way the real phenomena involved in the physical behaviour of buildings and HVAC plants and they provide a greater number of output data. Nevertheless, there are reasons why quasi-steady state methods are still used. In fact the quasi-steady state methods require less input data, they are simpler to be used, less time is needed to learn how to use them properly. Because of these reasons, they are typically used by building designers not confident with energy simulations, and generally they are what local legislations require, e.g. to obtain the energy performance

certificate (technical standard UNI/TS 11300:2008 in Italy).

A reasonable approach to calculation is to use quasi-steady state methods in the early stage of the design, in order to evaluate the first design hypotheses and to reject the worst ones, and to use dynamic methods afterwards in the definition of the final details, in order to produce an efficient and accurate design.

In this paper, a summary of a more complex research study is presented where some improvements have been proposed for the quasi-steady state methods described in Standard EN ISO 13790:2008 for the calculation of the energy performance of sunspaces.

2. Energy performance of sunspaces

First of all, it must be noticed that even dynamic models usually simplify very complex real situations, whose precise mechanisms are still not well known. For example, Voeltzel, A. et al. (2001) states that in simulating highly-glazed spaces “erroneous results can be explained by the poor modelling of some physical phenomena that is usually sufficient in conventional buildings. (..) This is, namely, that there are a number of simplifying assumptions regarding shortwave (SW) and longwave (LW) radiation heat transfer that cannot be applied to highly-glazed spaces. A significant fraction of the solar radiation entering a large highly-glazed room can be lost by direct transmission to the outside, direct transmission to other zones of the building, or diffuse retransmission to the outside.” Actually, the reflection to the outside is not necessary a perfect diffuse radiation, but it is generally modelled in this way (adopting a more realistic model would be extremely complicated).

Another simplification concerns temperature distribution of space: “standard thermal building simulation codes generally assume that a room can be treated as a single zone with homogeneous air temperature. Clearly, this does not apply to large highly-glazed spaces”.

In order to face this problem, authors have monitored and analysed the thermal behaviour of sunspaces through real scale prototypes (placed in Trento – Italy) for a period of one year. Surface temperatures, air temperatures and air velocities

(internal and external) were measured in different positions (Figure 1).



Fig. 1 – Sensors in the sunspace prototype during a monitoring campaign

Figure 2 shows some monitored data. It is possible to observe that, except for the floor, during the day/night cycle the temperature oscillations are very high. The floor temperatures are the lowest ones during the day and the highest ones during the night because of the thermal inertia of the ground.

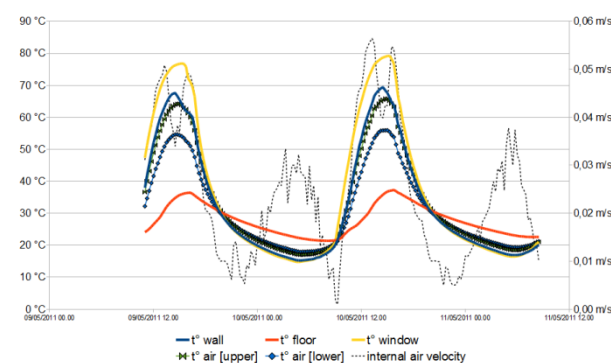


Fig. 2 – Surface temperatures and air velocities within a sunspace

Air temperatures were measured at two different heights. The temperatures of the lower sensor are obviously closer to the floor temperature. In some moments of the day, temperatures in different positions inside the sunspace are very similar: in those conditions, since the windows are closed, air velocity has its minimum values, while the maximum velocities are experienced in correspondence of the greatest differences in temperature among the internal surfaces between each other.

A model of the sunspace was created with the software IDA-ICE. Because of the big differences among the temperatures of the inner surfaces, the monitored air temperatures change a lot depending on the sensor position. However, the IDA-ICE model considers only uniform air temperature within a zone so in order to validate the model, a comparison between the surface temperatures trend of the model and the one of the real sunspace was performed (see Figure 3).

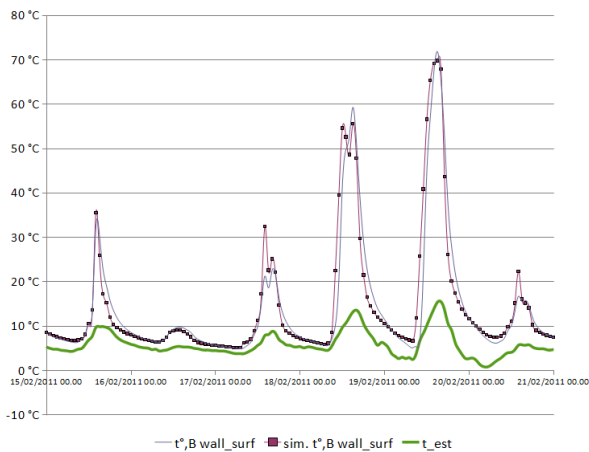


Fig. 3 – Wall temperatures: comparison between results of the model and monitored data

Average difference is very low, less than 3%, and temperature trends over the day fit very well. So the dynamic model was a good representation of the real situation, even if its proper definition and calibration was time consuming and required a lot of successive iteration. It is for this reason that usually designers prefer quasi-steady state methods even in the calculation of passive systems, requiring even greater approximations.

3. EN ISO 13790:2008

The Standard EN ISO 13790:2008 deals with passive solar systems in ANNEX E “Heat transfer and solar heat gains of special elements”. It proposes the calculation of energy performance of buildings through a quasi-steady state method, simpler than dynamic models. The calculation procedure of sunspaces proposed by the technical standard is illustrated in Figure 4.

In particular, thermal losses through a sunspace are calculated considering it as common unheated space, i.e. like an adjacent space that is unheated but whose temperature is higher than the external one because of buffer effect.

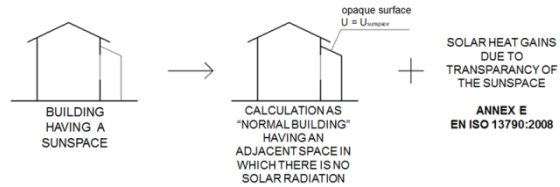


Fig. 4 – The calculation procedure of ANNEX E of EN ISO 13790:2008

On the other hand, the solar heat gains due to the presence of a sunspace have to be calculated in a different way than for common unheated spaces. In fact some phenomena that in “normal” unheated spaces are neglected have an important role in the energy behaviour of sunspaces. Such phenomena are presented in Figure 5.

Solar gains due to the presence of the sunspace must be multiplied by the utilization factor, as is usually done.

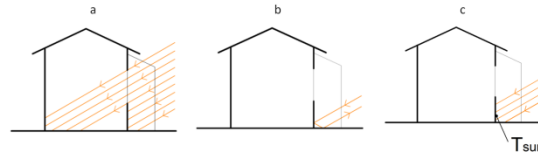


Fig. 5 – a. Part of the solar radiation enters directly the heated space; b. Part of the radiation is reflected to the external environment; c. Part of the radiation is absorbed by the opaque surfaces of the sunspace but it does not contribute to the increase of the sunspace temperature because it is conducted towards other environments.

The solar gain Q_{ss} , that the presence of the sunspace provides to the heated space, is considered as the sum of the direct gain Q_{sd} through the partitions that divide the heated space from the sunspace (both through transparent and through opaque parts) and the indirect gain Q_{si} relative to the increase of the sunspace temperature (i.e. Q_{si} is the increase of the buffer effect because of solar radiation):

$$Q_{ss} = Q_{sd} + Q_{si} \quad (1)$$

Figure 6 is a schematic representation of the physical quantities that ANNEX E considers in the calculation of the gain due to solar radiation in a sunspace adjacent to a heated space.

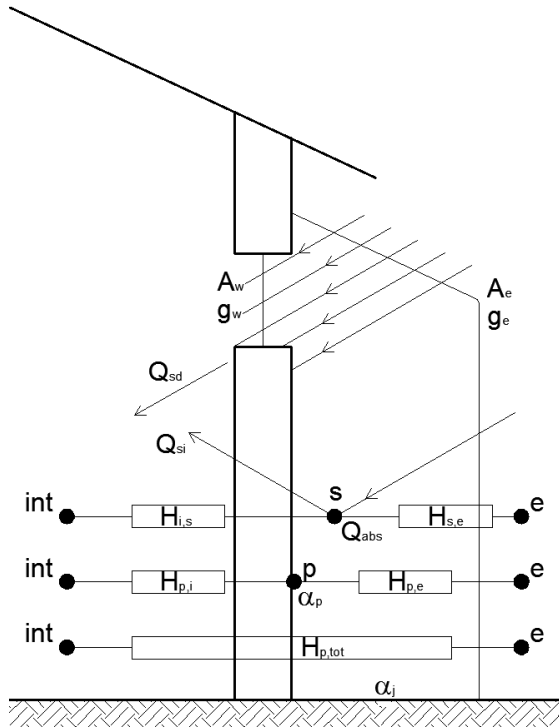


Fig. 6 –Calculation scheme proposed by ANNEX E of EN ISO 13790:2008 (image reviewed and modified by the authors)

The standard assumes that “the absorbing surfaces are all shaded in the same proportion by external obstacles and by the outer envelope of the sunspace”.

The direct solar heat gains, Q_{sd} , expressed in megajoules, are the sum of heat gains through the transparent and opaque parts of the partition wall.

Equation (E.2) in EN ISO 13790:2008 is:

$$Q_{sd} = F_{sh}(1 - F_{F,e})g_e \left[(1 - F_{F,w})g_w A_w + \alpha_p A_p \frac{H_{p,tot}}{H_{p,e}} \right] I_p t \quad (2)$$

where

subscript “w” is relative to the transparent part
between sunspace and heated space

subscript “e” is relative to the transparent part
between sunspace and external environment

subscript “p” is relative to the opaque part between
sunspace and heated space

F_{sh} is the shading correction factor

$F_{F,e}$ is the frame area fraction, i.e. the frame area to total surface ratio

g is the effective total solar energy transmittance of the glazing

A is relative to surfaces

α_j is the average solar absorption factor of absorbing surface j

$H_{p,tot}$ is the heat transfer coefficient by transmission from the internal environment, through the opaque part of the partition wall and through the sunspace, to the external environment (see paragraphs 8 and 9 of EN ISO 13790:2008 and Figure 6)

$H_{p,e}$ is the heat transfer coefficient by transmission from the absorbing surface of the partition wall, via the sunspace, to the external environment (see paragraphs 8 and 9 of EN ISO 13790:2008 and Figure 6)

I_i is the solar irradiance on surface i during the calculation step

ANNEX E states: "The indirect heat gains are calculated by summing the solar heat gains of each absorbing area, j , in the sunspace, but deducting the direct heat gains through the opaque part of the partition wall", while for "normal" unheated spaces solar gain is calculated from solar energy that enters through their external envelopes.

Equation (E.3) in EN ISO 13790:2008 is:

$$Q_{si} = (1 - b_{tr}) \cdot F_{sh,e} (1 - F_{F,e}) g_e \sum_j (I_j \alpha_j A_j) - F_{sh,e} (1 - F_{F,e}) g_e \alpha_p A_p \frac{H_{p,tot}}{H_{p,e}} I_p t \quad (3)$$

where b_{tr} is the adjustment factor ("The reduced temperature difference compared to heat transmission to the external environment is taken into account in ISO 13789 by an adjustment factor, $b_{tr,x}$, that reduces the heat transfer coefficient instead of the temperature difference").

For the other symbols that are presented in equation (3) the explanation of equation (2) can be considered. The heat gain due to solar radiation on the partitions between heated space and sunspace is subtracted because it was already calculated by equation (2) as direct heat gain.

But it is possible to observe that the equation (3) is not dimensionally consistent, because the time t multiplies only the subtrahend. So, a different calculation of Q_{si} is proposed in section "Analysis and proposals", subsection "Indirect heat gain".

4. Analysis and proposals

In this section specific aspects of the calculation of energy contribution of sunspaces are considered.

The method proposed by technical standard EN ISO 13790:2008 is critically analysed and some proposals for its modification are presented.

4.1 Solar heat entering through windows

Solar heat entering through windows regards both direct heat gains and indirect ones.

According to equation (47) of EN ISO 13790:2008, the total solar energy transmittance of the transparent part of a window can be expressed as

$$g_{gl} = F_w \cdot g_{gl,n} \quad (4)$$

where

$g_{gl,n}$ is the value of the total solar energy transmittance if the radiation has a direction normal to the window surface

F_w is a correction factor that was introduced in order to consider that “the time-averaged total solar energy transmittance is somewhat lower than g_n ”. In fact thermal energy transmittance is lower if solar radiation is not normal to the glazed surface.

In the absence of national values, the value of the correction factor F_w is fixed and it is recommended to be 0.9. Neither the European technical standard, nor the Italian (UNI/TS 11300-1:2008) nor the German one (DIN 18599-2:2007) take into consideration different values for different months.

Oliveti, G. (2009) proposed a linear regression that allows to estimate the correlation factor F_w as a linear function of the latitude:

$$F_w = a_1 L + a_2 \quad (5)$$

where

L is the latitude of the considered locality

a_1 and a_2 are parameters that depend on the month and on the orientation of the surface.

Since Oliveti shows that the linear regression improves in a significant way the calculation of the solar gains, next versions of the technical standards could provide parameters for it.

If data for the specific locality where the building is situated are available, the F_w value can be simply calculated even in a spreadsheet. According to Oliveti, the coefficient F_w relative to the time period Δt can be expressed as

$$F_w = \frac{\sum \left[\frac{g_b}{g_{gl,n}} I_b + \frac{g_d}{g_{gl,n}} I_d + \frac{g_r}{g_{gl,n}} I_r \right] \Delta t}{\sum [I_b + I_d + I_r] \Delta t} \quad (6)$$

where

I_b is the direct radiation on the external side of the window

I_d is the diffuse radiation from the sky on the external side of the window

I_r is the diffuse radiation coming from the ground on the external side of the window

g_b the total solar energy transmittance considering only the direct radiation

g_d the total solar energy transmittance considering only the diffuse radiation from the sky

g_r the total solar energy transmittance considering only the diffuse radiation coming from the ground

subscript “n” indicates radiation normal to the windowpane.

If $g_{b,n}$ is the total solar energy transmittance for normal radiation, the total solar energy transmittance for any other inclination of the radiation can be considered as

$$g_b = F_{w,dir}(\theta) \cdot g_{b,n} \quad (7)$$

where θ is the angle between the normal direction of the window and the solar radiation.

As example, in Figure 7, the model of $F_{w,dir}(\theta)$ that is present in the software for dynamic simulations IDA – ICE and the models presented in Karlsson, J. et al. (2000) for a window having a Ag+ coating layer and for a window having a SnO₂ coating layer are printed.

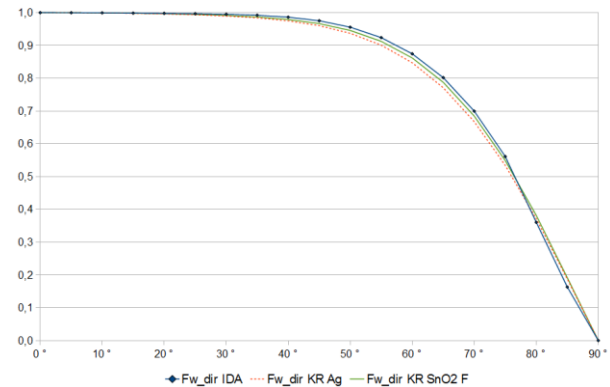


Fig. 7 – Three functions of the correction factor F_w . On the horizontal axis: angle between the radiation and the windowpane. On the vertical axis: the correction factor

The model proposed by IDA-ICE handles the angle dependence of $F_{w,dir}$ by using different trigonometric functions for three different angle intervals. For the diffuse radiation the reduction factor of the entering short-wave radiation is considered equal to 0,85 which derives from the average of $F_{w,dir}$ over the hemisphere.

For Bolzano the F_w values have been calculated both using the linear regression proposed by Oliveti and using the model of IDA-ICE (with climatic data from Comitato Termotecnico Italiano). The trend of the values is similar, as Figure 8 shows.

If F_w were calculated in this way for each Italian locality and printed in an atlas depending on the widely used commercial glasses, results of the Standard method could be much more accurate.

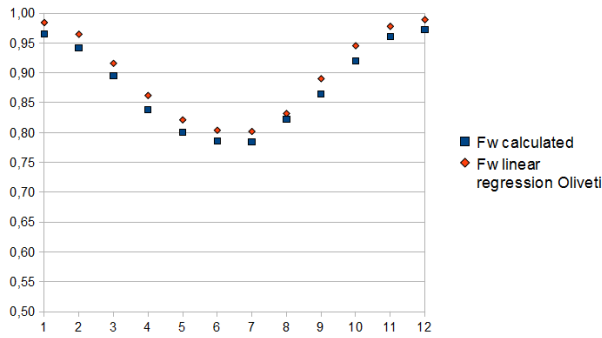


Fig. 8 – F_w trend throughout the year (monthly values)

4.2 Direct heat gain

Considering the solar radiation and the shading correction factor F_{sh} , which does not depend only on the external envelope, separately for every surface the equation (2) for the direct gain can be written in a new form:

$$Q_{sd} = (1 - F_{F,e})g_e \cdot \left[\sum_j (F_{sh,w} \cdot (1 - F_{F,w})g_w A_w I_w)_j + \sum_k \left(F_{sh,p} \cdot \alpha_p A_p I_p \frac{H_{p,tot}}{H_{p,e}} \right)_k \right] t \quad (8)$$

For the calculation of shading factors the Italian technical legislation refers to the paragraph 14.4 of UNI/TS 11300-1:2008, while the German legislation to ANNEX A of DIN V 18599-2:2007. Actually, if the geometry of the shading elements is complicated a precise calculation is possible only through a three-dimensional model.

For a more precise calculation, we could consider that for direct radiation in the heated space, the global solar transmittance of the sunspace external envelope g_e is not involved. In fact, g_e considers also the convective exchange. The solar direct transmittance τ_e , which considers only the solar heat that enters as radiation, could be taken in consideration. A heat proportional to $(g_e - \tau_e)$ could be considered released by the external window of the sunspace to sunspace air as convective exchange. It would increase the indirect heat gain.

4.3 Indirect heat gain

In this subsection a situation of absence of ventilation from and to the sunspace is considered, while some considerations concerning ventilation are presented in subsection “Ventilation”.

Here the floor slab is considered as adiabatic, because implicitly the technical standard considers it as such when it calculates the solar gain (but obviously it considers the heat losses through the floor when it calculates $H_{s,e}$, the heat transfer coefficients between the sunspace and the external environment). The issue of the heat losses through the ground is dealt with by subsection “Solar heat dispersion through opaque surfaces”.

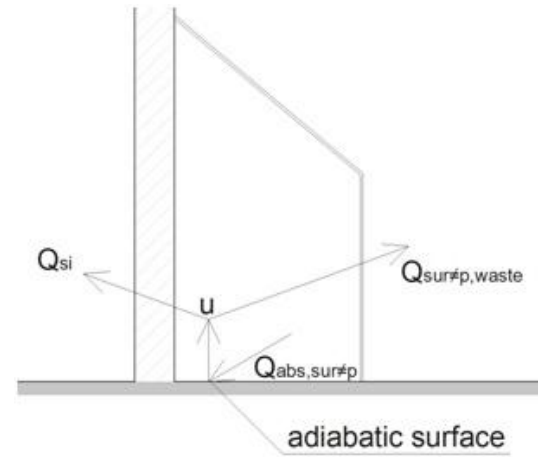


Fig. 9 – Indirect heat gain

The increase of the sunspace temperature due to solar radiation absorbed by the internal surfaces, except the partition, can be considered as:

$$(\Delta T_u)_{sol} = \frac{Q_{abs,sur\neq p}/t}{H_{i,s} + H_{s,e}} \quad (9)$$

where

$H_{i,s}$ is the heat transfer coefficient by transmission from the internal space to the sunspace (see Figure 6)

$H_{s,e}$ is the heat transfer coefficient by transmission from the sunspace to the external environment (see Figure 6)

$Q_{abs,sur\neq p}$ is the solar radiation that is absorbed by the surfaces inside the sunspace, except the partition walls, i.e.

$$Q_{abs,sur\neq p} = (1 - F_{F,e}) \cdot g_e \cdot \sum_{j \neq p} (F_{sh,j} I_j \alpha_j A_j) t \quad (10)$$

Solar radiation that is absorbed by partition walls is not considered because its contribution to the reduction of energy demand of the heated space is already considered in equation (7).

The indirect heat gain Q_{si} is the effect on the heat transmission through the wall (see Figure 6):

$$Q_{si} = H_{p,i} \cdot (\Delta T_p)_{sol} t = \frac{H_{p,i}}{H_{p,e} + H_{p,i}} \cdot Q_{abs,sur\neq p} \quad (11)$$

Considering equation (9), equation (10) can be written as

$$Q_{si} = \frac{H_{p,i}}{H_{p,e} + H_{p,i}} \cdot (1 - F_{F,e}) \cdot g_e \cdot \sum_{j \neq p} (F_{sh,j} I_j \alpha_j A_j) t \quad (12)$$

A different approach is presented by Wall, M. (1996): it presents values of the “solar collector property”, defined as the ratio between the solar heat that is absorbed by the sunspace and the solar radiation that enters through the external windows. Such values are results of dynamic simulations and are relative to different conditions (different properties of the windows, different shapes of the sunspace, different properties of the surfaces, and so on). Wall, M. (1996) regards the Swedish climate. A new similar study could be developed for other climatic conditions.

4.4 Ventilation

ANNEX E states that “if there is a permanent opening between the conditioned space and the

sunspace, it shall be considered as part of the conditioned space”. For a precise calculation of the ventilation losses in such a situation, the amount of heat absorbed by the air flow from the sunspace should be taken into consideration. The calculation, in order to be really accurate, needs to consider the convective exchange coefficients, the air stratification, the position of the openings through which there are air flows. The only way to achieve this accuracy is probably the use of Computational Fluid Dynamic simulations. Therefore the technical standard is not the proper tool to evaluate a situation with permanent ventilation through the sunspace. In a next study the supply air temperature in the heated space could be calculated through Computational Fluid Dynamic simulations for a great variety of situations, in order to give indications to the designers. For example, with the output of CFD analyses the study could present graphs or tables that provide the supply air temperature in the heated space as function of some variables and of some parameters (mean sunspace temperature, geometry, position of the openings, air flow and so on).

4.5 Solar heat dispersion through opaque surfaces

A part of the solar heat absorbed by the sunspace inner surfaces does not heat the air because it is lost directly to the external environment. For example, a part of the solar heat absorbed by the floor is lost directly through the ground. The technical standard does not consider this dispersion. In some cases, this approximation can be unacceptable, e.g. for sunspaces whose floor slab does not have insulating layers for some reason. A model having an uninsulated floor slab ($U_g = 1,34 \text{ Wm}^{-2}\text{K}^{-1}$) and another model with a well insulated one ($U_g = 0,32 \text{ Wm}^{-2}\text{K}^{-1}$) were simulated dynamically. The thermal transmittances were calculated through COMSOL Multiphysics, a FEM software. The sections of the models are presented in Figure 10 and in Figure 11. The test reference year of Bolzano provided by the Comitato Termotecnico Italiano was used.

In Figure 12 the calculated increases in air temperatures due to solar radiation are presented. The calculation was made through the software IDA-

ICE. It is evident that if there is no heat insulation, the temperatures are much lower.

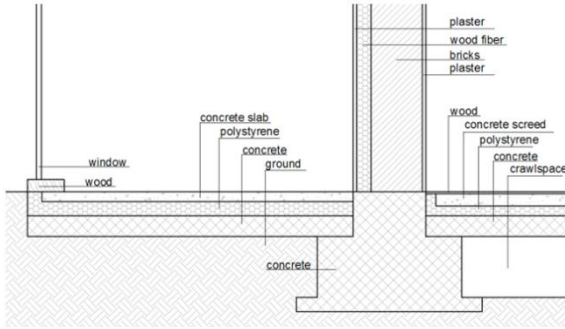


Fig. 10 – Sunspace with insulated floor slab

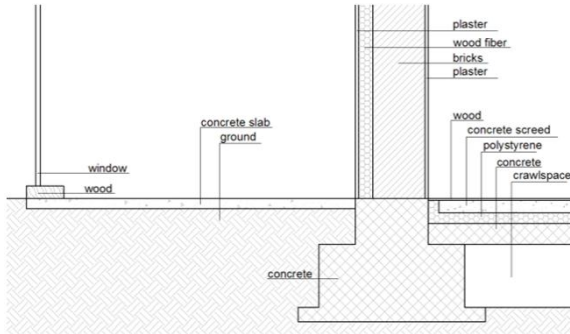


Fig. 11 – Sunspace with uninsulated floor slab

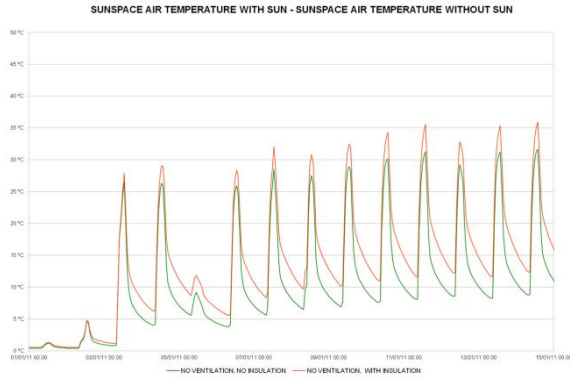


Fig. 12 – Temperature increase due to solar radiation in the case of insulated floor slab and in the case of uninsulated floor slab

Figure 13 represents schematically the heat exchanges from the point of view of the sunspace floor (as a simplification, there is no specific calculation for the IR exchange).

The temperature of the sunspace floor can be calculated as follow:

$$T_j = \frac{\frac{Q_{abs,j}}{t} + h_{ho}A_g \cdot (T_j - T_s) + U_{jo}A_g \cdot (T_j - T_o)}{h_{ho}A_g + U_{jo}A_g} \quad (13)$$

where

$Q_{abs,j}$ is the solar radiation that is absorbed by the sunspace floor

h_{ho} is the surface coefficient of heat transfer for internal horizontal surfaces

U_{jo} is the thermal transmittance between the sunspace floor and the external environment through the ground and it could be calculated through a FEM software or with technical standard EN ISO 13370:2008

A_g is the floor area

T_j is the floor temperature

T_s is the sunspace air temperature

T_o is the external air temperature.

Therefore the temperature increase due to solar radiation is:

$$(\Delta T_j)_{sol} = \frac{Q_{abs,j}/t}{h_{ho}A_g + U_{jo}A_g} \quad (14)$$

The part of heat due to solar radiation that is lost directly through the ground and that should be subtracted from $Q_{abs,surp}$ can be calculated as:

$$(Q_l)_{sol} = U_{jo}A_g \cdot (\Delta T_j)_{sol} = U_{jo}A_g \cdot \frac{Q_{abs,j}/t}{h_{ho}A_g + U_{jo}A_g} = U_{jo} \cdot \frac{Q_{abs,j}/t}{h_{ho} + U_{jo}} \quad (15)$$

It can be easily demonstrated that

$$\frac{U_{jo}}{h_{ho} + U_{jo}} = \frac{U_g}{h_{ho}} \quad (16)$$

where U_g is the thermal transmittance between the sunspace air and the external air.

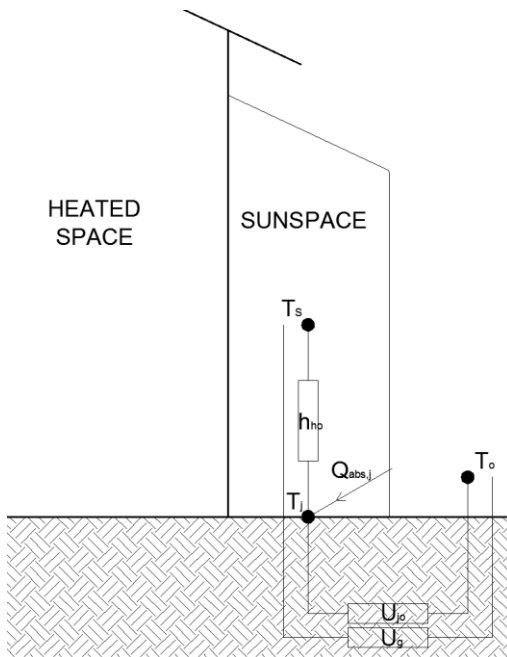


Fig. 13 – Schematic calculation of the floor temperature

Heat absorbed by the floor is

$$Q_{\text{abs},j} = (1 - F_{\text{F,e}}) \cdot g_{\text{e}} F_{\text{sh},j} I_{\text{j}} \alpha_{\text{j}} A_{\text{j}} t \quad (17)$$

Considering equations (16) and (17), equation (15) can be rewritten as

$$(Q_l)_{\text{sol}} = \frac{U_g}{h_{\text{ho}}} \cdot (1 - F_{\text{Fe}}) \cdot g_e F_{\text{sh},j} I_j \alpha_j A_j \quad (18)$$

5. Conclusion

The present paper presents the most important results of a wider research study on thermal behaviour of sunspaces. Sunspaces are architectonic elements and designers generally use quasi-steady state methods for calculating their thermal performances, for example in the energy certification procedure. Therefore the study focused on the quasi-steady state method proposed by the European technical standard EN ISO 13790:2008. The method was critically analysed and proposals for its modification were developed. Such proposals regard

the calculation of different aspects: solar heat entering through windows, direct heat gain, indirect heat gain, ventilation and solar heat dispersion through opaque surfaces.

The proposal is still in its initial stage. Future development concerns verification on real case studies and the comparison of the calculus results with energy performance monitored during specific campaign, together with a deeper analysis of costs and benefits in a great variety of cases.

6. Nomenclature

Symbols

A	surface (m^2)
F	correction factor
H	heat transfer coefficient (W/K)
I	solar irradiance (W/m^2)
L	latitude ($^\circ$)
Q	energy (J)
T	temperature ($^\circ\text{C}$)
b	adjustment factor
g	effective total solar energy transmittance
h	surface coefficient of heat transfer ($\text{Wm}^{-2}\text{K}^{-1}$)
t	time step (s)
α	solar absorption factor
θ	angle between the normal direction of the window and the solar radiation
τ	solar direct transmittance

Subscripts

F	frame
b	direct radiation
d	diffuse radiation
e	external environment
ho	horizontal
i	internal (heated) environment
n	normal
p	partition
r	radiation reflected by the ground
sh	Shading
w	transparent part

References

- A Report of Task 22 Building Energy Analysis Tools (1999) Models for Building Indoor Climate and Energy Simulation <www.iea-shc.org/task22/publications/t22brep.pdf>
- Karlsson, J. et al. (2000) "Modelling the angular behaviour of the total solar energy transmittance of windows", Solar Energy, Amsterdam, Elsevier Science Ltd., Volume 69, No. 4, pp. 321-329
- Oliveti, G. et al. (2008), "Evaluation of the absorption coefficient for solar radiation in sunspaces and windowed rooms", Solar Energy, Amsterdam, Elsevier Science Ltd., vol. 82, Issue 3, March 2008, pp. 212-219
- Oliveti, G. et al. (2009), Valutazione del coefficiente correttivo F_w della trasmittanza solare totale delle superfici vetrate, III Congresso Nazionale AIGE, Parma 4th-5th June 2009
- Oliveti, G. et al. (2011), "An accurate calculation model of solar heat gain through glazed surfaces", Energy and Buildings, Amsterdam, Elsevier Science Ltd., vol. 43, pp. 269-274
- Voeltzel, A. et al. (2001), "Thermal and ventilation modelling of large highly-glazed spaces", Energy and Buildings, Amsterdam, Elsevier Science Ltd., vol. 33, Issue: 2, January 2001, pp. 121-132
- Wall, M. (1996), Climate and energy use in glazed spaces. Lund: Building Science

Thermal performance of the building walls

Balaji N.C – Indian Institute of Science, Bangalore, India

Monto Mani – Indian Institute of Science, Bangalore, India

Venkatarama Reddy B.V. – Indian Institute of Science, Bangalore, India

Abstract

A building's climatic-response is determined by the prevalent exposure conditions (micro-climate) and the ability of the building envelope to regulate thermal transmittance (building physics). This ability to passively thermo-regulate indoor thermal comfort is determined by the materials configuring the envelope geometry. Various building envelope configurations are feasible depending on available/accessible building resources. In this study, the thermal performance of a building envelope, viz., a masonry wall has been investigated. The theoretical investigation is carried out under steady periodic conditions (occurring in natural building environments). A numerical model based on the implicit Finite Difference Method (FDM) has been developed for the computation of thermal transmittance. Six different wall configurations have been identified based on those typically used in commercial and residential buildings in India. The influences of both material thermal properties and external surface heat-transfer coefficient on the time lag and decrement factor have been investigated. The heat load transmission through the interior wall surface has also been studied. Most studies have arrived at time lag and decrement factor as critical performance measures of a building envelope, but under constant exterior surface heat transfer coefficient considerations. While it has been observed that the heat transfer coefficient does not remain constant, its variation has a bearing on both the time lag and decrement factor, and require careful investigation. The results of the numerical analysis show that decrement factor decreases while exterior heat transfer coefficient increases. Further, the thermal properties, thickness and material assembly are other important factors that determines interior surface instantaneous heat load. Further, it was observed that walls with the higher time lags and lower decrement factors were suited for adoption in tropical regions. The current study attempts to augment existing knowledge of building climatic-response leading to appropriate

envelope design-configurations for various climatic zones.

1. Introduction

Buildings are large energy consumers in many countries, and energy demand is growing every day. Energy required in building is mostly towards providing thermal comfort. Energy savings in a building can be achieved by appropriate energy efficient design of building envelopes. Building envelope comprise a configuration of building materials, the thermophysical properties of which determine the climatic response of the envelope. To reduce the energy consumption in buildings, it is necessary to understand the thermal performance of the building envelope on the indoor environment. The two parameters, which evaluate the thermal performance of walls are time lag and decrement factor (Xing Jin, 2012). These are influenced by the external and internal surface temperatures of the wall. In general, higher time lag and lower decrement factor is the preferred thermal performance in tropical regions to minimize energy consumption. The objective of the current study is to carry out thermal performance analysis of building walls attributed to the thermal properties of the construction materials.

2. Previous Studies

Salient studies that are related to the thermal performance of building walls are reviewed in this section. Asan and Sancaktar (1998) found that the thermophysical properties have a profound effect on the time lag and decrement factor, and they

computed time lag and decrement factor for different building materials. Asan (2006) found that the thickness and type of the material have a very profound effect on the time lag and decrement factor. Koray Ulgen (2002) investigated the effects of a wall's thermophysical properties on time lag and decrement factor experimentally and theoretically. Kontoleon and Bikas (2007) studied the effect of outdoor absorption coefficient of an opaque wall on time lag, decrement factor and temperature variations was investigated by employing a dynamic thermal-network model; Kontoleon and Eumorfopoulou (2008) studied to determine how time lag and decrement factor are affected by wall orientation and exterior surface solar absorptivity, for specific climatic conditions. Ozel (2012) studied the influence of exterior surface solar absorptivity on thermal characteristics and optimum insulation thickness of building walls, through an implicit finite difference method under steady periodic conditions.

Emad Al-Regib and Syed M. Zubair (1995) studied the transient effect of heat transfer through the walls used for the positioning of insulating materials by employing finite difference method (explicit method) to solve this problem. Asan (1998 and 2000) carried out analysis using finite difference methods (Crank-Nicolson method) for the investigating the insulation thickness and it optimum portion in wall for maximum time lag and minimum decrement factor. Al-Sanea (2000) developed a numerical model based on the finite-volume and implicit procedure developed for the computation of the time-dependent and nonlinear temperature variations through composite layers, and to evaluate thermal performance of building walls. Ozel and Pihtili (2007) carried out finite-difference analysis (implicit method) to determine optimum location and distribution of insulation in a wall. Ozel (2011) determined the thermal performance and optimum insulation thicknesses of building walls using an implicit finite difference method.

Vijayalakshmi et al. (2006) investigated the thermal behaviour of opaque wall materials under the influence of solar energy and analyzed the influence of thermophysical properties of different wall types on the interior environment. Finite

difference analysis was carried out and the results compared with the experimental findings.

In this study, the thermal performance of building wall has been investigated numerically. The effects of wall configurations on time lag and decrement factor, interior surface instantaneous heat load and the influence of exterior surface heat transfer coefficient on the time lag and decrement factors has been studied.

3. Time lag and decrement factor

Time lag and decrement factors are very important thermal performance characteristics that influence the heat storage capabilities of any materials. These can be obtained based on the materials' thermophysical properties (Asan, 1998).

Time lag (Φ) is the time difference between the temperature maximum at the outside and inside when subjected to periodic conditions of heat flow (IS 3792-1978), and a decrement factor is the ratio of the maximum outside and inside surface temperature amplitudes (Koenigsberger, 1973). The schematic of time lag and decrement factor is shown in Figure 1.

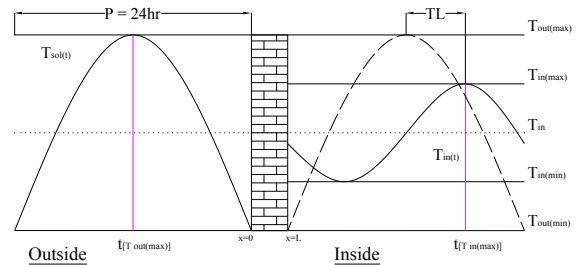


Fig. 1 – The schematic representation of time lag and decrement factor

$$\Phi = t_{[T_{in(max)}]} - t_{[T_{out(max)}]} \quad (1)$$

where, $t_{[T_{in(max)}]}$ and $t_{[T_{out(max)}]}$ are the time of day when the inside and outside surface temperatures reach maximum.

$$DF = \frac{T_{in(max)} - T_{in(min)}}{T_{out(max)} - T_{out(min)}} \quad (2)$$

where, $T_{in(max)}$ and $T_{in(min)}$ are the maximum and

minimum inside surface temperatures, $T_{out(max)}$ and $T_{out(min)}$ are the maximum and minimum outside surface temperatures.

4. Methods

The heat transfer through the walls is assumed one-dimensional. Figure 2 shows the schematic representation of heat transfer through the wall. Some of the wall sections consist of a number of layers with different thicknesses and thermal properties. The outside surface is exposed and subjected to the sol-air temperature. The inside wall surface is in contact with constant room air temperature. The sol-air temperature includes the combined effect of the outside temperature and solar radiation. The sol-air temperature is assumed to show sinusoidal variations during a 24-hour period.

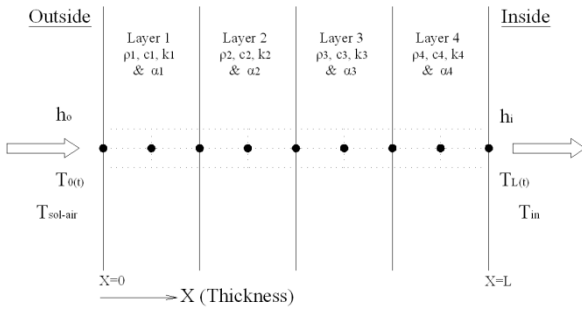


Fig. 2 – The schematic representation of heat transfer through the wall

The general governing one dimensional transient heat conduction equation is as follows:

$$k \frac{\partial^2 T}{\partial x^2} = \rho c p \frac{\partial T}{\partial t} \quad (3)$$

where, k is the thermal conductivity, ρ is the density and Cp is the specific heat capacity at constant pressure of the building wall materials.

To solve equation (3), it is necessary to specify two boundary conditions and one initial condition. Convection boundary conditions on both the inside and outside surface of a wall are present. The boundary condition at the inside surface is

$$k \left(\frac{\partial T}{\partial x} \right)_{x=0} = h_i [T_{x=0}(t) - T_i] \quad (4)$$

where, h_i is the inside surface heat transfer coefficient, for still air $h_{conv,in} = 9.36 \text{ Wm}^{-2}\text{K}^{-1}$ is considered in the study, as per Indian standard 3792-1978.

Similarly, the boundary condition at the outside surface can be written as

$$k \left(\frac{\partial T}{\partial x} \right)_{x=L} = h_o [T_{sa}(t) - T_{x=L}(t)] \quad (5)$$

where, h_o is the outside surface convective heat transfer coefficient. Ito et al. (1972) obtained h_o for an actual building as a function of wind speed (v) and direction as $h_o = 18.63 V^{0.605}$ in $\text{Wm}^{-2}\text{K}^{-1}$ (for the windward surface)

where,
$$V = \begin{cases} 0.25v & \text{for } v > 2\text{m/s} \\ 0.50v & \text{for } v < 2\text{m/s} \end{cases}$$

In this study the outside surface heat transfer coefficient is considered for the various wind speeds from 1 to 10 m/sec.

h_i is the wall inside surface heat transfer coefficient, h_o is the wall outside surface heat transfer coefficient, $T_{x=0}$ is the wall inside surface temperature, $T_{x=L}$ is the wall outside surface temperature and $T_{sol}(t)$ is the sol-air temperature (sol-air temperature).

The equation for sol-air temperature is taken as follows (Asan, 1998):

$$t_{sa}(\tau) = \frac{t_{max} - t_{min}}{2} \sin\left(\frac{2\pi\tau}{P} - \frac{\pi}{2}\right) + \frac{t_{max} - t_{min}}{2} + t_{min} \quad (6)$$

where, P is duration (24hrs), T_{max} and T_{min} are the maximum and minimum outdoor temperature, respectively.

Figure 3 illustrates the profile of this sol-air temperature and the one which was obtained from real climatological data by Threlkeld (1970) is presented. As seen from Figure 3, Eq. (4) has been found to be a very reasonable choice for sol-air temperature and also adopted by Asan (1998, 1998, 2000, 2006) and Xing Jin (2012).

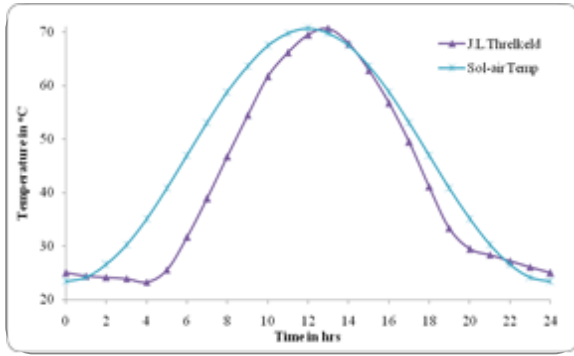


Fig. 3 – Comparison of sol-air temperatures

In this computation, indoor temperature T_{in} is taken to be constant ($T_{in} = 25^{\circ}\text{C}$), $T_{max} = 36.6^{\circ}\text{C}$, $T_{min} = 13^{\circ}\text{C}$, $h_i = 9.36 \text{ W/m}^2\text{K}$, as per IS 3792-1978, for inside surface heat transfer coefficient at still air.

As an initial condition, assuming the temperature distribution across the wall is constant at the beginning, so the initial condition is

$$T_{x(t=0)} = 25^{\circ}\text{C} \quad (7)$$

5. Numerical solution procedure

The one dimensional transient heat transfer problem is solved by the Finite Difference Method (FDM) using implicit method (backward difference). Although the implicit method needs more time to calculate, the advantage of this method has no limitation on time interval and is stable. The finite-difference equations systems are solved by using program in M.S Excel. The sol-air temperature is repeated on successive days until a steady periodic solution is obtained. The finite difference equations are derived for inside and outside surface boundary nodes, interior nodes and interface nodes between two layers as shown in figure 2 and solved.

The temperature distribution across the wall section is obtained under different outside surface heat transfer coefficients. The outside side heat transfer coefficient is influenced by the wind velocity and direction, surface shape and roughness and, temperature difference between surface and air (Cole and Sturrock, 1977). The heat flux taking place during the 24h period on the inside surface of the wall is calculated by the

following equations:

$$q_i = h_i(T_{in}(t) - T_{in}) \quad (8)$$

6. Building wall configurations and thermal properties

The wall structures investigated are shown schematically in Figures 4 to 9. These wall structures are commonly used in India. Thermal properties of materials used in the wall structures are given in Table 3. Fundamental thermo-physical properties are thermal conductivity, density and specific heat capacity. Derived thermal properties are thermal diffusivity, thermal inertia & thermal mass.

Thermal diffusivity is a measure of the rate at which a temperature propagates from one point to another point in a material. Thermal inertia is the degree of slowness with which the temperature of a body approaches that of its surroundings and which is dependent upon its absorptivity, its specific heat, thermal conductivity, dimensions and other factors.

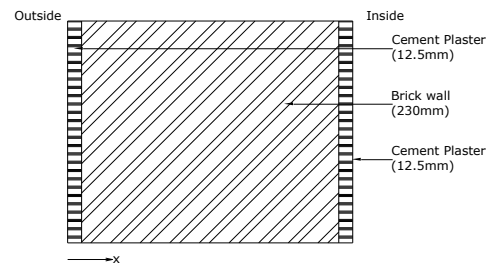


Fig.4 – Schematic of wall configuration W1

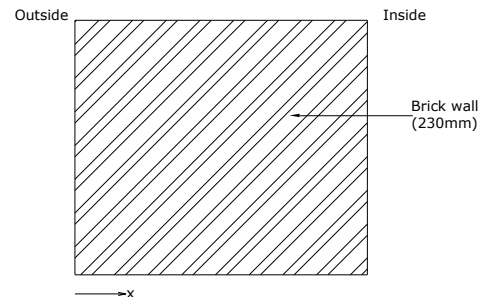


Fig.5 – Schematic of wall configuration W2

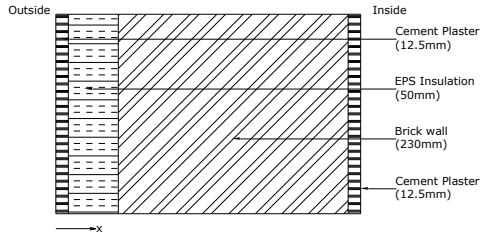


Fig.6 – Schematic of wall configuration W3

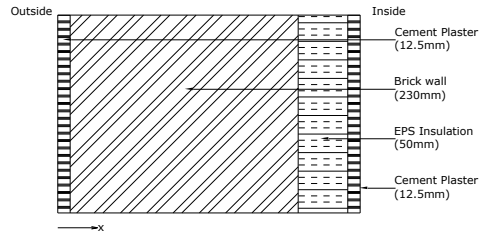


Fig.7 – Schematic of wall configuration W4

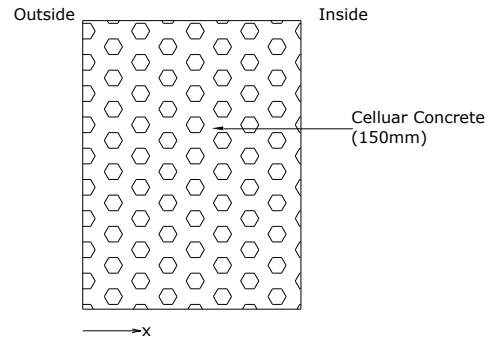


Fig.8 – Schematic of wall configuration W5

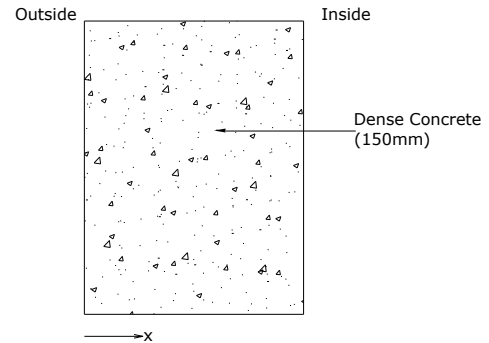


Fig.9 – Schematic of wall configuration W6

Material	k^* (W/m K)	ρ^* (kg/m ³)	C_p^* (J/kg K)	α ($\times 10^{-7}$) (m ² /s)	Thermal mass C (kJ/K m ²) (= ρC_p) ($\times 10^6$)	Thermal inertia ($k \rho C_p$) ^{1/2} (J m ⁻² K ⁻¹ S ^{-1/2})
Cement plastering	0.721	1762	840	4.87	1.480	1033.02
Brick wall	0.811	1820	880	5.06	1.601	1139.69
EPS insulation	0.035	24	1340	10.8	0.032	33.55
Cellular concrete	0.188	704	1050	2.54	0.739	372.78
Dense concrete	1.740	2410	880	8.20	2.120	1920.98

Table 1: – Thermal properties of wall building materials (Source: Indian Standard 3792-1978)

7. Results and discussions

Figure 10 groups the building materials based on thermal conductivity as low thermal conductivity materials such as Expanded Polystyrene (EPS) insulation and cellular concrete, and moderate thermal conductivity materials such as cement plastering, brick wall, and dense concrete walls have been adopted for the study.

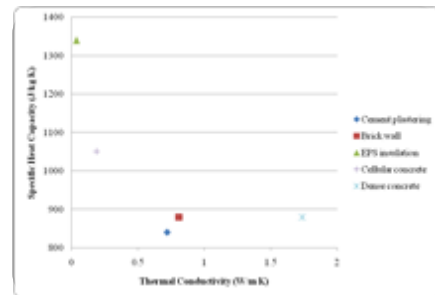


Fig. 10 – Specific heat capacity – thermal conductivity of building materials (compiled from Indian Standard 3792-1978)

8. Effects of wall configuration on time lag and decrement factor

The thermal performance of various walls configurations are tabulated in Table 2. The heat flow through the material is combined influence of the heat storing capacity and thermal resistance characteristics of the wall elements, which controls and regulates the indoor temperature conditions. The amount of heat stored in the wall depends largely on the thermal mass (volumetric heat capacity) of the material. The higher the thermal mass, the more heat it can store and the less heat will be transmitted on to the inside surface of wall (*van Straaten, 1967*).

The building envelope configuration and its thermophysical properties such as heat capacity and thermal diffusivity of the building wall material affect the time lag and decrement factor. Building walls with lower thermal transmittance (U) value

has better capability to reduce indoor surface temperature variations. Thermal transmittance (U) is a measure of the rate of heat loss of building component; it is expressed as $\text{Wm}^{-2}\text{K}^{-1}$.

From Table 2 it can be seen that the lower the value of thermal transmittance (U), the higher the time lag will be and the decrement factor is also reduced. Most of the studies show, to delay the temperature fluctuation on the inside surface compared with outside surface, and to reduce the inside temperature fluctuation amplitude. The walls should have a higher time lag and lower decrement factor, because it is required to maintain inside temperature fairly at constant temperature.

To achieve better thermal performance of the walls, it is desirable to combine different wall layers of materials having different thermophysical properties (*Koray Ullgen, 2002*), (*Vijayalakshmi, 2006*).

SI No.	Description of walls (from outside to inside)	Identification	U ($\text{Wm}^{-2}\text{K}^{-1}$)	R (m^2KW^{-1})	Time lag (hrs)	Decrement Factor
1	12.5mm CP + 230mm BW + 12.5mm CP	W1	2.09	0.478	7.262	0.174
2	230mm BW	W2	2.25	0.444	5.912	0.157
3	12.5mm CP + 50mm EPS + 230 BW + 12.5mm CP	W3	0.52	1.923	12.275	0.009
4	12.5mm CP + 230 BW + 50mm EPS + 12.5mm CP	W4	0.52	1.923	8.375	0.016
5	150mm Cellular concrete	W5	1.04	0.961	4.837	0.104
6	150mm Dense concrete	W6	3.63	0.275	2.512	0.488

Table 2: Thermal performance of various walls (Note: Outside surface heat transfer coefficient, $h_o = 18.63 \text{ Wm}^{-2}\text{K}^{-1}$ - Inside surface heat transfer coefficient, $h_i = 9.36 \text{ Wm}^{-2}\text{K}^{-1}$)

9. Effect of wall configuration on instantaneous transmission load

Figure 11 shows the variation of the inside surface heat fluxes with time for all six types of walls. The analysis is carried out for heat transfer coefficient values of $h_o = 18.63 \text{ Wm}^{-2}\text{K}^{-1}$ and $h_i = 9.36 \text{ Wm}^{-2}\text{K}^{-1}$. In the figure positive values indicate heat gain and negative values indicate heat loss through the wall from inside surface.

Figure 11 shows the variation of the inside surface heat fluxes with time for all six type of walls. The peak heat flux is obtained as 15.97, 11.81, -11.76, 2.17, 28.78 and 31.93 Wm^{-2} for W1, W2, W3, W4, W5 and W6 respectively. Results shows that the maximum peak loads occur for the wall made with W1, W2, W5 and W6.

Besides, it is seen that the highest heat gain and loss are obtained for the W6 (dense concrete) wall which has the highest thermal conductivity, while the lowest heat gain and loss are obtained for the W3 and W4 walls which has the highest thermal

resistivity. Similar kinds of conclusions were drawn by Ozel (2011) using the theoretical models.

The heat gained by the walls is stored inside the various layers of the structure and then dissipated to the inside. This has a great advantage in reducing the rate of heat flux transmission into the indoor environment as indicated in figure 11 for W3 and W4 walls by relatively small inside-surface heat flux.

In this study, it is clearly understood the importance of the materials' thermal properties and building envelope configuration, which significantly vary the dynamics of heat transfer through the building envelope. Significant improvement in the rate of heat loss/gain in the building can be achieved through multi-layered W3 and W4 wall types.

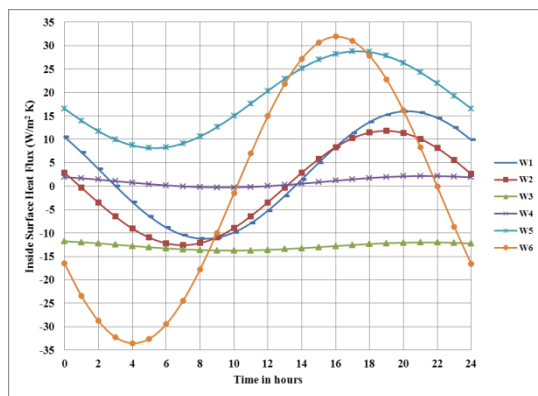


Fig. 11 – Variation of the inside surface heat fluxes with time for all walls

10. Effects of outside surface heat transfer coefficient on time lag and decrement factor

The higher the rate of air movement across a surface, the higher the rate of heat transfer will be and consequently the higher the surface coefficient. The outside surface convective boundary condition is a function of heat transfer coefficient (h_o) (Cole and Sturrock, 1977). The analysis of wall thermal performance is carried out under various wind speeds to study the effects of h_o on time lag and decrement factor.

The contribution of the convective heat transfer component at the outside surface shows a more complicated pattern; however, it has in general an adverse effect on the indoor cooling/ heating loads (Sami A. Al-Sanea, 2000). These loads depend on the

rate of heat transfer through the walls from the outside surface to inside surface. The rate of heat flow through the wall depends on thermal inertia of wall materials which depend on the material density (characteristic porosity), specific heat and thermal conductivity. Higher the thermal inertia of material; higher will be the heat flow rate through wall and also effects on the time lag and decrement factor.

Figures 12 and 13 show the variation of time lag and decrement factor with varying h_o for all six types of walls. It can be clearly seen from Figures 12 and 13 that there is not much influence/variation in the time lag and decrement factor under various outside surface convective heat transfer coefficient (h_o) conditions. The influence of surface heat transfer coefficient is negligible on the time lag and decrement factors. These mainly depend on the specific heat capacity and thermal diffusivity of the building materials and not on the surface heat transfer coefficient. From figure 13, W6 wall show a decreasing trend in the decrement factor as heat transfer coefficient increases. Due to the higher heat transfer coefficient and thermal inertia there will be a moderation in the temperature amplitude between outdoor and indoor temperature.

Thermal inertia of materials plays a major role in regulating the heat transfer from outdoor to indoor environment and vice-versa. These will influence time lag and decrement factor of building material.

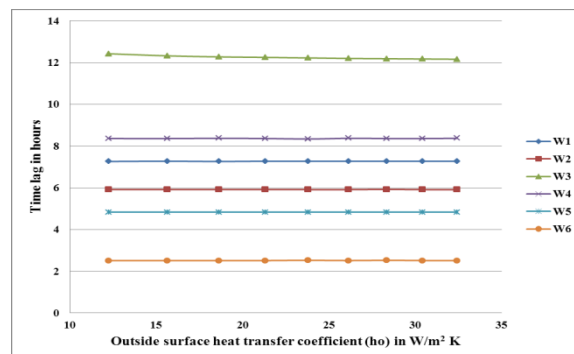
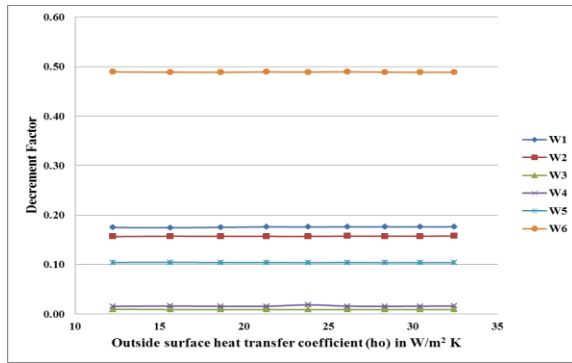


Fig. 12 – The variation of time lag with varying h_o for walls

Fig. 13 – The variation of decrement factor with varying h_o for walls

11. Conclusions

This study reveals the importance of the building wall configuration. To achieve a better thermal performance of the walls, it is desirable to have a multi-layered wall comprising materials of different thermophysical properties. It was found that different wall configurations have a strong effect on time lag and decrement factor. The inside surface heat flux in a building wall also depends on the wall configuration, its corresponding thermal transmittance and heat storage capacity. Further, from the results it can be concluded that the materials having higher thermal inertia when subjected to higher surface heat transfer coefficients, lower the decrement factor. The results obtained are useful for designing appropriate building envelope configurations for passive solar building.

12. Nomenclature

Symbols

k	Thermal Conductivity ($\text{Wm}^{-1}\text{K}^{-1}$)
ρ	Density (kgm^{-3})
C_p	Specific heat capacity ($\text{Jkg}^{-1}\text{K}^{-1}$)
t	Time (sec)
T	Temperature ($^{\circ}\text{C}$)
h	Heat transfer coefficient ($\text{Wm}^{-2}\text{K}^{-1}$)
v	Wind velocity / wind speed
α	Thermal diffusivity (m^2s^{-1})
C	Thermal mass ($\text{kJK}^{-1}\text{m}^{-2}$)
U	Thermal transmittance ($\text{Wm}^{-2}\text{K}^{-1}$)
R	Total thermal resistance (m^2KW^{-1})

Subscripts/Superscripts

i, in	Inside
o, out	Outside
sa	Sol-air temperature
min	Minimum
max	Maximum
t	time

References

- Al-Regib, E. and Zubair, S.M., (1995). Transient heat transfer through insulated walls, *Energy* 20(7): 687-694.
- Asan, H. (1998). Effects of wall's insulation thickness and position on time lag and decrement factor, *Energy and Buildings* 28(3): 299-305.
- Asan, H. and Sancaktar, Y.S. (1998). Effects of Wall's thermophysical properties on time lag and decrement factor, *Energy and Buildings* 28(2): 159-166.
- Asan, H. (2000). Investigation of wall's optimum insulation position from maximum time lag and minimum decrement factor point of view, *Energy and Buildings* 32(2): 197-203.
- Asan, H. (2006). Numerical computation of time lags and decrement factors for different building materials, *Building and Environment* 41(5): 615-620.
- Cole, R.J. and Sturrock, N.S. (1977), The convective heat exchange at the external surface of buildings, *Building and Environment* 12(4): 207-214.
- I.S. 3792 – 1978, Indian standard guide for heat insulation of non-industrial buildings, BIS, New Delhi, India.
- Ito, N. (1972). Field experiment study on the convective heat transfer coefficient on exterior surface of a building, *ASHRAE Trans*, Vol. 78, 184 – 191.
- Jin, X., Zhang, X. et al. (2012). Thermal performance evaluation of the wall using heat flux time lag and decrement factor, *Energy and Buildings* 47(0): 369-374.
- Koenigsberger. O.H., Ingersoll. T.G., Alan Mayhew and Szokolay. S.V., (1973), *Manual of Tropical*

- Housing and Building: Climatic Design, Universities Press.
- Kontoleon, K.J. and Bikas, D. K. (2007). The effect of south wall's outdoor absorption coefficient on time lag, decrement factor and temperature variations, *Energy and Buildings* 39: 1011–1018.
- Kontoleon, K.J. and Eumorfopoulou, E.A. (2008). The influence of wall orientation and exterior surface solar absorptivity on time lag and decrement factor in the Greek region, *Renewable Energy* 33: 1652–1664
- Ozel, M. and Pihtili, K. (2007). Optimum location and distribution of insulation layers on building walls with various orientations, *Building and Environment* 42(8): 3051-3059.
- Ozel, M. (2011). Thermal performance and optimum insulation thickness of building walls with different structure materials, *Applied Thermal Engineering* 31(17–18): 3854-3863.
- Ozel, M. (2012). The influence of exterior surface solar absorptivity on thermal characteristics and optimum insulation thickness, *Renewable Energy* 39(1): 347-355.
- Sami A. Al-Sanea. (2000). Evaluation of heat transfer characteristics of building wall elements, *Journal of King Saud University*, 12(2): 285–313
- Therkeld, J.L., (1970), *Thermal environmental engineering*, Englewood Cliffs, Prentice-Hall, New Jersey (NJ).
- Ulgen, K. (2002). Experimental and theoretical investigation of effects of wall's thermophysical properties on time lag and decrement factor, *Energy and Buildings* 34(3): 273-278.
- van Straaten, J.F. (1967), *Thermal Performance of Buildings*, Elsevier Publishing Company, Amsterdam.
- Vijayalakshmi, M.M., Natarajan, E. and Shanmugasundaram, V. (2006). Thermal behaviour of building wall elements, *International Journal of Applied Sciences*, ANSINET publishing, 6(15): 3128-3133.

Simulation of wind-driven ventilation in an urban underground station

Roberta Ansuini – Università Politecnica delle Marche, Ancona, Italia

Alberto Giretti – Università Politecnica delle Marche, Ancona, Italia

Roberto Larghetti – Università Politecnica delle Marche, Ancona, Italia

Costanzo Di Perna – Università Politecnica delle Marche, Ancona, Italia

Abstract

Sustainable Energy Management for Underground Stations (Seam4us) is a European research project aimed at developing adaptive control technologies to reduce energy consumption in subway stations. The research work is developed through a pilot subway station, the Passeig de Gracia – Line 3 station, in Barcelona, Spain. The entrances to the subway station are located along Passeig de Gracia, one of Barcelona's main avenues. In this type of location, evaluating the effects of wind in terms of underground ventilation, requires profound investigation. In the perspective of the Seam4us project, wind-driven ventilation must be known a priori in order to evaluate natural ventilation potentials and patterns related to wind-driven ventilation, and to compute wind pressure coefficients used in a synthetic lumped parameter model that is the training model for the control policy. In this perspective, an urban canyon model was built in a commercial CFD simulation environment. Different CFD modeling steps and simulations were faced in order to achieve reliable data, which was then compared with experimental data retrieved from an on-site survey. The results are discussed in the present paper.

1. Introduction

Evaluating the effects of wind, in terms of building ventilation, calls for profound investigation. Factors due to wind forces affecting the ventilation rate inside buildings include average speed, prevailing direction, seasonal and daily variation in speed and direction, and local obstructions such as nearby buildings, hills, trees, and shrubbery (Liddament, 1988).

(Horan et al., 2008) showed that assuming external airflow data on the basis of a single, mean wind speed, and an associated prevailing wind direction, could result in significant variations in ventilation rates, and in comfort conditions when other, external wind conditions prevail. Furthermore, the relationship between wind direction and air change rate proved to be non-linear in many cases. To model the effects of airflow in buildings, wind speed and direction frequency data are necessary. Generally, the turbulence or gustiness of approaching wind, and the unsteady character of separated flows, cause the fluctuation of surface pressures. (ASHRAE, 2005) states that although peak pressures are important with regards to structural loads, mean values are more appropriate for computing infiltration and ventilation rates. It considers time-averaged values for pressure, with the shortest averaging period of about 600s (approximately, the shortest time period considered to be a "steady-state" condition when considering atmospheric winds) and the longest 3600s. Instantaneous pressures may vary significantly above and below these averages. Peak pressures even doubled or tripled their mean values.

Furthermore, urban environments have drawbacks in terms of the application of natural ventilation: lower wind speed and higher temperatures due to the effect of urban heat island, noise and pollution (Ghiaus et al., 2006). The meteorological models currently available usually give the wind, temperature, and sky cover on a fictitious surface, usually measured at 10m above ground level, and on a several kilometre grid, approximately. These values need to be changed as a function of the

urban environment (Ghiaus et al., 2003) in order to be used for estimating natural ventilation airflow due to wind pressure and stack effect. An urban canyon is an urban environment artefact similar to a natural canyon. It is characterized by streets cutting through dense blocks of structures - generally heights (Santamouris et al. 1999). Airflow in street canyons has much lower values as compared to undisturbed wind. Lower wind velocity means reduced wind pressure on building facades and less effective cross ventilation. Experimental evaluation of the reduction of airflow rate in single-sided and cross-ventilated buildings in 10 urban canyons in Athens (Geros et al., 1999) showed that airflow rate might be reduced by 90%. Knowledge of the wind speed in urban canyons is a required input for estimating the natural ventilation potential of urban buildings, as well as thermal comfort in open areas. Wind flow inside canyons is driven and determined by the interaction of the flow field above buildings and the uniqueness of local effects such as topography, building geometry and dimensions, streets, traffic, and other local features.

Three approaches can be used to acquire data regarding urban canyon wind flows:

Measurements on site: This process requires months for the acquisition of data using anemometers and important instrument set-ups;

Wind tunnel tests: A slightly faster approach, but also a more expensive one, especially in terms of the construction of the neighbourhood and buildings' physical model ;

Computational Fluid Dynamics (CFD): a faster and cheaper approach, producing much more detailed information but also more "uncertain" data.

While the use of CFD in engineering practice is becoming a well-established procedure in indoor applications, they are used considerably less in outdoor applications; although numerical modeling with CFD is becoming a quite common approach for urban wind simulation. Indeed, CFD models can provide detailed information regarding relevant flow variables in the whole calculation domain ("whole-flow field data"), under well-controlled conditions and without similarity constraints. Furthermore, CFD models can avoid some of the limitations found in other models.

Even so, numerical and physical modeling errors need to be assessed by detailed verification and validation studies (Franke et al., 2007).

2. Urban Canyon Model in Seam4us

The development of a new class of energy control systems for underground public environments is one of the main objectives of the EU-funded R&D project called Sustainable Energy Management for Underground Stations (SEAM4US). The project aims at developing a fully featured pilot system, in Barcelona's "Passeig de Gracia" subway station, for the dynamic control of energy consumption, capable of setting up internal environments opportunistically and optimally, based on external environment forecasts, according to energy efficiency, comfort and regulation requirements.

The development of this class of advanced control system requires a robust modeling framework (Giretti et al., 2012) as the models are needed both for being embedded in the control system and for supporting the whole system design, especially the monitoring sensor network.

In this perspective, the model-engineering framework in SEAM4US is hybrid (Ansuini et al., 2012) as it includes different types of models (FEM, Lumped Parameter, and Probabilistic Models) and diverse processes (heat transfer, fluid dynamics, pollutant transport, lighting) at various scales (meteorological weather, local weather, indoor environments).

A very critical point is modelling the effect of meteorological weather conditions inside stations. Every subway station has numerous entrances, thus a local weather station deployed in each of the entrances is economically unsustainable. The idea currently being developed uses a third party weather forecasting service for gathering information pertaining to the climatic conditions within the city, and includes knowledge about local conditions related to a specific urban context as well as the entrances' geometric features, in embedded models. Thus, only one local weather station is deployed in each station (as part of the monitoring system) and used to check the weather model in real-time.

Two types of models are required:

A weather model including the third party weather service data and correlation among the aforementioned data and locally measured data,

A general model of the energetic behaviour of the station building, including the effect of external weather, using a thermal coefficient and a set of specifically computed Wind Pressure Coefficients (Costola et al., 2009).

The development of both the models requires the initial development of an urban canyon model.

This study presents the urban canyon model developed for the SEAM4US pilot station, located in Passeig de Gracia (PdG), Barcelona. Only a very preliminary set of experimental data is available to date, gathered during a two-day environmental survey. These data are used in this study for performing a preliminary calibration of the developed CFD models and for defining a methodology for selecting real-time experimental data to be used in the weather model check.

3. Model development

3.1 Model settings

Accuracy is an important matter of concern when using CFD for modeling urban blocks. Care is required in the geometrical implementation of the model, in grid generation and in selecting proper solution strategies (Franke et al., 2007).

An outdoor urban canyon model was developed. It encompasses the eight city blocks surrounding the station entrances. In order to be used to determine the velocity maps at the station entrances and inside the station, the model also contains the underground environments (Fig. 2).

Critical parameters were determined on the basis of the literature (Franke et al., 2004). Specifically, it emerged that the main decisions to be taken regarded:

- the general modeling approach (what was to be modelled) ;
- the computational domain;
- insertion of the “boundary layer” ;
- roughness of the material;
- geometrical detail level.

Regarding the modeling approach, according to (Franke et al., 2007), the final decision was to model only the volumes of fluid (air) included among the buildings and inside the station. Hence, a domain composed of a single material was inserted in the calculation software. Thus, all other components that really exist were excluded in order to obtain a simple geometry, capable of reducing the computational charges.

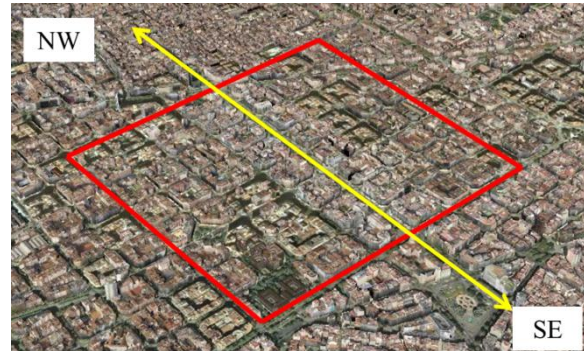


Fig. 1 – Urban Region around PdG modelled

The computational domain consists in a box measuring 2 km in length, 1.5 km in width and 220 m in height, where 20 m was the height of the ground and 200 m that of the air. The PdG underground station has eight entrances. It measures 630 m in length along the homonymous street and measures about 190 m in width in the perpendicular direction. Two different regions are defined in the computational domain (Fig. 1), a central box containing the real obstacles with their geometric shape and with a level of detail characterized by greater precision close to the points of interest, and a less detailed peripheral zone.

The boundary layer has not been included so far, because the width of the computational domain would generate a computationally uncontrollable number of degrees of freedom.

The roughness of the boundary material is considered, however, editing the speed of friction in the conduit. In particular, the B parameter (Comsol, 2011) is set to the value -3. This value was obtained calibrating internal models of the station with other data gathered in the station corridors during the preliminary survey.

Regarding the level of geometrical detail of the

representation, the buildings were considered with clean surfaces and street furniture in the area surrounding the entrances was included (Fig.2).

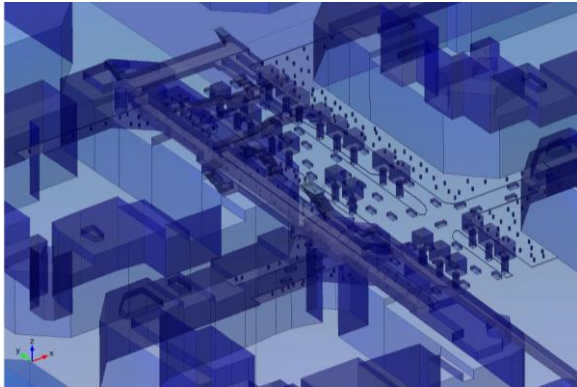


Fig. 2 – Detail of the model in the area surrounding the station entrances

3.2 Boundary Conditions

Four different types of boundary conditions were used (Fig. 3):

Slip condition, imposed on the sky of the computational domain to avoid viscous phenomena on the wall and assuming the continuity of the fluid;

Wall function condition, imposed on the surfaces of the air volume adjacent to a solid;

Inlet condition, applying a velocity profile to the surface of the air box the wind is arriving from;

Outlet condition “Pressure Zero”, which considers a pressure profile constant and equal to 0 on the surface, simulating the passage of flow from a tube that represents our computational domain in an undisturbed environment, as occurs in the surface opposite the inlet.

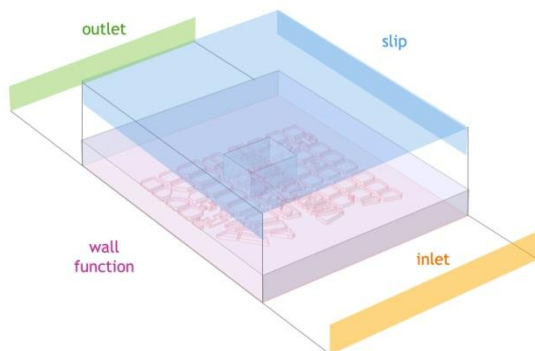


Fig. 3 – Boundary Conditions on different Surfaces

Two types of inlet conditions were considered, each required a different simulation for each

model, depending on the velocity profile. Of course, in reality, the wind speed profile along the atmosphere height has a logarithmic trend, but this profile is not fully known, as it will be measured only in one point. This point corresponds to the meteorological weather station. Thus, the definition of the logarithmic profile could include an error related to its trend. On the other hand, the linear profile (according to (Franke, 2004)) can ensure the development of a logarithmic profile due to friction with the ground if used soundly, but the overall effect may be underestimated.

The two profiles considered so far are:

$$\text{Linear WS}(z) = \text{WS}_{\text{Met}}$$

$$\text{Logarithmic WS}(z) = \text{WS}_{\text{Met}} * (z/10)^{0.2}.$$

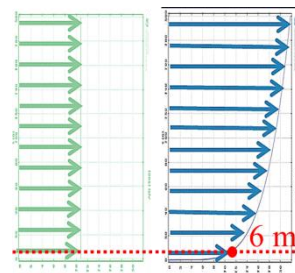


Fig. 4 – Linear and Logarithmic Speed Profile in relation to the experimental WSMet

3.3 Model definition by wind direction

In order to apply the inlet boundary condition efficiently, the surface in which it is applied must be normal to the wind vector direction. Thus, different models were developed for each of the sixteen, main wind directions, resulting in eight different geometrical models (opposite wind directions can use the same geometry).

3.4 Meshing

The results of the computation are strongly dependent on the grid that used to discretize the computational domain. In this case, two different meshes were used for the two different computational domains.

The discretization of the model is obtained by means of a free form mesh grid (normally tetrahedral), which varies in size according to the degree of accuracy to be obtained.

The CFD program used in this study allows two types of meshes: one, based on the general physical

behaviour that does not require a very accurate grid (the default size is then larger), and another, based on the fluid dynamic models' degree of accuracy (the default size is smaller) (Fig. 5). The two subsets include various grid default sizes ranging from an extremely detailed grid for the central region (with dimensions sub-centimetre), while the extreme regions are characterized by a much higher minimum dimension mesh (order of 50 m). In this modeling case, a grid size in the order of 30 meters in the peripheral areas and a centimetric grid size, with fluid-dynamic characteristics in the central region, is deemed necessary. Table 1 gives a summary of the meshing details.

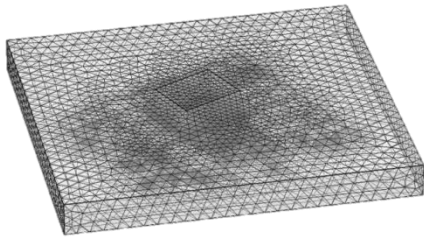


Fig. 5 – Model mesh

	Max elem. size (m)	Min elem. size (m)	Max elem. grow. rate	Resol. of curvature	Resol. of narrow regions
Central	20	0.05	1.5	0.6	0.5
Peripheral	69.5	2	1.2	0.7	0.6

Table 1 – Meshing details

In the post-processing phase, the quality of the mesh was checked, confirming that the variable “wall lift off” δ_w was equal to 11.06 on most of the walls, guaranteeing a good accuracy (Comsol, 2011).

In fact, the wall functions in COMSOL are such that the computational domain is assumed to start at distance δ_w from the wall, which is the distance from the wall where the logarithmic layer would meet the viscous sub-layer if there were no buffer layer in between.

3.5 Model solving

The simulations were carried out by means of COMSOL Multi-physics 4.3, 3D steady state analysis (Comsol, 2012).

The Physical Equations used are those related to the κ - ϵ Turbulence Model (Wilcox, 1998) in steady Reynolds-averaged Navier-Stokes (RANS) simulation, which is the commonly used method (Yoshie et al., 2007).

4. Experimentnal data

An environmental survey in PdG station was carried out on the 21st and 22nd of March 2012 to retrieve a very preliminary snapshot of the pilot station's environmental behaviour.

A number of different types of data were collected, including local weather data using a weather station (WS3600 LaCrosse Technology) placed close to the EN5 entrance (Fig. 6). The instrument has a resolution of 0.1 m/s for WS and 22.5 deg for WD. The data was acquired with a 1 minute time step from 9:00 a.m. to 6:00 p.m. during the first day and from 9:00 a.m. to 3:00 p.m. during the second one (Fig. 7).



Fig. 6 – Local Weather Station during the survey

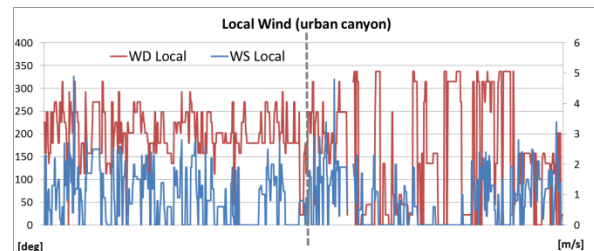


Fig. 7 – Original data acquired by the Local Weather Station during the survey.

4.1 Calibration approach

For the calibration of the weather models, the SEAM4US project uses two types of Wind Measurement (Fig. 8):

Local Wind data, similar to that retrieved during the preliminary survey, gathered from the Weather Station placed in the entrance EN5;

Meteorological Wind data retrieved by a third party weather service. The services considered so far, for the city of Barcelona, use mainly data gathered by the Barcelona El Prat Airport weather station, situated at an altitude of 6m, free field.

This data was also used for the preliminary calibration.

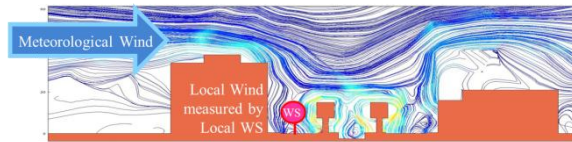


Fig. 8 – Diagram of the relation between Meteorological and Local Wind

4.2 Analysis of Meteorological Wind Data

Meteorological wind data, corresponding to the Local Weather Station's measurement time-period, was collected. The weather forecast services considered provide 30 minute averaged data, thus, 19 records for the first day, and 17 records for the second. Their distribution in terms of WD and WS are shown in Figure 9.

4.3 Definition of the CFD model set

The data available was analysed and 22 boundary conditions were identified on the basis of the winds occurring. The related models were developed and simulated.

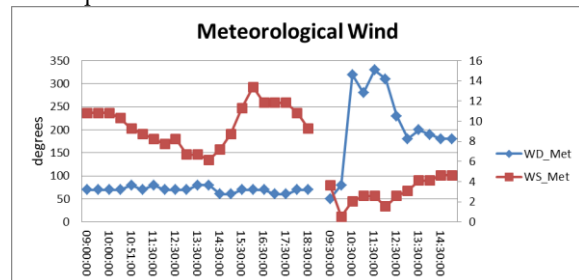


Fig. 9 – Data about the Meteorological Wind related to the survey period

4.4 Detailed analysis of local wind data

The critical part of the calibration process is then the analysis of local wind data. Weather stations, such as the one used in the survey, have a rather low accuracy: $\pm 10\%$ (AmbientWeather, 2012) that can increase to $\pm 30\%$ for $WS < 1$ m/s (Rossi, 2003). Furthermore, in terms of WD, they give a result even if $WS=0$ (no wind).

Hence, in the perspective of real-time checking/calibration, the definition of a protocol for defining data reliability is critical.

As the data are averaged for each half hour, 30 measures are expected for each interval. The analysis used in this study aims at defining the reliability of measures, depending on three parameters:

Validity: that is, computing the number of measures that are valid and correspondent to a wind ($WS > 0$). The interval set is defined valid if at least 10 measures are valid;

Reliability: that is, computing the number of measures corresponding to $WS > 1$ m/s. The interval set is defined reliable if the majority of the valid measures are also reliable;

Direction Prevalence: that is, computing the number of occurrences of each WD between the valid measures. If the most frequent WD, in terms of occurrence, has a number of measures greater than one-third the number of valid measures, and at least double of the number of the second WD cases, in terms of occurrences, it can be considered a prevalent direction (Fig. 10).

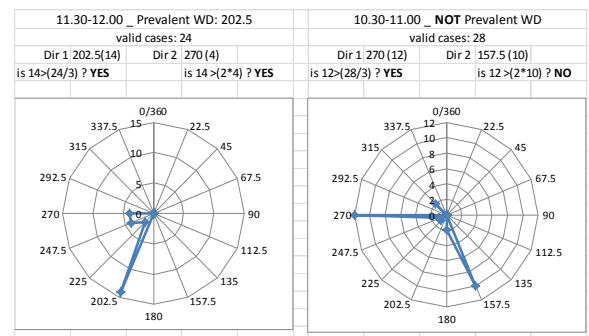


Fig. 10 – Example about the identification of Prevalent WD in a half hour interval

Setting the reliability threshold to 1 m/s is related to (Rossi, 2003) and can be considered plausible for our case given that its effect inside the station is not

very relevant when the outdoor wind speed is low. Based on these criteria, only reliable measures were considered, hence, 17 half-hour intervals from the survey data. For each interval, average WD_{Loc} and WS_{Loc} were computed.

WD_{Loc} was computed as the direction occurrence weighted average of the valid WD measures, paying particular attention to accounting properly the cases where the measures were around the 0/360 angle.

WS_{Loc} was computed differently depending on whether or not there was a single, prevailing wind direction: if a prevalent direction existed, the average, prevalent direction, WS was used. However, if a prevalent wind direction did not exist, the weighted average of all the average WS for each direction was used.

5. Results and discussion

5.1 Simulation Results

The whole CDF model set identified was developed and simulated. A line of plotting points was defined in each model, centred on the actual position of the Weather Station during the survey (Fig. 11).

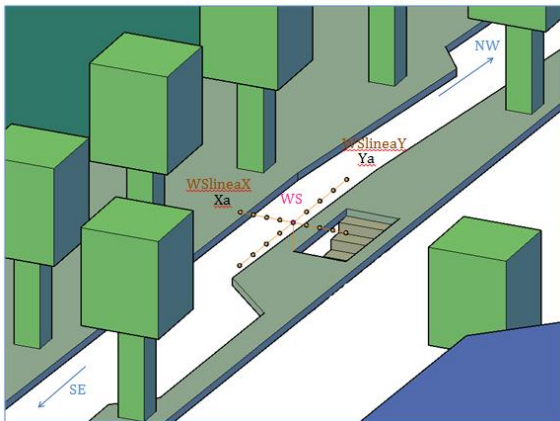


Fig. 11 – Plot points around the weather station

Table 2 reports the simulation results related to the reliable data of Local Wind, in both inlet conditions cases: linear (lin) and logarithmic (log) speed profile.

The analysis of the simulation performance was performed in terms of WD and WS .

In terms of WD , the results are very good as the mean errors obtained are ± 27.98 (lin) and ± 27.30 (log). Recalling that the weather station precision was ± 22.5 degrees, the results appropriateness is confirmed. In percentage terms, the relative errors are $\pm 14.9\%$ and $\pm 14.3\%$, which, considered in reference to 360 degrees, are $\pm 7.8\%$ and $\pm 7.6\%$.

In terms of WS , the mean errors obtained are ± 0.62 m/s (lin) and ± 0.41 m/s (log), corresponding to relative percentage errors of 36.8% and 26.8%.

time	WD_{S_Li} n	WS_{S_Lin}	WD_{S_Lo}	WS_{S_Log}
9.30-10.00	216.58	0.92	221.54	1.90
10.00-10.30	216.31	0.82	221.13	1.69
10.30-11.00	216.31	0.82	221.13	1.69
11.30-12.00	215.40	0.60	219.58	1.20
12.00-12.30	215.40	0.60	219.58	1.20
12.30-13.00	215.40	0.60	219.58	1.20
13.00-13.30	185.00	0.84	187.88	1.10
13.30-14.00	185.00	0.84	187.88	1.10
14.30-15.00	221.23	0.96	223.21	1.66
15.30-16.00	215.81	0.95	221.54	2.08
16.00-16.30	215.81	0.95	221.54	2.08
17.00-17.30	225.89	1.26	226.61	2.05
17.30-18.00	216.58	0.92	221.54	1.90
12.30-13.00	187.96	0.50	187.85	0.64
13.30-14.00	145.22	0.87	136.80	1.12
14.00-14.30	187.96	0.50	187.85	0.64
14.30-15.00	187.96	0.50	187.85	0.64

Table 2 – Simulation Results

5.2 Discussion

Figures 12-15 support a detailed analysis of the results.

Figure 12 represents WD and WS with the results ordered by WD_{Met} .

It emerges that the cases related to directions 80, 180 and 190 have recurrent problems, in terms of both WS and WD . In particular, the WS graph (Fig. 12b) shows that this problem is not related to the inlet condition and it should be related to the model. This behaviour has a physical explanation, as these directions are the most oblique to the city

block grids (and to the canyon) as showed in Figure 13.

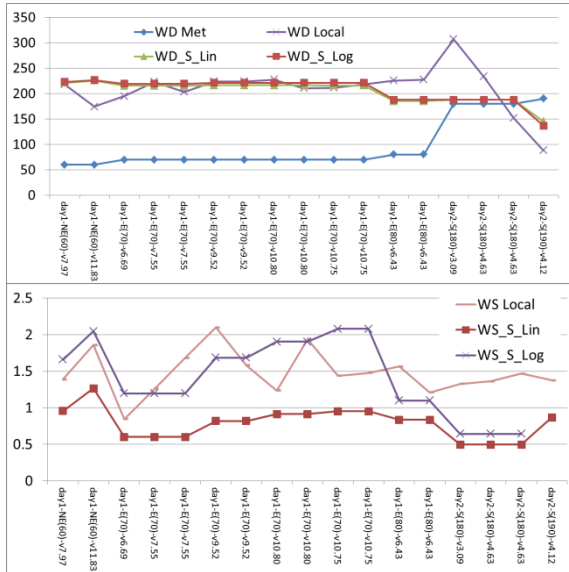


Fig. 12 – Simulation and Experimental Results ordered by WDMet:WD (a) and WS (b)

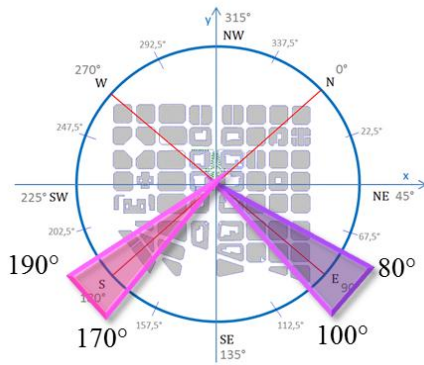


Fig. 13 – Superposition of cardinal axis to the urban canyon schema and identification of the oblique WD.

Furthermore, especially in regards to the south (180), there are two building blocks situated exactly perpendicular to this direction that could be causing the problems.

Solving the aforementioned problem is not easy, but taking it into consideration is very relevant in the perspective of defining a real-time checking/calibration protocol.

Figure 14 represents WD and WS with the results ordered by WSMet. It emerges that the WD gap between simulation and measurement clearly decreases while WSMet increases.

In terms of WS gap, it emerges that the worst cases are the cases related to WDMet = 180, as these are not only “oblique”, but they are also the ones with the lowest wind speed.

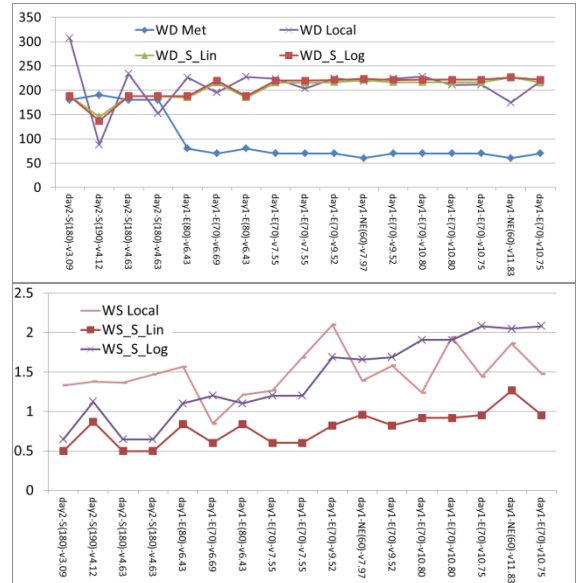


Fig. 14 – Simulation and Experimental Results ordered by WSMet:WD (a) and WS (b)

Finally, Figure 15 shows the relative percentage error for WS in the two cases, with simulations ordered by WDMet. It clearly shows that the two simulation sets’ trend is similar, but “shifted”, except for the “oblique” cases where they tend to overlap.

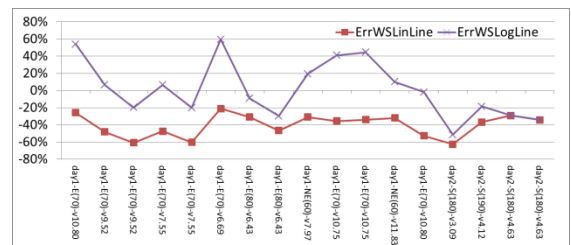


Fig. 15 – Relative Percentage Error for WS

“Shifting” is an expected behaviour because, as previously stated, the two inlet conditions relate to different average WSMet on the inlet surfaces. In fact, the two profiles have the same value in the point where height is 6m (altitude of the weather station at the airport) but the logarithmic profile then increases, resulting in a higher average value (Fig. 4). So far, the simulation using a logarithmic profile obtains better results. However, the existence of a “shifting” between linear and logarithmic model results also confirms that, in terms of WS, a further calibration might be required for both the cases. This calibration will be performed when a set of - statistically speaking -

more reliable experimental data is available. It also emerges that there is still a “fluctuation” of the model’s performance in terms of WS. In our opinion, this could be related to two main aspects. The first is “structural” in the process, and it is related to the action of “averaging” the wind. Averaging the wind speed, and defining the prevalent wind direction for both the two locations, is a very critical step in this process. So far, two different subjects conduct this step autonomously (the airport weather service and the authors) for two different sets of data. This procedure will be the same during the real-time phase, although, a deeper investigation regarding the averaging interval length could be useful. The 30-minute length chosen so far is related to the availability of real-time data from the meteorological weather services. The averaging interval could be modified to 10 minutes, if more detailed data from some weather service is made available.

The second aspect is the possible inaccuracy of some measurements in both the two weather stations (airport and canyon) during the survey. So far, the preliminary calibration is based on 17 cases, meaning possible “wrong” measures (not easy to be identified, especially if they are related to the weather station at the airport, not directly managed by the authors) highly affect overall performance. This aspect will be investigated further using statistical correlations when more experimental data is available from the local weather station. Thus, the weight of possible “anomalous” cases will be reduced statistically.

6. Conclusion

This paper presents the development and preliminary calibration of a CFD urban canyon model used in the EU funded project SEAM4US. The model aims at representing the relation between Meteorological Wind and local winds near subway station entrances; in this case, the pilot case used is the Passeig de Gracia subway station in Barcelona.

The preliminary calibration is based on a small experimental data set, thus the results will have to

be updated with a larger set of data. However, the preliminary results showed a very good convergence in terms of WD, with an average error of 27.30 deg, close to the precision of the instrument 22.5 deg. In terms of WS, the model would benefit from a further calibration (average error 0.41 m/s), which will be performed once more experimental data is available.

Furthermore, the paper discusses the data in the perspective of defining a protocol for the real-time comparison of experimental data concerning Meteorological and Local Wind, and simulation results, as this operation will have to be performed by the SEAM4US Control System.

7. Nomenclature

Symbols

WS	Wind Speed (m/s)
WD	Wind Direction (degree)

Subscripts/Superscripts

Loc	Local (in the urban canyon weather station)
Met	Meteorological (in the airport weather station)
S_Lin	Simulated/Linear Inlet Condition
S_Log	Simulated/Logarithmic Inlet Condition

References

- AmbientWeather.<http://ambientweather.wikispaces.com/Weather+Station+Comparison+Guide>
- Ansuini R., Larghetti R., Vaccarini M., Carbonari A., Giretti A., Ruffini S., Guo H., Lau S.L., “Hybrid Modeling for Energy Saving in Subway Stations”, in proceedings of: BSO12 - Building Simulation and Optimization 2012, Loughborough, UK, September 10-11, 2012
- ASHRAE 2005, Handbook Fundamentals, Atlanta.
- Comsol, 2011. CFD Module User’s Guide, p.162.
- Comsol, 2012. COMSOL Multiphysics Version 4.3.
- Costola D, Blocken B, Hensen JLM, 2009. Overview of pressure coefficient data in building energy simulation and airflow network programs. Build Environ 2009, 44: 2027-2036.

- Franke, J., Hirsch, C., Jensen, A.G., Krüs, H., Schatzmann, M., Westbury, P., Miles, S., Wisse, J., Wright, N., 2004. Recommendations on the use of CFD in wind engineering. In: van Beeck, J.P.A.J. (Ed.), Proc. of the International Conference on Urban Wind Engineering and Building Aerodynamics. COST Action C14., Sint-Genesius-Rode, Belgium.
- Franke J, Hellsten A., Schlünzen H., Carissimo B., 2007. Best practice guideline for the CFD simulation of flows in the urban environment. COST Office Brussels, ISBN 3-00-018312-4.
- Geros V, Santamouris M, Tsangrassoulis A, Guarracino G., 1999. Experimental evaluation of night ventilation phenomena. *Energy and Buildings* 1999;29:141–54.
- Ghiaus C, Allard F., 2003. Natural ventilation in an urban context. In: Santamouris M, editor. *Solar thermal technologies for buildings*. London: James and James; 2003. p. 116–39.
- Ghiaus C., Allard F., Santamouris M., Georgakis C., Nicol F., 2006. Urban environment influence on natural ventilation potential. *Building and Environment* 41 (2006) 395–406.
- Giretti A., Lemma M., Vaccarini M., Ansuini R., Larghetti R., Ruffini S., “Environmental Modelling for the Optimal Energy Control of Subway Stations”, *Gerontechnology* 11(2):168, 2012.
- Horan J.M., Finn D.P., 2008. Sensitivity of air change rates in a naturally ventilated atrium space subject to variations in external wind speed and direction. *Energy and Buildings* 40 (2008) 1577–1585.
- Liddament, M.W. 1988. The calculation of wind effect on ventilation. *ASHRAE Transactions* 94(2):1645-1660.
- Rossi N., 2003. *Manuale del Termotecnico*. Hoepli.
- Santamouris M., Papanikolaou N., Koronakis I., Livada I., Asimakopoulos D., 1999. Thermal and airflow characteristics in a deep pedestrian canyon under hot weather conditions. *Atmospheric Environment* 33 (1999) 4503:4521.
- Wilcox, D.C. 1998. *Turbulence Modeling for CFD*, 2nd ed., DCW Industries, 1998.
- Yoshie, R., Mochida, A., Tominaga, Y., Kataoka, H., Harimoto, K., Nozu, T., Shirasawa, T. 2007. Cooperative project for CFD prediction of pedestrian wind environment in the Architectural Institute of Japan. *J. Wind Eng. Ind. Aerodyn.* 95(9-11): 1551-1578.

Comfort and energy performance of a HVAC system under real conditions for an office block

Paolo Valdiserri – Università di Bologna, Bologna, Italy

Cosimo Marinosci – Università di Bologna – CIRI: Edilizia e Costruzioni, Bologna, Italy

Laura Pedretti – Università di Bologna – CIRI: Edilizia e Costruzioni, Bologna, Italy

Abstract

In the present work, we performed a dynamic simulation of an air-conditioning system for an office block using a mathematical model via Matlab-Simulink. Both the accomplishment of the desired human comfort within the conditioned space and the variation of energy request due to different measurements of volume flow rate have been evaluated, as requested by the European regulation EN 13779 on non-residential buildings. The model has been applied to an office block located in Bologna (Italy), but can also be used for other types of buildings, as well. The HVAC system in the study uses external air supply, with either constant or variable flow rate, and includes three different ways of air treatment: heating and humidification in winter, cooling and dehumidification in summer, and ventilation only, other ways. The study estimated: i) the conditions that can ensure the requested performances at the lowest energetic cost; ii) the energetic gain deriving from the installation of a heat recovery, or/and using carbon dioxide sensors within the conditioned space. The calculation of the energy required has been evaluated in both a typical winter and summer day.

1. Introduction

According to recent regulations on energy saving in buildings, all new structures should guarantee high energy performance [1, 2]. To this aim, the building envelope should be equipped with insulated walls and high efficiency windows. This approach leads to massive thermal insulation, but at the same time, it results in a worsening of indoor air quality, and in hygienic and environmental problems (such as mould growth and airborne diseases). A healthy quality of life imposes a good indoor air quality especially where people spend

most of their time [3], so it is mandatory to guarantee adequate air exchanges to reduce indoor pollution to “acceptable” levels. Energy-saving regulations should consider the indoor comfort not only intended as thermo-hygrometric parameters, but also air quality, conditions that are achieved with the emission of fresh and clean air. One solution for non-residential buildings is balanced mechanic ventilation to dilute and extract indoor pollutants. Moreover, using this strategy in an all air conditioning system, the air itself is the carrier to reduce or add thermal load, directly improving indoor comfort condition. The efficiency of this type of air control relies on project decisions, especially on the calculations of external mass flow rate. Actual indoor air quality recommendations enforce high quality standards, which demand high external airflow (in order to remove indoor pollutants) with the consequence of major energy consumption.

The aim of this work was to evaluate both the achievements of desired thermohygrometric requirements of the air-conditioned areas, and the variation of energy requirements according to different evaluations of airflow rate as requested by law for non-residential buildings. For this purpose, a dynamic simulation model of a HVAC system built in Matlab-Simulink, already applied for the evaluation of energy and comfort performance in hospital rooms [4] has been used. We hypothesized that, given the same indoor air quality: i) air-conditioning systems using a variable controlled ventilation ensure a better indoor comfort and air quality as well as a lower energy consumption than those using constant air flow rate, and ii) a CO₂-based demand-controlled ventilation allows higher energy saving than those

calculating airflow rate using a prescriptive approach. To calculate the airflow rate we used the European EN 13779 [5] regulation.

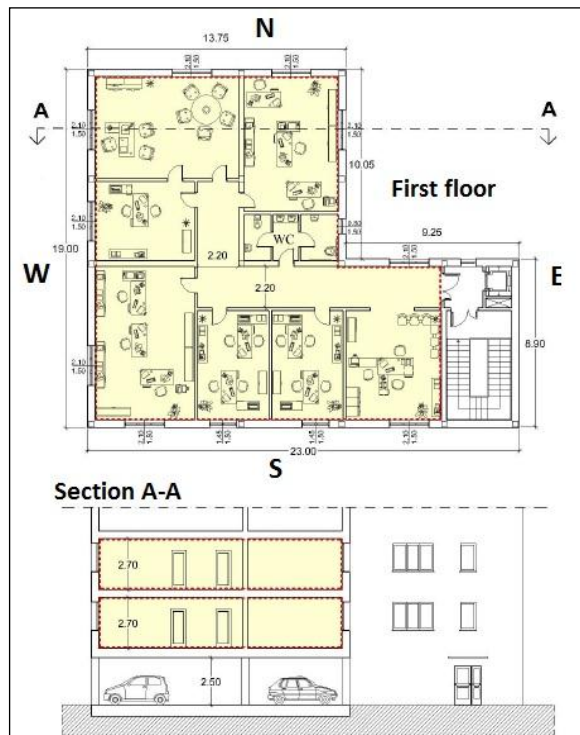


Fig. 1 – The office block

The mathematical model has been applied to a two-floor office of 533 m² floor area and having a volume of 1439 m³, as shown in Figure 1.

2. Description of the model

Air-conditioning systems are required to produce and maintain appropriate thermo-hygrometric conditions in buildings, accordingly to their final use. They ensure adequately comfortable conditions, defined by ASHRAE as satisfactory conditions for indoor environments [6]. Given the rate of metabolic heat production (according to people's physical activity), the major factors acting on thermo-hygrometric comfort are:

- dry air temperature (t);
- relative humidity (UR);
- air velocity.

The best technical solution is given by air conditioning systems which produce and maintain appropriate conditions of temperature, relative

humidity, velocity and air cleaning regardless of external air variations. Indoor temperature is maintained at the desired values either adding or removing heat, while the relative humidity control is preserved by air humidification in winter, and air dehumidification in summer.

As shown in Figure 2, the proposed model allows the simulation of an air conditioning system in a dynamic mode, and the analysis of the interaction between the indoor environment and its occupants.

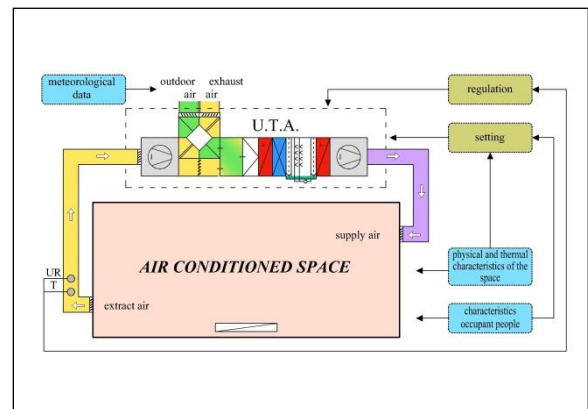


Fig. 2 – Organization of the office block system

To this aim, we used Simulink, a simulation software exploiting Matlab. The built model is characterized by fast calculation, simplicity, and ability to solve differential equations (introducing the temporal variable). It consists of (Figure 3) an:

- air conditioning system;
- air conditioned space.

The air conditioning system is a plant able to produce and maintain the required conditions for indoor comfort. It is modelled by Simulink as an air handling unit acting on equipment, and on constitutive devices.

The air conditioned space is a closed area that can be heated or cooled at specific set-points and can consist of a single room, several rooms on the same or on different floors, or the entire building. Within the Simulink model, the air conditioned space is divided into two parts describing indoor air quality and thermo-hygrometric conditions. Two more components allow the right operation:

- data acquisition;
- calibration and regulation.

During the simulation, data acquisition includes both outdoor and indoor air properties

(temperature, relative humidity, and air quality). The indoor environment is characterized by its dimensions, thermal features such as thermal transmittance, use (internal load), occupancy levels, and occupant characteristics (metabolic rate, carbon dioxide production etc.).

The calibration of the system was performed in a steady-state condition (the data were defined as constant during time); the dynamic condition of the system was obtained using the automatic regulation, to rectify the values previously defined on the modification of the data introduced.

3. filtering section;
4. preheat coil;
5. cooling coil;
6. humidifier;
7. reheat coil;
8. fan.

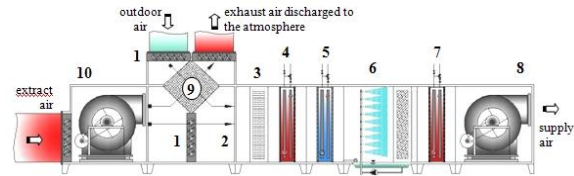


Fig. 4 – The air handling unit

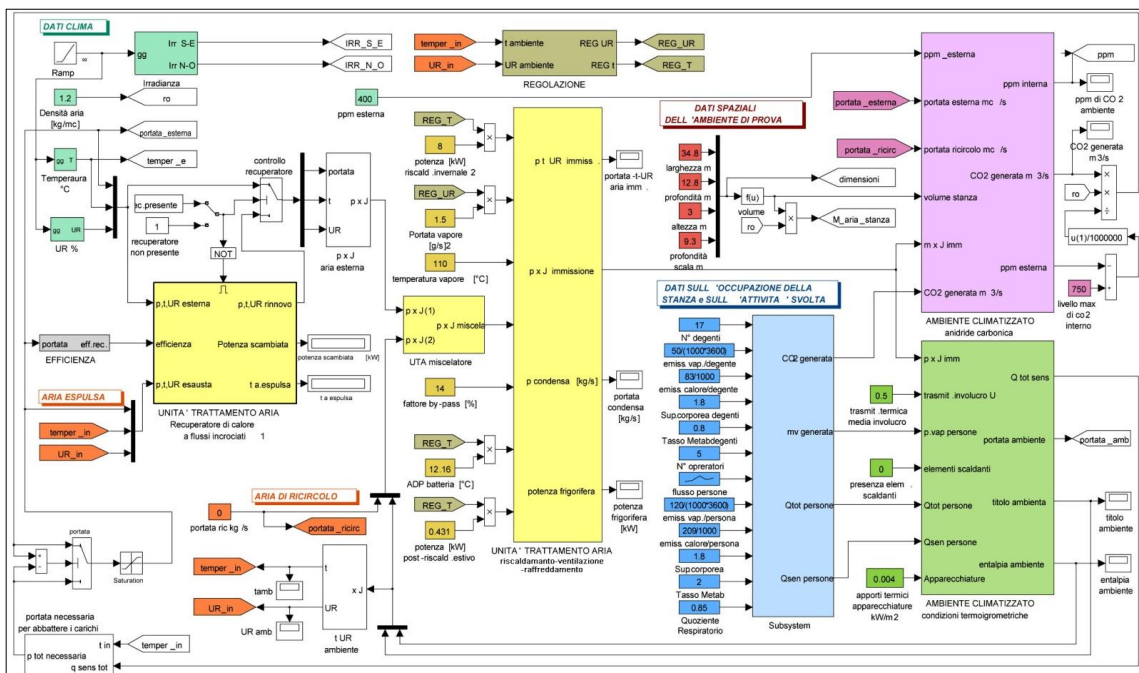


Fig. 3 – Model use for the office block

2.1 The air handling unit

The Air Handling Unit (AHU) consists of all the components of the system which take outdoor air, and filter and treat it to the required thermo-hygrometric indoor inlet characteristics.

Figure 4 shows a typical central system that supplies conditioned air to a single zone. During the process, the air encounters the following components:

1. dampers;
2. air mixers section;

Whenever an energy recovery is needed, the used AHU is equipped with a heat exchanger (9); in this case a second fan (10) is present. The reported application uses an all air conditioning system with water humidification. In the AHU, the air flow depends on external air temperature:

1. In winter time, when $t_e \leq 20$ °C, the air encounters: damper \Rightarrow heat recovery \Rightarrow mixing section \Rightarrow filters \Rightarrow preheat coil \Rightarrow humidifier \Rightarrow reheat coil \Rightarrow supply fan. Whenever the indoor temperature (produced, for example, by a high number of occupants) can heat the external air to the requested conditions of comfort, the heating

system is not activated, not operating the corresponding coil.

2. In summer time, when $t_e \geq 25$ °C, the air encounters: damper \Rightarrow heat recovery \Rightarrow mixing section \Rightarrow filter \Rightarrow cooling coil \Rightarrow reheat coil \Rightarrow supply fan.

3. In case of t_e intermediate values, no air treatment is needed and the system works only in ventilation mode.

Each component, containing a single air handling unit, operates only in the case of activation, which follows the comparison between t_e values and limit values as defined for the winter or summer regime. It is always possible to know the components which are active, for a better representation of the model and to reduce computational time during simulation.

2.2 Heat recovery system

The heat recovery system (which can be manually switched on or off) can save energy from the ejected air, Figure 5. The model employs a cross flow heat exchanger able to exchange both sensible and latent heat, but unable to exchange humidity since the two air fluxes are kept separate by specific sealing in the plates. Any air infiltration, contaminant gases (polluting materials), biological hazards and particulates are completely blocked.

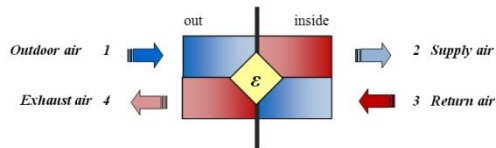


Fig. 5 – Scheme of preheat coil

The heat recovery system is activated only whenever the air is thermally treated. When only ventilation is present, the system is either useless or disadvantageous, since it can worsen indoor comfort, increasing the temperature. The heat flux exchanged (Eq.1) is proportional to the efficiency of the recovery system, to the air flow, and to the difference of the temperature of the fluxes according to the following equation:

$$\dot{Q}_r = \varepsilon [\dot{m}_a c_p (t_3 - t_1)] \quad (1)$$

2.3 Air mixers section

In the mixing box, the adiabatic mixing between outdoor air and the indoor air takes place only if the temperature of the outdoor air is uncomfortable.

2.4 Preheat coil

The heating takes place in the preheat coil, where an hot fluid exchanges heat with the flux of the moist air (Figure 6). The characteristics of supply air are obtained by a mass and energy balance of dry air and vapour.

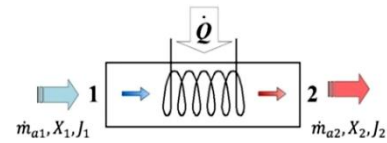


Fig. 6 – Scheme of the preheat coil

2.5 Humidifier

Air humidification is obtained by injecting water inside the air. The conditions of exiting air can be obtained from the mass and energy balance.

2.6 Cooling coil

In the cooling coil, Figure 7, the cooling and dehumidification of the air takes place, to reduce the temperature and the humidity ratio.

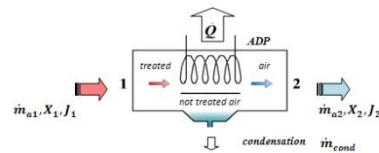


Fig. 7 – Scheme of the cooling coil

The cooling coil is characterized by the “By-pass Factor” (BF) which represents the ratio between not treated and total air flow. In the model a BF = 0.14 has been used.

3. The conditioned space

The conditioned space is a closed environment, with one or more rooms placed also on different floors, or the entire building, heated or cooled at specific temperatures (set-point). In the model, it corresponds to the two floor office block (Figure 1).

The conditioned space has been divided into:

- thermo-hygrometric component;
- CO₂ component.

3.1 Thermo-hygrometric component

The humidity ratio and the enthalpy for this component (Figure 8) is obtained by a mass and energy balance in transient regime (Eq. 2, 3).

$$M \frac{dX_{Amb}(\tau)}{d\tau} = \dot{m}_a X_{imm} + \dot{m}_v - \dot{m}_a X_{Amb}(\tau) \quad (2)$$

$$M \frac{dJ_{Amb}(\tau)}{d\tau} = \dot{Q}_{tot} + \dot{m}_a J_{imm} - \dot{m}_a J_{Amb}(\tau) \quad (3)$$

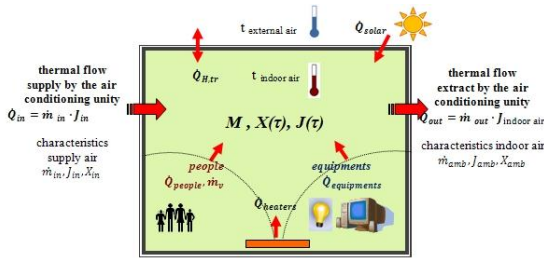


Fig. 8 – Interaction between the conditioned area and outside

3.2 CO₂ component

The study of thermal comfort cannot be separated by indoor air quality. There is a chemical-physical and biological balance between a person and the environment; therefore the air quality control (based on the degree of indoor pollution) is a peculiar part of environmental comfort. The diversity of pollutants potentially present in closed environments, excludes the possibility to identify a general marker of air pollution.

The bio effluents are considered the main responsible agents of indoor pollution [7], and they include gases produced by the body (through respiration and skin) such as CO₂, humidity, aromatic compounds, esters, and alcohols. Their concentration is in general difficult to be measured and limiting values are rarely found, with the exception of CO₂. Indeed, CO₂ concentration is an indicator of anthropic pollution since it is produced with respiration [8]. For the carbon dioxide calculation [9] it is necessary to know the number and the typology of people present each time in the environment. CO₂ produced by each person, Eq.4, is proportional to the oxygen

consumed during respiration (VO₂) which is related to body shape, (A_D), sex, age, Respiratory Quote (RQ) and physical activity (M):

$$\dot{G}_p = 0.83 \dot{V}_{O_2} = 0.83 \frac{0.00276 A_D M}{(0.23 RQ + 0.77)} \quad (4)$$

The variation of indoor carbon dioxide depends on its concentration in the inlet and outlet air, and on its indoor production (scheme on Figure 9) and it is calculated with Eq.4.

$$V \frac{dc_{amb}(\tau)}{d\tau} = (\dot{G} + \dot{Q}_v c_{imm}) - \dot{Q}_v c_{amb}(\tau) \quad (5)$$

The concentration of CO₂ in the supply air depends on the typology of air composing the flux (in the general case, there is both external and recirculated air). As an initial condition we used CO₂ concentration as obtained at 00.00 (midnight) of the day preceding the day of the simulation.

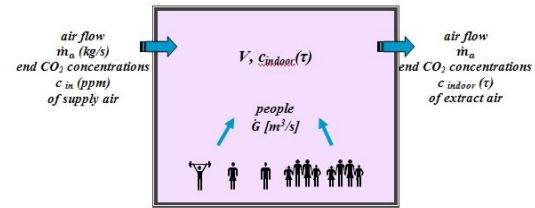


Fig. 9 – Correlation between indoor air quality and occupants

4. Calculation of the air flow and results of the simulations

The simulation of the office block was performed on two typical days in Bologna - Italy: one in winter time (January 17th), when the heating system is active the entire working day; and one in summer time (July 17th), when the cooling system works only during daylight hours when t_e>25°C, while in the remaining hours it only works as ventilation.

The system is supposed to maintain the following hygrometric parameters [10]:

Winter t = 20°C UR = 50%

Summer t = 26°C UR = 50%

and the internal air quality accomplishes IDA2 as defined by regulation [4].

Regarding the constructive characteristics, the thermal transmittance of the envelope was considered uniform and equal to 0.5 W/(m² K).

All the employees and the visitors are characterised by a metabolic rate of 1.2 met and with a vapour and heat emission per person evaluated as 50 g/h and 126 W. The working time is from 9 a.m. to 7 p.m. The outdoor concentration of CO₂ is of 400 ppm, whilst for the outside temperature the Arpa hourly data was used in the form of a sinusoidal function.

The calculation of the external airflow has been done according to the EN 13779. For each calculation methodology, the fulfilment of the thermo-hygrometric requirements (for indoor air conditioned environment) was verified. It was possible to calculate the energy required by the systems instantaneously and during the entire simulation, as well as the instantaneous concentration of CO₂ for the evaluation of indoor air quality (Fig.10) [5].

Category	Description	CO ₂ -LEVEL ABOVE LEVEL OF OUTDOOR AIR IN PPM	
		Typical range	Default value
IDA 1	High indoor air quality	≤ 400	350
IDA 2	Medium indoor air quality	400-600	500
IDA 3	Moderate indoor air quality	600-1000	800
IDA 4	Low indoor air quality	>1000	1200

Fig. 10 – Acceptable CO₂ concentration [5].

EN 13779 regulation allows to calculate the load both using the *prescriptive* and the *performance* related method.

1. The *prescriptive approach* defines the minimal air loading per person according to the final use of the building. In the case of offices it requires a minimal volumetric flow rate of 12.5 l·s⁻¹ per person (IDA2): 1.1. In the systems with constant air volume, the air flow per person is multiplied by the expected presence of employees and visitors in the office block (i.e. 50 people according to the dimension of the office and the EN 13779). From the simulations it is possible to obtain instantaneous values of the coil heat flux, with or without the insertion of the heat recovery as shown in figures 11 and 12.

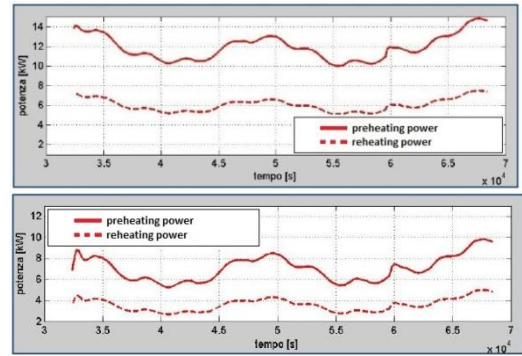


Fig. 11 – Coils power in a winter day (Jan 17th) without (a) and with (b) the heat recovery

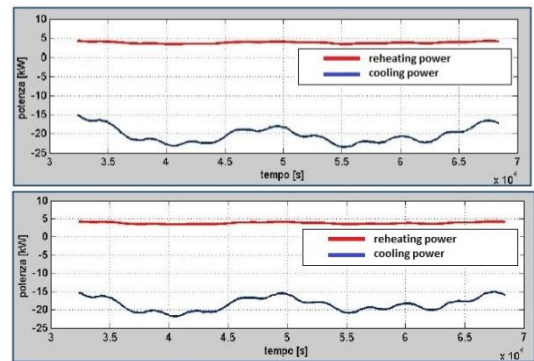


Fig. 12 – Coils power in a summer day (Jul 17th) without (a) and with (b) the heat recovery

Figure 13 shows carbon dioxide concentration produced by 50 people at 1.2 met. The simulation indicates *high* air quality classification always below the upper limit of IDA1.

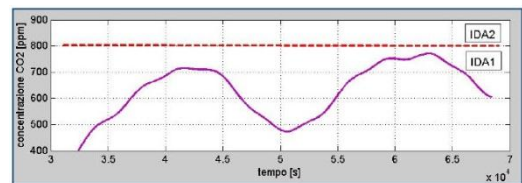


Fig. 13 – CO₂ concentration (50 people)

Given the indoor air classes of the regulation EN 13779 for offices (IDA2), the number of people has been reduced to the value of 30. In Figure 14 the indoor air quality results below the limit of IDA2.

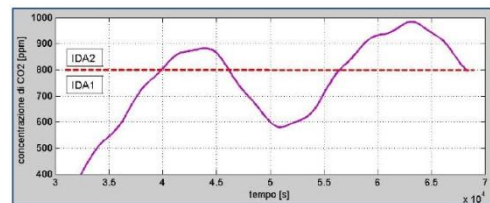


Fig. 14 – CO₂ concentration (30 people)

1.2. In the systems with Variable Air Volume (VAV), the air flow per person loading is multiplied by the number of people detected by specific sensors placed at the entrances of the office block. In Figure 15 the human occupancy profile for the entire office from 9 a.m. to 7 p.m is shown.

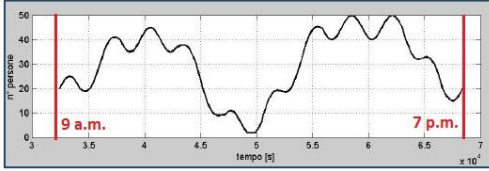


Fig. 15 – Office people occupancy



Fig. 16 – External mass flow rate

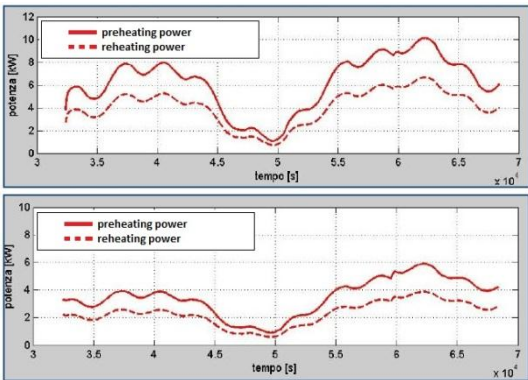


Fig. 17 – Coils power in a winter day (Jan 17th) without (a) and with (b) the heat recovery

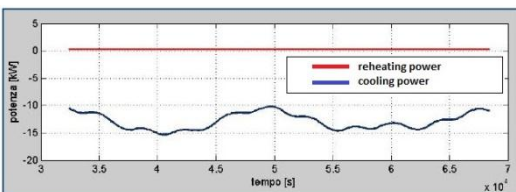


Fig. 18 – Coils power in a summer day (Jul 17th) with heat recovery

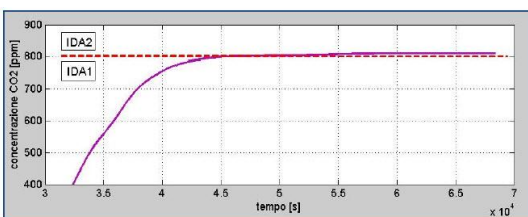


Fig. 19 – CO₂ concentration (VAV)

Using the people occupancy the mass flow rate is calculated multiplying the instantaneous value by

flow rate of 12.5 l·s⁻¹. The profile is reported in Figure 16.

The results of the simulation of the coil heat flux in the winter and summer days are reported in figures 17 and 18.

Carbon dioxide concentration is reported in Figure 19 for the simulation of an all air system with the variable air volume using the profile of Figure 16. Also in this condition the indoor air quality is *high* (IDA1 classification) except for almost four hours in the late afternoon in which indoor air quality is *medium* (IDA2).

2. The *performance related approach* defines the limits for CO₂ concentration and allows the calculation of outdoor air loading which ensures the limits in two different ways:

2.1. The first identifies the quantity of CO₂ produced by a “typical” occupant, and this value is multiplied by the number of people instantaneously detected by an automatic counting sensor. External air flow (Figure 20) is calculated to maintain indoor CO₂ concentration below the default value of 500 ppm above the level of the outdoor concentration (400 ppm).

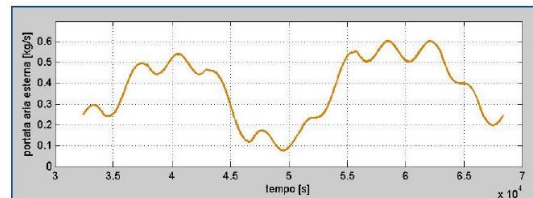


Fig. 20 – External mass flow rate

Heat flux and CO₂ concentrations obtained by the simulation are shown in figures 21 and 22.

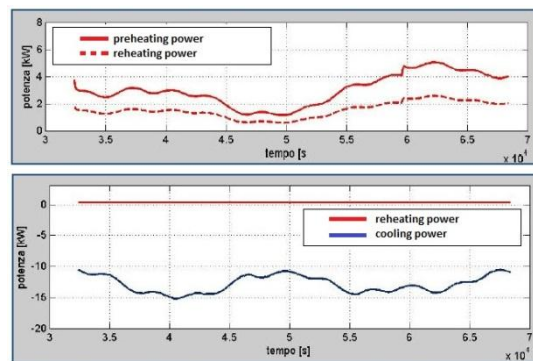


Fig. 21 – Coils power in a winter (a) (Jan 17th) and summer (b) day (Jul 17th) with heat recovery

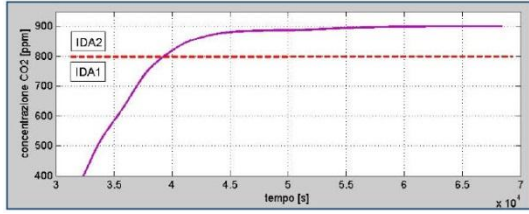


Fig. 22 – CO₂ concentration

2.2. The second way detects the carbon dioxide concentration using an indoor CO₂ sensor. This measured value is compared with the default one, 500 ppm above the outdoor concentration, corresponding to IDA 2 air category (Figure 10), and the range of ± 100 ppm is used by a proportional-integral regulator to determine the instantaneous external mass flow rate. Whenever the mass flow rate is below $0.24 \text{ kg}\cdot\text{s}^{-1}$ (that corresponds to 0.5 volume per hour exchange of indoor air) this value is set to $0.24 \text{ kg}\cdot\text{s}^{-1}$. Figure 23 shows the profile of the external mass flow rate.

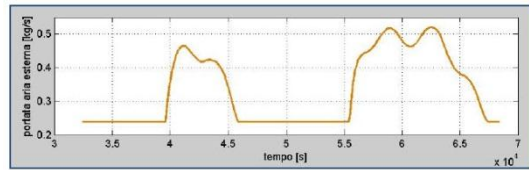


Fig. 23 – External mass flow rate

Heat flux and CO₂ concentrations obtained by the simulation are shown in figures 24 and 25.

The energy requirements for each approach during the representative winter (January 17th) or summer (July 17th) days are reported in tables 1 and 2.

The *prescriptive approach* allows both a constant and variable air flow rate. EN 13779 regulation specifies IDA2 air quality for office use and provides: i) typical value for human occupancy in terms of floor area per person based on the kind of building use; ii) the rate of outdoor air per person. In constant air flow systems the calculated values lead to a *high* air quality (IDA1). The reason is related to an overestimated number of people for the office object of this study. In the studied case the IDA2 air quality is reached with an occupancy of 30 people, that corresponds to 1 person each 18 m², instead of the 50 occupants given by the regulation.

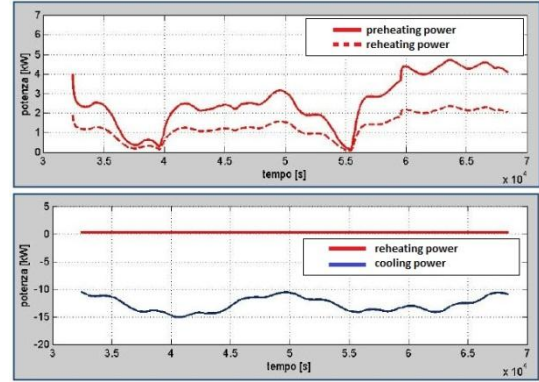


Fig. 24 – Coils power in a winter (a) (Jan 17th) and summer (b) day (Jul 17th) with heat recovery

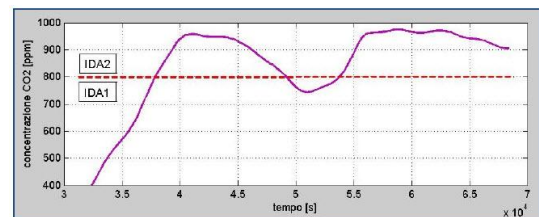


Figure 25 – CO₂ concentration

Category of indoor air reached:	IDA 1		IDA 2	
Outdoor air flow rate - calculation way:	without Heat Recovery	with Heat Recovery	without Heat Recovery	with Heat Recovery
Prescriptive approach				
Constant ventilation air flow (50 people)	179	106		
Constant ventilation air flow (30 people)			102	57
Variable air flow (Rate of outdoor air per person) with counting sensors			102	58
Performance related approach				
Variable air flow (Rate of outdoor air by CO ₂ level) with counting sensors			82	45
Variable air flow (Rate of outdoor air by CO ₂ level) with CO ₂ sensors			72	39

Table 1 – Energetic requirements - simulation on January 17th [kWh]

Category of indoor air reached:	IDA 1		IDA 2	
Outdoor air flow rate - calculation way:	without Heat Recovery	with Heat Recovery	without Heat Recovery	with Heat Recovery
Prescriptive approach				
Constant ventilation air flow (50 people)	241	224		
Constant ventilation air flow (30 people)			216	205
Variable air flow (Rate of outdoor air per person) with counting sensors			144	132
Performance related approach				
Variable air flow (Rate of outdoor air by CO ₂ level) with counting sensors			141	132
Variable air flow (Rate of outdoor air by CO ₂ level) with CO ₂ sensors			140	131

Table 2 – Energetic requirements - simulation on July 17th [kWh]

In the prescriptive approach the variable air flow rate is more reliable; the IDA2 air quality is always achieved. Notably, the default value of $12.5 \text{ l}\cdot\text{s}^{-1}$ recommended in the EN13779, as the rate of outdoor air per person, seems lightly overestimated for the office object of the present

study. It results in a CO₂ concentration that is either in the IDA1 range (in the morning), or in the lowest IDA2 range values.

The two *performance related approaches* always reach the required IDA2 air quality, since the calculated carbon dioxide level is used to compute the mass flow rate. To this aim, the proposed model is essential to calculate and adjust the outdoor airflow rate.

In order to achieve IDA2 air quality both i) *prescriptive* and *performance related approaches*, and ii) constant and variable air flow rate are suitable. The difference between the two approaches is evident in the consumption of energy. The employing of *performance* methods based on the CO₂ produced in the indoor environment is energetically more convenient than using prescriptive methods, especially in winter. Moreover the addition in the air handling unit of the heat recovery section reduces energy consumption in particular in winter.

5. Conclusion

From the results obtained by the numerical simulations, it is possible to conclude that:

- In order to achieve IDA2 air quality all the described methods are suitable;
- Variable volume systems are able to adjust to effective occupational loading and represent the best solution. Performance related methods based on the indoor pollution as the major input (evaluated as CO₂ produced by occupants), are more efficient since they always fulfil indoor standards of air quality with minor energy consumption.

6. Nomenclature

\dot{G}_p	Carbon dioxide production (per person)	m ³ /s
J	Specific enthalpy of moist air	kJ/kg _a
M	Total mass of air	kg
M	Rate of metabolic heat production	met
\dot{Q}	Heat flow rate	W

V	Total volume of air	m ³
X	Humidity ratio	kg _v /kg _{as}
c	Carbon dioxide concentration	ppm
c _p	Specific heat	kJ/kg K
h _v	Specific enthalpy of water vapor	kJ/kg _v
\dot{m}_a	Mass flow of dry air	kg _{as} /s
\dot{m}_v	Mass flow of water vapor	kg/s
t	Temperature of moist air	°C
t _e	Outdoor temperature	°C
t _i	Indoor design temperature	°C
M	Total mass of air in the air conditioned space	kg
ε	Heat recovery efficiency	-
τ	time	s

References

- [1] Directive 2002/91/EC of the European Parliament and of the Council of 16 December 2002 on the energy performance of buildings.
- [2] Directive 2009/28/EC of the European Parliament and of the Council of 23 April 2009 on the promotion of the use of energy from renewable sources and amending and subsequently repealing Directives 2001/77/EC and 2003/30/EC of 16 December 2002 on the energy performance of buildings.
- [3] Air quality guidelines – Global update 2005, World Health Organization, <http://www.euro.who.int>.
- [4] Valdiserri P., Pedretti L. 2012. Dynamic simulation of HVAC systems: evaluation of energy and comfort performance in hospital rooms, XXX UIT Conference, Bologna. June 25-27.
- [5] EN 13779:2007. Ventilation for non-residential buildings - Performance requirements for ventilation and room-conditioning system.
- [6] ANSI/ASHRAE Standard 62.1-2004. Ventilation for acceptable indoor air quality", American Society of Heating, Refrigeration and Air-Conditioning Engineers (ASHRAE), Atlanta.
- [7] Barbieri D., Pietrafesa M., Rizzo G. 1996. Qualità dell'aria interna e requisiti di ventilazione - Classificazione degli Inquinanti,

- Riferimenti Normativi, Metodi di Calcolo, Quaderni di Fisica tecnica ed energetica, serie: Memorie Scientifiche.
- [8] You Y., Bai Z., Jia C., Wan Z., Ran W., Zhang J. 2007., Measuring Air Exchanges Rates Using Continuous CO₂ Sensors, Proceedings of Clima 2007 WellBeing Indoors.
- [9] ASTM Standard: D6245-07. Standard Guide for Using Indoor Carbon Dioxide Concentrations to Evaluate Indoor Air Quality and Ventilation.
- [10] EN ISO 13790: 2008. Energy performance of buildings: Calculation of energy use for space heating and cooling.
- [11] UNI EN ISO 7730: 2006 Ergonomics of the thermal environment–Analytical determination and interpretation of thermal comfort using calculation of the PMV and PPD indices and local thermal comfort criteria.
- [12] ASHRAE Handbook 2009, Fundamentals, SI Edition.

Integrated BIPV performance assessment for tropical regions: a case study for Bangalore

Gayathri Aaditya – Indian Institute of Science, Bangalore, India

Rohitkumar Pillai – Indian Institute of Science, Bangalore, India

Monto Mani – Indian Institute of Science, Bangalore, India

Abstract

Building Integrated Photovoltaic (BIPV) are Photovoltaics (PVs) integrated as a building envelope. In addition to effectively generating energy, BIPV need to be energy efficient. They would need to passively regulate the responsiveness of the building envelope to the external environment to provide (natural) indoor thermal comfort, thus accomplishing the prime function of a building. Thermal comfort is an important parameter in building design as it contributes to overall health and productivity. Tropical regions, such as India, are generally characterized by high temperatures and humidity where passive designs need to integrate a combination of both, appropriate thermal massing and space orientation for adequate ventilation. BIPV poses unique considerations (and opportunities) as the inherent thermal mass is low and the radiative transmittance is high. Consequently, the BIPV also permits rapid heat-loss at night from the indoors through radiation, particularly when integrated as a roof. Regulating indoor thermal comfort in tropical regions poses a particular challenge under such conditions, as the Mean Radiant Temperature is likely to be high. Thermal comfort is also a key factor in assessing the energy efficiency of a building envelope as it determines the dependence on active (power-intensive) regulation for providing thermal comfort. Thus, building design strategies for optimizing BIPV performance would require an integrated consideration of three interdependencies, viz., maximizing PV performance, passive climate-responsive environment and natural thermal comfort. The paper investigates the performance of a 5.25 kWp roof integrated BIPV lab at the Indian Institute of Science, Bangalore (India) and is based on a year-long systematic study of parameters determining PV performance, indoor thermal comfort and building climate response. Regulating indoor thermal comfort is of particular concern as temperature stratification has been noted under BIPV roof. The current paper investigates

the influence of thermal comfort on building climate response and BIPV performance and suitable strategies have also been evaluated through a simulation model.

1. Introduction

Building Integrated Photovoltaic Systems (BIPV) represent a recent trend in building design where PV forms the part of the building structure and fabric. These modules can be utilized as roof, facade, walls, glass, sunscreen or sunshade. In addition to other functional (building) requirements, BIPV also harnesses (and generates) energy. The electrical output from a photovoltaic system follows the solar radiation trend thereby generating maximum power during the peak sunshine hours. Tropical regions are characterized by high annual solar insolation making them ideal for any photo-voltaic application. However, two major challenges, electrical and thermal, pertaining to the application of BIPV in tropical regions stem out upfront. Firstly, the cell temperatures (in the tropical region) increase phenomenally compared to the ambient temperature resulting in a power loss. Secondly, integrating solar panels into the building thereby transmits a lot of heat to the interiors raising the issue of thermal comfort of the occupants. An appropriate solution is to design a BIPV structure, which can resolve the above mentioned problems by regulating its own heat gain to provide comfort.

PV as an envelope has unique opportunities and challenges in tropical regions in contrast to northern cold regions. The energy efficiency of PV is a key factor, as it determines the dependence on active (power-intensive) regulation for providing

thermal comfort. The roof is the most exposed to impacts of solar radiation, with low thermal mass, as it receives sunlight for practically the whole day, and in the tropics, the angle of incidence is close to the normal in the hotter parts of the day. Heat gain through the roof elevates ceiling surface temperature and causes radiant heat load on the occupants (Kabre, 2010) which also stratifies the air in the room.

This paper attempts to investigate, through experiments and building simulation, the thermal comfort in a BiPV structure installed at the Indian Institute of Science, Bangalore (tropical region, moderate climate) by identifying critical factors determining thermal comfort and provide solutions for attaining thermal comfort in BIPV structures through passive techniques.

2. Thermal comfort

Thermal comfort is an important aspect of buildings as it contributes to overall health and productivity. The standards such as ISO 7730 and ASHRAE 55-2004, define thermal comfort as subjective response and according to ASHRAE 55-2004 thermal comfort is defined as the “state of mind that expresses satisfaction with existing environment”. There are many factors that influence the thermal comfort which can be broadly classified as environmental or physical factors (air temperature, humidity, air velocity and mean radiant temperature), physiological or personal factors (activity, clothing) and special factors (age, gender, asymmetrical radiation, draft, vertical temperatures, etc.). A single value integrating the various factors, which can assess the thermal environment, is called the thermal comfort index. Fanger’s PMV - PPD model considers the major factors influencing thermal sensation. It has also defined the thermal comfort zones on the psychrometric chart by applying Fanger’s laboratory based Predicted Mean Vote index (PMV) and Predicted Percentage Dissatisfied index (PPD) method. The results have been derived by controlling the three environmental variables viz., air velocity, mean radiant temperature and relative humidity and two personal variables viz.,

activity level and clothing insulation (Singh et.al., 2011) One of the important assumptions made by Fanger is that the mean radiant temperature is equal to the ambient temperature. The model rests in good agreement with HVAC buildings situated in cold temperatures. The limitation of this model, however, is that the PMV method overestimates the sensation of warmth than actual (Fanger, 2002). Many researchers have criticized the validity of PMV_PPD model for tropical countries. A study done by (Manikandan, 2011) elucidates that ASHRAE model is valid if the mean radiation inside the room is measured exactly then going by Fanger’s assumption mean radiant temperature equal to ambient temperature. But many researchers have proved that the tendency to adapt to a changing external climate is the important factor for deciding thermal comfort. Because of the adaptability of the body to different climatic zones, the range of indoor temperatures in which humans feel thermally comfortable is highly dependent on the outdoor temperature. (Humphreys and Nicol, 1998). Figure 1, adapted from ASHRAE 55-2007, depicts the ranges of temperature for thermal comfort, in a non-air conditioned space, varying with the average outdoor temperature. Table 1 shows the acceptable operative temperature ranges for naturally conditioned spaces for Bangalore, India.

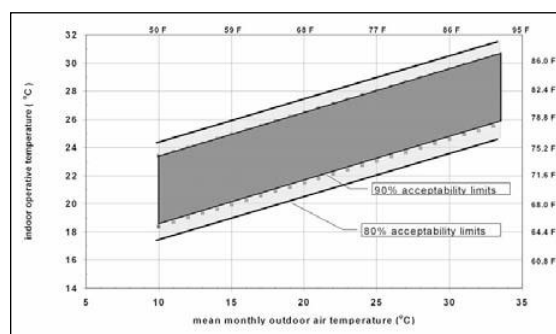


Fig. 1 – Acceptable operative temperature ranges for naturally conditioned space (Source: ASHRAE 55 - 2004)

3. Local thermal discomfort by ASHRAE standard 55-2004

It is necessary to understand and study the factors causing local thermal discomfort to determine

conditions for acceptable thermal comfort. These factors include draft, vertical air stratification, floor surface temperature and radiant temperature asymmetry. The acceptance criteria from all the local thermal discomfort factors must be met simultaneously in order to meet the thermal comfort requirements of the ASHRAE Standard 55-2004. The influence of these factors on the thermal comfort has been briefly discussed below.

Draft: Excessive air flow (or drafts) may result in an undesired body cooling. Sensitivity to drafts is greatest where the skin is not covered by clothing, especially the head region comprising the head, neck, and shoulders and the leg region comprising the ankles, feet, and legs. The requirements are

based on sensitivity to drafts in the head region with airflow from behind and may be conservative for some locations on the body and for some directions of airflow. (ASHRAE 55-2004)

Vertical Air Temperature Difference: Thermal stratification that results in the air temperature at the head level being warmer than at the ankle level may cause thermal discomfort. The allowable difference between the air temperature at head level and the air temperature at ankle level is 3°C. Thermal stratification in the opposite direction is rare, is perceived more favourably by occupants, and is not addressed in this standard. (ASHRAE 55-2004)

	Maximum Temperature deg C	Minimum Temperature deg C	Average	ASHRAE Naturally ventilated acceptable range	
Jan	30.2	13.6	21.9	26.601	22.368
Feb	33.4	14.1	23.75	27.417	22.4955
Mar	34.8	12.9	23.85	27.774	22.1895
Apr	33.9	21.2	27.55	27.5445	24.306
May	40.6	13.1	26.85	29.253	22.2405
Jun	30.4	19.6	25	26.652	23.898
Jul	31	13.8	22.4	26.805	22.419
Aug	31.3	17.4	24.35	26.8815	23.337
Sep	33.4	14.3	23.85	27.417	22.5465
Oct	30.4	18.4	24.4	26.652	23.592
Nov	32.2	13.2	22.7	27.111	22.266
Dec	33	10.9	21.95	27.315	21.6795

Table 1 – Acceptable operative temperature ranges for naturally ventilated spaces in Bangalore

Floor Surface Temperature: Occupants may feel uncomfortable due to contact with floor surfaces that are too warm or too cool. The allowable range of the floor temperature is 19-29 °C. (ASHRAE 55-2004)

Radiant Temperature Asymmetry: The thermal radiation field about the body may be non-uniform either due to hot and cold surfaces surrounding the body and exposure to direct sunlight. This asymmetry may cause local discomfort and reduce the thermal acceptability of the space. In general, people are more sensitive to asymmetric radiation caused by a warm ceiling than that caused by hot and cold vertical surfaces. ASHRAE 55 states a condition on the maximum temperature difference

from warm ceilings and suggests that it should be less the five degree centigrade, for obtaining the thermal comfort. (Christensen and Carr, 2012)

4. Case-Study: Building Integrated Photo-voltaic System at IISc

Bangalore lies in the south-east of the Indian state of Karnataka. It is positioned at 12.97°N 77.56°E, elevation of 1010 m. Winter temperatures rarely drop below 4°C, summer temperatures seldom exceed 30°C and it receives about 1300 mm of rain annually. The graph (figure 1) shows that for areas similar to Bangalore, thermal comfort will be

obtained if the operative temperature is between 21°C and 29°C. In the present analysis, an opaque type BIPV system installed on the roof (with no false ceiling or PV is not roof-mounted) of the experimental laboratory at the Centre for Sustainable Technologies (CST) of the Indian Institute of Science, Bangalore, India is considered. The lab is on the second floor of an existing load-bearing structure with one room measuring 18'2" x 17'10" and the other measuring 14'11" x 17'10". Stabilized Mud Blocks masonry has been adopted for the construction and is such that the south wall is not exposed to the sun. There are four windows in the experimental lab with an area of 14 square feet. The plan and section views of the BIPV lab are shown in Figure 2 and Figure 3. A photo-voltaic (PV) roof with a 15° slope true-south facing orientation for maximum solar gain is adopted. The mono crystalline silicon PV modules used are standard 150 W rated panels encapsulated in a toughened high transmittivity glass laminates. Rafters spanning a length of 6.3 m and a 0.2m depth fabricated from 2 mm galvanized iron sheets support these PV panels. A 0.2m air cavity below the PV panel permits effective extraction of warm air below the PVpanels. 35 panels run across the roof in a series-parallel combination to produce a desired maximum rated output of 5.25 kW_p at STC. The power generated is supplied to the grid directly through a grid-export conditioner equipped with an in-built inverter and a maximum power point tracker (MPPT). Daytime lighting in the rooms is taken care of by 10 glass panels symmetrically close to the edge of the roof, primarily to induce natural ventilation in the room below and also to extract hot air from below the panels. (Figure 4) The internal temperatures and humidity are measured using Suppco data loggers, which collect data at an interval of 5 minutes. The meteorological parameters have been monitored through a weather station appropriately installed on the BIPV lab. The weather station specification is provided in Table 2. Yearlong data is collected and analyzed to understand whether the temperatures inside are within the comfortable range (21 °C -- 29 °C). The internal temperatures were compared with ASHRAE specified comfort range values. The various discomfort factors are also assessed. The following sections deal with this appropriately.

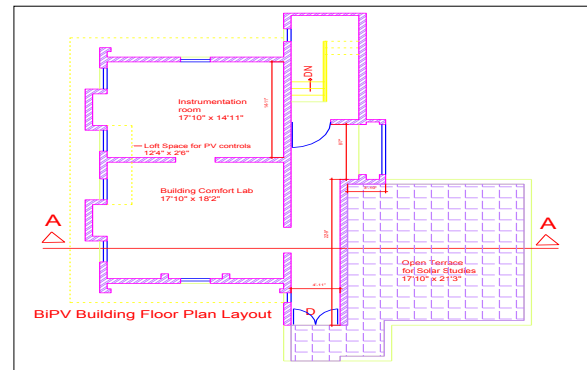


Fig. 2 – Plan of the BIPV Lab

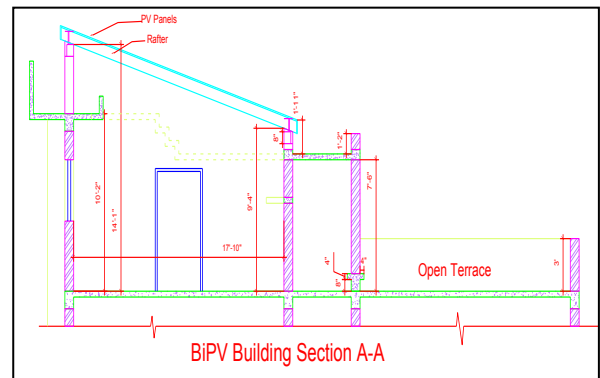


Fig. 3 – Section of BIPV lab



FFig. 4 – View of BIPV lab

Parameter	Measurement Range	Accuracy
Solar radiation	1-1250 W/m ²	±5%
Temperature	-20° to 70° C	±0.6° C
Relative Humidity	0-100% (non-condensing)	±2%

Table 2 – Specifications of weather station installed at the BIPV roof, IISc

5. Results and Discussion

The various modes of heat transfer on a human being in the BIPV structure is shown in Figure 5. All modes of heat transfer play a role in maintaining the thermal comfort level of a human body. Temperature is considered to be the most important parameter influencing the thermal comfort index. Emphasis has been made to look at all possible temperatures to find out the discomfort factors.

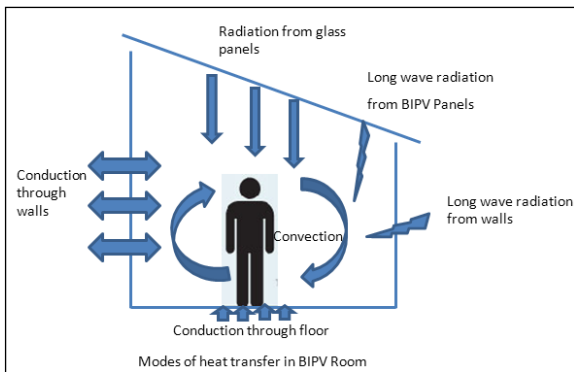


Fig. 5 – Heat exchange modes from the human body

Analyzing the temperature data (outdoor and indoor), the following observations are made.

1. The internal temperature of the BIPV structure is always higher than in a conventional building for eleven months. The figures below (Figure 9) show the comparison between internal and external temperatures for various months plotted for the different months in a year fortify the observation.
2. The maximum and minimum temperatures of

every month are plotted the graph of ASHRAE STANDARD 55-2004 acceptable operative temperature ranges for naturally conditioned as shown in Figure 6. It was found that except for one month, the rest is not within the comfort zone. The data is further analysed to find out what period of the day is not comfortable. It was found that during the winter months the temperatures during the night time are lower than the comfortable range whereas in the summer months the temperatures during the day time are hotter and only in the month of August is it completely in the comfortable range (Table 3).

3. The Radiant Temperature Asymmetry is high as the ceiling temperatures are high. Due to the low thermal mass of PV, the temperatures of the PV reach 60 -70°C. The inside panel temperature and the air temperature at different levels is shown in Figure 7 where the temperature T1 is near the roof and T8 is near the ground. (Cena and Clark, 1981) have compiled the studies done by Griffiths and McIntyre 1974, Berglund and Fobelets 1987 and found that exposure to heated panels above the subject produced a greater level of dissatisfaction than for cooled ceilings and walls or heated walls (Hodder and Parsons, 2008). It can be readily realized that due to the nature of the roofing material used, the thermal comfort environment within the BIPV Structure are most susceptible to changes of the local weather conditions and is the reason for thermal discomfort in the BIPV structure.

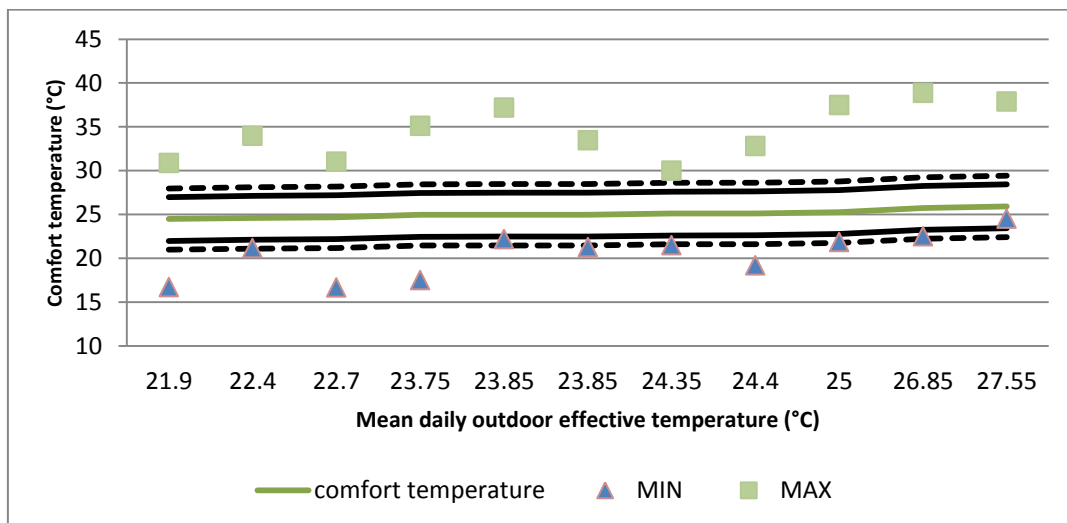


Fig. 6 – Minimum and maximum monthly temperatures on ASHRAE's acceptable operative temperature ranges

Month	Uncomfortable period	Time of the day when it is Cold	Time of the day when it is Hot	Minimum Temp. deg C	Maximum Temp. deg C
January	Day and Night	1 am to 9 am	--	16.7	30.87
February	Day and Night	1 am to 8 am	11am to 4 pm	17.5	35.1
March	Day and Night	--	11am to 6 pm	22.19	37.17
April	Day	--	10am to 7 pm	24.52	37.87
May	Day	--	11 am to 4 pm	22.51	38.85
June	Day	--	11pm to 6pm	21.86	37.48
July	Day	--	1pm -4 pm	21.15	33.96
August	Comfortable	Comfortable	Comfortable	21.48	30
September	Day	--	1pm to 3 pm	21.27	33.48
October	Day	--	1pm –3pm	19.2	32.82
November	Day and Night	4am -8am	1pm- 2pm	16.65	31.03

Table 3- Period during which the indoor temperatures are not within the comfortable range (for year 2012)

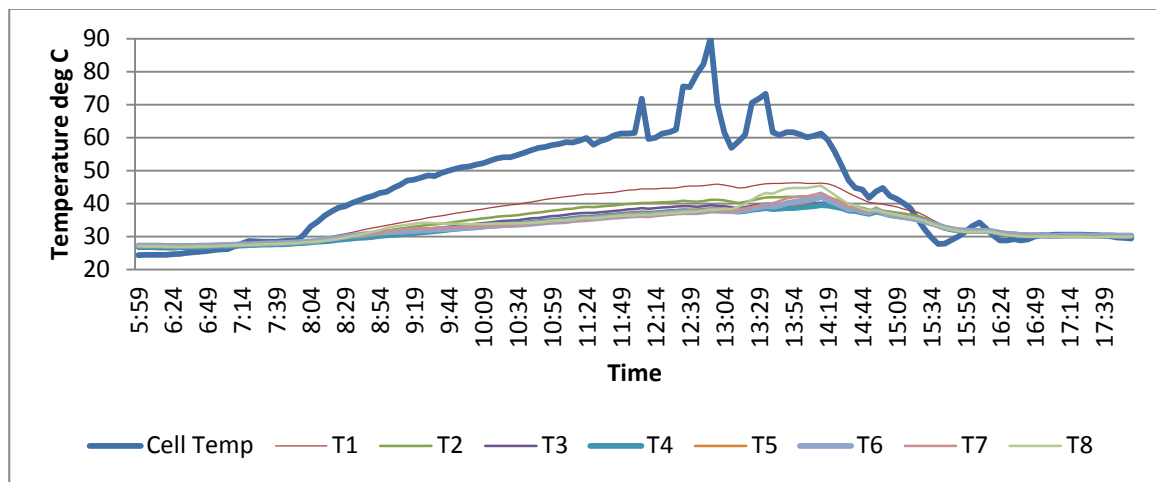


Fig. 7 – Air temperature at an interval of every 0.5m from the roof to the floor

6. Simulation

A computer-based building simulation model was developed in DesignBuilder (v 2.2.5), a CFD-based simulation package built over the successfully adopted EnergyPlus (Chowdhury et al and Wasilowski et al). Construction details, including general door window and heat gain from computer and inverter (power conditioning unit) etc., were given as input. The simulated temperatures were

compared with the real-time monitored data for four months. Since the simulation model responds to climate files (statistical data) and the real-time thermal monitoring responds to actual climatic conditions, one cannot expect an exact one-to-one temperature correlation. The correlation is more than 0.85 for both indoor and outdoor temperatures. Figure 8 shows the comparison between internal and external temperatures for various months both measured and simulated. The model is tested with various strategies for summer by reducing the glass

panels on top (two panels) of the roof and in winter by placing a false ceiling in the room and removed the ventilators. Figure 9 shows that the reducing the glass panels helps in summer by reducing the

temperature to 2-3° C, but in winter these strategies don't help as the temperature remains the same as shown in Figure 10.

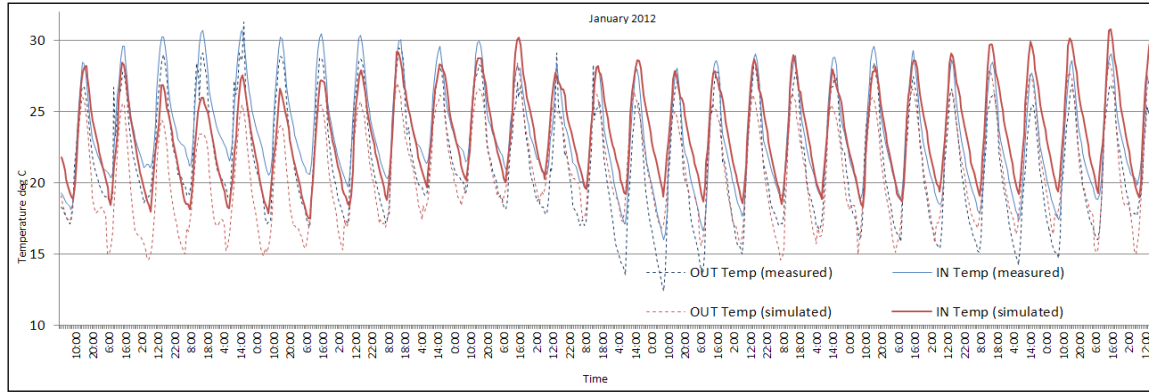


Fig. 8 – Comparison between internal and external temperatures for four months both measured and simulated (January 2012)

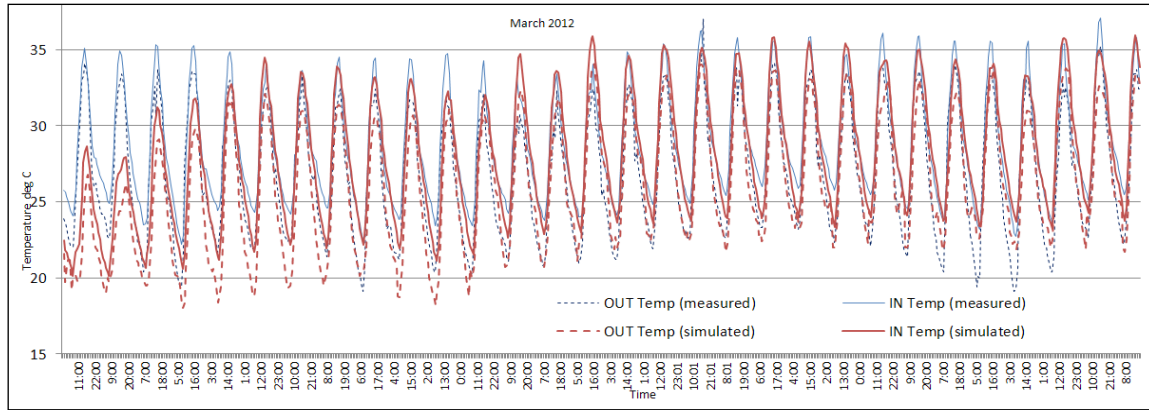


Fig. 9 – Comparison between internal and external temperatures for four months both measured and simulated (March 2012)

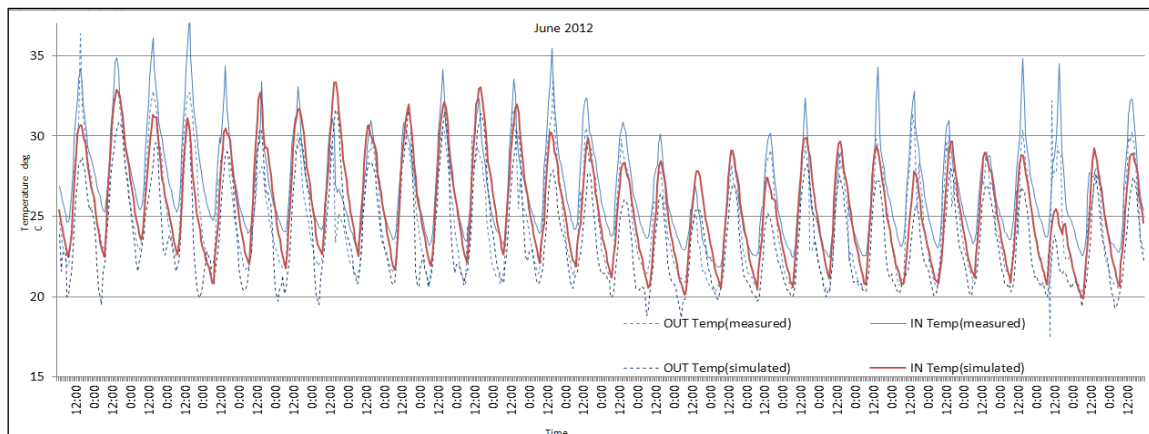


Fig. 10 – Comparison between internal and external temperatures for four months both measured and simulated (June 2012)

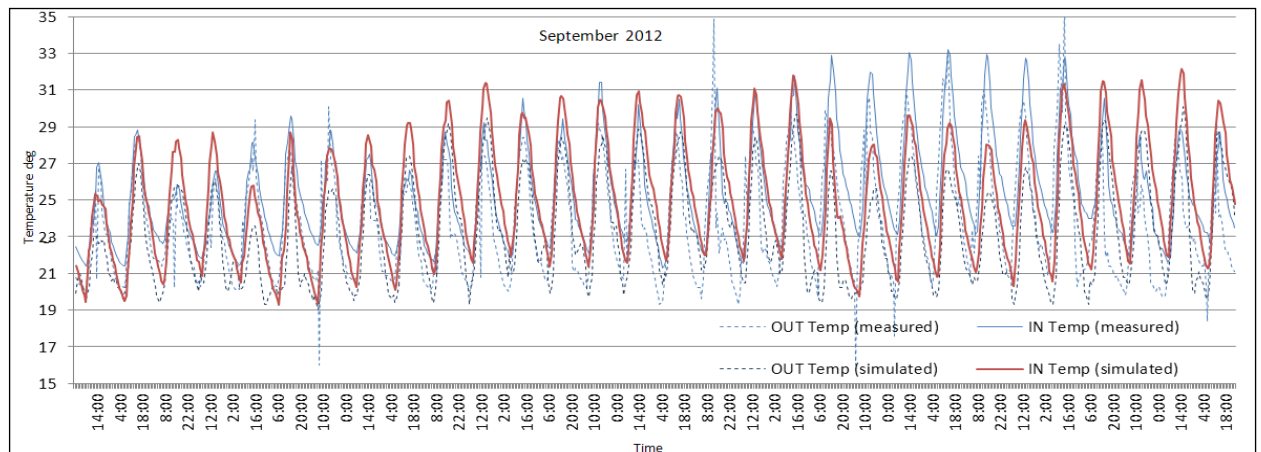


Fig. 11 – Comparison between internal and external temperatures for four months both measured and simulated (September 2012)

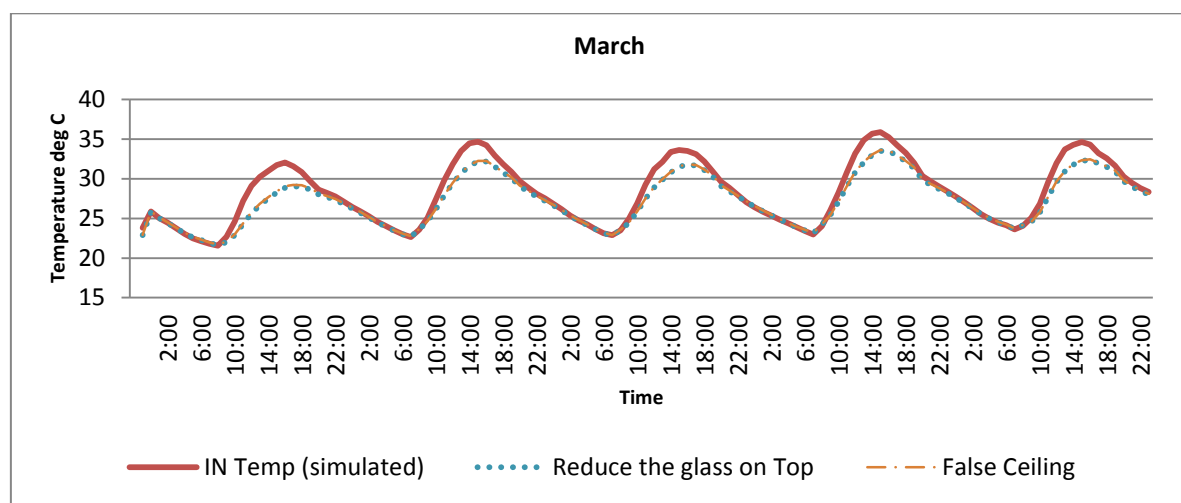


Fig. 12 – Simulated results of various strategies for summer months

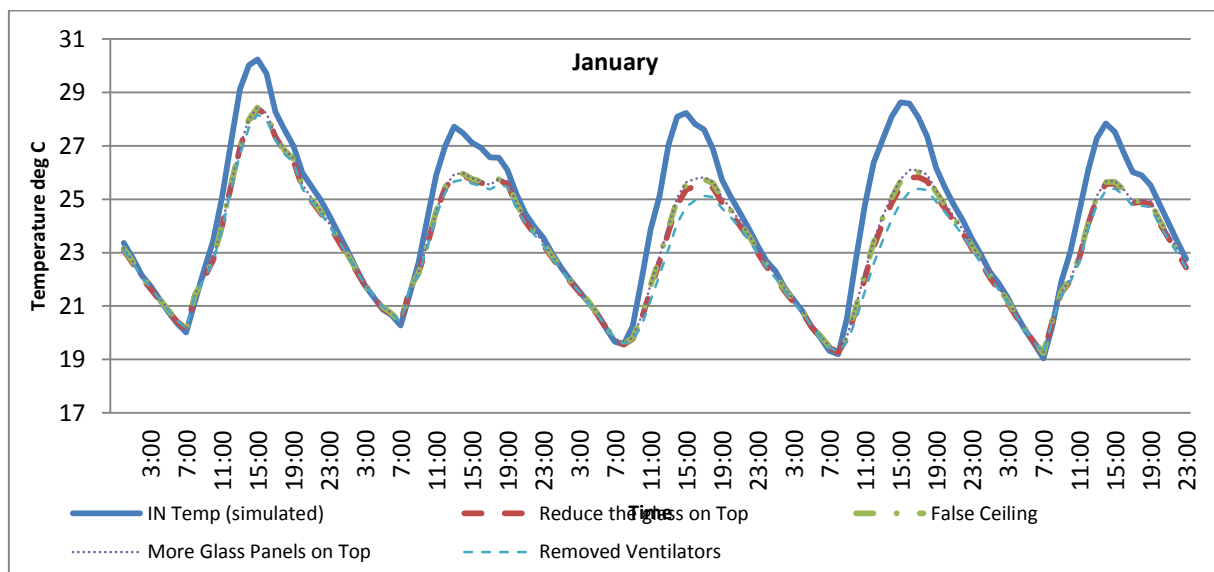


Fig. 13 – Simulated results of various strategies for winter months

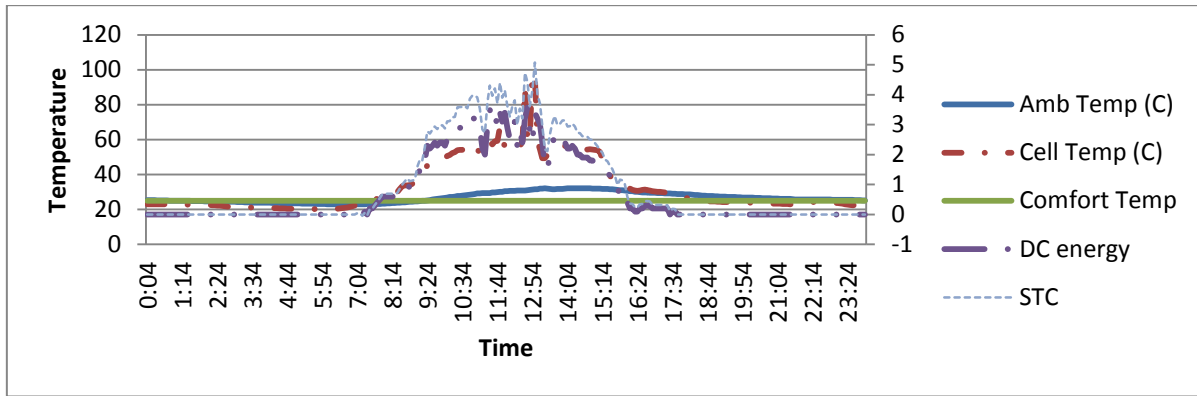


Fig. 14 – Comparison of electrical performance for regular and STC conditions and the thermal comfort temperature for a day in the month of September

7. Conclusion

- 1) Climatic-response in a BIPV structure depends on a complex correlation between PV performance and indoor thermal comfort.
- 2) In tropical regions, BIPV installations are required to tackle in design for the degrading effect of high PV (cell) temperatures and indoor radiant regimes (MRT); the former lowers energy generation efficiency and the latter causes indoor discomfort necessitating energy for maintaining thermal comfort particularly when the energy generation potential is the highest (Figure 11). The lower thermal mass of a PV building envelope permits a higher thermal transmittance and increases the indoor temperatures. With lower thermal mass, PV cell temperature is more sensitive to variations in solar insolation as compared to indoor temperature variations. Despite lower thermal mass, the radiation from the roof to the indoors offers consistent warming potential, which can be exploited in colder regions.
- 3) Solar passive designs for BIPV need to be considered to make BIPV structures thermally comfortable. However, completely neutral thermal comfort conditions may not be obtained in such a relatively uncontrolled environment because of the thermal mass of the PV and the nature of the construction at least the adaptable range should be obtained through passive strategies to reduce the temperature inside.
- 4) For the specific study various strategies are simulated that can provide opportunities to lower indoor temperatures during summer and to increase

the night temperatures during winter to regulate thermal comfort. The strategies, which were simulated for summer, hold positive, whereas the strategies tested for winter do not serve the intended purpose. Hence other effective strategies need to be tried and tested.

References

- Singh, M.K., Mahapatra, S., Atreya, S.K. 2011. Adaptive thermal comfort model for different climatic zones of North-East India. *Applied Energy* 88 (7): 2420-2428.
- Hodder, S., Parsons, K. 2008. The effects of solar radiation and black body re-radiation on thermal comfort, *Ergonomics*, 51(4): 476-491.
- Cena, K. and Clark J. A. 1981. *Bioengineering, thermal physiology and comfort*, Elsevier Scientific Publishing Company, 10, Amsterdam - Oxford - New York.
- Kabre, C. 2010. A new thermal performance index for dwelling roofs in the warm humid tropics, *Building and Environment*, 45: 727-738.
- Fanger, P.O., Toftum, J. 2002. Extension of the PMV model to non-air-conditioned buildings in warm climates, *Energy and Buildings*; 34: 533-536.
- Brian, Klejn-Christensen and Carr, S. 2012. *Movable Insulation for Passive Cooling of Roof Slab in the Tropics*, IEN Consultants, Malaysia.
- Manikandan, K. 2011. Computation of required wall emissivity for low energy consumption in buildings using ASHRAE model validated for Indian Thermal comfort. Indian Institute of Science, Bangalore.

- Humphreys, M.A. and Nicol, J.F. 2000. Outdoor temperature and indoor thermal comfort: raising the precision of the relationship for the 1998 ASHRAE database of field studies, *ASHRAE Transactions* 206(2): 485-492.
- ASHRAE (55) 2004. *Thermal Environmental Conditions for Human Occupancy*, Atlanta, Georgia.
- Chowdhury, A.A., Rasul, M.G., Khan, M.M.K. 2007. Modelling and simulation of building energy consumption: a case study on an institutional building in central Queensland, Australia: Proceedings of 10th International Building Performance Simulation Association (IBPSA) International Conference, Beijing, China, September 3–6, pp. 1916–1923.
- Wasilowski, H., Reinhart, C. 2009. Modelling an existing building in DesignBuilder/Ep: custom versus default inputs: Proceedings of Building Simulation 2009, Glasgow, Scotland, UK, July 27–30, 2009.

Multi-objective optimisation of external shading devices for energy efficiency and visual comfort

Gianluca Rapone – Ove Arup & Partners Ltd, London, UK

Onorio Saro – University of Udine, Udine, Italy

Giovanni Zemella – Ove Arup & Partners Ltd, London, UK

Abstract

In highly glazed office buildings, external shading devices represent a valuable option to limit solar gains and achieve better thermal performance during the summer. At the same time they impact the visual comfort of the occupants by reducing the clear view to the outside. Depending on the location of the building, maximising the external view may represent a key driver for the definition of the façade's architectural characteristics. Identifying the adequate geometry of external shadings is therefore a key aspect for the design of sustainable buildings. This article describes the application of a simulation-based optimisation tool to address this issue. Limiting solar gains and maximising the external view are two contradictory requirements, whose trade-off is investigated by means of multi-objective optimisation. Solar gains are assessed by means of dynamic thermal simulations: from the results of annual analyses, peak conditions are retrieved. For the quantitative assessment of the visual obstruction caused by the external shadings, an ad hoc script is employed. A Genetic Algorithm handles the results of these calculations and it searches for the optimum solutions that lie on the Pareto front. They all represent optimum options among which the preferred configuration can be selected during the decision making process. The optimisation algorithm, whose performance for this specific problem is validated, allows to identify the trade-off with a reasonable computational effort. From the results it is possible to determine the influence of the different variables – chosen in order to fully describe the geometric configuration of shading devices – on the balance between the two considered criteria. Calculations are run for different orientations in order to take into account the effect of variation in solar angle and exposure. In this way some general rules of thumb can be drawn for the design of effective shading elements.

1. Introduction

In designing office buildings, it is very important to limit solar gains as effectively as possible: this is because internal gains due to equipment, occupants and artificial lighting can already be very high. Only by limiting solar gains is it possible to achieve good targets of energy efficiency and to reduce the amount of carbon emissions.

These energy efficiency requirements are in direct contrast with current trends in contemporary architecture, which call for highly glazed buildings. In some situations, relying on high performance coatings on glazed elements is not enough to reduce solar gains. In these cases, using external shading devices may be a viable option. If considered properly during the early stages of the design process, shading devices can become an integral part of the architectural language of the façade. Shading devices can also be properly engineered to cut solar radiation during the cooling season, whilst allowing beneficial solar gains during winter.

Shading devices, however, do not simply limit solar gains: they also obstruct the building occupants' view towards the outside. This can be very detrimental to the value of the building, particularly if its location allows for prized views. Moreover, it can cause visual discomfort for the occupants.

It is therefore very important that the design team consider both the way shading devices limit solar gains and the amount of external view they obstruct. The main difficulty with this approach is that the two requirements are contradictory: the more shading devices there are to limit solar gains, the more they will also limit the view to the outside.

In order to design effective shading devices, it is important to consider as many options as possible.

This means that the research can be insurmountable if traditional design methodologies are employed: evolutionary optimisation algorithms offer a viable methodology, which allows for a wider spectrum of research to be made available, and, at the same time, can deal with the calculation process in a significantly shorter time. Evolutionary algorithms have been proven to be very effective in identifying optimum design solutions: they have been successfully applied to the integrated design of envelopes and building services (e.g. Znouda et al., 2007, Zhou et al., 2009, Ardakani et al., 2008), and to detailed design of façade elements (e.g. Rapone et al., 2012, Zemella et al., 2011). When more than one criterion is considered for the optimised design, two different approaches can be adopted. If a single-objective optimisation is carried out, the different criteria are assigned weights before the optimisation process (*a priori*). In the case of a multi-objective optimisation, a separate objective function is associated to each design criterion and the result is the identification of the optimum trade-off between the considered criteria. Weights to the different objective functions can be applied *a posteriori*, with no need to re-run the optimisation process (Wright et al., 2002).

Since it is not immediate to identify weights to combine solar gains and obstructed view, this paper describes a multi-objective optimisation process, carried out by means of Genetic Algorithms. The aim of the optimisation process is to identify the trade-off curve – i.e. the Pareto front – between these two contradictory requirements, expressed by two separate objective functions: annual peak solar gains and amount of obstructed view. All the options laying on the Pareto front represent optimum solutions, but they correspond to different compromises between the two objective functions. Once the optimisation process has identified all the optimum solutions, the design team can focus on them and consider other aspects, which may be difficult to quantify, e.g. aesthetical appearance, proportions with the other elements of the façade, and so on (e.g. Coley et al., 2002).

2. Methodology

For the analysis presented herein, a very generic module of a curtain wall façade has been considered. The façade module is 2.7m wide, with floor to ceiling glass 3.5m high and a slab zone of 0.5m. The 4.5m deep thermal zone considered in the calculation represents the typical perimeter zone of a building where the effects of the façade are relevant (BCO, 2009).

The research for the optimum geometry of shading devices considered a comprehensive range of different options. The following variables were considered:

- Number of louvres n : $4 \div 8$: this dictates the spacing between adjacent louvres S ;
- Rate of perforation of louvres p : $0 \div 50\%$ at 12.5% steps;
- Louvres depth D : $50 \div 300\text{mm}$ at 25mm steps;
- Louvres tilt angle α : $0 \div 50^\circ$ at 10° steps;
- Louvres inclination angle β : $0 \div 90^\circ$ at 15° steps.

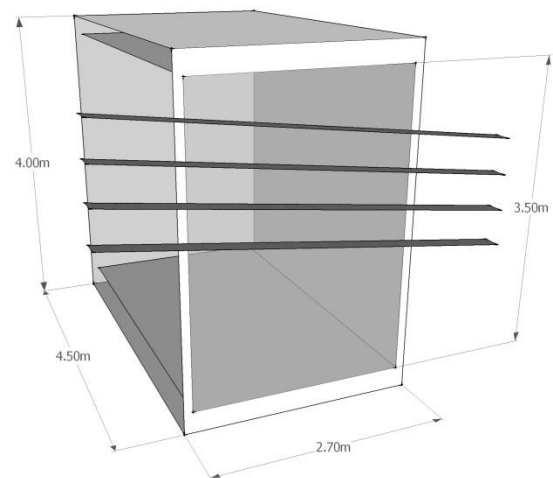


Fig. 1 – Overview of the thermal model

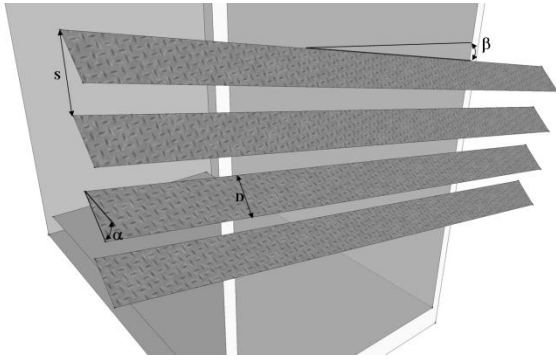


Fig. 2 – Shading devices, design variables

This leads to a total number of 11,550 possible options. Louvres are uniformly distributed along the height of the façade module, apart from the bottom 800mm, where no louvres are considered, since they would be ineffective in providing shading.

For the analysed options the following output data are calculated and represent the objective functions: peak annual solar gains and percentage of obstructed view.

2.1 Objective 1: Peak annual solar gains

The first objective function refers to the peak amount of solar gains, considering the 97.5 percentile (CIBSE, 2006). This calculation was carried out by means of annual energy simulations with the software tool EnergyPlus. Inter-reflections between louvres and between glass and louvres are taken into account. The ASHRAE weather file for London Gatwick was considered. The double glazed units considered for the vision area have a high performance coating that provides a g-value of 0.35, calculated in accordance with the standard EN 410. Solar gains are considered per unit of floor area. Calculations have been carried out for the south, east and west elevations.

2.2 Objective 2: Percentage of obstructed view

The way a shading configuration obstructs the view towards the outside was assessed by means of a script developed specifically for this type of applications. From an observation point – assumed to be in the centre of the room at a height of 1.2m corresponding to a seated position – an array of 2,500 view rays was considered, since this represents a good balance between accuracy of results and

calculation time. The rays are projected on a grid evenly distributed on the plane of glass, in the area where shading devices are located (i.e. everywhere apart for the bottom 0.8m zone). If the rays lie in a direction intercepted by the louvres, they are counted as obstructed taking into account the opacity of the louvres. The percentage of obstructed view is the ratio between the obstructed rays and the total amount of rays. Figure 3 shows diagrammatically how the methodology works (only a few rays are shown for clarity). From the coordinates of three vertices of a louvre (x_1, y_1, z_1 - x_2, y_2, z_2 and x_3, y_3, z_3), it is possible to identify the parameters a, b and c , defining the plane of the louvre, by means of equation 1 – where d can be assigned any value. Once these parameters are known, equation 2 can be used to calculate the coordinates x_i, y_i and z_i of the intersection between the plane where the louvre lies and the line defined by the coordinates of the observation point (x_o, y_o and z_o) and of the specific point on the grid (x_p, y_p and z_p).

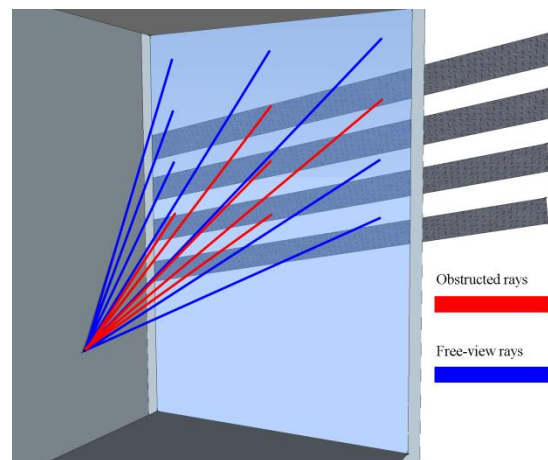


Fig. 3 – Evaluation of obstructed view

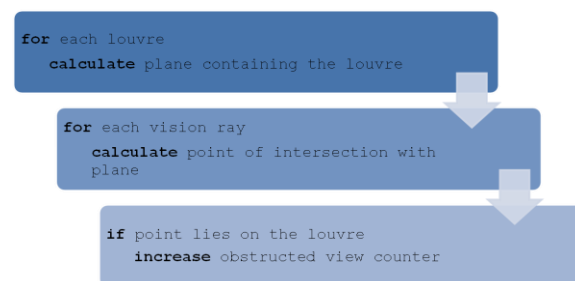


Fig. 4 – Outline of routine used to calculate obstructed view

$$\begin{bmatrix} x_1 & y_1 & z_1 \\ x_2 & y_2 & z_2 \\ x_3 & y_3 & z_3 \end{bmatrix} \cdot \begin{bmatrix} a \\ b \\ c \end{bmatrix} = \begin{bmatrix} d \\ d \\ d \end{bmatrix} \quad (1)$$

$$\begin{bmatrix} \frac{y_p - y_o}{x_p - x_o} & -1 & 0 \\ \frac{z_p - z_o}{x_p - x_o} & 0 & -1 \\ a & b & c \end{bmatrix} \cdot \begin{bmatrix} x_i \\ y_i \\ z_i \end{bmatrix} = \begin{bmatrix} x_o \frac{y_p - y_o}{x_p - x_o} - y_o \\ x_o \frac{z_p - z_o}{x_p - x_o} - z_o \\ d \end{bmatrix} \quad (2)$$

If the intersection point (x_i, y_i, z_i) lies on the louvre, the considered ray is obstructed. This procedure is repeated for each louvre and for each point on the grid, as shown by the outline algorithm in figure 4. This methodology is very flexible: for this paper, where general results are targeted, the grid where the “sight-rays” are projected is evenly spread across the glass. However, for project specific applications, the grid can be applied on a well-defined target, representing the most valuable view that the design team has identified in order to preserve it as much as possible.

2.3 Selection of optimisation algorithm

The simulation based optimisation problem has been solved by means of a self-developed Matlab software (Rapone, 2012), which couples the simulation program to a genetic algorithm allowing for a quick definition of the different settings involved through a graphical user interface. The interaction between the energy simulation software (EnergyPlus), the routine written to calculate the visual obstruction index and the genetic algorithm is fully automated. A Genetic Algorithm (GA) has been chosen because of its suitability in treating non-smooth, simulation based optimization problems where the objective function is highly discontinuous and non-differentiable (Wetter et al, 2004), which is the case when it is computed by external dynamic simulations.

Genetic Algorithms are based on natural selection and genetic recombination, the processes that drive biological evolution (Darwin, 1859), and are part of the evolutionary algorithms (Goldberg, 1989), a family of population-based probabilistic algorithms that also includes PSO (Particle Swarm

Optimisation) and ENN (Evolutionary Neural Networks) among many others.

In particular, a custom-modified version of the NSGA-II has been employed (Deb, 2001). The final Pareto front has been calculated on the individuals evaluated throughout all generations rather than on the last population only. This enabled the attainment of a more comprehensive and well distributed set of solutions.

In the case where the façade is oriented to the south, the whole design space (i.e. the total amount of potential solutions) was calculated in order to calibrate the algorithm and to assess its performance. A sensitivity analysis was carried out in order to estimate the values of the main parameters of the GA that guarantee satisfactory results in a limited amount of time. The aim was to achieve at least 50% of the real Pareto points after exploring no more than 5% of the whole design space, and not to miss areas of the real Pareto front: this is a simplified version of more rigorous methods (Zitler, 2003)..

Figure 5 shows the real Pareto front (in purple) and the Pareto found with the settings of the algorithm that yielded the best performance (in green). It can be observed that although there are some areas where the final solutions do not fall on the real Pareto set, from an overall point of view a good number of points of the latter are actually identified. Moreover, no areas of the actual Pareto front were missed during the optimisation process.

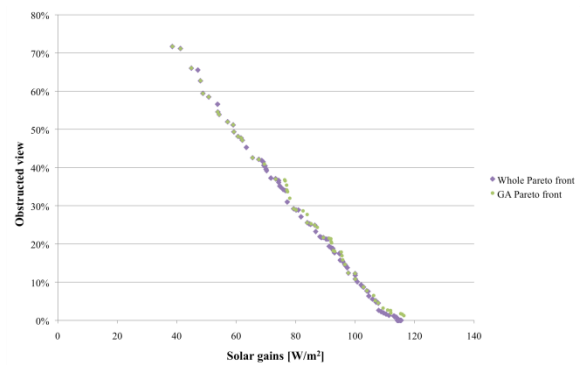


Fig. 5 – South orientation: found Pareto front and real Pareto front

According to the outcome of this analysis, the following settings for the GA were chosen: a population of 40 individuals, 15 generations, 80% crossover and 20% mutation. Since the Pareto has

been calculated on the individuals of all generations, no elite children were selected to be taken from one generation to the next.

3. Results

Figures 6, 7 and 8 display the results of the optimisation process for the different orientations. The optimum combinations are represented in the solution space in order to show the distribution of the Pareto front. The charts show all the optimum options; the points highlighted in red correspond to the options which meet the recommendation of limiting the peak solar gains to less than 65W/m^2 (BCO, 2009).

It is possible to see that the BCO requirement can be met only when the external shading devices obstruct at least 40% of the view towards the outside. Moreover, for the type of glass considered (g-value 0.35), the peak solar gains cannot be lower than about 40W/m^2 , and the percentage of obstructed view can be as high as 65 / 70% depending on the orientation.

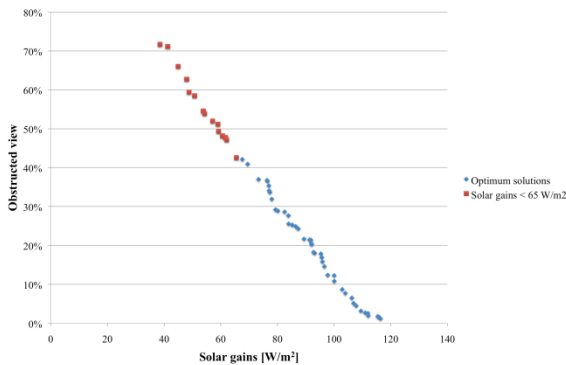


Fig. 6 – Pareto front, South orientation

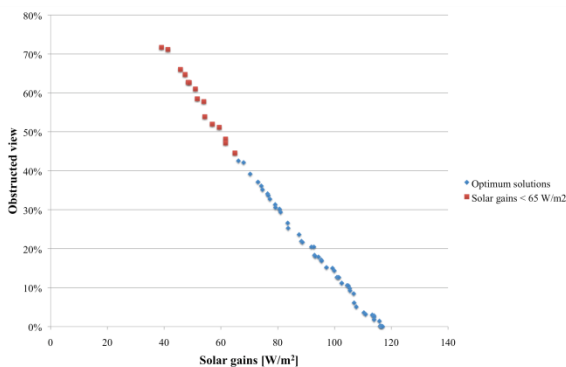


Fig. 7 – Pareto front, West orientation

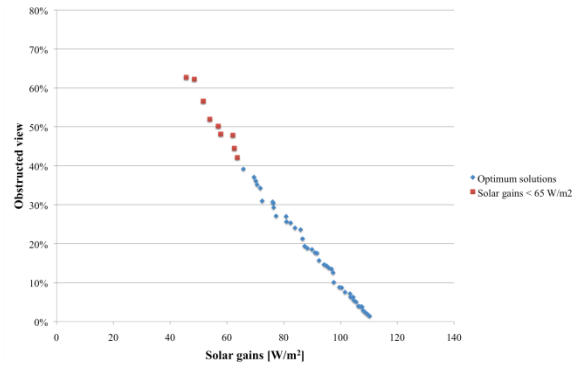


Fig. 8 – Pareto front, East orientation

This representation is valuable because it shows the performance of all the calculated optimum options in terms of the considered objective functions. In this way the trade-off between the different criteria is immediately understood. A big limitation of this representation is that it does not provide any information on the levels of the variables corresponding to the optimum solutions. It would be difficult for the design team therefore, to know how they can best develop the façade of a given project in order to achieve its optimum performance. Some works (e.g. Brownlee et al., 2012) aim to tackle this issue by providing indications of the impact that different variables have on the values of the objective functions. In this paper, we present a different approach to visualise the solution of a multi-objective optimisation procedure. The images below show the frequency with which the different levels of the considered variables occur in the Pareto front. In this way the measures that need to be considered in order to achieve optimum performance are immediately understandable. When the different levels of a variable are more or less evenly present within the Pareto front, it is possible to conclude that this specific variable has very little impact in the criteria considered for the optimisation. Therefore the design team can choose the level of this variable considering other criteria, such as aesthetics or economic reasons. On the other hand, some variables might appear in the Pareto front only with one level: in this case the design team has to accept a very definitive indication, if an optimum design is to be achieved. If this indication has implications that cannot be incorporated in the overall façade design, the whole optimisation

process has to be re-thought: either the types of variables are re-considered, or the design criteria (i.e. the objective functions) have to change.

3.1 Number of louvres

Figure 9 shows the frequency with which different numbers of louvres occur in the Pareto front for the considered orientations.



Fig. 9 – Occurrences in the Pareto front: number of louvres

Within the Pareto fronts there are solutions with a good variety of numbers of louvres; generally, optimum solutions have either the minimum amount of them (i.e. 4) or 7 (i.e. the second ‘most-dense’ option). It is better to avoid using intermediate amounts of louvres. There is little difference among the considered orientations.

3.2 Perforation rate

Figure 10 refers to the frequency of presence in the Pareto front of the different levels of perforation within the louvres.



Fig. 10 – Occurrences in the Pareto front: perforation rate

The design team can choose among many different levels of perforation rates, even if both for south and east orientations, fully solid louvres appear to be the most effective option. For the west orientation, on the other hand, the most common solution is with louvres being 37% perforated.

3.3 Depth of louvres

The occurrence of the different depths of louvres is shown in figure 11.

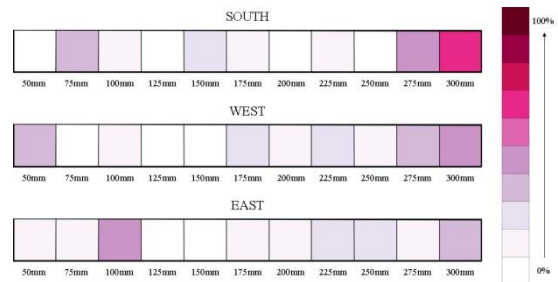


Fig. 11 – Occurrences in the Pareto front: depth of louvres

Overall, there is a relatively even distribution of different louvres’ depth along the Pareto fronts corresponding to the different orientations. In general, though, it is more likely to have an optimum solution if the depth is either kept to a minimum (corresponding to solutions at the bottom right area of the Pareto front), or to have deep louvres (for the solutions corresponding to low solar gains but high percentage of obstructed view).

3.4 Tilt angle

Figure 12 shows the frequency with which different tilt angles of the louvres occur in the Pareto front for the considered orientations.

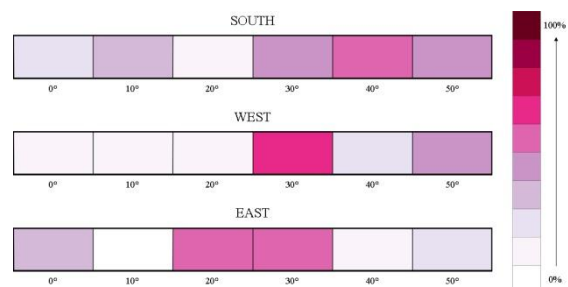


Fig. 12 – Occurrences in the Pareto front: louvres tilt angle

For this specific parameter, the results vary considerably for the different orientations. For the south elevation, there is a moderate indication for a tilt angle of 40°, but in general, all tilt angles are evenly present within the Pareto front: this indicates a weak influence of this parameter on the two criteria adopted for the optimisation process. For the west orientation on the other hand, there are very few optimum solutions for low tilt angles, and there is a strong preference for a tilt angle of 30°. On the

east elevation, tilt angles of 20° or 30° are the most frequent.

3.5 Louvres inclination

The most significant impact on the overall appearance of the façade is due to the inclination angle of the louvres. Figure 13 refers to the frequency of presence in the Pareto front of the different inclination angles.

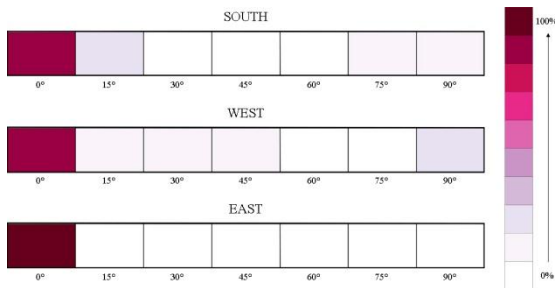


Fig. 13 – Occurrences in the Pareto front: louvres inclination

In this case, the optimisation process provides a very clear indication: the most effective inclination of the louvres is 0°, corresponding to horizontal elements. For the south and west orientations, horizontal louvres are the most frequent, but there are also other inclination angles within the Pareto fronts. For the east elevation, all the optimum solutions have horizontal louvres.

4. Conclusions

This work has presented the results of a multi-objective optimisation for the design of external shading devices of a typical curtain wall façade of an office building located in London. The calculations have been carried out for three different orientations. The trade-off between the ability of shading devices to limit the peak solar gains and their impact on view towards the outside has been assessed. Apart from the typical result output showing the Pareto front of the results space, this paper proposed a representation of results focused on the input data, rather than on the output. In this way the design team can derive more immediate answers from the analysis of results. The main indications provided by the analysis presented for the definition of the façade are:

- 1) For all the different orientations, horizontal louvres have proven to provide the best balance between reducing peak solar gains and keeping good levels of view to the outside.
- 2) For the east and west orientations, louvres have been found to be more effective when they are tilted at angles ranging between 30° and 40°.
- 3) In terms of louvre depth, it is preferable to have relatively large elements, or to keep them minimal: intermediate dimensions do not appear to provide substantial benefits.
- 4) Not very restrictive indications are given for the definition of the perforation rate and the number of louvres: the design team is relatively free to choose what best suits other considerations.

More in depth analyses of the output data are necessary to have a comprehensive understanding of the whole condition. For a specific project, it is important to consider the results on the solution space and on the input space together. Interactive tools are the most appropriate means to have a better understanding of all the information embedded in the considerable amount of data delivered during the optimisation process.

5. Future work

This paper only considered peak solar gains, therefore the focus of the analysis was on the impact of shading devices on the required capacity of the cooling system. It is also very important to assess how the cumulative solar gains during the whole cooling season are affected. It is expected that, in this case, the optimisation results will show more pronounced differences among the considered orientations.

6. Nomenclature

Symbols

n	number of louvres (-)
S	spacing between adjacent louvres (mm)
p	louvres perforation rate (%)
D	louvres depth (mm)
α	louvres tilt angle (°)
β	louvres inclination angle (°)
x	first coordinate (m)
y	second coordinate (m)
z	third coordinate (m)
a	first parameter defining the plane of the louver
b	second parameter defining the plane of the louver
c	third parameter defining the plane of the louver
d	fourth parameter defining the plane of the louver

Subscripts/Superscripts

1	of the first point
2	of the second point
3	of the third point
o	of the observation point
p	of the grid point
i	of the intersection point

References

- Ardakani, A. J., Ardakani, F.F., Hosseini, S.H. 2008. A novel approach for optimal chiller loading using particle swarm optimization, *Energy and Buildings* 40 (12), pp. 2177-2187.
- British Council for Offices 2009. Guide 2005 Best practice in the specification for offices.
- Brownlee, A., Wright, J. 2012. Solution analysis in multi-objective optimization, *Proc. of the Building Simulation and Optimization 2012 Conf.*, Loughborough, UK, 2012.
- CIBSE. 2006. Guide A. Environmental design. The Chartered Institution of Building Services Engineers.
- Coley, D.A., Schukat, S. 2002. Low-energy design: combining computer-based optimisation and human judgement, *Building and Environment* 37 (12), pp. 1241-1247.
- Darwin, C. 1859. *On the origin of species*. John Murray, London.
- Deb, K. 2001. *Multi-objective optimisation using evolutionary algorithms*. John Wiley & Sons, New York.
- Goldberg, D.E. 1989. *Genetic algorithms in search, optimization and machine learning*. Addison-Wesley, New York.
- Rapone, G. 2012. *Optimisation of office buildings façades by means of Genetic Algorithms*. PhD thesis, University of Udine, Italy.
- Rapone, G., Saro, O. 2012. Optimisation of curtain wall façades for office buildings by means of PSO algorithm. *Energy and Buildings*, 45 (2), pp. 189-196.
- Wetter, M., Wright, J. A. 2004. Comparison of deterministic and probabilistic optimization algorithms for non-smooth, simulation-based optimization. *Building and Environment* 39 (8), pp 989-99.
- Wright, J.A., Loosemore, H.A., Farmani, R. 2002. Optimization of building thermal design and control by multi-criterion genetic algorithm. *Energy and Buildings* 34 (9), pp. 959-972.
- Zemella, G., De March, D., Borrotti, M., Poli, I. 2011. Optimised design of energy efficient building façades via evolutionary neural networks. *Energy and Buildings*, 43(12), pp. 3297-3302.
- Zhou, L., Haghighat, F. 2009. Optimization of ventilation system design and operation in office environment. Part I. Methodology, *Building and Environment* 44 (4), pp. 651-656.
- Zitler, E., Thiele, L., Laumanns, M., Fonseca, C.A., Grunert de Fonseca, V. 2002. Performance assessment of multiobjective optimizers: an analysis and review. *TIK – Report No. 139*.
- Znouda, E., Ghrab-Morcos, N., Hadj-Alouane, A. 2007. Optimization of Mediterranean building design using genetic algorithms, *Energy and Buildings* 39 (1), pp. 148-1

Procedure for buildings' energy modelling suited for integrated control simulation

Chiara Dipasquale – University of Catania, Catania, Italy

Matteo D'Antoni – Eurac Research, Bolzano, Italy

Roberto Fedrizzi – Eurac Research, Bolzano, Italy

Michaël Kummert – École Polytechnique, Montréal, Canada

Luigi Marletta – University of Catania, Catania, Italy

Abstract

Numerical simulations are becoming more and more a key step in designing an integrated building + energy system. The use of a detailed numerical model and an accurate calculation algorithm permits us not only to study the influence of design parameters, but also to evaluate the building energy demand and indoor comfort conditions. The computational effort in modelling the building behaviour might become a limit in terms of simulation time, in particular in the case of complex systems. This is evident when an integrated control of building and thermal energy system is performed, because of the need of a short time step (1 to 5 minutes) for control purposes. In this sense, a clear edge between architectural and energy modelling has to be drawn. In this paper, a methodology for simplifying a detailed building model has been presented, by defining phases, quantitative figures, limits and uncertainty of the results. Such procedure is replicable and could be useful during any numerical modelling process. With reference to a three-story apartment building, the influence of (1) the algorithm for short- and long-wave radiation, (2) building and surrounding context's shadings, (3) different levels of geometric surface information have been investigated. For each phase, building's energy balance and simulation runtime has been reported. Additionally, the reliability and adherence of simulation outputs have been inspected by comparing the numerical model response with a whole year of monitoring data.

1. Introduction

Building models are being increasingly used for studying the influence of design parameters and for the evaluation of building energy demand and

indoor comfort conditions. Accurate building modelling might require computational efforts during simulations. The developing of a good building model requires focussing on the building's most important features (weather file, building size, energy loads...), to minimize the number of thermal zones, to properly characterize HVAC and controls (IBPSA-USA bis, 2012). Building models are commonly used to predict the energy consumption, and their accuracy is related to the phase of the design process (IBPSA-USA, 2012). Less importance is given to the design and operation of an integrated building energy and control systems model. When the interaction between the energy plant and building model is investigated, a strong reduction of computational effort is required.

The model needs to be as complex as needed to achieve its purpose. Good work is done when a balance between accuracy and model complexity is found. For this reason, it is important to define priorities and to individuate the features which have a greater impact on performances.

The main aim of this work is the elaboration of a simplified building model to be used in the study of an integrated control between building and energy supply system. To this end, (1) a detailed model has been created; (2) the calibration of the ventilation mass flow rate and infiltration rate has been carried out for a better agreement between the model and real case; (3) a simplification procedure for the reduction of the computational effort of the detailed model has been developed. A satisfying approximation of the heating demand between the detailed and the simplified model has

been reached with a strong reduction of the simulation runtime.

2. Case study

The building under investigation is located in Bronzolo, Italy, and it was built by IPES (a local social housing institution), in 2006, according to the “CasaClima A Plus” standard (Direttiva Casaclima, 2011). It is a residential building with 8 apartments for a total of 577 m² of conditioned living area distributed over three storeys. The building is oriented along the north-west to south-east axis, with a façade oriented to the south.

Domestic Hot Water (DHW) and heating demand are covered by a 15 kW pellet boiler. The hot water is stored in a tank-in-tank puffer of 800 L and then distributed to each apartment. A recirculation water system is also used in order to provide DHW during peak hours. For the supply air, a forced ventilation system with a heat recovery unit is used. External air is pre-heated by geothermal probes, to avoid the freezing of the ventilation fan; an AHU acts as heat recovery from the exhaust air to the fresh air and the supply air is then divided in three ducts, for the distribution on the three floors. A post-heating in each apartment is then provided through coils fed by a pellet boiler.

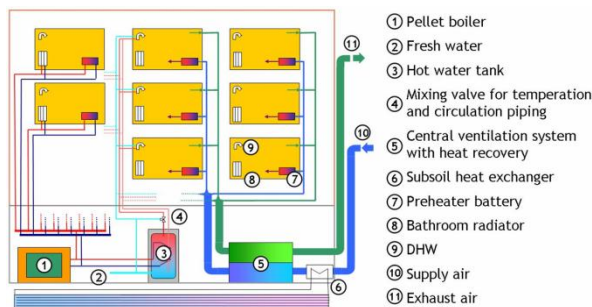


Fig. 1 – Ventilation and Domestic Hot Water (DHW) system (IPES, 2007)

A monitoring system has been installed and data of internal temperature, relative humidity and CO₂ levels, external temperature, relative humidity and solar radiation, electrical and thermal consumption have been collected for a whole year.

Geometrical and physical characteristics from

design have been employed to develop a detailed model which reproduces with high accuracy the real building. The large amount of monitored data have been used to define several boundary conditions and to calibrate the model.

3. Detailed model

The detailed model of the building was made in a previous work (Ecker, M., 2011) using Google SketchUp and Trnsys 3D plugin (Ellis, P., 2009). Walls and floors were defined according to the real geometry and orientation; for windows, a predefined window was used, whose characteristics reproduce the original ones. The envelope characteristics are reported in Table .

Due to calculation modes' requirements for running the detailed model, only convex zones have been accepted. Apartments 1, 2, 3, 5, 6 and 8 have a L-shape, so they have been divided in two zones. Fig. 2 shows the result of zone partitioning and the labels used to indicate the zones. The staircase has been modelled as a single zone with 4 stacked air-node, one for each storey. This zone is the only one not heated. In the 3D building model, self-building shadings and shadings due to the surrounding have been modelled with several shading groups. In Fig. 3, a picture of the real case and a view of the SketchUp model are shown.

3.1 Simulation boundary conditions

Simulations have been run with TRNSYS 17 (Klein S.A., 2009) and the following boundary conditions have been set:

- Weather: monitored weather file has been used. Data have been collected for one year with a timestep of 1 hour. The file format is an *.epw (Energy Plus format) and it has been read by Type 15.
- Infiltration: a yearly fixed value for each apartment has been defined after performing a building model calibration. It takes into account wind-driven leakages and average-users behaviour.

Wall type	U-value [W/m ² K]
Exterior walls	0.14
Roof	0.08
Cellar ceiling	0.15
Entrance door	0.7
Windows	0.86

Table 1 – U values of the building envelope (design values)

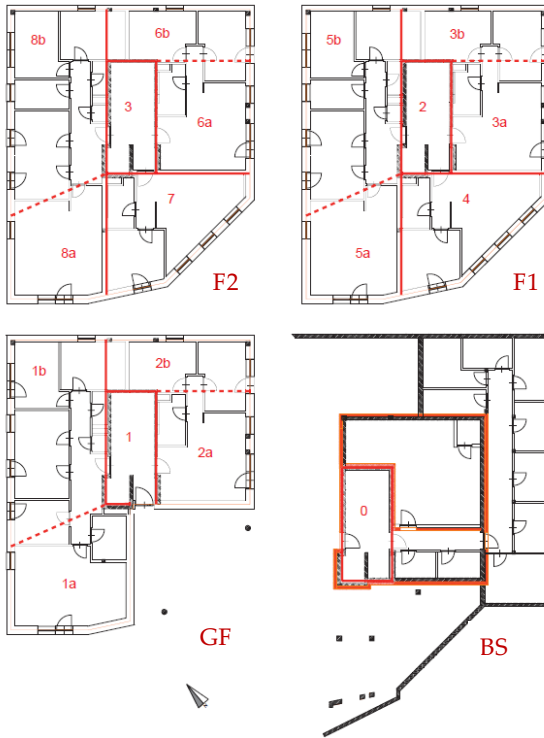


Fig. 2 – Zone partitioning of basement (BS), ground floor (GF), first (F1) and second (F2) floor



Fig. 3 – Picture of the real case (above) and view of SketchUp model (below)

- Ventilation: a fresh air supply flow rate has been defined for each apartment during the building

model calibration. A heat recovery of the 85% has been applied between the exhaust and the fresh air.

- Internal gains: monitored data of electrical consumption have been used to model internal gains due to electrical devices, lighting and cooking. The measured value is split into radiative (40%) and convective (60%) parts. Monitored data have been collected during a whole year with a timestep of 1 hour. Monitored data for users' occupancy are not available, so a schedule based on standard EN ISO 7730 (EN ISO 7730, 2007) has been used. The occupancy profile is assumed to be in accordance with power consumption profile; different user's activities during the day are also taken into account (Ecker M., 2011).

- Heating: an indoor air setpoint of 21°C is defined; the heating season is fixed from October to April;

- Cooling: an indoor air setpoint of 26°C is defined; the cooling season is fixed from May to September.

4. Detailed model calibration

The detailed model has been developed following all building characteristics available and monitoring data. Nevertheless, ventilation mass flow rate and infiltration rate needed to be further fixed through a model calibration because they are not directly measurable. The calibration process consists in an iterative process to match observed and simulated behaviours.

4.1 Ventilation

The coils' numerical model has been calibrated considering as boundaries the coil itself and using monitored data collected for one year with a time step of 1 hour: temperature and relative humidity of the supply air, air speed, water flow rate, inlet and outlet water temperature have been employed to this end. For each coil, an UA coefficient has been defined (Incropera et al., 2007). Rated values are available for fixed inlet air temperature (17°C), water flow-rate (180 m³/h) and inlet water temperature (70°C). Because of off-rated conditions of the air mass and fluid flow rate, the following expression can be adopted:

$$UA_{coil} = UA_{160} \cdot \left(1 + \left(\frac{\dot{m}_{water}}{\dot{m}_{design}} \right)^{0.8} \right) \quad (1)$$

Coils have been modelled as a counter-flow heat exchanger (Type 5) with water in the source side and air in the load side. The total air flow rate has been calculated from monitored air velocity in the channels; then the estimated air flow rate of each apartment has been defined multiplying the total air flow rate for design fractions (case VEN_1).

The discrepancy of the exchanged heat in each coil, between monitored consumption and VEN_1, is quite high in some apartments than in others. In apartments 1, 3, 6 and 8 the difference is less than 10%, whereas in apartments 4 and 7 (the smaller ones), the difference between the monitored and the simulated exchanged heat in the coils achieves 50%. This discrepancy is due to the wrong position of the sensor for the measurement of the air velocity. To solve such a discrepancy, the calibration of the air flow rate has been made with the process explained above. A corrective value of the guess rate (designed with Y) has been iteratively calculated up to obtain a match of simulated and monitored heat in each coil. The correct air flow rate has been calculated for each time step as follows:

$$\dot{m}_{air,calibrated} = \dot{m}_{air,guess} (1 + Y) \quad (2)$$

A constant yearly corrective value for each apartment has been individuated; in particular, the most frequent value has been chosen rather than an average value because not affected by measurements in transient conditions.

The yearly heating demand has been re-calculated with the corrected air fractions (case VEN_2) and a satisfactory approximation of the exchanged heat in the coils has been reached (Fig. 4).

An increase of 22% of the measured air mass flow is made, nevertheless, the total air flow still remains within the design value of 1440 m³/h (Castagna M., 2009).

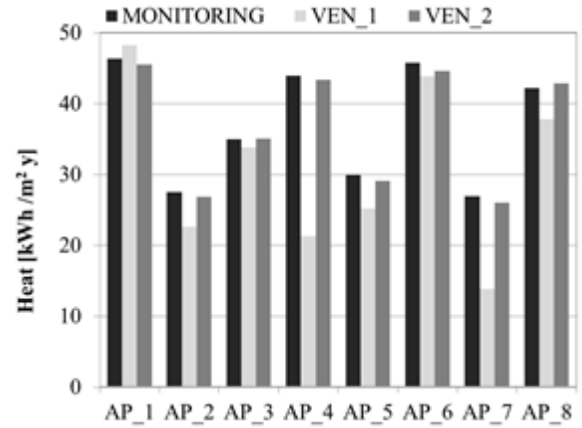


Fig. 4 – Comparison of ventilation rate from monitoring (MONITORING), before (VEN_1) and after calibration (VEN_2) in terms of exchanged heat

4.2 Infiltration

From monitoring, measurements on the instantaneous infiltration rate were not available, so the n_{50} value from the blower-door test has been assumed (case INFIL_1) as first attempt. In this case, the n_{50} value is equal to 0.8 h⁻¹ (IPES, 2006). Commonly, to calculate the infiltration rate from the n_{50} value, the Sherman equation is used (Sherman, 1987):

$$n = \frac{n_{50}}{20} = 0.04 \quad (3)$$

where n_{real} [h⁻¹] is the infiltration rate.

The calculated airtightness value gives an idea of the infiltration rate, but it does not take into account the building exposure to the wind direction, the ventilation strategy and occupants' behaviour. For this reason, a survey on the infiltration rate has been done, in order to fix an overall value for each apartment.

In the staircase, the infiltration rate has been assumed to be 0.35 h⁻¹ (Diamond R.C. et al, 1996) for considering the opening of the doors in the basement, in the ground floor and an air intake on the third floor. No calibration for the staircase infiltration rate has been done, because monitored data were not available.

For the definition of yearly fixed infiltration rate, the same procedure used for the ventilation rate has been applied. The calibration has been made by comparing simulated and monitored heating demand in each apartment. Monitored data have

been collected during a year with a time step of 1 hour. The iterative process individuated a corrective infiltration value (designed with X) for each time step up to obtain the match between simulated and monitored heating demand.

$$n_{calibrated} = n(1 + X) \quad (4)$$

Also in this case, the most frequent X value has been chosen for the definition of the constant yearly infiltration rate for each apartment. In particular, for apartments 3, 4 and 7, an infiltration rate of 0.34 h^{-1} has been individuated, while 0.44 h^{-1} has been taken for apartments 1, 2, 5, 6 and 8. These values are related to the apartment's size or to the occupancy.

New infiltration rate values have been set in the detailed model (case INFIL_2) and heating demands have been compared with case INFIL_1 and with the measured consumption.

The discrepancy in the heating demand, for the whole building, between monitored and calibrated case (INFIL_2) has been reduced to 1% (see Fig. 5). A slight difference between monitoring and simulation still remains due to the fact that (1) the occupancy profile is assumed (Ecker M., 2011); (2) the thermostat set point temperatures have been deduced from monitored indoor air temperature; (3) the infiltration rate value has been defined to be constant during the year. As a consequence, higher or lower heating demand with respect to the monitored consumption might occur.

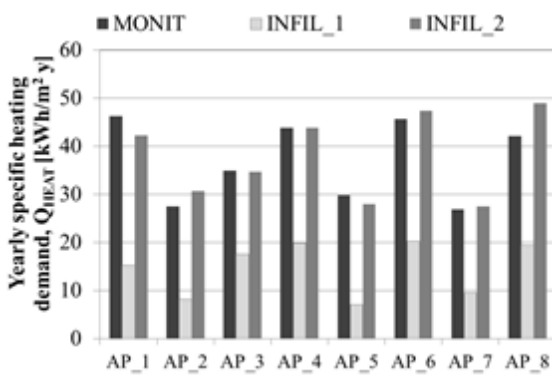


Fig. 5 – Specific heating demand calculated in each apartment from monitoring (MONIT), before (INFIL_1) and after (INFIL_2) calibration

5. Simplification procedure

The detailed model has been simulated with TRNSYS 17 (Klein S.A., 2009) for a whole year (8760 hours) with a time-step of 5 minutes. Although the real case has been reproduced with high accuracy, on the other hand, the complete simulation required 2.7 hours to run. In order to study the energy building model integrated with the supply energy system, a simplified model is therefore necessary. For this reason, a procedure has been individuated (see Table 2) starting from a detailed model and moving towards a simplified one. This process consists of three steps that analyze the main issues influencing the energy balance and the simulation runtime in a building model developed with TRNSYS. The impact of 1) radiation mode, 2) geometry mode and 3) shadings elements on building performance and simulation runtime have been analysed. Finally, a model, with reduced computational efforts which maintains sufficient accuracy, has been created. The analysed cases are reported in Table 2 where the used radiation mode, geometry mode and shading elements are specified.

For each step of Table 2, the incoming (denoted as positive terms) and the out-coming (denoted as negative terms) energy fluxes of each zone have been studied. Yearly energy losses and gains have been then calculated for the whole building according to the boundary conditions presented above.

CASE	Radiation mode	Shadings	Geometry mode
RAD_1	Detailed	Shad group	3D data
RAD_2	Standard	Shad group	3D data
SHD_1	Standard	Shad Factor	3D data
SHD_2		Type 34	3D data
GEO_1	Standard	Type 34	3D data
GEO_2			Manual

Table 2 – Steps of the simplification process

5.1 Radiation mode

In TRNSYS 17, two different modes for the distribution of the radiation within a zone are available, the standard and the detailed mode. In the case of the standard mode, the direct short-

wave radiation, is proportionally divided fixing a constant user-defined fraction (GEOSURF values), while the detailed mode calculates the distribution of the entering direct radiation according to shading and insolation matrices generated by an auxiliary program called TRNSHD (Hiller et al., 2000). The standard mode bases the diffuse radiation distribution on absorption-transmission weighted area ratios for all surfaces of a zone, while the detailed mode considers the multi-reflection too, thanks to the use of view factor matrix generated by an auxiliary program known as TRNVFM. Finally, the standard mode treats the long-wave radiation with the star-node approach (Seem, J.E., 1987). This approach takes into account no user defined emissivity of inside surfaces nor radiation exchange over more than one air-node. This aspect will be important for further considerations. For the treatment of long-wave radiation, the detailed radiation mode considers the multi-reflection too, using the view factor matrix generated by TRNVFM.

Comparing the energy balance for cases RAD_1 and RAD_2 (see Table 3), a difference in infiltration losses (Q_{INF}), ventilation gains (Q_{VENT}), transmission losses (Q_{TRANS}), heating (Q_{HEAT}) and cooling demand (Q_{COOL}) is shown.

		RAD_1	RAD_2
Q_{HEAT}	[kWh/m ² y]	37.6	34.1
Q_{COOL}	[kWh/m ² y]	-4.7	-6.9
Q_{INF}	[kWh/m ² y]	-35.0	-35.4
Q_{TRANS}	[kWh/m ² y]	-41.8	-34.8
Q_{GINT}	[kWh/m ² y]	41.9	41.9
Q_{SOL}	[kWh/m ² y]	23.8	23.7
Q_{VENT}	[kWh/m ² y]	-21.8	-22.6

Table 3 – Yearly energy gains and losses for the whole building in RAD_1 and RAD_2 cases

In order to understand the reason for this discrepancy, the radiation absorbed by all the apartments' walls has been analysed. The total radiation absorbed (and transmitted) in all inside (Q_{ABSI}) and outside (Q_{ABSO}) surfaces has been investigated. For the sake of clarity, the control volume is assumed to be the zone, so the term "inside" is referred to the radiation coming from

the zone, while the term "outside" concerns the radiation coming from outside the zone (Klein S.A. et al., 2009). In cases RAD_1 and RAD_2, the Q_{ABSI} differs less than 2%, while higher difference is verified in the Q_{ABSO} (see Table 4). Labels "EXT", "BND", "ADJ" are referred to the surface's categories, external, boundary or adjacent, respectively. The radiation mode refers to the inner radiation distribution, in fact the total external radiation absorbed at external surfaces (Q_{ABSO_EXT}) is the same in both cases. For the detailed mode, negative values indicate the absorption of radiation on a surface, whereas positive heat flux means a net emission. The main differences between standard and detailed mode have been pointed out by adjacent surfaces. In fact, all apartments border with an unconditioned multi air-node zone (the staircase and the lift), which influences the external absorbed radiation for adjacent walls. In particular, lower apartments are more affected by the exchange with staircase zone than higher.

	CASE	Q_{ABSO} [kWh]			
		TOT	EXT	BND	ADJ
AP_1	RAD_1	42495	42927	0	-432
	RAD_2	44004	42927	0	1077
AP_2	RAD_1	31353	32098	0	-745
	RAD_2	33164	32098	0	1066
AP_3	RAD_1	21297	21990	-	-693
	RAD_2	23691	21990	-	1701
AP_4	RAD_1	27831	27505	-	326
	RAD_2	28497	27505	-	993
AP_5	RAD_1	24763	25098	-	-335
	RAD_2	26902	25098	-	1804
AP_6	RAD_1	79724	79693	-	32
	RAD_2	80535	79693	-	843
AP_7	RAD_1	61442	61261	-	181
	RAD_2	61865	61261	-	604
AP_8	RAD_1	113303	113091	-	213
	RAD_2	114060	113091	-	969

Table 4 – Absorbed radiation on external walls

Maintaining all the boundary conditions unvaried and changing only the distribution of the radiation, the effect of the different heat transfer with multi air-node zones can be observed with the Mean

Radiant Temperature (T_{MR}) within the zone. This measure takes into account the area weighted mean temperature of all walls of the zone, so a variation in the air-node temperature might come out analyzing the different T_{MR} .

The cumulative frequency of the Mean Radiant Temperature for apartments 2 (situated in the GF) and 8 (situated in the F2) is shown in Fig. 6. The graph represents the yearly frequency distribution of the T_{MR} in the zones for cases RAD_1 and RAD_2. In apartment 2, the T_{MR} differs of about 0.7°C for the 40% of the year, while in apartment 8, there is a good overlapping of the two curves.

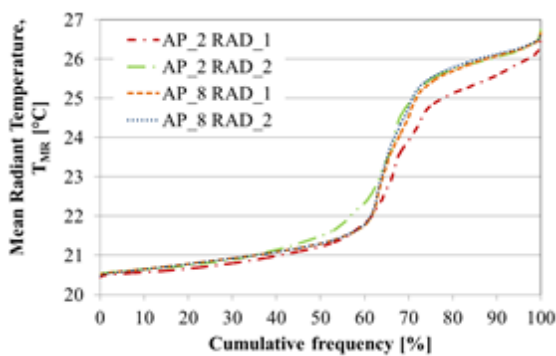


Fig. 6 – Cumulative distribution during a year of the Mean Radiant Temperature in apartment 2 and 8.

A different distribution of the radiation within the zone influences the ventilation load, the heating and cooling supply energy and the infiltration load. In particular, a discrepancy of about 9% is observed on the whole building heating load.

The radiation mode does not influence only internal air temperature within the zones, but also the simulation runtime. In fact, computational efforts are strongly affected and a reduction of 86% of runtime passing from the detailed to the standard radiation mode is observed.

In light of this, the choice of the radiation mode is very important for the reduction of computational effort, but attention should be paid when multi air-node zones are adjacent to single air-node zones.

5.2 Shading elements

External or internal shading elements may be defined for any transparent surface of a zone. To implement external shaders and self-shading of the building in the SketchUp building model, several “shading groups” have been used. At the

beginning of the simulation, TRNBuild generates a shading matrix which takes into account the presence of shading elements or surrounding structures. During the simulation, Type 56 determines the actual sunlit fraction of surfaces thanks to the use of the shading matrix file with respect to the sun's current position for each time step. If no shading group is present in the building model, external shadings might be modelled in TRNBuild itself. For an external window, the user can select an internal and/or external shading device, specifying its shading factor, which indicates the shaded fraction of the window element.

In this work, the effect of two different external shaders and self-shading of the building model have been investigated and compared with the case with the shading groups (RAD_2). A building with no shading elements has been modelled and the shadings' effect has been reproduced by External Shading Factors. An external file with shading factor obtained by the detailed model (case SHD_1) and a TRNSYS component, Type 34, (case SHD_2) have been used to determine the External Shading Factor inputs.

The use of both shading factors and Type 34 produces a difference of the yearly heating demand of the whole building, Q_{HEAT} , of 1% with the case of shading groups (case RAD_2). The use of Type 34 increases the cooling demand of the building, Q_{COOL} , of around the 8%.

In order to understand the different cooling demands needed in the two cases, single apartments have been analysed. As already seen, the detailed radiation mode does not consider irradiation from shade projected on exterior surfaces other than windows. For this reason, the incident radiation on windows only is taken into account.

Case SHD_1 has been considered to find out the difference of the simulation runtime when an external file with the sunlit portion area is used. Regarding the energy building balance, as the external file here used corresponds to the external shading factor of the RAD_2 case, no difference is shown.

The accuracy of the shadings modelled with Type 34 influences the agreement between cases SHD_2 and RAD_2. In Table 5, the incident radiation on all

apartments' windows for cases RAD_2 and SHD_2 is reported. The third column indicates the difference, in percentage, of incident radiation between the two cases.

CASE	RAD_2	SHD_2	Δ_{RAD_2, SHD_2}
	[MWh]	[MWh]	[MWh]
AP_1	6.2	6.2	-0.3%
AP_2	5.9	6.7	-12.8%
AP_3	7.2	6.7	7.6%
AP_4	3.6	4.9	-30.8%
AP_5	5.9	5.7	4.7%
AP_6	8.5	7.4	13.2%
AP_7	4.0	3.6	10.2%
AP_8	6.0	6.2	-3.6%

Table 5 – Incident radiation on all apartments' windows in RAD_2 and SHD_2 cases

Type 34 has been set to model the roof's overhangs and balconies, while surrounding contributions and the building's shadings (wall thickness, balconies on the adjacent sides) have not been reproduced. A high effect of this modelling is shown in apartment 4, where the difference with case RAD_2 is 31%, or in those apartments oriented to south-east, where the difference amounts to 8-13%.

Regarding the simulation runtime, the use of external file for the external shading factor (case SHD_1) reduces the simulation runtime of 6%, while the use of Type 34 (SHD_2) increases it by about 4%. The result of case SHD_2 also depends on the number of Type 34 units used into the model.

5.3 Geometry mode

For each zone, TRNBuild supports different levels of geometric surface information, known as "manual" and "3D data" mode. In the manual mode, the geometry of the building is individuated according to the definition of walls and floors and their boundary conditions. The advantage of modelling directly in TRNBuild is that no detailed shape definition is requested. Defining the area and the boundary conditions for each surface, the software automatically calculates the interactions between the surfaces and the zone. The walls' categories used in this case are external, boundary

and adjacent. "External" is referred to walls which border the outside, "boundary" is a wall in which boundary conditions of the first type can be specified and "adjacent" is a wall which borders another air-node.

The "3D data" mode provides, for all surfaces of the zone, three dimensional coordinates. Geometry model is designed in Google SketchUp with the Trnsys3D plugin and then an *.idf file is imported to the TRNBuild environment. If the detailed radiation mode is used, radiative zones must be convex polyhedrons.

Looking at yearly energy gains and losses in cases GEO_1 and GEO_2, no differences have been observed. For both cases, the simulation runtime is also unvaried.

For the calculation of the shadings' effects, the manual geometry mode does not use a shadings matrix. In fact, even if shading elements are inserted in the building model, the geometry mode does not consider this information. For this reason, if this mode is used, external inputs for modelling the shadings are required.

6. Simplified model

The steps analysed above have been used as a guide for the definition of a simplified building model. This new model has been conceived following the criteria of reducing the efforts during the numerical modelling design phase and the computational efforts:

- manual geometry mode has been applied in order to create zones in a flexible way because the walls' geometry and category are specified directly in the TRNBuild environment;
- standard radiation mode has been used to run the model, in order to reduce the simulation runtime and to draw the zones with any shape not necessarily convex;
- the use of Type 34 has allowed to model shading elements without any previous calculation for the definition of the sunlit portion area of the windows.

Building energy gains and losses of the simplified model have been compared with the reference case in order to verify the accuracy of the results.

With the use of standard radiation mode and manual geometry mode, a single zone for each apartment has been created. The staircase zone has been created as in the detailed model. All the characteristics and boundary conditions of the detailed mode have been set in the simplified model, too. The only exception has been the definition of windows because the total amount of glazed surface for each external wall has been taken into account.

The difference of heating demand of the whole building between reference case and the simplified case is around 8% (Fig. 7). Higher differences are observed in those apartments in which the constant infiltration value approximates with lower accuracy the real infiltration rate or in which the incident solar radiation differs more from the reference case (see Table 5).

Comparing the simulation runtime in the two cases, a strong reduction of 89% is observed decreasing from 2.7 hours to 20 minutes. This result is due to the fact that the standard radiation mode has been used and 9 zones (apartment zones + staircase zone) versus the 15 of the Reference case have been modelled.

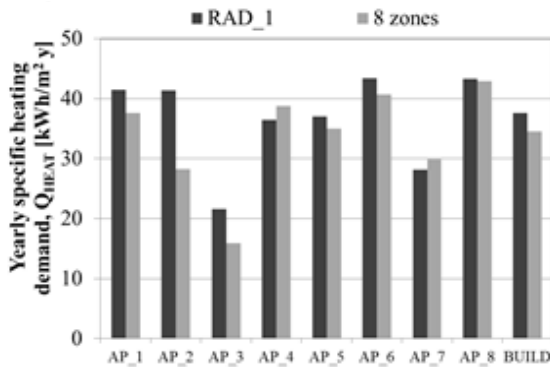


Fig. 7 – Yearly specific heating demand in the reference case (RAD_1) and in the 8 zones case

7. Conclusions

Building modelling integrated in supply energy systems are more and more challenging for the interdisciplinary of the treated aspects and the complexity of the model itself. A simplification procedure of a detailed building model has been presented in this work. The starting point has been a detailed model which has been calibrated with

monitored data to obtain an accurate model. The impact of radiation mode, geometry mode and shading elements on building performance and simulation runtime have then been analysed. A model with sufficient accuracy and reduced computational effort has been developed.

Simulations have been run in TRNSYS 17 and the following considerations have been made according to the calculation modes used by this simulation tool.

The use of the manual or 3D data geometry mode makes no changes in both simulation runtime and building energy response. An important reduction of computational efforts is instead observed in moving from a detailed radiation mode to a standard mode (around 85%). This simplification leads to a change in the air-node temperature in those zones which border with unconditioned multi air-node zones. When the standard mode is used, the building's heating and cooling demand differs by about 9% with respect to the detailed mode.

The modelling of External Shading Factor with external inputs does not significantly reduce the simulation runtime, which might have variations of around $\pm 5\%$. The influence on energy gains and losses using Type 34 depends on the apartment's orientation. Type 34 models shadings taking into account only overhangs or wing-walls of the building and not the shading effect of the surrounding.

The use of standard radiation mode leads to a significant reduction of simulation runtime maintaining the same solar radiation arriving on walls and windows, but neglecting the effect of multi-reflection within the zone. Differences might be observed in those cases in which conditioned zones border with unconditioned multi air-node zones. If a detailed radiation mode is used and the shadings' shape is not complex to be modelled, there are no advantages in using external inputs for the definition of the sunlit portion area. Indeed, if the geometry characteristics of the building are defined directly on TRNBuild and the manual geometry mode is set, the use of inputs for the External Shading Factor is requested. In particular, better results can be achieved with an external file which defines the sunlit portion area considering all

the shadings effects (for example obtained by a shader program (Nathaniel L. et al., 2006). If this information is not available, a good approximation of shading effect on windows can be made by Type 34.

A unique solution for the reduction of computational efforts does not exist because it is strictly related to the aim of the simulation and the parameters which have to be analysed. The main aim of the work presented here is the definition of a final building model which reproduces as well as possible the real building behaviour, reducing computational efforts and the time consumed during the design phase.

For this purpose, standard radiation mode, manual geometry mode and Types 34 have been selected for the simplified model.

The final simplified building model runs in 20 minutes with a reduction of the simulation runtime of 89%. A discrepancy of the heating demand of 9% has been found and, for the aim of the work, this might be considered suitable.

References

- Castagna, M. 2009. Studio di una Casa Passiva con un programma di simulazione dinamica. Università di Trento.
- Diamond, R. C., Feustel, H. E. and Dickerhoff, D. J. 1996. Ventilation and Infiltration in High-Rise Apartment Buildings. Technical report, Lawrence Berkley Laboratory, University of California, Berkley, California.
- Ecker, M. 2011. Modelling and Parametric Analysis for a Small-Scale Solar Heating and Cooling System. Master thesis, Fachhochschule Technikum, Wien.
- Ellis, P. 2009. OpenStudio plugin for Google SketchUp3D, Version 1.0, January. <http://sourceforge.net/projects/openstudio>
- EN ISO 13786:2007. Thermal performance of building components – Dynamic thermal characteristics – Calculation methods. International Organization for Standardization.
- IBPSA-USA. Energy Modeling of Buildings. IBPSA_US. <http://energymodeling.pbworks.com>
- IBPSA-USA bis. 2012. Modeling Best Practice. Building Energy Modelling. IBPSA-USA, Rocky Mountain Institute, ASHRAE. <http://bembook.ibpsa.us/>
- Gebhart, B. 1971. Heat Transfer, McGraw-Hill, New York.
- Hiller, M.D.E., Beckman, W.A, Mitchell, J.W. 2000. TRNSHD-a program for shading and insolation calculations, Building and Environment, Vol. 35.
- Incropera, F., Dewitt, D., Bergman T., Lavine A. 2007. Fundamentals of heat and mass transfer. John Wiley & sons, United States of America.
- IPES. 2006. La casa passiva Bronzolo. Istituto per l'edilizia sociale della Provincia Autonoma di Bolzano, Bolzano.
- Klein, S.A. et al. 2009. Trnsys 17. A transient simulation program. Solar Energy Laboratory, Univeristy of Wisconsin, Madison.
- Nathaniel, L.J., Donald, P. 2012. Hardware accelerated computation of direct solar radiation through transparent shades and screens. Program of Computer Graphics, Cornell University, Ithaca, New York, USA.
- Seem, J.E. 1987. Modeling of Heat in Buildings. PhD thesis, Solar Energy Laboratory, University of Wisconsin Madison.

Influence of the boundary conditions on the definition of a reference residential building for the Italian context

Davide Bettoni – Eurac Research Centre, Bolzano, Italy

Matteo D’Antoni – Eurac Research Centre, Bolzano, Italy

Roberto Fedrizzi – Eurac Research Centre, Bolzano, Italy

Abstract

Numerical simulation is nowadays a fast and well suited practice, useful to design buildings and thermal energy systems, being also recognized in international standards (e.g. UNI EN ISO 13790). However, monitoring data often show large divergences with respect to simulated data; this is especially true when highly efficient systems are considered. Moreover, when the effectiveness of a particular technical solution (e.g. thermal plant, insulation approach, etc.) has to be verified, an accurate prediction of the loads has to be computed. In this sense, the definition of a reference building is fundamental, as much as a correct assessment of constructive, climatic and inhabitants’ behavioural parameters that mostly affect system’s operation. This modelling phase represents, on the one hand, the main part of the simulation work, on the other, the way to adopt solutions that assure the lowest Primary Energy consumption. In this paper, a sensitivity analysis is presented with respect to the energy performance of a two-storey single family house; seasonal and yearly operations are reported, in terms of the final energy consumption. Two buildings placed in Bolzano and Rome, with the same size and construction characteristics according to the Italian standard (DM 26/01/2010), have been taken as reference points. Starting from these reference buildings, a number of parameters have been varied: the constructive characteristics (insulation properties and thickness, glazed area and infiltration), the management characteristics (natural free ventilation) and finally the climatic data used. The sensitivity analysis has been carried out with the Morris Method, by comparing average and standard deviation of the variation of the final energy with the aim to derive qualitative information on the effect of the single parameter on the model’s outputs. This process is fundamental for increasing the sensibility on the relevance of assumed boundary conditions and moreover, helpful for the

designer’s knowledge of what the parameters are to be tuned first in order to reach a given energy performance.

1. Introduction

The building sector is responsible for 40% of the total energy consumption at the European level (2020-2030-2050). To reduce the building’s energy need and plan an efficient integrated system, knowledge of the behaviour of the building is essential.

The numerical simulation models of buildings are well suited for understanding the energy consumption and predicting the time-varying loads for heating, cooling and lighting. In this context, the predicted energy needs are one of the key issues for the performance evaluation of different technical integrated solutions through dynamic simulations.

Results given by these models are strictly connected to the assumption made during the design phase. Furthermore, the boundary conditions imposed strongly affect the behaviour of the numerical model.

In order to understand the influence of a certain parameter on simulation outputs, a sensitivity analysis has been conducted by using the results of a residential building modelled in Trnsys for two different Italian climates.

Three main aspects have been investigated: (1) building inhabitant behaviour, (2) envelope construction and (3) climatic data. The first issue can affect the model results since, during the design phase, a typical profile of building usage has to be selected, for example the infiltration rate, the schedule of internal gains (occupants or

electrical appliances) and the adoption of the night ventilation strategy. The second aspect is related to the comparison between the building's numerical model and the constructed one. For this aspect, the focus is given to shading devices, internal walls and the real transmittance of opaque walls. Envelope could create a large difference not only in terms of energy demand between model results and real behaviour; this is even more visible when the performances of an integrated system have to be studied. Thirdly, huge difference could be found on simulation outputs using climatic data generated from different stochastic algorithms. In general, during design phases of a numerical model, inaccurate analysis are performed on the climatic data selected to use. Referring to a specific installation, the climatic profile data can affect the loads profile of the system.

The sensitivity analysis presented in this paper has been based on the Morris Method. This methodology can increase the awareness about the effect of the single parameter simulation results. It is used to prioritize the parameters, giving information related on their effects on the outputs (Morris, 1991). In the case studied here, the list of investigated parameters is described in detail in the next sections, with a specific focus on the heating and the cooling final energy.

2. Methodology

2.1 Sensitivity analysis with the Morris Method

The Morris Method (MM) belongs to the screening methods (Saltelli, 2005) where all parameters are varied "one at time" (OAT). The main objective is to isolate those inputs that can affect the response of the model by classifying their influence as (1) negligible, (2) linear or additive and finally (3) nonlinear or involved with some other factors.

The elementary effect of the MM is defined for the i parameters, on the k input analysed:

$$EE_i = \frac{[y(x_1, \dots, x_{i-1}, x_i + \Delta, x_{i+1}, \dots, x_k) - y(\bar{x})]}{\Delta} \quad (1)$$

Varying the x_i within a realistic range Δ , using r_i different number of steps for each i parameter, the Elementary Effects EE_i are evaluated. With the Elementary Effects of each input, the average μ_i and the standard deviation σ_i of the single elementary effect EE_i are then computed.

$$\mu_i = \frac{1}{r_i} \sum_{t=1}^{r_i} EE_{i,t} \quad (2)$$

$$\sigma_i = \sqrt{\frac{1}{r_i - 1} \sum_{t=1}^{r_i} (EE_{i,t} - \mu_i)^2} \quad (3)$$

The μ_i (eq. 2) is the mean parameter influence on the output, while the standard deviation σ_i (eq. 3) gives an idea on the nonlinear behaviour or interaction with other factors of the input.

The use of the average of the absolute elementary effect μ_i^* (eq. 4) is suggested (Campolongo, 2007), rather than μ_i , to prevent the possible error during the sum of the EE_i with a negative sign, which presents a decreasing effect. Plotting the value of σ_i related to the absolute value of the mean μ_i^* , the inputs closest to the origin indicate less influence on the output.

$$\mu_i^* = \frac{1}{r_i} \sum_{t=1}^{r_i} |EE_{i,t}| \quad (4)$$

2.2 Case study

The sensitivity analysis has been performed on the Trnsys numerical model of a residential building about 180 m² divided over two storeys. The net volume of the building is around 600 m³ and the ratio between external surface and gross volume (S/V) is around 0.7. The percentage of transparent surfaces on the different orientations is around 6% on the north, 10% on the east and west and 20% on the south. Heating and cooling are delivered to the internal zone through a radiative low temperature floor.

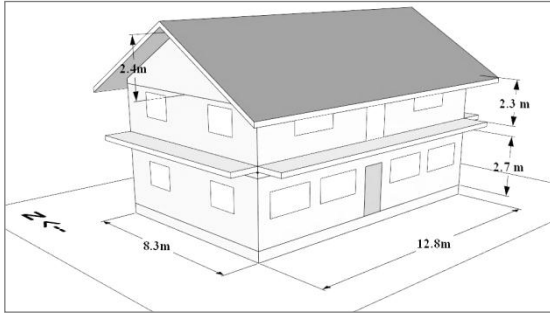


Fig. 1 – Residential building analysed.

The envelope characteristics considered are usual established massive wall stratigraphy, with an insulation thickness that allows to reach the limits imposed by the norm (DM 26/01/2010). The characteristics of the exterior walls, roof and floors are reported in the following table for the two Italian climatic zones analyzed (Rome and Bolzano).

Elements	Characteristics	Bolzano	Rome
External Walls	U [W/(m ² K)]	0.27	0.29
Roof	U [W/(m ² K)]	0.24	0.26
Ground Floor	U [W/(m ² K)]	0.30	0.34
Windows	U [W/(m ² K)]	1.80	2.00
	g [-]	0.597	0.613

Table 1 – Envelope characteristics for the two climatic zone (DM 26/01/2010).

In order to simulate balconies and roof overhang, on the south, west and east orientations a fixed shading is considered. Internal gains and the schedule of presence considered are in accordance with the UNI/TS 11300-1. These values are typical for residential buildings, assuming that 60% of the building area consists of bedrooms while the remaining 40% is for living space. This leads to a mean daily value for the internal gains of 5.2W/m². In both climates, an infiltration rate equal to 0.45 ACH is considered. During the night in summer, a free natural ventilation has been additionally considered. This night ventilation air change rate has been computed using a free driven tilted ventilation approach (Weber, 1997). The free night

ventilation is activated if the following conditions are met:

- Night time: between 21.00 and 08.00;
- Average of external temperature over 24 hours is greater than 12°C;
- Room temperature is above 23°C;
- Temperature difference between internal and external is above 2°C.

When this happens, an air exchange rate through the windows is calculated as a function of the internal-external temperature difference, the window shape and the opening tilt angle.

2.3 Weather data description

In building simulations, the weather data used for reproducing the climatic conditions affect the behaviour of the numerical model computed. In order to better understand the level of this influence, two “typical year” profiles have been considered. This climatic data, generated using the Meteonorm software (Meteonorm, 2012) are based on a stochastic analysis of 10 years of data for temperatures (from 2000 to 2009) and on 20 years of data for radiations (from 1986 to 2005). The two profiles considered are:

“Standard” weather data (STD), which is an hourly profile created using the models of (Remund, 2008) (Perez, 1991) for calculating solar radiation, while ambient air temperature is derived from the mean of extreme values over 10 years.

“Extreme” weather data (EXTR), which is an hourly profile generated by hourly extreme solar radiation and ambient air temperature, which correspond to extreme (minimum ambient temperature and radiation during wintertime and vice versa for summertime) values of the 10 years. With this approach, the year does not aim to represent a typical year, but to be a “worst” case scenario.

In the following graphs the frequency of the dry bulb temperature (DBT) and global horizontal radiation (GHR) are reported for the two locations analysed. The following graphs show columns related to frequency and curves that represents the cumulative frequency of the single series of data considered.

Analysing the distribution of DBT of Bolzano (Fig. 2) the EXTR data is clearly distributed in the low temperatures (extreme winter conditions) and in the high temperatures (extreme summer conditions). In winter, the number of hours where the temperature is below 0°C moves from 18% (790 h) to 32% (1300 h). During summer, analysing the temperature above 24°C, the hours move from 17% (770 h) to 35% (1600 h). The cumulative curve reflects this behaviour (higher at low temperature and lower at high temperature).

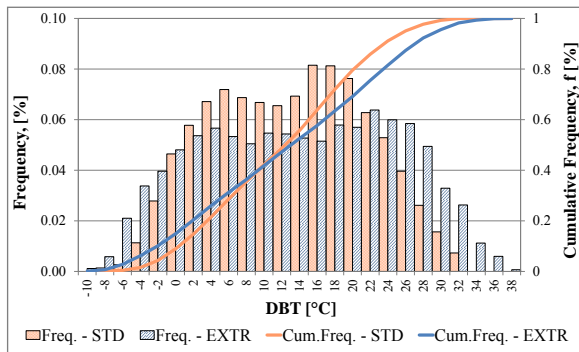


Fig. 2 – External Dry Bulb Temperature – Bolzano.

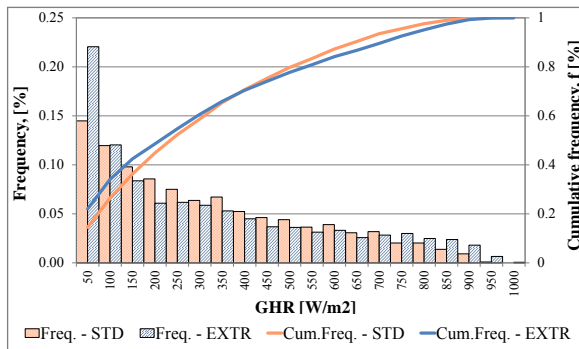


Fig. 3 – Global Horizontal Radiation – Bolzano.

Also the GHR for the EXTR data displays the percentage of radiation bigger for a higher level of GHR. It is interesting to note these differences also in Table 2, where the difference of the two climatic data is shown in terms of max. and min. temperatures, HDD and GHR computed for the whole year.

For Rome the differences between the two profiles are not so significant. Here, the two climatic data have almost the same distribution, with a small difference in the highest DBT and GHR. During the summer periods the extreme profile counts, for temperature above 28°C, 450 h, corresponding to 7% of the summer, while in the standard profile the

hours are 312 equal to 5%. The HDD analysis shows a small difference between STD profile and EXTR data analysis.

Bolzano		STD	EXTR
T_{min}	[°C]	-8.75	-11.13
T_{max}	[°C]	31.75	36.34
$I_{g,hor}$	[kWh/m²yr]	1251	1331
HDD $_{12/20}$		2711	2870

Table 2 – Temperature, total energy on the horizontal surface and HDD – Bolzano.

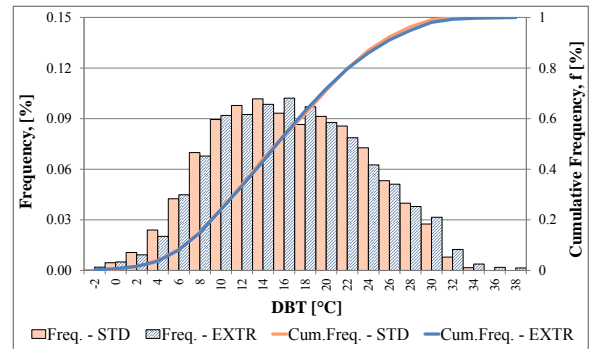


Fig. 4 – External Dry Bulb Temperature – Rome.

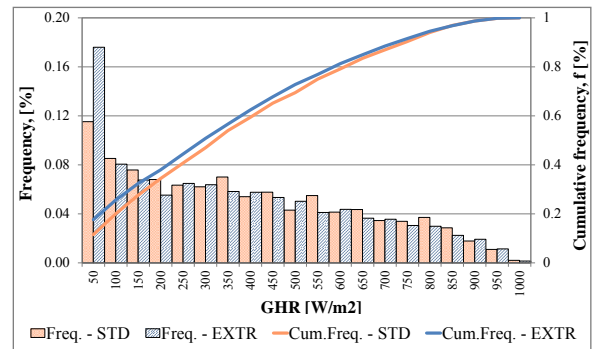


Fig. 5 – Global Horizontal Radiation – Rome.

Rome		STD	EXTR
T_{min}	[°C]	-2.3	-3.9
T_{max}	[°C]	33.1	37.4
$I_{g,hor}$	[kWh/m²yr]	1561	1562
HDD $_{12/20}$		1371	1299

Table 3 – Temperature, total energy on the horizontal surface and HDD – Rome.

2.4 Sensitivity analysis sets

The sensitivity analysis has been conducted through a campaign of simulations in Trnsys. The inputs of the model analyzed, the range and step considered are summarized in *Table 4*. The transmittance of opaque surfaces are the average of external walls, roof and floor weighted with the correspondent area of exchange for the two climatic zones studied. The overhang length is 1m, chosen for the simulation of the effect of balconies and roof overhangs. The internal gains are the average on the single day for a detailed approach (UNI EN ISO 13790). The night ventilation input is related to the operable window area ranging from 0 to 4 m². The orientation input is considered using the angle between the south orientation and the south façade of the reference. The fenestration ratio is the sum of all the windows on the different orientation.

n	Parameters	Ref.	Min	Max	Step
1	Overhang [m]	1	0.6	1.4	0.2
2	Internal Gains [W/m ²]	5.2	2.6	7.8	1.3
3	Infiltration rate [ACH]	0.45	0.25	0.65	0.1
4	Night ventilation [m ²]	4	0	4	1
5	Orientation [°]	0	0	360	45
6	Transmittance (Bolzano) [W/m ² K]	0.269	0.161	0.377	0.054
	Transmittance (Rome) [W/m ² K]	0.284	0.170	0.398	0.057
7	Fenestration ratio [m ²]	27	21.6	32.4	2.7
8	Thermal inertia [kJ/K]	2.2·10 ⁵	2·10 ⁵	2.5·10 ⁵	1·10 ⁴

Table 4 – Parameters investigated and range of variation for Bolzano and Rome.

The output used for sensitivity analysis of the system analyzed is the end energy demand for heating and cooling of the building with the set point of internal temperature of 20°C for winter and 24.5°C for summer. The distribution system considered is a radiative low temperature floor with the inlet temperature imposed using a climatic curve function of the external temperature.

3. Results and discussion

3.1 Analysis on weather data

A first analysis on the effect of the climatic data on the energy demand has been conducted and the comparison is reported in *Table 5*. Here, for Bolzano, the effects shown in the weather data description (higher frequency for low and high temperatures) are reflected in a twice cooling energy demand while the heating demand increased by about 20%.

Also for Rome, the effect of the analysis made on the weather data is visible on the heating and cooling demand. In this case, however, for the two climatic profile used, the heating and cooling energy needs are similar. A small difference between heating energy loads reflects the HDD analysis reported in Table 3.

	Weather	Unit	Bolzano	Rome
q_{heat}	STD	[kWh/(m ² yr)]	54	26
q_{heat}	EXTR	[kWh/(m ² yr)]	63	24
q_{cool}	STD	[kWh/(m ² yr)]	12	18
q_{cool}	EXTR	[kWh/(m ² yr)]	23	18

Table 5 – Final Energy for heating and cooling with different weather data.

3.2 Sensitivity analysis

Using as a reference the building with standard weather data, the results of the sensitivity analysis are presented here. The graphical representation of the MM is a scatter graph, where each point plotted is related to the elaboration on elementary effects of each parameter analyzed. The graph shows the absolute mean on the x-axis and the standard deviation on the y-axis. Values closer to the origin represent parameters with less influence

and linear effect on the output. A dotted line is also reported, representing the threshold between linear or non-linear influence on the output.

Two different outputs are evaluated in order to understand the effect of the parameters: seasonal cumulated heating and cooling demands.

Recalling the definition given for the elementary effect EE for a certain parameter analyzed, this represents the output variation when the input moves from a minimum to a maximum value.

Starting from the analysis on the heating demand, for both climatic locations (*Fig. 6* and *Fig. 7*), a linear effect with high mean value is visible in the graphs with regard to the envelope parameters (transmittance and infiltration) and inhabitants' behaviour (internal gains).

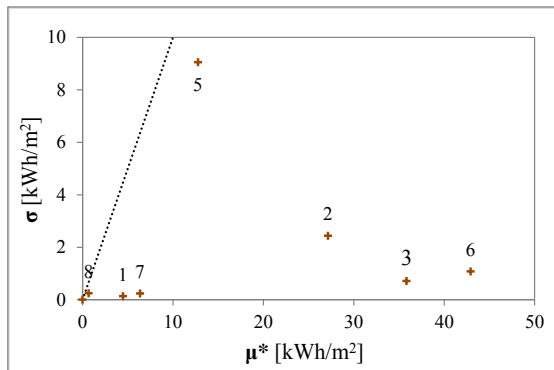


Fig. 6 – Estimated mean (μ^*) and standard deviation (σ) for each input factor on heating energy demand – Bolzano.

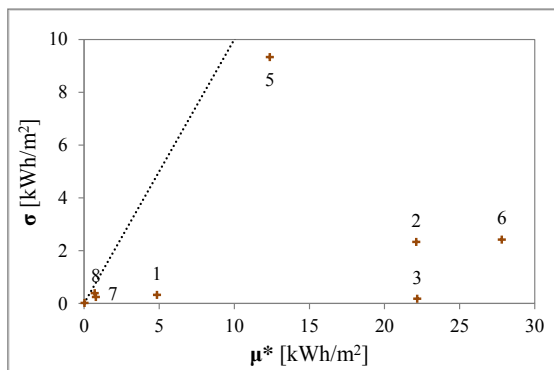


Fig. 7 – Estimated mean (μ^*) and standard deviation (σ) for each input factor on heating energy demand – Rome.

Secondarily the orientation of the building has an effect close to nonlinear behaviour or correlated with other parameters. A small linear effect is noticeable with regard to the two envelope parameters (variation of shading device and fenestration ratio); the effect of night ventilation is

null because the conditions for simulating this effect are not reached during winter, as reported in the case study description.

For the cooling analysis, the internal gains have the highest impact on the energy demand for both buildings located in Bolzano and in Rome (*Fig. 8* and *Fig. 9*). The variation of the fenestration ratio, differently from what is shown in the heating analysis, has a strong linear influence on the cooling energy because this parameter is directly connected to the solar gains. The orientation has a significant linear influence. The parameters that show a minor influence, compared with the analysis on the heating demand are the transmittance and the infiltration. Their minor effect is mainly due to the lower difference between internal and external temperature in the summer. For the same reason, also the variation of the operable window area, simulating the night ventilation, has a small impact on the cooling demand.

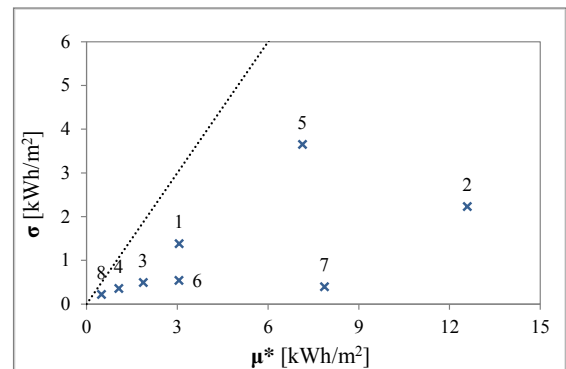


Fig. 8 - Estimated mean (μ^*) and standard deviation (σ) for each input factor on cooling energy demand – Bolzano.

A ranking of the design parameters influencing the sensitivity of the energy used for heating and cooling is reported in Table 6. Here, the predominant parameters are clearly reported for both output and climatic location considered. As mentioned before, the envelope characteristics and behavioural aspects have a strong influence, on the one hand, on the heating loads with transmittance of opaque walls, infiltrations and internal gains. On the other, the cooling demand is mainly affected by internal gains and fenestration ratio. The orientation of the building is an important

parameter for both analysis of the heating and cooling needs.

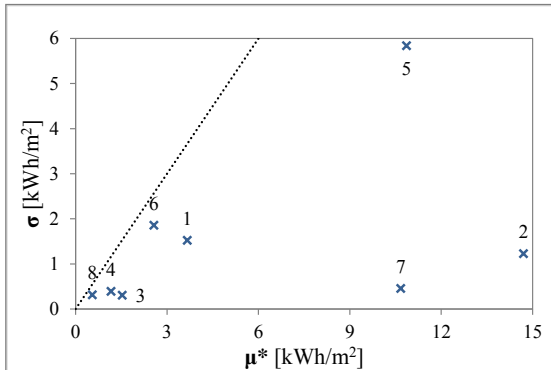


Fig. 9 – Estimated mean (μ^*) and standard deviation (σ) for each input factor on cooling energy demand– Rome.

Parameters	Rank Heating		Rank Cooling	
	Bolzano	Rome	Bolzano	Rome
Overhang [m]	6	5	4	4
Internal Gains [W/m²]	3	3	1	1
Infiltration rate [ACH]	2	2	6	6
Night ventilation [m²]	8	8	7	7
Orientation [°]	4	4	3	2
Transmittance [W/m²K]	1	1	5	5
Fenestration ratio [m²]	5	6	2	3
Thermal inertia [kJ/K]	7	7	8	8

Table 6. – Ranking parameters

4. Conclusions

Numerical simulation models are nowadays well suited for predicting the energy consumption of buildings and evaluating the performances of different technical integrated solutions. The building performances simulated are strictly connected to the boundary conditions chosen during the model's definition phase.

A correct choice of these parameters affect the building loads and the performances especially when an integrated solution is studied. In the early stage, a deeply analysis of the boundary conditions, e.g. the weather data used in the simulation, is strongly recommended in order to understand in which conditions the performance of the building is evaluated. The climatic data considered strongly affect the heating and cooling demand of the building.

The effects of the parameter's variation on the model's output is fundamental in order to understand the significance of each studied parameter. The Morris Method shows a strong influence of the envelope and construction aspects (transmittances, infiltration, orientation, fenestration ratio and shading devices) and behavioural aspects (internal gains) on the heating and cooling demand.

In order to reach a certain energy performance target or to modify the building numerical simulations, this awareness allows for the prioritization of the studied parameters and the tuning of the models starting from the most important parameters. Furthermore, the knowledge of the real value of these parameters and the effects produced when they move in a certain range of variability allow, in particular during the early design phases, for the following of a more or less conservative design approach to the building or the integrated system.

References

- UNI EN ISO 13790: Energy performance of buildings: Calculation of energy use for space heating and cooling.
- UNI TS 11300-1: Prestazioni energetiche degli edifici - Parte 1: Determinazione del fabbisogno di energia termica dell'edificio per la climatizzazione estiva ed invernale.
- DM 26/01/2010. Aggiornamento del decreto 11 marzo 2008 in materia di riqualificazione energetica degli edifici.
- 2020-20-30-2050: Common Vision for the Renewable Heating & Cooling sector in Europe. European Technology Platform on RHC.

- Mahabir Bhandari, Som Shrestha, Joshua New. 2012. Evaluation of weather datasets for building energy simulation. *Building and Environment* 49, 109-118
- Francesca Campolongo, Jessica Cariboni, Andrea Saltelli. 2007. An effective screening design for sensitivity analysis of large models. *Environmental Modelling & Software* 22, 1509-1518
- Francesca Campolongo, Roger Braddock. 1999. The use of graph theory in the sensitivity analysis of the model output: a second order screening method. *Reliability Engineering and System Safety* 64,1-12
- Joseph C. Lam, C. L. Tsang, L. Yang, Danny H. W. Li. 2005. Weather data analysis and design implications for different climatic zones in China. *Building and Environment* 40, 277-296
- Klein SA et al., 2002. TRNSYS Manual, University of Wisconsin (USA).
- Max D. Morris 1991. Factorial Sampling Plans for Preliminary Computational Experiments. *Technometrics* 33, 161-174.
- Meteonorm, 2012, Global meteorological database for engineers, planners and education, Version 7.0, www.meteonorm.com.
- Perez, R., P. Ineichen, E. Maxwell, R. Seals and A. Zelenka. 1991: Dynamic Models for hourly global-to-direct irradiance conversion. Edited in: *Solar World Congress 1991. Volume 1, Part II. Proceedings of the Biennial Congress of the International Solar Energy Society*, Denver, Colorado, USA, 19-23 August 1991.
- Remund, J. 2008. Quality of Meteonorm Version 6.0. *Proceedings of 10th World Renewable Energy Conference*, Glasgow
- Andrea Saltelli, Marco Ratto, Stefano Tarantola, Francesca Campolongo. 2005. *Sensitivity Analysis for Chemical Models*. Chemical Reviews
- Sanchez, B. Lacarrière, M. Musy, B. Bourges .2012. Application of sensitivity analysis in building energy simulations: Combining first- and second-order elementary effects methods. *Energy and buildings* (Article in press)
- Weber A., 1997. Modell für natürliche Lüftung durch Kippfenster, TRNSYS Usertag Stuttgart, 21. November 1997, EMPA Dübendorf
- Zuzanna B. Zajac. 2010. Global sensitivity and uncertainty analysis of spatially distributed watershed models. Thesis for degree of doctor of philosophy- University of Florida

Optimisation of an HVAC system for energy saving and thermal comfort in a university classroom

Giovanni Semprini – DIN / CIRI, University of Bologna, Bologna, Italy

Cosimo Marinosci – DIN / CIRI, University of Bologna, Bologna, Italy

Alessandro Gober – CIRI, University of Bologna, Bologna, Italy

Abstract

In university classrooms with air conditioning systems, as well as in conference rooms, thermo-hygrometric and air quality requests must deal with high energy consumption of the plant system. The whole plant management is sometimes critical due to the particular conditions of use of the rooms where the ventilation rate demand and thermal loads may change consistently during daily occupation. In this work an existing HVAC system unit is analyzed, serving two classrooms with a single zone distribution. The HVAC system is set to work with an external air supply at a constant rate, and includes air treatment sections with heating, cooling and vapour humidification. Experimental measurements of both thermal comfort parameters and real operating conditions of the HVAC unit gave information about critical aspects of the whole building-plant system design and management. In this work an energy dynamic simulation of the building-plant system using Energy-Plus software has been realized. After a proper calibration of the model based on experimental measurements, a dynamic simulation is used to carry out plant management strategies (e.g. free cooling, variable set points for intermediate occupational condition, mixing of the external air with recycled air, etc.) that combine energy savings with better indoor comfort. Several design alternatives are modelled through Energy-Plus to predict energy performance improvements associated with a different set of HVAC system configuration. Simulation results indicate up to 60% energy savings.

1. Introduction

Air conditioning plants are very energy consuming systems, especially in summer periods where the

control of internal humidity assumes an important role for hygrothermal comfort conditions. The possibility to adopt specific management controls of the plant system as a function of the effective occupation of each classroom can lead to an important reduction in the energy consumption. However, the effectiveness of adopted solutions is strongly dependent on external climatic conditions, especially when the HVAC system is connected to air condensing chillers for cooling water, as in the case study. Energy modelling of a building-plant system can be very difficult and can provide reliable results only if a detailed knowledge of the thermal characteristics of materials and plant components are available. Simulations of existing cases need a control or “calibration” with experimental measurements of physical parameters during the analysed period of study.

2. Description of case study

2.1 The building envelope

The investigated classrooms are two adjoining rooms with the same internal dimensions ($L=14.0 \times W=8.85 \times H=3.50$ m) located on the first floor of the Faculty of Engineering's new building in Bologna. Each one has a maximum occupancy of 96 students. Main external loads come from the external windowed façade (triple glazing for the lower fixed ribbon, quadruple glazing for the upper moveable ribbon, both with solar control properties in the outer glazing layer), oriented on the north-west side and protected by a solar screen on the top of the building, (Fig. 1 and 2).

Floor and opaque wall surfaces border internal conditioned areas, except south-east ones that are exposed to an unconditioned corridor



Fig. 1 – External view of the building

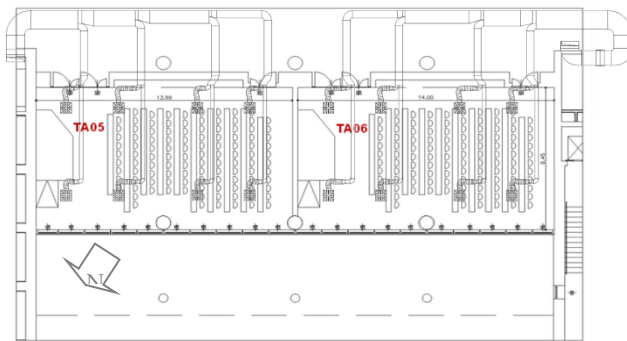


Fig. 2 – Plan of classrooms

2.2 HVAC System

The classrooms are conditioned by a single zone Air Handling Unit (AHU) of 8500 m³/h (constant air volume fan) where the inlet air (from ceiling air diffusers) is controlled by a thermostat that detects the temperature of the mixing air extracted from both classrooms (set point at 26°C). Typical operating conditions in summer provide a cooling coil section at a fixed temperature of about 14°C (connected to an external water chiller) and a post-heating coil section (powered by a gas boiler used also for hot water production). Scheduled times are from 6 am to 8 pm (Mon-Fri) and from 6 am to 2 pm (sat).

2.3 Thermal comfort conditions

During part of the summer period some experimental measurements were carried out in order to evaluate the internal comfort conditions

that are correlated to actual operating conditions of the AHU unit, by means:

- measurements of climatic parameters;
- questionnaires to students in different periods.

Results of PMV index evaluated from microclimatic measurements are comparable to results of questionnaires (Fig. 3), showing a small prevalence of slightly heating near windows in the afternoon period due to the thermal radiation of the glazed surfaces.

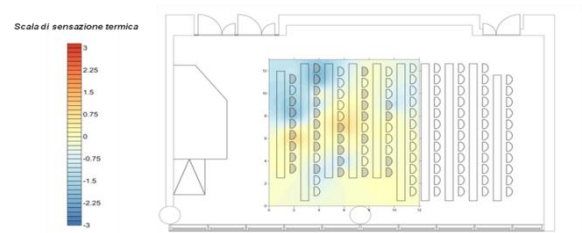


Fig. 3 – PMV map based on questionnaires (internal set point of 24°C)

The internal air distribution is quite uniform, even if little differences of the air temperature are detected; probably, those differences are due to asymmetric position of extraction grids.

The designed AHU can maintain a correct internal set point on both classrooms only when the same occupancy levels occur (same thermal loads); for a number of students, which differs from one classroom to the other, discomfort conditions occur in winter and summer periods, giving a general overheating condition in one of the two classrooms.

3. Energy modeling

Dynamic simulations are performed with “EnergyPlus” (version 7.2) software (energy calculation) and the corresponding “Legacy OpenStudio” plug-in (geometrical input data). The first step was the “calibration” of the energetic model of the building-HVAC plant system comparing the predicted data with the experimental measurements.

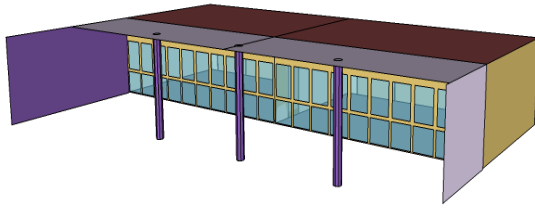


Fig. 4 – Sketch of simulated thermal zones

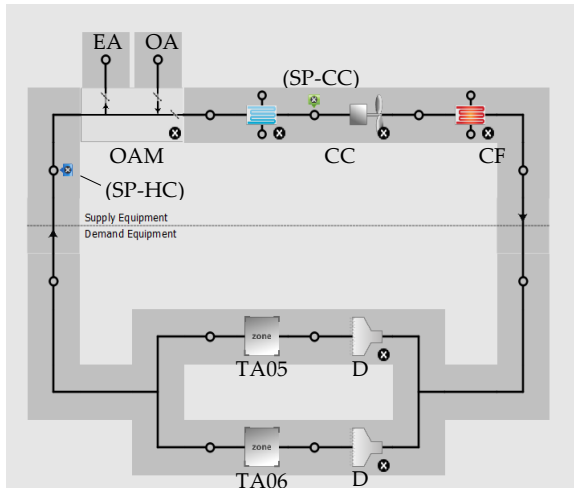


Fig. 5 - Model of the HVAC system

Figure 5 Legend:

CC	cooling coil
(SP-CC)	cooling coil dew point temperature controller
HC	post-heating coil
(SP-HC)	post-heating coil temperature controller
OAM	outdoor air mixer
EA	exhaust air
OA	outdoor air
TA05	TA05 classroom
TA06	TA06 classroom
D	diffusers

Then simulations are performed in order to evaluate energy consumption of the HVAC system both in the actual configuration, and using technical solution proposals to improve the plant system's efficiency. Fig. 4 shows the geometrical model of the building while fig. 5 shows the simplified model of the HVAC system. Due to the complexity of the water chiller and gas boiler plants, used also for other rooms and offices in the

building, they are modelled in order to simply supply the cooling and heating coils with the power they need at each time step calculation (5 min).

3.1 Calibration of the energetic model

The calibration of the model was not easy to achieve because of uncertainties about some thermal characteristics involved in the building envelope and, in addition, because of the non-uniform temperature of air in rooms caused by a not perfect balancing of the air inlet jets.

Due to our priority of energy analysis of the HVAC system, the model has been refined to achieve good correlation on internal temperatures and inlet temperatures. Fig. 6 and fig. 7 show measured and predicted temperature trends through days with a changing in set point temperature (27°C), used in the questionnaires experience.

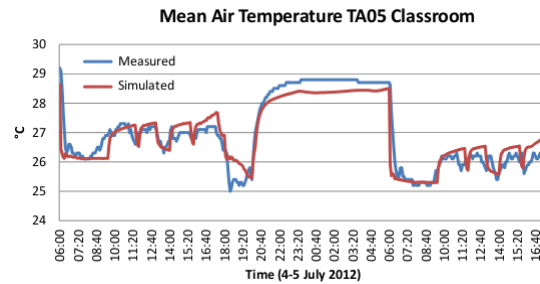


Fig. 6 – Comparison between predicted and measured mean indoor air temperature

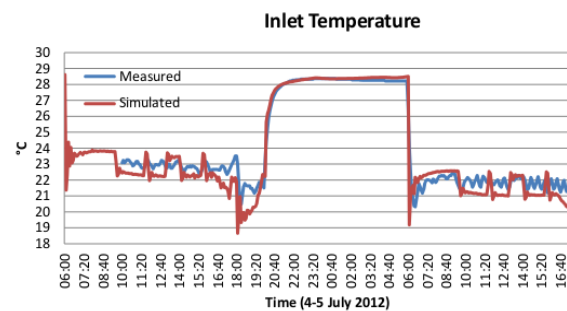


Fig. 7 – Comparison between predicted and measured inlet air temperature

Concerning the mean radiant temperature, there is a discrepancy of about 1°C between measured and predicted data (Fig. 8).

This discrepancy is due both to some simplifications adopted in roof/ceiling and corridor modelling, and also to specific conditions of

experimental measurements performed with the globo-thermometer. However, these results are deemed satisfactory for the purpose of this work.

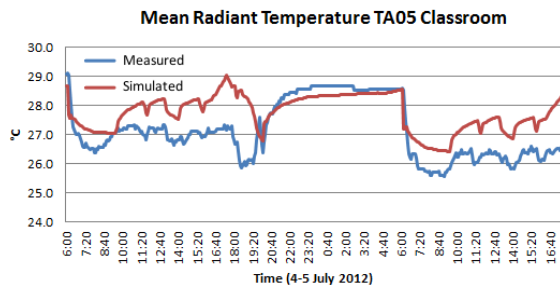


Fig. 8 – Comparison between predicted and measured mean radiant temperature

4. Energy optimisation of the hvac system

The energy consumption of the HVAC system is mainly related to the high air flow rate and to the low saturation temperature of the cooling coil; these situations, especially the second one, cause high energy consumption for the post-heating process when low internal thermal loads occur. In table 1 the basic setting parameters for actual situation (simulation starting point) are reported.

OCCUPANCY (BOTH CLASSROOMS)	Mon-Tue 20% Wed 100% Thu-Fri 80% Sat 10%
AHU OPERATION	Mon-Fri 06.00-20.00 Sat 06.00-14.00
INLET OUTDOOR AIR	100%
FIXED TEMP. COOLING COIL	13,5°C

Table 1 – Basic setting parameters for simulation starting point (actual situation - AS)

SOLUTION S1	
INLET OUTDOOR AIR	60%
SOLUTION S2	
FIXED TEMP. COOLING COIL	15°C

SOLUTION S3	
INLET OUTDOOR AIR	60% (with 100% occup.) 30% (with 50% occup.) 12% (with 20% occup.) 6% (with 10% occup.)
SOLUTION S4	
AHU OPERATION	Mon-Fri 07.00-20.00 Sat 07.00-14.00
AHU'S FAN OPERATION	Mon-Fri 05.00-06.00 Sat 05.00-06.00 (only if outside dry bulb temperature < 23°C)

Table 2 – Changed setting parameters to simulate different solutions (proposals from S1 to S4)

In order to reduce global energy consumption, four different managing solutions are analysed and compared to the actual situation (AS). Maintaining the AHU actual air flow rate of 8500 m³/h, the following cases are analysed (changed parameters are reported in Tab. 2):

S1 reducing the amount of external air flow to the minimum value of 7 l/s per person, as required to reference national standard (UNI 10339): the external air flow rate is then reduced to 60% of the total air flow;

S2 increasing the condensation set point temperature of cooling coil at values $\geq 15^{\circ}\text{C}$: this case results an increasing of indoor humidity, but not above 60% in the case of maximum occupancy of each classrooms;

S3 controlling the recirculated air flow of the AHU on the basis of the effective occupancy level of each classrooms;

S4 using free cooling in the first morning hours depending on the effective external air temperature.

C combining solutions S2, S3 and S4.

Each of the proposed solutions refers only to a different setting of one or more components of the existing AHU.

Further solutions concerning changes on components of the air handling unit are then analyzed.

First we considered a new smaller fan, designed

for a constant air flow rate of 4850 m³/h (which is enough to ensure the indoor air quality in conditions of full occupancy, as stated by UNI 10339 standard) and re-sized cooling and post-heating coils accordingly to the new air flow rate. Therefore, simulations with the new AHU are performed (new simulation starting point - NSP), applying the same previous managing solutions (respectively named S2R, S3R, S4R, CR). In the re-statement of the third solution (S3R), the correspondence between inlet outdoor air and occupancy is properly adjusted: both parameters have now the same percentages.

Lastly, it is supposed to modify the original concept of the HVAC control, adopting a multi-zone solution, where the single post-heating coil on the AHU is replaced by two half-power ones, located just upstream of the distribution air ducts of each classroom. A single thermostat for each classroom controls the power delivered from the corresponding post-heating coil, in order to maintain the internal set point at 26°C.

5. Simulation results

The evaluation of effective energy advantages for each proposed solution must be evaluated as a function of the specific temporal period of the analysis and correlated climatic data.

A first analysis related to a shorter and warm period (25th June – 1st July week), shows that all four solutions are effective energy savers, especially S3 where the high re-circulated air carries out a lower cooling coil energy consumption (Fig. 9). Adding the advantages related to a higher cooling coil temperature and the free cooling to this solution, the best performance is achieved (combination C of solutions from 2 to 4).

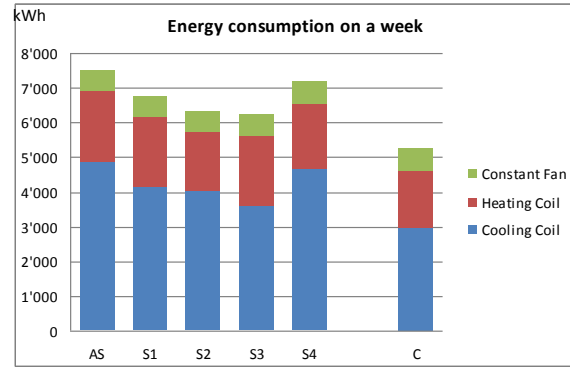


Fig. 9 – Energy consumption on a warm week (25th June - 1st July, IGDG weather data)

Energy saving of almost all solutions is higher when the period is warmer. Results from simulations run over the same week, but with the EPW climate data file built on the basis of measured 2012 data (detected by means of a weather station during the experimental measurement campaign), show improvements in energy saving, except in case S2 (Fig. 10 and Tab. 3).

	AS	Energy saving (%)				
		SOLUTIONS				
		S1	S2	S3	S4	C
IGDG	7'533 kWh	10.1	16.0	17.2	4.5	30.3
2012	8'302 kWh	13.4	14.0	25.4	5.1	38.0

Table 3 – Energy saving (%) for solution proposals respect to global consumption of the actual situation (AS) over two different warm weeks

Simulations were also performed over the whole cooling season, from 15th May to 30th September, considering that the HVAC system is switched off from 1st to 20th August (as scheduled by the school in the summer). Default EnergyPlus weather data for Bologna were used (resulting from the Gianni De Giorgio collection – IGDG).

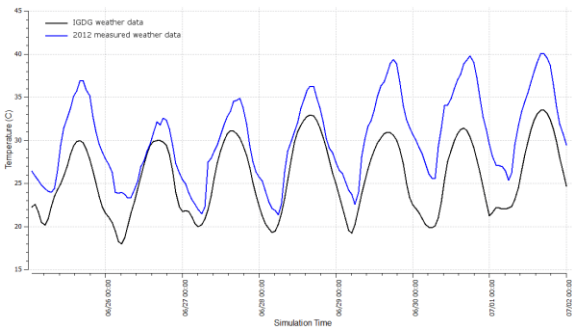


Fig. 10 – Comparison between IGDG and measured 2012 outdoor dry bulb temperature

Analysis of simulations over a whole summer season give a substantial difference on proposed solutions with respect to results obtained during the warm week previously analysed. From fig. 11 it can be seen that only in the middle of the season are climatic conditions advantageous for cooling strategies, while in other periods (the initial month and the last 15 days) when external temperatures are lower than the internal set point (26°C) energetic performances are worse than the actual situation. As shown in Fig. 12, solutions with air recirculation (S1 and S3) provide higher cooling coil consumptions. Only S2 solution is better than the initial situation AS.

But just simply looking at the energy consumptions of each components of the AHU, an improper design of the HVAC system should be pointed out: high values of the external air flow rate causes too high energy demands not only for the cooling coil but also for the post-heating coil.

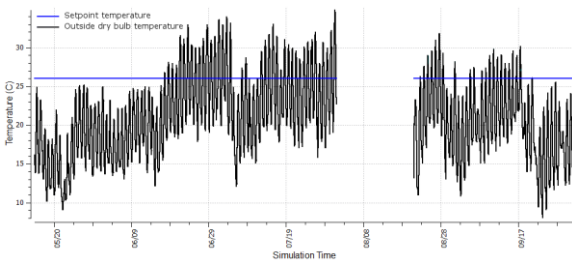


Fig. 11 – Outdoor dry bulb temperature (from IGDG climate data) compared to internal set point temperature

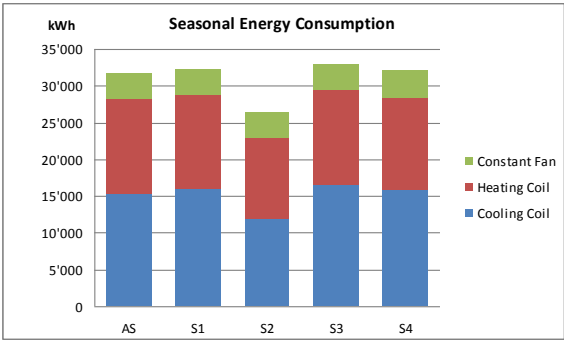


Fig. 12 – Energy consumption over standard cooling season (15th May - 30th September, IGDG weather data)

Now the reduced design air flow rate of 4850 m³/h is assumed, strictly meeting the minimum renewal requirements. Of course energy consumption is cut down and, with reference to the starting point of the actual situation, the savings are even greater, up to a maximum of 59.6% for the combined proposal in the warm week period (fig. 13 and table 4). Similar results are obtained over the standard cooling season (Fig. 14).

If the AHU works with a reduced air flow rate, more attention should be paid to the regulation of diffusers in the classrooms so that the inlet air jet at a lower temperature does not cause conditions of local discomfort for the occupants.

	AS	SOLUTIONS				
		NSP	S2R	S3R	S4R	CR
IGDG	7'533 kWh	45.4	54.4	51.8	47.2	59.6

Table 4 – Energy saving (%) for solution proposals respect to global consumption of the actual situation (AS) over the same week, but with the reduced total air flow rate (4'850 m³/h)

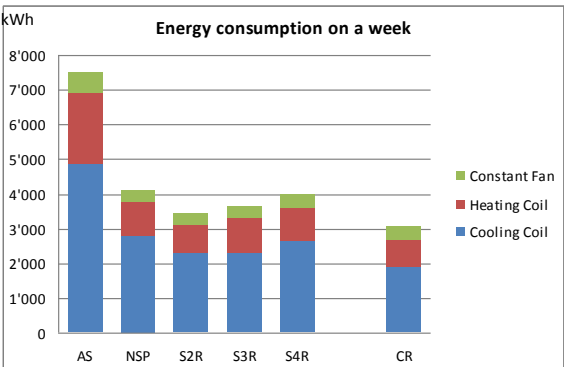


Fig. 13 – Energy consumption on a warm week with reduced total air flow rate (25th June - 1st July, IGDG weather data)

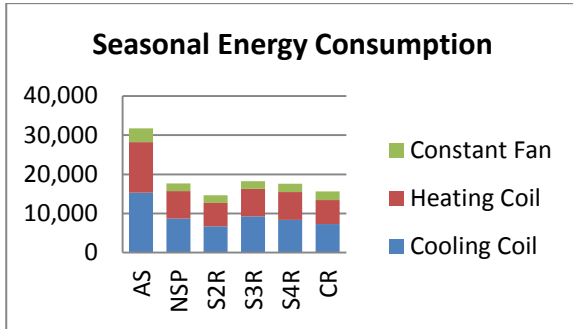


Fig. 14 – Energy consumption over standard cooling season with reduced total air flow rate (15th May - 30th September, IGDG weather data)

5.1 Comfort conditions

The actual configuration of the HVAC system can achieve comfort conditions in both classrooms only when they have the same occupancy level, because of the single heating coil controlled by the common return air temperature. However, a different number of students is very often present in the two classrooms, especially in the summer period. Fig. 14 shows that different occupancy levels (100% in TA05, and 10% in TA06) give mean air temperature differences between the two zones higher than 2 °C, and produce little discomfort in both classrooms.

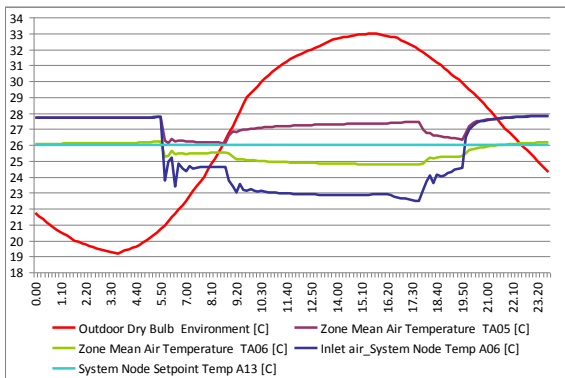


Fig. 15 - Trend of temperatures in a typical warm day when asymmetric occupancy occurs, for HVAC system in actual configuration

The replacement of the AHU fan could bring about energy savings, but would not improve HVAC system performance in terms of internal comfort when an asymmetric occupancy occurs. Instead, the HVAC configuration with the two separated post-heating coils would be able to ensure comfort conditions even for asymmetric occupancy levels. Fig. 15 shows that the same

previous different occupancy levels (100% in TA05, and 10% in TA06) are now correctly obtained.

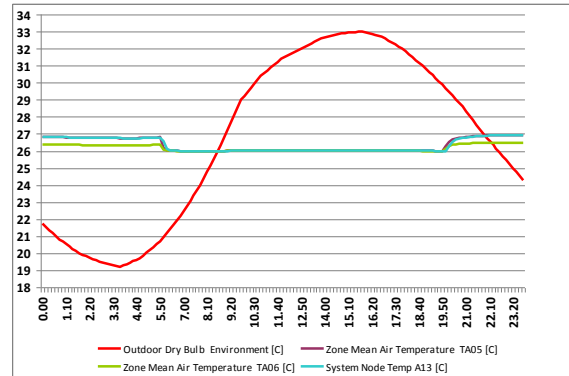


Fig. 16 – Trend of temperatures in a typical warm day when asymmetric occupancy occurs, for HVAC system configuration with split heating coils

6. Conclusion

Dynamic simulations software are very important tools for the energy analysis building-plant systems not only in design process but also in management decision for improve energy saving in existing buildings.

In the case study of a typical HVAC plant designed for hygrothermal and air quality control in university classrooms located in Bologna, energy simulations gave important information for the best setting of the air handling unit and for the evaluation of energy efficient solutions. Energy saving solutions must be evaluated depending on the effective external climatic conditions and daily scheduling of HVAC system.

Problems of the existing plant are related to excessive air renovation causing high energy consumptions and a lack of control of internal temperature of two classrooms treated as a single zone, creating discomfort when different occupancy of two rooms occurs.

The main and simplest solution is to increase the recirculating air flow rate (as for S1 and S3 solutions) that is an efficient strategy only if it is directed to reduce cooling loads. While in warmer summer periods this solution gives high energy savings (25%), no advantages are present in a seasonal analysis.

Other solutions analysed are the increasing of the cooling coil dew point temperature (controlling the

internal humidity) and reducing the volume total flow rate. Combining all those solutions, simulation results indicate up to 60% energy savings for a typical summer week in Bologna and 53% for a seasonal cooling period.

Further improvements can be achieved with a variable cooling coil dew point temperature

controlled by the measurements of the internal relative humidity.

References

UNI 10339, 1995: Impianti aeraulici per il benessere: Generalità, classificazione e requisiti EERE Energy Plus

An open access tool for building energy audits harmonizing European standards

Daniele Testi – DESTEC, University of Pisa, Italy

Elena Menchetti – Energy Manager Office, University of Pisa, Italy

Eva Schito – DESTEC, University of Pisa, Italy

Walter Grassi – DESTEC, University of Pisa, Italy

Abstract

SEAS (Simplified Energy Auditing Software) is an open access tool for energy audits of residential and office buildings, developed by the University of Pisa (Department of Energy, Systems, Territory, and Construction Engineering), in collaboration with ENEA (Italian National Agency for New Technologies, Energy, and Sustainable Economic Development), funded by the Italian Ministry of Economic Development. The analyzed services are: winter heating by hydronic systems, production of domestic hot water, and lighting and other electrical uses. Production of heat and electricity by renewable energy sources (solar thermal, photovoltaic, biomass heat generators, and heat pumps) is also calculated. The application assesses the different energy flows contributing to the energy balance of the building system on a monthly basis. The calculation methods are based on Italian and European technical standards, properly modified to take into account daily schedules of building usage. The tool has been developed with the intention of spreading energy auditing activities, thanks to the definition of a unified and inexpensive procedure, comprising the economic evaluation of retrofit actions by means of common investment metrics. All the worksheets are freely accessible to energy auditors, together with technical and user manuals (in Italian). Local Governments are expected to promote the use of SEAS, as part of their energy efficiency strategies. As for the reliability of energy calculations, they have been double-validated by both dynamic simulation results (tests have been run on TRNSYS 17) and comparison with actual energy billings. Two test cases are presented: a unit of a duplex house and a historical educational building, with classrooms and offices.

1. Introduction

As recognized by Directive 2010/31/EU, buildings account for 40% of total energy consumption in the European Union and the sector is expanding. Building energy audits are a necessary step towards the application of effective energy reduction measures in the Union.

As pointed out by Thumann and Younger, 2008, a single definition of “energy audit” is not available; its scope, the complexity of the calculations and of the employed energy models, and the level of detail of cost-benefit evaluations to be performed are all issues that each individual auditor can handle differently and that should be defined prior to starting any activity.

In any case, the goal of every building energy auditing process is to identify where energy is generated and exchanged between the zone under exam and its surroundings, considering the actual activities of the users in the building and how the energy systems are run. Besides, an integral part of each audit is to identify opportunities and provide recommendations of actions to be implemented for improving the overall energy performance of the building.

In order to avoid expensive on-site measurement and monitoring periods, the energy models on which the predictions of yearly thermal and electrical energy needs are based should be accurate and reliable, possibly validated by a documented history of energy vectors consumption.

In the present paper, a novel open access tool of building energy simulation specifically tailored to

energy audits is presented, together with two applications to existing buildings.

2. Description of the simulation tool and how to use it for an energy audit

SEAS (Simplified Energy Auditing Software) has been developed by DESTEC (Department of Energy, Systems, Territory, and Construction Engineering) of the University of Pisa, in collaboration with UTEE (Energy Efficiency Technical Unit) of ENEA (Italian National Agency for New Technologies, Energy, and Sustainable Economic Development). It analyzes hydronic heating, DHW (Domestic Hot Water) production, and electrical energy demands in residential and office buildings.

The energy simulation model is quasi-stationary, meaning that bihourly and weekly profiles in terms of presence and activities of the users (i.e., manual openings of the windows, use of the shutters) have to be added to obtain weighted averages for energy balances on a monthly basis. Attenuation of the internal set-point temperature as well as intermittent heating are also taken into account.

The architecture of the software – developed in a Microsoft Excel 2010 environment, making extensive use of Visual Basic macros – consists of a long series of worksheets included in a single file. Every worksheet has input fields and related intermediate results. For each input, the source and the level of uncertainty of the added value must be specified in order to filter the reliable fields and focus on the uncertain data for the subsequent tuning process, which will be described afterwards.

The main sections are listed below, in the same order they appear on SEAS:

- climatic data and internal set-points;
- occupancy and activities profiles;
- DHW uses;
- household and office electrical appliances;
- artificial lighting use;
- other non-electric internal loads;
- opaque envelope walls;

- windows;
- natural ventilation;
- ground-exchanging envelope elements;
- thermal bridges;
- building thermal capacity;
- building envelope monthly energy balance;
- scheme of the heating, DHW, and electrical systems;
- heat emission subsystem;
- heating system control;
- heat distribution subsystem;
- DHW distribution subsystem;
- storage subsystems;
- heat recoveries;
- solar thermal generation;
- heating and DHW generators (traditional boilers, biomass heat generators, electrical and absorption heat pumps, heat exchangers from district heating networks);
- photovoltaic system;
- estimated monthly uses of each energy vector for heating and DHW production;
- records of electrical and thermal energy and domestic water billings;
- comparison between energy billings and primary energy calculations.

The heat generators should be added in their order of priority, so that back-up generators are activated only when the power of the previous ones is not enough to fulfill the monthly thermal loads.

The building envelope monthly energy balance is the result of the following contributions:

- heat transmission through opaque elements towards external air, sky, unheated spaces, adjacent buildings, and ground;
- heat transmission through windows and external doors;
- heat transmission through thermal bridges;
- energy losses due to ventilation openings and infiltration cracks;
- internal gains from the electrical and lighting system, from occupants, and from other sources (e.g., cooking activities, stoves, fireplace);

- solar gains through opaque elements;
- solar gains through windows.

The dynamic response of the building is taken into account only by means of a monthly utilization factor for heat gains. In the case of intermittent or attenuated heating, an energy reduction factor is also employed. Both factors are calculated in accordance with ISO 13790:2008.

The entire calculation procedure, which attempts to harmonize a large number of Italian and European technical standards dealing with the topics covered by SEAS, is fully described in Conti et al., 2011.

Once the first energy calculation iteration is completed, deviations from actual energy billings can be reduced by reasonably adjusting the input data labeled with the highest uncertainty level. This tuning process ends when the discrepancies become acceptable. This phase is critical for the overall success of the auditing activity, as reliable subsequent cost-benefit analyses greatly depend on accurate estimates of energy consumptions.

The next SEAS-supported stage of the energy audit is the simulation of retrofit actions on the building envelope and on the heating, DHW production, and electrical systems, including possible use of renewable sources. The auditor identifies possible solutions and SEAS updates the energy consumptions. Besides, costs of the investments and other economic parameters are added (e.g., current and forecasted prices of energy vectors, discount rate, incentives for energy efficiency). Each measure is evaluated in terms of simple and discounted payback periods, NPV (Net Present Value), and PI (Profitability Index). Hence, the auditor completes its tasks, by recommending the most effective actions to the client, in terms of energy savings and economic investment.

3. Validation of seas: presentation of two test cases

3.1 Test Case 1: Historical Educational Building

Two SEAS-supported energy audits have been performed for validation purposes. The first

analyzed case is a historical educational building, property of the University of Pisa, having both classrooms and office spaces. This four-story building (gross volume: 4,370 m³) is located in the historical centre of Pisa and is bordered on the south by another university building and north with private buildings, while to the west and east there are two central streets of the city.

Natural gas and electricity billings are available for the past 4 years of the building's usage. The billing of electricity is shared with the adjacent building, where similar activities take place in classrooms and offices. It has been decided to divide the total electrical energy consumption proportionally to the buildings' gross volumes; this represents a critical assumption of the analysis.

The most uncertain input provided to the simulation tool is the presence profile of students in classrooms, also related to windows' opening and to the use of artificial lighting and other electrical equipment. Thus, the tuning process described in the previous section has been performed on these parameters.

Table 1 shows the comparison between average yearly consumption of electricity and natural gas – documented by the available billings – and SEAS estimates for the same energy vectors.

ENERGY VECTOR	BILLINGS	SEAS ESTIMATES	DEVI-ATION
Electricity	103.8 MWh/yr	95.5 MWh/yr	-8.0%
Natural gas	55.9 MWh/yr	56.8 MWh/yr	1.5%

Table 1 – Yearly consumption of energy vectors: billings vs. SEAS evaluations for Test Case 1

A DHW production and distribution system is not present, so natural gas is employed only for heating classrooms and offices. Thermal energy calculations are in satisfactory agreement with the billings. On the other hand, electrical energy consumption is underestimated, probably due to the above-mentioned splitting operation on electricity billings, which can be quite inaccurate, especially considering the presence of food and beverage vending machines only in the other building.

Table 2 reports the heating season energy balance of the building envelope. The main terms are heat losses through opaque walls and windows. A very large contribution is also given by internal gains, due to the intense use of the building during working hours.

ENERGY CONTRIBUTION	ESTIMATED VALUE
Heat losses through opaque walls (except for ground-facing elements) : $Q_{tr,o}$	-40.15 MWh
Heat losses through windows: $Q_{tr,w}$	-13.88 MWh
Heat losses via thermal bridges: $Q_{tr,tb}$	-1.03 MWh
Heat losses through ground-facing elements: $Q_{tr,g}$	-7.58 MWh
Air infiltration losses: Q_{inf}	-1.40 MWh
Natural ventilation losses: Q_{ve}	-3.28 MWh
Electrical internal gains: $Q_{int,el}$	7.87 MWh
Other internal gains: $Q_{int,ot}$	11.92 MWh
Solar gains from opaque walls: $Q_{sol,o}$	3.28 MWh
Solar gains from windows: $Q_{sol,w}$	5.93 MWh
Heating demand (from energy balance) : $Q_{H,nd}$	-38.32 MWh

Table 2 – Energy balance according to SEAS (heating season) for Test Case 1

As for the retrofit actions, it has to be remarked that the external envelope, as well as other building elements, cannot be modified due to the historical and artistic value of the construction. This notwithstanding, three recommendations have been given:

- thermal insulation of the garret (220 m²), with reduction of horizontal wall thermal transmittance from 1.60 to 0.32 W/(m²K); natural gas savings of 5.7% can be achieved and the calculated discounted payback period is 22 years (discount rate: 2%, lifespan of the structural solution: 50 years, NPV=7530 €, PI=1.8);
- installation of thermostatic valves on radiators and addition of a climatic control module on the heat generator; the efficiency of the heating control system increases from 93% to 97% and natural gas savings of 2.7% can be obtained (discounted payback period: 11 years,

lifespan of the control actuators: 15 years, NPV=550 €, PI=1.5);

- substitution of the existing traditional boiler with a biomass generator of reduced power (from 128 kW to 80 kW, lifespan: 15 years) and installation of an inertial storage tank; in spite of an 8.4% increase of heating energy consumption due to the lower efficiency of the biomass boiler, the discounted payback period is only 4 years, owing to the very low cost of biomasses, compared to natural gas (0.03 against 0.08 €/kWh), NPV=31200 €, PI=4.9.

The performed analysis shows that the latter recommendation leads to the best economic investment.

3.2 Test Case 2: Residential Unit of a Duplex House

The second energy audit was performed on a two-story residential unit (95.6 m²) of a duplex house built in the eighties and located in the town of Camaiore, Province of Lucca. The longer side of the building lies on the northeast-southwest direction. The zone under analysis is bordered on the northwest side with another house of similar size and thermo-structural characteristics, mostly unoccupied in winter and kept at a set-point temperature of 15°C. Another building, located in the northeast, screens the wall on that side to direct and diffuse solar gains and to long-wave radiation towards the sky. All the other external walls are unscreened.

The heating and DHW production systems have been recently retrofitted (in 2007), with the installation of a condensing boiler, thermostatic valves on all the radiators, two solar thermal collectors (dedicated to DHW production), and an inertial storage tank. The energy vector for producing thermal energy is LPG (Liquefied Petroleum Gas), due to lack of connection to the natural gas urban distribution network.

Building usage profiles obtained from interviews of the occupants, data recovered from design documents and technical sheets, and all the parameters recorded during the building

inspection have been inserted in the appropriate input worksheets of SEAS.

The tuning procedure has been performed on the following inputs:

- shutters utilization profiles;
- ventilation openings profiles;
- fireplace usage.

Electricity and LPG billings are available from 2009 to 2011. Table 3 shows the very good agreement between average yearly consumption of electricity and LPG and SEAS results.

ENERGY VECTOR	BILLINGS	SEAS ESTIMATES	DEVIATION
Electricity	2490 kWh/yr	2394 kWh/yr	-3.9%
LPG	8076 kWh/yr	7900 kWh/yr	-2.2%

Table 3 – Yearly consumption of energy vectors: billings vs. SEAS evaluations for Test Case 2

ENERGY CONTRIBUTION	ESTIMATED VALUE
Heat losses through opaque walls (except for ground-facing elements): Q_{tr_o}	-7103 kWh
Heat losses through windows: Q_{tr_w}	-1077 kWh
Heat losses via thermal bridges: $Q_{tr_{tb}}$	-507 kWh
Heat losses through ground-facing elements: Q_{tr_g}	-739 kWh
Natural ventilation and air infiltration losses: $Q_{ve}+Q_{inf}$	-797 kWh
Internal gains: Q_{int}	2406 kWh
Solar gains from opaque walls: Q_{sol_o}	1723 kWh
Solar gains from windows: Q_{sol_w}	675 kWh
Heating demand (from energy balance): $Q_{H_{nd}}$	-5418 kWh

Table 4 – Energy balance according to SEAS (heating season) for Test Case 2

Table 4 illustrates the heating season energy balance of the building envelope. As in Test Case 1, the main energy flow is heat transmission through opaque walls. Internal and solar gains (especially from opaque walls, owing to their high thermal transmittance) are also important contributions.

As far as DHW production is concerned, Table 5 shows the monthly fraction (f) of total load

supplied by the solar thermal system (SEAS implements the f -chart method described by Duffie and Beckman, 1991) and the residual energy to be generated by the boiler.

MONTH	F value	RESIDUAL ENERGY
January	0.30	132.3 kWh
February	0.43	98.4 kWh
March	0.77	38.9 kWh
April	0.91	7.9 kWh
May	1.00	0.00 kWh
June	1.00	0.00 kWh
July	1.00	0.00 kWh
August	0.97	0.00 kWh
September	0.99	0.00 kWh
October	0.74	43.1 kWh
November	0.33	125.3 kWh
December	0.19	142.9 kWh
Whole year	0.71	588.8 kWh

Table 5 – DHW production and solar thermal system: monthly f values and residual thermal energy for the boiler

As in Test Case 1, three retrofit actions are simulated and recommended:

- insulation of the roof (55.8 m²), with reduction of thermal transmittance from 1.46 to 0.32 W/(m²K); LPG savings of 24.9%, discounted payback period of 32 years (discount rate: 2%, lifespan of the solution: 50 years), NPV=7160 €, PI=1.4 (a grant from the Italian Government covering 55% of investments in energy efficiency is assumed to be obtained);
- installation of a climatic control module on the boiler; LPG savings of 2.7%, discounted payback period of 6 years (lifespan of the control actuator: 15 years), NPV=377 €, PI=2.5;
- installation of a photovoltaic system on the roof (electrical peak power: 2 kW, total area of the modules: 13.2 m²) and access to dedicated national incentives; yearly electrical energy production of 2410 kWh, discounted payback period of 15 years (lifespan of the photovoltaic modules: 25 years), NPV=5110 €, PI=1.4.

According to SEAS results, in spite of different initial investments and estimated payback periods, all the three proposed measures are profitable.

3.3 Test Case 2: Validation by Dynamic Simulations

The accordance between SEAS evaluations of energy vectors demands and actual energy billings on a yearly basis for the two presented test cases is not sufficient to conclude that SEAS is able to accurately predict every term of the energy balance. In order to exclude that positive and negative contributions conveniently cancel each other, a dynamic simulation of Test Case 2 has been executed on the software TRNSYS 17.

Hourly climatic data (temperature, solar irradiation, wind) of all the Italian provinces have been recently made available by CTI (Italian Committee of Thermotechnics). Thus, the typical meteorological year of the Province of Lucca has been used as an input of the building envelope dynamic simulation. The same correlation between external air temperature and sky temperature used in SEAS (and based on ISO 13791:2012) has been implemented in TRNSYS.

Two central winter months (January and February) have been simulated. Energy balances obtained by SEAS and TRNSYS are shown in Table 6. With respect to Table 4, some terms had to be aggregated for comparison purposes, as TRNSYS calculates the net heat flux through an opaque wall, superimposing heat losses to solar gains.

ENERGY CONTRIBUTION	ESTIMATED VALUE according to seas	ESTIMATED VALUE according to TRNSYS
$Q_{tr,o}+Q_{tr,w}+Q_{tr,tb}+Q_{tr,g}+Q_{sol,o}$	-3542 kWh	-3961 kWh
$Q_{ve}+Q_{inf}$	-357 kWh	-379 kWh
Q_{int}	913 kWh	861 kWh
$Q_{sol,w}$	271 kWh	486 kWh
$Q_{H,nd}$	-2715 kWh	-2992 kWh

Table 6 – SEAS vs. TRNSYS energy balances (January and February)

As expected, deviations of ventilation losses and internal gains estimates are very small (5.8% and

6.0%, respectively), since the same bihourly profiles of occupants conduct have been entered in both codes. Predictions of solar gains from windows disagree (44.2% deviation); specifically, they are overestimated by TRNSYS, in which the extensive usage of shutters during daylight hours and the presence of external obstructions have not been simulated, for the sake of simplifying the building model, as far as resistive envelope components have been concerned. As for net transmission losses, which represent the larger contribution to the building envelope energy balance, the origin of the observed discrepancies (10.6%) can be explained by analyzing the energy fluxes passing through each external component, as reported in Table 7. In particular, it has to be remarked that physical models of heat transfer through opaque walls are very different for the two codes:

- SEAS uses a quasi-stationary balance of the thermal zone, a single node where all the parameters are lumped, including heat capacity;
- TRNSYS calculates, for each wall, the time evolution of the temperature field across its thickness and also takes into account long-wave radiation heat exchanges between the internally-facing elements of the analyzed space; on the other hand, thermal bridges have to be simulated by properly increasing wall thermal transmittances.

Hence, acceptable agreement between SEAS and TRNSYS net transmission losses seasonal estimates represents an important verification of the reliability of the simplified methodology implemented by SEAS.

Figure 1 illustrates the evolution of internal and external air temperatures, sky temperature, and imposed set-point temperature profile (decreased during the night from 17°C to 16°C), according to the TRNSYS dynamic simulation. Apart from short overheating and overcooling phases, the internal air temperature remains within the target values of the control system.

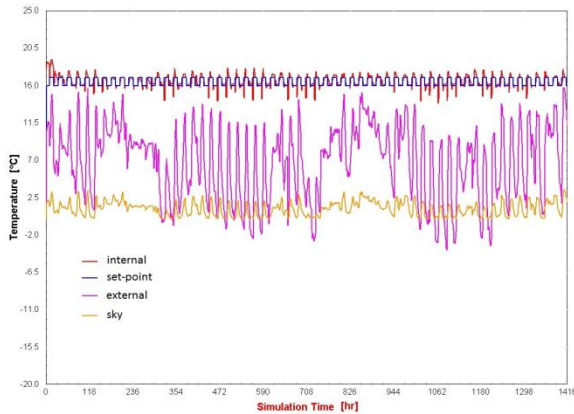


Fig. 1 – Evolution of internal and external air, sky, and set-point temperatures, according to TRNSYS

EXTERNAL WALL	seas ESTIMATE	TRNSYS ESTIMATE
Roof (55.8 m ²)	-1024 kWh	-1576 kWh
Floor (51.1 m ²)	-379 kWh	-303 kWh
North-East opaque wall (18.8 m ²)	-524 kWh	-501 kWh
South-East opaque wall (32.5 m ²)	-502 kWh	-610 kWh
South-West opaque wall (14.0 m ²)	-185 kWh	-193 kWh
North-West opaque wall (7.0 m ²)	-95 kWh	-160 kWh
Wall separating the two units of the duplex house (39.3 m ²)	-107 kWh	-135 kWh
South-East windows (6.8 m ²)	-355 kWh	-350 kWh
South-West windows (2.6 m ²)	-136 kWh	-133 kWh
Thermal bridges	-235 kWh	n/a
Total energy flux through external walls	-3542 kWh	-3961 kWh

Table 7 – SEAS vs. TRNSYS energy fluxes through each external component (January and February)

The element giving the largest deviation between SEAS and TRNSYS results is the roof. This is coherent with the more accurate TRNSYS building physical model. In fact, in winter, the roof is particularly cold, even on the internal side, not only because of its low conductance, but also due to low solar gains and high long-wave thermal radiation towards the sky. All the other opaque

elements of the room – which are warmer – transfer heat to the roof, causing increased transmission losses. Therefore, SEAS, using a simplified model that does not take into account heat exchange between internal surfaces, tends to underestimate these losses. On the other hand, the floor is warmer than the other external walls, due to the higher temperature of the ground, with respect to external air. Thus, for the same reasons explained above for the roof and taking care of changing the sign of heat fluxes, SEAS tends to overestimate transmission losses towards the ground.

Figure 2 reports the temperature evolution of the external face of the roof obtained by TRNSYS dynamic simulation, showing values always higher than the sky temperature, but generally lower than the external air temperature.

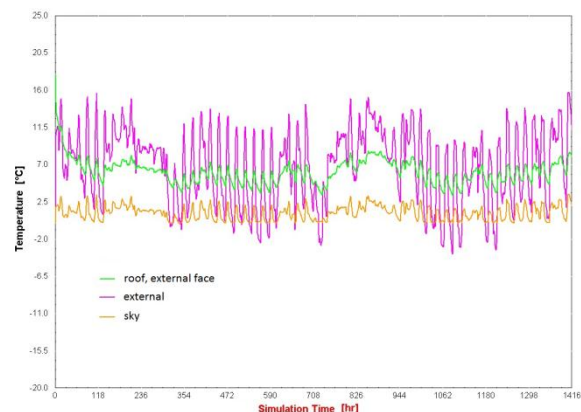


Fig. 2 – Evolution of roof (external face), external air, and sky temperatures according to TRNSYS

In spite of the observed differences between SEAS and TRNSYS estimates of energy flows through single external envelope elements, a satisfactory agreement of the total transmitted energy – as well as of the other terms involved in the building energy balance – is reached, indicating that SEAS predictions are consistent not only with energy billings, but also with overall dynamic simulation results.

4. Conclusion

The presented energy auditing software, intended to be open, flexible, and user-friendly, has proven to be suitable for accurately assessing the electrical and thermal energy flows in residential and office buildings and in hydronic heating systems. Consequently, SEAS can evaluate energy and economic savings introduced by possible retrofit actions.

The calculation procedure makes use of the most recent technical standards, performing small integrations and modifications intended to optimally simulate real usage of the building envelope and systems. Besides, the energy auditor can modify climatic data and other standard input parameters, in order to increase the accuracy of energy consumption predictions.

Like every new tool, SEAS will have to be monitored and periodically updated. Further validation of energy estimates is in sight, to be performed on other test cases and exploring different types of buildings and systems.

5. Acknowledgement

The funding of the Italian Ministry of Economic Development and the collaboration of ENEA is gratefully acknowledged, particularly for the fruitful discussions with Ing. Paolo Signoretti and Arch. Gaetano Fasano of the ENEA Energy Efficiency Technical Unit. The technical support of Ing. Paolo Conti and Ing. Davide Della Vista (DESTEC, University of Pisa) during the

development phase of SEAS is thankfully acknowledged as well.

References

- Conti, P., Della Vista, D., Fantozzi, F., Fasano, G., Grassi, W., Manetti, R., Menchetti, E., Schito, E., Signoretti, P., Testi, D. 2011. Definizione di una Metodologia per l'Audit Energetico negli Edifici ad Uso Residenziale e Terziario, Ricerca di Sistema Elettrico, Report RdS/2011/143, 178 pp.
- Duffie, J.A., Beckman, W.A. 1991. Solar Engineering of Thermal Processes, 2nd Edition, John Wiley & Sons, New York, USA.
- European Parliament and Council of the European Union. 2010. Directive 2010/31/EU on the Energy Performance of Buildings (Recast), Official Journal of the European Union.
- International Organization for Standardization. 2008. ISO 13790:2008 – Energy Performance of Buildings – Calculation of Energy Use for Space Heating and Cooling. ISO Standards Catalogue.
- International Organization for Standardization. 2012. ISO 13791:2012 – Thermal Performance of Buildings – Calculation of Internal Temperatures of a Room in Summer without Mechanical Cooling – General Criteria and Validation Procedures. ISO Standards Catalogue.
- Thumann, A., Younger, W.J. 2008. Handbook of Energy Audits, 7th Edition, The Fairmont Press, Lilburn, GA, USA.

Energy performance of shading devices for thermal and lighting comfort in offices

Anna Maria Atzeri – Free University of Bozen-Bolzano, Bolzano, Italy
Giovanni Pernigotto – University of Padova, Vicenza, Italy
Francesca Cappelletti – University IUAV of Venezia, Venezia, Italy
Andrea Gasparella – Free University of Bozen-Bolzano, Bolzano, Italy
Athanasios Tzempelikos – Purdue University, West Lafayette, Indiana (USA)

Abstract

In this paper, the effect of the windows shading systems both on visual and thermal comfort and on the total building energy needs (for heating, cooling and artificial lighting) has been analysed. An open-space office module with different window characteristics has been simulated with EnergyPlus 7.1, controlling the internal conditions with appropriate comfort setpoints. Different window distributions (on a single façade or on opposite façades), and two orientations have been analysed, varying the glazed area and the glazing type. Two moveable shading systems have been considered (roller shades and venetian blinds), controlled by two setpoint variables: the glare index and the total solar radiation incident on the windows.

1. Introduction

The office building category is often characterized by an extensive use of glazing façades. The presence of large transparent components and the application of shading devices have usually been the object of analysis because solar gain values can largely influence the building thermal energy balance both in summer and winter, the lighting energy demand and both the thermal and visual comfort. Some authors have compared the influence of different kinds of glazing and shades on the heating and cooling energy needs in office buildings with a parametrical approach in order to evaluate different opaque envelope composition, floor shape ratio, windows area (Eskin and Türkmen, 2008; Shen and Tzempelikos, 2012a; Shen and Tzempelikos, 2012b;

Zhu *et al.*, 2013). Tsikaloudaki *et al.* (2012) carried out a similar analysis on a residential building and proposed some correlations.

Some studies focus on the assessment of the thermal and visual efficiency of different shading devices (David *et al.*, 2011 Kuhn, 2006). David *et al.* (2011), calculated by means of dynamic simulations, and evaluate their relation with the solar shading coefficient, cooling energy demand, daylight autonomy and sun patch index on work plane. Tzempelikos *et al.* (2010) introduced a transient thermal comfort model to investigate separately the impact of different shades and three kinds of glazing on mean radiant temperature, operative temperature, thermal discomfort index, radiant asymmetry, and daily heating needs for a perimeter office with a high window area. Two representative days for winter conditions in Montreal (Canada) have been taken into consideration.

The relation between the use of shading devices and availability of natural light was investigated by Kim *et al.* (2012) who suggest that optimal shading systems should increase daylight levels while controlling the amount of excessive sunlight.

The effect of different shading devices has been often analysed considering different control strategies in order to optimize the visual comfort and minimizing the artificial lighting demand (Ihm *et al.*, 2011; Mahdavi and Dervishi, 2011; Correia da Silva *et al.*, 2012; Oh *et al.*, 2012). Moreover, some authors optimized the selection of the window size and of the properties of shades with reference to the heating, cooling and lighting energy performance

considering different control strategies (Tzempelikos and Athienitis, 2007).

In general, all the literature on solar shading devices is oriented to the evaluation of the strategies for the daylight harvesting in order to reduce lighting consumption, for the cooling or heating energy saving and for the indoor thermal comfort, but only a few authors analyse all these aspects together (Nielsen et al., 2011). By means of dynamic simulation, they calculate the energy demand and the daylight level of a single office comparing different situations of shading (none, fixed, dynamic), modifying some variables such as the orientation and the size of windows. They also imposed an internal setpoint for heating/cooling and air flow rates for mechanical ventilation coherent with the comfort conditions of class II in the Standard EN ISO 15251:2007 (CEN, 2007).

Also, Poirazis *et al.* (2008) used a comfort setpoint strategy for temperature and lighting. A minimum acceptable level for thermal comfort satisfaction was defined.

Finally, Ochoa *et al.* (2012) compared multi-objective optimization criteria for low energy consumption and high visual criteria. Frontini and Kuhn (2012) proposed a new method to evaluate the impact on mean radiant temperature in office spaces of four different internal blinds combined with four kinds of glazing and considering an on-off strategy during two typical days for winter and two for summer.

In this paper, the effect of the windows shading systems both on visual and thermal comfort and on the total building energy needs (for heating, cooling and artificial lighting) of an open office module has been analysed. The thermal comfort has been controlled by fixing the operative temperature setpoint consistent with the comfort conditions of class II of EN ISO 15251:2007. The visual comfort requirements have been taken into account by fixing a maximum limit value for the glare index and a minimum illuminance level to be met through the shading system control and artificial lighting integration.

The windows have been distributed on a single façade or on opposite façades, and the room oriented towards 2 different orientations, varying the glazed area (2 sizes) and the glazing systems (4 types).

Three different moveable shading systems have been compared (two kinds of venetian blinds and roller shades), controlled by two criteria – the glare index and the total solar radiation incident on the windows.

One locality in southern Europe (Rome) has been selected for the investigation. The comfort indexes have been calculated for each hour of occupation of the whole year assuming two seasons as regards the setpoint conditions and clothing level. The evaluation of the long-term comfort conditions (on seasonal basis) has been conducted by computing the hourly value of the Predicted Mean Vote index in 9 different positions in the office and considering some statistical indicators of distribution (the median, minimum, maximum and the interquartile range). The energy performance for heating, cooling and lighting of the different solutions has been compared accounting for comfort considerations. Energetic, comfort and lighting simulations have been carried out with EnergyPlus 7.1.

2. Simulation assumptions

2.1 Office model

The model is an open office space of 100 m² of floor area and 3 m of interior height. Vertical walls and roof are exposed to the outdoor environment. The floor is considered as adiabatic, assuming that it is located above a zone with the same indoor thermal conditions.

The composition of all the opaque elements, both vertical walls and roof slab, is identical, with a clay block internal layer 20 cm thick and an external insulation layer 5 cm thick and a thermal transmittance of 0.45 W m⁻² K⁻¹.

The solar absorptance coefficients have been set to 0.6 for the floor (internal side) and 0.3 for the vertical walls and the roof (both sides). The wall emissivity is 0.9, both for the internal and the external side.

The considered venetian blinds have a high and low reflectivity. A roller shade with 0.4 solar transmittance was evaluated as an intermediate solution between the alone glazing system and the null transmittance of venetian blind, preserving the occupants clear vision of large objects outside. A full

factorial parametrical analysis has been performed by varying the parameters as summarized in Table 1.

Factor	Values
Location	Rome: Lat. N 42° 54' 39'' Heating Degree-Days HDD ₁₈ : 1420 K d Cooling Degree-Days CDD ₁₈ : 827 K d
Glazings	DH: Double Glazings with high SHGC $U_{gl} = 1.140 \text{ W m}^{-2} \text{ K}^{-1}$; SHGC = 0.608; $\tau_d = 0.439$ DL: Double glazing with low SHGC $U_{gl} = 1.099 \text{ W m}^{-2} \text{ K}^{-1}$; SHGC = 0.352; $\tau_d = 0.205$ TH: Triple Glazings with high SHGC $U_{gl} = 0.613 \text{ W m}^{-2} \text{ K}^{-1}$; SHGC = 0.575; $\tau_d = 0.391$ TL: Triple Glazings with low SHGC $U_{gl} = 0.602 \text{ W m}^{-2} \text{ K}^{-1}$; SHGC = 0.343; $\tau_d = 0.191$
Window Size	S1: width = 9; height = 1.5 m; area = 13.5 m ² S2: width = 9; height = 2.5 m; area = 22.5 m ²
Window distribution	East (E) East + West (E+W) South (S) South + North (S+N)
External shadings	WITHOUT SHADES (WO): - ROLLER SHADE (RS): Roller Shade; $\rho_s = 0.5$; $\tau_s = 0.4$ BLIND-H (BH): Venetian Blind with high reflectivity slats; $\rho_s = 0.8$ BLIND-L (BL): Venetian Blind with low reflectivity slats; $\rho_s = 0.2$

Table 1 – Variables set for the analysis

2.2 Internal gains and schedule

The office occupation period is from 8:00 am to 6:00 pm, Monday to Friday. According to the Italian Technical Standard UNI 10339:1995 (UNI, 1995) the occupancy index for an open office can be fixed at 0.12 people/m², which corresponds to 12 occupants.

The occupants' activity is defined as sedentary with a metabolic flux equal to 70 W m⁻² or 1.2 met. The heat flow is divided into the sensible portion of 75 W (58% as radiant exchange) and latent heat of 55 W.

The unit thermal resistance of clothing is 1 clo (such as typical work clothing with long trousers, shirt, tie and jacket) during the winter season, and 0.5 clo (such as lightweight summer trousers and a light

long-sleeved shirt during the summer). The conventional winter season is from 1st October to 31st March while the summer season is from 1st April to 30th September.

The considered Light Power Density (LPD) is 12 W m⁻², with T-8 fluorescent lamps installed on the ceiling.

The internal loads related to electrical equipment are quantified considering 12 computers, 12 monitors, a laser printer and a copier, with constant average power during the occupation period.

Lighting and Thermal comfort control

The lights are turned on only during occupation hours. A control system operates on the artificial lighting in such a way that the integration, and consequently the electric power required, increases or decreases continuously and linearly, depending on the level of illumination provided by natural light, in order to maintain 500 lux of illuminance level, as prescribed by EN ISO 12464-1:2002 (CEN, 2002).

In order to guarantee the visual comfort, the shading devices are closed in relation to the amount of incident radiation on the outdoor surface of the windows: when the total radiation overcomes 150 W m⁻² the shadings are closed. This setpoint value has been chosen considering that people do not usually shut the shades when solar radiation is below 50-60 W m⁻² while normally they need to close them above 250-300 W m⁻² (Inoue *et al.*, 1998; Farber Associates, 1992; Newsham, 1994; Reinhart and Voss, 2003). Venetian blinds tilt is also controlled in order to reject beam solar radiation. A second control criterion based on the DGI (Daylight Glare Index) is assumed. A DGI limit value of 22 for the position 2 (Figure 1) has been selected, which corresponds to a value of Unified Glare Rating (UGR) of 19 as required by the standard EN ISO 15251:2007 to ensure the comfort of light inside the confined spaces for office use.

The control strategy of the heating and cooling system ensures the compliance with the limits imposed by the EN ISO 15251:2007 or by the EN ISO 7730:2005 by imposing operative temperature conditions during the weekdays within 20°C to 24°C for winter and from 23° to 26°C for summer, which are the described ranges Category II or B respectively, for a normal level of expectation about

the conditions of comfort for users. A setpoint of 15 °C has been considered for the night-time and for weekends. Referring to the cooling setpoints during the unoccupied periods, the setpoint is equal to 38 °C until 6:00 am and then is gradually reduced to the occupational setpoint. To determine the variability of thermal and visual comfort conditions inside the office, a grid consisting of 9 points, each one at 0.8 m from the floor level was considered. For each of these points, specific indicators for the evaluation of thermal and lighting comfort were calculated.

Through the analysis of the spatial distribution of the indices of thermal and visual comfort, it is possible to estimate their variation both from a geometrical point of view, thus evaluating the uniformity of the environment, and over the time period considered.

Figure 1 represents the positions considered for the comfort analysis. For reasons of space, the point P5, located at the centre of square floor, and the points P2 (for South oriented) and P6 (for East oriented buildings), which are the most representative or critical positions have been analysed respectively for the thermal comfort and for the glare discomfort. The comfort conditions have been analysed only during the occupancy period.

2.3 Thermal and daylight simulation

EnergyPlus enables both thermal and daylighting simulation of complex glazing and moveable shading systems. Detailed evaluation of the system optical properties and heat balance considering the contribution of each layer is considered for the thermal balance. Daylight and glare analysis is performed through the calculation of proper hour daylight factors (daylight coefficients method) for the reference sky types which are then interpolated and used with the actual outside conditions.

3. Results and discussion

At the end of the paper the results of the thermal comfort analysis and of the energy simulations have been represented for the winter season (Figure 2) and for summer season (Figure 3). Figure 4 shows

the results concerning the indoor glaring and the corresponding energy needs for artificial lighting.

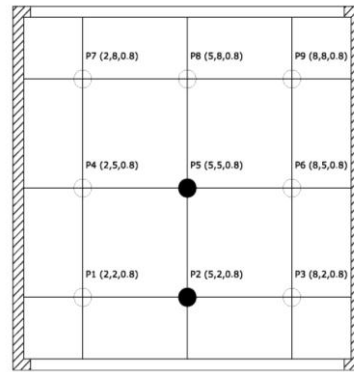


Figure 1 – Plan of the office model and occupants' positions for the PMV calculations (orientation South/North)

3.1 Indoor thermal comfort

In Figures 2a and 2c the distribution of the Predicted Mean Vote for small and large windows is plotted for the winter season. The upper lines represent the maximum values, the lower lines the minimum, the points in the middle the medians and the rectangular boxes the range between the first quartile and the third quartile of all the values calculated during the occupied hours. Because of the temperature control strategy, 75% of the PMV values remain, in all configurations, within the range ± 0.5 . Nevertheless the PMVs have a greater dispersion during the winter season. The application of the external shading devices reduces the variability of the comfort index.

The standard deviation between the PMV values of each hour over the 9 positions has been calculated and its maximum values during the occupied hours have been evaluated for each configuration.

The maximum standard deviations for the winter and summer seasons have been reported in Table 2 for the windows without shades (WO) and with the different kinds of shades analysed (roller shades/RS, high reflectivity/BH and low reflectivity/BL venetian blinds). It can be seen that the standard deviation never overcomes the value of 0.09 and it decreases when shading devices are used.

	WO	RS	BH	BL
Winter	0.081	0.049	0.036	0.019
Summer	0.089	0.054	0.047	0.030

Table 2 – Maximum standard deviations between the PMV values at the 9 positions all over the office

3.2 Heating and cooling energy use

During the winter season, both heating and cooling needs are present (Figure 2). The use of sun protection systems with the considered control strategy leads to increasing heating needs and decreasing cooling needs. Considering the smaller windows, almost for all the cases the increasing in heating needs overcomes the decreasing in cooling needs. In fact, the shading control results in a reduction of the contribution of solar gains without affecting night thermal losses. However for larger windows, the reduction of cooling needs due to shades overcome the increment of heating needs.

During the summer, heating energy needs are almost null (Figure 3). Shading devices are fundamental for the reduction of cooling needs and elimination of glare. For each shading device, size and kind of glazings, it can be seen that for the E and E/W orientations of windows the cooling energy needs are larger. Regarding the windows size, the larger the windows, the larger the cooling needs, but the increase is not the same in percentage for all the shading conditions: the increment is maximum for glazings without shades (from 107% to 23%) and it is minimum for the venetian blinds with low reflectivity (from 55% to 3%). Roller shades and blinds with high reflectivity have a similar behaviour even if the blinds give the lower energy needs.

Comparing the shaded cases to the ones without shading, the use of glazings with a high SHGC gets the largest advantages from the shading device. Considering the shading devices for the same glazing type, orientation and window size, it can be seen that the best performing shades are the venetian blinds with low reflectivity slats.

Lighting needs and Indoor visual comfort

The annual lighting energy needs have been plotted out computing the number of occupied hours for which the DGI exceeds the limit value of 22 (Figure 4). For reference, annually the hours of occupation are 2500.

Regarding the discomfort from glare associated with configurations without sunscreen, it can be noticed that, for the South or South/North orientation, the hours of glare discomfort are approximately in the range 760-600. This means that the occupants will

find themselves under conditions of visual stress for about 30% of their working time (Figures 4a and 4c). The use of blinds with slats at high or low reflectivity, reduces to zero (or near to zero) the hours of discomfort. As could be expected from the quite large solar transmittance, the roller shades do not allow to reach the same results, with even an increasing time of glare discomfort when considering window size S2 and E or E/W orientation. In general the sun protection systems, if adjusted depending on the amount of radiation incident and on the glare index, lead to an increase of artificial lighting needs. However, the control system set for the artificial lighting is usually able to reduce the consumption of electricity from 30% to 60% compared to a system switched on and off manually (Galasiu *et al.*, 2004).

Figure 5 suggests that although the use of shading devices results in an increase in primary energy demand for the winter season in each configuration, their use always leads to a reduction in total needs.

4. Conclusions

In this paper, different shading devices have been compared in relation to the energy needs for equivalent thermal comfort conditions and under an equivalent regulation setup for the glare control. The use of solar shading systems has resulted in an increase in final energy demand for artificial lighting, in the net energy demand for heating mostly in winter, a decrease in net energy demand for cooling during both summer and winter in all configurations. The primary energy need of each configuration allows to compare the overall performance of the different shading systems. The shading system which gives the lowest energy demand is strictly related to the orientation of the windows, to the windows size and position and to the glazing system to which it is coupled. It is quite difficult to generalize the results in terms of optimal configuration, but it is clear that for Rome's climatic conditions the shading devices are essential to contain the total primary energy demand and limit glare. Further investigations will be carried out on different roller shades, configurations and climatic context.

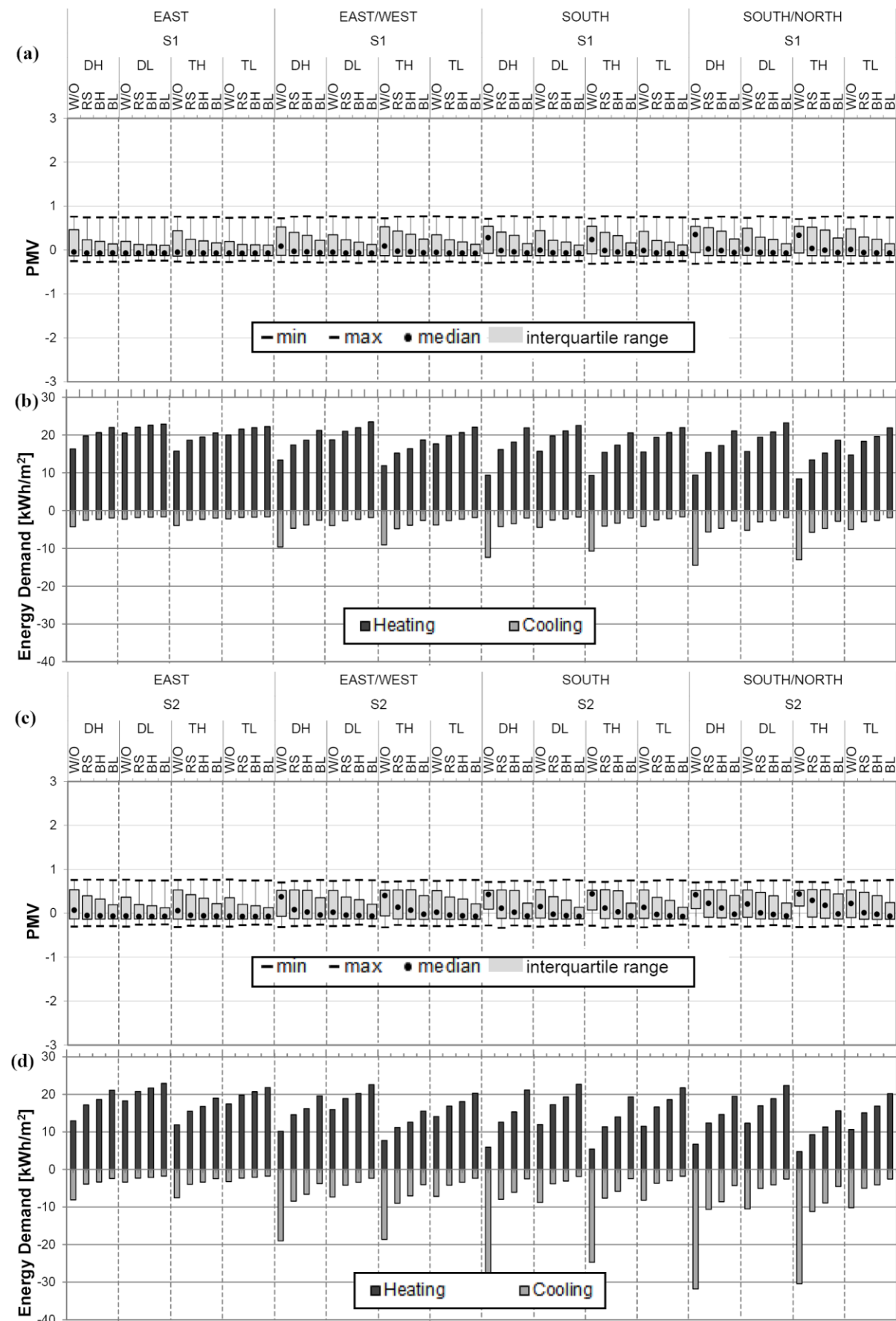


Figure 2 – Winter distributions of PMV for small (a) and large windows (c) and Energy needs for small (b) and large windows (d)

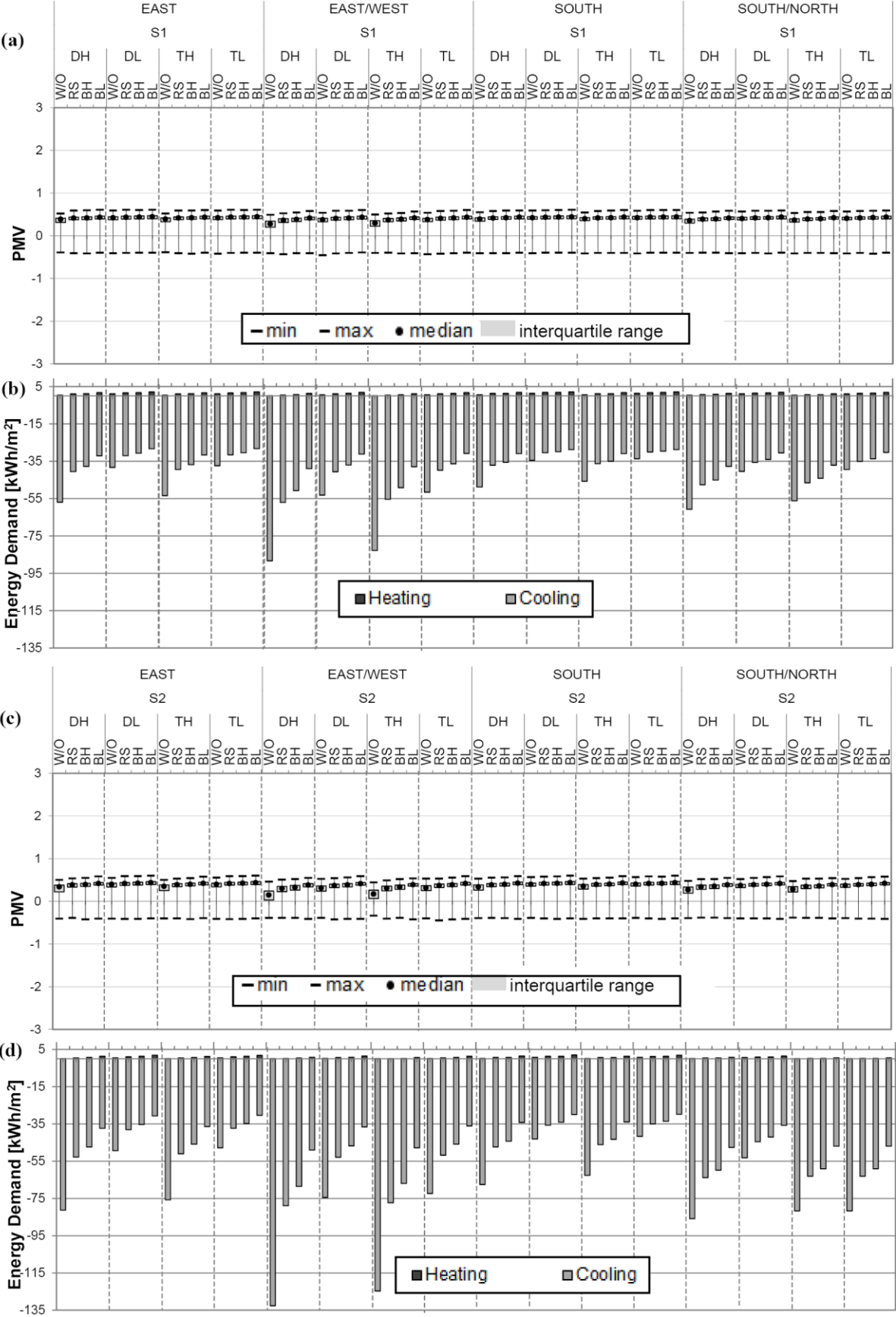


Figure 3 – Summer distributions of PMV for small (a) and large windows (c) and Energy needs for small (b) and large windows (d)

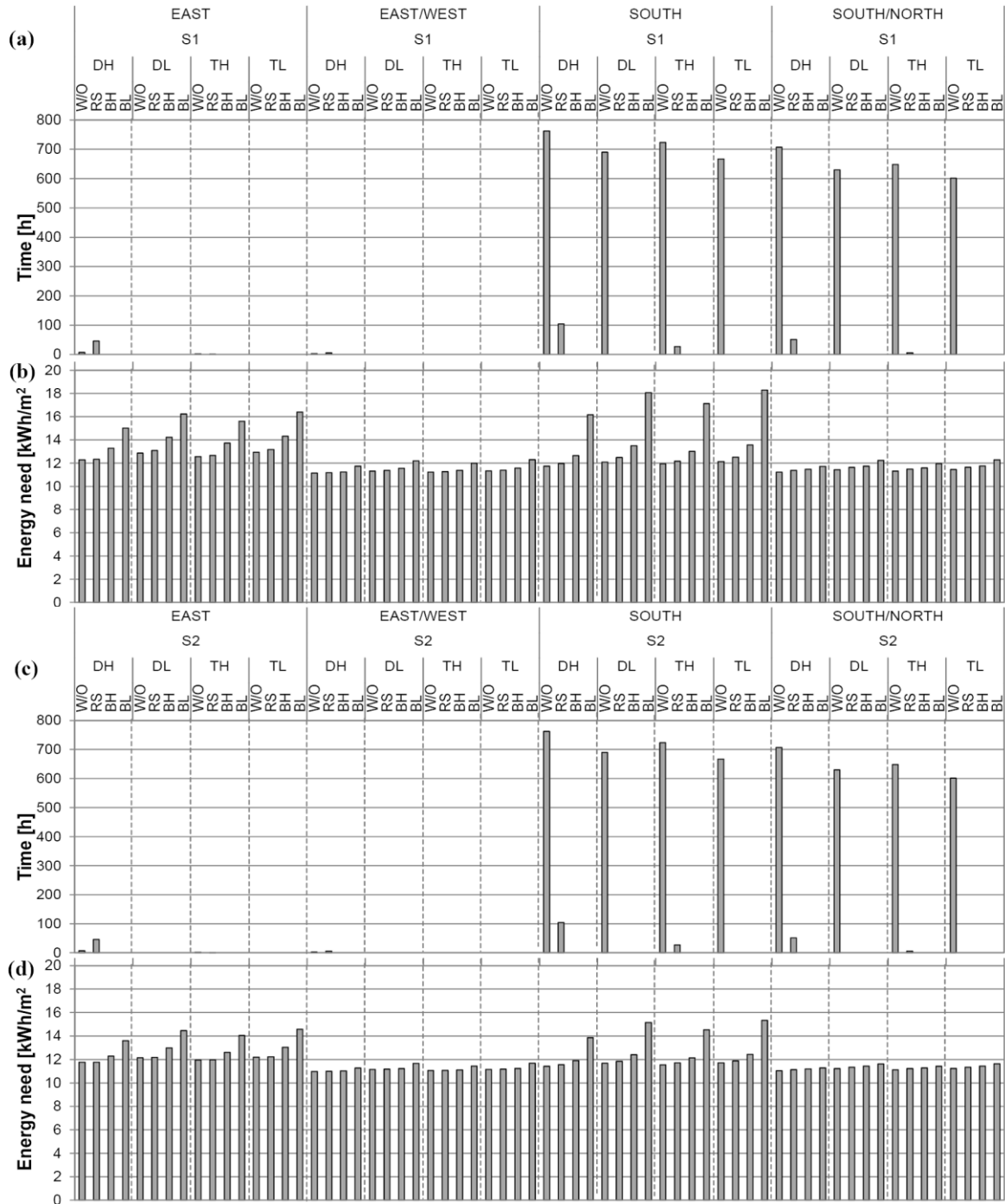


Figure 4 – Hours of visual discomfort and lighting energy needs for small (a,b) and large windows (c,d)

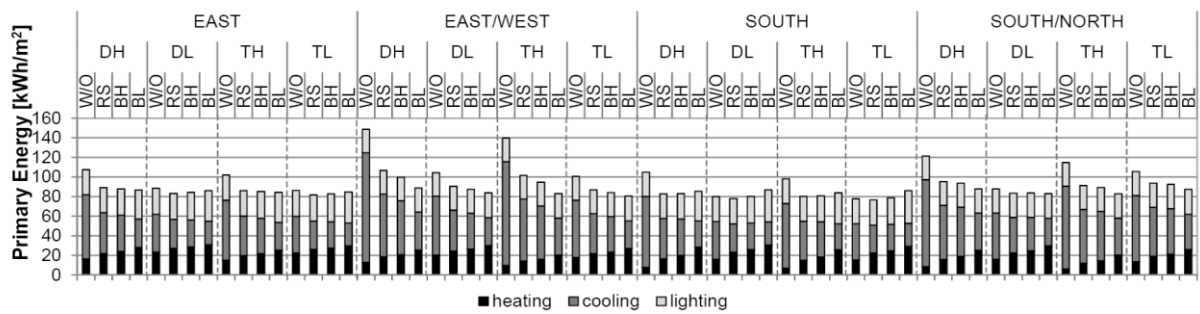


Figure 5 – Total Primary Energy need for larger windows (S2)

References

- CEN, 2005, Standard EN 7730:2005 Ergonomics of the thermal environment – Analytical determination and interpretation of thermal comfort using calculation of the PMV and PPD indices and local thermal comfort criteria.
- CEN, 2002, Standard EN 12464-1:2002: Lighting of work places Part 1: Indoor work places.
- CEN, 2007, Standard EN 15251:2007 Indoor environmental input parameters for design and assessment of energy performance of buildings addressing indoor air quality, thermal environment, lighting and acoustics.
- Correia da Silva P., Leal V. & Andersen M. 2012. Influence of shading control patterns on the energy assessment of office spaces. *Energy and Buildings*, 50.
- David M., Donn M., Garde F. & Lenoir A. 2011. Assessment of the thermal and visual efficiency of solar shades, *Building and Environment*, 46(7).
- Eskin N. & Türkmen H. 2008. Analysis of annual heating and cooling energy requirements for office buildings in different climates in Turkey. *Energy and Buildings*, 40(5).
- Frontini F. & Kuhn T. E. 2012. The influence of various internal blinds on thermal comfort: A new method for calculating the mean radiant temperature in office spaces. *Energy and Buildings*.
- Galasiu A.D., Atif M.R. & MacDonald R.A. 2004. Impact of window blinds on daylight-linked dimming and automatic on/off lighting controls, *Solar Energy*, 76 (5).
- Ihm P. & Krarti M. 2012. Design optimization of energy efficient residential buildings in Tunisia. *Building and Environment*, 58.
- Inoue T., Kawase T., Ibamoto T. & Takakusa S., Matsuo Y. 1988. The development of an optimal control system for window shading devices based on investigations in office buildings, *ASHRAE Transactions*, 94.
- Kim G., Lim H. S., Lim T. S., Shaefer L. & Kim T. J. 2012. Comparative advantage of an exterior shading device in thermal performance for residential buildings, *Energy and buildings*, 46.
- Kuhn T. E. 2006. Solar control: A general evaluation method for facades with venetian blinds or other solar control systems, *Energy and Buildings*, 38(6).
- Mahdavi A. & Dervishi S. 2011. Exploring the energy performance of simulation-powered lighting and shading systems controls in buildings, *Proc. of Building Simulation 2011*, Sydney, Australia.
- Newsham G.R. 1994. Manual control of window blinds and electric lighting: implications for comfort and energy consumption, *Indoor Environment*, 3 (3).
- Nielsen M. V., Svendsen S. & Jensen B. L. 2011. Quantifying the potential of automated dynamic solar shading in office buildings through integrated simulations of energy and daylight, *Solar Energy*, 85(5).
- Ochoa C. E., Aries M. B. C., van Loenen E. J. & Hensen J. L. M. 2012. Considerations on design optimization criteria for windows providing low energy consumption and high visual comfort. *Applied Energy*, 95.
- Oh M. H., Lee K. H. & Yoon J. H. 2012. Automated control strategies of inside slat-type blind considering visual comfort and building energy performance. *Energy and Buildings*.
- Poirazis H., Blomsterberg Å. & Wall M. 2008. Energy simulations for glazed office buildings in Sweden. *Energy and Buildings*, 40(7).
- Reinhart C.F. & Voss K. 2003. Monitoring manual control of electric lighting and blinds, *Lighting Research and Technology*, 35 (3).
- Shen H. & Tzempelikos A. 2012a. Daylighting and energy analysis of private offices with automated interior roller shades. *Solar Energy*, 86(2).
- Shen H. & Tzempelikos A. 2012b. Sensitivity analysis on daylighting and energy performance of perimeter offices with automated shading. *Building and Environment*.
- Tsikaloudaki K., Theodosiou T., Laskos K. & Bikas D. 2012. Assessing cooling energy performance of windows for residential buildings in the Mediterranean zone. *Energy Conversion and Management*, 64.

- Tzempelikos A. & Athienitis A. K. 2007. The impact of shading design and control on building cooling and lighting demand, *Solar Energy*, 81.
- Tzempelikos A., Bessoudo M., Athienitis A. K. & Zmeureanu R. 2010. Indoor thermal environmental conditions near glazed facades with shading devices – Part II: Thermal comfort simulation and impact of glazing and shading properties. *Building and Environment*, 45(11).
- Zhu J., Chew D. a. S., Lv S. & Wu W. 2013. Optimization method for building envelope design to minimize carbon emissions of building operational energy consumption using orthogonal experimental design (OED). *Habitat International*, 37.
- UNI, 1995, UNI 10339:2005 Impianti aeraulici a fini di benessere. Generalità. Classif. e requisiti.

Parametrical analysis for the evaluation of the technical and economic effectiveness of different refurbishment measures

Francesca Cappelletti – University IUAV of Venice, Venice, Italy

Paola Penna – Free University of Bozen/Bolzano, Bolzano, Italy

Piercarlo Romagnoni – University IUAV of Venice, Venice, Italy

Andrea Gasparella – Free University of Bozen/Bolzano, Bolzano, Italy

Abstract

One of the major aims in building energy refurbishment is to compare different solutions in order to achieve requirements of the law or improve the energy efficiency, but the priority of interventions and their effectiveness can be affected by the initial situation (weather conditions, geometry and shape of building, entity of transparent surfaces, and so on). In the present paper a reference building model has been simulated in order to calculate the primary energy need for heating and DHW production. The initial configuration of the building has been varied concerning the windows' size and orientation, the S/V ratio, the materials of the opaque envelope and the location. A total of 54 different reference buildings were obtained from the combination of the above alternatives. About 360 refurbishment packages have been analyzed for each reference building combining improvement measures on the opaque envelope and the transparent components, on the ventilation losses, and on the energy production system. The improvement packages have been analyzed from an economic and energetic perspective in order to draw up a priority list of investments and retrofit measurements.

1. Introduction

According to the International Energy Agency, the residential sector is mainly responsible for energy consumption (about 40% of the final energy demand). For that reason the Annex 56 activity has been recently approved with the purpose of analysing the potentiality of building renovation in energy saving.

In Italy two-thirds of the buildings were built before the adoption of the first energy legislations (Law no. 373 of 1976), and their energy

performances are much lower than the law's prescriptions. For this reason energy retrofit actions present an huge potential in energy saving and they will represent the ever more predominant commitment of construction designers. To improve the energy behaviour of a building, a large number of interventions could be considered to achieve more energy-efficiency targets. The measures on the building envelope could reduce its global energy consumption significantly, by minimizing the thermal losses during the heating season and the solar gains through the windows during the cooling season. At the same time, the use of a more efficient system and RES-based solutions can lead to consistent energy savings. One of the major obstacles in building renovation is due to the financial aspect. For a single owner it is not clear how long it will take to get a return on the initial investment. Policy makers also aim to support the interventions which give the best energy advantages with the smallest need for economic incentives. Recently the European Commission has published the Commission Delegated Regulation EU 244/2012 (European Commission, 2012) which proposes a multi-objective methodology to find reasonable new energy requirements for buildings. In this methodology, called cost-optimal analysis, the aim is to identify the combination of strategies giving the best advantage in primary energy saving with the minimum life cycle cost, or Net Present Value (NPV). The optimal solution and the intermediate ones, as well as the optimal combination of retrofit measures, will depend on the characteristics of the starting reference case. Many approaches are described in the literature for comparing different retrofit measurements. In

some cases a great number of energy efficiency solutions is compared by means of simulation: this is the case of the analysis on the optimal thickness of insulation carried out for different buildings' characteristics, especially the glazing area and the glazing type (Kaynakli 2008, Kaynakli 2012, Özkan and Onan, 2011), and under different climatic conditions (Bolattürk 2008, Lollini *et al.* 2006). When a set of possibilities is composed in order to choose the best among them, some other methods have been investigated: some authors use the multi-criteria analysis (Alanne 2004, Ray 2004, Kaklauskas *et al.* 2005), others the multi-objective optimization (Asadi *et al.* 2012, Hamdy *et al.* 2012, Yang and Wang 2012, Zhu *et al.* 2012, Ihm and Krarti 2012) or the statistical sensitivity analysis (Heiselberg *et al.* 2009, Jaffal *et al.* 2009, Yildiz and Arsan 2011). Just a few authors have carried out a cost-benefit analysis (Hamdy *et al.* 2012, Ihm and Krarti 2012, Asadi *et al.* 2012, Diakaki *et al.* 2010). Some of them analyze real cases studies (Jaggs and Palmer 2000, Alanne 2004, Kaklauskas *et al.* 2005, Asadi *et al.* 2012), some other uses many virtual models (Diakaki *et al.* 2010).

This paper analyzes a residential building model whose characteristics have been changed one at a time in order to obtain many reference models. The aim is to evaluate the contribution of each individual retrofit measure on a set of reference buildings, considering the energy needs and the corresponding cost impact, in order to list the measurement packages with reference to the Net Present Value, the energy performance and also the investment cost. The starting building models are obtained from an uninsulated single-storey module, by modifying the windows' size and orientation, the envelope materials and the ratio between the dispersing envelope and the conditioned volume. The analysis has been performed for three Italian localities situated in different climatic zones (Belluno, climatic zone F, Milan, climatic zone E and Pisa, climatic zone D) representative of the parts of Italy with relevant heating needs. Different retrofitting interventions such as the improvement of the thermal transmittance of the opaque and transparent envelope, the use of efficient energy conversion technologies and RES-based solutions, have been

combined and each combination evaluated considering the energy needs and the total cost of the investment. The cost-optimal approach has been applied to all the cases and the Pareto front has been calculated for each reference building. Finally, the results have been elaborated to identify the combinations of the solutions which are the more cost and energy effective.

2. Reference buildings and energy efficiency measures

2.1 The reference cases

The reference case is a module with a squared floor of 100 m² and 3 m of internal height. The vertical walls are oriented towards the cardinal orientations and the opaque envelope is a simplified structure composed of a single massive layer of clay with a thermal resistance equal to 0.8 m² K W⁻¹. For windows a single-pane glass and a standard timber frame have been considered. A standard boiler coupled with radiators with an on-off regulation system has been considered. The characteristics of the envelope and the heating system have been summarized in Table 1.

Three different ratios between the dispersing envelope and the conditioned volume have been considered:

- $S/V = 0.97$ (one wall adjacent to another conditioned zone, considered as adiabatic);
- $S/V = 0.63$ (one wall and the floor adjacent to another conditioned zone, as adiabatic);
- $S/V = 0.30$ (one wall, the floor and the ceiling adjacent to another conditioned zone, as adiabatic)

Two different windows to floor ratio have been analysed (14.4 % and 28.8 %) and three possible orientations for all the windows have been considered (East, South, North). The considered climates were Belluno (HDD₂₀ = 3043 K d), Milan (HDD₂₀ = 2404 K d) and Pisa (HDD₂₀ = 1694 K d), in the three colder Italian climatic areas (F, E and D respectively in the Italian classification; Dfc, Cfa and Cfa according to the Köppen classification).

The effect of the thermal bridges has been

considered, with a fixed value of $0.15 \text{ W m}^{-1} \text{ K}^{-1}$ for the walls, ceiling and floor corners and of $0.2 \text{ W m}^{-1} \text{ K}^{-1}$ for the windows perimeter, for all the examined cases. The infiltration rates have been calculated according to EN 12207:1999 (CEN, 1999) and EN 15242:2007 (CEN, 2007). The reference air tightness n_{50} is 7 (h^{-1}) and the infiltration rates, for the different glazing sizes and S/V ratios, are reported in Table 2.

CHARACTERISTICS OF OPAQUE ENVELOPE		
Thickness d (m)		0.2
Conductivity λ (W m ⁻¹ K ⁻¹)		0.25
Thermal Resistance R (m ² K W ⁻¹)		0.80
Areal heat capacity κ (kJ m ⁻² K ⁻¹)		150
Density ρ (kg m ⁻³)		893
Specific heat capacity c (J kg ⁻¹ K ⁻¹)		840
CHARACTERISTICS OF WINDOWS		
Glazing	Single-pane glass $U_{gl} = 5.693 \text{ W m}^{-2} \text{ K}^{-1}$	
Frame	Metal without thermal break $U_f = 3.2 \text{ W m}^{-2} \text{ K}^{-1}$	
Ratio A_{win}/A_{fl}	Size 1: 14.4%	
	Size 2: 28.8%	
Orientation	East (E) / South (S) / North (N)	
CHARACTERISTICS OF HEATING SYSTEM		
	Max	Min
Power (kW)	24.3	10.7
On cycle flue losses	8.6 %	8.6 %
Off cycle flue losses	0.1 %	-
Jacket losses	1.2 %	-

Table 1 – Characteristics of the reference cases

Ratio S/V	Size 1 (14.4%)	Size 2 (28.8%)
0.3	0.062	0.124
0.63	0.130	0.260
0.97	0.200	0.400

Table 2 – Infiltration Rate (ach h⁻¹) values according to the different characteristics of the reference buildings

2.2 Energy Efficiency Measures (EEMs)

To improve the thermal performance of the envelope, the following EEMs have been considered (Table 4):

- Application of external insulation layer (EPS with conductivity $\lambda=0.04 \text{ W m}^{-1} \text{ K}^{-1}$, specific heat $c=1470 \text{ J kg}^{-1} \text{ K}^{-1}$ and density

$\rho=40 \text{ kg m}^{-3}$) with five different thicknesses: 0.05 m, 0.10 m, 0.15 m, 0.20 m, 0.25 m;

- Substitution of the existing with better performing windows: two double and two triple respectively with two different solar heat gain coefficients and an aluminium frame with thermal break;
- Replacement of the boiler with a modulating or a condensing boiler and climatic regulation;
- Introduction of flat-plate solar thermal collectors coupled with a water storage tank of 300 l for Domestic Hot Water (DHW);
- Introduction of a mechanical ventilation system with heat recovery.

Although the replacement of the boiler is considered, the substitution of the emission system (kind and nominal capacity, in particular) is not planned. The air tightness of the building is assumed to improve with the substitution of the windows: in this case the infiltration rates become half of the values in Table 2. The reference for the prices of the different EEMs (Table 4) is the Regional Price List, RPL, of Lazio which has been chosen as a benchmark because it represents a possible reference for North and Central Italy.

3. The COST-EFFECTIVE analysis

The Primary Energy demand for space and DHW Heating (EPH) was calculated, according to the monthly quasi-steady-state method of UNI/TS 11300:2008, the Italian specification for the application of EN ISO 13790:2008. This allowed for the calculation of a consistent number of cases over a short time. The cost-effective analysis was carried out for each reference building according to the methodology proposed by the EU 244/2012. The Net Present Value (NPV) was evaluated for a calculation period of 30 years, considering the initial Investment Cost (IC), the annual running costs (composed by the Energy Cost and Maintenance Cost), the replacement cost (due to the periodic substitution of building elements) and

the residual value for the equipment with longer lifetimes.

The investment and operative costs and economic parameters are reported in Tables 3 and 4. The lifespan of the building elements and the maintenance costs refer to the values suggested by the EN 15459:2009 (CEN, 2009). A cost of 1000 euros has been considered for the replacement of a standard boiler. Each one of the 360 interventions per reference case has been evaluated in terms of NPV and EPH. The Pareto front (the configurations with the best NPV for a given EPH) has been isolated (Figure 1). In order to check the accuracy of the results, the Pareto front points of three reference cases with smaller windows oriented towards the east (S/V=0.3 Pisa, S/V=0.63 Milano, S/V=0.97 Belluno) were calculated by dynamic simulations with TRNSYS v.17.1 (SEL, 2012) showing good agreement (Figure 2). The interventions for the Pareto front points, ranked by decreasing energy demand, have been listed for the different starting buildings (tables 7a to 7c), just for the cases with small windows because of space reasons. From the tables, it can be noticed that the cost of the investment is continuously increasing. The optimal combination (in bold) and so the investment costs, depends largely on the locality and just in some cases on the S/V ratio, on the windows' orientation and size. In some cases the investment cost of the optimum is similar, but the EPH reached is different: for example in Belluno the optimal EEMs are the same for east as for south orientation but the EPH demand reached is lower for south orientation as can be seen in Table 5.

In particular, in Milan the optimal intervention set remains the same in all the considered cases with the application of 15 cm of insulation, the substitution of the existing windows with DH window and the replacement of the standard boiler with a condensing one. The situation in Belluno does not present a single trend. What the common feature is for this location is that the solar collectors are never considered in the optimal configuration, nor the mechanical ventilation. In general for east and south orientation the cost-optimal combination is 15 cm of insulation, DH windows and

condensing boiler, except for the case with S/V ratio of 0.97 where TH glazing is needed.

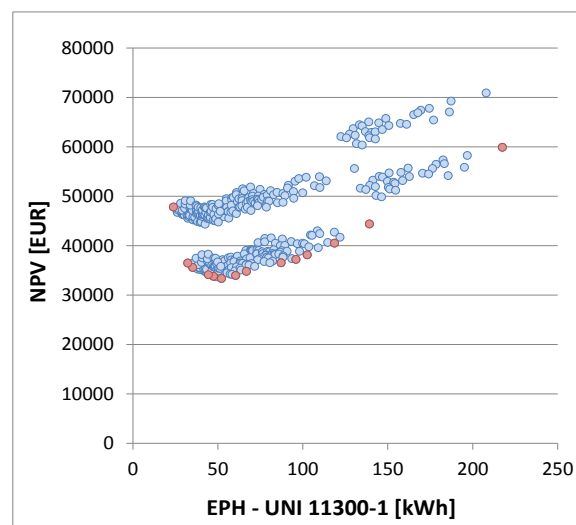


Fig. 1 – NPV and EPH [kWh year⁻¹ m⁻²] for the case of Milan, Ratio S/V=0.63, windows East exposed with smaller dimension.

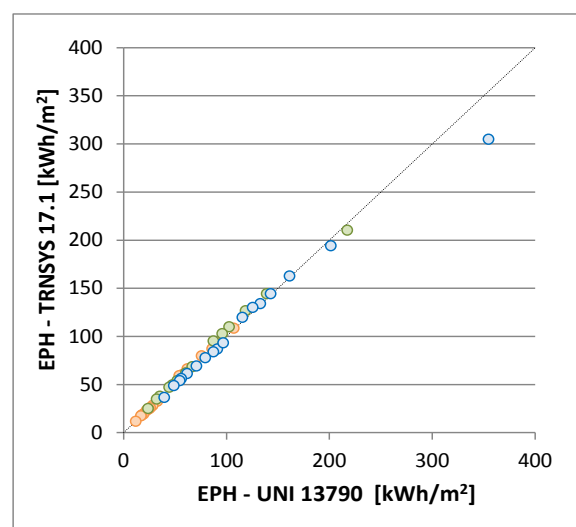


Fig. 2 – Comparison between the Primary Energy Demand for Heating and DHW (EPH) calculated according to EN 13790 and with Trnsys17.1

For Pisa the optimal combination of EEMs depends on the windows' size and orientation. In particular, for east and south orientations the optimal solution of EEMs requires the introduction of the solar collectors, while for north orientation the boiler replacement with a condensing one becomes a preferable solution. Considering the insulation, 10 or 15 cm are needed depending on the size of windows and on their orientation. Regarding the type of glazing the DH is needed for all the orientation except for south.

Opaque Envelope: insulation layer thermal characteristic						Cost (EUR m ⁻²)
thickness x* (cm)	5	10	15	20	25	IC _{VW} = 1.6 x* + 38.53
U (W m ⁻² K ⁻¹)	0.45	0.29	0.21	0.17	0.14	IC _{HW} = 1.88 x* + 8.19
Windows			U _{gl} - U _f (W m ⁻² K ⁻¹)	SHGC	Cost (EUR m ⁻²)	
DH – Double, high SHGC (4/9/4, krypton, low-e)			1.140 – 1.2		0.608	IC _{DH} = 404.33
DL – Double, low SHGC (6/16/6, krypton, low-e)			1.099 – 1.2		0.352	IC _{DL} = 439.06
TH – Triple, high SHGC (6/12/6/12/6 krypton, low-e)			0.613 – 1.2		0.575	IC _{TH} = 477.65
TL – Triple, low SHGC (6/14/4/14/6 argon, low-e)			0.602 – 1.2		0.343	IC _{TL} = 454.49
Heating System: Boiler						
	Power max/min (kW)	On cycle flue losses	Off cycle flue losses	Jacket losses	Cost (EUR)	
Modulating MDL	26.7/11.7	6%	0.1%	1.2%	IC _{MDL} = 1500	
Condensing CND	24.3/8.4	2.1/0.3%	0.1%	0.3%	IC _{CND} = 2000	
Thermal Solar System (SS)						
Absorber area (m ²)	Orientation	Slope	Heat loss coefficients a ₁ / a ₂ (W m ⁻² K ⁻²)	Zero-loss efficiency	Cost (EUR) including tank	
4.66	South	30°	4.16 / 0.0073	84 %	IC _{SS} = 2500	
Mechanical ventilation system (MVS)						
Ventilation Rate (m ³ h ⁻¹)			Power (W)		Cost (EUR)	
150			59.7		IC _{MV} = 6000	

Table 3 – Energy Efficiency Measures and the related Investment Costs without VAT.

Fuel Cost ⁽¹⁾	85 EUR cent Sm ⁻³
Fuel Lower Heating Value ⁽²⁾	32.724 MJ Sm ⁻³
Electricity Cost ⁽¹⁾	6.94 EUR cent MJ _{el} ⁻³
Increase Fuel price ⁽³⁾	2.8%
Increase Electricity price ⁽³⁾	1.71%
VAT	10%
Real Interest Rate	3%

⁽¹⁾ Autorità per l'Energia Elettrica e il Gas, 2011, *Relazione annuale sullo stato dei servizi e sull'attività svolta*, Milan, Italy

⁽²⁾ Ministry of Economic Development, 2011, *Bilancio Energetico Nazionale 2010*, Rome.

⁽³⁾ EU Energy Trends to 2030, update 2009. European Union 2010.

Table 4 – Costs and Parameters for the economic analysis

	S/V	North	East	South
Belluno	0.3	52	45	34
	0.63	65	59	47
	0.97	72	71	59
Milan	0.3	49	41	31
	0.63	61	52	41
	0.97	75	65	54
Pisa	0.3	33	26	41
	0.63	47	35	56
	0.97	49	58	61

 Table 5 – Primary Energy demand for Heating and DHW for cost-optimal cases (small windows) in kWh/m²

In this case the replacement of the windows is not needed to achieve the cost-optimal level.

4. Conclusions

In this paper a cost-optimal analysis has been carried out on a set of reference residential building models in order to define a list of prior retrofit interventions. The primary energy demand for heating and DHW and the Net Present Value have been calculated for different localities. For each reference case it was possible to identify the cost-optimal solution and the configurations with the best *NPV* for a given *EPH* which lay on the Pareto front. The investment cost, always increasing with decreasing *EPH* demand, for the optimal combination of EEMs depends on the locality. In some climates (e.g. Milan) the starting case configuration (*S/V* ratio, windows size and orientation) does not influence the optimal combination of EEMs. This methodology can give a contribution in guiding the choices of interventions for the existing buildings' refurbishment.

5. Nomenclature

Symbols

A	area	(m ²)
HDD ₂₀	heating degree days	(K d)
IC	investment cost	(Eur m ⁻²)
NPV	Net Present Value	(Eur)
EPH	Primary Energy for Heating	(kWh/m ²)
SHGC	solar heat gain coefficient	(-)
S	dispersing envelope surface	(m ²)
U	thermal transmittance	(W m ⁻² K ⁻¹)
V	conditioned volume of building	(m ³)
VAT	Value Added Tax	(%)

Greek symbols

α	solar absorptance	(-)
λ	thermal conductivity	(W m ⁻¹ K ⁻¹)

Subscripts

f	frame	H	horizontal
fl	floor	W	wall
gl	glazings	win	window
V	vertical		

References

- Alanne, K. 2004. Selection of renovation actions using multi-criteria knapsack model, *Automation in construction*, 13, 377–391.
- Asadi, E., Gameiro, M., Henggeler, C., & Dias, L. 2012. A multi-objective optimization model for building retrofit strategies using TRNSYS simulations, GenOpt and MATLAB. *Building and Environment*, 56, 370–378.
- Asadi, E., Gameiro, M., Henggeler, C., & Dias, L. 2012. Multi-objective optimization for building retrofit strategies : A model and an application. *Energy & Buildings*, 44, 81–87.
- Bolattürk A., 2008. Optimization insulation thickness for building walls with respect to cooling and heating degree-hours in the warmest zone of the Turkey, *Building Environment*, vol. 43.
- Diakaki, C., Grigoroudis, E., Kabelis, N., Kolokotsa, D., Kalaitzakis, K., & Stavrakakis, G. 2010. A multi-objective decision model for the improvement of energy efficiency in buildings. *Energy*, 35(12).
- European Commission, 2012. Commission Delegated Regulation EU 244/2012, *Official Journal of European Union*, L81/18, 20/03/2012.
- Hamdy, M., Hasan, A., & Siren, K. 2011. Applying a multi-objective optimization approach for Design of low-emission cost-effective dwellings. *Building and Environment*, 46(1), 109–123.
- Heiselberg P., Brohus H., Hesselholt H., Rasmussen H., Seinre E., Thomas S. 2009, Application of sensitivity analysis in design of sustainable buildings, *Renewable Energy*, vol. 34, p. 2030–2036.
- Ihm, P., & Krarti, M. 2012. Design optimization of energy efficient residential buildings in Tunisia. *Building and Environment*, 58, 81–90.
- Jaffal, I., Inard, C., & Ghiaus, C. 2009. Fast method to predict building heating demand based on the design of experiments, 41, 669–677.
- Jaggs, M., & Palmer, J. 2000. Energy performance indoor environmental quality retrofit — a European diagnosis and decision making method for building refurbishment, 97–101.
- Kaynakli O., 2008. A study on residential heating energy requirement and optimum insulation thickness, *Renewable Energy*, vol. 33.

- Kaynakli O., 2012. A review of the economical and optimum thermal insulation thickness for building applications, *Renewable and Sustainable Energy Review*, vol. 16.
- Kaklauskas, A., Zavadskas, E. K., & Raslanas, S. 2005. Multivariant design and multiple criteria analysis of building refurbishments, 37.
- Lollini R., Barozzi B., Fasano G., Meroni I., Zinzi M., 2006. Optimization of opaque components of the building envelope. *Energy, economic and environmental issues, Building Environment*, vol. 41, p. 1001-1013.
- Özkan D.B., Onan C., 2011. Optimization of insulation thickness for different glazing areas in buildings for various climatic regions in Turkey, *Applied Energy*, vol. 88, p. 1331-1342.
- Rey, E. 2004. Office building retrofitting strategies: multicriteria approach of an architectural and technical issue, 36, 367–372.
- Solar Energy Laboratory, 2012. TRNSYS 17.1 Documentation, Madison, Wisconsin.
- Yang, R., & Wang, L. 2012. Multi-objective optimization for decision-making of energy and comfort management in building automation and control. *Sustainable Cities and Society*, 2(1).
- Yıldız, Y., & Durmus, Z. 2011. Identification of the building parameters that influence heating and cooling energy loads for apartment buildings in hot-humid climates, 36, 4287–4296.
- Zhu, J., Chew, D. A. S., Lv, S., & Wu, W. 2012. Optimization method for building envelope design to minimize carbon emissions of building operational energy consumption using orthogonal experimental design (OED). *Habitat International*, 1–7.

INSULATION		GLAZING SYSTEM		BOILER		Domestic Hot Water		VENTILATION	
INS		GL		BOI		DHW		V	
0	No insulation	0	Single pane	0	Standard	0	Standard boiler	0	Natural
1	5 cm	1	Double H	1	Modulating	1	Solar system	1	Mechanical
2	10 cm	2	Double L	2	Condensing				
3	15 cm	3	Triple H						
4	20 cm	4	Triple L						
5	25 cm								

Table 6 – Reading code for tables 7

	N						E/W						S					
S/V = 0.3	INS	GL	BOI	DHW	MV	I	INS	GL	BOI	DHW	MV	I	INS	GL	BOI	DHW	MV	I
	0	0	0	0	0	382	0	0	0	0	0	382	0	0	0	0	0	382
	2	0	0	0	0	4917	2	0	0	0	0	4917	2	0	0	0	0	4917
	3	0	0	0	0	5582	3	0	0	0	0	5582	3	0	0	0	0	5582
	2	0	1	0	0	6758	2	0	1	0	0	6758	2	0	1	0	0	6758
	2	0	2	0	0	7500	3	0	1	0	0	7424	3	0	1	0	0	7424
	3	0	2	0	0	8165	2	0	2	0	0	7500	2	0	2	0	0	7500
	4	0	2	0	0	8830	3	0	2	0	0	8165	3	0	2	0	0	8165
	2	1	0	0	0	11322	4	0	2	0	0	8830	4	0	2	0	0	8830
	3	1	0	0	0	11987	2	1	0	0	0	11322	2	1	0	0	0	11322
	4	1	0	0	0	12652	3	1	0	0	0	11987	3	1	0	0	0	11987
	2	1	1	0	0	13163	2	1	1	0	0	13163	2	1	1	0	0	13163
	2	1	2	0	0	13904	3	1	1	0	0	13828	3	1	1	0	0	13828
	3	1	2	0	0	14569	2	1	2	0	0	13904	2	1	2	0	0	13904
	4	1	2	0	0	15235	3	1	2	0	0	14569	3	1	2	0	0	14569
	4	3	2	0	0	16396	4	3	2	0	0	16396	4	1	2	0	0	15235
	5	3	2	0	0	17061	5	3	2	0	0	17061	4	3	2	0	0	16396
	5	3	2	1	0	20768	5	3	2	1	0	20768	5	3	2	0	0	17061
	5	3	2	1	1	29662	5	3	2	1	1	29662	4	3	2	1	0	20102
													5	3	2	1	0	20768
													5	3	2	1	1	29662
S/V = 0.63	INS	GL	BOI	DHW	MV	I	INS	GL	BOI	DHW	MV	I	INS	GL	BOI	DHW	MV	I
	0	0	0	0	0	382	0	0	0	0	0	382	0	0	0	0	0	382
	1	0	0	0	0	6187	1	0	0	0	0	6187	1	0	0	0	0	6187
	2	0	0	0	0	7886	2	0	0	0	0	7886	2	0	0	0	0	7886
	2	0	1	0	0	9727	2	0	1	0	0	9727	3	0	0	0	0	9585
	2	0	2	0	0	10469	2	0	2	0	0	10469	2	0	1	0	0	9727
	3	0	1	0	0	11427	3	0	1	0	0	11427	2	0	2	0	0	10469
	3	0	2	0	0	12168	3	0	2	0	0	12168	3	0	1	0	0	11427
	2	1	0	0	0	14291	2	1	0	0	0	14291	3	0	2	0	0	12168
	3	1	0	0	0	15990	3	1	0	0	0	15990	3	1	0	0	0	15990
	2	1	1	0	0	16132	2	1	1	0	0	16132	2	1	1	0	0	16132
	2	1	2	0	0	16873	2	1	2	0	0	16873	2	1	2	0	0	16873
	2	3	2	0	0	18034	3	1	2	0	0	18572	3	1	2	0	0	18572
	3	1	2	0	0	18572	4	1	2	0	0	20272	4	1	2	0	0	20272
	3	3	2	0	0	19734	4	3	2	0	0	21433	4	3	2	0	0	21433
	4	3	2	0	0	21433	5	3	2	0	0	23132	5	1	2	0	0	21971
	5	3	2	0	0	23132	4	3	2	1	0	25139	5	3	2	0	0	23132
	4	3	2	1	0	25139	5	3	2	1	0	26838	4	3	2	1	0	25139
	5	3	2	1	0	26838	5	3	2	1	1	35733	5	3	2	1	0	26838
	5	4	2	1	1	35366							5	3	2	1	1	35733
S/V = 0.97	INS	GL	BOI	DHW	MV	I	INS	GL	BOI	DHW	MV	I	INS	GL	BOI	DHW	MV	I
	0	0	0	0	0	382	0	0	0	0	0	382	0	0	0	0	0	382
	1	0	0	0	0	8122	1	0	0	0	0	8122	1	0	0	0	0	8122
	2	0	0	0	0	10855	2	0	0	0	0	10855	2	0	0	0	0	10855
	2	0	1	0	0	12696	2	0	1	0	0	12696	2	0	1	0	0	12696
	2	0	2	0	0	13437	2	0	2	0	0	13437	2	0	2	0	0	13437
	3	0	1	0	0	15429	3	0	1	0	0	15429	3	0	1	0	0	15429
	3	0	2	0	0	16171	3	0	2	0	0	16171	3	0	2	0	0	16171
	4	0	2	0	0	18904	2	1	2	0	0	19842	2	3	1	0	0	20262
	2	1	2	0	0	19842	2	3	1	0	0	20262	2	3	2	0	0	21003
	2	3	1	0	0	20262	2	3	2	0	0	21003	3	3	1	0	0	22995
	2	4	2	0	0	20637	3	3	1	0	0	22995	3	3	2	0	0	23737
	2	3	2	0	0	21003	3	3	2	0	0	23737	4	3	2	0	0	26470
	3	3	1	0	0	22995	4	3	2	0	0	26470	5	3	2	0	0	29203
	3	4	2	0	0	23370	5	3	2	0	0	29203	4	3	2	1	0	30176
	3	3	2	0	0	23737	4	3	2	1	0	30176	5	3	2	1	0	32909
	4	3	2	0	0	26470	5	3	2	1	0	32909	5	3	2	1	1	41804
	5	3	2	0	0	29203	5	3	2	1	1	41804						
	5	3	2	1	0	32909												
	5	4	2	1	1	41437												

Tables 7a-7b-7c - Measures Packages ordered by Energy Demand for Heating and DHW from the higher till the lower. 7a- Belluno - Cases with small windows(S1).

	N						E/W						S					
	INS	GL	BOI	DHW	MV	I	INS	GL	BOI	DHW	MV	I	INS	GL	BOI	DHW	MV	I
S/V = 0.3	0	0	0	0	0	382	0	0	0	0	0	382	0	0	0	0	0	382
	2	0	0	0	0	4917	2	0	0	0	0	4917	2	0	0	0	0	4917
	3	0	0	0	0	5582	3	0	0	0	0	5582	3	0	0	0	0	5582
	2	0	1	0	0	6758	2	0	1	0	0	6758	2	0	1	0	0	6758
	2	0	2	0	0	7500	2	0	2	0	0	7500	2	0	2	0	0	7500
	3	0	2	0	0	8165	3	0	2	0	0	8165	3	0	2	0	0	8165
	2	1	0	0	0	11322	2	1	0	0	0	11322	2	1	1	0	0	13163
	3	1	0	0	0	11987	3	1	0	0	0	11987	2	1	2	0	0	13904
	2	1	1	0	0	13163	2	1	1	0	0	13163	3	1	2	0	0	14569
	3	1	1	0	0	13828	2	1	2	0	0	13904	3	1	0	1	0	15693
	2	1	2	0	0	13904	3	1	2	0	0	14569	4	1	0	1	0	16358
	3	1	2	0	0	14569	4	3	0	1	0	17520	5	1	0	1	0	17024
	4	1	2	0	0	15235	5	3	0	1	0	18185	4	3	0	1	0	17520
	4	3	2	0	0	16396	4	3	2	1	0	20102	5	3	0	1	0	18185
	4	3	0	1	0	17520	5	3	2	1	0	20768	3	1	2	1	0	18276
	5	3	0	1	0	18185	5	3	2	1	1	29662	4	1	2	1	0	18941
	4	3	2	1	0	20102							5	1	2	1	0	19606
	5	3	2	1	0	20768							4	3	2	1	0	20102
	5	3	2	1	1	29662							5	3	2	1	0	20768
													4	3	2	1	1	28997
													5	3	2	1	1	29662
S/V = 0.63	0	0	0	0	0	382	0	0	0	0	0	382	0	0	0	0	0	382
	1	0	0	0	0	6187	1	0	0	0	0	6187	1	0	0	0	0	6187
	2	0	0	0	0	7886	2	0	0	0	0	7886	2	0	0	0	0	7886
	2	0	1	0	0	9727	2	0	1	0	0	9727	2	0	1	0	0	9727
	2	0	2	0	0	10469	2	0	2	0	0	10469	2	0	2	0	0	10469
	3	0	2	0	0	12168	3	0	2	0	0	12168	3	0	1	0	0	11427
	2	1	0	0	0	14291	2	1	1	0	0	16132	3	0	2	0	0	12168
	2	1	1	0	0	16132	2	1	2	0	0	16873	2	1	1	0	0	16132
	2	1	2	0	0	16873	3	1	2	0	0	18572	2	1	2	0	0	16873
	3	1	2	0	0	18572	4	1	2	0	0	20272	3	1	2	0	0	18572
	3	3	2	0	0	19734	4	3	2	0	0	21433	4	1	0	1	0	21395
	4	3	2	0	0	21433	4	3	2	1	0	25139	4	3	0	1	0	22557
	4	3	2	1	0	25139	5	3	2	1	0	26838	4	1	2	1	0	23978
	5	3	2	1	0	26838	5	3	2	1	1	35733	4	3	2	1	0	25139
	5	3	2	1	1	35733							5	1	2	1	0	25677
													5	3	2	1	0	26838
													4	3	2	1	1	34034
													5	3	2	1	1	35733
S/V = 0.97	0	0	0	0	0	382	0	0	0	0	0	382	0	0	0	0	0	382
	1	0	0	0	0	8122	1	0	0	0	0	8122	1	0	0	0	0	8122
	2	0	0	0	0	10855	2	0	0	0	0	10855	2	0	0	0	0	10855
	2	0	1	0	0	12696	2	0	1	0	0	12696	2	0	1	0	0	12696
	2	0	2	0	0	13437	2	0	2	0	0	13437	2	0	2	0	0	13437
	3	0	1	0	0	15429	3	0	1	0	0	15429	3	0	1	0	0	15429
	3	0	2	0	0	16171	3	0	2	0	0	16171	3	0	2	0	0	16171
	2	1	1	0	0	19101	2	1	1	0	0	19101	2	1	1	0	0	19101
	2	1	2	0	0	19842	2	1	2	0	0	19842	2	1	2	0	0	19842
	3	1	1	0	0	21834	3	1	1	0	0	21834	3	1	2	0	0	22575
	3	1	2	0	0	22575	3	1	2	0	0	22575	4	1	2	0	0	25309
	4	3	2	0	0	23737	4	1	2	0	0	25309	4	3	2	0	0	26470
	4	3	2	0	0	26470	4	3	2	0	0	26470	4	1	2	1	0	29015
	4	3	2	1	0	30176	4	3	2	1	0	30176	4	3	2	1	0	30176
	5	3	2	1	0	32909	5	3	2	1	0	32909	5	1	2	1	0	31748
	5	3	2	1	1	41804	5	3	2	1	1	41804	5	3	2	1	0	32909
													5	3	2	1	1	41804

7b – Milano - Cases with small windows(S1).

	N						E/W						S					
	INS	GL	BOI	DHW	MV	I	INS	GL	BOI	DHW	MV	I	INS	GL	BOI	DHW	MV	I
$S/V = 0.3$	0	0	0	0	0	382	0	0	0	0	0	382	0	0	0	0	0	382
	0	0	1	0	0	2224	0	0	1	0	0	2224	0	0	1	0	0	2224
	0	0	2	0	0	2965	0	0	2	0	0	2965	0	0	2	0	0	2965
	2	0	0	0	0	4917	2	0	0	0	0	4917	2	0	1	0	0	6758
	2	0	1	0	0	6758	2	0	1	0	0	6758	2	0	2	0	0	7500
	2	0	2	0	0	7500	2	0	2	0	0	7500	3	0	2	0	0	8165
	3	0	2	0	0	8165	3	0	2	0	0	8165	3	0	0	1	0	9289
	2	1	1	0	0	13163	2	1	2	0	0	13904	4	0	0	1	0	9954
	2	1	2	0	0	13904	2	1	0	1	0	15028	2	1	0	1	0	15028
	3	1	2	0	0	14569	3	1	0	1	0	15693	3	1	0	1	0	15693
	3	1	0	1	0	15693	4	1	0	1	0	16358	4	1	0	1	0	16358
	4	1	0	1	0	16358	4	3	0	1	0	17520	3	3	0	1	0	16855
	4	3	0	1	0	17520	4	1	2	1	0	18941	5	1	0	1	0	17024
	5	3	0	1	0	18185	4	3	2	1	0	20102	3	1	1	1	0	17534
	4	3	2	1	0	20102	5	3	2	1	0	20768	3	1	2	1	0	18276
	5	3	2	1	0	20768	5	3	2	1	1	29662	4	1	2	1	0	18941
	5	3	2	1	1	29662							3	3	2	1	0	19437
													5	1	2	1	0	19606
													4	3	2	1	0	20102
													5	3	2	1	0	20768
													3	1	2	1	1	27170
													4	1	2	1	1	27836
$S/V = 0.63$	0	0	0	0	0	382	0	0	0	0	0	382	0	0	0	0	0	382
	1	0	0	0	0	6187	1	0	0	0	0	6187	1	0	0	0	0	6187
	2	0	0	0	0	7886	2	0	0	0	0	7886	2	0	0	0	0	7886
	2	0	1	0	0	9727	2	0	1	0	0	9727	2	0	1	0	0	9727
	2	0	2	0	0	10469	2	0	2	0	0	10469	2	0	2	0	0	10469
	3	0	2	0	0	12168	3	0	2	0	0	12168	3	0	2	0	0	12168
	2	1	1	0	0	16132	2	1	2	0	0	16873	3	0	0	1	0	13291
	2	1	2	0	0	16873	3	1	2	0	0	18572	2	1	0	1	0	17997
	3	1	2	0	0	18572	3	1	0	1	0	19696	3	1	0	1	0	19696
	3	1	0	1	0	19696	4	1	0	1	0	21395	3	3	0	1	0	20857
	3	3	0	1	0	20857	4	3	0	1	0	22557	4	1	0	1	0	21395
	4	1	0	1	0	21395	4	1	2	1	0	23978	3	1	2	1	0	22279
	4	3	0	1	0	22557	4	3	2	1	0	25139	4	1	1	1	0	23237
	3	3	2	1	0	23440	5	3	2	1	0	26838	3	3	2	1	0	23440
	4	3	2	1	0	25139	4	3	2	1	1	34034	4	1	2	1	0	23978
	5	3	2	1	0	26838	5	3	2	1	1	35733	4	3	2	1	0	25139
	5	3	2	1	1	35733							5	1	2	1	0	25677
													5	3	2	1	0	26838
													4	1	2	1	1	32872
													4	3	2	1	1	34034
													5	1	2	1	1	34572
													5	3	2	1	1	35733
$S/V = 0.97$	0	0	0	0	0	382	0	0	0	0	0	382	0	0	0	0	0	382
	1	0	0	0	0	8122	1	0	0	0	0	8122	1	0	0	0	0	8122
	2	0	0	0	0	10855	2	0	0	0	0	10855	2	0	0	0	0	10855
	2	0	1	0	0	12696	2	0	1	0	0	12696	2	0	1	0	0	12696
	2	0	2	0	0	13437	2	0	2	0	0	13437	2	0	2	0	0	13437
	3	0	2	0	0	16171	3	0	2	0	0	16171	3	0	2	0	0	16171
	2	1	1	0	0	19101	2	1	2	0	0	19842	3	1	0	1	0	23699
	2	1	2	0	0	19842	3	1	2	0	0	22575	3	3	0	1	0	24860
	3	1	2	0	0	22575	3	1	0	1	0	23699	4	1	0	1	0	26432
	3	3	2	0	0	23737	3	3	0	1	0	24860	4	3	0	1	0	27594
	3	3	0	1	0	24860	4	1	0	1	0	26432	4	1	1	1	0	28273
	4	3	0	1	0	27594	3	1	2	1	0	26281	4	1	2	1	0	29015
	3	3	2	1	0	27443	4	3	0	1	0	27594	4	3	2	1	0	30176
	4	3	2	1	0	30176	4	1	2	1	0	29015	5	1	2	1	0	31748
	5	3	2	1	0	32909	4	3	2	1	0	30176	5	3	2	1	0	32909
	5	3	2	1	1	41804	5	1	2	1	0	31748	4	3	2	1	1	39071
							5	3	2	1	0	32909	5	1	2	1	1	40643
							5	3	2	1	1	41804	5	3	2	1	1	41804

7c - Pisa – Cases with small windows(S1)

Buildings and biomass cogeneration systems: integrated simulation approach

Dario Prando – Free University of Bozen-Bolzano, Bolzano, Italy

Francesco Patuzzi – Free University of Bozen-Bolzano, Bolzano, Italy

Giovanni Pernigotto – University of Padova, Vicenza, Italy

Andrea Gasparella – Free University of Bozen-Bolzano, Bolzano, Italy

Marco Baratieri – Free University of Bozen-Bolzano, Bolzano, Italy

Abstract

The aim of this work is the energy efficiency assessment of cogeneration systems based on biomass gasification for residential applications, using a multistage modelling approach. The gasification stage has been modelled through an enhanced (i.e., gas-solid) thermodynamic approach using the Cantera solver and the Gri-Mech thermodynamic properties. Several values of temperature and amounts of gasifying agent have been taken into account for the simulations. The efficiency of the whole CHP system has been evaluated supplementing the simulation of the gasification stage with the energy balance of the cogeneration set (i.e., internal combustion engine) and implementing the developed routines in the Matlab-Simulink environment. The CHP plant is considered to supply thermal energy to residential buildings. Dynamic simulations by means of EnergyPlus 7.1 code have been performed considering three main building configurations given by three different thermal resistances for the opaque building envelope. The building-system interactions have been performed for the climate of Milan. Domestic hot water consumption has been chosen in agreement with EN 15316-3-1:2007. The resulting building-system scenarios have been compared with a conventional scenario of separated production by means of PES (primary energy saving). The paper shows the system size range for the chosen residential applications and the optimal operating conditions. The economic return of a such power plant has been discussed. The results of this work confirm the gasification-based CHP technology allows energetic and economic benefits. It can have substantial room for improvement with respect to conventional separated generation systems at the same size.

1. Introduction

Combined heat and power (CHP) production systems based on biomass gasification represent a promising technological solution and a feasible alternative to biomass combustion, especially for small-scale applications. In this perspective, the integration of biomass gasification with high efficiency power generation systems is able to define competitive scenarios even if compared with conventional biomass cogeneration systems. The increase of the systems' efficiency, given by the application of this alternative technology, makes feasible the development of energy models based on distributed cogeneration at sizes that have never been sufficiently efficient until now.

The research concerning the coupling of biomass gasification with traditional power generators (gas engines and gas turbines) and with innovative generation systems (fuel cells) is well documented in the literature (M. Baratieri et al., 2009; Dong et al., 2009; Fagbenle et al., 2007). Besides the development of mathematical models for a given biomass processing systems, the simulation of a complete energy conversion plant is usually carried out through process simulators that offer advantages in the evaluation of the process performance in different operating conditions (Ahmed et al., 2012). The evaluation of the overall system performance still requires further development to assess the technologies integrated in their complete chain (biomass pre-processing, biomass energy conversion, energy distribution, final use).

Micro cogeneration systems based on biomass are not largely diffused in residential applications due to the high price and complex operation for residential end-users (Dong et al., 2009). Systems

based on gasification are commercially available for micro generation but the heat production does not match a single apartment (Prando et al., 2012). The aim of this work is the energy efficiency assessment of a micro cogeneration system based

on biomass gasification for residential applications. For this purpose a multistage model has been developed and used to assess the balance of plant and its performance.

moisture	ash	C	H	O	N	LHV	Ref.
[%wt _{ar}]						[MJ/kg _{ar}]	
15.0	1.1	41.2	5.0	37.2	0.4	14.936	(Van Ree et al., 1995)

Table 1 – Characteristics of poplar wood

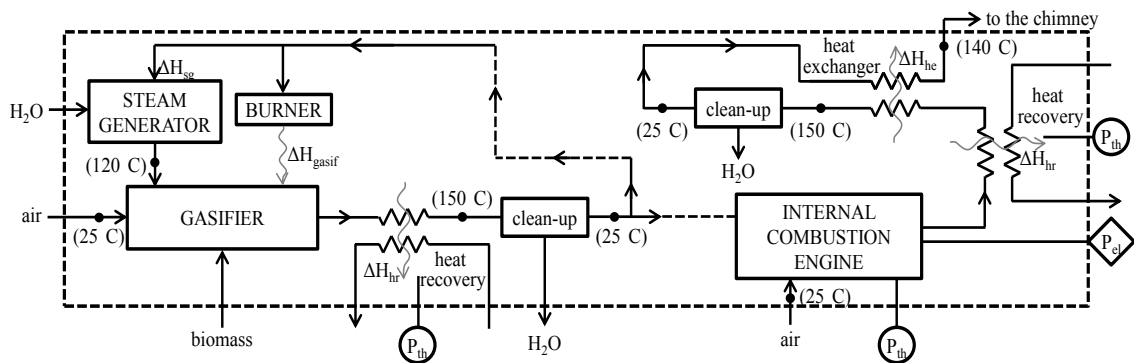


Fig. 1 – Schematic diagram of the power plant layout

2. Material and Methods

2.1 Power plant layout

The power plant layout (Figure 1) consists of the production and use of the syngas to generate electrical and thermal power. The syngas production section has been modelled as a fixed bed air gasifier operating in ideal conditions which can simulate the pyrolysis and air gasification process. The chemical reaction can be endothermic or exothermic depending on the process conditions. For an endothermic process the heat is provided by a burner fed by a syngas spilling. For an exothermic process the heat is supposed to be discharged. The pressure inside the gasifier is considered to be atmospheric. Before feeding the CHP, syngas is piped through heat recovery and clean-up sections. Heat exchangers are assumed to be adiabatic; the syngas is cooled from gasification temperature to 150 °C. This temperature has been chosen to minimize tar condensation that would clog up the heat

exchanger. The clean-up section can be considered a condenser where tar and water vapour are condensed and cooled to 25 °C. The heat extracted from the clean-up section is not recovered but lost in the atmosphere. Electricity consumption and pressure losses due to the ancillary equipment and to the filters, respectively, have not been considered. In this work, poplar wood has been used as feedstock for the gasification process. Its elemental composition, moisture content and heating value have been used as an input of the thermochemical equilibrium model. The characteristics of the feedstock have been reported in Table 1 on “as received” base (ar). Synthesis gas coming from gasification of biomass is used in an internal combustion engine (ICE) based on the Otto cycle. Like the gasifier, also the CHP has been modelled in a MATLAB-SIMULINK environment (M. Baratieri et al., 2009). The exhaust gases from CHP are processed by means of a heat exchanger and clean-up as previously described for the gasification section. Purified exhaust gas is then ready to be heated up to

140 °C through a heat exchanger and sent to the chimney.

The Otto cycle has been implemented in the simulation model in ideal conditions. Process air and synthesis gas are compressed in isentropic conditions according to a specified volume ratio (v_1/v_2). Then complete combustion occurs at constant volume, followed by an isentropic expansion of exhaust gases and a discharge of exhaust gases at a constant volume. Mechanical power is calculated considering the expansion work reduced by the compression work. The thermal power is considered to be produced by the exhaust gas cooling and the cylinder cooling. The cylinder is assumed to transfer 20% of the heat generated by the combustion to the cooling water. The Otto cycle is optimized in order to operate with gasoline which has different properties with respect to syngas. If compared to gasoline, syngas has a higher auto-ignition temperature, hence it enables the adoption of a higher volumetric ratio for the engine. In this work, volume ratio has been fixed to 15 in agreement with the scientific literature (Porpatham et al., 2012). Electrical power is converted from mechanical power considering an ideal electric generator. Thermal power is recovered by means of adiabatic heat exchangers, from both the gasifier and CHP sections. Electrical and thermal power have been computed to assess the electrical and thermal efficiency that have been calculated respectively as:

$$\eta_{el} = \frac{P_{el}}{LHV_{biom} \cdot Q_{m,biom}} \quad [1]$$

$$\eta_{th} = \frac{P_{th}}{LHV_{biom} \cdot Q_{m,biom}} \quad [2]$$

where LHV_{biom} is the lower heating value of the biomass and $Q_{m,biom}$ is the mass flow rate of biomass, P_{el} is the CHP electrical power and P_{th} is the thermal power recovered from both the gasifier and CHP.

2.2 Characteristics of the buildings

In this work the produced heat is supposed to be provided to four buildings, each one with ten floors. Each floor consists of one flat with the following characteristics: 100 m² of floor area without internal partitions, 3 m of internal height. The ratio between the surface area and the volume of the building (S/V) is equal to 0.47. The residential dwelling is supposed

to be located in Milan (2404 Heating Degree Days with a base temperature of 20°C).

The vertical surfaces of the envelope are oriented towards the cardinal points. The basement of the building has been considered to be in contact with an unheated basement with high ventilation rate. All the surfaces are light coloured both on the internal and the external sides (absorption coefficient equals to 0.3), with the exception of the internal floor and the external roof (absorption coefficient equals to 0.6). The opaque elements present a simplified two-layer structure with a massive clay block layer with a thermal resistance equal to 0.8 m² K W⁻¹ on the internal side and an insulating polystyrene layer (thermal conductivity 0.04 W m⁻¹ K⁻¹, density 40 kg m⁻³, specific heat capacity 1470 J kg⁻¹ K⁻¹) on the external side. The effect of the thermal bridges has been neglected. The ratio between the area of the glazings and the internal floor is equal to 11.67 %. The windows are double-glazed with a thermal transmittance of the glazing area equals to 1.1 Wm⁻²K⁻¹. The frame area is 19.9% of the whole window area (14.56 m²) and its thermal transmittance is 1.2 Wm⁻²K⁻¹. The ventilation rate has been fixed in 0.3 ach/h in accordance with the Italian technical standard UNI/TS 11300-1:2008 and the internal gains have been assumed as constant and equal to 4 Wm⁻², half radiant and half convective.

Several building configurations have been simulated considering different levels for the characteristics mentioned below. Four thicknesses of the thermal insulation layer have been considered: 0, 5, 10 and 15 cm. The thermal transmittances are respectively: 1.03, 0.45, 0.29 and 0.21 Wm⁻²K⁻¹. The glazing components are supposed to be all in a single façade East oriented or West oriented. Two glazings with different solar heat gain coefficients (0.608 and 0.352) have been considered. Combining the four different opaque structures, the two different glazings and the two orientation of the windows, 16 different cases have been simulated. The simulation of the building's behaviour have been performed by means of EnergyPlus 7.1 (U.S. DoE, 2011) with a time step of 1 minute. The heating air temperature set point has been fixed to 20 °C in accordance with the UNI/TS 11300-1:2008 prescriptions for residential buildings. The building-system dynamic simulations have been performed for three selected

configurations of buildings. The thermal insulation of the opaque components has been detected to be the parameter that mainly influences the load profile of the buildings. Therefore, the three selected cases have west-oriented windows with high solar transmittance but different thermal resistance of the opaque envelope (0, 5, 15 cm of thermal insulation).

2.3 Buildings Coupling with the Power Plant

For the building-system analysis, the buildings have been considered to be served by the same power plant (central system). Domestic hot water consumption has been determined in agreement with EN 15316-3-1:2007; it is representative of an average daily tapping pattern for a family with shower use. Heating and domestic hot water system consists of two main parts, the power production unit already presented and the power delivery system presented in this section.

Thermal losses of the delivery section have been considered constant for the whole year in agreement with the technical specification UNI TS 11300-2:2008. The domestic hot water system is characterized by an emission efficiency equals to 0.95 because no devices for the control of the supply are considered in the system. The distribution thermal loss has been considered negligible thanks to the thermal insulation of the distribution pipes. Concerning the heating system, the emission and distribution efficiencies depend on the envelope performance in agreement with the technical specification UNI TS 11300-2:2008. Three values are mentioned below: the first value refers to the building without thermal insulation, the second one to 5 cm of insulation and the third one to 15 cm. The emission efficiency has been considered equal to 0.90/0.93/0.95; it refers to the amount of heat transferred by means of radiators. The control efficiency can be considered the same for the three analysed buildings and equals to 0.94; it refers to an on/off temperature control for each room of the building. The distribution efficiency has been considered equals to 0.97/0.98/0.99; it depends on the insulation distribution of the building.

The experience shows that most of the gasifiers run as much as possible without care to the dissipated

heat due to the high interest to the electricity production. Actually, from the economical point of view, there is more interest in the electricity valorisation (comprehensive incentive) than the heat valorisation. Furthermore most of the gasifiers require complex operations to reach the steady state performance hence a partial or on/off operational mode is still considered a future development. In this work the power plant is supposed to run without stops for the whole operational time of the year. The selected operational times are considered to be centred on the coldest day of the reference year. The entire electricity production is given to the electrical grid that can act as an infinite storage facility while only part of the thermal production is useful. When the buildings have no heat demand, heat has to be dissipated. In this perspective, PES (primary energy saving) has been calculated to evaluate the energetic convenience to adopt a cogeneration system instead of the separated production of heat and power. In agreement with the Directive 2004/8/EC (European Parliament, 2004), PES has been calculated as:

$$PES = 1 - \frac{1}{\frac{CHP H\eta}{Ref H\eta} + \frac{CHP E\eta}{Ref E\eta}} \quad [3]$$

where $CHP H\eta$ and $CHP E\eta$ are respectively the thermal and electrical efficiencies of the CHP calculated with the simulation model, $Ref H\eta$ is the efficiency reference value for separate heat production, $Ref E\eta$ is the efficiency reference value for separate electricity production. The efficiency reference values depend on the year of construction of the power plant and on the type of fuel; they have been determined in agreement with Italian law (European Parliament, 2004). Considering the plant construction at the present year and wood as fuel, $Ref E\eta$ is 0.3 and $Ref H\eta$ is 0.86.

2.4 Economic Analysis

The differential cash flow has been evaluated between the CHP plant and a traditional boiler, both systems have the same thermal power. The payback time (PBT) and the annual worth (AW) have been calculated considering the gasifier as a reference for the lifespan of the whole power plant. Both the economic indexes consider a real interest rate equals

to 3 %. The discounted PBT estimates the time required to recover the investment cost and AW estimates the revenue per year of owning and operating an asset over its entire lifespan. Table 2 reports the costs and revenues required to perform the economic analysis. The heat economic valorisation has been calculated considering the natural gas LHV equals to 32.724 MJ/Sm³ and the natural gas cost for residential use equals to 0.85 €/Sm³. With the previous hypothesis, thermal power is valorised at 0.094 €/kWh. The cogeneration bonus is paid for the electricity that is produced if the heat is used in the proper way. In particular the cogenerative electricity coming from a cogenerative operation is calculated according to the Directive 2004/8/EC (European Parliament, 2004). The lifespan of the power plant has been considered to be 80 000 hours for the gasifier and 40 000 hours for the engine.

3. Results and Discussion

3.1 Syngas Production Section

The air gasification process has been simulated for different values of gasification temperature and equivalence ratio to define an optimum theoretical condition (Figure 2). The gasification temperature has been evaluated between 500 °C and 1000 °C. The equivalence ratio has been evaluated between 0.0 and 0.6. The optimization has been based on the

electrical efficiency. The maximum electrical power has been obtained for a gasification temperature of 800 °C and ER of 0.1. In this configuration the CHP electrical efficiency is 0.23 and the CHP global efficiency is 0.79. The global efficiency has been computed as the sum of the electrical and the thermal efficiency. The optimal configuration corresponds to the complete conversion of carbon. The gasifier uses 26% of the produced syngas to feed the heater that keeps the gasification temperature. A share of 15% of the total thermal power is recovered in the heat recovery section of the gasifier, while a further share of 85% is recovered in the correspondent section of the CHP system.

parameter	value
IC, gasifier + engine ⁽¹⁾ [€/kW _{el}]	4500
IC, engine ⁽¹⁾ [€/kW _{el}]	2200
maintenance cost ⁽¹⁾ [€/kWh _{el}]	0.080
biomass cost ⁽²⁾ [€/kg]	0.133
electricity revenue ⁽³⁾ [€/kW _{el}]	0.229
heat valorisation ^(4,5) [€/kW _{th}]	0.094
cogeneration bonus ⁽³⁾ [€/kW _{el}]	0.040
real interest rate [%]	3.00

⁽¹⁾M. Prussi, personal communications, October 2012, C.R.E.A.R. University of Firenze; ⁽²⁾Agriforenergy n.3/2012; ⁽³⁾D.lgs 6th July 2012 n. 159; ⁽⁴⁾Autorità per l'Energia Elettrica e il Gas, 2011, Relazione annuale sullo stato dei servizi e sull'attività svolta, Milan; ⁽⁵⁾Ministry of Economic Development, 2011, Bilancio Energetico Nazionale 2010, Rome.

Table 2 – Parameters for the economic analysis

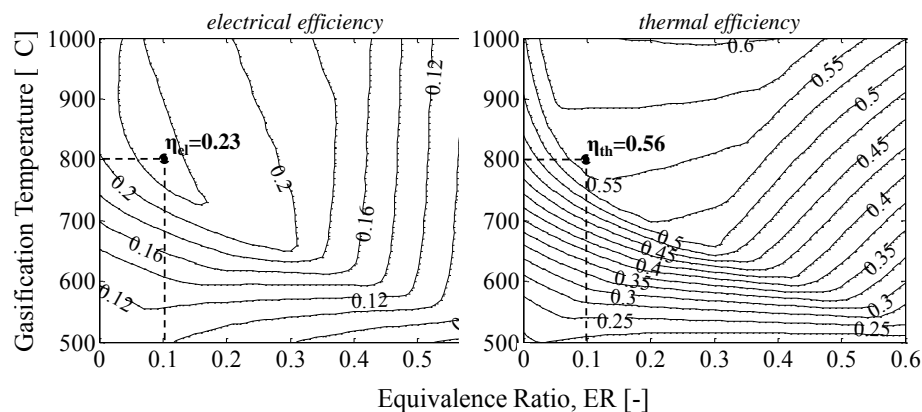


Fig. 2 – Electrical and thermal efficiency of the whole power plant layout

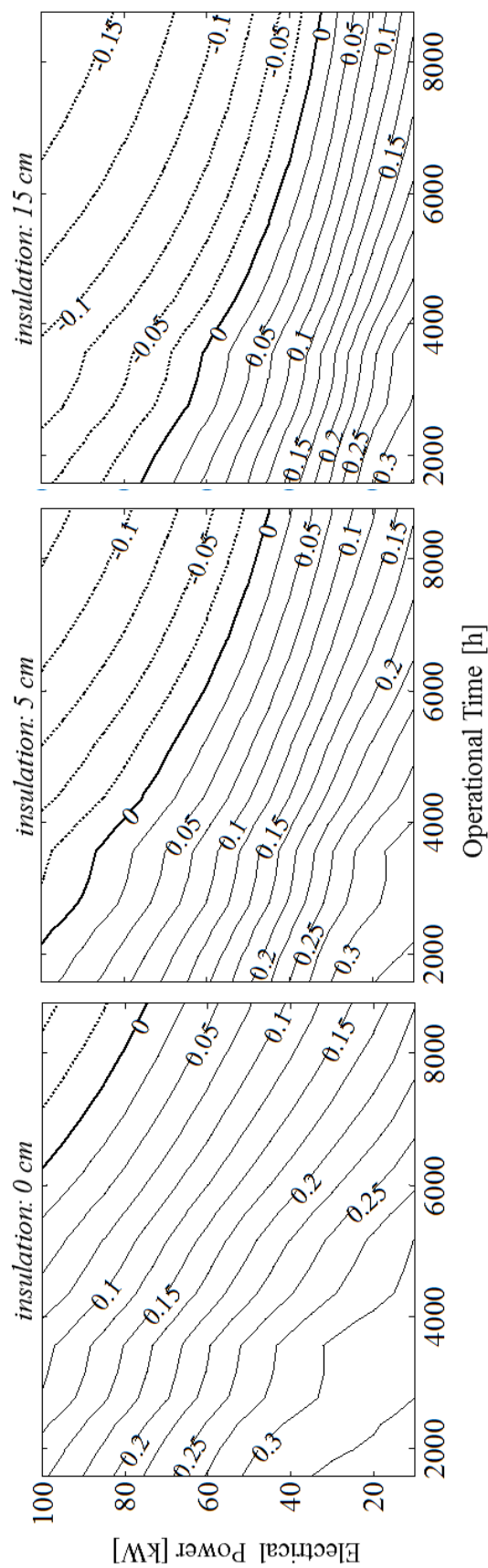


Fig. 3 – PES depending on the power plant size and the operational time for different building configurations

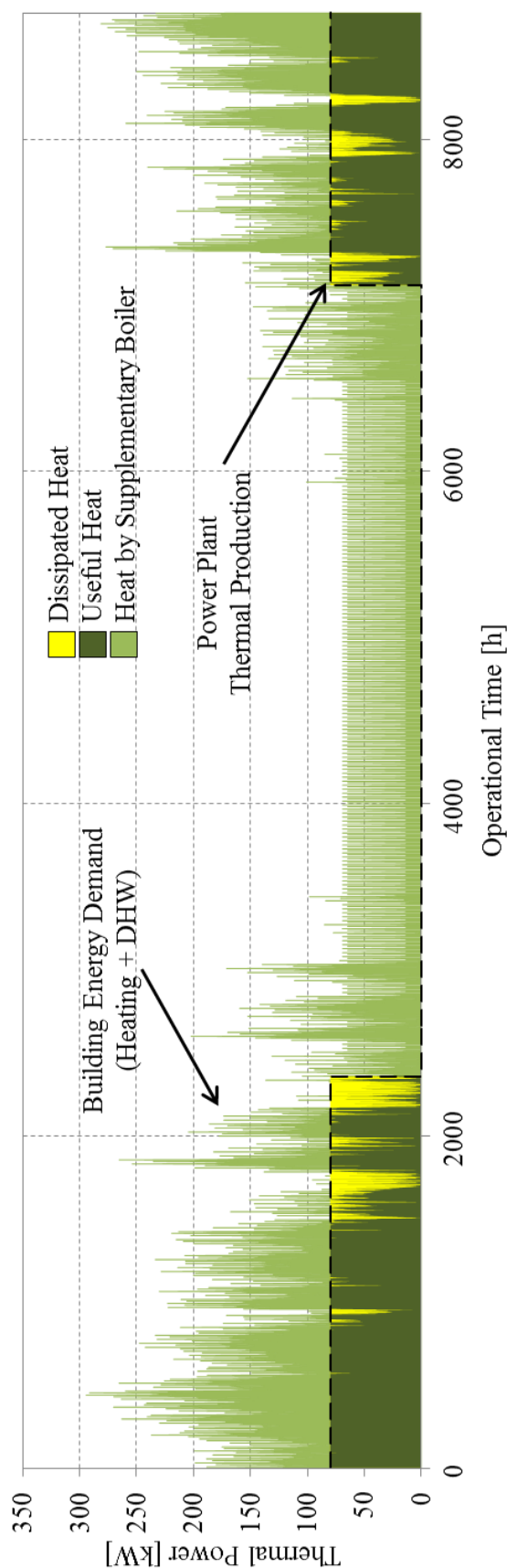


Fig. 4 – Heat demand of the building without envelope insulation and thermal power produced by a power plant of 30 kWel operating for 4000 hours per year

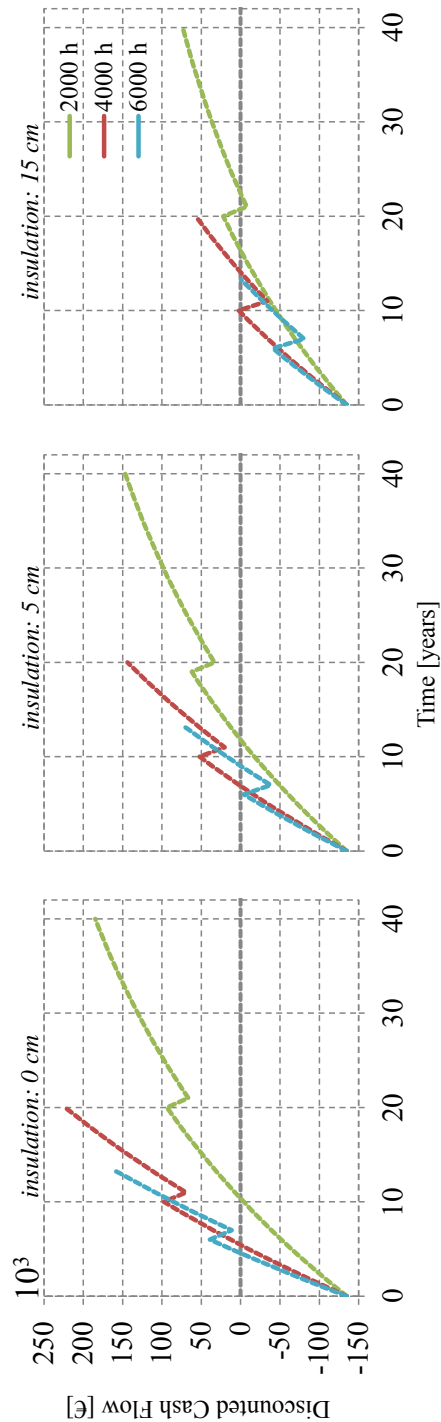


Fig. 5 – Payback time for a 30 kWel power plant, considering different operational times and building configurations

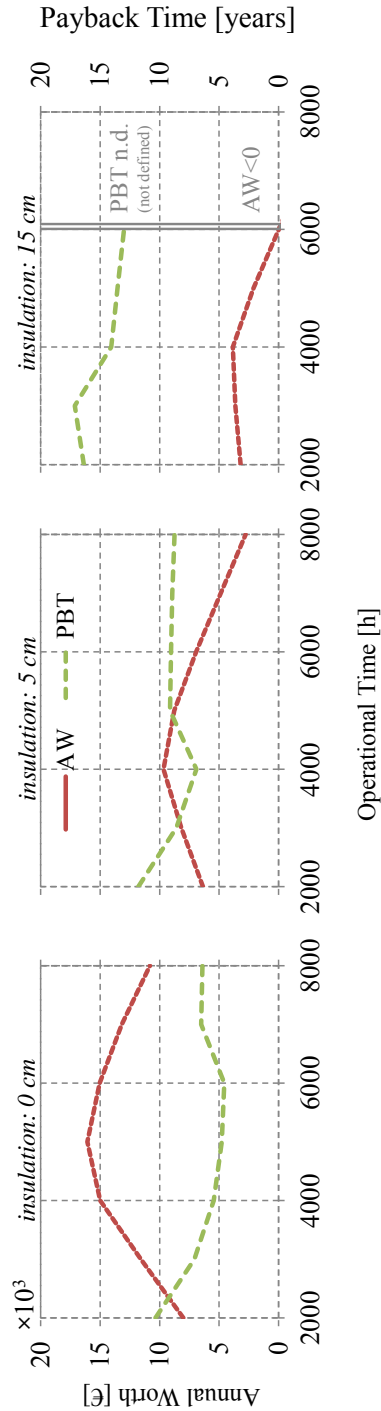
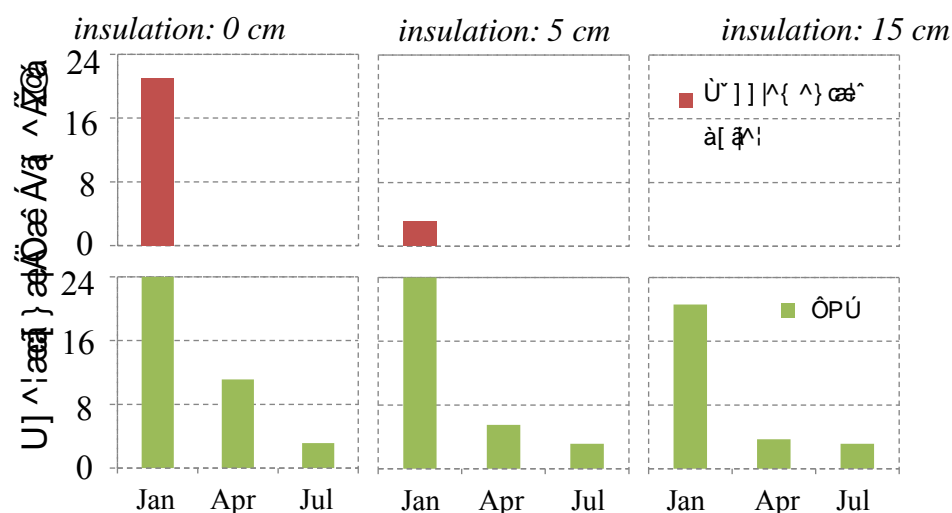


Fig. 6 – Annual Worth (AW) and Payback Time (PBT) for a 30 kWel power plant, considering different operational times and building configurations

Building Configurations:	Insulation: 0 cm	Insulation: 5 cm	Insulation: 15 cm
PES	0.29	0.23	0.15
Disposed Heat	14 %	29 %	46 %
Heat demand covering	52 %	70 %	73 %

Table 3 – Indexes summary for 30 kW_{el} (plant size) and 4000 hours (operational time)Fig. 7 – Operational time for a 30 kW_{el} (80 kW_{th}) power plant. Three average days (January, April, July) are considered for different building configurations. Supplementary boiler is supposed to be 80 kW_{th}

3.2 Power Plant and Buildings

The primary energy saving (PES) of the power plant layouts is analysed in this section. The index has been calculated for several power plant sizes and operational times in order to trace some performance charts. Figure 3 shows areas of positive values of PES for all the three building configuration solutions. As the index is related to the exploitation of the produced heat, the less heat that is discharged, the larger the PES. Short operational time and small plant size reach higher primary energy saving values, but there are some limitations to consider, such as that no commercial plants smaller than 30 kW_{el} exist. Furthermore, operational times shorter than 4000 hours could lead to a high payback time. Figure 4 shows the thermal load of a building (i.e. building without envelope insulation) and the heat produced by a power plant for the whole year. As previously mentioned, a higher thermal power production could be entirely exploited only during the coolest months. For most of the operational time

the produced heat would be discharged. Considering the smallest plant size (30 kW_{el}), Figure 5 shows the discounted cash flow for a power plant of 30 kW_{el} that runs for 2000 h, 4000 h and 6000 h. The economic analysis has been performed for the three analysed building configurations (0/5/15 cm of the envelope insulation) and it confirms what has already been mentioned: power plants operating for 4000 hours have an interesting payback time that becomes less attractive decreasing the operational time. Furthermore, the supplementary boiler would run more frequently decreasing the operational time of the CHP: this means that the global efficiency of the power plant decreases due to the separated production of heat and power.

Figure 6 shows the payback time (PBT) and the annual worth (AW) for the three analysed building configurations. The choice of the optimal operational time could be based on the AW rather than the PBT depending on the optimization target. Considering the AW, the optimal operational time corresponds to 5000 h (16072 €/y) for the building without envelope

insulation, 4000 h (9674 €/y) for the building with 5 cm of insulation and 4000 h (3838 €/y) for the building with 15 cm of insulation. Considering the PBT, the optimal operational time corresponds to 6000 h (4.6 y) for the building without envelope insulation, 4000 h (6.9 y) for the building with 5 cm of insulation and 6000 h (13 y) for the building with 15 cm of insulation. Both economic indexes show that the optimal operational times correspond with values between 4000 h and 6000 h for the three building configurations. Some detailed results are shown in Table 3 considering a power plant of 30 kW_{el} and 4000 hours of operational time. PES is greater than zero for the three building configurations. The discharged heat is considerably high for the building with 15 cm of insulation, which means that the power plant size does not match with the application. A better exploitation of heat could be reached increasing the number of users that are served by the power plant but in that case a district heating system is a more realistic approach. Heat demand covering represents the amount of heat demand that is covered by the cogeneration system. The complementary percentage should be provided by a supplementary boiler. A high operation of the supplementary boiler would decrease the global efficiency of the whole system due to the separated production of heat and power. An on/off operational mode seems a possible solution to reduce the wasted heat. In this perspective, Figure 7 shows the operational time of a 30 kW_{el} CHP system for three average days (January, April and July). The graph shows that for the winter months (i.e. January) the supplementary boiler is required to meet the building energy demand. For the summer, the spring and the autumn months the supplementary boiler is not required and an on/off operational mode could decrease the dissipated heat. Nevertheless, a power off followed by a power on in a short time span could lead to an energetic waste considering the energy lost to reach the steady state conditions. In fact the system starts to produce electricity as soon as the syngas meets the chemical composition required by the internal combustion engine. Further development has to be carried out for an exhaustive assessment of the on/off operational mode.

4. Conclusion

The analysed CHP gasifier presents an optimal operation for gasification temperature equals to 800°C and ER equals to 0.1. Electrical efficiency is 0.23 and global efficiency is 0.79. Gasification power plants smaller than 30 kW_{el} are not commercially available. Considering the smallest power plant (30 kW_{el}), the PES is positive for all the building configurations but the economic benefits are more interesting for the building with 5 cm of insulation and even more for the building without insulation. In the latter case the power plant has the lowest heat discharge (14 %) and a high operation of the supplementary boiler. In fact 52 % of the heat demand is provided by the non-cogenerative system, decreasing the global efficiency of the whole system. Both the annual worth (AW) and the payback time (BPT) show that the optimal operational times correspond with values between 4000 h and 6000 h for the three building configurations.

Further developments of this work foresee the assessment of an on-off operational mode of the gasifier to increase the efficiency of the whole power plant. In fact, this operational mode can be considered as a feasible way to reduce wasted heat, even if a careful assessment of the energy losses - needed to reach the nominal condition - has to be carried out.

References

- Ahmed, T.Y. et al., 2012. Mathematical and computational approaches for design of biomass gasification for hydrogen production: A review. *Renewable and Sustainable Energy Reviews*, 16(4), pp.2304–2315.
- Baratieri, M. et al., 2009. The use of biomass syngas in IC engines and CCGT plants: A comparative analysis. *Applied Thermal Engineering*, 29(16), pp.3309–3318. Available at: <http://linkinghub.elsevier.com/retrieve/pii/S1359431109001446> [Accessed October 14, 2011].
- Dong, L., Liu, H. & Riffat, S., 2009. Development of small-scale and micro-scale biomass-fuelled CHP systems – A literature review. *Applied Thermal Engineering*, 29(11-12), pp.2119–2126. Available at: <http://linkinghub.elsevier.com/retrieve/pii/S1359431108004766> [Accessed August 3, 2011].

- European Parliament, 2004. Directive 2004/8/CE of the European Parliament and of the council of 11 February 2004. , pp.50–60.
- Fagbenle, R.L., Oguaka, a. B.C. & Olakoyejo, O.T., 2007. A thermodynamic analysis of a biogas-fired integrated gasification steam injected gas turbine (BIG/STIG) plant. *Applied Thermal Engineering*, 27(13), pp.2220–2225.
- Porpatham, E., Ramesh, a. & Nagalingam, B., 2012. Effect of compression ratio on the performance and combustion of a biogas fuelled spark ignition engine. *Fuel*, 95, pp.247–256.
- Prando, D. et al., 2012. Modeling analysis of biomass gasification MCHP systems for residential applications. In E. Florence, ed. *European Biomass Conference and Exhibition - Setting the course for a biobased economy*. Milan, Italy, pp. 1058–1064.
- Van Ree, R. et al., 1995. Modelling of a biomass-integrated-gasifier/combined-cycle (BIG/CC) system with the flowsheet simulation programme ASPEN+,
- UNI EN 15316-3-1 Impianti per la produzione di acqua calda sanitaria, caratterizzazione dei fabbisogni.
- UNI/TS 11300-1 Determinazione del fabbisogno di energia termica dell' edificio per la climatizzazione estiva ed invernale.
- UNI/TS 11300-2 Determinazione del fabbisogno di energia primaria e dei rendimenti per la climatizzazione invernale e per la produzione di acqua calda sanitaria.

On the influence of several parameters in energy model calibration: the case of a historical building

Roberta Perneti – University of Pavia, Pavia, Italy

Alessandro Prada – Free University of Bolzano, Bolzano, Italy

Paolo Baggio – University of Trento, Trento, Italy

Abstract

The aim of this work is to investigate the extent to which several different variables (e.g. climate conditions, infiltration rates and envelope characteristics) could affect the calibration process and, consequently, the reliability of the simulation outcomes. In this regard, in this paper the calibration phases of a dynamic hourly energy model for an existing building are presented. The test case is a historical construction built at the end of the nineteenth century in northern Italy. The building, originally designed for tobacco processing, has a massive envelope and it has no HVAC system. Therefore, the simulation model is calibrated using the actual air and wall surface temperature as control variables. Finally, a sensitivity analysis is carried out in order to assess the incidence of different inputs in building thermal behaviour and to identify which parameters have to be refined with the aim of optimizing the model calibration.

1. Introduction

Energy simulation represents a useful tool to describe building actual behaviour; hence it is used not only in the design process but also in the post occupancy analysis with the purpose of evaluating the actual energy efficiency of a building. In fact, the recast Energy Performance Building Directive (*EPBD 2010/31/EU*) highlights that residential and commercial buildings account for more than one third of total annual energy consumption. Since significant energy savings can be achieved through energy conservation measures (ECM) for existing building stock, the importance of refurbishment has been growing. Consequently, simulations have been applied to existing constructions to assess their energy performance and to define effective

ECM. However, the large number of required parameters affects the reliability of a simulation and significant discrepancies between predicted and real data could occur. For this reason, model calibration with monitored data is often appropriate in order to refine models and to develop more realistic energy-behaviour simulations.

In this regard, a new European standard is going to be developed by CEN Technical Committee 89 (Working Group 14) and it will provide for calibration strategies and measurements post processing procedures for building energy models. Currently, three standards define general criteria and tolerance ranges for model calibration:

- International Performance Measurement and Verification Protocol (IPMVP 2012),
- Measurement and Verification (M&V Guidelines 2008);
- ASHRAE Guideline 14/2002: Measure of energy and demand savings.

However, none of these protocols establish an operative methodology to calibrate building models. In the literature, several studies face the model calibration issues using actual energy consumption either from in situ measurements during the calibration period (e.g. Raftery et al. 2011; Norford et al. 1994) or from the analysis of monthly utility bills (e.g. Yoon et al. 2009). Only a few works adopt the internal temperature as a calibration goal (e.g. Tian et al. 2009). In fact, in this approach the monitoring data could be affected by a series of uncertainties and interactions with the indoor environment, such as occupant behaviour, internal gain and building equipment. Besides, the measurement of several variables can be an

expensive and time consuming activity. However, the model calibration using temperature as a control variable is the only viable procedure when no operating HVAC are present in a building. Taking into account these considerations, an issue closely related to calibration activity becomes the sensitivity analysis (SA) of the model to the input data. This calculation technique is applied for the evaluation of building thermal response according to a given perturbation of inputs in order to assess the parameter influence on the building energy performance. Hence the results of the sensitivity analysis reveal the strategy to refine a building simulation model (e.g. Lam et al, 1996).

This paper aims firstly to define a suitable calibration procedure of an existing building model using temperatures as control variables. Secondly, starting from the model calibrated against the experimental data, a sensitivity analysis is carried out with the aim of investigating the extent to which several parameters affect the energy model. The purpose of this investigation is to discover which parameters, if experimentally measured, can improve the model calibration.

2. Case study

The case study is a historical manufacturing facility built in Rovereto in northern Italy. The overall surface of the construction is 3650 m² and it has four levels and one basement. The envelope has a high thermal mass with a homogeneous ratio of the glazing over an opaque surface, which is equal to 0.3.

Since the building has no HVAC system, the internal temperatures have been monitored in order to calibrate the simulation model. In particular, both the surface and air temperatures have been collected every 10 minutes in the control thermal zone (i.e. P3_Z1) that is placed on the 4th floor next to the roof (Figure 1). The measurement campaign was carried out from March to June 2012.

In Figure 1 the instrument position is shown: the heat flux meter (HFM) apparatus (two HFM and two thermo-resistance pt100) is installed in B, while the points from S1 to S5 indicate the

thermistors employed for the surface temperature recording.

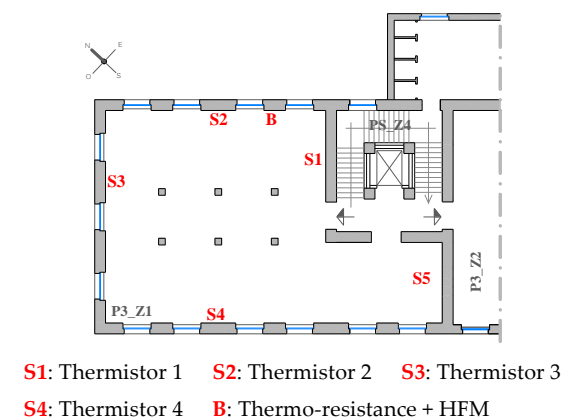


Fig. 1 – Control thermal zone

3. The calibration procedure

Model calibration is an iterative process which, through the assessment of a series of simulations with different inputs, aims to reduce the discrepancies between simulated and actual building energy behaviour.

The main steps of a calibration procedure are as follows:

- Simulation plan: aim of calibration, availability of data and validation criteria;
- data gathering: input and calibration parameters have to be collected
- simulation runs
- comparison between predicted and actual values

If the results of the validation indices are in agreement with the tolerance range, the model is correctly calibrated, otherwise the model has to be revised in order to reach the calibration target. Inputs have to be refined according to the source hierarchy, which must be defined for each case study as a function of the accuracy and the reliability of the data source. Further, a sensitivity analysis can be carried out to investigate the most influent inputs and refine them.

3.1 Model calibration criteria

The calibration protocols employ some validation indices to quantify the calibration of the model. Then, the calibration indices have to consider both the gap between actual and predicted values and their correlation.

Defining M the monitored data, S the simulation outcomes and N the number of data, the following indices are applied:

Mean Bias Error MBE

$$MBE = \frac{\sum_{i=1}^N (S_i - M_i)}{N} \quad (1)$$

MBE provides for a general gap between predicted and actual values. This index can give a misleading indication due to the sign error compensation.

Root Mean Square Error RMSE

$$RMSE = \sqrt{\frac{\sum_{i=1}^N (S_i - M_i)^2}{N}} \quad (2)$$

It overcomes MBE weakness, since it considers the absolute error values.

Pearson's Index r

$$r = \frac{\sum (S_i \cdot M_i) - \sum (M_i) \cdot \sum (S_i / N)}{\sqrt{\left(\sum (M_i^2) - \frac{\sum (M_i)^2}{N} \right) \left(\sum (S_i^2) - \frac{\sum (S_i)^2}{N} \right)}} \quad (3)$$

It represents a measure of the correlation between two variables. The Pearson's index ranges from -1 to 1, where a negative value means an opposite correlation.

3.2 Building model input

The calibration procedure aims to optimize the model and to reduce the discrepancies between predicted and real values. In order to reach this target a set of simulations is defined. In particular, due to the building characteristics, three variables are assumed as main inputs of the energy model:

- weather data;
- air-change rates;
- thermo-physical properties of the envelope.

Since weather variables (temperature, solar

radiation, relative humidity and wind speed) are the external solicitation and the main cause of heat losses/gains, they play an important role in the building energy model. Consequently a reliable dataset is necessary to assess a correct energy simulation.

Regarding the case study, three different sets of data were available.

The first source of data is the Test Reference Year (TRY), which reports hourly standard values for weather variables defined according to EN 15927-4. This standard defines a method to develop a reference year starting from long period measurements (at least ten years). In a recent study (Baggio et. al, 2010), the TRY for the Italian provinces are developed and the TRY are now provided by Thermo-technical Italian Committee (C.T.I.). The other two datasets are collected by a meteorological station in Rovereto close to the building location but on two different sides of the valley: Meteo Trentino (45.88° N, 11.05° E) and IASMA (45.89° N, 11.65° E). Figure 2 and Figure 3 show respectively the temperature and the solar radiation trends for the three datasets over three days (i.e. March 17th - 19th) which represent both sunny and cloudy conditions. Despite the different exposure, Meteo Trentino and IASMA show consistent trends for every day while, obviously, the TRY presents significant discrepancies, especially during the second day.

The second analysed variable is the air change rate, in fact, since the building has no HVAC system, natural ventilation is considered. In particular the effect of infiltration is taken into account since it represents the only source of ventilation.

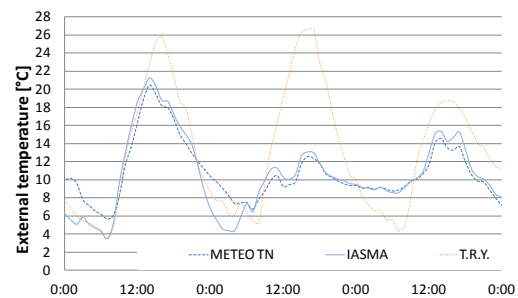


Fig. 2 – External temperature (March 17th - 19th)

Table 1 shows the different air change rates applied in the calculation. The standard values (0.3 and 0.5 ach) are adopted even if they are used for global natural ventilation because the envelope presents numerous cracks and leakages. EN 15242 and the ASHRAE Handbook define standard methods to estimate the infiltration air-change rates, according to envelope features and to local weather data (temperature and wind speed).

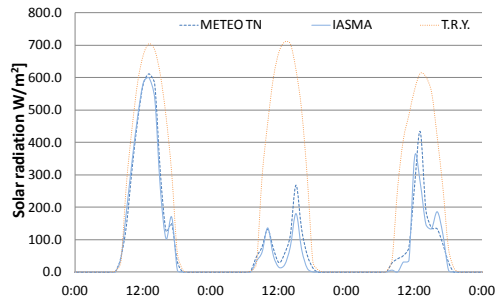


Fig. 3 – Solar radiation (March 17th - 19th)

Code	Air-change rate [h ⁻¹]	Standard source
0.3	0.3	UNI/TS 11300-1
0.5	0.5	-
EN	variable	UNI EN 15242:2008
ASH	variable	ASHRAE Handbook

Table 1 – Air change rates

Finally, the thermo-physical properties of the envelope are evaluated both through standard and experimental analysis. The external wall in zone P3_Z1 is 65 cm thick, it has a high thermal mass and it is built of bricks and sand. Therefore, according to UNI TS 11300-1, the reference structure CO-01 is chosen. Moreover an experimental analysis was carried out conforming to ISO 9869; two couples of HFM and thermo-resistance pt100 were positioned on internal and external surfaces in order to measure surface temperatures, inward and outward heat fluxes. The measurements were carried out over 70 days (March 2nd - May 10th) in order to obtain stable results. The monitored data were post processed with the average method described in standard ISO 9869. The values of conductance for standard

and experimental method are reported in Table 2.

Λ [W m ⁻² K ⁻¹]	
Standard approach (STD)	Experimental approach (MS)
1.372	1.552

Table 2- Thermal conductance

Starting from the different sources of input data, a series of simulations was carried out with the TRNSYS software. A code identifies each model and it describes which kind of parameter is applied in the analysis. Table 3 shows the set of simulations and it explains which inputs have been implemented.

4. Results of Model Calibration

After the run of the simulation set shown in Table 3, the discrepancies between simulated and real values are evaluated in terms of MBE, RMSE and Pearson's index, for the hourly temperature measured during the monitoring period (March 2nd - June 26th).

The indices give information both for air (air) and for the envelope surfaces (S1 - S2 - S3 - S4 - S5) temperature in the control thermal zone P3_Z1.

MBE in Figure 4 highlights a general underestimation of the predicted temperature with respect to actual data. Moreover, the results of TRY simulations present high discrepancies; in fact MBE generally ranges from 0.05°C to 0.8°C for positive values and between - 0.05 to - 1.4 for negative ones, except for TRY results, whose MBE account for -0.8°C -3.4°C. Obviously, the end of the TRY, and consequently of its calculation procedure, is to be representative of the average weather conditions of the location. For this reason, the TRY does not lend itself to an accurate punctual assessment as it is instead the model calibration. Considering MBE error compensation, this index is not exhaustive to evaluate the reliability of simulations.

RMSE overcomes this problem, because it reveals

the absolute discrepancies between real and simulated values. In this case RMSE indices confirm the previous considerations: in fact TRY simulations have RMSE values next to 4°C (5°C for S2 temperature surface), while the other simulations carried out with real weather datasets range from 1°C to 1.7°C (Figure 5). The other parameters (thermo-physical properties of external walls and air change rates) do not significantly affect the RMSE values.

Input data		IAS 03 STD	TN 03 STD	TRY 03 STD	IAS 05 STD	TN 05 STD	TRY 05 STD	IAS EN STD	TN EN STD	TRY EN STD	IAS ASH STD	TN ASH STD	TRY ASH STD
Weather data	IASMA	x			x			x			x		
	MeteoTn		x			x			x			x	
	TRY			x			x			x			x
Air change rates	0.3	x	x	x									
	0.5				x	x	x						
	EN ISO 15242:2008								x	x	x		
	ASHRAE										x	x	x
	Standard	x	x	x	x	x	x	x	x	x	x	x	x
Envelope properties		Measured											
Input data		IAS 03 MS	TN 03 MS	TRY 03 MS	IAS 05 MS	TN 05 MS	TRY 05 MS	IAS EN MS	TN EN MS	TRY EN MS	IAS ASH MS	TN ASH MS	TRY ASH MS
Weather data	IASMA	x			x			x			x		
	MeteoTn		x			x			x			x	
	TRY			x			x			x			x
Air change rates	0.3	x	x	x									
	0.5				x	x	x						
	EN ISO 15242:2008								x	x	x		
	ASHRAE										x	x	x
	Standard												
Envelope properties		Measured	x	x	x	x	x	x	x	x	x	x	x

Table 3 - Set of simulations

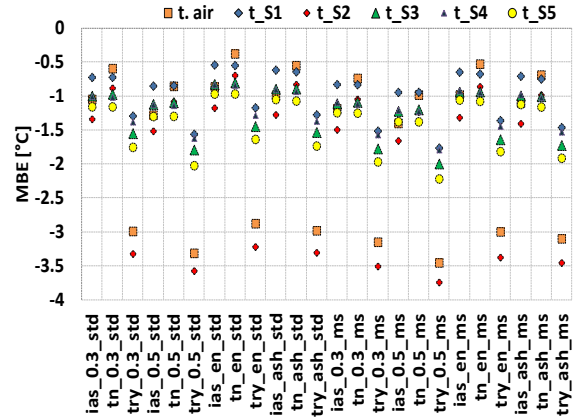


Fig. 4 – Mean Bias Error

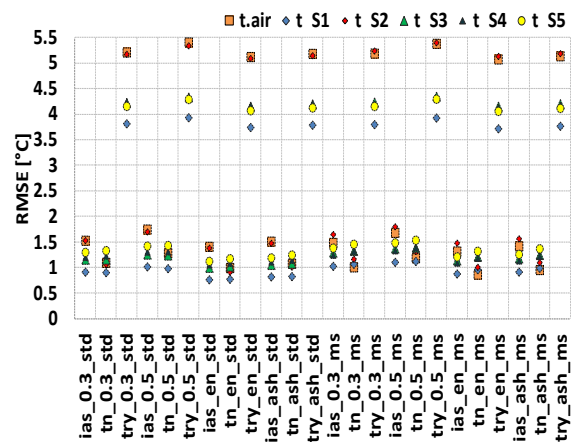
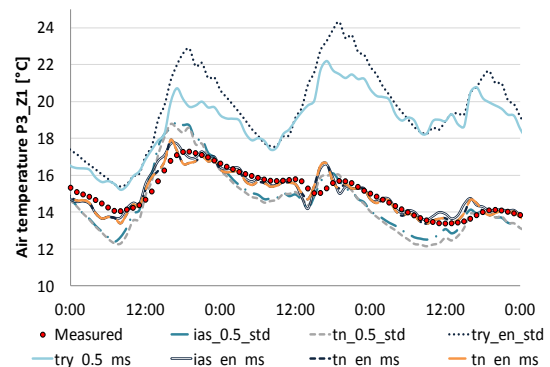


Fig. 5 – Root Mean Square Error

Nevertheless, error indices give information about the global gap between actual and predicted temperature and, in order to understand the reliability of building simulations, it is necessary to evaluate the hourly temperature trends in the control thermal zone, comparing the monitored values and the simulation results.

Fig. 6 – Air temperature - April 23rd - 24th

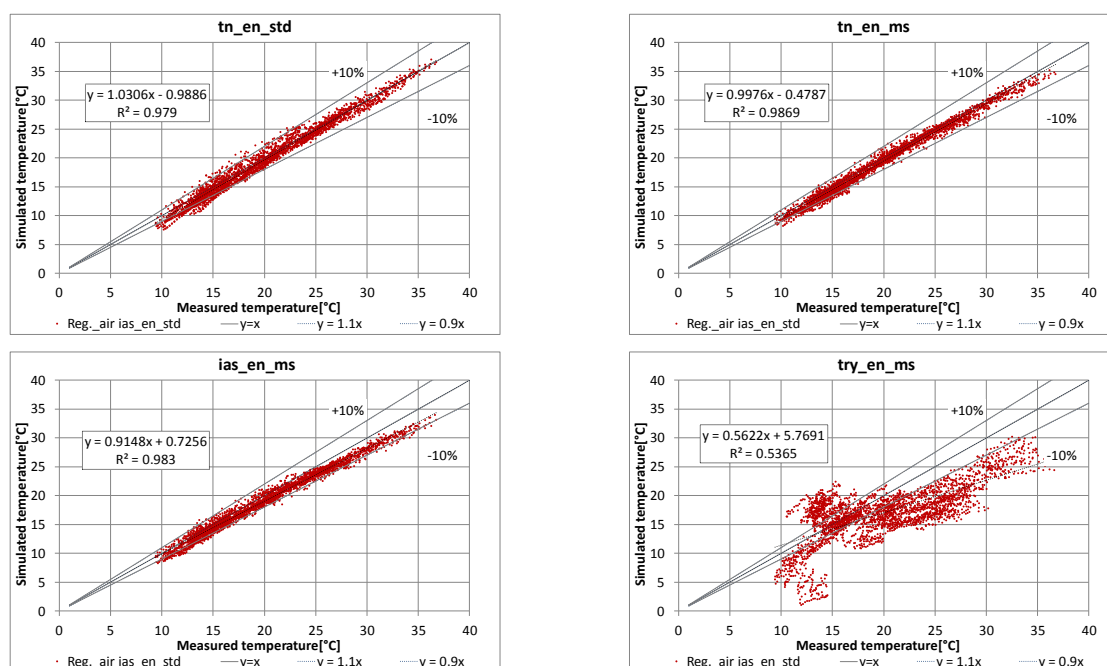


Fig. 7 – Regression analysis t. air P3_Z1 - measured and predicted values

ias_03_std	tn_03_std	try_03_std	ias_03_ms	tn_03_ms	try_03_ms
0.982	0.988	0.711	0.988	0.990	0.742
ias_05_std	tn_05_std	try_05_std	ias_05_ms	tn_05_ms	try_05_ms
0.979	0.987	0.711	0.988	0.991	0.742
ias_en_std	tn_en_std	try_en_std	ias_en_ms	tn_en_ms	try_en_ms
0.982	0.989	0.715	0.989	0.992	0.746
ias_ash_std	tn_ash_std	try_ash_std	ias_ash_ms	tn_ash_ms	try_ash_ms
0.981	0.988	0.715	0.989	0.991	0.746

Table 4 – Pearson's Index for air temperature

In Figure 6 some representative air temperature trends are reported for three days of the calibration period (April 21st-23rd). TRY simulations are featured by different thermal behaviours of the zone, according to the different weather conditions of the standard dataset. The other simulations have more reliable trends, but the models with standard thermo-physical properties reproduce positive and negative temperature peaks higher than real ones, probably caused by the different thermal capacitance of the walls.

Pearson's indices (Table 4) confirm the previous considerations; in fact weather data strongly affect the model results while the other parameters cause slight variations in r : air-change rates determine negligible differences, and measured thermo-

physical properties increase the correlation between real and predicted values.

Finally, in order to identify the most reliable simulation for internal air temperature, also a regression analysis between measured and simulated temperature is developed. The simulations with air change rates computed by means of EN 15242 are reported in Figure 7.

It clearly appears that simulations with standard weather data have low R^2 values, and a significant spread of results, which indicates low correlation between the two variables. The models with real datasets have regression indices close to 1 and a more regular distribution across the regression line; in fact most of the values are include in the tolerance interval of $\pm 10\%$. In particular, the simulation tn_ash_ms could be considered the most reliable simulation which is obtained applying the calibration procedure. Nevertheless, some discrepancies between predicted and real temperature still affect the model, therefore, in order to refine the model, deeper analysis are necessary. Hence a sensitivity analysis is carried out in order to identify the parameters with an high impact on the model results.

5. Sensitivity analysis

The sensitivity analysis aims to evaluate the influence of input data on the dependent variables which, in the case of building simulations, represent the energy behaviour of constructions. Since in the test case there are no energy systems, the dependent variables are related to the air temperature of the control thermal zone (i.e. P3_Z1). In particular, since the final goal of the energy model will be the system sizing and the evaluation of energy demand, four different indexes are herein adopted and investigated from January 1st to September 30th.

- Minimum temperature (t_{\min})
- Maximum temperature (t_{\max})
- Zone Heating Degree Hour (HDH_{18})
- Zone Cooling Degree Hour (CDH_{26})

Heating and Cooling Zone Degree Hour indicate the sum of hourly difference between internal set point temperature (i.e. 18°C for heating and 26°C for cooling) and the simulated values for P3_Z1 thermal zone; they are evaluated with the following equations and to a certain extent they are proportional to the heating and cooling demand, as well as minimum and maximum temperature are closely related to the required size of energy system.

$$HDH_{18} = \sum_{i=1}^n (\vartheta_{i,H,set} - \vartheta_{i,H,sim}) \quad (4)$$

$$CDH_{26} = \sum_{i=1}^n (\vartheta_{i,C,sim} - \vartheta_{i,C,set}) \quad (5)$$

In this work, a sensitivity analysis has been carried out with a local external approach using two different procedures, i.e. differential sensitivity analysis and factorial method, with the aim of evaluating which parameters have to be refined in order to improve the model results, according to the limited resources in terms of experimental analysis.

5.1 Differential sensitivity analysis

The Differential Sensitivity Analysis (DSA) works by perturbing an input data around the mean value while all the other parameters remain fixed. For each perturbed value the numerical simulation is carried out and the model response is calculated.

Due to its robustness and simplicity, the DSA is the most diffused method for a local uncertainty evaluation. The effects of an uncertain parameter are estimated by comparing the results of these simulations against those with unperturbed inputs. Consequently, a sensitivity index of the model prediction to the uncertain parameter is defined as:

$$s = \frac{\Delta O}{\Delta I} \quad (6)$$

where O is the model output and I is the perturbed input (the other parameters influencing the output are held fixed).

Since the absolute sensitivity index depends on the magnitude of parameter perturbation, a direct comparison between different variable influences is not possible. In order to overcome this aspect, a percentage sensitivity index is defined as

$$s_{\%} = \frac{\Delta O / O_{un}}{\Delta I / I_{un}} \quad (7)$$

where O_{un} is the model output with unperturbed input and I_{un} is the unperturbed input.

For the analysed building, the following inputs are perturbed applying a $\pm 10\%$ variation to the original value of:

- Infiltration air change rates (Q_{4Pa})
- Roof thermal transmittance (U_{roof})
- Wall thermal transmittance (U_{wall})
- Intermediate Floor thermal transmittance (U_{floor})
- Roof thermal capacitance (K_{roof})
- Wall thermal capacitance (K_{wall})
- Floor thermal capacitance (K_{floor})
- g-value for glazing systems (g-value)

In Figure 8 the computed $s_{\%}$ for HDH_{18} and CDH_{26} are reported for each case analysed. Note that for CDH_{26} , g-value and roof thermal transmittance are the most influent parameters. Besides, for these variables, the indices have a positive sign which indicates a direct correlation. The greater the input values the higher the CDH_{26} and, consequently, the cooling demand. The other indices are negative but the magnitudes of sensitivity index are close to zero and therefore they indicate an inverse correlation. The graphs highlight the role of thermal capacitance both of the wall and roof in smoothing over the cooling demand. It is also interesting to note the negative correlation between

CDH₂₆ and the wall thermal transmittance. This means that for the test case the night heat losses prevail on the inward heat losses.

Similarly, the graph shows the percentage sensitivity indexes for HDH₁₈. Figure 8 highlights again the role of g-value in the building energy demand. It should be emphasized that a direct comparison between the percentage sensitivity index of CDH₂₆ and HDH₁₈ is not possible. In fact, the low value of CDH₂₆ for unperturbed input stresses the magnitude of the percentage sensitivity index. In order to understand if each input affects

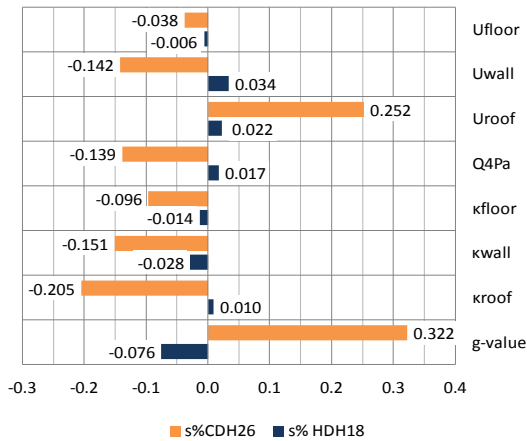


Fig. 8 – s% for Cooling and Heating Degree Hour

	HDH ₁₈	CDH ₂₆	s(HDH ₁₈)	s(CDH ₂₆)	
Base	26316.8	8568.2			
U_f	26301.6	8535.5	-211.6	-98.6	°Ch [W/(m²K)] ⁻¹
U_w	26405.5	8446.5	733.9	-1005.6	°Ch [W/(m²K)] ⁻¹
U_r	26375.4	8783.9	453.7	1670.5	°Ch [W/(m²K)] ⁻¹
Q_{4Pa}	26362.5	8449.3	76.1	-197.9	°Ch (m³/h) ⁻¹
κ_f	26362.5	8449.3	-7.5	-17.3	°Ch [kJ/(m²K)] ⁻¹
κ_w	26241.9	8438.7	-11.5	-19.9	°Ch [kJ/(m²K)] ⁻¹
κ_r	26342.1	8392.1	3.0	-21.2	°Ch [kJ/(m²K)] ⁻¹
g	26118.1	8843.9	-2450.4	3401.5	°Ch

Table 5 – Sensitivity index (s) for HDH₁₈ and CDH₂₆

more deeply HDH₁₈ or CDH₂₆, the dimensional index s has to be adopted (Table 5).

In Figure 9 percentage sensitivity indices for minimum and maximum air temperatures are reported for each perturbed input.

The graph shows that thermal capacitance of the envelope strongly affects both minimum and maximum temperature. Lower magnitude is registered for the other parameters and in particular is interesting to note the low effects of g-

values on CDH₂₆ with respect to envelope capacitance.

Even in this case, in order to define if a single input causes higher differences for t_{min} than for t_{max}, the sensitivity analysis has to be integrated by s index (Table6).

The main weakness of differential analysis is the assumption of perfect independency among all parameters. Consequently, the combined effects can be estimated by a superposition only in case of a linear problem. With the aim of overcoming this issue, the Factorial Method (FM) is also applied in this work. This analysis allows to investigate the extent to which input data have a synergic effect on the simulation results.

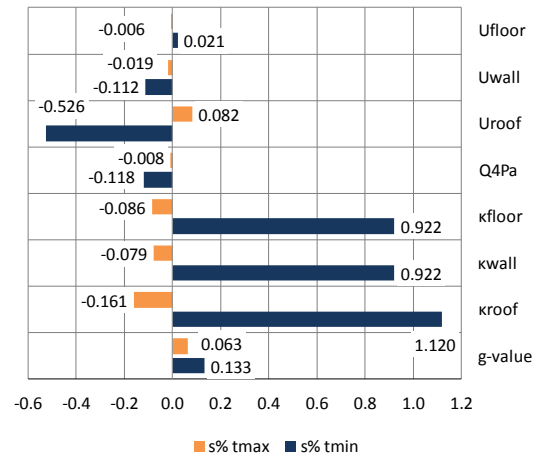


Fig. 9 – s% for minimum and maximum air temperatures

	t _{max} [°C]	t _{min} [°C]	s(t _{max})	s(t _{min})	
Base	36.270	-2.710			
U_{floor}	36.250	-2.702	-0.132	0.037	°C/[W/(m²°C)]
U_{wall}	36.250	-2.702	-0.563	-0.25	°C/[W/(m²°C)]
U_{roof}	36.568	-2.851	2.303	-1.102	°C/[W/(m²°C)]
Q_{4Pa}	36.241	-2.740	-0.048	-0.053	°C/(m³/h)
κ_{floor}	35.959	-2.458	-0.065	0.052	°C/[kJ/(m²°C)]
κ_{wall}	35.984	-2.458	-0.044	0.038	°C/[kJ/(m²°C)]
κ_{roof}	35.685	-2.405	-0.070	0.037	°C/[kJ/(m²°C)]
g-value	36.500	-2.672	2.829	0.443	°C

Table 6 – Sensitivity index (s) for t_{min} and t_{max}

5.2 Factorial analysis

The FM is a further development of the DSA approach, which includes the interactions between parameters and permits the estimation of the high order effects. In this procedure three parameters

are perturbed simultaneously around their mean values: wall thermal capacity, floor thermal capacity and g-value for glazing surfaces.

In this case two different perturbation levels are considered: +5% and -5%. The drawback of this technique is the number of simulations required that is factorially related to the number of inputs.

The implementation of the factorial method is essentially the same as for the differential method. The main difference is that multiple parameters are perturbed simultaneously in the same simulation process. Consequently, the possible synergistic effects of variable perturbations can be observed. The factorial design scheme is developed according to three-variables analysis (e.g. MacDonald 2002 and Prada 2012).

The first order effects of each variable perturbation can be determined by combining the simulation results as reported in the following equations:

$$F_{kf} = \frac{(Z_2+Z_4+Z_6+Z_8)-(Z_1+Z_3+Z_5+Z_7)}{4} \quad (8)$$

$$F_{kw} = \frac{(Z_3+Z_4+Z_7+Z_8)-(Z_1+Z_2+Z_5+Z_6)}{4} \quad (9)$$

$$F_g = \frac{(Z_5+Z_6+Z_7+Z_8)-(Z_1+Z_2+Z_3+Z_4)}{4} \quad (10)$$

Similarly, the high order effects are given using the signs founded by multiplying the sign of the individual variable state (e.g. MacDonald 2002) and the indices are determined as:

$$F_{kf-kw} = \frac{(Z_1+Z_4+Z_5+Z_8)-(Z_2+Z_3+Z_6+Z_7)}{4} \quad (11)$$

$$F_{kf-g} = \frac{(Z_1+Z_3+Z_6+Z_8)-(Z_2+Z_4+Z_5+Z_7)}{4} \quad (12)$$

$$F_{kw-g} = \frac{(Z_1+Z_2+Z_7+Z_8)-(Z_3+Z_4+Z_5+Z_6)}{4} \quad (13)$$

$$F_{kwkf-g} = \frac{(Z_2+Z_3+Z_5+Z_8)-(Z_1+Z_4+Z_6+Z_7)}{4} \quad (14)$$

In order to compare the results both for degree hour indices and for internal peak temperatures, also the relative factorial factors are used; these indices are calculated by dividing the results of the previous equations for the unperturbed output. The indices reported in Table 7-8 are consistent with the results of differential analysis.

Regarding first order, the factorial method confirms that HDH₁₈ and CDH₂₆ are less affected by thermal capacitance of floor, whose index is of an order of magnitude lower than F_{kw} and F_{g-value}

(both the absolute and the relative ones). The results of factorial analysis show weak second order effects and the link between variables has generally a negative sign, which means that there is not a synergic effect. Therefore the assumption of perfect independent variables of the DSA approach has been proved.

	CDH ₂₆ [Ch]	HDH ₁₈ [Ch]	t _{max} [°C]	t _{min} [°C]
F_{kf}	-32.87	-24.58	-0.055	0.060
F_{kw}	-258.62	-110.72	-0.525	0.495
F_g	612.88	-444.06	0.500	0.085
F_{kf-kw}	3.52	1.97	0.000	0.000
F_{kf-g}	-0.10	-0.06	-0.005	0.000
F_{kw-g}	-5.66	-3.59	-0.015	0.005
F_{kwkf-g}	0.12	-0.69	0.000	0.000

Table 7- Factorial analyses - dimensional indices

	CDH ₂₆	HDH ₁₈	t _{max}	t _{min}
F_{kf}	-0.0038	-0.0009	-0.0015	0.0221
F_{kw}	-0.0302	-0.0042	-0.0145	0.1827
F_g	0.0715	-0.0169	0.0138	0.0314
F_{kf-kw}	0.0004	0.0001	0.0000	0.0000
F_{kf-g}	0.0000	0.0000	-0.0001	0.0000
F_{kw-g}	-0.0007	-0.0001	-0.0004	0.0018
F_{kwkf-g}	0.0000	0.0000	0.0000	0.0000

Table 8- Factorial analyses - relative indices

6. Conclusion

The thermal behaviour of a historical building without HVAC system is investigated, therefore a calibration procedure using the internal temperature measured in a control thermal zone is developed.

MBE and RMSE, and Pearson's index with regression analysis are employed to assess the errors and the correlation between predicted and real temperature. With these indexes, the set of main parameters that ensure the best prediction of air and surface temperature compared against actual data has been determined.

Nevertheless there are still some discrepancies between predicted and real temperature so, in order to understand the most influent parameters, a sensitivity analysis has been carried out.

The sensitivity analysis highlights that the necessity to improve the knowledge of input data depends on the final goal of the energy model. In fact, if the model is to be used for energy system sizing, the reliable estimation of the thermal capacitance of the envelope will assume a key role. On the other hand, for the consistent calculation of the building energy performance the estimation of the glazing solar transmittance and of the roof thermal transmittance becomes more important.

In particular g-value for glazing system and roof thermo-physical properties affects both summer and winter energy demand; and thermal capacitance of the roof significantly influences the temperature peaks. Finally, the Factorial Method confirms the negligibility of the high order effect of the input data analysed. Consequently these parameters have not a synergic effect in the model predictions.

Further investigations are necessary and, according to the aim of the optimization, different parameters have to be refined, according to the results of the sensitivity analysis.

7. Nomenclature

Symbols

CDH ₂₆	Cooling degree hours base on 26°C
F	Sensitivity index for factorial method
HDH ₁₈	Heating degree hours base on 18°C
k	Specific heat capacitance [$\text{J m}^{-2} \text{K}^{-1}$]
n	Number of Simulation Steps (hours)
s	Sensitivity Index (DSA)
R ²	Regression Index
U	Thermal transmittance [$\text{W m}^{-2} \text{K}^{-1}$]
Z_j	Model response of the j-th simulation

Greek symbols

Λ	Thermal Conductance [$\text{W m}^{-2} \text{K}^{-1}$]
θ	Dry bulb temperature [K]

Subscripts

C	Cooling
f	Floor
H	Heating
I	Internal

r	Roof
sim	Simulated
set	Setpoint
w	wall

References

- Baggio P., Corrado V., Murano G., Riva G. (2010). "Definizione degli anni tipo climatici delle provincie del Nord Italia", *La Termotecnica* vol.11, 61-68
- Lam J., Hui S. (1996). "Sensitivity analysis of energy performance of office buildings", *Building and environment*, vol 31, 27-39.
- Macdonald I.A. (2002) "Uncertainty in building simulation". *Ph.d. dissertation*, University of Strathclyde, Glasgow UK.
- Norford L.K., Socolow R.H., Hsieh E.S., Spadaro G.V. (1994). "Two-to-one discrepancy between measured and predicted performance of a 'low-energy' office building: insights from a reconciliation based on the DOE-2 model", *Energy and Buildings*, vol. 21, 121-131
- Prada, A. (2012). *Energy performance of buildings: modeling of dynamic summer behavior*. Ph.D. Thesis, University of Trento, Civil and Environmental Engineering, Trento.
<http://eprints-phd.biblio.unitn.it/770/>
- Seem, J. (1987). *Modeling of heat transfer in buildings*. Ph.D. Thesis, Madison, Wisconsin (USA).
- Tian, W., and deWilde, P. (2011). Uncertainty, sensitivity analysis of building performance probabilistic climate projections: a UK case study. *Automation in construction*, 20(8), 1096-1109.
- Raftery P., Keane M., O'Donnell J. (2011). "Calibrating whole building energy models: An evidence-based methodology", *Energy and Buildings*, vol. 43, 2356–2364.
- Tian Z., Love J.A. (2009). "Energy performance optimization of radiant slab cooling using building simulation and field measurements", *Energy and Buildings*, vol. 41, no. 3, 320-330.
- Yoon J., Lee E.J., Claridge D.E. (2003). "Calibration procedure for energy performance simulation of a commercial building", *Journal of Solar Energy Engineering*, vol. 125, 251–257.

Energy simulation and design of a hot box suitable for dynamic tests of building envelope opaque components

Alessandro Prada – Free University of Bolzano, Bolzano, Italy

Davide S. Gigli – Free University of Bolzano, Bolzano, Italy

Andrea Gasparella – Free University of Bolzano, Bolzano, Italy

Marco Baratieri – Free University of Bolzano, Bolzano, Italy

Abstract

The aim of this work is to set up a procedure for the evaluation of dynamic thermal characteristics starting from experimental data collected by means of a hot box apparatus. The system involved is a calibrated and guarded hot box, available at the Free University of Bolzano, equipped with air cooling and heating systems capable of keeping stable conditions at the boundary of an opaque envelope structure. Since the experimental tests require dynamic boundary conditions (e.g. periodic temperature variations), an upgrade of the apparatus is then necessary. Consequently, a thermo-fluid dynamic model of the hot box apparatus is developed with the purpose of designing an effective improvement in the appliance. In addition, this model is also applied for the simulation of the hot box operation during the dynamic test and the numerical results are validated versus the experimental data. The numerical analysis also enables the correct understanding of the operation of the whole equipment. The paper firstly describes the methodology involved in the implementation of the numerical analysis and in the system design. Following on from this point, the experimental tests carried out on several timber components, subjected to periodic boundary conditions and the model validation, are presented.

1. Introduction

In the last few years the use of dynamic simulation has increased due to the purpose of better modelling the dynamic interaction between building and energy systems. A reliable evaluation of the thermal behaviour of building envelopes requires dynamic simulations to take into account their thermal capacity. An improvement of experimental methods to measure the dynamic

thermal characteristics of the components is then needed to test calculations.

In this regard, while it is well known how to measure the steady-state thermal transmission properties - both regarding the standard procedures (EN 1934:1998) and in terms of the performance of different approaches (Asdrubali and Baldinelli, 2011) - there are no standard technical rules for the evaluation of dynamic parameters (e.g., periodic thermal transmittance and time shift) by means of experimental laboratory tests.

In the literature there are few examples of dynamic tests on envelope components carried out in the laboratory.

Ulgen (2002), has investigated the behaviour of opaque wall materials by means of a simulation unit, consisting of two volumes separated by the wall sample. One volume has adiabatic boundaries and no heat generation, while in the other volume a heat generation device generates a sinusoidal temperature signal. The aim of the study is to measure time lag and decrement factor for different wall compositions.

A calibrated guarded hot-box unit has been adjusted to measure the dynamic thermal properties of insulated brick walls (Sala et al., 2008). The forcing temperature follows a triangular signal of 10 °C amplitude in an interval of 2 hours. The results are compared with those obtained from a finite volume simulation. By means of the same apparatus also the response factors of a wall have been obtained (Martin et al., 2010). The designed procedure does not require the measurement of the material properties.

Furthermore, the analysis of transient heat transfer

data has also been applied to compare effective thermal transmittances of both isotropic and anisotropic building materials (Yesilata and Turgut, 2007). In particular, sample measurements with ordinary concrete and rubberized concretes have been performed in an adiabatic hot box apparatus.

The present work can be divided into two sections, the former relevant to the experimental tests carried out through a hot box apparatus equipped with a heat-flow meter and the latter regarding the system modelling validated through the collected data. The goal of the experimental tests is to describe the thermal behaviour of sample envelope components (i.e., section of a timber wall) under dynamic boundary conditions. The amplitude variations of the heat flux on the internal side and the amplitude variations of the surface temperature on the external side have been recorded. According to EN ISO 13786:2007 it has been possible to compute the delay time and decrement factor of the sample. A thermo-fluid dynamic model (based on finite element method, f.e.m.) of the hot box apparatus has been developed for the hot box design and for the simulation of the system operation during the dynamic test. The simulation results have been validated versus the experimental data.

2. Materials and methods

2.1 Hot box apparatus description

According to the EN 1934 standard, the hot box apparatus - designed and constructed for the purpose of the present research - is an insulated box (aluminium plates filled with 10 cm of polyurethane insulation) of a height of 170 cm, a width of 170 cm and a 110 cm length, with one side left open (Figure 1). A black screen separates the inner volume of the hot box from the test wall to avoid heat exchange by radiation between the hot box and the sample.

The box is equipped with an evaporator (the cooling unit), an electrical resistance (the heating unit) and a cylindrical horizontal fan, which generates a regular-shaped air flow stream on the

surface of the component, also reducing the surface thermal resistance. The evaporator and the electrical resistance work together adjusted by a PID type regulation unit, tuned up in order to keep an internal constant temperature in a range of ± 0.05 °C with respect to the set point value. The tuning of the system allows for stable conditions and a satisfying uniformity of temperature on the sample surface, in the measurement area. Peripheral inhomogeneity is due to viscosity effects of the air flow near the hot box perimeter and to geometrical thermal bridges. According to the standard, these phenomena have to be assessed and if they are kept within the prescribed ranges they have negligible effects on the measured physical quantities.

For a steady state operation, the hot box is used in its standard configuration having two twin chambers kept at a constant temperature (usually 20°C and -10°C) in order to measure the thermal conductance (C_s) of the envelope component. For the transient operation one of the two chambers has been set up to keep steady-state conditions: the set point was at 20°C, with an air flow rate of 3.5 m s⁻¹ and relative humidity that ranges between 45% and 65%.

An electrical heater has been used to impose the forcing temperature signal on one side of the test wall considered as the external side. The electrical heater is a 120 x 120 cm copper coil crossed by an electric current of 6.5 A, which can generate a nominal thermal power of 1500 W. At the present time the control system only allows an on/off behaviour of the heater, as a first step to simulate a dynamic forcing temperature on the external side of the component.

The hot box has been designed with reduced dimensions with respect to traditional hot box systems, in order to have a reduced mass and, thus, reducing the thermal inertia of the system. This allows for a higher precision in controlling the operation conditions and, consequently, more precise measurements of the dynamic response of a component due to imposed thermal variation.

The heat flow variation on the internal side of the component has been measured by the use of a heat-flow meter, namely a thermopile made of 250 type T thermocouples, which measures the heat

flux on a component surface by means of the variation of electric potential through the two sides of the flow meter. The thermometric quantity, i.e., the electric potential in mV, is converted into W m^{-2} through calibration values obtained by means of guarded hotplate tests, suitable for conductivity measurements.

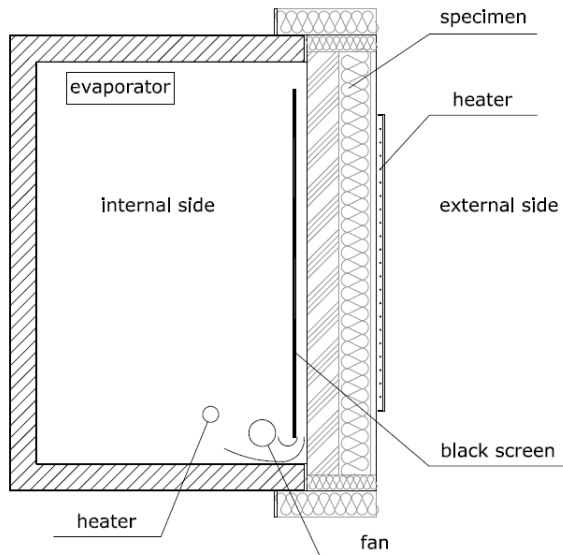


Fig. 1 – Hot box apparatus

The heat-flow meter has been surrounded by a guard ring having thermal properties similar to the heat flow meter. On the internal side of the component, 8 type T thermocouples measure the temperature on the layer between the inner side of the sample and the guard ring, a further 4 thermocouples measure the temperature in the layer between the inner side of the sample and the heat-flow meter. On the external side, there are 12 thermocouples in the same position of the opposite side, which measure the external surface temperatures. The thermocouples are placed 1 mm under the external surface of the component sample, to avoid the influence of direct radiation due to the electrical heater.

2.2 Experimental tests

The test envelope components are characterized by timber frame structures. Two different samples (i.e., sample n. 1 and 2) have been chosen. Table 1 and 2 show the main characteristics and physical properties of the samples. The sample geometry and structural characteristics have been reported in

Figure 2. The internal side temperature (with respect to the test component, see Figure 2) is held at a constant value of 20°C by means of the hot box apparatus. The power of the inner electrical resistance is usually limited to 45%, to reduce the thermal variations inside the hot box, allowing for a quick convergence of the PID controller and consequently a finer tuning of the setup point. The air stream flow rate is set to 3.5 m s^{-1} , while the relative humidity is not controlled. After the time necessary to obtain the steady state conditions in the inner side (i.e., usually 24 hours) - also dependent on the balance with the temperature of the lab also set up to 20°C - the external side is then subjected to a 1500 W thermal radiation for 2 hours, followed by 22 hours of rest. The 24 period on/off thermal power signal is controlled by a programmable switch. The electrical heater is placed very close to the external surface, to minimize the influence of air buoyancy effects, which could cause temperature gradients between the lower and the higher part of the sample.

Material	Code	Density (kg m^{-3})	Conductivity ($\text{W m}^{-1} \text{K}^{-1}$)
Gypsum-Fibreboard	CG	900	0.21
Low density wood fibre	F1	40	0.038
Low density wood fibre	F2	50	0.038
High density wood fibre	F3	160	0.040
Timber structure (beam)	W	450	0.13
Timber structure (pillar)	LW	450	0.13
Timber multilayer panel LVL	LV	530	0.20
Plaster	PL	1000	1.0

Table 1 – Wall samples materials library

The test was usually carried out over two weeks, in order to minimize the influence of the initial conditions due to thermal inertia of the specimen and thus ensuring the achievement of periodic

steady state. The transient effects were observed to be negligible usually after 3 or 4 days starting from the first thermal forcing signal. Once reached the periodic steady state – i.e., when the amplitude of either the thermal flux or the temperature variations have constant amplitude between two periods - the heat flux on the internal side and the external surface temperatures were recorded and used for the further analysis.

Table 2 – Wall samples characteristics

code	thickness (cm)	n. sample
CG	2.5	1 - 2
F1	4	1 - 2
LW	16	1 - 2
F2	10	1
F1	5	2
W	10	1
LV	1.25	1 - 2
F1	4	1 - 2
W	4	1 - 2
LV	1.25	1 - 2
F3	8	1 - 2
PL	0.8	1 - 2

TOP SECTIONS

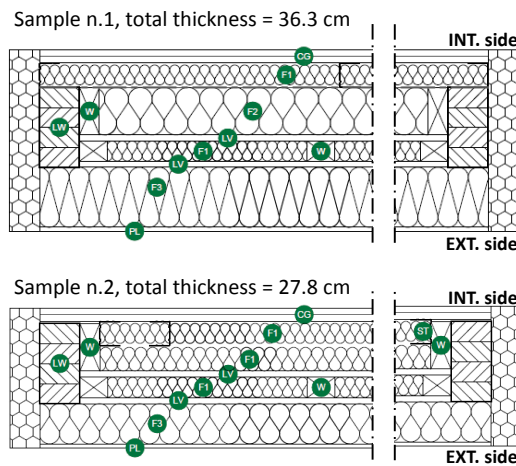


Fig. 2 – Sample geometry and structural characteristics

2.3 Dynamic parameters: experimental evaluation

A set of 4 days in a periodic steady state was chosen to record the external surface temperature (i.e., forcing temperature signal) and the internal heat flux. The Fast Fourier Transform (FFT)

algorithm (Press et al., 2007) was applied, computing the first 720 harmonics of the experimental temperature and heat flux. The fundamental signals (first term of the Fourier approximation) were then used to compute the decrement factor and the time shift in agreement with the EN ISO 13786 standard. It is worth pointing out that in the calculation the surface thermal resistances have been not taken into account, thus considering thermal conductance instead of transmittance. This assumption is acceptable, as far as the internal surface temperature is approximately constant. In particular the periodic thermal conductance (1) has been computed as the ratio between the amplitude of the first harmonic of the internal heat flux ($\phi_{i,1}$) and the amplitude of the first harmonic of the external surface temperature ($\theta_{e,1}$). The decrement factor (f) has been then computed (2) dividing the obtained periodic thermal conductance by the thermal conductance relevant to the steady state (C_s), measured by means of the hot box in agreement with EN 1934.

$$C_{ie} = \frac{\phi_{i,1}}{\theta_{e,1}} \quad (1)$$

$$f = \frac{C_{ie}}{C_s} \quad (2)$$

The time shift (5) has also been calculated using the phase displacements (φ and ψ) of the fundamental signals.

$$\theta_e \approx \bar{\theta}_e + \theta_{e,1} \cos(\omega t + \varphi) \quad (3)$$

$$\phi_i \approx \bar{\phi}_i + \phi_{i,1} \cos(\omega t + \psi) \quad (4)$$

$$\Delta t_f = \frac{\psi - \varphi}{\omega} = \frac{\psi - \varphi}{2\pi} \times 24[h] \quad (5)$$

Both in the case of the decrement factor and of the time shift, the values of each day of the chosen set (4 days) and the average values have been computed.

2.4 Simulation model

With the purpose of modelling the behaviour of the hot-box apparatus when a dynamic test is carried out, an unsteady thermo-fluid dynamic

model has been developed. This numerical analysis investigates the applicability of the hot-box upgrade appliances for the experimental estimation of the wall dynamic characteristics according to EN ISO 13786. In particular, the numerical model has been herein applied to a well-insulated timber wall (sample 1) when a sinusoidal variation of the wall surface temperature is imposed. The domain is discretized by means of an unstructured triangular mesh. Globally, 20268 triangular elements are used to discretize the whole domain with a greater thickening in the zone of the convective heat exchange between the air flow and the wall surface.

In order to model the behaviour of the turbulent system with a low computational cost, the Reynolds-averaged Navier Stokes (RANS) equations are used. Adopting the weakly compressible hypothesis (i.e. compressibility is taken into account only in continuity equation) and the Newtonian behaviour of the fluid, the system of partial differential equations describing the problem becomes:

Conservation of mass for fluid

$$\frac{\partial \rho}{\partial t} + \nabla \cdot (\rho u) = 0 \quad (6)$$

Momentum equation with the eddy closure relation

$$\rho \left(\frac{\partial u}{\partial t} + u \cdot \nabla u \right) = \nabla \cdot \left[\begin{array}{c} -pI + (\eta + \eta_T) \\ \left(\nabla u + (\nabla u)^T - \frac{2}{3} (\nabla \cdot u) I \right) - \frac{2}{3} \rho k I \end{array} \right] + F \quad (7)$$

Heat equation for solid domain

$$\rho c_p \frac{\partial T}{\partial t} + \nabla \cdot (-\lambda \nabla T) = 0 \quad (8)$$

Heat equation for fluid domain

$$\rho c_p \frac{\partial T}{\partial t} + \nabla \cdot (-(\lambda + \lambda_T) \nabla T) = -\rho c_p u \nabla T \quad (9)$$

Transport equation of the turbulent kinetic energy

$$\rho \left(\frac{\partial k}{\partial t} + u \cdot \nabla k \right) = \nabla \cdot [(\eta + \eta_T) \nabla k] +$$

$$+ \frac{1}{2} \eta_T (\nabla u + (\nabla u)^T)^2 - \rho \varepsilon \quad (10)$$

Transport equation of the turbulent energy dissipation rate

$$\rho \left(\frac{\partial \varepsilon}{\partial t} + u \cdot \nabla \varepsilon \right) = -\rho C_{\varepsilon 2} \frac{\varepsilon^2}{k} \nabla \cdot \left[\left(\eta + \frac{\eta_T}{1.3} \right) \nabla \varepsilon \right] + \frac{1}{2} C_{\varepsilon 1} \frac{\varepsilon}{k} \eta_T (\nabla u + (\nabla u)^T)^2 \quad (11)$$

where η_T and λ_T are respectively the eddy viscosity and the eddy conductivity computed as:

$$\eta_T = \rho C_\eta \frac{\varepsilon^2}{k} \quad (12)$$

$$\lambda_T = \eta_T c_p Pr_t \quad (13)$$

where Pr_t is the turbulent Prandtl number computed with the Kays-Crawford relation. In particular, the values of the constant adopted in the $k - \varepsilon$ model are reported in Table 3.

C_η	$C_{\varepsilon 1}$	$C_{\varepsilon 2}$
0.09	1.44	1.92

Table 3 – Constant adopted in the k-ε model

Since the momentum equations are nonlinear, the solution of the coupled heat and fluid dynamic problem become unstable if the Galerkin finite element method is adopted for the spatial discretization of the domain (Hauke, 2002). Consequently, in all the turbulent simulations herein reported an artificial diffusion is introduced. The diffusion is required in order to ensure the numerical convergence of the problem solution. However, the artificial diffusion parameter is kept to as low a value as possible while still getting a converged simulation. The key aspect in the numerical model of the hot box behaviour is the definition of the initial and boundary conditions. While the steady state solution at the time $t=0$ is imposed as initial conditions, several boundary conditions are defined both for heat transfer and RANS equations. In particular, while for the solid domain the Newton-Robin equation with the convective heat coefficients defined by EN ISO 6946 are used, Table 4 shows the BC applied for the ventilation channel.

INLET	OUTLET	WALL
$u = u_0$	$p = p_0$ no normal stress	Logarithmic wall function
$k = \tilde{k}(t)$	-	-
$\varepsilon = \tilde{\varepsilon}(t)$	-	-
$T = \tilde{T}(t)$	$\hat{n} \cdot (\lambda \nabla T) = 0$	Robin –Newton with radiative exchanges

Table 4 – BC of the ventilation cavity

3. Results and discussion

3.1 Experimental tests

The first experimental runs have been carried out in standard steady state conditions with the complete double hot box, in order to measure the thermal conductance (i.e., EN ISO 1934) of the two envelope components (Table 5).

The two samples have then been tested under dynamic conditions. An example of the measurements performed on sample n.1 is reported in figure 3, where the external forcing temperature and the internal heat flux have been plotted versus time. In the same figure also the reconstruction obtained through the FFT procedure (i.e., using 720 harmonics) has been pointed out and the first term of the approximation (i.e., the fundamental signal). The decrement factor and time shift have then been computed using the amplitudes and phase displacements of the fundamentals signals of temperature and heat flux. Table 6 shows the values of the dynamic parameters obtained for each day of the chosen set and the relevant average value.

Sample	Thermal conductance (W m ⁻² K ⁻¹)
n.1	0.172
n.2	0.240

Table 5 – Thermal conductance of the samples, measured in agreement with EN ISO 1934

	C_{ie} (W m ⁻¹ K ⁻¹)	f (-)	Δt_f (hours)
Sample n.1			
Day 1	0.0326	0.1894	8.82
Day 2	0.0269	0.1566	9.20
Day 3	0.0311	0.1806	9.40
Day 4	0.0346	0.2012	9.32
Average	0.0312	0.1819	9.18
Sample n.2			
Day 1	0.1029	0.4288	6.65
Day 2	0.1004	0.4183	6.75
Day 3	0.1018	0.4242	6.67
Day 4	0.0997	0.4213	6.87
Average	0.1011	0.4215	6.73

Table 6 – Dynamic parameters obtained from the experimental measurements (4 days set)

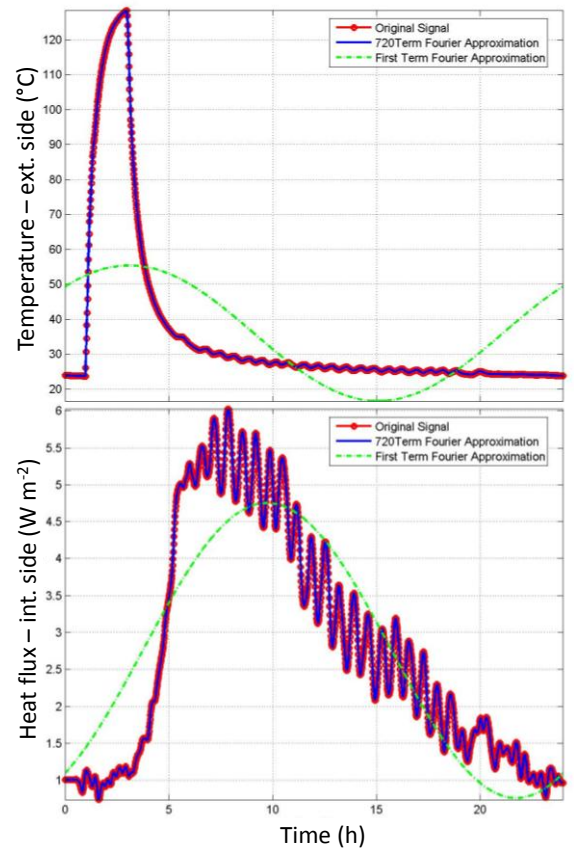


Fig. 3 – Surface temperature (ext. side) and heat flux (int. side) recorded on the first day of periodic steady state - sample 1

3.2 Model test

The finite element model has been applied to the sample no.1 case. The simulation was carried out during the same period of the measured test

obtaining a comparison on the same time basis (day 1 to 4).

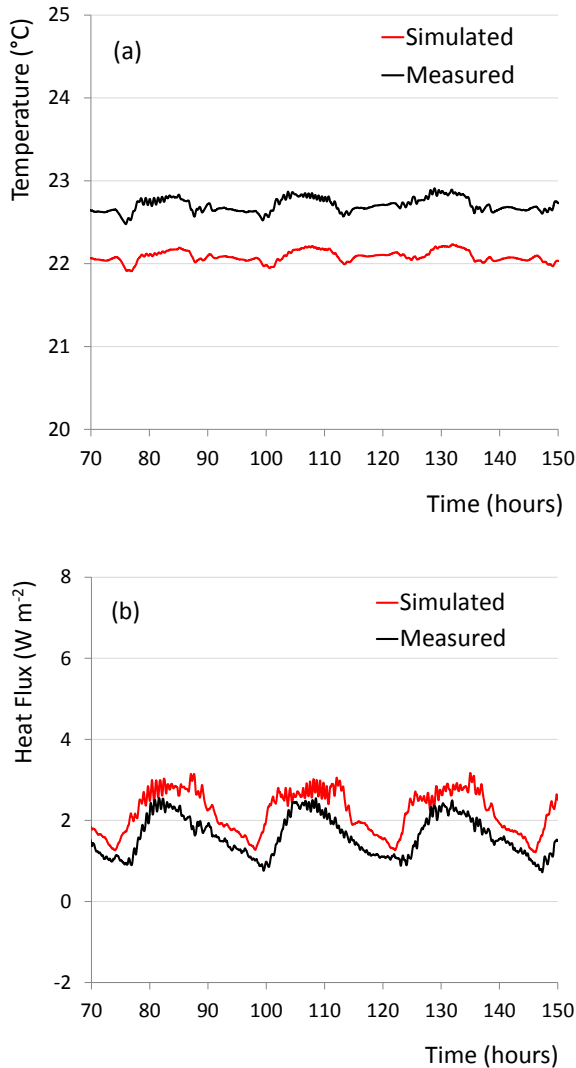


Fig. 4 – Surface temperature (a) and heat flux (b) on the wall internal side: comparison between simulated and measured values (sample n.1)

Figure 4 shows the comparison between the simulated and measured surface temperature and heat flux on the internal side of the test wall (the signals have been subjected to a proper filtering). Although the shape and the trend of the curves show a satisfying agreement, a constant deviation has been observed between the measured and simulated signals. The same behaviour is consequently obtained, and further clarified, by computing the first harmonic of the simulated heat flux when compared with the measured one (figure 5). The detected constant deviation (i.e., measured Vs simulated signal) can be explained on

a purely steady state basis, since the periodic signals show a very similar phase during the tests. In particular, the average difference of temperature is approx. 0.6 K, while the average deviation of the heat flux has been assessed at 0.5 W m^{-2} .

The values of the periodic thermal conductance, decrement factor and time shift have been computed using the first harmonic of the simulated heat flux and of the measured forcing temperature. As for the measured values, the calculation has been carried out on a 4-day basis also obtaining the average values (table 7). The comparison between the average values is shown in figure 6.

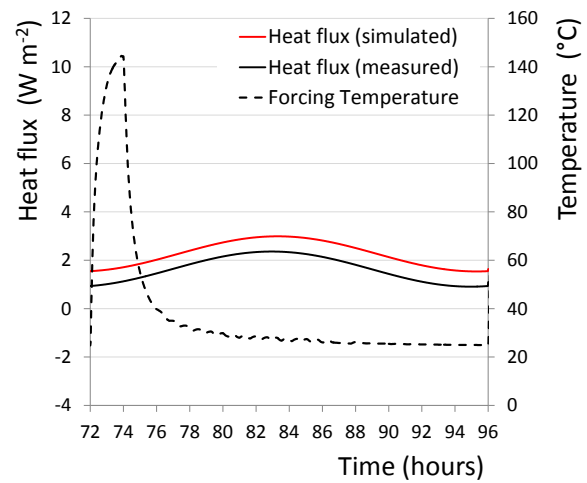


Fig. 5 – First harmonic signals of heat flux on the wall internal side: comparison between simulated and measured values (sample n.1)

	C_{ie} ($\text{W m}^{-1} \text{K}^{-1}$)	f (-)	Δt_f (hours)
Sample n.1			
Day 1	0.0299	0.1738	8.68
Day 2	0.0303	0.1763	8.91
Day 3	0.0219	0.1275	10.35
Day 4	0.0188	0.1092	10.75
Average	0.0252	0.1467	9.67

Table 7 – Dynamic parameters obtained by means of the FEM model (4 days set, sample n.1)

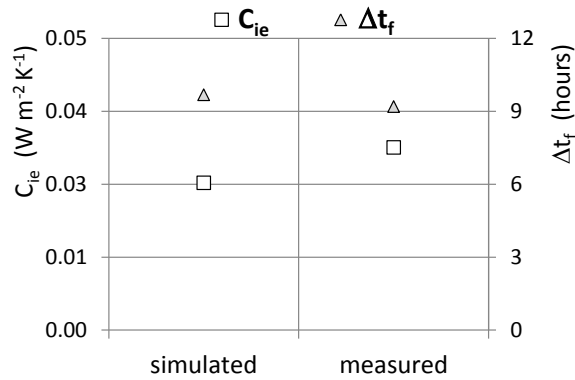


Fig. 6 – Periodic thermal conductance and time shift: comparison between simulated and measured data (4 days set, sample n.1)

3.3 Remarks

The calculation of the decrement factor and time shift using the experimental data lies on the assumption that it is possible to consider a periodic thermal conductance instead of a transmittance. This has been considered an acceptable assumption, since the definition of the periodic thermal conductance implies a constant internal surface temperature, which it has been measured to be in the range of $0.5^{\circ}C$ (i.e., approx. 1% of the first harmonic amplitude relevant to the external forcing temperature). Further analysis will foresee a set of two runs per sample - using forcing temperature signals of different amplitude and shape - in order to be able to estimate the decrement factor and the periodic thermal transmittance starting from the heat transfer matrix as defined in EN ISO 13786.

The deviations resulting between the measured and the simulated surface temperature and heat flux (on the wall internal side) deviations can be attributed to steady state effects. In particular a calibration of the model has to be carried out as a further development, for example, tuning the thermo-physical properties of the wall materials or using a 2D-time dependent air velocity profile as boundary condition in the hot box cavity.

4. Conclusion

A hot box laboratory apparatus has been upgraded and used for the dynamic testing of timber opaque components. Two types of timber components have been tested using a time dependent

temperature signal. The decrement factor and the time shift have been computed using the measured heat fluxes. The experimental data have then been compared with the results of a simulation carried out by means of a thermo-fluid dynamic model. The resulting comparison is satisfying, even if a further calibration of the model is needed to achieve a better agreement.

The developed model seems to be a suitable tool for the further planning of the research activity. In particular, by applying a sinusoidal forcing temperature it will be possible to validate the results obtained using only the first harmonic and also to point out a range of applicability of this procedure with varying wall characteristics.

An assessment of the periodic thermal transmittance and of the time shift will also be possible only through the experimental data, by performing a series of tests (i.e., two at least) on the same wall sample, using different forcing signal (e.g., using different amplitudes) and solving the equation system with the transfer matrix as reported in Annex B of EN 13786.

5. Nomenclature

Symbols

C_{ie}	Periodic thermal conductance of the component [$W m^{-2} K^{-1}$]
C_s	Thermal conductance [$W m^{-2} K^{-1}$]
F	Volume force vector [$N m^{-3}$]
I	Identity tensor [-]
T	Temperature [K]
c_p	Specific heat [$J kg^{-1} K^{-1}$]
F	Decrement factor [-]
k	Turbulent kinetic energy
\hat{n}	Surface normal versor [-]
p	Pressure [Pa]
t	time [s]
u	Vector of velocity [$m s^{-1}$]

Greek

ϕ	Specific heat flux [$W m^{-2}$]
ε	Turbulent kinetic energy dissipation rate [-]
φ	Phase difference [rad]

η	Dynamic viscosity [Pa s]
λ	Thermal conductivity [$\text{W m}^{-1} \text{K}^{-1}$]
θ	Temperature [$^{\circ}\text{C}$]
ρ	Specific mass [kg m^{-3}]
ω	Angular frequency [rad s^{-1}]
ψ	Phase difference [rad]

Subscripts/Superscripts

0	initial condition
1	the first harmonic of the signal
i	internal side of the sample
e	external side of the sample
T	referred to turbulent quantity

References

- Asdrubali, F., Baldinelli, G., Thermal Transmittance measurements with the hot box method; Calibration, experimental procedures, and uncertainty analyses of three different approaches, *Energy Build*, 43 (2011) 1618-1626
- CEN 1998. EN 1934:1998, Thermal performance of buildings - Determination of thermal resistance by hot box method using heat flow meter
- CEN 2007. EN ISO 13786:2007, Thermal performance of building components - Dynamic thermal characteristics - Calculation methods.
- CEN 2008. EN ISO 6946:2008, Building components and building elements - Thermal resistance and thermal transmittance -Calculation method
- Hauke, G., 2002. A simple subgrid scale stabilized method for the advection-diffusion-reaction equation, *Computer Methods in Applied Mechanics and Engineering*, 191, pag. 2925-2947
- Martín, K., Flores, I., Escudero, C., Apaolaza, A., Sala, J.M., Methodology for the calculation of response factors through experimental tests and validation with simulation, *Energy and Buildings*, 42 (2010) 461–467
- Press, W.H., Teukolsky, S.A., Vetterling, W.T., Flannery, B.P., *Numerical Recipes 3rd Edition: The Art of Scientific Computing*, Cambridge University Press, Cambridge, 2007.
- Sala, J.M., Urresti, A., Martín, K, Flores, I., Apaolaza, A., Static and dynamic thermal characterisation of a hollow brick wall: Tests and numerical analysis, *Energy and Buildings*, 40 (2008) 1513-1520
- Ulgen K., Experimental and theoretical investigation of effects of wall's thermophysical properties on time lag and decrement factor, *Energy Build*, 34 (2002) 273-278
- Yesilata, B., Turgut, P., A simple dynamic measurement technique for comparing thermal insulation performances of anisotropic building materials, *Energy and Buildings* 39 (2007) 1027–1034

The effect of material uncertainties on envelope heat transfer simulations

Alessandro Prada – Free University of Bolzano, Bolzano, Italy

Paolo Baggio – Free University of Bolzano, Bolzano, Italy

Marco Baratieri – Free University of Bolzano, Bolzano, Italy

Andrea Gasparella – Free University of Bolzano, Bolzano, Italy

Abstract

In this paper, the influence of thermo-physical properties on the heat flux transmitted through the envelope is investigated. In fact, the retrieval of reliable thermo-physical properties is one of the major difficulties in the early stage of energy simulations. This issue is further emphasized if the model refers to existing buildings, when usually reference thermo-physical properties are used in lieu of declared and certified values (i.e. 90 % fractile). Moreover, the thermal characteristics, especially for porous media, are closely related to the water content and, to a lesser extent, to temperature and age. In addition to this, the uncertainties due to simplifying assumptions, commonly made in thermal analysis, should not be forgotten. For instance, the material apparent conductivities, as well as the other thermo-physical properties, are the macroscopic results of various basic mechanisms such as the solid and gas conduction, the gas convection and the long wave radiation.

The question then addresses to what extent the uncertainties of thermo-physical properties affect the reliability of the heat transfer through envelope and, consequently, of the energy simulation predictions. In order to answer this question, an uncertainty analysis has been carried out by means of a Monte Carlo approach. This procedure is applied for the recursive numerical solution of the partial differential equation of the heat conduction.

Different Italian climates (i.e. Trento and Palermo) and typical wall typologies are adopted in order to broaden the representativeness of the results. Furthermore, two methods widely used in hourly simulation code (i.e. Conduction Transfer Function and Finite Difference Method) are herein analysed.

1. Introduction

Dynamic energy simulation has the potential to provide relevant information about the building energy behaviour and to indicate the possible conservation measures for the reduction of energy consumption. In fact, these enhanced methods allow for better modelling of the dynamic interactions between building, occupants and energy systems. On the other hand, one of the problems in the application of enhanced simulation models, which can sometimes undermine the reliability of their results, is the difficulty to gather reliable input data. The reliability of simulation outcomes hinges upon the accuracy of input data, simulation models and energy modellers all together. Without these characteristics, significant deviations between the actual and the simulated energy performance can be found. Therefore, an estimation of the sensitivity and of the degree of uncertainty introduced by each factor can help to increase the awareness of the result reliability and of the robustness of the whole simulation process.

In the last few years, increasing attention has been paid to the uncertainty and sensitivity analyses on building energy simulations. In one of the earliest works (Lomas and Eppel, 1992), the authors compared three different techniques for sensitivity analysis. Following on from this work, Macdonald (Macdonald, 2002) integrated some uncertainty procedures in the software Esp-r. In addition, in (Costola, Blocken and Hensen, 2009) the effect of uncertainties in wind-pressure coefficients on the infiltration and ventilation rates is investigated. Further research dealing with uncertainty is reported in (Holm and Kuenzel, 2002), where the

authors investigated the impacts of materials properties and surface coefficients on hygro-thermal building simulation using a Monte Carlo technique.

More recently, in (Corrado and Mechri, 2009) a sensitivity analysis of the quasi steady state approach proposed by EN ISO 13790:2008 (CEN, 2008) is proposed for the calculation of the energy performance for heating. Similarly, Tian and deWilde (2011) explored the uncertainties of climate, construction material properties, infiltration rates, internal loads and equipment efficiency for building simulations of an office building in the UK.

In (Hopfe and Hensen, 2007) and in (Hopfe and Hensen, 2011), the influence of uncertainty in the early stage of design process is analyzed, while, in (Dominguez-Munoz, Cejudo-Lopez, and Carrilo-Andres, 2011) a study about the impacts of suboptimal design parameters on the simulated peak-cooling loads is presented.

Often in the literature, the authors analyze the simultaneous effect of several parameters on the simulations outcomes. However, due to their different nature, it is dangerous to combine different sorts of uncertainties (Hopfe and Hensen, 2011). Furthermore, since the energy behaviour is not always linear, in order to draw reliable considerations from results, a realistic distribution of the input data is required. Unfortunately, the literature review shows there are limited data available describing uncertainties for design parameters in building energy simulation.

For these reasons, this work focuses on the effects of perturbations in the thermo-physical properties on the numerical solutions of the heat transfer equation. In particular, the primary goal is the investigation of the robustness of different calculation procedures such as finite difference method (FD) and conduction transfer functions (CTF) when suboptimal thermo-physical properties are used. Besides, this work aims to clarify if different calculation procedures can respond in different ways to perturbed input data. To this purpose, the analysis focuses on the heat transfer through the envelope (i.e. inward and outward heat losses) computed both with FD and CTF approaches, when Gaussian distributions of

the material thermo-physical properties are imposed.

2. Calculation procedure

2.1 The Monte Carlo method

In this paper, the sensitivity analysis of the calculation procedures for the numerical solution of the heat transfer partial differential equation is carried out using the Monte Carlo method. The idea behind the Monte Carlo approach is that if a set of data with the same statistic of the population can randomly be found, these data can be used as deterministic input in the heat transfer model and, subsequently, the distribution of the model expectation could be generated (Fig.)

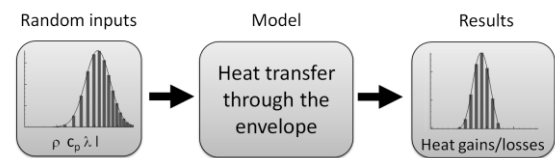


Fig. 1 – Scheme of research analysis carried on

A Monte Carlo method entails full random selection, out of all possible values of the inputs in a correct statistical combination. When the selection of data is improved, the number of simulations can be reduced (Macdonald, 2002). However, with enhanced sampling methods, unbiased results cannot be taken for granted and, consequently, it should be verified with additional computational costs. Therefore, in this work a simple random sampling method is adopted (Prada, 2012). It is the most basic method, which works by generating random numbers in agreement with the probability distribution and scaling this to the target value. The results are an unbiased estimation of the population variance.

2.2 The numerical solution of heat transfer equation

Since the analytical solution of heat equation is known only for simple domain and boundary conditions, in building simulations numerical methods are adopted. Among the possible ways to

numerically solve the partial differential equation, the main strategies are the domain discretization and the use of a frequency analysis for the calculation of the time series terms, which are called conduction transfer function.

The key obstacle in using a finite difference approach (FD) is finding a stable and not time consuming procedure. In this work, with the purpose of ensuring the stability of the solution, a semi-implicit scheme (i.e. Crank-Nicholson) is adopted. However, building thermal simulation software uses to a large extent the CTF method for the evaluation of transient heat conduction. Despite the simplicity of the equations, the complexity of the procedure lies in the evaluation of the CTF coefficients. Several calculation techniques have been proposed. Nevertheless, those that are largely diffused are the Direct Root Finding approach (Hittle, 1979) and the State Space method (Seem, 1987). In this paper the DRF method is adopted for the analysis with perturbed thermo-physical properties. Both the calculation procedure and the Monte Carlo routine are implemented by means of a Fortran code.

2.3 Boundary conditions

The heat transfer transmitted through the envelope is evaluated performing a hourly simulation over an annual period. With the FD approach a variable spatial discretization (max 3 cm) is chosen. Moreover, even if the Von Neumann stability analysis shows that semi-implicit scheme is unconditionally stable, a time discretization, which ensures to meet the condition Fourier number lower than 0.5, is herein adopted. In order to numerically solve the partial differential equation, initial and boundary conditions are imposed. While the steady state solution at the starting time is adopted as initial values, hourly temperatures are imposed on the external environment. In particular, in order to take into account the effect of both convective and radiative exchanges, the temperature adopted is the so-called sol-air temperature (ASHRAE, 2009). The sol-air temperature is a simplification that allows to greatly reduce the computational cost of the dynamic simulations and it can be computed as:

$$T_{solair} = T_{db} + \frac{\alpha \cdot G_{solar}}{h_0} - \frac{\varepsilon \Delta R}{h_0} \quad (1)$$

where ΔR is the difference between long-wave radiation incident on surface from sky and surroundings and radiation emitted by blackbody at outdoor air temperature. Because of the multiple sources of long-wave radiation, for vertical surfaces accurate ΔR values are difficult to determine. For instance, in (Gasparella et al. 2011) the predicted heat fluxes obtained by means of hourly dynamic simulations are used for the estimation of the sol-air temperature. However, according to the ASHRAE Handbooks (ASHRAE, 2009) when solar radiation intensity is high, surfaces of terrestrial objects usually have a higher temperature than the outdoor air. Thus, their long-wave radiation compensates to some extent for the long-wave radiation to the sky. Since in this work a vertical south orientated wall is analysed, a ΔR equal to zero is adopted. Besides, the other parameters are the surface absorptance equal to 0.6 and h_0 of $17 \text{ W m}^{-2} \text{ K}^{-1}$. Starting from the test reference year (TRY) for the analyzed cities, the hourly values of the sol-air temperature are therefore computed and used in the external boundary conditions. On the inner surface a Robin-Newton condition is used by assigning a surface convective and long wave radiation coefficient (i.e. $7.69 \text{ W m}^{-2} \text{ K}^{-1}$) and a fixed internal temperature (i.e. 20°C for winter and 26°C for summer). In order to have a consistent comparison between the calculation procedures, similar boundary conditions are imposed also in the CTF approach. Therefore the air to air CTFs are evaluated by introducing the additional resistive layers at the internal and external surfaces. Then, the heat transfer through the envelope, using the sol-air and the internal fixed temperature, is computed.

2.4 The test cases

The choice of the envelope typology is a key point in the uncertainty analysis. Besides, since the unsteady heat conduction through the envelope is strictly connected to the thermal inertia of the component, also the arrangement of layers has an important role in the envelope dynamic behaviour.

The most common types of building envelope in Italy are investigated and adopted. In particular, in Italy about 20% of the housing stock was built before the 20th century. In this period the construction type is various and includes brick and stone walls (Fig. 2). The latter (SW case), due to the high thickness and mass, is of particular interest to the uncertainty analysis. While the SW case is representative of existing buildings, for new constructions, which must meet energy requirements, the typology most widely diffused in low rise residential buildings is the ME case. This opaque structure is a multilayer wall with external insulation (Fig. 3). For both test cases, reasonable physical properties are chosen, by analysing either the manufacturer technical sheets or reference standard values. The properties adopted and used in this work are reported in Table .

In order to ensure a greater representativeness of the Monte Carlo simulation results, two different climates are analysed. More specifically, Trento, and Palermo test reference years are used with the purpose of modelling both warm and mixed climates. The coordinates and the main characteristics of the sites used in the Monte Carlo simulations are shown in Table 2. Since the work focuses on the effect of suboptimal input data, one of the key aspects, in order to obtain meaningful results from the stochastic simulation, is the quantification of the input variability. Besides, it should not be forgotten that there is a strong correlation between the material properties. For example, moisture content would impact upon the conductivity, density and specific heat capacity simultaneously. Further the specific mass for insulation material is strictly connected to conductivity as shown in (Dominguez-Munoz et al., 2010). However, in this study the cross correlations are not taken into account and each thermo-physical property is treated as an independent variable. A realistic quantification of the parameter variability can become difficult and time consuming due to the lack of information.

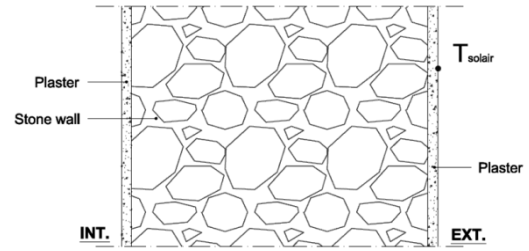


Fig. 2 – Poorly insulated wall (SW case)

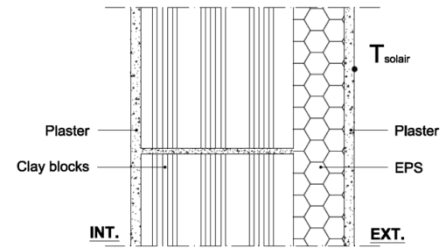


Fig. 3 – Well insulated wall (ME case)

Layer	λ	ρ	c_p	l
Internal Plaster	0.70	1400	1010	0.01
Clay Blocks	0.26	600	840	0.30
Insulation	0.036	30	1500	0.10
Stone wall	2.20	2000	1000	0.70
External Plaster	0.90	1800	910	0.02

Table 1 – Average values of adopted properties

City	Lat.	Elev.	HDD ₂₀	CDD ₂₀
Trento	46°.02 N	185 m	2798	197
Palermo	38°.13 N	50 m	994	704

Table 2 – Climate feature of reference cities

In fact, handbooks, data sheets and technical standards provide safe values but they do not usually declare the variability of these characteristics. Besides, in the literature only a few works have formally dealt with the issue of uncertainty (e.g. Dominguez-Munoz et al., 2010). For this study, a Gaussian distribution of thermo-physical properties is used. The normal distribution is adopted in order to correctly represent the variability of material characteristic caused by random errors. Mean and variance are

defined for each material based on the comparison between manufacturer data sheets and on data reported in the literature (Prada, 2012). The variability of each material property is herein summarized in Table 3, where the 1 % and 99 % fractiles are highlighted.

Layer	Clay Blocks	Insulation	Stone wall
λ	0.17÷0.36	0.031÷0.041	1.75÷2.70
ρ	510÷700	26.5÷33.5	1551÷2503
c_p	620÷1090	1060÷2000	670÷1370
l	0.28÷0.31	0.08÷0.12	0.59÷0.83

Table 3 – Fractiles 1 % and 99 % of distributions

2.5 Postprocessing of results

The last step in the analysis involves the investigation of the monthly heat losses distribution. For both cities, January and August are identified as the most representative months respectively for outward and inward heat losses. To do this analysis, a postprocessing code is implemented by means of Matlab.

Starting from the hourly values of transmitted heat flux through the envelope, computed either with FD or CTF approaches, the terms are firstly separated in inward heat losses and outward heat loss contributions and assigned to one of the 90 bins in which the output variability range is divided.

Finally, the code fits one of three probability distributions (i.e. Normal, Log-normal and Weibull) to the output data distributions. The distribution that best fits the data is selected automatically. The sum of point by point square differences between outputs and the values of each distribution function is assumed as measure of goodness of fit. The lower the squared 2-norm of residual, the better the fit. The code estimates the parameters of the curve that best approximate the actual output distribution, and in particular μ and σ for normal and lognormal distribution or α and β for the Weibull distribution.

3. Results and Discussions

3.1 Shapes of probability density functions (PDF)

As a first step in the result comparison, the PDF shapes are herein presented. The PDF shape analysis firstly highlights that the use of Gaussian random fields as inputs does not imply a Gaussian structure of the heat loss distributions. The distortion of the PDF shape may be represented as a propagation of probability distributions through the model, and the uncertainty is propagated through the DRF and FD methods. In fact, while thickness uncertainty always induces a normal distribution of the simulation outcomes, a perturbation of material conductivity causes a Weibull distribution. Nonetheless, due to the low skewness of these Weibull distributions, the result PDFs are close to normal distributions.

Otherwise, when the perturbed parameters are either specific heat or specific mass, a preponderance of asymmetrical curves, in particular log-normal distributions, is noted. It should be stressed that the shapes of the distributions vary according to the wall typology and to climate conditions. In any case the perturbation of either specific mass or specific heat induces the same output distributions.

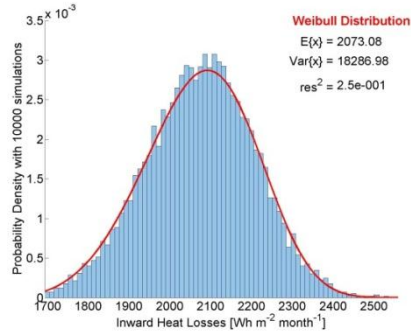
3.2 Sensitivity of calculation procedures

As is to be expected, the CTF and FD methods give consistent results with deviations within $\pm 5\%$ when deterministic inputs are used. Based on this result, this work investigates the extent to which CTF and FD methods are sensitive to the perturbation of the input data. Both calculation procedures show similar responses to the perturbation of the material thermo-physical parameters. Indeed, similar results are obtained both in the shape of the PDF and in the moment of distributions, e.g. the expected values and the variances (Fig. 4a and Fig. 4b).

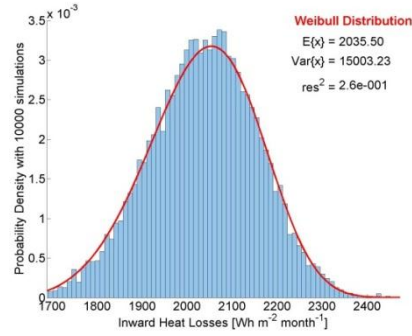
However, Fig. 4c and Fig. 4d show a greater sensitivity of the CTF approach with respect to the FD method when an uncertain specific mass is used as input data. This result, however, is found only in the SW case, which is a massive wall

characterized by a high thickness. Therefore, this higher sensitivity is probably related to the well-known numerical issues associated with the root searching in the Laplace space of the Direct Root Finding method used in the CTF approach. Since a substantial agreement of the methods has been

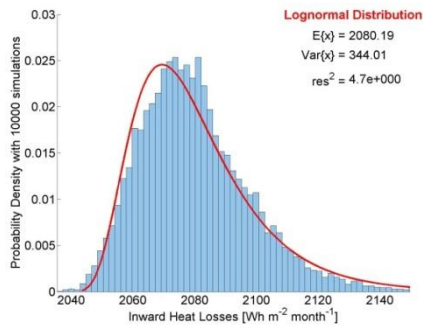
proved by comparing the monthly inward and outward heat losses computed for several wall typologies and climate conditions, the following considerations are herein presented only for the finite difference method. However, similar results are found for the CTF calculation procedure.



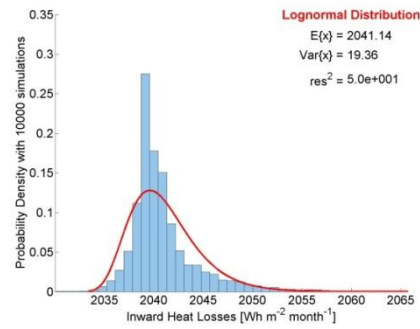
λ perturbations with CTF method in Trento



λ perturbations with FD method in Trento



ρ perturbations with CTF method in Trento



ρ perturbations with FD method in Trento

Fig. 4 – August output PDF of case SW in Trento as a function of calculation procedure.

3.3 Influence of climate conditions on PDF shape

The second part of the comparison focuses on the investigation of the interaction between climate and uncertainty in the thermo-physical parameters. For this reason, two different climates are investigated with the purpose of quantifying the extent to which a higher fluctuation of the sol-air temperature around the internal setpoint can affect the reliability of the simulation outcomes.

In Fig. 5 the PDF curves obtained for the ME case when uncertain specific mass is used either in Trento or Palermo are presented. Notice that there is an opposite change in the PDF shapes in Trento with respect to Palermo. In fact, while in Trento the

Gaussian distribution of the inward heat losses in the winter months becomes skewed for the outward heat losses in August, in Palermo an opposite trend is registered. This can be explained taking into account the role of the specific mass. In fact, specific mass together with specific heat assume a primary role in the heat transfer because of describing the capability of the wall to work as a thermal storage. Nevertheless, if the oscillation of the sol-air temperature around the internal set-point is limited, the heat flux has a prevailing direction and the effect of accumulation is less. This is what happens for example in the winter months in colder climates (e.g. Trento) and in the summer months in warm climates (e.g. Palermo). In these cases, therefore, the effect of perturbed specific mass on the heat capacitance are

not highlighted and, consequently, the output does not assume the characteristic log-normal distribution that instead occurs when the role of the thermal capacitance grows (Fig. 5). These changes in PDF shapes due to variations in climate conditions are not found instead for the perturbations of either thermal conductivity or thickness. In fact, these characteristics primarily affect the thermal resistance of the wall and, consequently, the stationary part of the solution of the heat transfer problem.

3.4 Spread comparison of model predictions

With the purpose of comparing the sensitivity of the models to the perturbation of different input, the same variability of thermo-physical properties is

required. Although this is not strictly observed in this analysis, the ranges of percentage variability of the different parameters used are similar (within $\pm 30\%$) and therefore a preliminary and qualitative analysis can be carried out. In order to better graphically represent the variability of the heat losses through the envelope, a box plot is adopted. The box plot leads to describe the degree of dispersion and skewness in the distribution of simulation outcomes by means of the simultaneous representation of the 1 % fractiles of observation, lower quartile, median, upper quartile and the 99 % fractiles of observation. Besides, with the aim of directly comparing the results obtained in different climate conditions and in different test cases, a normalization of the results is adopted.

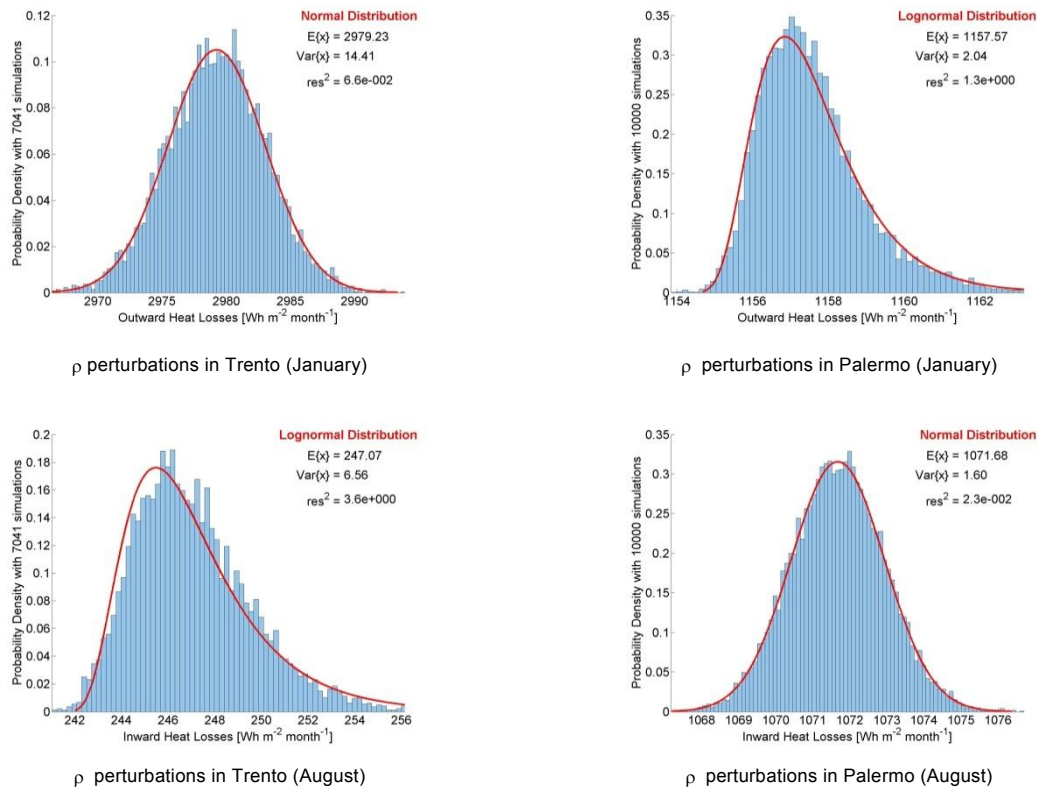


Fig. 5 – Output PDF of case ME with FD approach as a function of climate conditions.

In particular, the perturbed heat losses have been divided by the unperturbed one, thus highlighting the differences from predictions of the model with deterministic input.

The box plots in Fig. 6a and Fig. 6b show the spread of the predicted monthly inward heat losses in

August of the ME test, when suboptimal input data are used respectively for clay blocks and insulation layer. For both figures notice that a negligible dependence of normalized heat losses on specific mass and on specific heat is found. Only in Trento, due to the high daily temperature range, is there a

light influence of specific mass and specific heat with respect to clay block while, of course, variations of these parameters on the insulation layer are negligible.

Moreover, while in clay block contained variations emerge due to the perturbation of layer thickness, the FD model seems to be more sensitive to insulation thickness. In reality this is mainly caused by the effect of thickness perturbation on the total thermal resistance of the element. In fact, while the variation of the insulation thickness alters by about $\pm 14\%$ the total resistance, the clay blocks change it by only $\pm 2\%$. Instead, the uncertainties of thermal conductivity induce a variation of the total thermal resistance between $\pm 10\%$ for both materials and this produces an equal sensitivity of the method and, consequently, an equal data dispersion.

The graph in Fig. 6a also shows how, with increasing amplitude of daily fluctuations of sol-air temperature, around the internal set-point temperature (e.g. in Trento), also the results

variability caused by the perturbations of either the thickness or the thermal conductivity increases. This is because the thickness affects both the thermal resistance and the thermal capacitance of the wall. As well as the thermal conductivity, perturbation produces an alteration of the thermal diffusivity, which is the main parameter in the description of the transient part of the solution of heat transfer problem. A similar comparison is also carried out for the SW case and the results are shown in Fig. 6c.

In contrast with the ME case with uncertain clay block properties, no significant variations of the normalized inward heat losses are noted between Trento and Palermo. In addition, notice that despite the similar percentage perturbations of specific mass and specific heat in the ME case, it produces less spread in predicted inward heat losses (Fig. 6c). This is probably caused by the high thermal capacitance of the SW wall, which may result much higher than the capacitance required to accumulate and release the daily variations of heat flux.

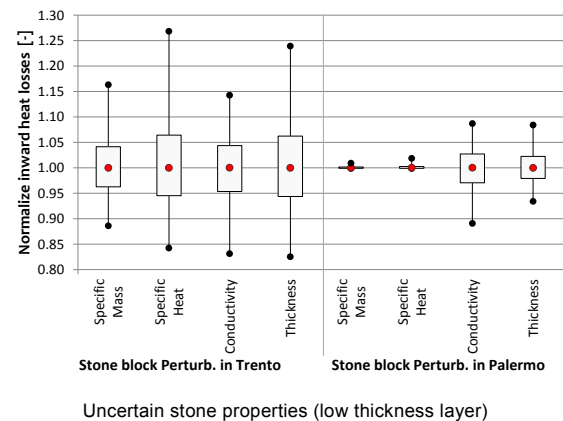
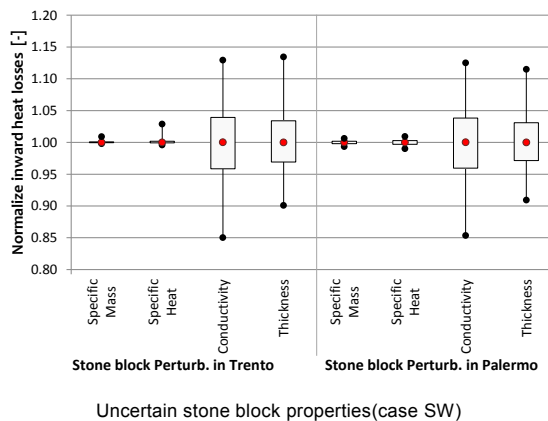
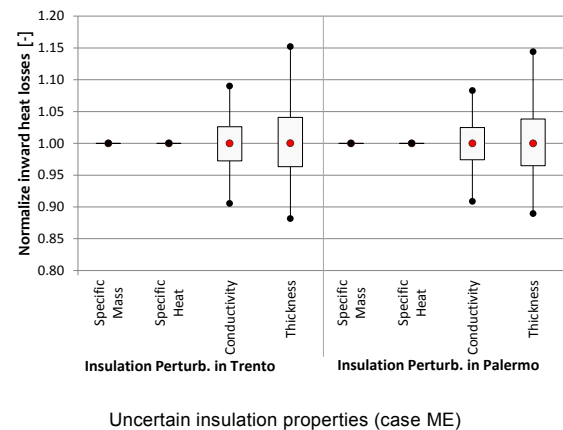
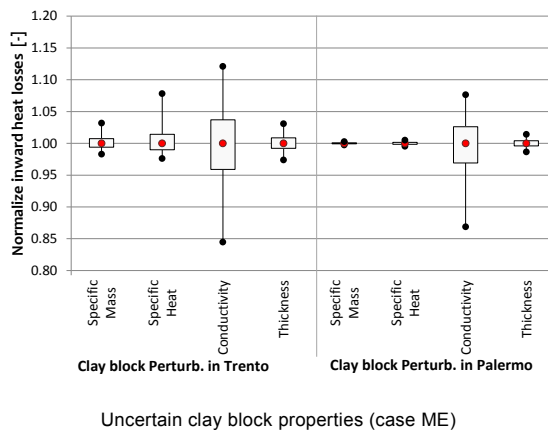


Fig. 6 – Normalized heat losses(FD approach) due to uncertain clay block properties (case ME).

Therefore, even if the wall behaviour is greatly influenced by the thermal capacitance, the perturbations of specific mass and specific heat do not induce changes in the used thermal capacitance. This is confirmed by the analysis carried out on a wall similar to the SW case, in which, however, the thickness of the stone layer is 30 cm. The other thermo-physical parameters and the percentage perturbation of the input data are kept unchanged with respect to the SW case. Fig. 6d stresses the role of specific mass and specific heat perturbations in temperate climates such as Trento. The box plot shows how the variability on the inward heat transfer in Trento, due to either uncertain specific mass or specific heat, becomes comparable to those caused by the conductivity and thickness perturbations. Because of the warmer climate, this does not happen in Palermo. Therefore the weight of the heat capacitance in the wall thermal response decreases and, consequently, the role of the perturbations imposed on specific mass and specific heat drops off.

The results obtained in this work are summarized in Table 4, where the distance between the upper and lower quartile (i.e. interquartile range) of the inward heat losses distributions is reported for each test case and for each uncertain parameter.

			Specific Mass	Specific Heat	Conductivity	Thickness
SW	Trento	CTF	4.26%	7.39%	30.19%	27.29%
		FD	1.12%	3.29%	27.91%	23.36%
	Palermo	CTF	0.07%	0.11%	27.92%	22.10%
		FD	1.29%	1.91%	27.15%	20.57%
ME clay block perturb.	Trento	CTF	5.15%	10.53%	28.37%	5.80%
		FD	4.88%	10.21%	27.65%	5.70%
	Palermo	CTF	0.01%	0.03%	21.59%	3.04%
		FD	0.54%	0.96%	20.77%	2.74%
ME insulation perturb.	Trento	CTF	0.01%	0.04%	18.29%	26.86%
		FD	0.02%	0.04%	18.47%	27.04%
	Palermo	CTF	0.01%	0.01%	17.54%	25.64%
		FD	0.01%	0.04%	17.44%	25.48%
SW with L=30 cm	Trento	CTF	25.81%	39.98%	30.28%	39.51%
		FD	27.73%	42.60%	31.15%	41.42%
	Palermo	CTF	4.43%	6.80%	21.28%	18.45%
		FD	1.03%	2.01%	19.62%	15.02%

Table 4 – Percentage interquartile range for inward heat losses

4. Conclusions

The present work investigates the extent to which uncertain thermo-physical properties of envelope

materials can affect the reliability of predicted heat transfer through the envelope.

Firstly, the comparison between the Finite Different method and the Conduction Transfer Function approach demonstrates that the two calculation procedures provide consistent results both with deterministic and uncertain parameters. Only a little deviation in sensitivity to either specific mass or specific heat is registered for the massive envelope. This is probably caused by the numerical issues in the Direct Root Finding technique.

Secondly, the results of Monte Carlo simulations reveal that the outcomes of calculation procedures are not always normally distributed when Gaussian distributions of input data are adopted. This skewness is highlighted especially for perturbed specific mass or specific heat. Moreover, these parameters show a greater correlation with the external climate conditions. In particular, since specific mass and specific heat primarily affect the thermal capacitance of the wall, the output uncertainty is emphasized by the amplitude of daily oscillation of the sol-air temperature around the internal set-point temperature. However, for the SW case the sensitivity to the perturbations of specific mass and specific heat is smoothed over. In fact, the uncertainty of these parameters significantly affects the results only when the thermal capacitance needed to absorb the daily changes in sol-air temperature is modified.

For non-insulated but high massive walls, although the behaviour is mainly governed by the thermal capacitance, the uncertainties of specific mass and specific heat have limited influence on the results.

5. Nomenclature

Symbols

C_p	Specific Heat ($\text{J kg}^{-1} \text{K}^{-1}$)
CDD_{20}	Cooling degree days base on 20°C
$E\{x\}$	Expected value of x
G_{solar}	Global solar irradiation (W m^{-2})
HDD_{20}	Heating degree days base on 20°C
L	Layer thickness (m)
T_{db}	Dry Bulb Temperature (K)

Var{x}	Variance of the x variable distribution
h_0	Heat transfer coefficient ($\text{W m}^{-2} \text{K}^{-1}$)
res ²	Residuals 2-norm of the fitting
x	Random variable

Greek symbols

α	Wall solar absorptance (-)
ε	Wall hemispherical emissivity (-)
λ	Thermal conductivity ($\text{W m}^{-1} \text{K}^{-1}$)
ρ	Specific mass (kg m^{-3})

References

- ASHRAE. (2009). ASHRAE Handbook-Fundamentals (SI Edition). Atlanta (USA): American Society of Heating, Refrigerating and Air-Conditioning Engineers, Inc.
- CEN. (2008). EN ISO 13790. European Committee for Standardization.
- Corrado, V., and Mechri, H. (2009). Uncertainty and sensitivity analysis for building energy rating. *Journal of building physics*, 33(2), 125-156.
- Costola, D., Blocken, B., and Hensen, J. (2009). Overview of pressure coefficient data in building energy simulation and airflow network programs. *Building and Environment*, 44(10), 2027-2036.
- Dominguez-Munoz, F., Anderson, B., Cejudo-Lopez, J., and Carrillo-Andres, A. (2010). Uncertainty in the thermal conductivity of insulation materials. *Energy and Buildings*, 42(11), 2159-2168.
- Dominguez-Munoz, F., Cejudo-Lopez, J., and Carrillo-Andres, A. (2011). Uncertainty in peak cooling load calculations. *Energy and Buildings*, 42(7), 2798-2805.
- Gasparella, A., Pernigotto, G., Baratieri, M. and Baggio, P. (2011). Thermal dynamic transfer properties of the opaque envelope: analytical and numerical tools for the assessment of the response to summer outdoor conditions. *Energy and Buildings*, 43, 2509-2517.
- Hittle, D. (1979). Building loads analysis and system thermodynamics program BLAST user's manual. Champaign, Illinois (USA): U.S. Army Construction Engineering Research Laboratory.
- Holm, A., and Kuenzel, H. (2002). Practical application of an uncertainty approach for hygrothermal building simulations—drying of an AAC flat roof. *Building and Environment*, 37(8-9), 883-889.
- Hopfe, C., and Hensen, J. (2007). Uncertainty analysis for building performance simulation - a comparison of four tools. *Building Simulation*, (pp. 1383-1388). Beijing (China).
- Hopfe, C., and Hensen, J. (2011). Uncertainty analysis in building performance simulation. *Energy and Buildings*, 43(10), 2798-2805.
- Lomas, K., and Eppel, H. (1992). Sensitivity analysis techniques for building thermal simulation programs. *Energy and Buildings*, 19(1), 21-44.
- Macdonald, I. (2002). Uncertainty in building simulations. Glasgow UK: University of Strathclyde.
- Prada, A. (2012). Energy performance of buildings: modeling of dynamic summer behavior. Ph.D. Thesis, University of Trento, Civil and Environmental Engineering, Trento.
- HYPERLINK ["http://eprints-phd.biblio.unitn.it/770/"](http://eprints-phd.biblio.unitn.it/770/) <http://eprints-phd.biblio.unitn.it/770/>
- Seem, J. (1987). Modeling of heat transfer in buildings. Ph.D. Thesis, Madison, Wisconsin (USA).
- Tian, W., and deWilde, P. (2011). Uncertainty, sensitivity analysis of building performance probabilistic climate projections: a UK case study. *Automation in construction*, 20(8), 1096-1109.

Quasi-steady state and dynamic simulation approaches for the calculation of building energy needs: Part 1 thermal losses

Giovanni Pernigotto – University of Padova, Vicenza, Italy

Andrea Gasparella – Free University of Bozen-Bolzano, Bolzano, Italy

Abstract

In order to assess the coherence between the dynamic simulation and the EN ISO 13790:2008 quasi-steady state method, the authors, differently from previous works in literature, analysed the discrepancy sources directly for thermal losses and gains instead of considering only the final result in term of energy needs. In this first part, the deviations between the thermal losses are evaluated by means of an extensive use of simulation. More than 2000 configurations obtained by the factorial combination of different values for the building shape, envelope insulation and composition, window type and size, ventilation rate and climatic conditions, have been considered to identify the most important discrepancy sources and to improve the correspondence between simulation and quasi-steady state methods.

1. Introduction

According to the Energy Performance of Building (EPB) Directive 2010/31/EU and the former 2002/91/EC (European Parliament, 2010; European Parliament, 2002), in order to implement the energy labelling of buildings, the energy performance can be evaluated either with analytical approaches or with enhanced simulation tools. As observed by Tronchin and Fabbri (2008), the coherence of the methods is of crucial importance in order to obtain a perception of the reliability of this instrument by the market and to ensure the EPB Directive effectiveness. Moreover, the European Standard EN ISO 13790:2008 (CEN, 2008) suggests to use the dynamic simulation in improving and tuning the proposed quasi-steady state method, by refining the estimation of the utilization factor (i.e., the dynamic parameters that reduce the thermal gains for heating need

calculation and the thermal losses for cooling). The utilization factor is considered as a function of the ratio between the thermal losses and the thermal gains. Those are calculated through conventional expressions. Extending the method of studying the dynamic factor by van Dijk and Arkesteijn (1987), the Standard proposes the recourse to dynamic simulation also in determining the thermal losses and gains. Many authors have already made some efforts in calibrating the EN ISO 13790:2008 approach, such as Jokisalo and Kurnitski (2007), Corrado and Fabrizio (2007), Orosa and Oliveira (2010) and Oliveira Panão *et al.* (2011). They proposed some changes on the correlations in order to adapt the method to the climatic conditions, especially for the cooling season, and the building stock characteristics in their respective countries but the general problem appears to be still unsolved, as large discrepancies have been found.

The comparison between the dynamic simulation results and the analytical approaches (detailed or simplified) can be helpful in looking for disagreement sources, which can lead to mismatches and errors in the quasi-steady state method refinement. Referring to the thermal losses, among the causes of error or discrepancies, the ones depending on the definition of the boundary conditions and on the calculation of the thermal losses appear to play a crucial role (Judkoff *et al.*, 2008).

For the transmission losses, which represent the first component of thermal losses, the quasi-steady state model linearizes and considers the internal long wave radiation exchanges in parallel with the convection exchange with the air node, assuming an equivalent operative temperature setpoint. This is a weighted average of the air temperature of the

conditioned zone and the mean radiant temperature of the envelope delimiting the zone itself. In contrast, many of the simulation codes perform a detailed analysis of the internal long wave radiation exchange and refer to an air heat balance approach. This method considers an air temperature setpoint, as it is generally more reliable when simulating real operative conditions. As regards the ventilation losses, the actual driving temperature difference is given by the one between the internal and external air temperatures. Using an operative setpoint for ventilation losses evaluation, as indicated by the quasi-steady state approach of the technical Standard, leads to incorrect results, in particular with large ventilation rates. Previous studies (Pietrzyk, 2010) have stressed the importance of distinguishing the total losses into those by transmission and the ones by ventilation in defining statistical models. The evaluation of the link between the transmission heat losses and ventilation losses has also been investigated in relation to the reduction of the building energy need (Zhou *et al.*, 2008). Other authors (Soleimani-Mohseni *et al.*, 2006) have studied the ventilation flow rate in order to derive some interactions with the operative temperature. In a previous work, Gasparella and Pernigotto (2012), the authors compared the thermal losses calculated in accordance with the quasi-steady state method to the ones simulated with TRNSYS 16.1, considering the effect of using an air temperature or an operative temperature setpoint, calculated both with balanced and unbalanced weights. In the present work, in addition to the sources of discrepancies between the air and the operative temperature already analysed, the presence of envelope insulation and the ventilation rate, different amounts of adiabatic surfaces have been considered. A statistically derived correction factor has been determined in order to improve the estimation of an operative equivalent temperature starting from the air temperature setpoint. This allowed to improve the agreement with the results of simulation by TRNSYS and air temperature setpoint.

2. Methods

2.1 EN ISO 13790:2008 model

In accordance with the Standard EN ISO 13790:2008, the thermal losses Q_{ht} through the envelope and by ventilation can be calculated with the Eq. (1).

$$Q_{ht} = Q_{tr} + Q_{ve} \quad (1)$$

The thermal transmission losses through the envelope directly exposed to the outdoors are:

$$Q_{tr} = H_{tr} \cdot (\theta_{i,set} - \theta_e) \cdot t \quad (2)$$

Considering only dispersions of the heated zone towards the outside environment and neglecting the thermal bridges, the overall transmission heat transfer coefficient is:

$$H_{tr} = H_D = \sum_{k=1}^n A_k U_k \quad (3)$$

Due to the adopted simplifications, as the surface long wave radiation exchanges are linearized and superimposed to the convective ones, and in coherence with the definition of H_D and of the thermal transmittance U , the setpoint should be considered an operative temperature. It can be assumed as a weighted average of the air and mean radiant temperatures, considering equal weights if complying with the EN ISO 13790:2008:

$$\theta_{op} = 0.5 \cdot \theta_{air} + 0.5 \cdot \theta_{mr} \quad (4)$$

The ventilation thermal losses are defined as:

$$Q_{ve} = H_{ve} \cdot (\theta_{i,set} - \theta_e) \cdot t \quad (5)$$

where:

$$H_{ve} = \rho_a c_a \left(\sum_{k=1}^n b_{ve,k} \dot{V}_k \right) \quad (6)$$

In the considered cases the temperature adjustment factor $b_{ve,k}$ is 1 because the supply air temperature is equal to the external air temperature.

The use of an operative temperature setpoint also for the calculation of ventilation losses is not strictly correct. For that reason it is expected that some discrepancies arise between simulation and simplified calculation results even if the same operative temperature setpoint is used, and that

those differences increase for increasing ventilation rates. The second issue is that generally the operative temperature is not known when using the method, in particular when air temperature setpoints are considered.

2.2 TRNSYS air heat balance

TRNSYS, as many of the most widespread simulation codes, solves the heat balance calculation with respect to the air node, considering separately the convective and the radiative exchanges. The air node balance is expressed as function of the convective thermal exchanges:

$$\phi_{c,i} + \phi_{ve} + \phi_{gc} + \phi_{sys} = C_{air} \frac{d\theta_{air}}{dt} \quad (7)$$

The surface convective exchange is determined solving the surface heat balance, per unit of surface, for the internal side:

$$\dot{q}_{c,i} + \dot{q}_{sol,i} + \dot{q}_{gswr,i} + \dot{q}_{IR,i} + \dot{q}_{glwr,i} + \dot{q}_{tr,i} = 0 \quad (8)$$

In particular, the internal long wave radiation is evaluated by Seem's equivalent star network approach (Seem, 1987). The conduction heat through the envelope is usually calculated by the simulation codes with a numerical approach, such as the transfer function method (TFM): in TRNSYS the method implemented is the Direct Root-Finding (DRF). The external boundary conditions are defined by the balance equation:

$$\dot{q}_{c,o} + \dot{q}_{sol,o} + \dot{q}_{IR,o} + \dot{q}_{tr,o} = 0 \quad (9)$$

The external long wave radiation is calculated considering the exchanges with the external surrounding elements (ground, other buildings, sky vault).

2.3 Thermal losses calculation procedure with the dynamic simulation approach

In order to evaluate the thermal losses by means of dynamic simulation, the EN ISO 13790:2008 prescribes to calculate the energy needs setting to zero the internal gains, the solar gains and the infrared extraflow to the sky vault. The simulation heating and cooling setpoints have to be the same

(null regulation band). The thermal losses can be calculated from the heating energy need and the cooling energy need:

$$Q_{ht} = Q_{H,nd} - Q_{C,nd} \quad (10)$$

In order to compare the simulated losses to the quasi-steady state results, boundary conditions and calculation parameters for the simulation have to be coherent with the ones assumed in the quasi-steady state approach. Regarding the external conditions, the hourly weather data have been calculated by means of the subroutine Type 54 starting from the monthly average values reported by the Italian technical Standard UNI 10349:1994 (UNI, 1994). Regarding the internal conditions, because in the TRNSYS subroutine Type 56 only an air temperature setpoint is allowed, an iterative approach was adopted in the simulation in the cases with an operative temperature setpoint:

- imposing the weighting factors to the internal air temperature and the mean radiative temperature calculated at each timestep, the resulting operative temperature was calculated;
- the air temperature setpoint in Type 56 was then corrected given the target operative temperature setpoint, repeating the calculations again, till convergence.

Since the aim of this work is to deepen the analysis of the elements of disagreement and to make the two approaches coherent, only balanced weights have been considered, as defined in Eq. (4).

According to the EN ISO 6946:2007 (CEN, 2007) for quasi-steady state methods, the global surface heat transfer coefficients are distinguished in convective and radiative coefficients. Due to the detailed long wave radiation models adopted by TRNSYS, only the convective coefficients could be set to the values prescribed by the Standard also in the simulation: 20 W m⁻² K⁻¹ for the external side, and 5.0, 0.7 or 2.5 W m⁻² K⁻¹ respectively for upward, downward and horizontal flow on the internal side.

As far as the radiation exchanges are concerned, both internal ($\epsilon=1$) and external emissivity values ($\epsilon=0.9$) are non-modifiable in TRNSYS. In principle, attempting to improve the coherence between

detailed simulation and quasi-steady state calculation, the internal long wave radiation heat transfer coefficient used in the quasi-steady state approach could be calculated according to:

$$h_r = 4 \cdot \sigma \cdot \varepsilon \cdot T_{mr}^3 \quad (11)$$

The same unitary internal emissivity used in TRNSYS can be assumed, but the surfaces temperature is not known in advance and can only be approximated with the temperature setpoint, as suggested by the Standard itself. Thus, different surface radiative heat transfer coefficients have been considered coherently with the chosen setpoints.

2.4 Reference building model and set of configurations

The difference between the air and the operative temperature, which impacts on the correspondence between the transmission losses calculated with quasi-steady state approach or detailed simulation when using an air temperature setpoint, is largely affected by the insulation level of the envelope. Moreover, as is also pointed out by the Standard EN ISO 13790:2008 itself, it is expected that also large ventilation rates lead to relevant discrepancies with the quasi-steady state methods, and not only when using air temperature setpoint for the simulation. Therefore, in this first part of the analysis we focused on different ventilation rates and insulation levels of the envelope, as well as on the kind of temperature setpoint. The simulations were performed considering air temperature and operative temperature setpoints and then compared with the ones calculated with quasi-steady state method. Concerning the values of setpoint, a typical heating season setpoint temperature for residential applications (20 °C) and the second one with a typical cooling setpoint temperature (26 °C) have been assumed, in accordance with the prescriptions by the EN ISO 13790:2008.

A single base building module has been considered and a selected group of parameters has been varied within a predefined set of values, obtaining a variety of configurations. With the perspective of the second part of this work on thermal gains, we

also paid attention to some component properties, such as the thermal capacity of the walls or the SHGC of the glazings, not related to the thermal losses but affecting the selection the components themselves.

The considered module is single-storey with 100 m² of floor area and a horizontal roof. The opaque envelope is composed by a two-layer structure, whose thermo-physical characteristics are reported in Table 1. An insulation layer, with a thickness depending on the simulation plan, is positioned on the external side. Three possible materials have been considered for the internal layer (timber, clay-block or concrete) with a thickness chosen to have a thermal resistance around 0.8 m² K W⁻¹, as 0.2 m of clay-block. The window frame is a timber frame with a low performance ($U_f = 3.2 \text{ W m}^{-2} \text{ K}^{-1}$) if coupled with the single glass and high performance ($U_f = 1.2 \text{ W m}^{-2} \text{ K}^{-1}$) in the other cases. The frame area covers about the 20 % of the whole window area.

	Timber	Clay-Block	Concrete	Insulation
λ	0.13	0.25	0.37	0.04
c	1880	840	840	1470
ρ	399	893	1190	40
s	0.1	0.2	0.3	0/0.05/0.10
R	0.77	0.80	0.81	0/1.25/2.5

Table 1 – Properties of the opaque components

The following geometrical and thermo-physical characteristics have been determined in accordance with the factorial plan:

1. the amount of envelope surface exposed to the external conditions;
2. the ventilation rate;
3. the level of insulation added to the internal layer;
4. the base material of the opaque envelope (taken into account in this part of the analysis because of the small differences of the three layers thermal resistances);
5. the percentage ratio of glazings A_{gl} to floor area A_f ;
6. the kind of glazings;
7. the climatic conditions.

For each of the above factors, a certain number of

alternatives (levels) were considered as reported in Table 2. The presence of thermal bridges has been neglected in this study, as they can be considered to play a neutral role comparing the simulation and the quasi-steady state approaches. As the aim was to evaluate the losses by thermal transmission through opaque and transparent elements directly exposed to the outdoor air (i.e. with external air convection boundary conditions), when the floor is not adiabatic, it has been assumed as directly in contact with the external air without any solar contribution, as if it was on a well-ventilated cavity.

The first factor allows to consider different ratios between the dispersing surface and the effect of different percentages of adiabatic surface in the total envelope. The second one analyses the ventilation rates, taking into account also its absence (e.g., thermal losses only by transmission). The variation of the thickness of the insulation layer from 0 to 10 cm (factor 3) and the kind of glazings (factor 6), allow to evaluate configurations ranging from non-insulated buildings to well insulated ones. The factors 1, 5 and 6 allow to analyse the internal infrared exchanges between the glazings and the adiabatic surface and their effects on the mean radiant temperature of the thermal zone. Two climates have been considered to calculate the thermal losses for different profiles of external temperatures

Considering 3 shape ratios, 4 ventilation rates, 3 possible insulation thicknesses, 3 base materials, 2 different ratios between the window surface and the floor and 5 types of glazings, 1080 different configurations have been evaluated for each month of each climate. 25920 monthly values have been elaborated for each of the 4 setpoint conditions (air temperatures 20 °C and 26 °C, operative temperatures 20 °C and 26 °C).

3. Results and discussion

The different setpoint temperature strategies have been considered, assuming the EN ISO 13790:2008 results as a benchmark. Firstly the different setpoint strategies have been compared for a null ventilation rate, in order to investigate the

deviation induced by choosing air temperature

1	a	one wall, floor and ceiling adiabatic; $S/V=0.30 \text{ m}^{-1}$
	b	one wall and floor adiabatic; $S/V=0.63 \text{ m}^{-1}$
	c	one wall adiabatic; $S/V=0.97 \text{ m}^{-1}$
2	a	0 ACH (no ventilation rate)
	b	0.3 ACH (as for residential dwellings in accordance with the Italian technical Specification UNI/TS 11300-1:2008)
	c	0.6 ACH
	d	0.9 ACH
3	a	0 cm – $U_{env} = 1.03 \text{ W m}^{-2} \text{ K}^{-1}$
	b	5 cm – $U_{env} = 0.45 \text{ W m}^{-2} \text{ K}^{-1}$
	c	10 cm – $U_{env} = 0.29 \text{ W m}^{-2} \text{ K}^{-1}$
4	a	Timber
	b	Clay-block
	c	Concrete
5	a	11.7%
	b	23.4%
6	a	(S) single glass $U_{gl} = 5.68 \text{ W m}^{-2} \text{ K}^{-1}$, $SHGC = 0.855$
	b	(DH) double glazing high solar transmittance $U_{gl} = 1.140 \text{ W m}^{-2} \text{ K}^{-1}$, $SHGC = 0.608$
	c	(DL) double glazing low solar transmittance $U_{gl} = 1.099 \text{ W m}^{-2} \text{ K}^{-1}$, $SHGC = 0.352$
	d	(TH) triple glazing high solar transmittance $U_{gl} = 0.613 \text{ W m}^{-2} \text{ K}^{-1}$, $SHGC = 0.575$
	e	(TL) triple glazing low solar transmittance $U_{gl} = 0.602 \text{ W m}^{-2} \text{ K}^{-1}$, $SHGC = 0.343$
7	a	Messina – HDD_{20} : 707 K d
	b	Milan – HDD_{20} : 2 404 K d

Table 2 – Factors and levels in the simulation plan

setpoint or operative setpoint in dynamic simulation. Then the effects of different the ventilation rates have been analysed.

3.1 Transmission heat losses

In Figure 1, the transmission thermal losses simulated with the air temperature setpoints and with the operative temperature setpoints have been plotted against the quasi-steady state results for the case of 20 °C. The cases with a 26 °C setpoint present similar trends and behaviours.

For both setpoint strategies, the results have been first distinguished by S/V ratio. The cases without insulation have been highlighted in a darker colour and regression lines have been added to distinguish trends and deviations. The linear regressions always show a very high index of determination R-squared in all the considered conditions, given that the results have been distinguished by shape ratio and presence of insulation. All other factors, such as window size, kind of glazings, climate and also the thickness of insulation for the insulated cases, seem rather ineffective in spreading the results away from the trendlines. Apart from the coefficient of determination, the equations of the trendlines reported in the charts enable to quantify the deviation of the results of the simulation from the ones of the quasi-steady state method: the more the slope coefficient is different from 1, the more the deviation of the simulation results will be.

The largest deviations are shown when using an air temperature setpoint for the simulations, whose results underestimate the absolute value of thermal losses. As one could expect, the differences are particularly large for the non-insulated cases with a high S/V ratio, with an undervaluation around 22%, but also in the insulated cases, the use of air temperature setpoint leads to absolute simulated losses larger than 10% with respect of the ones of the quasi-steady state method. Reducing the S/V ratio (i.e., increasing the percentage of adiabatic surface), the mean radiant temperature becomes higher, together with the operative temperature, and so the deviations between the simulations and the EN ISO 13790:2008 method get lower. With a S/V equal to 0.3, the underestimation is around 7% for the uninsulated cases and less than 3% for the insulated ones. The operative temperature setpoint enlarges the difference between internal and external air temperature, giving higher absolute transmission and ventilation losses. For the high S/V, the underestimation is less than 7% for the uninsulated cases and around 1% for the insulated ones. For more compact structures (e.g., $S/V=0.3$), instead, there is a slight overestimation in the simulated results, around 2% for the uninsulated cases and more than 6% for the insulated ones.

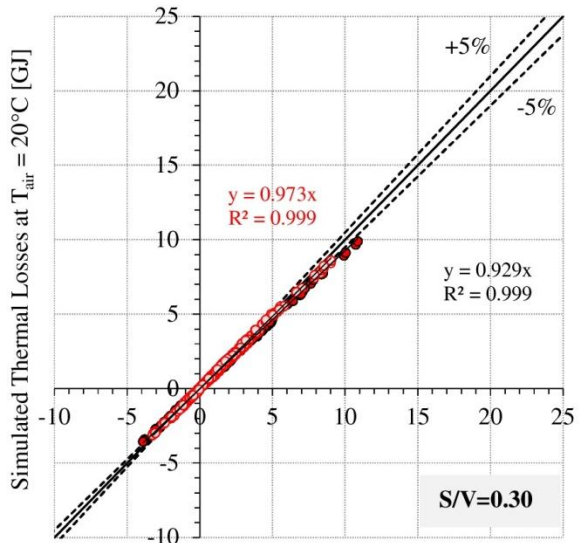
3.2 Effects of the ventilation rate

The histograms in Figure 2 represent the percent deviation of the linear trendline slopes from the unitary value for a 20 °C setpoint.

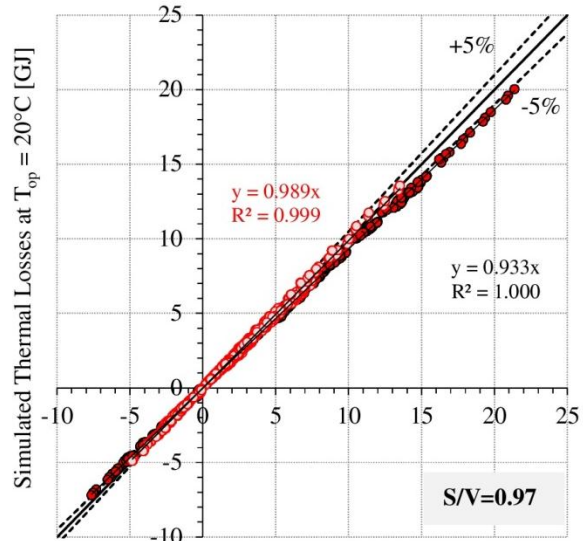
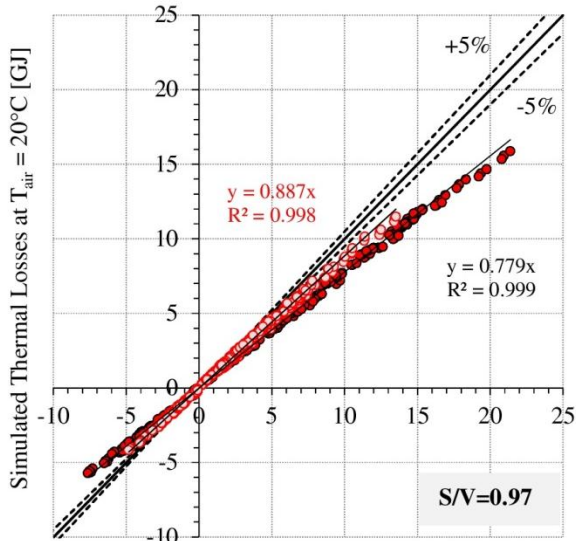
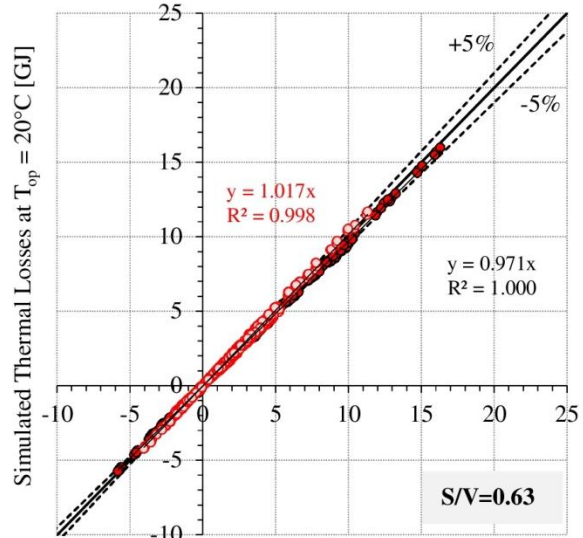
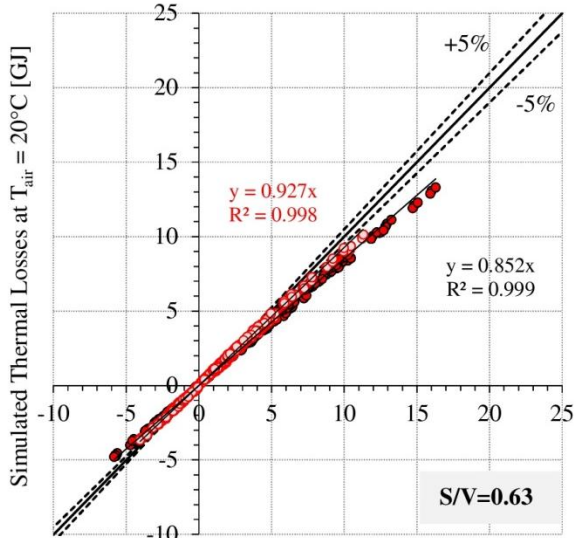
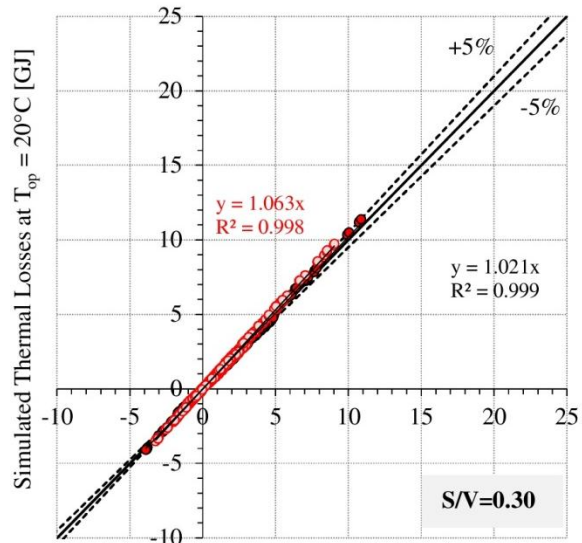
When considering an air temperature setpoint, increasing the ventilation rate reduces the difference with the estimation of the thermal losses by the simulation approach, whatever the amount of adiabatic surfaces. This is due to the fact that larger absolute ventilation losses tend to compensate more the difference between transmission losses.

For S/V larger than 0.3, the air temperature setpoint still remains critical for all the considered ventilation rates, in particular in the non-insulated cases whose deviations are always larger than 10%. When using an operative temperature setpoint, the trend is generally the same but in that case the effect does not compensate for the already positive deviation of transmission losses. The ventilation losses are underestimated in absolute value by the quasi-steady state approach: the more the ventilation rate increases, the lower the absolute ventilation losses in the quasi-steady state method than in the simulations. The only exception to this behaviour is for the insulated cases with aspect ratio equal to 0.3 and 20 °C setpoint and the insulated ones with the same aspect ratio but a 26 °C setpoint and ventilation rate larger than 0.6 ACH, where increasing the ventilation rate the deviations slightly decrease. Since the mean radiant temperature is independent from the ventilation rate and it is larger than the operative temperature setpoint in many of these last cases, the air temperature setpoint used by TRNSYS in the air-heat balance is lower than the setpoint of 20 or 26 °C (indeed, the thermal losses estimated by TRNSYS are lower than the ones calculated with the EN ISO 13790:2008 method). That also affects the ventilation thermal losses which are overestimated by the quasi-steady state approach and make the global percentage deviation decrease in absolute terms. With the operative temperature setpoint, the deviations are generally within a range of 5%, except for the uninsulated cases

without ventilation and $S/V=0.97$ and for the



insulated ones with $S/V=0.3$.



Thermal Losses at 20°C - EN ISO 13790 [GJ]

Thermal Losses at 20°C - EN ISO 13790 [GJ]

Fig. 1 – Simulated thermal losses with air temperature setpoint (on the left) and operative setpoint (on the right), without ventilation a for the different S/V. Insulated cases in lighter colours

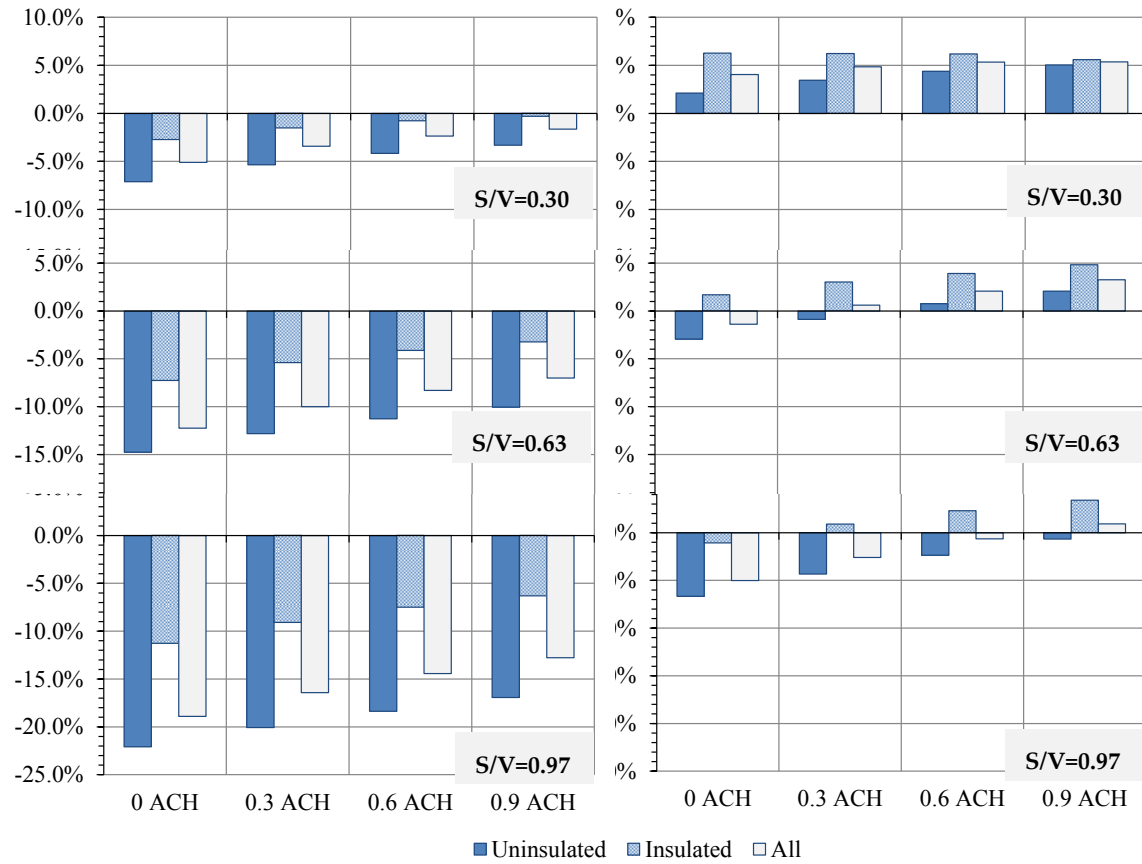


Fig. 2 – Percent deviation of the simulated thermal losses with air temperature setpoint (on the left) and operative setpoint (on the right) respect to the losses calculated with the quasi-steady state approach for different airchange rates and S/V ratios

k_0	k_1	k_2	k_3	k_4	k_5	k_6	k_7	k_8	k_9	k_{10}
1.031	-1.456E-3	2.091E-3	2.451E-3	-0.01465	-0.2093	0.01022	-0.1044	4.518E-3	0.05882	-2.084E-3

Table 3 – Regression coefficients

3.3 Setpoint correction factor for the calculation of thermal losses by transmission

As observed in the previous paragraphs, the main source of discrepancy is the kind of temperature considered as setpoint. The operative temperature setpoint is not realistic in most of the applications and so a correction factor has been calculated for all cases and a regression analysis has been performed in order to find a general equation for determining the correction starting from the envelope characteristics. The developed model is reported in Eq. (12) and it is characterized by an

adjusted determination index R^2_{adj} equal to 0.85. The 11 coefficients have been reported in Table 3 and Figure 3 represents an example of its application. The sample used for the regression consists mainly in positive thermal losses (e.g., when the average external temperature is lower than the air temperature setpoint of 20 or 26 °C: negative values are, actually, thermal gains). In consequence of that, Eq. (12) should be used only for setpoints close to the range 20 – 26 °C and when the average external temperature is lower than the setpoint.

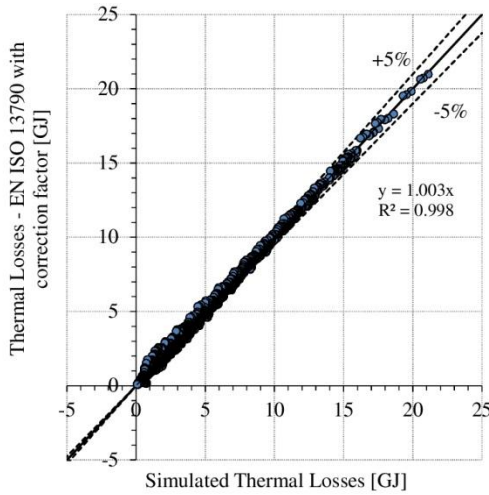


Fig. 3 – Comparison between the corrected EN ISO 13790 method and the air temperature setpoint simulations

The correspondence between the new thermal losses and the simulated ones is good (+0.3%), with larger errors for low values of the thermal losses.

$$\begin{aligned}
 f = & k_0 + \theta_e \cdot (k_1 + k_2 \cdot x_{env} + k_3 \cdot x_{win}) + \\
 & + U_{env} (k_4 + k_5 \cdot x_{env} + k_6 \cdot x_{env} \cdot \theta_e) + \\
 & + U_{win} (k_7 \cdot x_{win} + k_8 \cdot x_{win} \cdot \theta_e) + \\
 & + k_9 \cdot x_{ad} + k_{10} \cdot \theta_{i,set}
 \end{aligned} \quad (12)$$

4. Conclusion

In the present work two thermal losses estimation methods have been analysed: the EN ISO 13790:2008 quasi-steady state approach and dynamic simulations, both with air and operative temperature setpoints. In addition 301rdert kind of setpoint, the most important sources of discrepancies, the building aspect ratio, the envelope insulation and the ventilation rate, have been analysed. A correction 301rdert estimation of the operative temperature for the quasi-steady state method has been proposed in 301rdert o correctly evaluate the thermal losses by transmission in presence of air temperature setpoint.

5. Nomenclature

Symbols

A	area (m ²)
c	specific heat capacity (J kg ⁻¹ K ⁻¹)
f	correction factor (-)
h	heat transfer surf. Coeff. (W m ⁻² K ⁻¹)
H	overall heat transfer coeff. (W K ⁻¹)
HDD	heating degree-days (K d)
Q	energy (GJ)
\dot{q}	thermal flux (W m ⁻²)
R	thermal resistance (W m ² K ⁻¹)
s	thickness (m)
S	dispersing surface (m ²)
$SHGC$	solar heat gain coefficient (-)
t	time (s)
U	thermal transmittance (W m ⁻² K ⁻¹)
V	conditioned volume (m ³)
\dot{V}	air change flow (m ³ s ⁻¹)
x	surface fraction (-)
ϵ	surface emissivity (-)
ϕ	thermal flow (W)
λ	thermal conductivity (W m ⁻¹ K ⁻¹)
ρ	density (kg m ⁻³)
σ	Stefan-Boltzmann constant (5.67·10 ⁻⁸ W m ⁻² K ⁻⁴)
θ/T	temperature (°C) (K if absolute)

Subscripts/Superscripts

a/air	internal air
ad	adiabatic
c	convective
C	cooling
D	towards external air
e/o	external/external side
env	opaque envelope
f	frame
fl	floor
gc	convective gains
gl	glazing
H	heating
ht	heat transfer
i	internal/internal side
i,set	setpoint
IR	infrared radiation
glwr	longwave radiative gains
gswr	shortwave radiative gains

op	operative
mr	mean radiant
nd	energy need
r	radiative
sol	solar
sys	system
tr	transmission
Ve	ventilation
win	window

References

- Corrado V. and Fabrizio E. 2007. Assessment of building cooling energy need through a quasi-steady state model: Simplified correlation for gain-loss mismatch. *Energy and Buildings* 39.
- Gasparella A. and Pernigotto G. 2012. Comparison of quasi-steady state and dynamic simulation approaches for the calculation of building energy needs: thermal losses. *Proc. of the 2nd High Performance Buildings Conference at Purdue, West Lafayette, Indiana (U.S.)*.
- Jokisalo J. and Kurnitski J. 2007. Performance of EN ISO 13790 utilisation factor heat demand calculation method in a cold climate. *Energy and Buildings* (39).
- Judkoff R., Wortman D., O'Doherty B. and Burch J. 2008. A methodology for validating building energy analysis simulations. Technical Report NREL/TP-550-42059.
- Oliveira Panão M.J.N., Camelo S.M.L. and Gonçalves, H.J.P. 2011. Assessment of the Portuguese building thermal code: Newly revised requirements for cooling energy needs used to prevent the overheating of buildings in the summer. *Energy* (36).
- Orosa J.A. and Oliveira, A.C. 2010. Implementation of a method in EN ISO 13790 for calculating the utilisation factor taking into account different permeability levels of internal coverings. *Energy and Buildings* (42).
- Pietrzyk K. 2010. Thermal Performance of a Building Envelope – A Probabilistic Approach. *Journal of Building Physics* (34).
- Seem, J.E. 1987, Modeling of Heat in Buildings, Ph.D. thesis. University of Wisconsin Madison, Solar Energy Laboratory, Madison, Wisconsin.
- Soleimani-Mohseni M., Thomas, B. and Fahlén P. 2006. Estimation of operative temperature in buildings using artificial neural networks. *Energy and Buildings* (38).
- Tronchin L. and Fabbri K. 2008. Energy performance building evaluation in Mediterranean countries: Comparison between software simulations and operating rating simulation. *Energy and Buildings* (40).
- van Dijk H.A.L. and Arkesteijn C.A.M. 1987. Windows and space heating requirements; Parameter studies leading to a simplified calculation method. The Netherland national report on activities within step 5. TNO Institute of Applied Physics.
- Zhou J., Zhang G., Lin Y. and Li Y. 2008. Coupling of thermal mass and natural ventilation in buildings. *Energy and Buildings* (40).

Quasi-steady state and dynamic simulation approaches for the calculation of building energy needs: Part 2 thermal gains

Giovanni Pernigotto – University of Padova, Vicenza, Italy

Andrea Gasparella – Free University of Bozen-Bolzano, Bolzano, Italy

Abstract

In order to assess the coherence between the dynamic simulation and the EN ISO 13790:2008 quasi-steady state method, this paper, differently from previous works in literature, analysed the discrepancy sources directly for thermal losses and gains instead of considering only the final result in term of energy needs. In the first part, the deviations between the thermal losses were evaluated. In this second part, the authors investigate the deviations between the estimation of thermal gains, both solar and internal ones, by means of an extensive use of dynamic simulation. More than 800 configurations obtained by the factorial combination of different values for building shape, envelope insulation and composition, window type, size and orientation and climatic conditions, are considered to identify the most important discrepancy sources and to improve the correspondence between simulation and quasi-steady state methods.

1. Introduction

According to the Energy Performance of Building (EPB) Directive 2010/31/EU and the former 2002/91/EC (European Parliament, 2010; European Parliament, 2002), in order to implement the energy labelling of buildings, the energy performance can be evaluated either with simplified approaches or with enhanced simulation tools. As reminded in the first part of this work, the coherence of the methods is of crucial importance in order to obtain a perception of the reliability of energy certification by the market and to ensure the EPB Directive effectiveness (Tronchin and Fabbri, 2008). Moreover, the European Standard EN ISO 13790:2008 (CEN, 2008) suggests to use the dynamic simulation in improving and tuning the proposed quasi-steady state method, by refining

the estimation of the utilization factors, i.e. the dynamic parameters that reduce the thermal gains for heating need calculation and the thermal losses for cooling when evaluating the balance between thermal losses and thermal gains. The utilization factor is considered as a function of the ratio between the thermal losses and the thermal gains. Those are calculated through conventional expressions reported in the technical Standard. Extending the method of studying the dynamic factor by van Dijk and Arkesteijn (1987), the Standard proposes the recourse to dynamic simulation also in determining the thermal losses and gains. As indicated by van Dijk and Arkesteijn (1987) and remarked by Corrado and Fabrizio (2007), the utilization factor considers the mismatch between heat losses and gains leading to heating or cooling energy needs. What is of crucial importance, then, is that the heat losses and gains are determined accurately.

According to the quasi-steady state method, the heat gains consist in all thermal fluxes to the internal air node not driven by the temperature gradient between indoor and outdoor environment. Those can be distinguished in solar gains, internal gains and infrared extra flow towards the sky vault.

In many applications, the solar heat flow entering through the transparent envelope is the most relevant thermal gain component. The control of the entering solar radiation is becoming more and more important in designing passive systems (Orosa and Oliveira, 2012). For instance, Gasparella *et al.* (2011) simulated a well-insulated building with different kinds of glazing systems, with or without fixed shading overhangs and fins for different window sizes, orientations and European localities, showing the influence of the choice of the

glazing on the heating and cooling energy needs and peak loads. The correct estimation of the entering solar radiation is necessary since the early stages of the design process, in particular when using the simplified quasi-steady methods. Moreover, as underlined by Oliveti *et al.* (2011), the black body cavity hypothesis adopted by the EN ISO 13790:2008 method, according to which the whole solar radiation entering into the thermal zone is absorbed, is not representative of the real physical phenomena. In many cases a certain amount of the radiation is reflected by the walls and dispersed through the windows themselves. Thus, Oliveti *et al.* proposed a correction to the solar transmittance of the glazings in order to take into account the radiation lost because of the reflections. In addition to the entering radiation, the solar gains by transmission through the opaque envelope have also been studied by many researchers in different contexts. Some of them (Oliveira Pañao *et al.*, 2012; Oliveti *et al.*, 2012a) focused on the sunspaces and analysed the EN ISO 13790:2008 calculation method. Other authors paid particular attention to the roofs, underling the importance of the solar absorption coefficient (Suehrcke *et al.*, 2008), especially for the cooling energy needs. Finally, Oliveti *et al.* (2012b) assessed the methods proposed by the EN ISO 13790:2008 for the calculation of the infrared extra flow towards the sky dome, comparing the Standard with the empirical collected data and finding inaccuracies in the Standard estimations.

In the present work, a large number of configurations have been simulated with TRNSYS in order to calculate the different components of the heat gains and to compare them with the EN ISO 13790:2008 monthly procedure. By means of different statistical analyses, some correction factors have been determined to improve the accuracy of the technical Standard, estimating the actual amount of heat gains.

2. Methods

2.1 EN ISO 13790:2008 model

The technical Standard EN ISO 13790:2008 considers as heat gains Q_{gn} the term of the heat

balance that is independent of the difference of temperature between the indoor and the outdoor environments. A positive sign is assumed for heat added to the air node, while negative for subtracted. The thermal gains are defined as:

$$Q_{gn} = Q_{int} + Q_{sol} \quad (1)$$

The internal heat gains are:

$$Q_{int} = t \cdot \sum_k \Phi_{int,m,k} + t \cdot \sum_l (1 - b_{tr,l}) \Phi_{int,m,u,l} \quad (2)$$

where the effect of the heat sources from adjacent unconditioned thermal zones is considered with a contribution weighed by the reduction factor $b_{tr,l}$ defined in the Standard ISO 13789:2007 (CEN, 2007). Different heat sources (occupants, appliances, lighting, hot and mains water, HVAC system, processes and goods) can be identified:

$$\Phi_{int} = \left(\begin{array}{l} \Phi_{int,Oc} + \Phi_{int,A} + \Phi_{int,L} + \\ + \Phi_{int,WA} + \Phi_{int,HVAC} + \Phi_{int,Proc} \end{array} \right) \quad (3)$$

Case by case, it is possible to estimate the heat gain due to each single source, even if national typical values are generally proposed by national annexes or technical Standards. Whatever the entity of the internal gains, the EN ISO 13790:2008 states that they should be considered as half radiative and half convective gains.

Similar to the internal gains, the solar gains are estimated considering also the solar gains of the adjacent unconditioned thermal zones, properly weighed by the reduction factor $b_{tr,l}$:

$$Q_{sol} = t \cdot \sum_k \Phi_{sol,m,k} + t \cdot \sum_l (1 - b_{tr,l}) \Phi_{sol,m,u,l} \quad (4)$$

In particular, the heat flow by solar gains consists in the solar gains transmitted through a general element k of the building envelope, in which the infrared extra flow towards the sky-dome is subtracted:

$$\Phi_{sol,k} = F_{sh,ob,k} A_{sol,k} I_{sol,k} - F_{r,k} \Phi_{r,k} \quad (5)$$

where $F_{sh,ob,k}$ is the shading reduction factor for the external obstacles on $A_{sol,k}$, the effective solar collecting area of the element k , with a view factor of the sky $F_{r,k}$. $I_{sol,k}$ is the solar irradiance on the element k and $\Phi_{r,k}$ its infrared extra flow.

The effective solar collecting area is defined differently depending on the type of element.

For the glazings, it is calculated as:

$$A_{sol} = F_{sh,gl} g_{gl} (1 - F_f) A_{win,p} \quad (6)$$

The overall projected window area $A_{win,p}$ is reduced in order to take into account the frame factor F_f , the

total solar transmittance of the glazing g_{gl} and the shading reduction factor for movable shadings $F_{sh,gl}$, neglected in this work. The term g_{gl} is calculated in accordance with Eq. (7):

$$g_{gl} = F_w g_{gl,n} \quad (7)$$

where $g_{gl,n}$ is the solar energy transmittance for radiation perpendicular to the glazing and F_w is the correction factor for non-scattering glazings which takes into account for the different incidence angles. The scattered glazings are not considered in this work and are treated separately also by the Standard. An approximated value of F_w is 0.9 but, if available, the values indicated by the technical Standard of the EU Member States should be used. The values reported by the draft of the revUNI/TS 11300-1:2012 have been considered.

For the opaque surfaces:

$$A_{sol} = \alpha_{S,env,k} R_{se} U_{env,k} A_{env,k} \quad (8)$$

where $A_{env,k}$ and $U_{env,k}$ are, respectively, the projected area and the thermal transmittance of the opaque component k , R_{se} its external surface resistance and $\alpha_{S,env,k}$ its absorption coefficient.

The infrared extra flow can be calculated by means of Eq. (9):

$$\dot{Q}_r = R_{se} \cdot U_{env,k} \cdot A_{env,k} \cdot h_{re} \cdot (\theta_e - \theta_{sky}) \quad (9)$$

The average difference between the air temperature θ_e and the sky fictive temperature θ_{sky} can be approximated as 11 K at the latitudes of interest. Assuming an external surface temperature equal to the air temperature, the surface radiative heat exchange coefficient h_{re} can be calculated as:

$$h_{re} = 4 \cdot \sigma \cdot \varepsilon \cdot \left(273.15 + \frac{\theta_e + \theta_{sky}}{2} \right)^3 \quad (10)$$

2.2 TRNSYS heat gains

As observed in the first part of this work, TRNSYS implements and solves an air heat balance model as function of the convective thermal exchanges:

$$\phi_{c,i} + \phi_{ve} + \phi_{gc} + \phi_{sys} = C_{air} \frac{d\theta_{air}}{dt} \quad (11)$$

The convective part ϕ_{gc} of the internal gains is the only one directly involved in the balance of Eq. (11). The other gains indirectly affect the air heat balance through the radiation exchanges with the internal surface of the envelope. Per unit of surface:

$$\dot{q}_{c,i} + \dot{q}_{sol,i} + \dot{q}_{gswr,i} + \dot{q}_{lr,i} + \dot{q}_{glwr,i} + \dot{q}_{tr,i} = 0 \quad (12)$$

The radiative part of the internal gains (both shortwave $\dot{q}_{gswr,i}$, for instance from internal lighting, and longwave $\dot{q}_{glwr,i}$) and $\dot{q}_{sol,i}$, the solar irradiance entering through the glazings are considered here. In particular, in TRNSYS, the diffuse entering solar radiation is distributed homogeneously on the various surfaces of the envelope and the beam entering component is controlled by a distribution parameter called *geosurf*. Following more detailed models implemented in other simulation tools (as EnergyPlus) and the suggestions of the BESTEST procedure (Judkoff and Neymark, 1995), the *geosurf* is imposed equal to 1 for the floor and 0 for the other surfaces, so that the entering beam solar radiation first falls entirely on this surface. The solar radiation is then partially absorbed by each surface in accordance with its absorption coefficient and partially reflected as diffuse solar radiation. Due to the reflections, a certain amount of the total entering solar radiation is lost through the transparent surfaces. It is also clear that the whole heat gains involved in the internal surface heat balance do not affect the air heat balance because a fraction of the absorbed terms is lost by transmission. All these effects have been recognized by the EN ISO 13790:2008 as sources of disagreement between the quasi-steady state approach and detailed simulations.

The temperatures of the external surfaces are defined by the following balance equation:

$$\dot{q}_{c,o} + \dot{q}_{sol,o} + \dot{q}_{lr,o} + \dot{q}_{tr,o} = 0 \quad (13)$$

The extra flow infrared radiation towards the sky vault is considered in the total external long wave radiation $\dot{q}_{lr,o}$. Also in this case, the estimation of the effect on the indoor air heat balance of the solar heat gains for the opaque components and the infrared extra flow are affected by the heat transfer between the internal and the external surfaces of the envelope.

2.3 Thermal gains calculation procedure with the dynamic simulation approach

In order to evaluate the thermal gains by means of dynamic simulation, the EN ISO 13790:2008 prescribes first to calculate the thermal losses, as in

the first part of this work (Pernigotto and Gasparella, 2013). This time the internal gains, the solar gains and the infrared extra flow to the sky vault are set as in a standard simulation but the heating and cooling setpoints have to assume the same value (as for the calculation of the thermal losses). The thermal gains can be calculated from the previously determined thermal losses and from the heating and cooling energy needs of this second set of simulations:

$$Q_{gn} = Q_{ht} - (Q_{H,nd} - Q_{C,nd}) \quad (14)$$

Since the heat gains are independent from the chosen simulation setpoint, using either air or operative temperatures is irrelevant, as well as considering a value of 20 °C or 26 °C. In this analysis an air temperature setpoint of 20 °C has been assumed and the results have been used in Eq. (14), together with the correspondent set of thermal losses.

As in the first part, in order to compare simulated and quasi-steady state results, boundary conditions and calculation parameters for the simulation have been selected coherently with the ones assumed in the quasi-steady state approach. As regards the external conditions, the hourly weather data have been calculated by means of the subroutine Type 54 starting from the monthly average values reported by the Italian technical Standard UNI 10349:1994 (UNI, 1994) and used in the simplified method. The horizontal global solar radiation is split into the beam and the diffuse components in accordance with the Erbs' algorithm implemented in the Type 54. The diffuse components of the solar radiation on the vertical façades have been calculated in accordance with the algorithm by Perez *et al.* (1990). The mean daily solar radiation on a monthly basis has been calculated for each orientation and used in the quasi-steady state method instead of the ones reported in the UNI 10349:1994. Starting from the horizontal infrared flux reported in the EPW weather files, the fictive sky temperature has been calculated for each timestep and used in TRNSYS simulations. As for the solar radiation, monthly averages have been calculated for the quasi-steady state method, in place of the gradient of 11 K suggested by the EN ISO 13790:2008. Constant internal heat gains equal to 4 W m⁻² have been set in TRNSYS, half

convective and half radiative as the Standard prescribes.

The same surface convective coefficients have been considered both in TRNSYS and in the quasi-steady state method: 20 W m⁻² K⁻¹ for the external side, and 5.0, 0.7 or 2.5 W m⁻² K⁻¹ respectively for upward, downward and horizontal flow on the internal side, as in the EN ISO 6946:2007 (CEN, 2007). As underlined in the first part of the analysis, in TRNSYS, both internal ($\epsilon=1$) and external emissivity values ($\epsilon=0.9$) are non-modifiable and so the internal long wave radiation heat transfer coefficient used in the quasi-steady state approach has been recalculated by means of Eq. (15), assuming a mean radiant temperature equal to the setpoint value.

$$h_{ri} = 4 \cdot \sigma \cdot \epsilon \cdot T_{mr}^3 \quad (15)$$

2.4 Reference building model and set of configurations

The simulation plan presented in (Pernigotto and Gasparella, 2013) has been modified in order to study the heat gain problem. The plan considers a single base building module and a selected group of parameters varied within a predefined set of values, in order to develop a variety of configurations. The module is single-storey with 100 m² of floor area and a horizontal roof.

The opaque envelope is composed by a two-layer structure, whose thermo-physical characteristics are reported in Table 1. An insulation layer, with a thickness depending on the simulation plan, is positioned on the external side. Three possible materials have been considered for the internal layer (timber, clay-block or concrete) with a thickness chosen to have a thermal resistance around 0.8 m² K W⁻¹, as 0.2 m of clay-block. The absorption coefficients of the sun-exposed walls are 0.3 for the vertical walls (both sides) and for the ceiling (internal side), 0.6 for the roof (external side) and for the internal floor. When a surface is exposed to the external environment but not to the sun, its coefficient is 0. It is the case of the non-adiabatic floors directly in contact with the external air, modelled as if they are on a well-ventilated cavity. Coherently with the first part, the presence of thermal bridges has been neglected.

	Timber	Clay Block	Concrete	Insulation
λ	0.13	0.25	0.37	0.04
c	1880	840	840	1470
ρ	399	893	1190	40
s	0.1	0.2	0.3	0/0.05/0.10
R	0.77	0.80	0.81	0/1.25/2.5

Table 1 – Properties of the opaque components

The window frame is a timber frame with a low performance ($U_f = 3.2 \text{ W m}^{-2} \text{ K}^{-1}$) when coupled with the single glass or high performance ($U_f = 1.2 \text{ W m}^{-2} \text{ K}^{-1}$) in the other cases. The frame area covers about 20 % of the whole window area and its absorption coefficient is 0.6.

The following geometrical and thermo-physical characteristics have been determined in accordance with the factorial plan:

8. the amount of envelope surface exposed to the external conditions;
9. the level of insulation added to the internal layer;
10. the base material of the opaque envelope;
11. the percentage ratio of glazings A_{gl} to floor area A_f ;
12. the orientation of the windows, all positioned in the same façade;
13. the kind of glazings;
14. the climatic conditions.

For each of the above factors, a certain number of levels were considered as reported in Table 2. Since not pertinent with the topic of the second part, the ventilation rate has been neglected as variable and the simulations have been performed considering 0 ACH. The orientation of the windows has been introduced in particular to assess more profiles of entering radiation.

The first factor allows to consider different ratios between the dispersing surface and so can influence the amount of solar gains received by the opaque components and the infrared extra flow (from the external side) and the dispersion of the entering solar radiation absorbed (on the internal side). Similarly, the variation of the thickness of the insulation layer from 0 to 10 cm (factor 2) affects the heat exchanges from the internal and external

1	a	one wall, floor and ceiling adiabatic; $S/V=0.30 \text{ m}^{-1}$
	b	one wall and floor adiabatic; $S/V=0.63 \text{ m}^{-1}$
	c	one wall adiabatic; $S/V=0.97 \text{ m}^{-1}$
2	a	0 cm – $U_{env} = 1.03 \text{ W m}^{-2} \text{ K}^{-1}$
	b	5 cm – $U_{env} = 0.45 \text{ W m}^{-2} \text{ K}^{-1}$
	c	10 cm – $U_{env} = 0.29 \text{ W m}^{-2} \text{ K}^{-1}$
3	a	Timber
	b	Clay-block
	c	Concrete
4	a	11.7%
	b	23.4%
5	a	(S) single glass $U_{gl} = 5.68 \text{ W m}^{-2} \text{ K}^{-1}$, $SHGC = 0.855$
	b	(DH) double glazing high solar transmittance $U_{gl} = 1.140 \text{ W m}^{-2} \text{ K}^{-1}$, $SHGC = 0.608$
	c	(DL) double glazing low solar transmittance $U_{gl} = 1.099 \text{ W m}^{-2} \text{ K}^{-1}$, $SHGC = 0.352$
	d	(TH) triple glazing high solar transmittance $U_{gl} = 0.613 \text{ W m}^{-2} \text{ K}^{-1}$, $SHGC = 0.575$
	e	(TL) triple glazing low solar transmittance $U_{gl} = 0.602 \text{ W m}^{-2} \text{ K}^{-1}$, $SHGC = 0.343$
6	a	East
	b	South
	c	West
7	a	Messina – $HDD_{20}: 707 \text{ K d}$
	b	Milan – $HDD_{20}: 2\,404 \text{ K d}$

Table 2 – Factors and levels in the simulation plan

surfaces. The kind of glazings (factor 6), is probably the most important in this analysis because it strongly influences the entering solar radiation, which is generally the major heat gain source, together with factors 4 and 5. Factor 5 is also important in affecting the profile of the entering solar radiation during the day. Two climates have been considered to calculate the thermal losses for different profiles of external temperatures. Since the comparison is on a thermal flow and on a monthly basis, as stated in the thermal losses part, the heat capacity of the opaque envelope (factor 3) is not supposed to be relevant and it has been considered as variable because of the small deviations in the thermal resistance of the 3 alternatives and with the

perspective of further development on the calculation of the utilization factor.

Considering 3 shape ratios, 3 possible insulation thicknesses, 3 base materials, 2 different ratios between the window surface and the floor, 5 types of glazings and 3 orientations, 810 different configurations have been evaluated for each month of each climate. 19440 monthly values have been elaborated.

3. Results and discussion

The thermal gains have been analysed considering separately their 4 main components (entering solar gains through the glazings, solar gains transmitted through the opaque elements, internal gains and infrared extra flow towards the sky vault) and some correction factors based on the envelope properties have been developed. In Figures 1 and 2 the thermal gains evaluated in accordance with the EN ISO 13790:2008 method and the simulated ones have been compared, as well as the corrected results and the simulated ones. The coefficients of the regressions performed to correlate the correction factors with the envelope characteristics are reported in Table 3.

3.1 Entering solar heat gains

The entering solar radiation gains are clearly overestimated by the EN ISO 13790:2008. As we observed before, this is consistent with the lack of consideration for the redispersion of these gains by transmission or by radiation through the windows. The deviations are strongly dependent on the amount of dispersing surface (i.e., the S/V ratio) and, in particular, on the insulation level, which is also the variable considered in Figure 1 to distinguish the results in two groups: insulated one in light red and uninsulated one in dark red. The spread of the points of these two groups around the trend line is mainly due to S/V ratio. As it can be seen, the trend line of the uninsulated cases demonstrates a general overestimation of +51.2% given by the EN ISO 13790:2008 method. In case of insulation, it is reduced to +28.5%. For the analysed cases, a correction factor $f_{sol,gl}$ has been determined and a

regression has been performed in order to correlate $f_{sol,gl}$ with the characteristics of the envelope.

$$f_{sol,gl} = k_0 + U_{env} \cdot (k_1 + k_2 \cdot x_{env}) + x_{win} \cdot (k_3 + k_4 \cdot U_{win}) + k_5 \cdot x_{ad} \quad (16)$$

The regression, with an adjusted index of determination R^2_{adj} of 0.957, underlines also the importance of the interactions between the windowed fraction (calculated with respect of the whole envelope, including the adiabatic surfaces) with the window thermal transmittance and the opaque dispersing fraction with the mean opaque thermal transmittance (with a standardized coefficient of -0.527 and -0.448, respectively). By using Eq. (16) the quasi-steady state results have been corrected, obtaining a percentage deviation within the 5% respect of the simulations.

3.2 Solar heat gains by transmission

For the solar gains transmitted through the opaque envelope, the EN ISO 13790:2008 underestimates the results respect of the simulations. The trend is the same both for insulated and uninsulated cases and it is around -25%. The spreads of the results around the trend lines are similar in both cases (a little larger for the insulated ones).

$$f_{sol,env} = k_0 + k_1 \cdot A_{env} + x_{env} \cdot (k_2 \cdot x_{ad} + k_3 \cdot U_{env} + k_4 \cdot \theta_e) + k_5 \cdot U_{env} + k_6 \cdot U_{win} \quad (17)$$

The regression has an adjusted R^2_{adj} of 0.948 and the most influencing parameters are the opaque dispersing surface (with a standardized coefficient of 1.165) and the interaction between the opaque and the adiabatic fractions (0.609). By using Eq. (17) the quasi-steady state results have been corrected, and brought close to the 5% range of deviation respect of the simulations.

3.3 Internal gains

The convective internal gains are the same in both calculation methods and the deviations are due to the radiative part. The variability in the EN ISO 13790:2008 results is simply due to the different lengths of the months and a trend line cannot be defined. In simulation results, also the partial

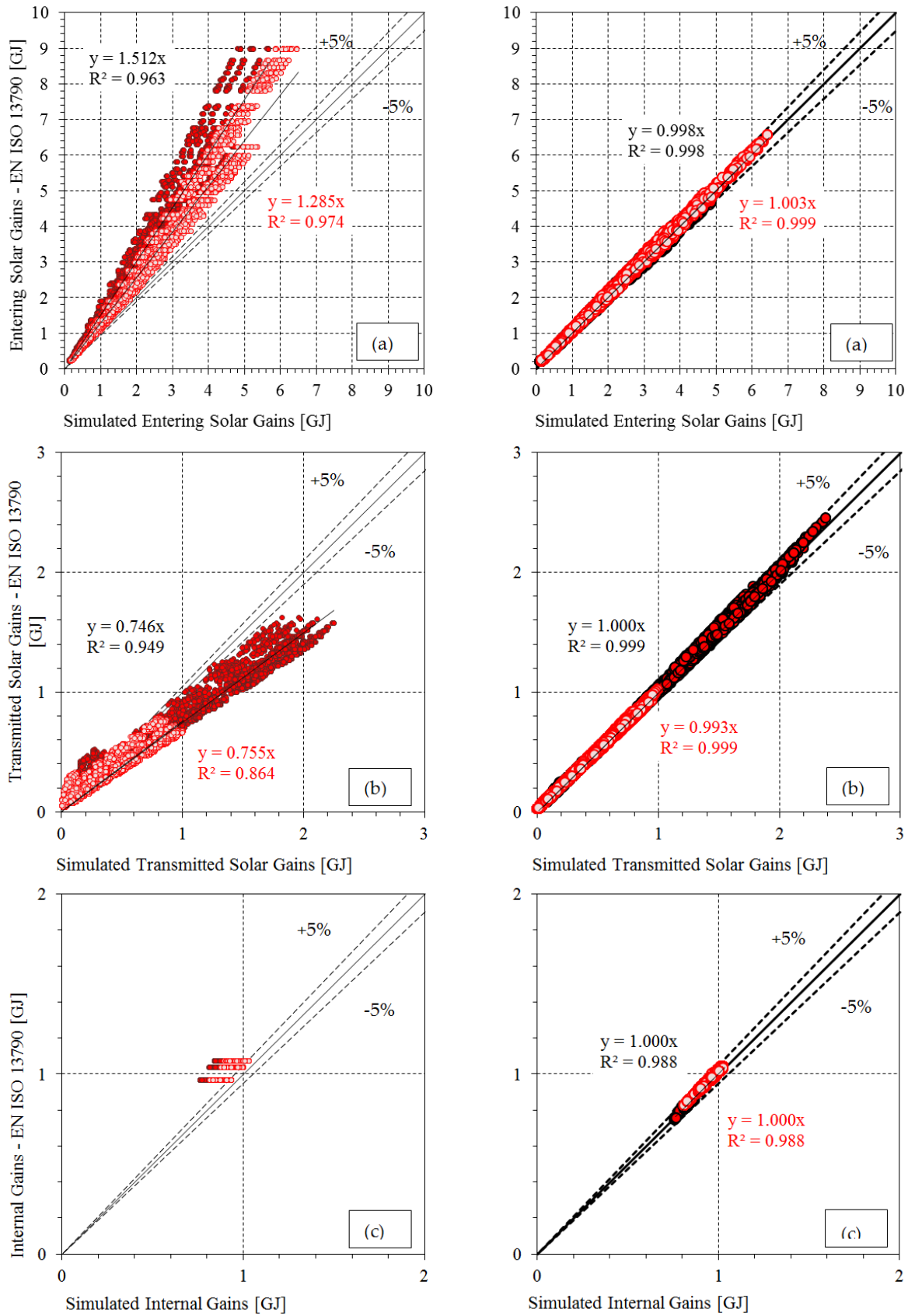


Fig. 1 – EN ISO 13790:2008 entering solar gains (a), transmitted solar gains (b) and internal gains (c), calculated according to the Standard (on the left) and using the correction coefficients (right) compared to the simulated gains. Insulated cases in lighter colours

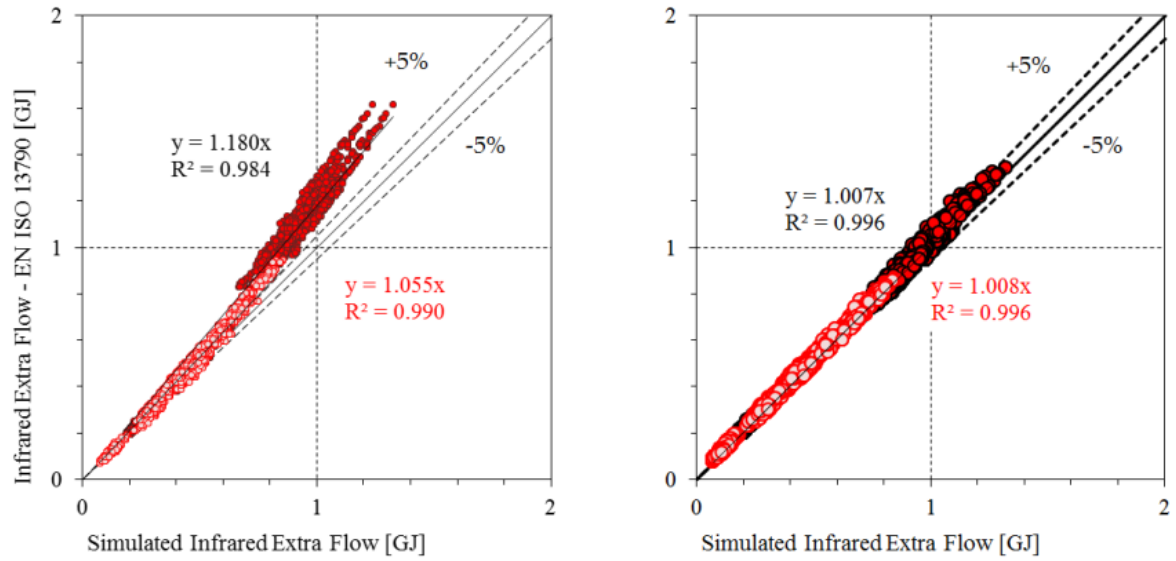


Fig. 2 – EN ISO 13790:2008 infrared extra flow towards the sky vault, calculated according to the Standard (on the left) and using the correction coefficients (right) compared to the simulated gains. Insulated cases in lighter colours

Entering solar gains

k_0	k_1	k_2	k_3	k_4	k_5
0.9346	-0.1014	0.1531	-0.2889	-0.3248	2.487E-2

Transmitted solar gains

k_0	k_1	k_2	k_3	k_4	k_5	k_6
-0.3265	4.964E-3	3.780	-0.4017	6.765E-3	0.3228	-5.766E-2

Internal gains

k_0	k_1	k_2	k_3
0.9885	-4.610E-2	-9.773E-2	-0.1709

Infrared extra flow towards the sky vault

k_0	k_1	k_2	k_3	k_4	k_5	k_6	k_7	k_8
1.044	-0.3144	-0.1433	2.217E-3	7.914E-3	-0.1562	0.2187	-3.738E-3	-5.795E-2

Table 3 – Regression coefficients

dispersion of the radiative part is considered. The overestimation provided by the Standard is between 10-20% for uninsulated cases and 5-10% for the insulated ones.

Also the S/V ratios, as expected, are relevant.

The regression adjusted R^2_{adj} is 0.99 and the

interactions between the fraction of opaque surface and its mean thermal transmittance and the one between the fraction of window surface and its thermal transmittance have the same standardized coefficients (around -0.5).

$$f_{int} = k_0 + U_{env} \cdot (k_1 + k_2 \cdot x_{env}) + k_3 \cdot U_{win} \cdot x_{win} \quad (18)$$

3.4 Infrared extra flow towards the sky vault

In the calculation of the infrared extra flow towards the sky dome, a different behaviour from the insulated to the uninsulated cases can be noticed: while for the insulated cases a good agreement is registered, for the uninsulated ones the EN ISO 13790:2008 overestimates (+18%). The difference is probably due to the estimation of the surface temperature for the calculation of h_{re} . The

adjusted determination index is 0.878 and the most influencing parameters are the interaction between the thermal transmittance of the opaque envelope and its fraction (standardized coefficient equal to -0.418) and the fraction of adiabatic surface (0.665).

$$f_{IR,sky} = \frac{k_0 + x_{env} \cdot (k_1 \cdot x_{ad} + k_2 \cdot U_{env} + k_3 \cdot \theta_e) + U_{win} \cdot (k_4 + k_5 \cdot x_{win}) + k_6 \cdot x_{ad} + k_7 \cdot \theta_e + k_8 \cdot U_{env}}{(19)}$$

4. Conclusions

In the present work two thermal gains estimation methods have been analysed: the EN ISO 13790:2008 quasi-steady state approach and dynamic simulations. The most important sources of discrepancies, due to the dispersion of the thermal gains involved in the surface balance of the envelope, such as the amount of dispersing surface and the envelope insulation, have been analysed. A correction, which takes into account this phenomenon, has been proposed for each heat gain component, in order to improve the coherence between dynamic simulation and quasi-steady state approach.

5. Nomenclature

Symbols

A	area (m ²)
b/F	reduction factor (-)
C	heat capacity (J K ⁻¹)
c	specific heat capacity (J kg ⁻¹ K ⁻¹)
F	view factor (-)

g	g-factor (-)
f	correction factor (-)
h	heat transfer surf. coeff. (W m ⁻² K ⁻¹)
HDD	heating degree-days (K d)
I	solar irradiance (W m ⁻²)
Q	energy (GJ)
\dot{q}	thermal flux (W m ⁻²)
R	thermal resistance (W m ⁻² K ⁻¹)
s	thickness (m)
S	dispersing surface (m ²)
$SHGC$	solar heat gain coefficient (-)
t	time (s)
U	thermal transmittance (W m ⁻² K ⁻¹)
V	conditioned volume (m ³)
x	surface fraction: $x_{env} + x_{win} + x_{ad} = 1$ (-)
α	absorption coefficient (-)
ϵ	surface emissivity (-)
Φ/ϕ	thermal flow (W)
λ	thermal conductivity (W m ⁻¹ K ⁻¹)
ρ	density (kg m ⁻³)
σ	Stefan-Boltzmann constant (5.67·10 ⁻⁸ W m ⁻² K ⁻⁴)
θ/T	temperature (°C) (K if absolute)

Subscripts/Superscripts

A	appliances
a/air	internal air
ad	adiabatic
c	convective
C	cooling
e/o	external/external side
env	opaque envelope
f	frame
fl	floor
gn	heat gain
gc	convective gains
gl	glazing
H	heating
ht	heat transfer
i	internal/internal side
int	internal heat gain
IR	infrared radiation
$glwr$	longwave radiative gains
$gswr$	shortwave radiative gains
L	lighting
$Proc$	processes
ob	obstacles

<i>Oc</i>	occupants
<i>mr</i>	mean radiant
<i>n</i>	normal incidence
<i>nd</i>	energy need
<i>r</i>	radiative
<i>sh</i>	shading
<i>sky</i>	sky vault
<i>sol/S</i>	solar
<i>sys/HVAC</i>	system
<i>tr</i>	transmission
<i>u</i>	unconditioned
<i>ve</i>	ventilation
<i>WA</i>	water mains
<i>win/w</i>	window

References

- Corrado V. and Fabrizio E. 2007. Assessment of building cooling energy need through a quasi-steady state model: Simplified correlation for gain-loss mismatch. *Energy and Buildings* (39).
- Gasparella A., Pernigotto G., Cappelletti F., Romagnoni P., Baggio P. 2011. Analysis and modelling of window and glazing systems energy performance for a well insulated residential building. *Energy and Buildings*, 43.
- Pernigotto G., Gasparella A. 2013. Quasi-steady state and dynamic simulation approaches for the calculation of building energy needs: part 1 thermal losses. *Proceedings of BSA2013 1st IBPSA Italy Conference*, January 30th February 1st 2013, Bolzano, Italy.
- Oliveira Panão M.J.N., Camelo S.M.L. and Gonçalves, H.J.P. 2012. Solar Load Ratio and ISO 13790 methodologies: Indirect gains from sunspaces. *Energy and Buildings* (51).
- Oliveti G., Arcuri N., De Simone M. and Bruno R. 2012a. Solar heat gains and operative temperature in attached sunspaces. *Ren. En.* (39)
- Oliveti G., Arcuri N., De Simone M. and Bruno R. 2012b. Experimental evaluations of the building shell radiant exchange in clear sky conditions. *Solar Energy* (86).
- Oliveti G., Arcuri N., Bruno R. and De Simone M. 2011. An accurate calculation model of solar heat gain through glazed surfaces. *Energy and Buildings* (43).
- Orosa J.A. and Oliveira, A.C. 2012. A field study on building inertia and its effects on indoor thermal environment. *Renewable Energy* (37).
- Suehrcke H., Peterson E.L. and Selby N. 2008. Effect of roof solar reflectance on the building heat gain in a hot climate. *Energy and Buildings* (40).
- Tronchin L. and Fabbri K. 2008. Energy performance building evaluation in Mediterranean countries: Comparison between software simulations and operating rating simulation. *En. & Build.* (40).
- van Dijk H.A.L. and Arkesteijn C.A.M. 1987. Windows and space heating requirements; Parameter studies leading to a simplified calculation method. The Netherland national report on activities within step 5. TNO Institute of Applied Physics.

Improving summer energy performance of highly insulated buildings through the application of a thermal analysis by numerical simulation

Ilaria Ballarini – Politecnico di Torino, Torino, Italy

Vincenzo Corrado – Politecnico di Torino, Torino, Italy

Abstract

The work presented in this paper is aimed at deepening the optimisation of the energy performance of highly insulated buildings in summer conditions through the application of an original methodology of thermal analysis.

The methodology, already presented in a previous work (Ballarini *et al.*, 2011), allows us to investigate the building energy balance and identify the most important parameters affecting the energy performance under certain conditions. The analysis is developed through the application of a dynamic simulation tool (*EnergyPlus*). The methodology consists of analysing the different contributions to the convective energy balance on internal air and their interrelations with different boundary conditions. Each contribution is split according to the dynamic driving forces of outdoor and indoor environment, i.e. external air temperature, solar radiation, internal air temperature and internal heat sources, and it is referred separately to the specific groups of components that exchange heat with internal air.

This work focuses on the application of the above thermal analysis to a highly insulated single-family house in summer conditions, in two different Italian climatic zones. The methodology provides the mean values and the standard deviations of the contributions to the convective energy balance on internal air, and allows both to identify the main causes of low energy performance and to quantify the effects of possible retrofit or operational measures.

As an exemplification, the effect of increasing the air change rate by natural ventilation during the night is investigated. The results show how the energy performance could be improved also in highly insulated buildings located in warm climates.

1. Introduction

Since the Seventies, the principles of energy efficiency and environmental sustainability have been progressively applied to buildings in Europe. Some experimental demonstrations and codes of practice were carried out, like *Passivhaus* (Germany), *Maison autonome en énergie* (France), *Green Building* (England). These examples show some common design strategies and building technologies, but they differ regarding the socio-economic, cultural and climate contexts and the habits of construction (Filippi *et al.*, 2011).

The concept of *Passivhaus*, proposed in 1988, was the first systematised concept in order of time. The typical *Passivhaus* is a residential building built according to a precise standard (*Passivhaus Standard*), obtaining a drastic reduction of the energy consumption mostly by means of a high level of thermal insulation. Since 2007, when the *Passivhaus Standard* was extended to southern European countries, the design solutions commonly implemented in the Central European passive houses have been adopted: high thermal insulation, avoiding thermal bridges, mechanical ventilation with thermal recovery from the exhaust air. In addition, further strategies of the passive cooling were introduced (Pagliano *et al.*, 2007).

Recently, a further boost towards nearly zero energy consumption has been given by the European Directive 2010/31/EU (*EPBD recast*), which requires the Member States to draw up national plans to guarantee that all the new buildings will be *Nearly Zero Energy Building* from January 2021.

More severe requirements of energy performance imply an optimisation of the building and its services, through the use of new strategies that

enable high energy efficiency and exploit renewable energy sources, taking into account the geographical and social context specificities.

The improvement of the energy performance also involves the optimisation of the traditional technologies, such as the traditional building envelope components. For instance, the application of thermal insulation material in the building envelope is generally considered the most effective way of increasing the thermal resistance of a building component, even under a dynamic driving force (Al-Turki *et al.*, 1991). However, some studies show that the building thermal insulation is a complex issue when analysed on an annual basis, because of different feedback on thermal load components when the insulation degree is increased. A higher insulation level does not always lead to lower yearly energy consumption. Some of the thermal load components show a significant dependence on user profiles and on site dependent and locally dependent climatic conditions. This dependence induces an inversion on the thermal load component sign, changing a loss into a gain and vice versa, making it impossible to have generalised conclusions only related to the insulation degree (Mazzarella *et al.*, 2011).

A detailed analysis of the thermal flows through the building envelope can show how the building energy performance in summer can worsen due to a different response of the various heat load components for the increase of the insulation degree, (Mazzarella, 2011). It was demonstrated that the energy need for the cooling of offices and commercial buildings is generally more affected by the internal gains than by the heat transfer through the building envelope, while the transparent envelope affects the energy performance in summer more than the opaque envelope in residential buildings (Ballarini *et al.*, 2012).

Taking into account these premises, the present work is aimed at identifying and quantifying strategies for the optimisation of the energy performance of highly insulated buildings in summer conditions. The analysis is carried out applying a methodology of thermal analysis presented in a previous work (Ballarini *et al.*, 2011). The analysis is developed by means of a dynamic

simulation tool (*EnergyPlus*) which allows us to find out the most important parameters affecting the energy performance of buildings under certain conditions, through the investigation of different contributions to the convective energy balance on internal air and their interrelations with different boundary conditions and driving forces.

The thermal analysis methodology is applied to a highly insulated single-family house, built according to the standards of a *passive house*. The case study is supposed to be located in two different Italian climatic zones.

The causes of low energy performance in summer are identified and some strategies for improving the energy performance are proposed. The effects of the application of a higher air change rate by natural ventilation during the night is also quantified, using the same investigation method.

2. Analysis of a case study

2.1 Methodology of thermal analysis

The proposed methodology of thermal analysis is based on the classification of the convective heat balance terms as functions of the different dynamic driving forces of indoor and outdoor environments, in order to find out the elements that mainly affect the building energy performance under certain conditions. Each contribution to the heat balance equation (the effect) is split according to the driving forces (the causes), among which the external temperature, the solar radiation and the internal heat sources are mentioned (Table 1).

Each contribution can also be referred separately to specific groups of building components exchanging heat with internal air (e.g. opaque envelope components, transparent envelope components, internal partitions of the building), as shown in Fig. .

The thermal analysis of the building is carried out by means of the numerical simulation code *EnergyPlus*. The principle of superposition of the effects is applied in order to identify each contribution to the convective heat balance to be attributed to each driving force. Five simulations are sequentially run on the same model and in the

Acronym	Driving force	Phenomenon
$T_{tr,op}$	External temperature	Heat transfer by thermal transmission through the opaque envelope
$T_{tr,w}$	External temperature	Heat transfer by thermal transmission through the transparent envelope
T_{ve}	External temperature	Heat transfer by ventilation
Int	Internal sources	Internal heat gains
Sol_{op}	Solar radiation	Solar radiation incident on the opaque envelope, partially absorbed and transmitted indoor
Sol_w	Solar radiation	Solar radiation entering indoor through the transparent envelope

Table 1 – Driving forces and associated phenomena

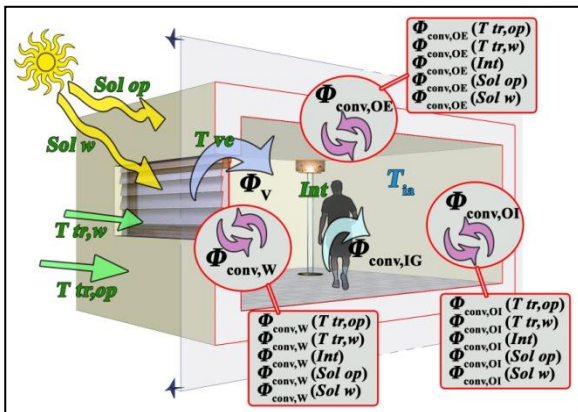


Fig. 1 – Driving forces and convective heat flows

same conditions, but adding a different driving force each time.

In simulations no. 1 and no. 2, the solar radiation and the internal heat sources are removed, so the only driving force considered is the outdoor air

temperature. Moreover, in simulation no. 1 the windows are considered adiabatic by introducing null values of thermal conductivity and thermal emissivity of glass and frame. In this way, only the effect of the outdoor air temperature ($T_{tr,op}$) on the convective heat balance of the internal air, considering only the thermal transmission through the opaque envelope components, is obtained. This effect is referred separately to the convective heat exchange of the internal surfaces of the opaque envelope, $\Phi_{conv,OE}(T_{tr,op})$, of the transparent envelope $\Phi_{conv,W}(T_{tr,op})$ and of the surfaces of the internal partitions $\Phi_{conv,OI}(T_{tr,op})$.

In simulation no. 2, the effect of the outdoor air temperature is fully considered including also the heat transmission through the transparent envelope components ($T_{tr,w}$), by re-establishing the correct values of the thermal/solar parameters of glass and frame. In this way, it is possible to obtain the contribution of the outdoor air temperature on the convective heat balance of the internal air in relation to the heat transfer through the transparent building envelope, by difference from simulation no. 1. Also this contribution is separately referred to the internal surfaces of the opaque envelope $\Phi_{conv,OE}(T_{tr,w})$, of the transparent envelope $\Phi_{conv,W}(T_{tr,w})$ and to the surfaces of the internal partitions $\Phi_{conv,OI}(T_{tr,w})$.

In the first two simulations, also the effect of the outdoor air temperature (T_{ve}) on the heat flow by ventilation (Φ_v) is directly obtained.

In simulation no. 3, the internal heat sources (Int) are added. The effect of the internal heat sources on the convective heat balance of the internal air is shown by a difference from simulation no. 2. This effect is both the convective part of the internal heat sources $\Phi_{conv,IG}(Int)$, and the convective heat flow exchanged between the internal air and the internal surfaces of the opaque envelope $\Phi_{conv,OE}(Int)$, of the transparent envelope $\Phi_{conv,W}(Int)$ and of the internal partitions $\Phi_{conv,OI}(Int)$, resulting from subsequent heat transfer by thermal radiation from the internal heat sources to the room surfaces. In simulation no. 4, the contribution of the solar radiation is added (Sol_{op}), by considering completely reflective glazing. In such a way the effect of the solar radiation incident on the opaque envelope on

the convective heat balance is obtained by a difference from simulation no. 3. This effect is split with reference to the internal surfaces of the opaque envelope $\Phi_{\text{conv,OE}}(\text{Sol op})$, to the internal surfaces of the transparent envelope $\Phi_{\text{conv,W}}(\text{Sol op})$ and to the surfaces of the internal partitions $\Phi_{\text{conv,OI}}(\text{Sol op})$.

In simulation no. 5, the solar radiation through the windows is also considered ($Sol w$). The effect of this driving force on the convective heat balance is obtained by a difference from simulation no. 4. Also this effect is split with reference to the internal surfaces of the opaque envelope $\Phi_{\text{conv,OE}}(Sol w)$, of the transparent envelope $\Phi_{\text{conv,W}}(Sol w)$ and to the surfaces of the internal partitions $\Phi_{\text{conv,OI}}(Sol w)$.

The same hourly profile of the indoor air temperature is applied in all the simulations, in order to assure the consistency of the results. This temperature profile is obtained by running a simulation no. 0, in which all the driving forces are considered and a dead-band thermostat with a lower limit equal to the heating set-point temperature (20 °C) and an upper limit equal to the cooling set-point temperature (26 °C) is applied.

2.2 Description of the building

The simulated building is a two-storey detached single-family house: the first floor includes the kitchen, the dining room, the living room and some service rooms. Two bedrooms and two bathrooms are located on the second floor. Part of the first floor, coincident with the living room, has a double height. The vertical section of the building is shown in Fig. 2. The main geometrical data of the building are listed in Table .

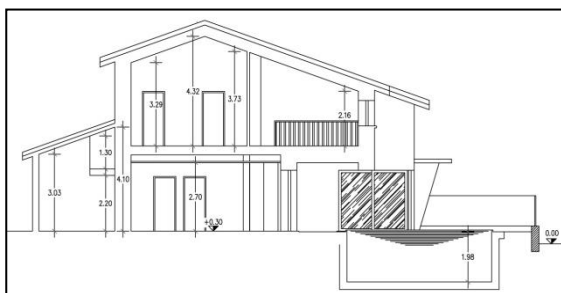


Fig. 2 – Vertical section of the building

Parameter	Value
A_f	192.4 m ²
V_n	758 m ³
V_g	1191 m ³
A_{env}	710 m ²
A_w	37.3 m ²
A_{env}/V_g	0.6 m ⁻¹
A_w/A_{env}	0.05
A_w/A_f	0.19
A_{env}/A_f	3.69

Table 1 – Main geometrical data of the case study

The building was designed applying solutions commonly implemented in a *passive house*, in order to obtain a high energy performance both in winter and summer seasons. The main data of the building referred to the construction features are listed in Table 2.

Upper horizontal enclosure	U	$[\text{W}\cdot\text{m}^{-2}\cdot\text{K}^{-1}]$	0.084
	Stot	$[\text{m}]$	0.50
	Sins	$[\text{m}]$	0.40
	λ_{ins}	$[\text{W}\cdot\text{m}^{-1}\cdot\text{K}^{-1}]$	0.035
Lower horizontal enclosure (on ground)	U	$[\text{W}\cdot\text{m}^{-2}\cdot\text{K}^{-1}]$	0.083
	Stot	$[\text{m}]$	0.98
	Sins	$[\text{m}]$	0.25
	λ_{ins}	$[\text{W}\cdot\text{m}^{-1}\cdot\text{K}^{-1}]$	0.027
Opaque vertical enclosure	U	$[\text{W}\cdot\text{m}^{-2}\cdot\text{K}^{-1}]$	0.091
	Stot	$[\text{m}]$	0.66
	Sins	$[\text{m}]$	0.24
	λ_{ins}	$[\text{W}\cdot\text{m}^{-1}\cdot\text{K}^{-1}]$	0.036
Transparent vertical enclosure	U_w	$[\text{W}\cdot\text{m}^{-2}\cdot\text{K}^{-1}]$	0.69
	$g_{\text{gl,n}}$	$[-]$	0.60

Table 2 – Main construction data of the case study

2.3 Energy performance of the building in summer

The methodology of thermal analysis was applied to the analysed building to determine the net energy need for cooling and the contributions to the heat balance on internal air split by the different driving forces. In this way, it is possible to identify the terms that have the greatest influence on the summer energy performance of the building and the causes of a low energy

performance. The analysis does not embrace the calculation of the delivered energy.

The building is located in northern Italy, near Bologna. The numerical simulations were carried out for the month of July considering the climatic data of Bologna, as the nearest city with available hourly climatic data ("G. De Giorgio" weather file). A conventional occupancy was considered in the simulations. Both the mean monthly value of the internal heat gains and the use profile (hourly values) were determined according to technical Standard EN ISO 13790, considering a conventional use. The internal heat gains of the building have a mean value of 2.4 W/m² and a maximum value of 8.2 W/m².

The ventilation of the indoor environment was set according to indoor air quality requirements. It was established that the indoor air quality was always guaranteed through hybrid ventilation. The minimum air flow rate was calculated applying technical Standard EN 15251, differentiating the occupied time from the unoccupied hours. In this way, it ensued a mean value of 0.34 h⁻¹ and a maximum value of 0.54 h⁻¹ of the air change rate.

The results of the application of the thermal analysis applied to the case study are shown in Fig. 3, concerning the monthly mean values of the contributions to the convective heat balance equation on the internal air, expressed in terms of mean heat flow rate normalised on the conditioned net floor area. The contributions to the energy balance are split according to the driving forces of the internal and external environment. These terms are identifiable in the graph of Fig. 3 with the same colour.

The sums of the terms characterized respectively by positive values and negative values are represented in the box at the top right of the graph (see Fig. 3). In the same box is the value of the mean monthly net cooling load (corresponding to an energy need of 2.94 kWh/m²) and the number of hours in July in which cooling is required (724 hours on a total amount of 744 hours).

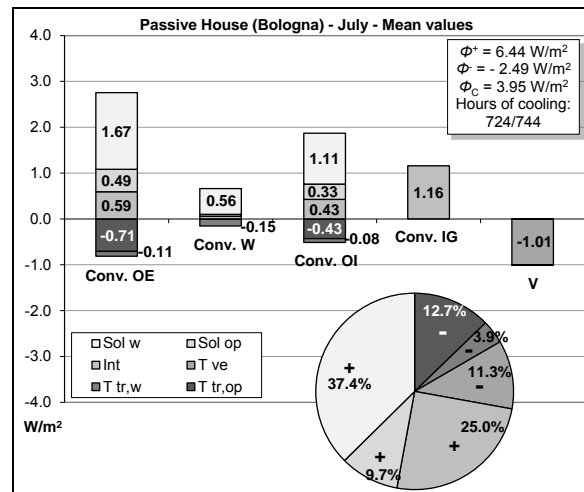


Fig. 3 – Mean monthly values of the convective heat balance contributions split by driving force and corresponding percentage weight of each driving force (July - Bologna)

From the analysis of Fig. 3, it can be pointed out that the main convective contributions to the cooling need are due to the solar radiation entering through the transparent envelope and the internal heat sources.

On the other hand, the outdoor air temperature gives a limited contribution. It induces a heat loss both by thermal transmission and by ventilation, because the outdoor temperature is lower than the indoor temperature on monthly average. For this reason, the effect of the outdoor temperature is characterised by a negative value, as shown in the pie chart of Fig. 3, in which the contributions to the heat balance are aggregated by driving force distinctly.

The standard deviations of the different contributions to the convective heat balance equation on the internal air are shown in Fig. 4. The standard deviation of the building's cooling load depends both on the internal heat capacity of the building structure and on the variability of the thermal driving forces. So this graph is a useful tool to identify critical situations and to adopt coherent solutions in order to improve the thermal performance of buildings under dynamic conditions. In particular, this representation allows to verify the effectiveness of a retrofit strategy finalized to reduce the variability of the thermal load and limit the load peaks through the increment of thermal inertia.

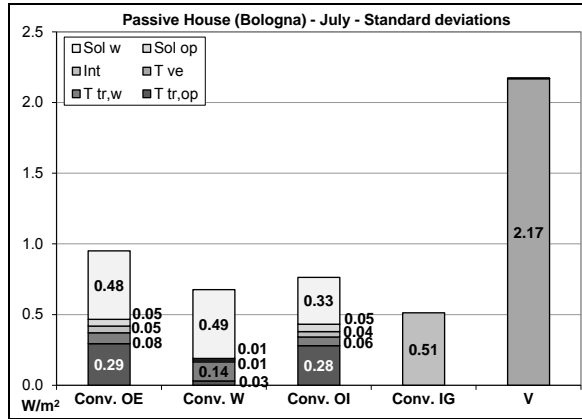


Fig. 4 – Mean standard deviation of the convective heat balance contributions split by driving force (July - Bologna)

Analysing the results of Fig. 4, the contributions characterised by the greatest deviation from the mean value refer to the internal heat sources and to ventilation. Another contribution with high standard deviation is the solar radiation entering through the transparent envelope. In order to reduce this last term, a design measure might consider the position of the window shading devices. The venetian blinds should be positioned outside and not in the cavity of the glass, as occurs in the case study.

The extremely limited deviation of the contribution of the heat transmission through the opaque envelope can be explained by the high heat capacity of the opaque building components together with their high insulation level.

2.4 Analysis under a different climatic context

In this section, the methodology of thermal analysis is applied to the same case study, but considering its collocation in the climatic context of Palermo, in southern Italy. The hourly weather file IWEC (*International Weather for Energy Calculations*) was applied in the numerical simulations.

The results are shown in Fig. 5, regarding the monthly mean values of the contributions to the convective heat balance equation on the internal air, and in Fig. 6, with regard to the mean standard deviations of the same contributions.

Comparing Fig. 3 and Fig. 5, the same building in Palermo shows higher mean monthly cooling loads than in Bologna (more than 27%). This is mainly due to the reduction of the heat transfer through

the building envelope and of the heat flow by ventilation (around 53%).

The negative value of the effect of the outdoor air temperature (see Fig. 5) depends on the fact that in both locations the mean monthly outdoor air temperature is lower than the indoor air temperature and that both the thermal transmission through the building envelope and the ventilation cause a reduction of the energy need. For this reason the high insulation level of the building components contributes to reduce the heat transfer by thermal transmission through the opaque envelope and to increase the cooling energy need.

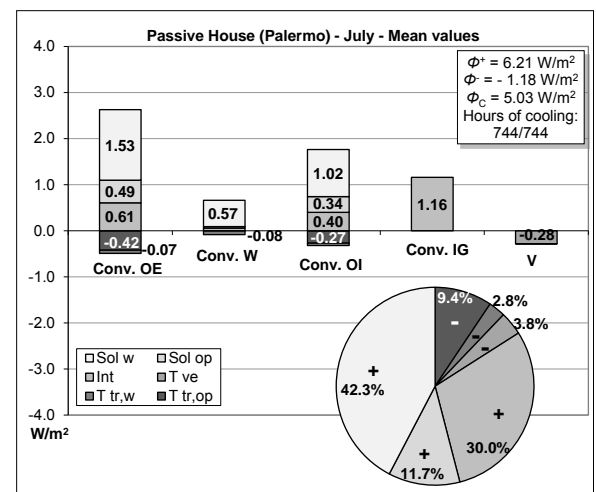


Fig. 5 – Mean monthly values of the convective heat balance contributions split by driving force and corresponding percentage weight of each driving force (July - Palermo)

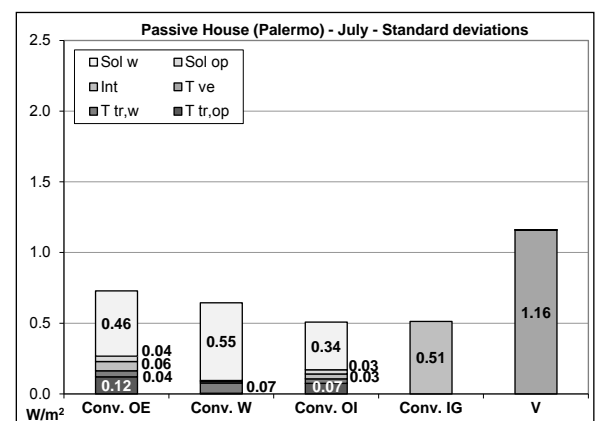


Fig. 6 – Mean standard deviation of the convective heat balance contributions split by driving force (July - Palermo)

Also the mean standard deviation of the ventilation contribution decreases for the building in Palermo compared to the same building in

Bologna, as shown in Fig. 6. This mainly depends on the limited variation of the external temperature in July in Palermo.

3. Strategies for improving energy performance

The results of the thermal analysis applied to the passive house show a satisfactory energy performance in summer. However, it is possible to identify some measures to further reduce the energy need for cooling, especially considering the location of the building in warmer climates (e.g. Palermo).

The choice of the best strategies should take into account the results of the thermal analysis and considering the contributions that mostly affect the energy need of the building in summer. However, it is chosen neither to modify the internal heat sources because they are fixed according to the building use, nor the technology of the building envelope, which is established by design choices.

As an exemplification, it is proposed to increment the air change rate fixed previously in the analysis to a value of 2 h^{-1} in the hours of July in which the outdoor air temperature is lower than the indoor air temperature (*free cooling*). This condition occurs in nearly all the days of July from about 10 p.m. to 9 a.m., in both locations. It is assumed that the fixed air change rate is always guaranteed, if necessary by means of fans. As the analysis only takes into account the net energy need for cooling, the electrical energy consumption of the fans is not considered in the study.

The thermal analysis is applied to the passive house both in Bologna and in Palermo, in order to evaluate the effects of the strategy. The results for Bologna are shown in Fig. 7 and in Fig. 8; for Palermo in Fig. 9 and in Fig. 10.

Compared to the original condition, the mean monthly thermal load of the building in Bologna decreases nearly 74% and the hours of cooling became 225, i.e. 30% of the total hours of July. The activation of the natural ventilation at night determines a decrement of the thermal load due to the increase of the negative contributions to the heat balance (Φ^-). The heat transfer by ventilation

increases, while the heat transfer by thermal transmission through the building envelope decreases slightly, as a result of the reduction of the indoor air temperature for the *free cooling* effect. The greatest deviation of the loads from the mean value occurs firstly in the ventilation contribution, and secondly in the heat flow transferred through the opaque envelope. The latter aspect is ascribable to the variability of the indoor-outdoor temperature difference linked to the high variability of the indoor temperature due to the increase of the natural ventilation.

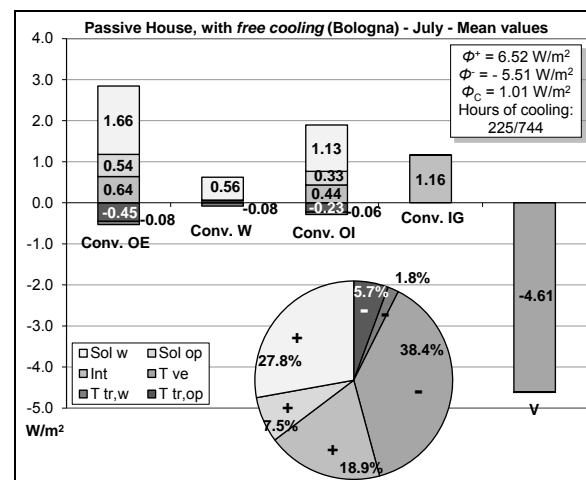


Fig. 7 – Mean monthly values of the convective heat balance contributions split by driving force and corresponding percentage weight of each driving force (case with free cooling, July – Bologna)

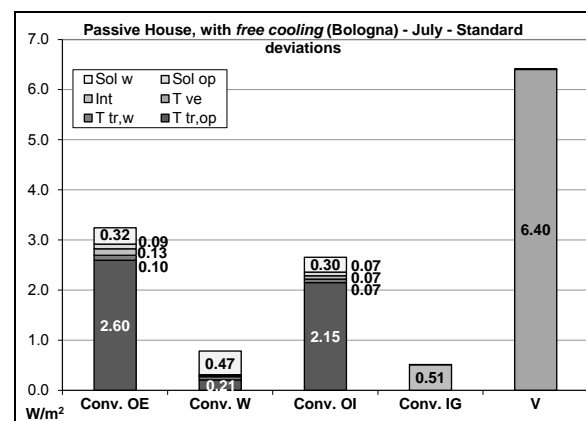


Fig. 8 – Mean standard deviation of the convective heat balance contributions split by driving force (case with free cooling, July – Bologna)

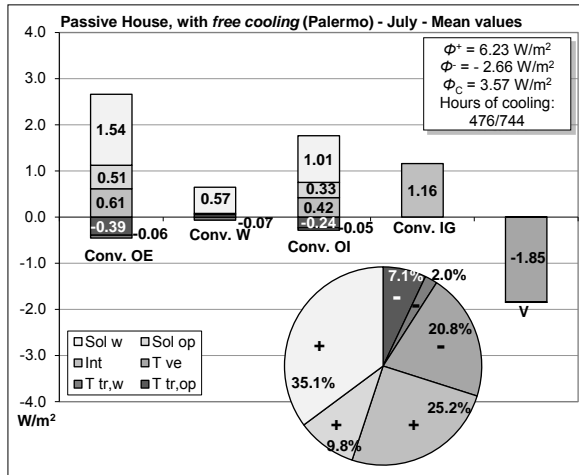


Fig. 9 – Mean monthly values of the convective heat balance contributions split by driving force and corresponding percentage weight of each driving force (case with free cooling, July – Palermo)

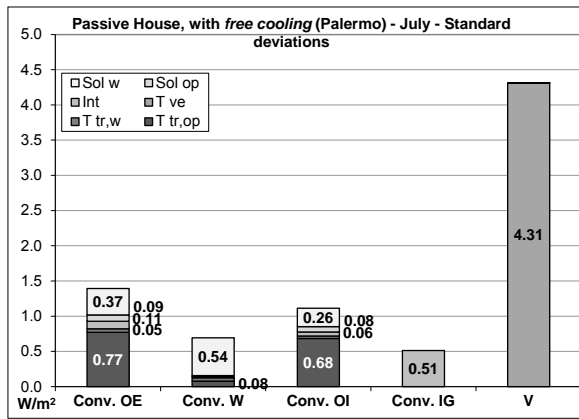


Fig. 10 – Mean standard deviation of the convective heat balance contributions split by driving force (case with free cooling, July – Palermo)

The increment of the air change rate causes an improvement of the summer energy performance of the case study in Palermo as well. However, the effect is less significant because the hourly values of the external temperature in Palermo are higher than in Bologna. In addition, they are characterized by a reduced variability (limited thermal excursion).

The building energy need for cooling in July decreases by 29% approximately, compared to the case without *free cooling*. The hours of cooling activation decrease by 36%, due to the increase of the convective heat flow by ventilation (561%), which is also characterised by the greatest standard deviation, compared to all the terms of the convective heat balance on internal air.

Considering thermal comfort implications, the

mean monthly values of the indoor air temperature and their standard deviations are, respectively, 24.3 °C and 1.5 °C for the building in Bologna, and 25.7 °C and 0.5 °C for the same building in Palermo.

The relation between the cooling need reduction due to *free cooling* and the positive cumulative indoor- outdoor hourly temperature difference in July is shown in Fig. 11.

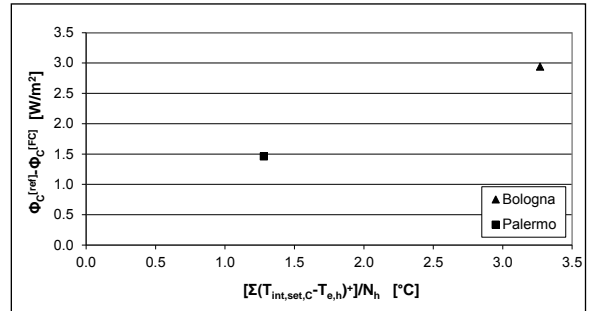


Fig. 11 – Cooling need reduction due to free cooling vs. positive cumulative indoor-outdoor hourly temperature difference (July)

4. Conclusion

The analysis presented in the paper is aimed at identifying and quantifying strategies for the optimisation of the energy performance of highly insulated buildings in summer conditions. A methodology of thermal analysis presented in a previous work (Ballarini *et al.*, 2011) has been applied to a *passive house* supposed to be located in two different Italian climatic zones (Bologna and Palermo).

The analysis was developed by means of a dynamic simulation tool (*EnergyPlus*) and the most important parameters affecting the energy performance of the case study in July were identified.

In order to reduce the mean monthly thermal load of the building, the effects of the application of a higher air change rate by natural ventilation were investigated through the same methodology.

The reduction of the net energy need for cooling (74% for the building in Bologna, 29% for the same building in Palermo) is linked to the increase of the convective heat flow by ventilation, as clearly shown in the graphical representation of the methodology of analysis. However, it is necessary

to point out that the effectiveness of the night ventilation is strongly linked to the specificity of the climate. For an effective *free cooling* strategy, the outside air temperature should be lower than the indoor air temperature, guaranteeing however a correct dimensioning of the air flow and avoiding draft risk.

The effectiveness of the use of *free cooling* was correlated to the thermal excursion of the outside air temperature in summer.

5. Nomenclature

Symbols

A	area (m ²)
g	total solar energy transmittance (-)
s	thickness (m)
T	temperature (°C)
U	thermal transmittance (W·m ⁻² ·K ⁻¹)
V	volume (m ³)
λ	thermal conductivity (W·m ⁻¹ ·K ⁻¹)
Φ	heat flow (W)

Subscripts/Superscripts

ia	internal air
C	cooling
conv	convection
e	external
env	envelope
f	floor
g	gross
gl	glass
h	hour
ins	insulation
int	internal
IG	internal gains
n	net, normal
OE	opaque external
OI	opaque internal
set	set-point (temperature)
tot	total
W,w	windows
V	ventilation

References

- AA. VV. 1989. Climatic Data “Giovanni De Giorgio”. Internal report. CNR Istituto di Fisica dell’Atmosfera, Milano, 1989.
- Al-Khawaja, M.J. 2004. Determination and selecting the optimum thickness of insulation for buildings in hot countries by accounting for solar radiation. *Applied Thermal Engineering* 24, 2601-2610.
- Al-Turki, A., Zaki, G.M. 1991. Cooling load response for building walls comprising heat storing and thermal insulating layers. *Energy Conversion and Management* 32, 235-247.
- Ballarini, I., Corrado, V. 2011. A new thermal analysis by numerical simulation to investigate the energy performance of buildings. *Proc. of Building Simulation 2011 Conference*, Sydney, Australia.
- Ballarini, I., Corrado, V. 2012. Analysis of the building energy balance to investigate the effect of thermal insulation in summer conditions. *Energy and Buildings* 52, 168-180.
- Bolattürk, A. 2008. Optimum insulation thicknesses for building walls with respect to cooling and heating degree hours in the warmest zone of Turkey. *Building and Environment* 43, 1055-1064.
- CEN 2007. Indoor Environmental Input Parameters for Design and Assessment of Energy Performance of Buildings Addressing Indoor Air Quality, Thermal Environment, Lighting and Acoustics. EN 15251:2007. European Committee for Standardization.
- CEN 2008. Energy Performance of Buildings – Calculation of Energy use for Space Heating and Cooling. EN ISO 13790:2008. European Committee for Standardization.
- European Union 2010. Directive 2010/31/EU of the European Parliament and of the Council of 19 May 2010 on the energy performance of buildings (recast). *Official Journal of the European Union*, 18 June 2010.
- Filippi, M., Fabrizio, E. 2011. Il concetto di Zero Energy Building. *Proc. of “Verso gli edifici ad energia quasi-zero: le tecnologie disponibili”*, AiCARR 2011 Conference, Bologna, Italy.

- Ghiaus, C., Allard, F. 2006. Potential for free-cooling by ventilation. *Solar Energy* 80, 402-413.
- Karlsson, F., Moshfegh, B. 2006. Energy demand and indoor climate in a low energy building – changed control strategies and boundary conditions. *Energy and Buildings* 38, 315-326.
- Mazzarella, L. 2011. Problematiche nell’ottimizzazione energetica degli edifici: possibili soluzioni e prospettive. Proc. of “Verso gli edifici ad energia quasi-zero: le tecnologie disponibili”, AiCARR 2011 Conference, Bologna, Italy.
- Mazzarella, L., Romagnoni, P. 2011. Annual based performance analysis of buildings thermal insulation. Proc. of “Energy refurbishment of existing buildings: which solutions for an integrated system, envelope, plant, control”, AiCARR 2011 Conference, Baveno, Italy.
- Pagliano, L., Carlucci, S., Toppi, T., Zangheri, P. 2007. The Passivhaus Standard in European warm climates: Design guidelines for comfortable low energy homes. Part 2. National proposals in detail: Italy, “Passive-on Project” [<http://www.passive-on.org/en/cd.php>].

Energy performance characterisation of vented opaque envelope through simplified methodologies

Vincenzo Corrado – Politecnico of Torino, Italy

Alice Gorrino – Politecnico of Torino, Italy

Simona Paduos – Politecnico of Torino, Italy

Abstract

Opaque vented façades are innovative and widely-used technological systems adopted both in new constructions and in building renovations. According to European Directive 2010/31/EU (EPBD recast) on the energy performance of buildings, each Member State should give priority to passive cooling techniques in order to enhance building performance during the summer period. For this purpose opaque vented envelope could be an appropriate technological solution to reduce the summer peak loads and the energy consumption. Although the EPBD recast has submitted the development of calculation methods for the energy performance evaluation to the European Committee of Standardisation (CEN), there is a lack in European Standards on the calculation of non-conventional building envelope performance, including vented façades.

The object of the present work is the thermal performance characterization of vented vertical opaque enclosures in real conditions of use, through simplified parameters.

Starting from EN ISO 6946 and EN ISO 13786, new equivalent thermal parameters are defined, such as the equivalent steady state thermal transmittance, the equivalent periodical thermal transmittance and the time shift.

Equivalent parameters are obtained by evaluating surface inside face conduction in the opaque components, under stabilized periodic external conditions, for the summer design day. An equivalent outside temperature is used, which considers both the convective and the radiative thermal exchanges (solar and infrared waves), for different boundary conditions (orientation). The tool used for calculations is based on the conduction transfer function – CTF – method, as implemented in the thermal dynamic simulation program *Energy Plus*.

Through a sensitivity analysis, different opaque

enclosures are analyzed, varying the design parameters such as the thickness, the height and the length of the vented cavity.

1. Introduction

Opaque vented façades are largely used both for existing buildings' renovations and for new buildings to improve the thermal performance of the envelope and the architectural design quality of the external skin.

An opaque vented façade is a double skin façade made up of two opaque building elements separated by an air gap. The outer component (baffle) is generally a thin layer attached to the load bearing wall by specific mechanical systems. The inner component is the wall itself, traditionally composed of a massive layer (brick, concrete etc.) coated by a thermal insulation layer. Through the gap a natural air flow is created through specific openings by means of the combined effect of the wind forces and the stack effect.

In summer period the advantages of an opaque vented façade are related to the reduction of the thermal load due to direct solar radiation by means of the shading effect of the baffle and of the natural convection inside the air gap.

In order to calculate the opaque vented wall performance, several works focus on CFD analysis (Sanjuan et al. 2011, Patania et al. 2010) while others apply a zonal approach (Marinosci et al. 2011, Chan et al. 2009) which is simpler than the CFD approach but quite precise. Both the numerical models are validated through experimental data (Peci López et al. 2012, Giocola et al. 2012, Sanjuan et al. 2011).

The detailed evaluation of the vented façade thermal performance is quite complex and requires a complete thermofluid-dynamic analysis of the vented air gap, an accurate knowledge of heat transfer coefficients and the knowledge of each input parameter affecting the results. On the other hand simple calculation methods can be applied.

Despite the growing interest in this technological solution and the correlated scientific research based on detailed calculation methods, only a few studies (Balocco 2002, Ciampi et al. 2003) refer to simplified methods, which enable the estimation of the vented façade performances in an easy but rigorous way.

In this paper a simplified calculation method is presented in order to provide equivalent dynamic thermal parameters (periodic thermal transmittance, time shift) for different vented façade configurations.

The use of these thermal parameters can be a useful simple tool for designers and industries to evaluate the performance of this technology.

2. Case study

In order to evaluate the thermal performance of the opaque vented solution, a test-room has been considered (Figure 1).

The test room is surrounded by opaque adiabatic components except for the analyzed vented façade. No window has been considered.

The layers constituting the adiabatic components have been chosen according to EN ISO 13791 while their thermophysical properties have been adopted according to UNI 10351.

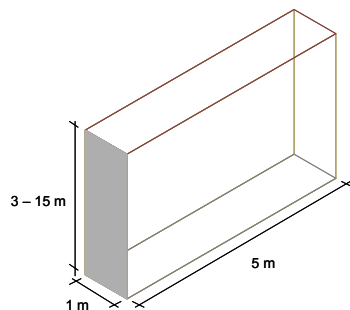


Fig. 1 – 3D model of the test-room analyzed. In grey colour the vented façade

Layers			s	ρ	c	λ
(ext-int)			c m	kg/ m ³	J/(kg K)	W/(m K)
INTERNAL WALL	I	Gypsum plasterboard	1,2	900	880	0,21
	II	Thermal insulation	10	30	840	0,04
	II I	Gypsum plasterboard	1,2	900	880	0,21
FLOOR	I	Waterproofing	0,4	1500	1500	0,23
	II	Concrete	6	2000	880	1,40
	II I	Thermal insulation	4	50	840	0,04
	I V	Concrete	18	2400	880	2,10
	V	Thermal insulation	10	50	840	0,04
	V I	Acoustic underlay	2	400	880	0,06
ROOF	I	Waterproofing	0,4	1500	1300	0,23
	II	Thermal insulation	8	50	840	0,04
	II I	Concrete	20	2400	880	2,10

Table 1 – Thermo physical characteristics of adiabatic components

For each simulation, the thermophysical properties (thermal conductivity, thickness, density and specific heat) of the external vented massive layer as well as the case study height (3 and 15 m respectively) have been changed, while the adiabatic components have been set as constant. See Table 1.

Moreover the test-cell has been considered South, North, East and West oriented in order to evaluate the influence of the orientation on the energy performance of the vented façade, while the indoor air temperature is maintained constant at 26 °C.

2.1 Naturally vented wall

The analysed wall is a naturally vented wall. It is composed of a massive layer (dotted in Figure 2), a

thermal insulation layer, a naturally vented cavity and a baffle.

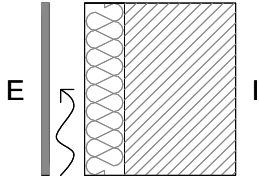


Fig. 2 – Vented façade layers.

In order to evaluate the influence of the main thermophysical properties of the massive layer on the dynamic thermal parameters of the vented wall, a sensitivity analysis has been carried out varying the thermal conductivity (λ), the thickness (s), the density (ρ) and the specific heat (c).

The four parameters have been varied simultaneously within specific range values according to a random analysis as implemented in *SimLab 2.2*. A hundred solutions have been chosen. Table 2 shows the maximum and minimum values of the thermal parameters range.

		Min	Max
s	[m]	0,10	0,50
λ	[W/(m K)]	0,15	2,00
ρ	[kg/m ³]	400	2400
c	[J/(kg K)]	840	2700

Table 2 – Minimum and maximum values of thermo-physical characteristic of the massive layer

Surfaces properties influencing convective and radiative heat transfer have been chosen as constant values.

Concerning the thermal insulation layer, fixed thermophysical properties have been chosen: $\lambda = 0,04$ W/(m K); $\rho = 30$ kg/m³; $c = 840$ J/(kg K) with a constant thickness of 0,08 m.

The thermal transmittance of the wall is calculated according to EN ISO 6946 for each configuration and varies from 0,22 to 0,43 W/(m²K).

It is important to point out that the thermophysical properties of the massive layer have been chosen to consider most of the existing building material (wood, concrete, brick etc.). Moreover, the range of variation of vented façade thermal transmittance as well as the range of its dynamic thermal properties

have been chosen with respect to the national current limit values.

In order to evaluate the influence of the geometrical characteristic of the air cavity on the vented façade performance, three thicknesses of the air gap have been considered: 5 – 10 – 15 cm. The ventilation openings at the top and at the bottom of the wall are considered to be of the same length and depth of the baffle and of the air cavity respectively.

3. Calculation methods

The *EnergyPlus* dynamic simulation tool has been used to calculate the conductive heat flux through the inner surface of the vented wall by means of the conduction transfer function calculation method.

3.1 Exterior naturally vented cavity

The opaque vented envelope is a traditional opaque wall whose outer layer consists of a thin and only resistive coat (baffle) separated from the load bearing wall by a vented air cavity.

As the baffle is sufficiently thin and highly conductive, it is possible to consider a single temperature for both sides and along its area. Moreover, the baffle is opaque to shortwave and longwave radiation and it completely covers the underlying layers avoiding solar energy to reach the underlying layers. The baffle is a continuous surface: the natural ventilation of the gap only depends on the openings at the top and at the bottom of the cavity.

The baffle temperature is calculated through the heat balance equation in the baffle surface's control volume (see Figure 3) as in equation

$$\theta_{s,baff} = \frac{(I\alpha + h_{cv}\theta_{ae} + h_{t,air}\theta_{ae} + h_{t,sk}\theta_{sk} + h_{t,gr}\theta_{gr} + h_{t,cav}\theta_{se} + h_{cv,cav}\theta_{cav})}{(h_{cv} + h_{t,air} + h_{t,sk} + h_{t,gr} + h_{t,cav} + h_{cv,cav})} \quad (1)$$

where I is the solar irradiance reaching the outer side of the baffle; $h_{cv}\theta_{ae}$ and $h_{cv,cav}\theta_{cav}$ are the convective heat exchanges of the baffle with the external environment and the air cavity respectively; $h_{t,air}\theta_{air}$, $h_{t,sk}\theta_{sk}$, $h_{t,gr}\theta_{gr}$, $h_{t,cav}\theta_{se}$ are the radiative heat exchanges between the baffle and

the external air, the sky, the ground and the underlying component surface respectively.

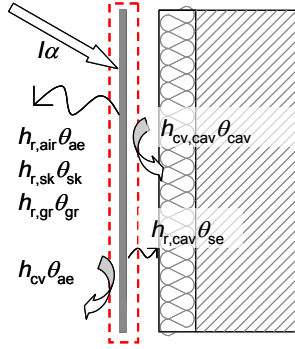


Fig. 3 – Baffle surface heat balance scheme

The volume of air located between the baffle and the underlying wall components is the cavity. It is possible to calculate a uniform air temperature of the air cavity through the heat balance equation (2) (see Figure 4).

$$\theta_{cav} = \frac{Ah_{cv,cav}\theta_{se} + Ah_{cv,cav}\theta_{s,baff} + \dot{m}c\theta_{ae}}{(Ah_{cv,cav} + Ah_{cv,cav} + \dot{m}c)} \quad (2)$$

where A is the surface surrounding the cavity involved in convective heat exchange. The heat balance equation takes into account the baffle ($Ah_{cv,cav}\theta_{s,baffle}$) and the outer surface of the massive wall ($Ah_{cv,cav}\theta_{se}$) convective heat exchange within the cavity, as well as the heat exchange due to the air mass flow from natural forces ($\dot{m}c\theta_{ae}$).

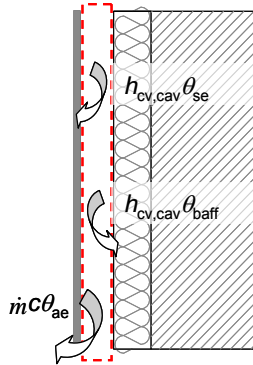


Fig. 4 – Cavity air heat balance scheme

In order to take into account natural ventilation air exchanges, the ASHRAE HOF (2009) model has been considered.

According to this model, the air mass flow from natural forces is calculated through equation

$$\dot{m} = \rho \dot{V}_{tot} \quad (3)$$

where ρ is the density of the air and \dot{V}_{tot} is the total

volumetric flow rate of air ventilating in and out of the cavity due to natural buoyancy and wind forces:

$$\dot{V}_{tot} = \dot{V}_{wind} + \dot{V}_{thermal} \quad (4)$$

Wind forces are calculated as:

$$\dot{V}_{wind} = C_v A_{in} w \quad (5)$$

where C_v is the effectiveness of the openings that depends on opening geometry and opening orientation respect to the wind direction; A_{in} is the half of the total area of the openings; w is the local wind speed.

A typical range of C_v values is 0,25 – 0,35 for diagonal wind and 0,5 – 0,6 for perpendicular wind.

Natural buoyancy phenomena are taken into account according to equation (6) or (7).

$$\dot{V}_{thermal} = C_D A_{in} \sqrt{2g\Delta H_{NPL}(\theta_{cav} - \theta_{ae})/\theta_{cav}} \quad (6)$$

if $\theta_{cav} > \theta_{ae}$

$$\dot{V}_{thermal} = C_D A_{in} \sqrt{2g\Delta H_{NPL}(\theta_{ae} - \theta_{cav})/\theta_{ae}} \quad (7)$$

if $\theta_{ae} > \theta_{cav}$ and baffle is vertical.

where C_D is the discharge coefficient for the opening and it depends on opening geometry; g is the gravitational constant; ΔH_{NPL} is the height from the midpoint of the lower opening to the Neutral Pressure Level and is equal to $1/4$ of the height of the component (in case of vertical component) or $1/4 \sin\beta$ where β is the component tilt.

ASHRAE HOF provides a typical range of C_D values varying from 0 to 1,5 and a fixed value (0,65) for unidirectional air flow rate.

In order to investigate the influence of the vented opaque component design on its dynamic thermal performance, different geometrical characteristics of the air gap have been considered: three thicknesses of vented cavity (0,05 – 0,10 – 0,15 m) and two heights of the wall (3 – 15 m) as described in previous section.

In Table 3 the input parameters considered for the simulations are shown.

Input data	Values		
Height of the wall (m)	3	15	
Thermal emissivity of exterior baffle material ε [-]	0,9		
Solar absorptivity of exterior baffle α [-]	0,6		
Height scale for buoyancy – driven ventilation ΔH_{NPL} [-]	0,75	3,75	
Effective thickness of cavity behind exterior baffle [m]	0,05	0,10	0,15
Roughness of exterior surface	Smooth		
C_V [-]	0,25		
C_D [-]	0,65		

Table 3 – Input parameters considered for the simulations

3.2 Equivalent dynamic thermal parameters

EN ISO 13786 has been considered. This technical standard is based on the admittance method introduced by N.O. Milbank and J. Harrington-Lynn (1974), and supplies a simplified calculation model that considers 24 h sinusoidal boundary conditions.

The main simplification of the model is due to the use of a sinusoidal trend of external temperature varying cyclically around a mean value (Baratieri et al. 2009).

In order to represent in a more realistic way the boundary conditions influencing the heat flow through a wall, an equivalent external temperature has been considered ($\theta_{e,eq}$) as in equation.

$$\theta_{e,eq} = \theta_{ae} + \frac{I\alpha + h_{r,gr}(\theta_{gr} - \theta_{ae}) + h_{r,sk}(\theta_{sk} - \theta_{ae})}{h_e} \quad (8)$$

The use of an equivalent external temperature allows us to take into account as driven forces not only the external temperature θ_{ae} , but also the effects of the solar radiation $I\alpha$, the radiative heat exchange between the component and the ground $h_{r,gr}(\theta_{gr} - \theta_{ae})$ and between the component and the sky $h_{r,sk}(\theta_{sk} - \theta_{ae})$.

h_e is the outdoor surface heat transfer coefficient, that includes the convection coefficient h_{cv} and the radiative ones, between the component and the air $h_{r,air}$, the ground $h_{r,gr}$ and the sky $h_{r,sk}$ respectively

$$h_e = h_{cv} + h_{r,air} + h_{r,gr} + h_{r,sk} \quad (9)$$

In order to calculate the equivalent dynamic thermal properties of a naturally vented wall, a

summer design day has been considered for the city of Turin.

In Table 4 the geographical data of the location and the climatic data of the summer design day are shown.

PLACE	Location	Turin
	Longitude	45,08 [°]
	Latitude	7,68 [°]
	Altitude	239 [m]
SUMMER DESIGN DAY	$\theta_{db,max}$	30,7 [°C]
	$\Delta\theta_{ae}$	11 [°C]
	$I_{m,North}$	79,8 [W/m ²]
	$I_{m,South}$	150,0 [W/m ²]
	$I_{m,East}$	177,3 [W/m ²]
	$I_{m,West}$	211,5 [W/m ²]
	Wind speed	0,8 [m/s]

Table 4 – Geographical data and climatic data of summer design day for Turin

In the summer design day of Turin, the equivalent external temperature varies according to exposure as shown in Figure 5.

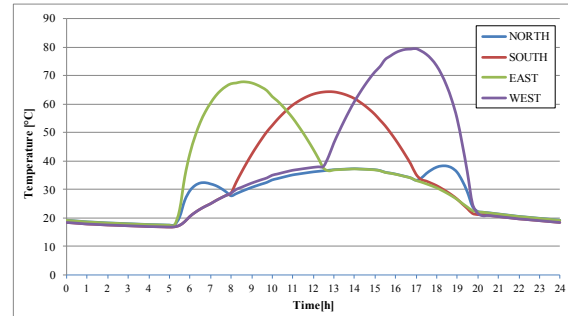


Fig. 5 – Profiles of external equivalent temperature on summer design day for different exposures.

The equivalent dynamic thermal properties taken into account are periodic thermal transmittance Y_{ie} and the time shift φ .

According to the definition in EN ISO 13786, the equivalent periodic thermal transmittance has been defined as the ratio between the daily maximum $\Phi_{cd,si,max}^{dyn}$ and minimum $\Phi_{cd,si,min}^{dyn}$ opaque inner surface heat flux difference, and the outdoor detailed equivalent temperature maximum $\theta_{e,eq,max}$ and minimum $\theta_{e,eq,min}$ difference (Corrado and Paduos, 2009).

$$Y_{ie} = \frac{(\Phi_{cd,max} - \Phi_{cd,min})_{si}^{dyn,CTF}}{(\theta_{e,eq,max} - \theta_{e,eq,min})} \quad (10)$$

The conductive heat flux has been calculated through the *EnergyPlus* dynamic model using the conduction transfer function calculation heat balance algorithm.

The equivalent time shift is defined as the delay between the daily maximum conductive heat flux value on the inner surface $\Phi_{cd,si,max}^{dyn}$ and its correspondent heat flux maximum value not considering components thermal inertia $\Phi_{cd,si,max}^{st}$, corresponding to the maximum of the external equivalent temperature.

Time shift has been calculate as in equation (11)

$$\begin{cases} t_{\phi_{cd,si,max}}^{dyn} > t_{\phi_{cd,si,max}}^{st} \Rightarrow t_{\phi_{cd,si,max}}^{dyn} - t_{\phi_{cd,si,max}}^{st} \\ t_{\phi_{cd,si,max}}^{dyn} \leq t_{\phi_{cd,si,max}}^{st} \Rightarrow t_{\phi_{cd,si,max}}^{dyn} - t_{\phi_{cd,si,max}}^{st} + 24 \end{cases} \quad (11)$$

where $t_{\phi_{cd,si,max}}^{dyn}$ is the hour of the design day in which the maximum conductive heat flux occurs; $t_{\phi_{cd,si,max}}^{st}$ is the time of the design day at which the maximum conductive heat flux occurs through the same wall neglecting its thermal inertia, that is the time of the maximum external equivalent temperature.

The equivalent time shift would be the same as the EN ISO 13786 time shift only if the external equivalent temperature profile were a sine curve with a period of 24 hours.

In order to obtain the equivalent time shift, the conductive heat flux has been calculated through the *EnergyPlus* dynamic simulation tool twice: the first time the thermal inertia of opaque components has been considered while the second time it has been neglected.

In Figure 6 the difference between the conductive heat flux profile is shown by considering (_MASS) or not (_NO MASS) the thermal inertia of the wall, for a light solution corresponding to the lowest ζ value.

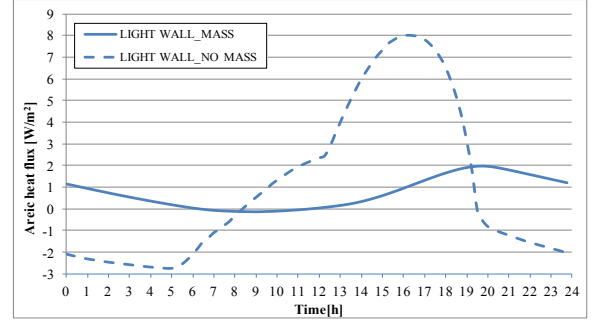


Fig. 6 – Conductive heat flux trend: comparison between light and heavy walls.

4. Results

4.1 Dynamic thermal parameters

The dynamic equivalent thermal parameters are represented versus ζ . EN ISO 13786 introduces ζ as the parameter representing the ratio between the thickness of the considered layer and its penetration depth δ . The penetration depth is a function of the thermal diffusivity a related to the considered time period T :

$$\zeta = \frac{d}{\delta} = \frac{d}{\sqrt{a \frac{T}{\pi}}} = \frac{d}{\sqrt{\frac{\lambda \cdot T}{\rho \cdot c \cdot \pi}}} \quad (12)$$

Applying equation (12) to the massive layer of the opaque envelope technical solutions derived from the random analysis, the corresponding ζ values lies within the range 0,64 to 10,49. Higher ζ values correspond to higher thermal inertia of the technical solutions.

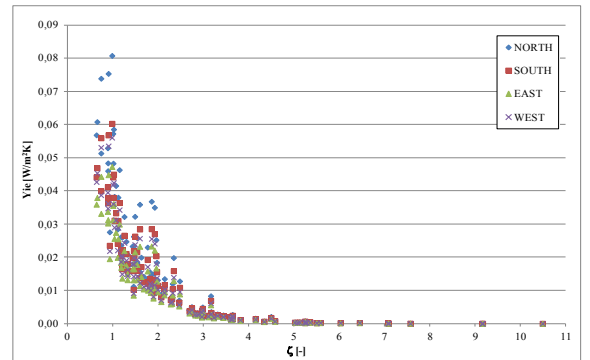


Fig. 7 – Equivalent periodic thermal transmittance versus ζ for different exposures (one storey wall with 0.05m vented cavity)

The results show the periodic thermal transmittance exponentially decreases for increasing values of ζ . The light solutions give the

highest Y_{ie} values, for heavy solutions Y_{ie} tends to zero; the dynamic thermal performance could be generally considered very good independently from ζ (values lower than $0,08 \text{ W}/(\text{m}^2\text{K})$).

By increasing the thickness of the vented cavity from 0.05 m to 0.15 m , both the one storey and the five storey wall do not get significant deviations from the results shown in Figure 7.

The influence of the exposure on the periodic thermal transmittance is noticeable for low values of ζ . By considering the same solution ($\zeta = 0,9$) for different exposures, the north side gives the highest Y_{ie} value (around $0,08 \text{ W}/(\text{m}^2\text{K})$) while the east side the lowest one (around $0,04 \text{ W}/(\text{m}^2\text{K})$).

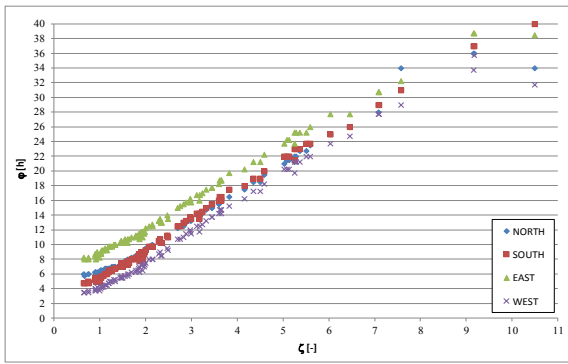


Fig. 8 – Time lag versus ζ for different exposures (one storey wall with 0.05m vented cavity).

The analysis shows that time shift is an increasing function of ζ and the trend is linear: heavy solutions obtain highest ϕ values, for light solutions ϕ tends to zero; for values of ζ higher than $5,5$, the time shift exceeds 24 hours.

As for the periodic thermal transmittance, by increasing the thickness of the vented cavity from 0.05 m to 0.15 m , both the one storey and the five storey wall do not show significant deviations from the results shown in Figure 8.

Despite the periodic thermal transmittance, the exposure influence on the time shift is noticeable both for heavy and light solutions: for increasing ζ the time shift deviation among exposures is maintained constant. North and south exposures obtains similar results; east side obtains the highest values of time shift because of the external equivalent temperature trend: despite from its high value, the peak is relevant during the early hours of the morning, when the wall is discharged because of the night thermal exchange; exactly the

opposite reasoning could be argued for the west exposure.

From what has been observed, it is possible to conclude that ventilation reduces the conductive heat flux entering the opaque component.

4.2 Equivalent thermal transmittance

Rather than in terms of periodic thermal transmittance, the variation of the conductive heat flux can be better performed introducing a parameter defined as the "equivalent thermal transmittance" U_{eq} representing the ratio between the summer design day conductive heat flux mean value and the average temperatures difference between the internal and external environments in the same design day:

$$U_{eq} = \frac{\overline{\Phi}_{cd,si}}{\overline{\theta}_{e,eq} - \theta_{ai}} \quad (13)$$

Therefore, the equivalent thermal transmittance considers the effect of the vented cavity on the stationary conductive heat flux : as being evaluated in daily average conditions, U_{eq} is not influenced by the thermal inertia of the component.

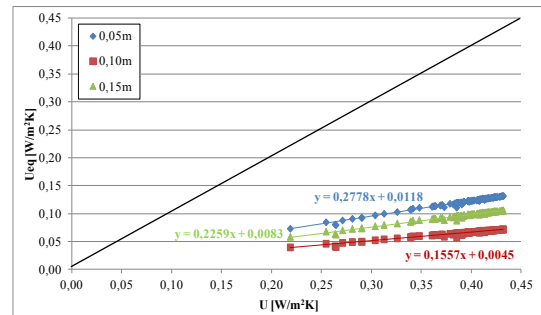


Fig. 9 – Equivalent versus theoretical thermal transmittance for West oriented 5 storey opaque vented wall, and different cavity thickness

Figure 9 shows the relation between the thermal transmittance U evaluated in steady state conditions – according to EN ISO 6946 – and the equivalent thermal transmittance U_{eq} defined in dynamic conditions. The introduction of a vented cavity deeply reduce the conductive heat flux and consequently U_{eq} .

Increasing the thermal conductance, the ratio between the steady state and the equivalent thermal transmittance shows a rising linear function and the deviation depends on the

thickness of the vented cavity: by considering medium resistive solutions, for each exposition the 0.05 m cavity reduces the thermal transmittance of about 3.5 times, the 0.10 m cavity 6.5 times and the 0.15 m cavity around 4.5 times.

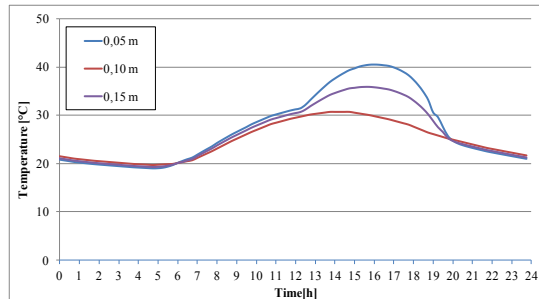


Fig. 10 – Summer design day trends of the cavity temperature for a West oriented 5 storey wall, for 0.05 m, 0.10 m and 0.15 m thickness of the cavity

Solutions characterized by 0.15 m thickness of the vented cavity present U_{eq} values higher than the 0, 10 m ones; Figure 10 shows results depending on the temperatures within the vented cavity: increasing the cavity thickness from 0.10 m to 0.15 m the conductive heat flux referred to solutions with the same resistive and massive thermal characteristics increases too, because of the cavity overheating. That means the vented cavity of 0.10 m thickness shows better thermal performances. The same considerations could be made for each orientation, cavity thickness and number of storey considered.

5. Conclusion

The present work introduces a methodology to evaluate the thermal performances of opaque vented solutions. A case study has been evaluated for different heights of the component, vented cavity thickness and exposures. The thermal performance has been evaluated in dynamic conditions, referring to the Turin summer design day. Equivalent thermal parameters have been then calculated for the case study, like periodic thermal transmittance, time shift and thermal transmittance.

The results show the equivalent periodic thermal transmittance is a decreasing exponential function of ζ , that represents the ratio of the thickness of the

massive layer to the penetration depth. For really massive solutions Y_{ie} tends to zero. The vented cavity thickness and the boundary conditions only influence light solutions, but deviations are not significant.

The results also show the time shift is an increasing linear function of ζ ; for really massive solutions φ exceed the 24 hours. The time shift does not seem to be significantly influenced by the thickness of the cavity or the height of the panel. Indeed, the same technical solutions with different exposures show deviations that remain constant with increasing ζ values and depend on the joint between the thermal inertia of the component and the daily trend of the equivalent external temperature.

The introduction of a vented cavity deeply influences the conductive heat flux; the parameter that better represents the phenomenon is the equivalent thermal transmittance.

The proposed methodology could be a valid tool for industries and designers to easily perform opaque vented innovative technologies for different boundary conditions.

6. Nomenclature

Symbols

a	thermal diffusivity (m^2/s)
A	surface (m^2)
c	specific heat ($\text{J}/(\text{kg K})$)
g	gravitational constant ($= 9,81 \text{ m/s}^2$)
h	surface heat transfer coefficient ($\text{W}/(\text{m}^2\text{K})$)
I	solar irradiance (W/m^2)
\dot{m}	air mass flow (kg/s)
R	thermal resistance ($(\text{m}^2\text{K})/\text{W}$)
s	thickness (m)
U	thermal transmittance ($\text{W}/(\text{m}^2\text{K})$)
\dot{V}	volumetric flow rate (m^3/s)
Y_{ie}	periodic thermal transmittance ($\text{W}/(\text{m}^2\text{K})$)
α	solar absorptivity (-)
δ	periodic penetration depth of a heat wave in a material (m)
Φ	heat flux (W)
φ	time shift (h)
λ	thermal conductivity ($\text{W}/(\text{m K})$)

θ	temperature (°C)
ρ	density (kg/m ³)
ζ	ratio of the thickness of the layer to the penetration depth

Subscripts/Superscripts

ae	external air
ai	internal air
baff	baffle
cav	cavity
cd	conduction
cv	convection
dyn	dynamic
e	external
eq	equivalent
gr	ground
i	internal
in	inlet
max	maximum
min	minimum
r	radiative
s	surface
sk	sky

References

- ASHRAE. 2009. Ventilation and Infiltration, ASHRAE Handbook – Fundamentals, Chapter 27, American Society of Heating, Refrigerating, and Air-Conditioning Engineers, Inc. Atlanta.
- C. Balocco. 2002. A simple model to study vented façades energy performance, *Energy and Buildings* 34, pp. 469-475.
- M. Baratieri, A. Prada, P. Baggio, A. Gasparella. 2009. Comportamento dinamico dell'involucro edilizio: previsioni teoriche e analisi sperimentale. Atti del 64° Congresso Nazionale ATI. L'Aquila, Italia.
- V. Corrado, S. Paduos. 2009. Building envelope analysis in summer: dynamic thermal parameters and calculation methods. *Proceedings of the 4th International Building Physics Conference*. Istanbul. pag. 151-158.
- A.L.S. Chan, T.T. Chow, K.F. Fong, Z. Lin. 2009. Investigation on energy performance of double skin façade in Hong Kong, *Energy and Building* 41, pp. 1135-1142.
- CEN. 2007. EN ISO 6946:2007, Building components and building elements - Thermal resistance and thermal transmittance - Calculation method. European Committee for Standardization.
- CEN. 2007. EN ISO 13786:2007, Thermal performance of building components - Dynamic thermal characteristics - Calculation methods. European Committee for Standardization.
- CEN. 2012. EN ISO 13791:2012, Thermal performance of buildings - Calculation of internal temperatures of a room in summer without mechanical cooling - General criteria and validation procedures. European Committee for Standardization.
- M. Ciampi, F. Leccese, G. Tuoni. 2003. Vented façades energy performance in summer cooling of buildings, *Solar Energy* 75, pp. 491-502.
- European Parliament and Council of 19 May 2010, 2010, Directive 2010/31/EU on the energy performance of buildings (recast).
- E. Giocola, C. Sanjuan, E Blanco, M.R. Heras. 2012. Experimental assessment and modelling of the performance of an open joint vented façade during actual operating conditions in Mediterranean climate, *Energy and Buildings* 54, pp. 363-375.
- European Commission JRC. Sensitivity Analysis. SW SIMLAB. <http://simlab.jrc.ec.europa.eu/>
- Italian Government 2007. Legislative Decree no. 311 of December 29th 2006. Disposizioni correttive ed integrative al decreto legislativo 19 agosto 2005, n. 192, recante attuazione della direttiva 2002/91/CE, relativa al rendimento energetico nell'edilizia. Ordinary Supplement to the Italian Official Gazette no. 26 of February 1st 2007.
- C. Marinosci, P.A. Strachan, G. Semprini, G.L. Morini. 2011. Empirical validation and modelling of a naturally vented rainscreen façade, *Energy and Buildings* 43, pp. 853-863.
- N.O. Milbank, J. Harrington-Lynn J. 1974, Thermal response and admittance procedure, *Building Services Engineering* 42, pp. 38-51.
- F. Patania, A. Gagliano, F. Nocera, A. Ferlito, A. Galesi. 2010. Thermofluid-dynamic analysis of vented façades, *Energy and Buildings* 42, pp. 1148-1155.

- F. Peci López, R.L. Jensen, P. Heiselberg, M. Riuz da Adana Santiago. 2012. Experimental analysis and model validation of an opaque vented façade, *Building and Environment* 56, pp. 265-275.
- C. Sanjuan, M.J. Suárez, E. Blanco, M.R. Heras. 2011. Development and experimental validation of a simulation model for open joint vented façades, *Energy and Buildings* 43, pp. 3446-3456.
- C. Sanjuan, M.J. Suárez, M. González, J. Pistono, E. Blanco. 2011. Energy performance of an open-joint vented façade compared with a conventional sealed cavity façade, *Solar Energy* 85, pp. 1851-1863.
- UNI. 1994. UNI 10351:1994, Materiali da costruzione - Conduttività termica e permeabilità al vapore. Ente Nazionale italiano di Unificazione.
- United States Department of Energy, 2012, EnergyPlus, Version 7.2

Impact of using cool paints on energy demand and thermal comfort of a residential building

Diana Dias – Universidade do Porto, Portugal & CIN, Corporação Industrial do Norte, Maia, Portugal

João Machado – CIN, Corporação Industrial do Norte, Maia, Portugal

Vítor Leal – Universidade do Porto, Portugal

Adélio Mendes – Universidade do Porto, Portugal

Abstract

This work studies the role of using cool paints and/or thermal insulation on the thermal behaviour and energy demand of a residential building. Buildings with thermal characteristics representing both old and new constructions are considered; the results were obtained using the dynamic computer simulator ESP-r.

For a case-study building in Portugal, in the summer, it was found that an increase in roof and façade value of total solar reflectance from 50 % to 92 % reduces the maximum free-float indoor temperature between 2.0 °C and 3.0 °C in old construction (without thermal insulation), and between 1.2 °C and 2.2 °C in new construction (with thermal insulation). This has as a trade-off effect the decrease of the minimum indoor temperature of up to 1.5 °C. The results of annual energy demand for heating show a maximum penalization of about 30 % when using cool paints. However, it was demonstrated that the cooling demand almost disappears, thus eliminating the need to install air-conditioning devices.

The analysis of two specific hot periods of real summer weather data shows that the sun's altitude is critical on which solution originates the highest temperature reduction.

1. Introduction

Since the 90s, the frequency and intensity of heat waves have increased (IM-I.P., 2012) and weather events like these are expected to be more severe in the future (Meehl et al., 2004). These phenomena have a negative impact on human health, decreasing indoor-thermal comfort in buildings and thus increasing energy consumption.

The worldwide energy consumption, particularly to obtain indoor thermal comfort in buildings, has had a constant growth. In Europe, between 1990 and 2005, the absolute level of final household energy consumption rose by an average of 1.0 % per year and, in 2005, the residential sector accounted for 26.6 % of the final energy consumption (EEA, 2008). In Portugal, the fraction of energy for indoor thermal comfort already has a significant impact in global energy demand, approximately 22 % of the energy used in residential buildings (INE et al., 2011).

Until 2020, the European Union (EU) is committed to reduce energy use by 20 %, referred to 1990 (EPC, 2010). To achieve this goal, the EU has imposed that all Member States must implement measures to apply minimum energy performance requirements for buildings and ensure the certification of building energy performance (EPC, 2002). According to these guidelines, the Portuguese government decided to classify buildings according to their thermal efficiency (MEI, 2006, MOPTC, 2006, MOPTC, 2006).

One of the strategies that can be used to decrease energy consumption is coating not only the façades, but also the roofs of buildings with special coatings called cool paints. There are two ways in which cool paints may contribute to control the heat load of a building: reflect the incident solar radiation and release heat by thermal emittance, where the heated surface dissipates the heat absorbed by emitting infrared (IR) radiation.

The reflectance is normally characterized by the so-called TSR index (total solar reflectance). The value of TSR is obtained by analyzing the reflectance

over twenty specific wavelengths, which covers the solar spectrum (Lind et al., 1980).

The colour of a paint film depends on its visible reflectance spectrum. However, increasing the IR reflectance of coatings, which accounts for almost 52 % of the total solar radiation energy – see Figure 1, it is possible to make it to reflect more energy without interfering with the surface colour.

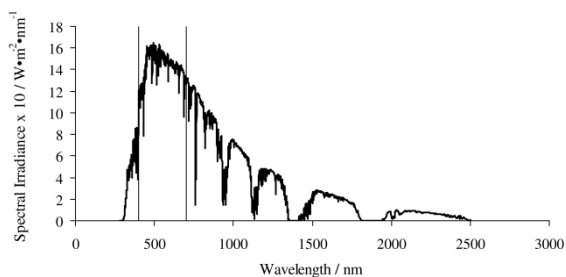


Fig. 1 – Terrestrial global spectrum, AM 1.5, 1000 W·m⁻² – based on ASTM G173-03 (ASTM, 2008)

The so-called cool pigments can dramatically contribute to the TSR increase of paints, increasing the reflectance of the IR radiation. Another approach to make a paint film reflect solar radiation energy is to make the paint transparent to the IR radiation and use it over a high reflective primer.

Most of organic paints show a very high emittance. Usual exterior paints show normal emittance in the range of 90 %. It means that a paint film when heated radiates in the IR spectrum 90 % of the energy that a black body would do. The emittance is mostly not disturbed by the surface aging or cleanness.

A large number of studies were performed focusing on cool pigments, their incorporation in paints, the impact and the simulation of their use and their behaviour regarding aging. In 1931, Paul Kubelka and Franz Munk published an article of great relevance in this area, where they derived a mathematical equation for the reflectance of an achromatic paint as a function of the reflectance of the substrate and the coating thickness (Kubelka et al., 1931). Later, in 1947, Kubelka determined the validation range of the Kubelka-Munk theory and developed new formulas more adapted for practical use (Kubelka, 1947).

More recently, a great deal of research in this area has been conducted by Lawrence Berkeley National Laboratory (LBNL). For example, in 1998

and also in 2003, Akbari et al. studied the impact of a cool roof real application on the energy savings and comfort performance in buildings, at different locations in the United States (three commercial buildings in California and two small non-residential buildings in Nevada) (Akbari et al., 1998, Akbari, 2003). Both articles show cooling energy savings and drop of temperature in the summer. In 2004 and 2005, researchers from the same laboratory identified, characterized and studied the application of pigments to roof products in order to determine the effects of climate and solar exposure on the reflectance and the variability in colour over time (Miller et al., 2004, Levinson et al., 2005, Levinson et al., 2005). These studies have allowed LBNL to create a pigment database, which has free access (LBNL, 2012). In addition, the same workgroup, in 2005, assessed the effect of soiling and cleaning (wiping, rinsing, washing and bleaching) on the value of reflectance of roof coating samples (Levinson et al., 2005). They concluded that wiping restores some of the initial reflectance, but rinsing and/or washing are more effective and bleaching does not greatly increase the solar reflectance of a washed roof. Later, in 2010, the same authors presented the results of solar reflectance evaluation of three-year weathering tests on asphalt shingles, located in Berkeley, California, and in Houston, Texas (Berdahl et al., 2012) and they observed that, after six months, changes in solar reflectance are small and reduce by as much as 0.06 at three years. They also described methods for creating solar-reflective surfaces, first in 2007, presenting how to create non-white surfaces and their application to a wide variety of residential roofing materials, including metal, clay tile, concrete tile, wood and asphalt shingle (Levinson et al., 2007) and, in 2010, creating a prototype with the demonstration of a new process for coating concrete tile and asphalt shingle roofing products that uses a two-layer spray coating (Levinson et al., 2010).

Other authors made similar studies, for example, Ichinose et al., in 2009, performed an interesting study about the paint performance over time with respect to surface contamination and degradation of reflectivity through environmental exposure tests (Ichinose et al., 2009). This study

demonstrates that panels coated with high-reflectivity paint can preserve thermal conditioning effects longer than the conventional coating panels. In 2011, Romeo and Zinzi also studied the impact of a cool roof application on the energy and comfort performance in an existing non-residential building located on the west coast of Sicily (Romeo et al., 2011). The effect of cool coatings in mitigating the thermal conditions was demonstrated and an average reduction of 2.3 °C of the operative temperature, during the cooling season, was observed. This study also registered a 54 % reduction of the cooling energy demand.

Moreover, studies of cool roof performance have been carried out by computer simulation. Building simulation serves not only to predict indoor thermal behaviour of buildings and their energy consumption (annual cooling and heating load), but also to make environmentally-friendly design options possible. For example, in 2005, Luxmoore et al. used a dynamic and detailed energy simulation tool, DEROB-LTH, to create recommendation actions and strategies to mitigate temperature increase in residential buildings in Queensland, Australia (Luxmoore et al., 2005). Authors concluded that the heat island impacts can be mitigated through the use of light coloured or high albedo surfaces (roofs, walls, roads and other paved areas). Also Wang et al., in 2008, used dynamic thermal simulation software, EDSL Tas, to assess a retail shed, located in six different locations around the world, and with external surfaces painted with reflective coatings (Wang et al., 2008). The authors prove that the use of solar reflective coatings is effective in reducing cooling loads and overall electricity consumption, in particular in hot climates.

In this work, the application of cool coatings on a building was assessed using an open source simulator, ESP-r (ESRU, 2012). ESP-r is an integrated energy modelling tool for the simulation of the thermal, visual and acoustic performance of buildings and evaluation of their energy use associated with environmental control systems.

This paper focuses mainly on assessing the impact of cool coatings on the thermal behaviour and on the energy demand of a residential building. The study was conducted in buildings with different

thermal comfort solutions and with cool coatings applied both on roof and façade surfaces. The results are especially relevant for addressing the thermal comfort during the renovation of old buildings since the introduction of insulation elements is normally significantly more expensive.

2. Simulation

In this work, a single villa was modelled on a yearly basis; it has two floors and a partially inhabited attic, as indicated in Figure 2. The ground floor has a living room (LR), a dining room (DR), a kitchen (KT), a toilet (TL), a hall (HL) and stairs (ST). The first floor consists of three bedrooms (BD), a suite (ST), a toilet, a bathroom (BR), a corridor (CR) and stairs. The attic has two parts that are inhabited, a playroom (PL) and stairs. Although all these zones were considered during the simulations, only some of them were used to obtain the average indoor temperature per floor. The zones considered are the living room, dining room and the kitchen on the ground floor, three bedrooms and the suite on the first floor and the playroom in the attic.

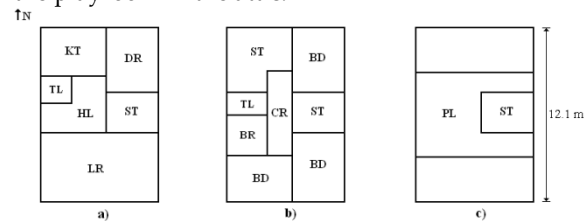


Figure 2 - Plant of the building: a) ground floor, b) first floor and c) attic

According to Portuguese law (MOPTC, 2006) a constant value of 0.6 air changes per hour was considered. The internal gains of the zones considered in the calculation of the indoor temperature were settled to 4 W·m⁻², following the recommendations of Portuguese law (MOPTC, 2006); for the remaining zones it was assumed to have 1 W·m⁻² of internal gains (except for the two inhabited zones of the attic that were assumed to have no internal gains).

The building has a total area of 26.3 m² of windows with clear glass. Taking into account the seasons, the existence of venetian blinds on windows was considered. These venetian blinds were considered

as an additional layer over the windows, without any control system. Between June and September, exterior shading layers cover 75 % of each window, while during the rest of the year it was assumed 50 % of coverage.

3. Discussion and result analysis

The thermal behaviour and energy demand of a residential building were assessed using the dynamic computer simulator ESP-r (ESRU, 2012). The results were obtained in two steps: first a free float simulation was performed to evaluate the indoor temperature over the year and the second one with an HVAC system to assess the annual energy demand of the building. Two old constructions types, without thermal insulation, were assessed: single wall façade and double wall façade. A building with modern construction was also assessed: single wall façade with thermal insulation. The next sections detail the simulation results of a building located in Porto, Portugal (41°9'N 8°37'W). The weather data of Porto was obtained from the website of the Energy Efficiency and Renewable Energy (EERE).

3.1 Building 1 – single wall

Building 1 (BD1) is a single wall building (building whose exterior walls have masonry composed by single dense layer – the brick layer), with no thermal insulation, neither on the façades (external walls) nor on the roof (roof slab). The construction details are presented in Table 1, where all layers that compose the construction are described, from the exterior to the interior. This table also shows the thickness of each layer and the overall heat transfer coefficient – U . The specifications of each layer (e.g. conductivity, density, specific heat, emissivity and absorption) follows (Santos et al., 2006).

In the base case, the façades were assumed to have 50 % of TSR and 0.90 of emissivity; the roof was assumed to have 40 % of TSR and 0.90 of emissivity (clay tile). Simulations of a full year were performed, but for the thermal behaviour analysis only two specific periods were selected, one typical

summer and winter week. According to the ESP-r Cookbook, typical weeks are determined taking into account, for each week of the year, the average and total heating and cooling degree days and solar radiation data. These values are compared with the seasonal values and the weeks with the least deviation (using user supplied weighting factors) are reported (ESRU, 2010). In Porto, the

Const.	Layer	Thick. (MM)	U (W·M ⁻² ·K ⁻¹)
External wall	Coating	0.2	1.3
	Plaster	30	
	Brick	190	
	Plaster	10	
Internal wall	Plaster	10	2.1
	Brick	110	
	Plaster	10	
Ground floor	Earth	300	0.7
	Gravel	300	
	Concrete	300	
	Asphalt	10	
	Concrete	20	
	Wood floor	20	
Slab	Plaster	10	2.0
	Concrete	240	
	Plaster	10	
Window	Clear glass	8	5.6
Roof slab	Clay tile	5	1.6
	Air	3	
	Plaster	5	
	Brick	110	
	Plaster	5	

Table 1 – Construction details of the building with a single wall façade (BD1)

typical weeks considered were from June 26th to July 2nd and from January 22nd to 28th.

To analyze the energy demand, the annual cooling and heating needs to keep the temperature within the Portuguese reference values for residential buildings (MOPTC, 2006), between 20 °C and 25 °C, were taken into account. These values were obtained assuming an HVAC system working all over the year.

Two different studies were performed based on BD1: i) the impact of using cool paints, both on roof and façade surfaces, named BD1-CP, and ii) the impact of using thermal insulation, named BD1-TI.

3.1.1 Impact of using cool paints

The cool paint considered has 92 % of TSR and 0.90 of thermal emissivity; these correspond to experimental values obtained for a high quality white exterior paint. The thermal results of Porto location are presented in Table 6 and in Table 7 related to the typical summer week and the typical winter week, respectively. In these tables, T_{\max} is the week average daily maximum temperature and T_{\min} is the week average daily minimum temperature.

The indoor temperatures of the ground floor, first floor and second floor were separately determined as well as the exterior temperature of the building. According to the summer results, one can conclude that the thermal impact of cool paints is more significant on the second floor, followed by the first floor and finally the ground floor. Since the second floor has a larger exposed area to solar radiation, the cool paints can promote a higher cooling effect, 3.0 °C on T_{\max} . On the ground floor the cooling effect was smaller, 2.1 °C.

In the typical winter week there is a non-desirable reduction of T_{\min} between 0.8 °C and 1.4 °C due to the cool paint. Since cool paints are related to radiation control and the level of radiation in winter is expected to be low, these values show otherwise. Indeed, Figure 3 shows the daily direct solar radiation for both typical weeks; the winter irradiation is just 38 % smaller than the summer irradiation.

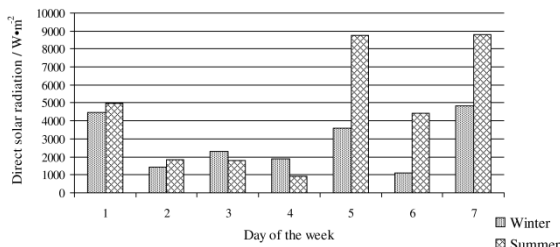


Figure 3 - Daily direct solar radiation over the typical weeks.

Table 8 shows annual cooling and heating demand of Porto and, although the annual energy demand has a heating load penalization of about 2.9 MWh per year, it was demonstrated that the cooling demand almost disappears, i.e. the building is comfortable even during the peak summer without mechanical cooling.

3.1.2 Impact of using thermal insulation

The impact of thermal insulation on the thermal comfort of BD1 was assessed assuming the use of 60 mm of expanded polystyrene (EPS) insulation, both on external walls and on the roof slab, as shown in Table 2. The conductivity value of this material was considered to be 0.042 W·m⁻¹·K⁻¹.

Const.	Layer	Thick. (MM)	U (W·M ⁻² ·K ⁻¹)
External wall	Coating	0.2	0.5
	Plaster	30	
	Insulation	60	
	Brick	190	
Roof slab	Plaster	10	0.5
	Clay tile	5	
	Air	3	
	Plaster	5	
	Insulation	60	
	Brick	110	
	Plaster	5	

Table 2 – Construction details of BD1-TI – in bold the differences from BD1

Table 7 shows the results of the typical winter week and it was found that the use of thermal insulation leads to an increase between 0.7 °C and 2.1 °C on T_{\min} . On the other hand, Table 6 presents the values of T_{\max} in the typical summer week, where one can see that on the ground floor there was a reduction of 0.4 °C, while on the first and second floors there was a temperature increase of 0.4 °C. The temperature reduction on the ground floor is due to the thermal inertia of the ground, which leads to a lower ground temperature compared to the exterior air temperature. Therefore, the use of thermal insulation helps to keep or to reduce the indoor temperature of the ground floor. Table 8 shows that these temperature variations have an impact on the energy demand of

the building; a not very significant reduction of the cooling demand was observed, while a drop in the heating demand of about 1.2 MWh per year was noted.

In order to perform a comparison of thermal insulation (BD1-TI) with the other two previous cases (base case – BD1 – and cool paints – BD1-CP), Figure 4 shows the hourly temperature history over the typical summer week. The exterior air temperature history is also presented.

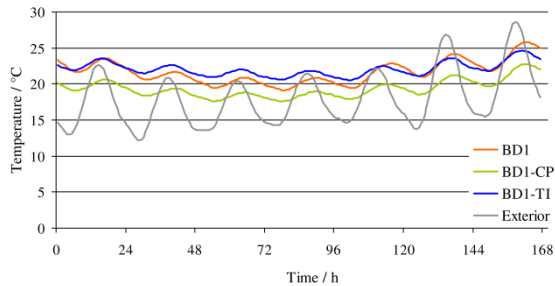


Fig. 4 – Hourly temperature history, over the typical summer week, for a single wall façade building.

Although the use of thermal insulation has the greatest reduction on the impact of exterior air temperature variations, decreasing the indoor temperature range, BD1-TI exhibits, most of the time, the highest indoor temperature. On the other hand, cool paints lead to a permanent and significant reduction in the indoor temperature.

3.2 Building 2 – double wall

BD2 has a double wall façade and no thermal insulation neither on the façades (external walls) nor on the roof (roof slab). Differences on construction details are indicated in bold in Table 3.

Const.	Layer	Thick. (MM)	U (W·M ⁻² ·K ⁻¹)
External wall	Coating	0.2	1.0
	Plaster	30	
	Brick	110	
	Air	60	
	Brick	110	
Window	Plaster	10	2.8
	Clear glass	8	
	Air	16	
	Clear glass	5	

Table 3 – Construction details of the double wall façade building (BD2) – differences from BD1 highlighted in bold

Similarly to the previous case, two different studies were performed: i) the impact of using cool paints, both on roof and façade surfaces, named BD2-CP, and ii) the impact of using thermal insulation, named BD2-TI.

3.2.1 Impact of using cool paints

Results of BD2-CP are similar to those obtained for BD1-CP. The typical summer week shows a T_{max} reduction between 2.0 °C and 3.0 °C and between 0.8 °C and 1.5 °C on T_{min} in the typical winter week – see Tables 6 and 7. Table 8 shows that also in this case the cooling demand almost disappears and the annual heating demand has an increase of about 2.8 MWh per year.

3.2.2 Impact of using thermal insulation

The impact of thermal insulation on BD2 was assessed assuming again 60 mm of EPS insulation, both on external walls and on the roof slab, as shown in Table 4.

Table 7 shows that in the typical winter week T_{min} has an increase between 0.6 °C and 2.7 °C. In the typical summer week occurs a slight reduction of 0.2 °C of T_{max} on the ground floor and an increase of 0.8 °C on each of the other floors – see Table 6. In Table 8, one can see that these results lead to a decrease of about 4.1 MWh per year on heating demand and to a not significant variation of the annual cooling demand.

Const.	Layer	Thick. (MM)	U (W·M ⁻² ·K ⁻¹)
External wall	Coating	0.2	0.4
	Plaster	30	
	Insulation	60	
	Brick	110	
	Air	60	
	Brick	110	
Roof slab	Plaster	10	0.5
	Clay tile	5	
	Air	3	
	Plaster	5	
	Insulation	60	
	Brick	110	
	Plaster	5	

Table 4 – Construction details of BD2-TI, where differences from BD2 are highlighted in bold

3.3 Building 3 – single wall with thermal insulation

BD3 follows the present Portuguese laws (MOPTC, 2006) concerning overall heat transfer coefficients. BD3 has a single wall façade with thermal insulation both on external walls and on the roof slab - construction details given in Table 5.

As BD3 already considers thermal insulation the impact of using cool paints, both on roof and façade surfaces, named BD3-CP was only assessed. Values of TSR and thermal emissivity of cool paints were 92 % and 0.90 respectively, as before. Tables 6 and 7 show that in the typical summer week BD3-CP exhibits a T_{\max} decreasing between 1.2 °C and 2.2 °C and, in the typical winter week, a maximum reduction in T_{\min} of 1.1 °C was observed. In Table 8, it was also observed that annual demand has a heating load penalization of about 1.2 MWh per year, although it was demonstrated that cooling demand almost vanishes.

3.4 Thermal comfort analysis in two specific real weather periods

Since ESP-r uses averaged weather data, hot or cool weeks especially do not happen, although in reality they occur. These outliers' conditions significantly influence the decision of house-owners in terms of deciding for one or another architectural solution. In the following, two real and specific hot periods in Porto, from July 4th to 7th of 2010 and from September 2nd to 6th of 2012, are considered – Figure 5 and 6. Data shows daily maximum values of global solar radiation of about 1000 W·m⁻² and maximum temperatures overpassing 30 °C.

Simulations considering the building with a single wall façade (BD1) were performed and the indoor temperature difference between the base case (BD1) and, the base case with thermal insulation (BD1-TI) and the base case coated with cool paints (BD1-CP) were calculated. The average of these temperature differences, $\Delta T_{\text{average}}$, for each period of time are shown in Tables 9 and 10.

Const.	Layer	Thick. (MM)	U (W·M ⁻² ·K ⁻¹)
External wall	Coating	0.2	0.5
	Plaster	30	
	Insulation	60	
	Brick	190	
	Plaster	10	
Ground floor	Earth	300	0.5
	Gravel	300	
	Concrete	300	
	Asphalt	200	
	Concrete	200	
	Wood floor	20	
Window	Clear glass	8	2.8
	Air	16	
	Clear glass	5	
Roof slab	Clay tile	5	0.5
	Plaster	10	
	Insulation	60	
	Brick	110	
	Plaster	10	

Table 5 – Construction details of BD3

Case	Temp. (°C)	G. F.	1 st F.	2 nd F.
BD1	T_{\max}	22.0	23.2	23.2
BD1-CP	T_{\max}	19.9	20.7	20.2
	ΔT_{\max}	- 2.1	- 2.5	- 3.0
BD1-TI	T_{\max}	21.6	23.6	23.6
	ΔT_{\max}	- 0.4	+ 0.4	+ 0.4
BD2	T_{\max}	22.0	23.5	23.3
BD2-CP	T_{\max}	20.0	21.0	20.3
	ΔT_{\max}	- 2.0	- 2.5	- 3.0
BD2-TI	T_{\max}	21.8	24.3	24.1
	ΔT_{\max}	- 0.2	+ 0.8	+ 0.8
BD3	T_{\max}	22.2	24.3	24.1
BD3-CP	T_{\max}	21.0	22.5	21.9
	ΔT_{\max}	- 1.2	- 1.8	- 2.2

Table 6 – T_{\max} over the typical summer week of Porto

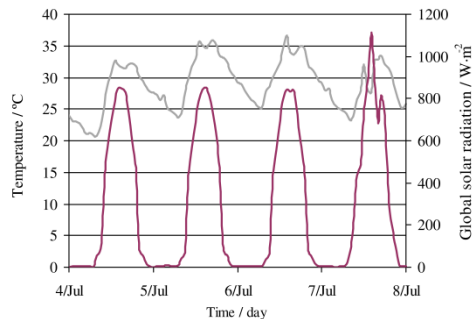
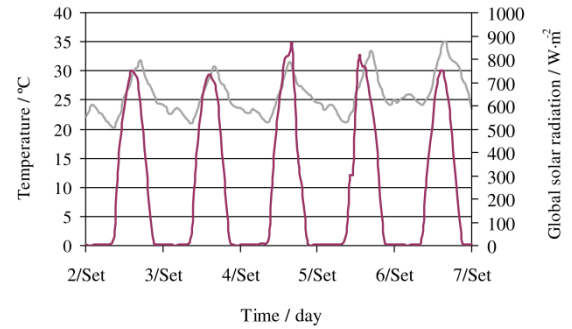
Case	Temp. (°C)	G. F.	1 st F.	2 nd F.
BD1	T_{min}	9.5	10.6	9.1
BD1-CP	T_{min}	8.7	9.2	8.2
	ΔT_{min}	- 0.8	- 1.4	- 0.9
BD1-TI	T_{min}	10.2	11.8	11.2
	ΔT_{min}	+ 0.7	+ 1.2	+ 2.1
BD2	T_{min}	10.1	11.5	9.5
BD2-CP	T_{min}	9.3	10.0	8.5
	ΔT_{min}	- 0.8	- 1.5	- 1.0
BD2-TI	T_{min}	10.7	13.0	12.2
	ΔT_{min}	+ 0.6	+ 1.5	+ 2.7
BD3	T_{min}	10.8	12.6	11.9
BD3-CP	T_{min}	10.3	11.5	11.2
	ΔT_{min}	- 0.5	- 1.1	- 0.7

Table 7 – T_{min} over the typical winter week of Porto

Case	Energy demand (MWh/year)		
	cooling	heating	total
BD1	0.4	11.2	11.6
BD1-CP	≈ 0	14.1	14.1
BD1-TI	0.3	10.0	10.3
BD2	0.4	8.9	9.3
BD2-CP	≈ 0	11.7	11.7
BD2-TI	0.4	4.8	5.2
BD3	0.4	4.8	5.2
BD3-CP	≈ 0	6.0	6.0

Table 8 – Annual energy demand for studied cases

For the first period (July 4th to 7th), the building with thermal insulation (BD1-TI) shows the greatest indoor temperature reduction compared with the base case. However, it should be noted that on the second floor, the use of cool paints shows the highest temperature reduction, 4.2 °C.

Fig. 5 – Exterior air temperature and global solar radiation histories from July 4th to 7th, 2010.Fig. 6 – Exterior air temperature and global solar radiation histories from September 2nd to 6th, 2012.

Case	Temp. (°C)	G. F.	1 st F.	2 nd F.	BD.
BD1	$T_{average}$	27.9	30.1	32.6	30.2
BD1-CP	$T_{average}$	26.1	27.9	28.4	27.5
	$\Delta T_{average}$	- 1.8	- 2.2	- 4.2	- 2.7
BD1-TI	$T_{average}$	24.9	26.6	29.0	26.8
	$\Delta T_{average}$	- 3.0	- 3.5	- 3.6	- 3.4

Table 9 – $\Delta T_{average}$ for the period of July 4th to 7th, 2010

Case	Temp. (°C)	G. F.	1 st F.	2 nd F.	BD.
BD1	$T_{average}$	25.7	27.1	27.5	26.8
BD1-CP	$T_{average}$	24.1	25.0	24.5	24.6
	$\Delta T_{average}$	- 1.6	- 2.1	- 3.0	- 2.2
BD1-TI	$T_{average}$	24.6	26.3	27.5	26.1
	$\Delta T_{average}$	- 1.1	- 0.8	≈ 0	- 0.7

Table 10 – $\Delta T_{average}$ for the period of September 2nd to 6th, 2012

Interestingly, the opposite is observed in the second period (September 2nd to 6th): the greatest indoor temperature reductions are obtained always with cool paints. To understand these results it is necessary to note that the first period of time is close to the summer solstice, when the sun reaches 71° of altitude, and the second period happens when the sun reaches 55° of altitude. Since for the second period the sun strikes more strongly on the house's walls, the cool paint originates higher temperature reductions. The previous sections dealt with average results using an averaged weather database. However, real weather data originates a more complex reality where the effect of the proposed thermal comfort architectural solutions blurs.

4. Conclusion

The thermal performance of a residential building was simulated, assessing the impact of using cool paints and/or thermal insulation. In Porto – Portugal, although the use of cool paints shows that no annual cooling demand is required, the heating load penalization of about 30 % increases the total energy demand of the residential building.

The analysis of two specific hot periods of real summer weather data, not averaged, shows that the sun's altitude is critical as to which cool paint or thermal insulation solution originates the highest temperature reduction; it was concluded that for lower sun altitudes the cool paints performed better.

5. Acknowledgement

The authors acknowledge the Portuguese Foundation for Science and Technology (FCT) and CIN, S.A. for the financial support of Diana Dias's Ph.D. grant (SFRH/BDE/33548/2009). The authors would also like to acknowledge the technical support of LEPAE, IDMEC and ARCP (Associação Rede de Competência em Polímeros).

References

- Akbari, H., 2003, Measured energy savings from the application of reflective roofs in two small non-residential buildings, *Energy*, 28 (9) p. 953-967.
- Akbari, H., Gartland, L., Konopacki, S., 1998, Measured Energy Savings of Light-colored Roofs: Results from Three California Demonstration Sites, *Energy Efficiency in Buildings*, 3.
- ASTM, American Society for Testing and Materials, 2008, ASTM G173-03: Standard Tables for Reference Solar Spectral Irradiances: Direct Normal and Hemispherical on 37 ° Tilted Surfaces.
- Berdahl, P., Akbari, H., Levinson, R., Jacobs, J., Klink, F., Everman, R., 2012, Three-year weathering tests on asphalt shingles: Solar reflectance, *Solar Energy Materials and Solar Cells*, 99 (0) p. 277-281.
- EEA, European Environment Agency, 2008, Energy and environment report 2008, Report n.º: 978-92-9167-980-5, Copenhagen, Denmark.
- EPC, European Parliament and of the Council, 2002, Directive 2002/91/CE Official Journal of the European Communities.
- EPC, European Parliament and of the Council, 2010, Directive 2010/31/UE Official Journal of the European Communities.
- ESRU, Energy Systems Research Unit, University of Strathclyde, The ESP-r Cookbook, <http://www.esru.strath.ac.uk/Documents/ESP-r_cookbook_dec_2010.pdf> (accessed September 2012).
- ESRU, Energy Systems Research Unit, University of Strathclyde, ESP-r - ESRU, <<http://www.esru.strath.ac.uk/Programs/ESP-r.htm>> (accessed September 2012).
- Ichinose, M., Inoue, T., Sakamoto, Y., 2009, Long-term performance of high-reflectivity exterior panels, *Building and Environment*, 44 (8) p. 1601-1608.
- IM-I.P., Portuguese Meteorological Institute, Ministry of Education and Science, <<http://www.meteo.pt/pt/areaeducativa/otempo.eoclima/onda.calor/index.html>> (accessed September 2012).
- INE, Statistics Portugal, DGEG, Directorate General for Energy and Geology, 2011, Inquérito ao Consumo de Energia no Sector Doméstico 2010 (Residential Energy Consumption Survey, 2010), Lisbon, Portugal.
- Kubelka, P., 1947, New Contributions to the Optics of Intensely Light-Scattering Materials. Part I, *Journal of the Optical Society of America*, 38 (5) p. 448-457.
- Kubelka, P., Munk, F., 1931, An Article on Optics of Paint Layers, *Zeits. f. Techn. Physik*, 12 p. 593-601.
- LBNL, Lawrence Berkeley National Laboratory, Pigment Database, <<http://coolcolors.lbl.gov/LBNL-Pigment-Database/database.html>> (accessed October 2012).
- Levinson, R., Akbari, H., Berdahl, P., Wood, K., Skilton, W., Petersheim, J., 2010, A novel technique for the production of cool colored

- concrete tile and asphalt shingle roofing products, *Solar Energy Materials and Solar Cells*, 94 (6) p. 946-954.
- Levinson, R., Berdahl, P., Akbari, H., 2005, Solar spectral optical properties of pigments-Part I: model for deriving scattering and absorption coefficients from transmittance and reflectance measurements, *Solar Energy Materials and Solar Cells*, 89 (4) p. 319-349.
- Levinson, R., Berdahl, P., Akbari, H., 2005, Solar spectral optical properties of pigments-Part II: survey of common colorants, *Solar Energy Materials and Solar Cells*, 89 (4) p. 351-389.
- Levinson, R., Berdahl, P., Akbari, H., Miller, W., Joedicke, I., Reilly, J., Suzuki, Y., Vondran, M., 2007, Methods of creating solar-reflective nonwhite surfaces and their application to residential roofing materials, *Solar Energy Materials and Solar Cells*, 91 (4) p. 304-314.
- Levinson, R., Berdahl, P., Asefaw Berhe, A., Akbari, H., 2005, Effects of soiling and cleaning on the reflectance and solar heat gain of a light-colored roofing membrane, *Atmospheric Environment*, 39 (40) p. 7807-7824.
- Lind, M. A., Pettit, R. B., Masterson, K. D., 1980, The Sensitivity of Solar Transmittance, Reflectance and Absorptance to Selected Averaging Procedures and Solar Irradiance Distributions, *Journal of Solar Energy Engineering*, 102 (1) p. 34.
- Luxmoore, D. A., Jayasinghe, M. T. R., Mahendran, M., 2005, Mitigating temperature increases in high lot density sub-tropical residential developments, *Energy and Buildings*, 37 (12) p. 1212-1224.
- Meehl, G. A., Tebaldi, C., 2004, More Intense, More Frequent, and Longer Lasting Heat Waves in the 21st Century, *Science*, 305 (5686) p. 994-997.
- MEI, Ministry of the Economy and Innovation, 2006, Decree-Law No 78/2006 of April 4, *Diário da República - I Série - A* (Official Gazette).
- Miller, W., Loye, K. T. L., Desjarlais, A., Akbari, H., Kriner, S., Wiel, S., Levinson, R., Scichili, R. G. S., Berdahl, P., 2004, Special Infrared Reflective Pigments Make a Dark Roof Reflect Almost Like a White Roof, *ASHRAE - Buildings IX*, p. 11.
- MOPTC, Ministry of Public Works Transport and Communications, 2006, Decree-Law No 79/2006 of April 4 - Regulamento dos Sistemas Energéticos de Climatização em Edifícios (Regulation for Energetic Systems related to Building Climatization), *Diário da República - I Série - A* (Official Gazette).
- MOPTC, Ministry of Public Works Transport and Communications, 2006, Decree-Law No 80/2006 of April 4 - Regulamento das Características de Comportamento Térmicos dos Edifícios (Regulation on Thermal Insulation in Buildings), *Diário da República - I Série - A* (Official Gazette).
- Romeo, C., Zinzi, M., 2011, Impact of a cool roof application on the energy and comfort performance in an existing non-residential building. A Sicilian case study, *Energy and Buildings*.
- Santos, C. A. P., Matias, L., 2006, Coeficiente de Transmissão Térmica de Elementos da Envolvente dos Edifícios - Verão actualizada 2006 (U-values/Building envelope elements), *Laboratório Nacional de Engenharia Civil* (National Laboratory for Civil Engineering), Lisbon, Portugal.
- Wang, X., Kendrick, C., Ogden, R., Maxted, J., 2008, Dynamic thermal simulation of a retail shed with solar reflective coatings, *Applied Thermal Engineering*, 28 (8-9) p. 1066-1073.

Long term evaluation of building energy performance: comparison of the test reference year and historical data series in the North Italian climates

Giovanni Pernigotto – University of Padova, Vicenza, Italy & Eindhoven University of Technology, Eindhoven, The Netherlands

Gianluca Antonacci – CISMA Srl, Bolzano, Italy

Paolo Baggio – University of Trento, Trento, Italy

Andrea Gasparella – Free University of Bozen-Bolzano, Bolzano, Italy

Jan Hensen – Eindhoven University of Technology, Eindhoven, The Netherlands

Abstract

The pursuit of better energy performance of buildings led to the recourse to more detailed instruments of analysis, requiring more complex and detailed inputs, such as the hourly weather data. In this work, the representativeness of the *test reference year* (TRY_{EN}) weather data, recently developed in Italy in accordance with the procedure proposed by EN ISO 15927-4:2005, has been studied evaluating the energy performance – energy needs and peak loads – of a set of different simplified reference buildings by means of TRNSYS simulation code, using both the TRY_{EN} and the TRY_{EN} source multi-year collected weather series for 5 north Italian locations.

The results have been analysed by means of both descriptive and inferential statistics. The variability of energy performance has also been correlated with the envelope characteristics, in order to estimate a sensitivity of the different buildings to the weather data variability.

1. Introduction

In many design applications, the use of simplified calculation methods, such as the quasi-steady state method proposed by the EN ISO 13790:2008 (CEN, 2008) for the evaluation of a building energy consumption, cannot provide results detailed enough to allow advanced investigations aimed at achieving both a high energy efficiency and an adequate occupants' visual and thermal comfort. This fact is making recourse to the detailed dynamic simulation tools by professionals more and more frequent.

The higher capability in calculating detailed

outputs by simulations codes requires more complex and detailed inputs. As regards the weather data, while in simplified methods the user needs only a dataset of monthly mean values of dry bulb temperature, solar radiation and relative humidity, like the ones in the Italian Standard UNI 10349:1994 (UNI, 1994), in simulation tools the weather data inputs generally require at least an hourly discretization.

We can distinguish three kinds of data for dynamic simulation (Keeble, 1990): the multi-year weather data, the typical year and the representative days. The multi-year weather data are the best solution, in case of trend and sensitivity analyses of the building performance to the variability of the weather solicitations, aimed at a design which is robust to climatic changes (Struck *et al.*, 2009). Complete multi-year series, with low measurement errors and a good representativeness, are available for a limited number of localities in Italy, since the local environmental protection agencies (ARPA) have started to collect weather data in the urban areas only 20 years ago, in the best cases (Baggio *et al.*, 2010).

The use of typical years instead of multi-year weather data leads to a loss of information but is required to mitigate the impact of missing and wrong data and to provide a single standard weather condition for assessing the energy performance of a building in a particular location. One of the first definitions of typical reference years (TRY) was given by Lund (1974 and 1991) and Lund and Eidorff (1980): the reference years have to be characterized by *true frequencies* (i.e., the

TRY should be a good approximation of the mean values derived from a long period of measurements), *true sequences* (i.e., the weather situations must follow each other in a similar manner to the recorded data) and *true correlations* (i.e., the weather data are cross-correlated variables). The last feature is probably one of the most important, as also noted by Guan (2009).

Different approaches are available in the literature for the construction of a TRY but each one starts from the calculation of some weather parameters (e.g., daily solar radiation) for the selection of the representative month from the collected data, as suggested by Hall *et al.* (1978).

In accordance with Harriman *et al.* (1999), the choice of the main variables should be made with the perspective of the final use of the TRY, distinguishing the sizing and the energy assessment. Moreover, Hensen (1999) remarked that a proper statistical weighting for the primary parameters should be used, based on the type of building which will be analysed.

In Italy, the procedure selected for developing the new TRY_{EN} starting from ARPA's data is the one described in the European technical Standard EN ISO 15927-4:2005 (CEN, 2005). Its selection method is based on the dry bulb temperature, the solar radiation and the relative humidity as primary variables and the wind speed as secondary one.

In this work, the representativeness of the test reference year has been studied by carrying out different dynamic simulations with both TRY_{EN} and multi-year data series and analysing the annual energy needs and peak loads (both cooling and heating) of a set of reference buildings characterized by different insulation levels, thermal inertia, sizes and orientations of windows and kind of glazing. In addition, the sensitivity of the different building envelope characteristics to the variability of 5 north Italian climates has been evaluated.

2. Methods

2.1 Analysis and selection of the weather data

The raw data were available for the capital cities of each province in four north Italian Regions: Emilia-Romagna, Lombardia, Trentino-Alto Adige/Südtirol and Valle d'Aosta. They have been first analysed in order to identify the outliers, according to the following criteria:

- *horizontal global solar radiation*: the values exceeding the solar constant or positive during the night-time;
- *dry bulb temperature*:
 - the values exceeding 50% of the 99th percentile;
 - the data with a derivative larger than $\pm 4 \text{ K h}^{-1}$;
 - periods with constant values for more than 5 h;
- *relative humidity*:
 - the values exceeding 100% or null;
 - periods with constant values for more than 5 h (if lower than the 75th percentile);
- *wind velocity*:
 - the values exceeding 50% of the 99th percentile or negative;
 - periods with constant values for more than 5 h (if the registered speed is larger than the anemometer's minimum speed).

Known bias errors have been corrected.

In order to follow as closely as possible the prescription by the EN ISO 15927-4:2005, which recommends having at least 10 years for the development of a TRY_{EN}, only locations with at least 8 years in the data series and with less than 10% of wrong/missing data for each variable and each year were considered. Wrong and/or missing data have been replaced using the linear interpolation for the temperature, the relative humidity and the wind speed when the consecutive data to correct were less than 6, otherwise a cyclic interpolation has been considered (Prada, 2012).

The selection procedure led to identify 5 cities:

Aosta (with 8 years available), Bergamo (10 years), Monza (9 years), Trento (10 years) and Varese (9 years).

2.2 TRY_{EN} calculation

For each location, a TRY_{EN} has been built in accordance with the EN ISO 15927-4:2005 procedure following the steps described below:

1. calculation of the daily averages \bar{p} for each primary climatic parameter p , month m and year y of the series;
2. sorting of all the \bar{p} for a specific month m of all the available years in increasing order and calculation the cumulative distribution function $\Phi(p, m, i)$ for each parameter and i^{th} day as:

$$\Phi(p, m, i) = \frac{K(i)}{N + 1} \quad (1)$$

where $K(i)$ is the rank order of the i^{th} day and N is the total number of days for a month over all the available years.

3. sorting of all the \bar{p} for a specific month m and year y in increasing order and calculating the cumulative distribution function $F(p, y, m, i)$ for each parameter and i^{th} day, as

$$F(p, y, m, i) = \frac{J(i)}{n + 1} \quad (2)$$

where $J(i)$ is the rank order of the i^{th} day and n is the number of days for a specific month.

4. calculation of the statistics by Finkelstein-Schafer for each month m and year y as

$$F_S(p, y, m) = \sum_{i=1}^n |F(p, y, m, i) - \Phi(p, m, i)| \quad (3)$$

5. sorting of the months for increasing values of F_S for each parameter, calculating the ranks for each month and parameter and summing them in order to calculate the total ranking.
6. for each month among the first 3 months with the lowest ranking sum, calculate the deviation between the mean wind speed of the

month m of the year y and the mean multi-year wind speed: the month with the lowest deviation can be chosen for a TRY_{EN}.

The final 8 hours of a month and the first 8 hours of the next one are smoothed by means of a cubic spline interpolation in order to avoid discontinuities.

2.3 Set of reference buildings

A sample of 48 different simplified thermal zones has been developed in accordance with a full factorial plan.

The base module consists in single thermal zone with 100 m² of squared floor, 3 m of internal height and the façades oriented towards the main cardinal directions. The thermal bridges have been neglected and the floor has been modelled as on a ventilated cave (i.e., without sun exposition and infrared thermal losses towards the sky dome), instead of in touch with the ground, whose sensitivity and response to the variability of the external conditions are very low considering a limited number of years because of its very high thermal inertia. All the opaque components have been modelled with a two-layer structure with insulation on the external side and a massive layer on the internal one, with a thermal resistance around 0.8 m² K W⁻¹. The solar absorptance is 0.3 for both sides of the vertical walls and for the internal side of the roof, 0.6 for the external side of the roof and the internal side of the floor and 0 for the external side of the floor. The thermal properties of the considered material are shown in Table 1. The windows are positioned all on the same façade and consist in a double-pane glazing ($U_{gl} = 1.1$ W m⁻² K⁻¹) and in a timber frame ($U_f = 1.2$ W m⁻² K⁻¹), whose area is 20% of the whole window area. The internal gains have been assumed equal to 4 W m⁻², half radiative and half convective, as indicated by the EN ISO 13790:2008 for residential dwellings. The ventilation has a constant rate of 0.3 ACH, as suggested by the Italian technical Specification UNI/TS 11300-1:2008 (UNI, 2008).

The considered variables are the most relevant building envelope parameters and, with the exception of the window orientation, each one presents a high and a low level:

- the insulation level of the envelope components (5 cm or 15 cm of polystyrene) in order to have two levels of thermal transmittance (e.g., for the vertical walls, $U= 0.45 \text{ W m}^{-2} \text{ K}^{-1}$ and $U= 0.21 \text{ W m}^{-2} \text{ K}^{-1}$);
- the thermal inertia of the opaque elements (area specific heat capacity of the internal layer equal to $75 \text{ kJ m}^{-2} \text{ K}^{-1}$ for the timber structure and equal to $300 \text{ kJ m}^{-2} \text{ K}^{-1}$ for the concrete);
- the solar heat gain coefficient of the glazing (equal to 0.608 or 0.352);
- size of the windows (14.56 m^2 or 29.12 m^2);
- the orientations of the windows (East, South or West).

Property	Timber	Concrete	Insulation
Thermal conductivity $\lambda \text{ [W m}^{-1} \text{ K}^{-1}]$	0.13	0.37	0.04
Specific Heat Capacity $c \text{ [J kg}^{-1} \text{ K}^{-1}]$	1880	840	1470
Density $\rho \text{ [kg m}^{-3}]$	399	1190	40
Thickness $s \text{ [m]}$	0.1	0.3	0.05/0.15
Thermal resistance $R \text{ [m}^2 \text{ K W}^{-1}]$	0.77	0.81	1.25/3.75

Table 1 – Properties of the opaque components

The different cases have been simulated with TRNSYS, considering the following assumptions:

- the timestep is coherent with the hourly discretization of the weather data, in order to avoid interpolation strategy influencing, in particular, the peak load results;
- constant convection coefficients have been selected in accordance with the Standard EN ISO 6946:2007 (CEN, 2007);
- the long wave radiation exchanges are considered according to the star network approach by TRNSYS;
- the heating and the cooling set-point have been fixed to 20°C and 26°C in accordance with the UNI/TS 11300-1:2008 prescriptions for residential buildings, but they are applied all

year long, i.e. no heating and cooling seasons have been defined.

3. Results and discussion

3.1 Average monthly data

The monthly values of average dry bulb temperature, daily horizontal solar radiation and relative humidity of the different years and TRY_{EN} have been calculated and compared, as in Figure 1 for the location of Trento.

Generally, the TRY_{EN} monthly value is within the range between Q_1 and Q_3 but it is rarely close with the median for the three climatic parameters at the same time. This is a consequence of the statistical method proposed by EN ISO 15927-4:2005 for the selection of each month, which tries to minimize the sum of the differences of the three parameters together.

3.2 Annual energy needs and peak loads

In Figure 2 the results for the energy needs of 48 thermal zones of the sample have been represented for the analysed localities. For the heating energy needs, the average values are generally within the $\pm 10\%$ range, which means that the error provided by the TRY_{EN} weather data respect to the average of multi-year real data is under 10%.

In the five locations, the general trend of the deviation is not the same:

- in Bergamo and in Trento the TRY_{EN} weather files lead to overestimations of the heating energy needs with respect of average over the multi-year series;
- in Monza the TRY_{EN} weather file shows an underestimation;
- in Aosta and in Varese there is a good agreement between results simulated with the TRY_{EN} file and average values on the multi-year series.

Also for the cooling energy needs, the differences between the TRY_{EN} results and the averages on the multi-year series are generally within $\pm 10\%$:

- by using the TRY_{EN} weather data, in Aosta, Bergamo, Monza and, in particular, Trent

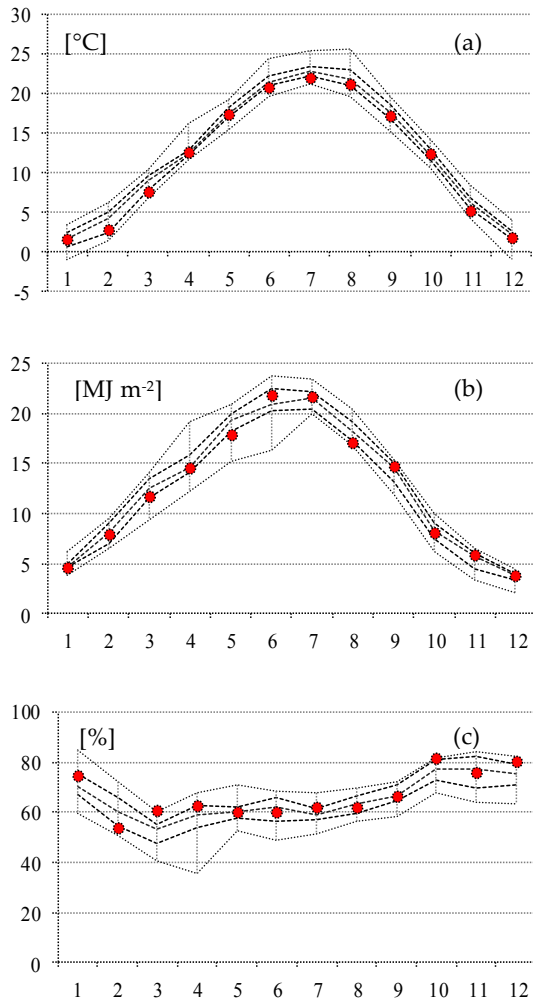


Fig. 1 – (a) Average monthly temperature (b) average daily horizontal global radiation and (c) average monthly relative humidity for Trento. The red dots represent the TRY_{EN} monthly values, the external dotted lines represent the maximum and the minimum for the multi-year series, the internal dotted lines the first and the third quartile (Q_1 and Q_3), while the continuous line is the median.

- there are underestimations of the cooling needs;
 - in Varese a slight overestimation is registered.
- The peak loads are represented in Figure 3. For the heating peak loads, the deviations between the TRY_{EN} results and the averages over the multi-year series are within a range of 10%:
- for all locations except Bergamo the TRY_{EN} weather file causes a slight underestimation, which is more marked for Trento;
 - in Bergamo there is an overestimation by the TRY_{EN} weather file.

Also for the cooling peak loads, the results are generally within the $\pm 10\%$ range but the deviations present a larger variability. The TRY_{EN} weather file causes an underestimation for Aosta while for the other locations there is a good agreement.

Both for the energy needs and the peak loads, for the heating analysis the results are well aligned while for the cooling one a certain variability can be observed, demonstrating that the considered buildings present different responses to the use of a TRY_{EN} weather file instead of the multi-years data.

3.3 Statistical analysis

In order to study the variability of the energy performance and its correlation with the building envelope characteristics, the results with the TRY_{EN} weather files have been considered as a benchmark and the deviations between the energy needs and peak loads simulated in each year and the ones of the TRY_{EN} have been calculated. The deviations have been analysed by means of Pearson's correlation index, distinguishing the positive and the negative differences because of the linear definition of the index. The considered variables have been distinguished into the ones describing the envelope characteristics and the ones describing the external solicitation.

For the energy need deviations, the considered variables are:

- the variables aimed at describing the dynamic behaviour of the opaque envelope, such as $Y_{ie,env}$ [$\text{W m}^{-2} \text{K}^{-1}$], the area-weighted average periodic thermal transmittance, $\Delta t_{ie,env}$ [h], the area-weighted average time shift, and $k_i \cdot A_{tot}$ [kJ K^{-1}], the total internal heat capacity;
- U_{env} [$\text{W m}^{-2} \text{K}^{-1}$], the area-weighted average thermal transmittance of the opaque envelope;
- $SHGC$ [-], the solar heat gain coefficient of the glazing;
- A_{gl} [m^2], the glazing area;
- the deviation between the area-weighted *Heating/Cooling Degree Days* [K d] calculated using a particular year and the ones of the TRY_{EN} (both for the opaque envelope and for the transparent one).

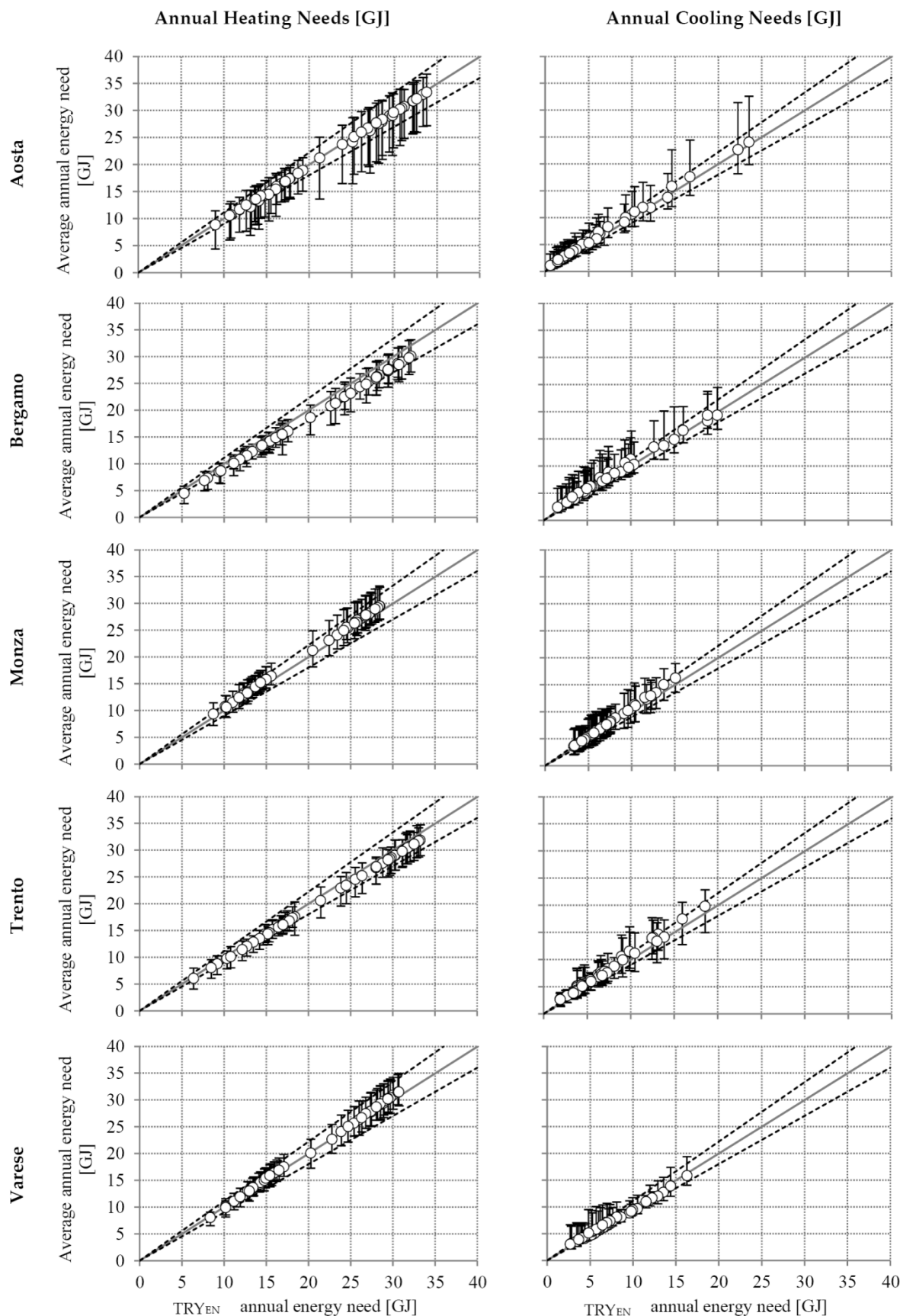


Fig. 2 – Heating and cooling energy needs: the dots are the average energy needs for the considered 10 years, the bars represent the maximum and the minimum in the multi-year series and the dotted lines a deviation of $\pm 10\%$ respect of the TRY_{EN} values

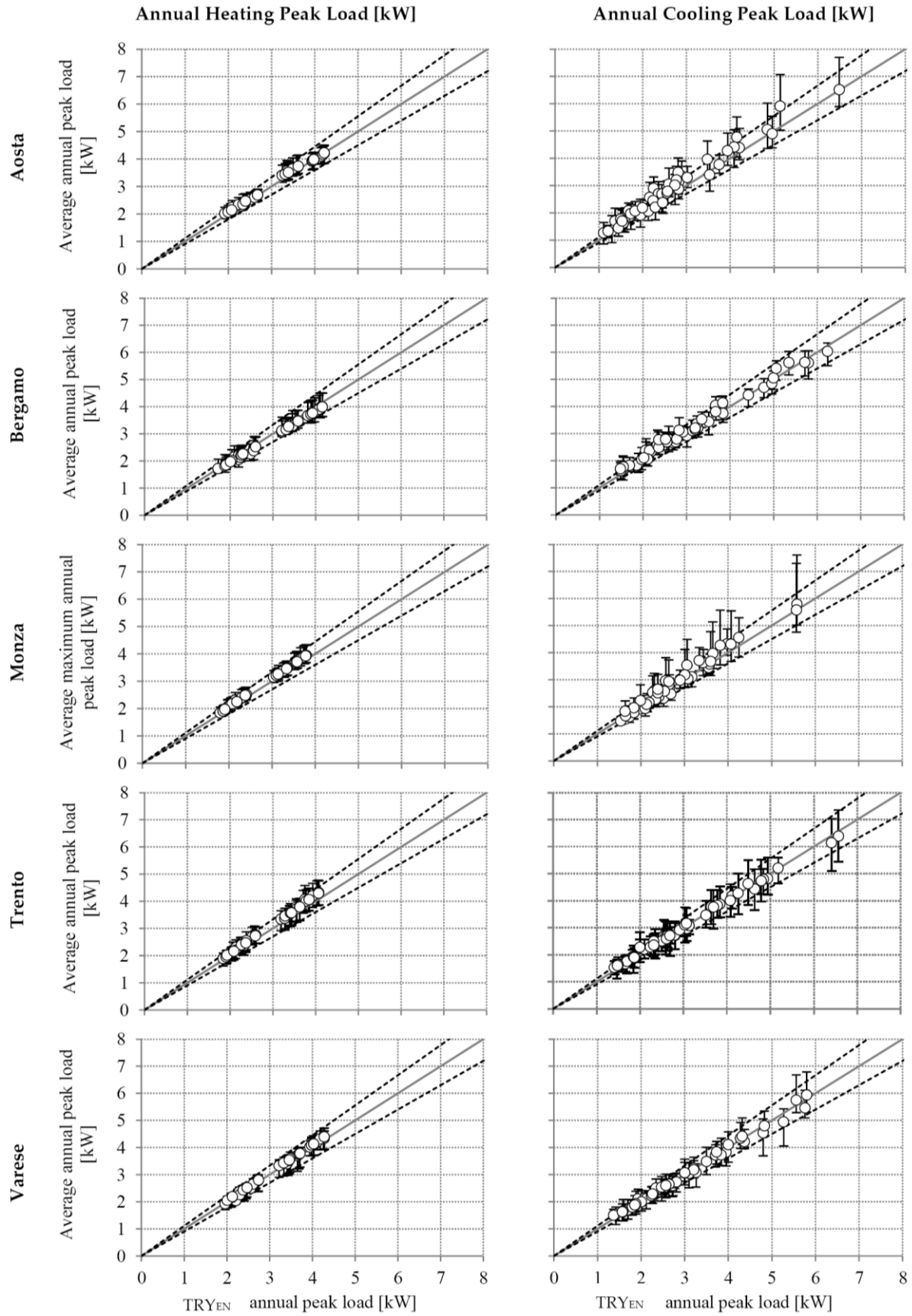


Fig. 3 – Heating and cooling peak loads: the dots are the average energy needs for the considered 10 years, the bars represent the maximum and the minimum in the multi-year series and the dotted lines a deviation of $\pm 10\%$ respect of the TRY_{EN} value

The HDD_{env} , CDD_{env} , HDD_{gl} and CDD_{gl} have been calculated for each orientation considering respectively the sol-air temperature for the opaque components and the equivalent sol-air temperature for the transparent components, according to the Eq. 4 and 5 (Gasparella *et al.*, 2011):

$$\theta_{sol-air, env} = \theta_e + \frac{I\alpha + h_{r,sky}(\theta_{sky} - \theta_e)}{h_{se}} \quad (4)$$

$$\theta_{sol-air, gl} = \theta_e + \frac{SHGC \cdot I}{U_{gl}} + \frac{h_{r,sky}(\theta_{sky} - \theta_e)}{h_{se}} \quad (5)$$

Area-weighted heating/cooling degree days have then been calculated per each year and used for determining the deviations ΔHDD_{env} , ΔCDD_{env} , ΔHDD_{gl} and ΔCDD_{gl} .

For the peak load deviations, the variables are the same, with the exception of the ones describing the variability of the external solicitation:

- $\Delta\theta_{min}$ [°C], the deviation between the minimum annual external temperature for a considered year and the one for the TRY_{EN} has been used instead of ΔHDD_{env} and ΔHDD_{gl} ;
- ΔH_{hor} [MJ m⁻²], the deviation between the total horizontal solar radiation per square meter and $\Delta \hat{H}_{2dd}$ [MJ m⁻²], the deviation between the annual peak of the 2-days cumulated solar radiation incident on the windows for a considered year and the one for the TRY_{EN}, instead of ΔCDD_{env} and ΔCDD_{gl} .

The indexes for the energy needs deviation have been represented in Figure 4 and the ones for the peak loads in Figure 5. The most influencing parameter on the variability of the heating energy needs is, as expected, the deviation of the heating degree days. In the reduction of the variability, an important role belongs to the characteristics of the opaque components (limiting U , $Y_{ie,env}$ and $\Delta t_{ie,env}$ the variability of the energy needs is reduced). For the cooling deviations, the most influencing parameter, besides the deviation of the cooling degree days, is the solar heat gain coefficient. Also the glazing area appears to have a light correlation for the positive deviations. For the heating peak loads the most influencing parameter on the variability is the deviation of the minimum

external temperature. The opaque components are the most correlated with the variability of the peak deviations, both on the steady and dynamic point of view. For the cooling peak loads, the variables chosen for describing the external forcing solicitation are not able to fully justify the variability by themselves. With the exception of the glazing area, the correlations appear very weak, suggesting that interactions between the different characteristics (dynamics of the opaque components and entering solar radiation through the glazings) could be pursued to reduce the variability of the cooling peak loads.

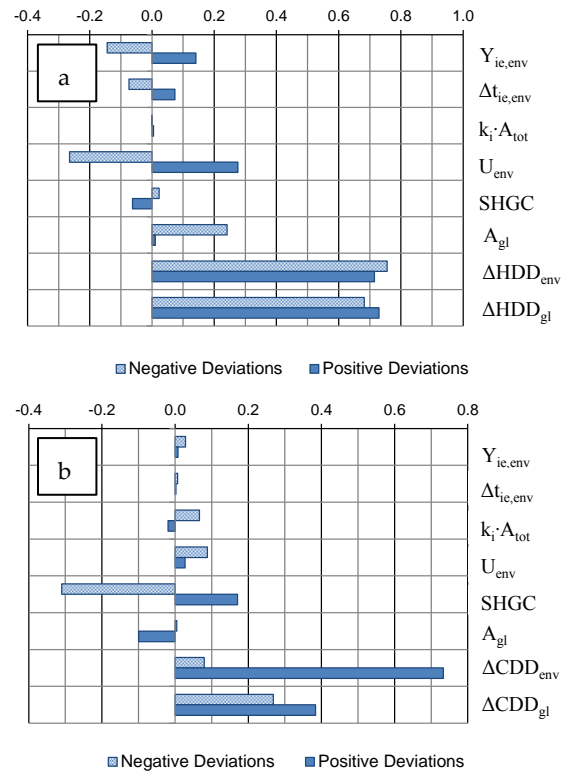


Fig. 4 – Pearson's indexes for (a) the heating needs deviations and (b) for the cooling needs deviations

4. Conclusion

In this work the TRY_{EN} weather files have been compared with the multi-year series of the data collected in 5 north Italian locations, analysing the annual energy needs and the peak loads of a set of reference buildings. Analysing the monthly average temperatures, solar radiation and humidity it can be noticed that the correspondence with the TRY_{EN} values and the averages is not good

for the three parameters at the same time. That

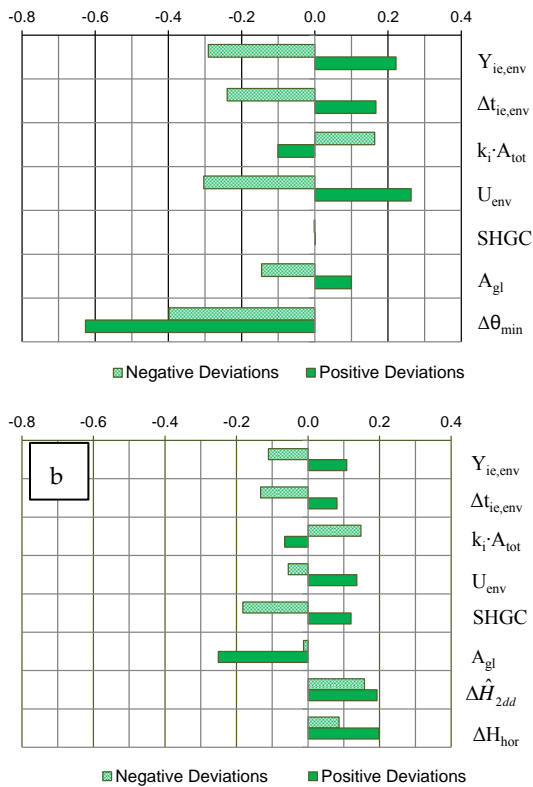


Fig. 5 – Pearson's indexes for (a) the heating peak loads deviations and (b) for the cooling ones

suggests a possible change of the Standard procedure by introducing weighting coefficients, in order to develop different TRY_{EN} to use for specific purposes, as already underlined in literature. The mean of the results of the multi-year series are within a 10% deviation from the TRY_{EN} results but in some cases (Trento and Bergamo) the TRY_{EN} overestimates/underestimates.

The correlations between the building envelope characteristics and the variability of the energy performances in a multi-year analysis have been also considered. The thermal transmittance and also the dynamic parameters can be considered for reducing the variability of the heating energy needs and peak loads. The solar heat gain coefficients and the window size are correlated with the cooling energy needs and peak loads (and, so, generally speaking, the reduction of the entering solar radiation can limit the variability of the cooling energy performance).

5. Nomenclature

Symbols

A	area (m ²)
c	specific heat capacity (J kg ⁻¹ K ⁻¹)
CDD	cooling degree-days (K d)
F, Φ	cumulative distribution functions (-)
F_s	Finkelstein-Schafer's statistics (-)
H	solar global radiation (MJ m ⁻²)
HDD	heating degree-days (K d)
I	solar global irradiance (W m ⁻²)
J, K	rank order (-)
k	internal heat capacity (kJ m ⁻² K ⁻¹)
Q	quartile (-)
R	thermal resistance (m ² K W ⁻¹)
s	thickness (m)
$SHGC$	Solar Heat Gain Coefficient (-)
U	thermal transmittance (W m ⁻² K ⁻¹)
Y_{ie}	periodic transmittance (W m ⁻² K ⁻¹)
α	solar absorptance (-)
Δt_{ie}	time-shift (h)
λ	thermal conductivity (W m ⁻¹ K ⁻¹)
ρ	density (kg m ⁻³)
θ	temperature (K)

Subscripts/Superscripts

$2dd$	2-day cumulated
e	external
env	referred to the opaque envelope
f	referred to the frame
gl	referred to the glazings
hor	horizontal
i	internal
r	radiative
s	surface
sky	referred to the sky-dome
$sol-air$	referred to the sol-air temperature
tot	total

References

- Baggio P., Corrado V., Murano G., and Riva G. 2010. Definizione degli anni tipo climatici delle province del Nord Italia. La Termotecnica, 61 (9).
- European Committee for Standardization (CEN). 2005. EN ISO 15927-4:2005 Hygrothermal performance of buildings - Calculation and

- presentation of climatic data - Part 4: Hourly data for assessing the annual energy use for heating and cooling. Brussels. Belgium.
- Gasparella A., Pernigotto G., Cappelletti F., Romagnoni P., Baggio P. 2011. Analysis and modelling of window and glazing systems energy performance for a well insulated residential building. *Energy & Building*, 43(4).
- Guan L. 2009. Preparation of future weather data to study the impact of climate change on buildings. *Building & Environment*, 44(4).
- Hall I., Prairie R., Anferson H. and Boes E. 1978. Generation of a typical meteorological year for 26 SOLMET stations. Technical Report SAND - 78-1601, Sandia Lab., Albuquerque, U.S.
- Harriman L.G., Colliver D.G. and Quinn H.K. 1999. New weather data for energy calculations. *ASHRAE Transactions*, 41(3).
- Hensen J. 1999. Simulation of building energy and indoor environmental quality - some weather data issues. Proc. Int. Workshop on Climate data and their applications in engineering. Prague.
- Keeble E. 1990. Availability of UK climatic data for use in simulation. BEPAC Technical Note 1, Building Research Establishment.
- Lund H. 1974. The reference year a set of climate data for environmental engineering. In 2nd Symposium on the use of computers for environmental engineering. Paris, France.
- Lund H. 1991. The design reference year. In 3rd IBPSA Conference. Nice, France.
- Lund H. and Eidorff S. 1980. Selection methods for a production of test reference year. Technical Report ES DK - 248-7., Copenhagen, Denmark.
- Prada A. 2012. Energy performance of buildings: modeling of dynamic summer behavior. Ph.D. Thesis, University of Trento, Trento.
- Struck C., de Wilde P., Evers J. E. J., Hensen J. and Plokker W. 2009. On selecting weather data sets to estimate a building design's robustness to climate variations. Proc of the 11th IBPSA Building Simulation Conference. Glasgow, U.K.

Analysis of the impact of ventilated cavities on the performance of opaque components

Alessandro Prada – Free University of Bolzano, Bolzano, Italy

Marco Baratieri – Free University of Bolzano, Bolzano, Italy

Andrea Gasparella – Free University of Bolzano, Bolzano, Italy

Abstract

The energy performance of buildings depends on the behaviour of the different components under transient conditions, as it happens in particular for the opaque envelope both through its stationary and through its dynamic response to the external solicitations.

Some attempts to improve especially the summer performance of such elements are related to the insertion of air cavities, both still air or naturally ventilated through external openings. In those cases the annual performance evaluation becomes quite difficult, in particular when quasi steady state approaches are considered.

A large number of papers in the literature consider theoretical and experimental analysis of different ventilated components (opaque ventilated walls, roofs, double skin facades, ventilated floors). Daily and annual variations of boundary conditions and their dependence on the specific climatic context further increase the generalization of the results.

Summer improvement of comfort conditions and the reduction of cooling energy needs should be compared with the possible drawbacks during the heating season. This evaluation requires us to consider the entire building envelope and can be generalized only by means of a parametric analysis of the cavities impacts in relation to the composition, geometry, orientation and climatic context both of the cavities and of the building envelope.

In the present paper a thermal and fluid-dynamic analysis of ventilated air cavities is performed under different flow patterns and external conditions. The aim is to analyse the impact on the energy performance of the opaque building components. The values calculated by means of the enhanced model are compared with the predictions obtained with the reference standards.

1. Introduction

Heat transfer modelling of building envelope components with a ventilated air cavity requires the knowledge of the air change rates.

The air motion inside the ventilation channel is closely related to cavity shape, weather conditions (i.e. wind velocity, solar irradiation, air pressure and dry bulb temperature) and to the heat flux transmitted through the envelope. Therefore, to correctly model the wall behaviour, a coupled thermo-fluid dynamic analysis is needed.

In the literature, a large number of papers deal with the problem of modelling the effects of a ventilated air cavity on the summer heat transfer through the envelope (e.g. Ciampi et al., 1998, Ciampi et al., 2003 and Gagliano et al. 2012). Further, since there are few experimental measurements of air velocity in ventilation channels (e.g. Susanti et al., 2008 and Falk et al., 2012), few of these models are validated against experimental data. For this reason, several authors in the past investigated the role of the choice of CFD models and computation domain in the reliability of CFD predictions coupled with heat transfer solutions (e.g. Gan 2010, Nore et al., 2010 and Pasut et al. 2012).

However, in view of the reduction of cooling loads, ventilated air cavities present some drawbacks in winter months. In fact, in cold and humid locations some problems related to moisture infiltration in the opaque components can often occur. Consequently, a high ventilation rate is often required in order to dispose of the excess moisture in the wall. On the other hand, an increase in the heat transmission could be caused by the high air velocity in the cavity. Despite these considerations,

the winter performance of a ventilated wall has been barely investigated up until now.

Therefore, this paper focuses on the investigation of the winter performances of ventilated walls evaluated by means of a thermal-fluid dynamic analysis. In particular the CFD model is used to describe the turbulent air flow rate in the vented cavity caused by a buoyancy effect.

Starting from the heat fluxes calculated by means of the enhanced model, the average surface thermal resistance is then computed. This data, applied in the simple quasi steady state approaches, is then compared with the reference values proposed by the standard EN ISO 6946.

2. Test cases

Since this work aims to investigate the heat exchanges through the wall when ventilated channels are present, numerical simulations with several variants of the cavity are adopted. In particular, the different conditions aim to take into account the influence factors of the heat transfer mechanisms and of the boundary conditions. Two different wall typologies are used with the purpose of analysing both insulated (i.e. Case I) and not insulated (i.e. Case U) constructions (Figure 1). In fact, since in insulated walls the inner surface of the cavity could have lower temperature, the driving factor behind the ventilation flow is greatly reduced.

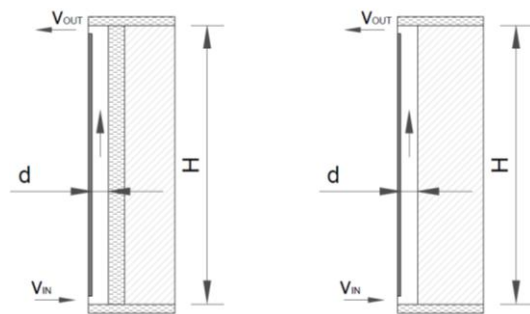


Fig. 1 – Test cases used in the analysis (case I on the left and case U on the right)

Therefore, in the test cases, particular attention is paid to the choice of the characteristics of the wall internal layer. In particular, the thermo-physical

properties, used for steady state analysis, which are adopted in this work are shown in Table 1.

Material	Thickness [m]	Conductivity [$\text{W m}^{-1} \text{K}^{-1}$]
Concrete Cover	0.02	0.90
EPS insulation	0.05	0.036
Brick block (case I)	0.25	0.34
Brick block (case U)	0.30	0.34

Table 1 – Material property of the solid layer

In addition to the two types just described, the cases analysed are expanded by varying certain parameters. For both cases, the external air temperatures, the emissivity of the cavity inner surface and the shape ratio of the cavity are changed with the purpose of investigating the extent to which each parameter affects the air motion in the channel and, consequently, the heat transfer. The parameter values adopted in the various configurations are reported in Table 2

Variable	Levels
T_{ext} [$^{\circ}\text{C}$]	-10, -5, 0, 5, 10, 15
e_2 [-]	0.1, 0.9
H [m]	3, 6
d [cm]	0.6, 0.10, 0.15

Table 2 – Cavity configuration parameters

The outdoor wind hardly influences the ventilation flow in the cavity. However, the study of the inlet velocity caused by wind forces is strictly connected with site characteristics. For this reason, in this work only the stack effect is investigated by assuming no wind external forces.

3. Simulation model

3.1 Governing equations

In order to model the behaviour of the turbulent system with a low computational cost, the Reynolds-averaged Navier Stokes (RANS) equations are used. Adopting the weakly

compressible hypothesis (i.e. compressibility is taken into account only in continuity equation) and the Newtonian behaviour of the fluid, the system of solved partial differential equations becomes:

Conservation of fluid mass

$$\frac{\partial \rho}{\partial t} + \nabla \cdot (\rho u) = 0 \quad (1)$$

Momentum equation with the eddy closure relation

$$\rho \left(\frac{\partial u}{\partial t} + u \cdot \nabla u \right) = \nabla \cdot \left[-pI + (\eta + \eta_T) (\nabla u + (\nabla u)^T - \frac{2}{3} (\nabla \cdot u) I) - \frac{2}{3} \rho k I \right] + F \quad (2)$$

Heat equation for solid domain

$$\rho c_p \frac{\partial T}{\partial t} + \nabla \cdot (-\lambda \nabla T) = 0 \quad (3)$$

Heat equation for fluid domain

$$\rho c_p \frac{\partial T}{\partial t} + \nabla \cdot (-(\lambda + \lambda_T) \nabla T) = -\rho c_p u \nabla T \quad (4)$$

Transport equation of the turbulent kinetic energy

$$\rho \left(\frac{\partial k}{\partial t} + u \cdot \nabla k \right) = \nabla \cdot [(\eta + \eta_T) \nabla k] + \frac{1}{2} \eta_T (\nabla u + (\nabla u)^T)^2 - \rho \varepsilon \quad (5)$$

Transport equation of the turbulent energy dissipation rate

$$\rho \left(\frac{\partial \varepsilon}{\partial t} + u \cdot \nabla \varepsilon \right) = -\rho C_{\varepsilon 2} \frac{\varepsilon^2}{k} \nabla \cdot \left[\left(\eta + \frac{\eta_T}{1.3} \right) \nabla \varepsilon \right] + \frac{1}{2} C_{\varepsilon 1} \frac{\varepsilon}{k} \eta_T (\nabla u + (\nabla u)^T)^2 \quad (6)$$

where η_T is the eddy viscosity computed as:

$$\eta_T = \rho C_{\eta} \frac{\varepsilon^2}{k} \quad (7)$$

3.2 Numerical discretization

The first step in the problem solution is the numerical discretization of the problem of air motion and of heat transfer through the ventilated channel. Figure 2 visualizes the spatial discretization by means of triangular finite element of the upper part of the 2D model reported in Figure 1.

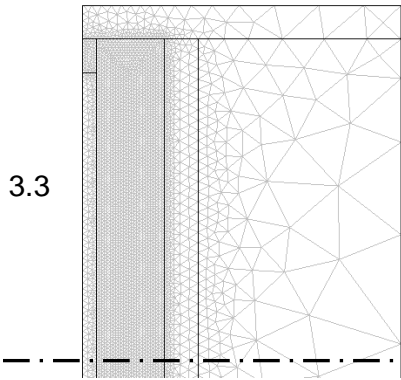


Fig. 2 – Typical mesh discretization adopted.

Note that, with the purpose of increasing the simulation accuracy and at the same time limiting the computational cost, the domain is discretized with a greater thickening in the zone of the convective heat exchange between the air flow and the wall surface.

Since the momentum equations (eq. 2) are nonlinear, the solution of the coupled heat and fluid dynamic problem becomes unstable if the Galerkin finite element method is adopted for the spatial discretization of the domain (Hauke, 2002). Consequently, in all the turbulent simulations herein reported an artificial diffusion is introduced. The diffusion is required in order to ensure the numerical convergence of the problem solution. However, the artificial diffusion parameter is kept to as low a value as possible while still getting a converged simulation.

3.4 Boundary conditions

In order to univocally solve the problem, boundary conditions are required. For instance, for the RANS equations the pressure at the inlet and outlet sections is imposed (Table 3). In addition to the pressure condition, at the outlet section also the condition of vanishing viscous stress along the boundary is imposed.

Boundary	RANS	Heat trans.
Inlet	$p = p_{atm}$	$T = T_{ext}$
Outlet	$p = p_{atm} - \rho g H$	$-\hat{n} \cdot (-\lambda \nabla T) = 0$
Wall	$-\hat{n} \cdot u = 0$ Log. wall function	Log. wall function

Table 3 – RANS e heat transfer BC for fluid domain

For the other boundaries, the turbulence close to the solid wall is very different from isotropic free-stream turbulence and this should be taken into account. In this work the adopted approach is the so-called wall functions. In this method, an empirical logarithmic relation between the value of velocity and wall friction replaces the thin boundary layer close to the wall. Then, for the heat transfer problem, the inlet temperature and the convective BC are imposed respectively at the inlet and outlet sections. Similarly, a series of boundary

conditions are imposed also for the solid domain (Table 4).

Boundary	Heat transfer
Internal surface	$-\hat{n} \cdot (-\lambda \nabla T) = h_{int}(T - 20^\circ\text{C})$
External surface	$-\hat{n} \cdot (-\lambda \nabla T) = h_{ext}(T - T_{ext})$
Cut-off	$-\hat{n} \cdot (-\lambda \nabla T) = 0$

Table 4 – Heat transfer BC for solid domain

In particular, while for the internal and external surfaces the Robin-Newton condition is used, for the cut off plane (i.e. the bottom and upper surfaces) the adiabatic conditions are adopted.

4. Results

As a first step in the result analysis the velocity field is herein presented. Figure 3 shows the velocity field and the streamline obtained at the inlet and outlet sections for the case I. The figure clearly shows the stagnant region in the inlet portion of the cavity that produces an increasing velocity on the other side of the ventilation channel. Similarly, due to the narrowing, the air speed increases at the cavity outlet.

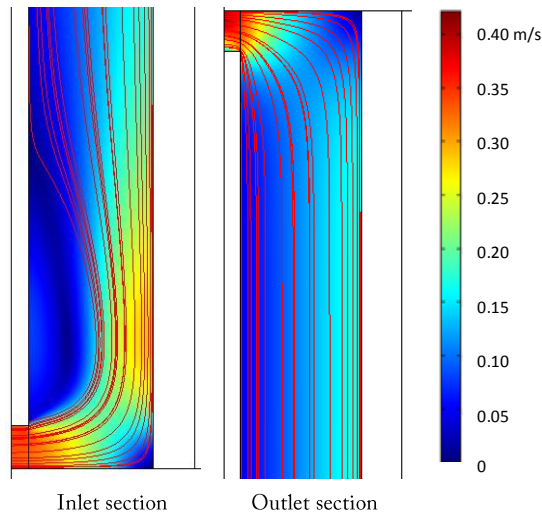


Fig. 3 – Velocity field in the channel at inlet and outlet (case I with $d=15$ cm, $e_2=0.1$ and $T_{ext}=0^\circ\text{C}$)

Besides, it is interesting to note that in areas far from the edge regions, the air speed induced by the stack effect settles around $0.15 - 0.20$ [m s⁻¹].

In the following paragraphs the results of the comparisons between the surface thermal resistances, provided by the annex A of the standard EN ISO 6946, and the values obtained from the post-processing of thermo-fluid dynamics simulations are reported. In particular, starting from the heat flux density computed by means of the finite element method, the surface thermal resistance is computed by means of equation 8.

$$R_{se} = \frac{T_i - T_e}{\phi} - \sum_j \frac{S_j}{\lambda_j} - R_{si} \quad (8)$$

Using this relation for each configuration an equivalent average thermal resistance of the vented cavity are computed. The values obtained are reported in Table 5

Besides, a study of the influence of cavity parameters on the surface thermal resistance is herein presented. In these sections, the way in which the boundary configurations affect the reduction of the surface resistance is analysed. In particular, the parameter investigated are the cavity height, the emissivity of the cavity inner surface, the insulation level of the wall behind the ventilation channel and the inlet air temperature.

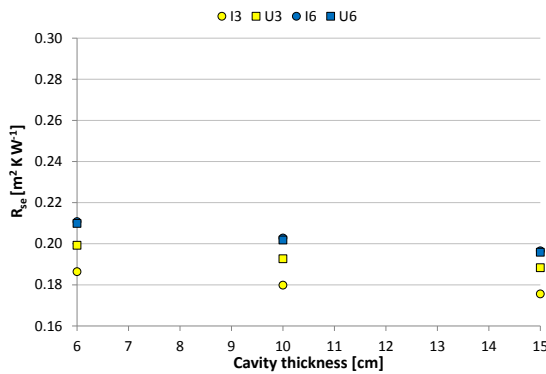
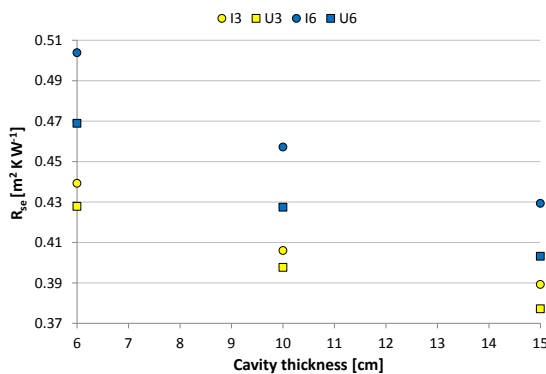
4.1 Effect of cavity thickness

The increasing of cavity thickness induces an adjustment in the air motion characteristics. In fact, air passes from a laminar flow to a transition regime or turbulent motion. Consequently, it also increases the heat transfer between the fluid and the inner cavity surface.

Figure 4 and Figure 5 show respectively the trends of surface thermal resistance as a function of cavity thickness for high and low emissivity of the inner surface. The points names represent the parameters used in the configuration adopted, i.e. insulated (I) or uninsulated (U) wall combined with either 3 or 6 metres of cavity height. Both figures show increasing surface thermal resistance for high cavity height. In fact, the higher the cavity height the lower the influence of inlet and outlet turbulent region. Further, for long ventilation channels, in the top region the temperature difference and, consequently, the convective heat transfer decrease.

		$e_2 = 0.1$				$e_2 = 0.9$			
	T_e [°C]	U3	I3	U6	I6	U3	I3	U6	I6
$d = 6$ cm	-10	0.367	0.374	0.400	0.428	0.199	0.186	0.210	0.211
	-5	0.375	0.383	0.411	0.439	0.198	0.185	0.208	0.209
	0	0.386	0.395	0.424	0.454	0.197	0.184	0.208	0.207
	5	0.401	0.412	0.439	0.472	0.197	0.184	0.208	0.207
	10	0.428	0.439	0.469	0.504	0.199	0.185	0.210	0.210
	15	0.480	0.492	0.534	0.573	0.206	0.185	0.209	0.209
$d = 10$ cm	-10	0.341	0.346	0.365	0.388	0.193	0.180	0.202	0.203
	-5	0.348	0.354	0.374	0.399	0.192	0.179	0.201	0.201
	0	0.358	0.365	0.386	0.413	0.191	0.178	0.201	0.201
	5	0.373	0.381	0.401	0.429	0.191	0.179	0.201	0.201
	10	0.398	0.406	0.427	0.457	0.195	0.182	0.205	0.205
	15	0.453	0.462	0.486	0.520	0.203	0.189	0.213	0.213
$d = 15$ cm	-10	0.327	0.329	0.344	0.365	0.188	0.176	0.196	0.197
	-5	0.333	0.337	0.352	0.374	0.187	0.175	0.197	0.197
	0	0.342	0.349	0.363	0.386	0.187	0.176	0.195	0.195
	5	0.355	0.364	0.378	0.402	0.187	0.176	0.196	0.195
	10	0.377	0.389	0.403	0.429	0.191	0.180	0.196	0.195
	15	0.423	0.441	0.459	0.489	0.200	0.187	0.204	0.203

Table 5 – Surface thermal resistance obtained by thermo fluid-dynamic analysis

Fig. 4 – Surface resistance as a function of cavity thickness ($e_2 = 0.9$ and $T_e = -10^\circ\text{C}$)Fig. 5 – Surface resistance as a function of cavity thickness ($e_2 = 0.1$ and $T_e = -10^\circ\text{C}$)

Similarly the surface equivalent thermal resistance of the cavity decreases for high cavity thickness, as is shown both in figure 4 and in figure 5. Also in this case, the reduction of the average surface equivalent resistance is caused by the increasing vorticity of the air motion.

It should be remarked that the values plotted in Figure 4 and in Figure 5 are in quite a good agreement with the surface resistance obtained by means of the calculation procedure provide by the annex A of EN ISO 6946. In fact, the standard values using an outside temperature of -10°C are $0.170 [\text{m}^2 \text{K W}^{-1}]$ and $0.344 [\text{m}^2 \text{K W}^{-1}]$, respectively adopting an emissivity of 0.9 and 0.1 for the inner cavity surface.

Furthermore, Figure 4 points out the different behaviour between 3 and 6 metres of cavity height. In fact, while no appreciable differences are noted between cases U6 and I6, case I3 shows lower equivalent resistance with respect to case U3. These results suggest that for tall cavities the pressure difference between the outlet and inlet section is the primary cause of the air motion. Therefore, no appreciable variations in the mean air speed are noted even if the surface temperature changes between cases I and U. On the contrary, in short cavities the pressure gradient is limited and

the air motion is mainly induced by the variation of air specific mass. In fact, Figure 4 highlights lower resistance for case I3 where the cavity inner surface temperature is higher. This behaviour is not found, however, when the cavity inner surface has low emissivity (Figure 5). In these configurations, the component of radiative thermal resistance increases and, therefore, the behaviour is closely related to the shape aspect ratio. In addition, despite the high surface temperature, the increase radiative thermal resistance ensure a high thermal resistance in the cases I with respect to uninsulated cases.

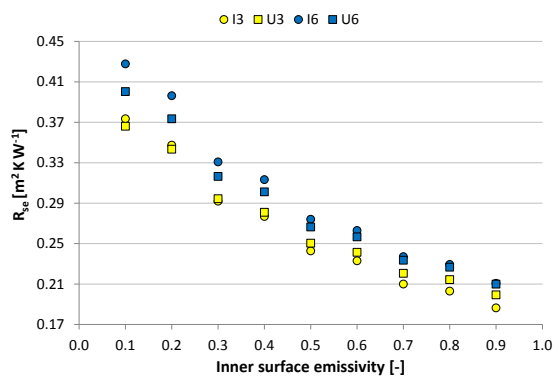


Fig. 6 – Surface resistance as a function of inner surface emissivity ($d = 6$ cm, $T_e = -10^\circ\text{C}$)

These preliminary results therefore show two different behaviours of the vented cavity that are influenced by the surface characteristics and by boundary conditions. These variations are even more visible by analysing the equivalent resistance plotted as a function of the inner surface emissivity of the cavity (Figure 6). In fact low surface emissivity ensures high radiative thermal resistance and higher temperature of the inner surface of the vented channel. However, these high temperatures help the air motion inside the cavity and, consequently, they reduce the convective thermal resistance.

Therefore for 3 metre cavities when the inner surface has emissivity lower than 0.3 despite the higher surface temperature of case I3 that favours the air motion, the low emissivity value coupled with the reduced difference between the fourth powers of the surface temperatures greatly reduce the heat exchange by radiation. Consequently case

I3 shows a value of total equivalent thermal resistance higher than case U3.

On the other hand, if the inner surface emissivity is greater than 0.3, the increase of radiative heat transfer prevails on the reduction of the convective exchange. For this reason, the case U3 shows a total equivalent thermal resistance higher than case I3.

The threshold for the transition between the first and the second behaviour of the ventilation channel will of course depend on the characteristics of the motion and therefore on the cavity shape. For example in Figure 6 it seems that, for the 6 metre length, the transition occurs for emissivity of 0.9. Hence the increasing of the cavity height induces a greater emissivity threshold. In fact, as already pointed out and better described for the velocity profiles (Figure 7), the lower inner surface emissivity favours the motion of the fluid and therefore the convective heat transfer.

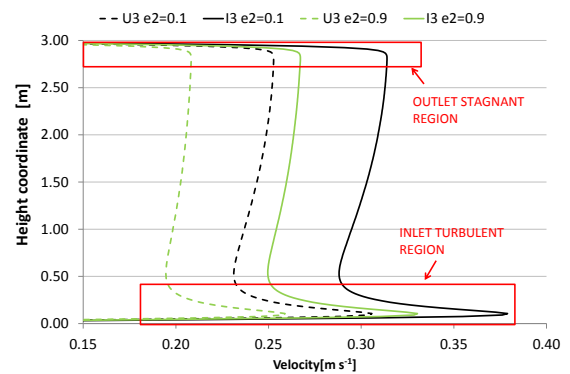


Fig. 7 – Velocity profiles for cases U3 and I3 close to the cavity inner surface.

4.2 Effect of outdoor air temperature

In addition to the cavity thickness and height and to the surface emissivity, also the influence of air temperature on the surface thermal resistance is investigated.

Figure 8 shows the trend of the surface thermal resistance as a function of temperature for the case studies already presented. In addition to this, the graph also shows the surface resistances computed by the method provided in annexe A of the standard EN ISO 6946. The latter considers the dependence of the temperature only in the radiative contribution, while the convective resistance is assumed to be constant.

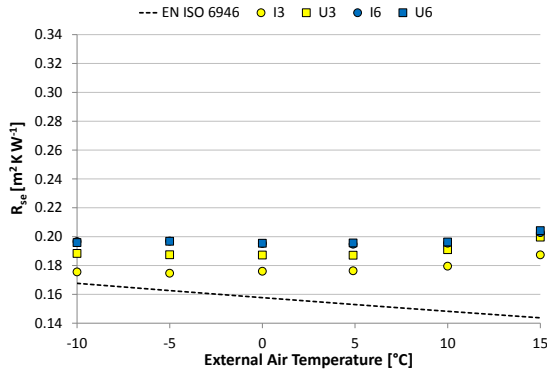


Fig. 8 – Surface resistance as a function of T_e ($d=15$ cm, $e_2=0.9$)

The graph points out a slight underestimation of the resistance computed by means of the standard correlation. This obviously occurs because the convective resistance of the standard takes into account the unfavourable condition of motion caused by wind forces. In this case the higher air velocity in the channel greatly reduces the convective thermal resistance. However, it can be seen that the gap between EN ISO 6949 and thermo-fluid dynamic simulations increases for high external temperatures.

In fact, from the comparison among the data obtained from the thermo-fluid dynamic model a weak dependence of the total thermal resistance on the outdoor temperature emerges. This is probably linked to the compensation between the increase of the convective flow, tied to the higher air velocity, with the decrease of exchange by radiation.

Therefore the standard relation for the calculation of the radiative thermal resistance, obtained by linearizing the equation of the radiative heat exchange, describes in an opposite way the resistance trend linked to temperature variations. This emerges even more clearly if the behaviour of cavity with low emissivity surface is analysed (Figure 9).

Note that while the resistance calculated from the thermo-fluid dynamic analysis tends to increase with an increase in outside temperature, the EN ISO 6946 approach shows a downward trend.

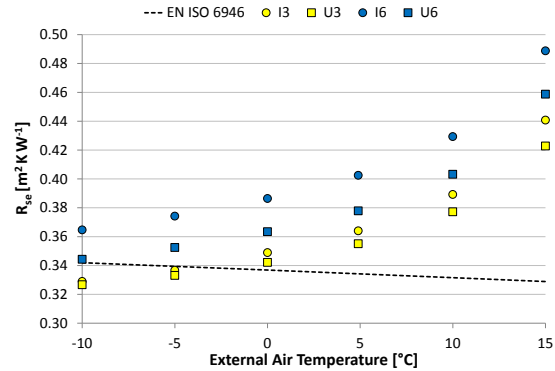


Fig. 9 – Surface resistance as a function of T_e ($d=15$ cm, $e_2=0.1$)

4.3 Resistance data dispersion

Finally, the paper focuses on the analysis of the dispersion of the surface thermal resistances. Assuming the development of a relationship that binds the surface thermal resistance to some parameters such as surface emissivity and cavity thickness, the purpose is to investigate the data dispersion induced by other parameters. Therefore, the spreads in the values caused by the outside air temperature, by the height of the ventilation channel and by the insulation level of the wall behind the cavity are studied.

The simulation results are summarized in the box plot (Figure 10 and Figure 11) where the degree of dispersion and skewness in the distribution are fully described by means of the minimum, lower quartile, median, upper quartile and the maximum of observations.

The graph in Figure 10 shows the box plot obtained for several configurations using an emissivity of the inner surface of the cavity of 0.9. The box plot clearly shows a limited symmetrical dispersion of the data. Only when the thickness is equal to 6 cm, does the distribution assume a slightly asymmetric shape with an approach of the maximum value to the upper quartile. Besides, the difference between various thicknesses seems to be linked to a mere translation of the graph around another median value.

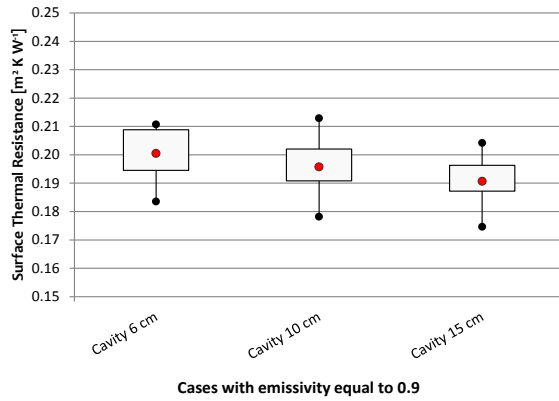


Fig. 10 – Variability of surface thermal resistance.

The distribution features change, however, if the resistance to irradiation increases due to reduced emissivity of the cavity inner surface (Figure 11). The graph indeed shows a high skewness of the distribution for all the thickness analysed. In particular, there is a greater distance between the maximum value and the upper quartile. This is mainly related to the high dependence of the radiative thermal resistance on the temperature. Since in low emissivity cases the ratio of radiative resistance over total thermal resistance increases, this dependency becomes more visible. Moreover, the chart in Figure 11 stresses again the limited dependence of the results variability on the cavity thickness. In fact, when the cavity thickness increases the box plot simply translates to a lower median resistance.

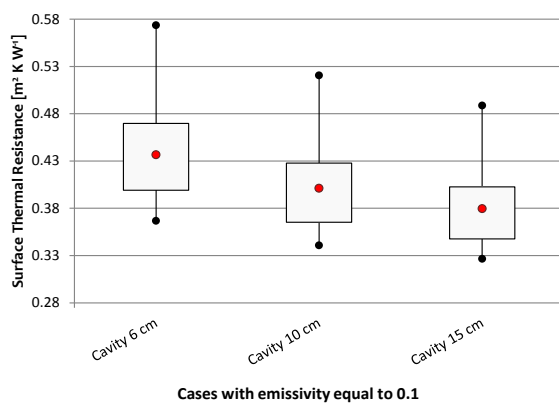


Fig. 11 – Variability of surface thermal resistance.

5. Conclusion

This paper has shown an analysis about the vented cavity behaviour under winter conditions. In particular the energy performances of several configurations are investigated by means of a coupled thermo-fluid dynamics model.

In addition to the cavity behaviour as a function of aspect ratio (e.g. thickness and length of the ventilation channel), the results stress a high dependence on the emissivity of the inner surface of the cavity. Results point out that, due to the higher surface temperature, when the emissivity decreases in insulated walls, the surface resistance increases much faster with respect to uninsulated cases. Therefore, these results highlight the effectiveness of reflective foil coupled with both traditional insulation and ventilation cavity.

Another result obtained regards the variability of the resistance to the boundary temperatures. While for normal emissivity (of the order of 0.9) the resistances show a poor temperature dependence, when the emissivity decreases the total thermal resistance is strictly connected to the boundary temperatures.

Thus, for these cases the simplified approach for the surface resistance calculation should be refined. In fact, an incorrect modelling of the thermal resistance trend caused by the outside temperature emerges from the comparison between the simplified approach of the standard EN ISO 6946 and enhanced calculation method. However, it should be stressed that in insulated walls the contribution of the ventilated cavity on the total thermal resistance is smoothed over by the insulating layers. Consequently, the dispersion of surface thermal resistance may have a limited effect on the energy demands.

In conclusion, this work has enabled us to deepen our understanding of the mechanisms of heat transfer in the ventilated cavity under steady state conditions. In future developments, this model can be applied to transient regimes in order to evaluate the behaviour under real external conditions.

6. Nomenclature

Symbols

F	Volume force vector [N m^{-3}]
H	Cavity height [m]
I	Identity tensor [-]
T	Temperature [K]
c_p	Specific heat [$\text{J kg}^{-1} \text{K}^{-1}$]
d	Cavity thickness [cm]
ϵ_2	Emissivity of the internal surface of the ventilated channel [-]
f	Decrement factor [-]
g	Gravity acceleration constant [m s^{-2}]
k	Turbulent kinetic energy
\hat{n}	Surface normal versor [-]
p	Pressure [Pa]
s	Thickness [m]
t	time [s]
u	Vector of velocity [m s^{-1}]

Greek

ϕ	Specific heat flux [W m^{-2}]
ε	Turbulent kinetic energy dissipation rate [-]
η	Dynamic viscosity [Pa s]
λ	Thermal conductivity [$\text{W m}^{-1} \text{K}^{-1}$]
ρ	Specific mass [kg m^{-3}]

Subscripts/Superscripts

0	initial condition
i	internal side of the sample
e	external side of the sample
s	referred to surface quantities
T	referred to turbulent quantity

References

CEN 2008. EN ISO 6946:2008, Building components and building elements - Thermal resistance and thermal transmittance -Calculation method

Ciampi, M., Tuoni, G. 1998. Periodic heat flow through ventilated walls. *La Termotecnica*, 9, p. 79-87

Ciampi, M., Leccese, F., Tuoni, G. 2003. Ventilated facades energy performance in summer cooling of buildings. *Solar Energy*, 75, p. 491-502

Falk, J. Sandin, K., 2012. Ventilated rain screen cladding: Measurements of cavity air velocity estimation of air change rates and evaluation of driving forces. *Building and Environment*.

Gagliano, A., Patania, F., Nocera, F., Ferlito, A., Galesi, A. 2012. Thermal performance of ventilated roofs during summer period. *Energy and Buildings*, 49, p. 611-618

Gan, G., 2010. Simulation of buoyancy-driven natural ventilation of buildings—Impact of computational domain. *Energy and Buildings*, 42, p. 1290–1300

Hauke, G., 2002. A simple subgrid scale stabilized method for the advection-diffusion-reaction equation, *Computer Methods in Applied Mechanics and Engineering*, 191, p. 2925-2947

Nore, K. Blocken, B. Thue, J.V., 2010. On CFD simulation of wind-induced airflow in narrow ventilated façade cavities: Coupled and decoupled simulations and modeling limitations. *Building and Environment*, 45, p. 1834-1846

Pasut, W., De Carli, M., 2012. Evaluation of various CFD modeling strategies in prediction airflow and temperature in a naturally ventilated double skin facade. *Applied thermal engineering*, 37, p. 267-274

Susanti, L., Hommab, H. , Matsumoto, H. , Suzuki, Y. , Shimizu, M., 2008. A laboratory experiment on natural ventilation through a roof cavity for reduction of solar heat gain. *Energy and Buildings*, 40, p. 2196–220

GA-optimisation of a curtain wall façade for different orientations and climates

Debora Bogar – Università degli Studi di Udine, Udine, Italy

Gianluca Rapone – Ove Arup & Partners Ltd, London, United Kingdom

Ardeshir Mahdavi – Technische Universität Wien, Vienna, Austria

Onorio Saro – Università degli Studi di Udine, Udine, Italy

Abstract

The importance of considering the environmental performance of buildings since the conceptual stages of the design process is growing as a consequence of the restrictive requirements of building regulations and energy certification. The building envelope plays a central role in controlling the thermal, the acoustic and the light flows exchanged between the indoor and the external environment. Therefore designing a good façade system and installing it properly is fundamental to increase the overall performance of the building.

This study focused on a modular curtain wall façade that can integrate photovoltaic panels on its opaque areas. The aim was to identify the layouts that minimise total cost, calculated as the sum of investment and operation costs, and at the same time maximise daylighting in the rooms. The methodology consisted in a simulation based multi-objective optimisation solved by means of Genetic Algorithms, whose behaviour is inspired by Darwin's Theory of Evolution.

An office room was modelled and its façade divided into twelve modules of equal size, two of which were fixed glazed elements and the remaining ten having three possible construction types: glazing, spandrel or photovoltaic elements. The optimisation process assigned a specific construction to each of the ten modules in order to obtain a set of façade layouts that fulfill both objective functions. Different climatic scenarios and orientations were considered.

The dynamic thermal simulations were carried out with *EnergyPlus* while the optimisation employed a modified version of the widely used NSGA-II Genetic Algorithm. A custom-made software was written in *Matlab* in order to interface the simulation and optimisation processes, to automate their interaction and to make the input of the problem's parameters easier through a graphical user interface.

1. Introduction

The façade plays a key role in the design of buildings that need to meet strict requirements of energy efficiency and provide internal comfort conditions at the same time. In air-conditioned buildings, and especially in office buildings that have highly glazed curtain wall façades, the energy consumption levels for heating, cooling and artificial lighting strongly depend on solar exposure and on the performance of the building envelope. The latter is responsible for heat losses, solar heat gains and it allows for daylighting. The design of a good façade is a very challenging task because of the complicated interactions between the various parameters involved.

Traditionally different variable assignments on building operation were compared by parametric studies, often employing dynamic energy simulation programs. In this study an automated search for one or more optimal solutions is performed through a procedure that couples an optimisation program to a simulation program. This solving method is known as simulation based optimisation.

In the field of building design, the simulation can be carried out by any program that can evaluate a model of the object under study, such as available dynamic energy simulation programs (*EnergyPlus*, *TRNSYS*, etc.). The optimisation is usually based on evolutionary algorithms, a family of population based probabilistic algorithms that proved to be suitable in solving problems where the objective function is calculated by external simulation programs.

A Genetic Algorithm (GA) and an artificial neural network were used in a multi-objective optimisation in order to find envelope and HVAC parameters that minimise energy consumption and guarantee the internal comfort at the same time (Magnier et al., 2010). Particle swarm (PSO) algorithms were applied to optimise life-cycle cost of a single detached house in Finland (Hasan et al., 2008).

Narrowing down to envelopes, some authors focused on residential buildings optimising the size of windows (Caldas et al., 2002), some considered the characteristics of the envelope (Znouda E. et al., 2007) and others took into account also the shape of the building (Tuhus-Dubrow D. et al., 2010).

In the present work the layouts of a curtain wall façade of an office building that optimise cost and at the same time guarantee good daylight provision are researched. This is accomplished by coupling an open source dynamic energy simulation program, *EnergyPlus*, to a NSGA-II Genetic Algorithms implemented in *Matlab*. A specific program, *ePlusOpt*, was written to couple *EnergyPlus* and *Matlab* and a graphical user interface was created to simplify its use.

2. Optimisation

2.1 Mathematical background

Optimisation is a process aimed at finding the best solutions of a problem by means of minimising (or maximising) one or more objective functions that describe the problem itself. The procedure comprises a model of the problem and an optimisation algorithm that minimises the objective function. The optimisation model comprehends variables, constraints and the aforementioned objective function.

When conflicting aims need to be satisfied at the same time, a single objective function is not enough to describe the problem. In this case, a multi-objective optimisation made up by two or more objective functions must be set up.

In mathematical terms, a multi-objective problem can be written as:

$$\begin{aligned} \Omega &\subset \mathbb{R}^n \times \mathbb{R}^n && \text{parameter space} \\ Z &\subset \mathbb{R}^k \times \mathbb{R}^k \subset \mathbb{R}^n && \text{image of } X \\ \mathbf{x} &\in \Omega && \text{vector of decision variables} \\ \mathbf{z} &= F(\mathbf{x}) && \text{performance vector} \end{aligned}$$

The problem has no unique solution and the concept of non-inferiority (Zadeh, 1963), also known as Pareto optimality (Censor, 1977), must be introduced to characterize the objectives. A non-inferior solution is one in which an improvement in one objective requires a degradation of another. A point $\mathbf{z}^* \in \Omega$ is defined as a non-inferior solution if for some neighbourhood of \mathbf{x}^* there does not exist a $\Delta \mathbf{x}$ such that:

$$\begin{aligned} (\mathbf{x}^* + \Delta \mathbf{x}) &\in \Omega \\ F_i(\mathbf{x}^* + \Delta \mathbf{x}) &\leq F_i(\mathbf{x}^*), i=1, \dots, m \quad \square \\ F_j(\mathbf{x}^* + \Delta \mathbf{x}) &< F_j(\mathbf{x}^*), \text{ for at least one } j. \end{aligned}$$

Multi-objective optimisation is concerned with the generation and selection of non-inferior solution points, also called Pareto optima.

2.2 Genetic Algorithms

In simulation based optimisation, where external dynamic simulations are employed to compute the value of the objective function, the latter is highly discontinuous and non-differentiable. Evolutionary algorithms have proved to be particularly suitable in this field and they offer the additional advantage of their capability in handling huge amounts of variables and potential solutions (Wetter & Wright, 2004). Genetic algorithms are part of this family of population-based probabilistic methods. Their behaviour is inspired by the biological evolution, based on natural selection and genetic recombination. A population of individuals, possible solutions, is first randomly generated and then repeatedly modified through genetic operators (selection, crossover and mutation). At each step, the GA selects individuals with the best fitness function value from the current population to be parents of the children for the next generation. Over successive generations, the population evolves toward an optimal solution.

2.3 ePlusOpt

In optimisation problems where the value of the objective function depends on the results obtained by an external simulation program, there is the need to configure the correct communication between the latter and the optimisation solver. To simplify and to automate this operation a specific program, named *ePlusOpt*, that couples *EnergyPlus* and *Matlab* was developed.

Given that the user has already prepared the energy simulation model to be employed for the dynamic thermal simulations, *ePlusOpt* guarantees the communication between the GA in *Matlab* and the *EnergyPlus* software through a series of functions and scripts. The core of this interaction happens inside the fitness function, which is called by the GA to compute the objectives of the optimisation.

The combination of the variables encoded in the chromosome of each individual is passed to a function that writes them inside a data set that is part of the energy model used for the simulations. Subsequently another function starts the simulation of the updated input file by calling the *EnergyPlus* executable file. When the simulation ends and the output files are produced, a third function retrieves from them the values of the output variables that were requested by the user. The fitness function finally uses these values to compute the objective(s). Figure 1 shows how these interactions work.

A graphical user interface was programmed to make the definition of an optimisation process and the management of the data easier and faster.

A standard version of the NSGA-II was modified by supplying some bespoke functions in order to make it work with a custom-built data type.

For more details about the routines and the interaction between the two programs, see Rapone, 2011.

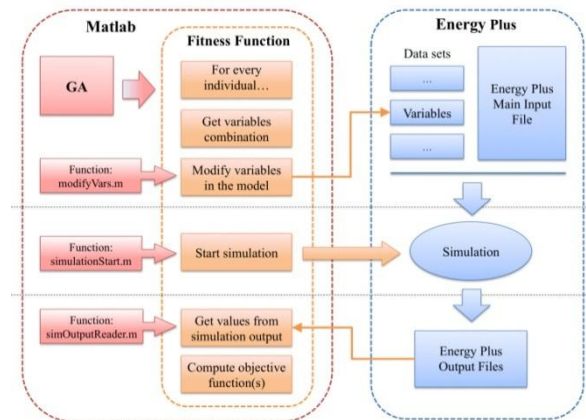


Fig. 1 – Coupling of the GA and EnergyPlus

3. Case study

To prove the effectiveness of *ePlusOpt*, a curtain wall façade of an office room was optimised in order to find the layouts that guarantee minimum total cost and maximum daylighting at the same time.

To see how climate and tariffs affect the results, additional optimisations were carried out for different European countries.

3.1 Thermal model

An *EnergyPlus* thermal model of an office room was built and used for the simulation based optimisation.

The room has a floor area of 50 m² and an overall height of 4.1 m. It is placed in the corner of an intermediate floor, so it has two sides facing outside. Both the internal partitions in plasterboard and the floors in reinforced concrete are modelled as adiabatic (Table 1); the smaller façade facing outdoors is completely opaque with a thermal transmittance of 0.25 W/m²K. The main façade is a curtain wall façade modelled with a backing surface that embodies the behaviour of the aluminium frames of the curtain wall units. The thermal transmittance of this part is a mean value of the real transmittance of the frames, calculated as 4.2 W/m²K. All modules are sub-surfaces cut-out in this backing surface, with characteristics described in the following paragraph.

Two reference points positioned at desk level

inside the room, as pictured in Figure 2, are used to control the daylighting in the zone. Based on the levels of daylight coming in from the windows, they trigger the use of artificial lights in the room. When the glare index is greater than 22 the venetian blinds are closed automatically.

The plant system is considered to have unlimited capacity and can thus always maintain the required setpoint temperatures during the periods of peak heating and cooling loads.

The overall annual efficiency of the heating system is assumed to be 0.8, while for the coefficient of performance of the cooling system a value of 2.5 is taken. Other properties of HVAC system are shown in Table 2 together with the internal gains.

The simulations were carried out for a year time period using the weather files downloadable from the U.S. Energy Department's website.

Floors				
Layer	c_v [J/kg K]	ρ [kg/m ³]	λ [W/mK]	s [m]
Concrete slab	1000	2000	1.13	0.25
Double ceiling (plasterboard)	840	950	0.16	0.025
Double floor (tile)	800	1900	0.84	0.025
Internal Partitions				
Layer	c_v [J/kg K]	ρ [kg/m ³]	λ [W/mK]	s [m]
Plasterboard	840	950	0.16	0.025

Table 1 – Properties of adiabatic walls and floors

INTERNAL GAINS		VALUE
People (max 6 people)		126 W/person
Electric equipment		15W/m ²
Lights		8 W/m ²
HVAC SYSTEM		VALUE
Infiltration		0.15 ach
Mechanical ventilation		max 1 ach
Heating setpoint / setback		20°C / 12°C
Cooling setpoint / setback		25°C / 32°C

Table 2 – Model assumption: internal gains and HVAC system

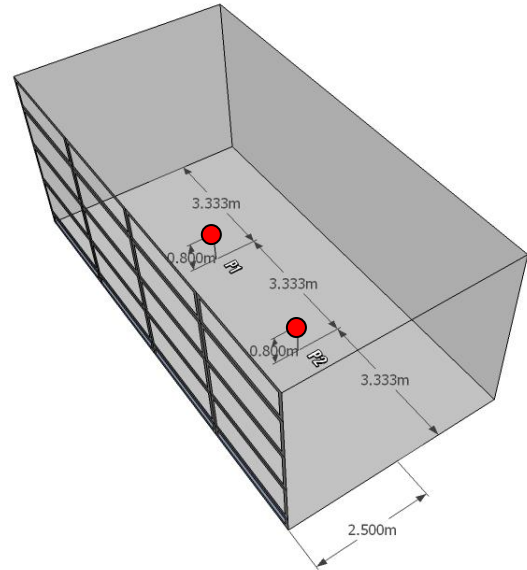


Fig. 2 – Disposition of daylighting reference points in the model

3.2 Façade description and variables

The assembly of the main façade, sketched out in Figure 3, consists in a central area made up of variable panels and in two strips of spandrel panels covering the service spaces above and below.

The central area is subdivided in three rows and four columns, thus generating a grid of twelve equal modules with an area of 2.5 m² each. The two central ones were assumed to be fixed and glazed in order to provide a minimum window area that corresponds to 10% of the floor area, while the other ten modules were allowed to vary and consist in any of the three following construction types:

- Spandrel panel

The construction is that of a simple opaque panel consisting in an outer cladding layer, an insulation layer and a vapour barrier followed by an internal gypsum board (see Table 4). Since the climate changes for every city, the thickness of the insulation is calculated according to the limit of U-value imposed by national energy building codes. The thickness values adopted are shown in Table 3.

- Glazed panel

It is constituted by a double glazed unit with a clear internal glass pane and an

external pane with a solar control coating. The thermal, solar and visual characteristics are reported in Table 5.

- Photovoltaic Panel

The BiPV panels construction is the same as the spandrel panel with the addition of the layer containing polycrystalline silicon photovoltaic cells on the external surface (see Table 4). The efficiency of the cells is assumed to be 14%.

The PV panels are modelled in *EnergyPlus* with objects that simply apply their overall energy conversion efficiency to the incident solar radiation. They are then connected to an *inverter* object with an efficiency of 0.9.

COUNTRY	Insulation thickness [m]	LAW
Austria	0.15	OIB RICHTLINIE 2008
Germany	0.18	EnEV 2009
Greece	0.08	B 407/2010
Italy	0.13	DM 26/01/2010
Spain	0.06	Ahorro de Energia
UK	0.15	Building Regulations 2010

Table 3 – Insulation thickness

SPANDREL PANEL				
Layer	c_v [J/kg K]	ρ [kg/m ³]	λ [W/mK]	S [m]
Cladding	840	2500	0.7	0.015
Insulation	840	80	0.04	0.15
Gypsum board	830	785	0.16	0.015
PV PANEL				
Layer	c_v [J/kg K]	ρ [kg/m ³]	λ [W/mK]	S [m]
PV cells	840	2700	0.78	0.010
Insulation	840	80	0.04	0.15
Gypsum board	830	785	0.16	0.015

Table 4 – Panels properties

U-VALUE	g-VALUE	LT
1.14 W/m ² K	0.58	75%

Table 5 - Characteristics of the glazing modelled

Ten variable modules that can assume three different values means that the possible combinations are $3^{10} = 59049$. To increase the daylighting a rule was implemented in the algorithm so that when glazed panels are present, they are first positioned in the two upper rows and only subsequently in the lower one.

A base configuration where all the variable modules were chosen to be simple spandrel panels was taken as reference case. The energy consumption levels for space heating, cooling and artificial lights stemming from the energy simulation of this case were recorded to be later compared with the ones arising from all other possible compositions generated during the optimisation process.

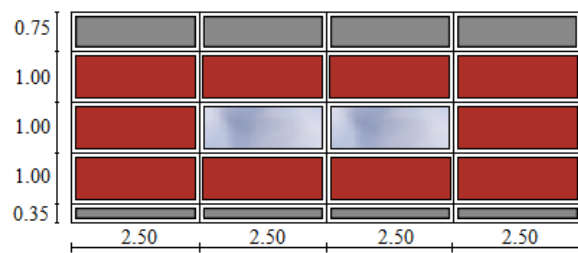


Fig. 3 – Layout of the curtain wall façade

3.3 Algorithm properties

As a result of a sensitivity analysis done by applying different algorithm properties to the same case study, the optimisations are performed with a population of 30 individuals and each process is repeated for 20 generations. The elite children are two and the cross-over fraction is 0.8.

3.4 Objective functions

The double-objective optimisation aim is to investigate the trade-off between the costs related to the improvement of the façade and the daylighting performance.

The first objective function is defined by the sum of investment and operation costs to be faced when upgrading the reference façade with more glazed panels or with building integrated photovoltaics:

$$F_1 = C_{tot} = C_{inv} + C_{op} \quad (1)$$

The investment costs are estimated as:

$$C_{inv} = n_G \cdot p_G + n_{PV} \cdot p_{PV} \quad (2)$$

The differential costs between spandrel modules and the other panels taken in account are estimated by averaging product prices in European countries. The assumptions made are shown in Table 6.

Replacement of a spandrel panel	price
With a glazed panel	+200€
With a PV panel	+600€

Table 6 – Prices assumptions

The operation costs are evaluated in 20 years as:

$$C_{op} = UPV^* \cdot [dE_{heat} \cdot t_{gas} + (dE_{cool} + dE_{lights}) \cdot t_{el}] - 20 \cdot E_{PV} \cdot t_{feed} \quad (3)$$

The electricity produced by PV panels as well as the energy consumption are retrieved from *EnergyPlus* output files. Then the differential energy demands between the reference case and the other possible façade layouts are calculated in *Matlab*. The values obtained are multiplied for the energy tariffs: natural gas (used for space heating) and electricity (used for space cooling and artificial lighting) prices are taken from Eurostat 2012 (except gas rates for Athens, taken from www.aerioattikis.gr). The energy rates are reported in Table 7.

The feed-in tariffs are taken from current national standards; the values are shown in Table 8.

The operating costs are considered for a period of twenty years in order to correspond to the average duration of the feed-in contracts for PV production prefigured by national laws. Since the feed-in tariff value is guaranteed during this period, the yearly savings arising from PV energy production are just multiplied by twenty. On the other hand, the yearly operation costs cannot be considered constant over the years because the energy prices are likely to rise during a twenty year period. Besides, since the evaluation of the costs is done at the present time, there is the need to calculate the present value of these non-uniform amounts

recurring over the period considered. Hence, using life-cycle cost analysis concepts, the modified uniform present value factor is calculated with the following formula:

$$UPV^* = \frac{1+e}{d-e} \cdot \left[1 - \left(\frac{1+e}{1+d} \right)^y \right] = 18.08 \quad 4)$$

where the assumed real interest rate d is 3% and the escalation in energy price is 2%.

COUNTRY	Gas tariff [€/kWh]	Electricity tariff [€/kWh]
Austria	0.072	0.197
Germany	0.064	0.253
Greece	0.078	0.124
Italy	0.088	0.208
Spain	0.054	0.209
UK	0.052	0.158

Table 7 – Natural gas and electricity tariffs (including taxes)

COUNTRY	tariff [€/kWh]	Years	LAW
Austria	0.276	13	ÖSET-VO 2012
Germany	0.243	20	EEG 2012
Greece	0.305	20	3468/2006 and adjournments
Italy	0.282	20	V Conto Energia
Spain	0.3357	25	BOE num.315, p.146709
UK	0.22	20	Energy Act

Table 8 – Feed-in tariffs

The second objective function is an indicator of daylighting performance: the number of hours during a whole year in which the illuminance in both reference points is higher than the target value of 500 lux. This is a straightforward approach to evaluate the quantity of daylight entering the room, as it is directly related to the number and position of glazing panels on the façade. The minus sign is used because the aim is to maximise this amount of hours.

$$F_2 = - h_{ill>500} \quad (5)$$

4. Results

Optimisations were run for every city and every orientation in order to explore how climate and tariffs affect the results. At the end of each process a set of twelve solutions is found (in some cases two or more solutions are coincident). The results obtained for every city together with the Pareto front, represented as a polynomial trend line, are shown in Figures 4-9. In all countries, despite the differences in climate and feed-in tariffs, the best benefits are achieved for the southern orientation: most of the results suggest the use photovoltaic panels and this is why the Pareto front reaches towards higher gains. Furthermore, southern exposures, likewise western ones, guarantee a high number of hours when daylight exceeds the target value of 500lux. On the contrary, the Pareto front resulting for the northern orientation is narrow.

The total 288 possible layouts found are not reported in detail but the properties of an “average solution” of each case study are shown in Figures 10-12.

These solutions were worked out by averaging the characteristics (panel typology, energy demands and costs) of the twelve solutions obtained for each orientation in each city.

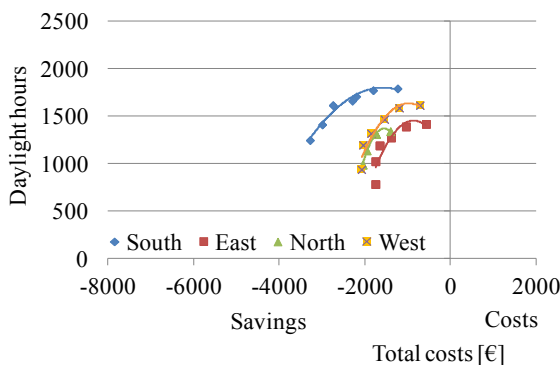


Fig. 4 – Results obtained for Berlin

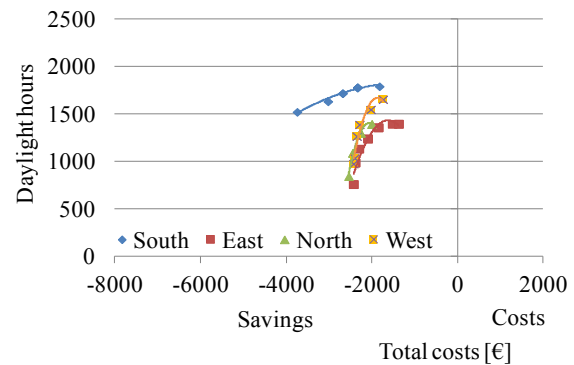


Fig. 5 – Results obtained for London

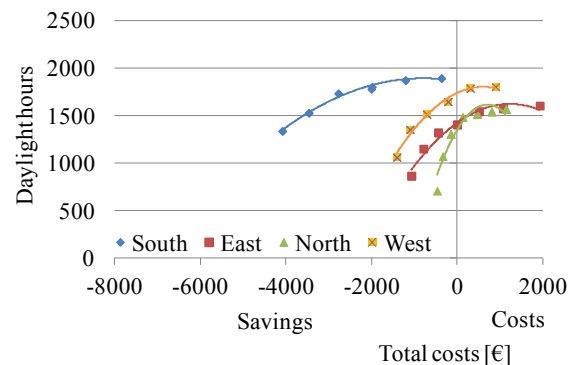


Fig. 6 – Results obtained for Vienna

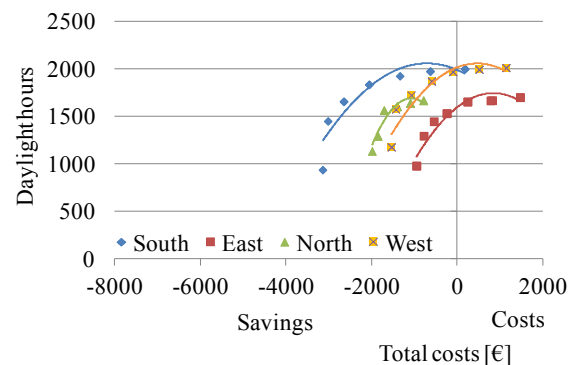


Fig. 7 – Results obtained for Rome

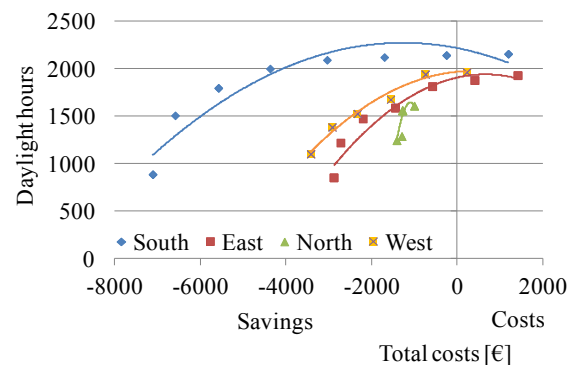


Fig. 8 – Results obtained for Madrid

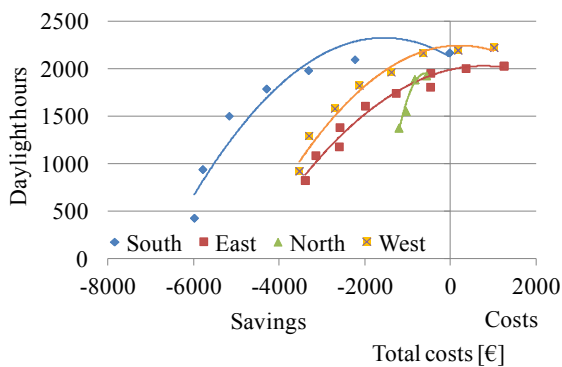


Fig. 9 – Results obtained for Athens

The average number of each kind of module assigned by every optimisation is shown in Figure 10. As expected, the number of photovoltaic panels strongly depends on climate, exposure and tariffs. It is remarkable that the results of all optimisation processes suggest the installation of additional glazed panels compared to the reference case.

The number of spandrels modules that should be replaced by glazed ones varies, on average, from 3 (Athens, southern exposure) to 6 (Rome, northern exposure).

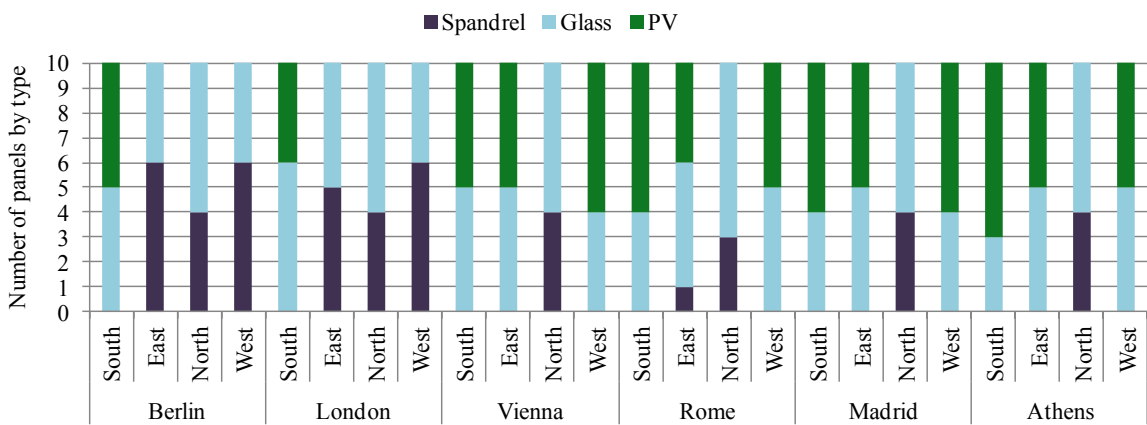


Fig. 10 – Average number of each kind of module assigned in the set of twelve solutions

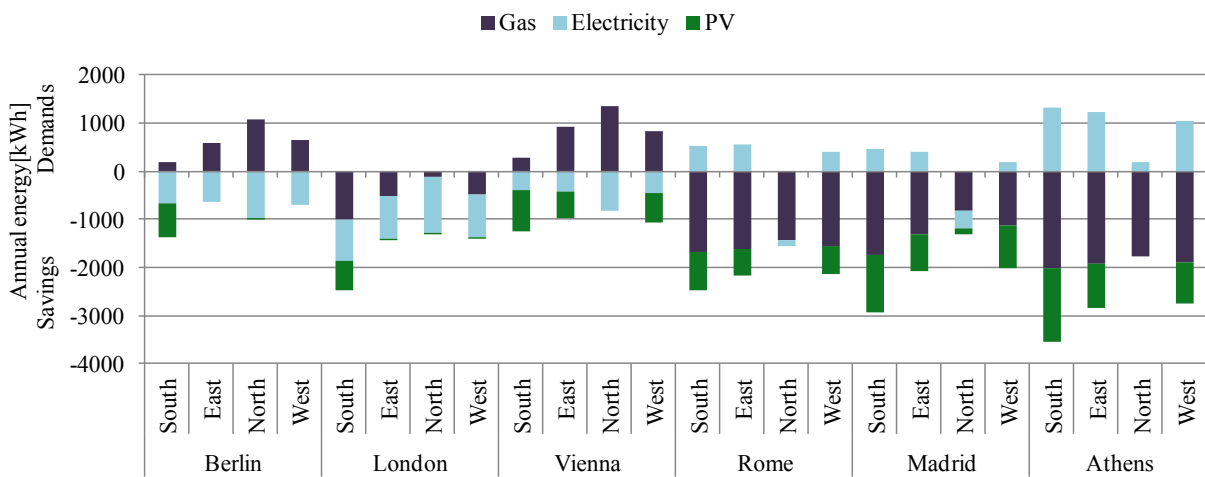


Fig. 11 – Average annual energy demands and savings (compared to reference case)

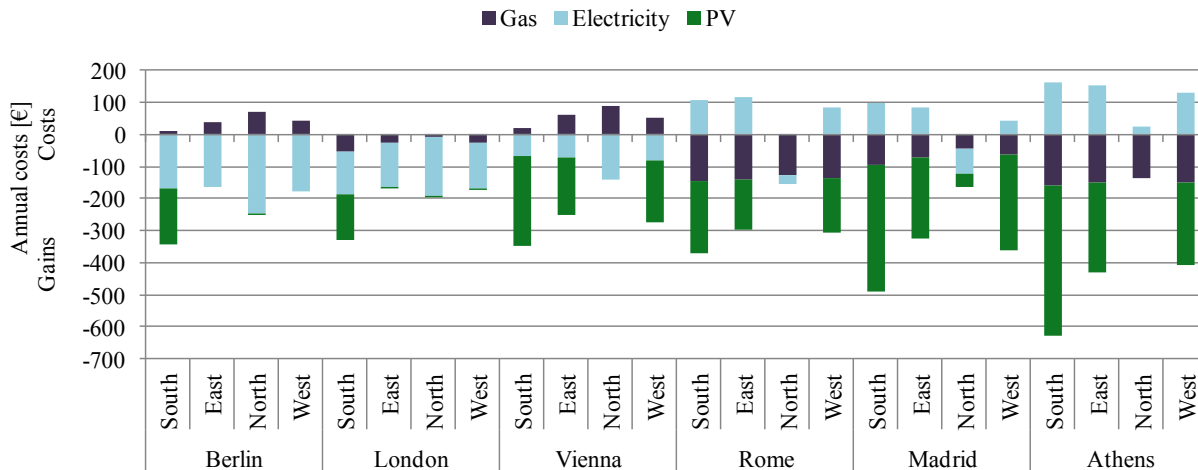


Fig. 12 – Average annual costs (compared to reference case)

Energy consumption and the related costs are displayed in figures 11 and 12. The comparison of the results underlines that choosing one of the optimal solutions in hot climates allows achieving more savings for heating, which means lower yearly natural gas costs. On the other hand, the layouts suggested for cold climates guarantee lower consumptions for cooling, then less electricity costs.

All solutions with improved daylight, besides the advantages they bring in terms of visual comfort, also help cutting the energy consumption related to artificial lights, which has a positive impact on electricity costs.

5. Conclusions

In this paper an optimisation-simulation tool developed in *Matlab*, *ePlusOpt*, is presented. Its main feature is the automatic integration within the optimisation process of energy simulations to be performed with *EnergyPlus*.

The program was employed to carry out optimisations of a curtain wall façade of an office room placed in different climates. The aim of the study was to find the façade layouts that minimise costs and maximise daylight by varying the type of panels installed. The optimised solutions found provide diverse design alternatives, as they represent different trade-offs between the two objectives.

The encouraging results found for the case studies confirm that simulation based optimisation can be a valuable instrument in the early design stages of energy efficient façades because it can provide a number of optimised solutions to be presented to the decision makers for the ultimate choice. Moreover, the developed program *ePlusOpt*, thanks to its graphical user interface and the automatic coupling of the programs, has proven to be a good tool to set up and carry out simulation based optimisation processes.

6. Nomenclature

Symbols

c_v	specific heat capacity (J/kg K)
ρ	density (kg/m ³)
λ	conductivity (W/mK)
s	thickness (m)
F	objective function
c	cost (€)
n	number (-)
p	price of replacement (€)
a	side length (m)
dE	differential energy consumptions
E	energy produced
t	Tariff
UPV^*	modified uniform present value factor
e	escalation in energy price
d	real interest rate
y	number of years
h	Hours

Subscripts/Superscripts

1	first objective function (€)
2	second objective function (hr)
in	Investment
tot	Total
op	Operation
G	Glazed
PV	Photovoltaic
heat	Heating
cool	Cooling
lights	artificial lights
gas	natural gas
el	Electricity
feed	feed-in
ill>500	illuminance greater than 500 lux

References

- Caldas LG., Norford LK. 2002. A design optimization tool based on a genetic algorithm, *Automation in Construction*, Volume , pp. 173-84.
- Censor Y. 1977. Pareto Optimality in Multiobjective Problems. *Applied Math Optimization*, Vol. 4, pp 41–59,
- Hasan A, Vuolle M, Siren K. 2008. Minimisation of life cycle cost of a detached house using combined simulation and optimisation, *Building and Environment*, Volume 43(12), pp. 2022-34.
- Magnier L., Haghighat F. March 2010. Multiobjective optimization of building design using TRNSYS simulations, genetic algorithm, and Artificial Neural Network, *Energy and Buildings*, Volume 45, Number 3, pp. 739-746.
- Rapone G. 2011. Optimisation of office building façades by mean of genetic algorithms. PhD thesis, University of Udine.
- Tuhus-Dubrow D., Krarti M. 2010. Genetic algorithm based approach to optimize building envelope design for residential buildings, *Building and Environment*, Volume 45, pp. 1574-81.
- Various authors. 2012. Household electricity prices in EU27 rose by 6.3% and gas prices by 12.6%, *Eurostat News release*, 78/2012.
- Wetter M, Wright J. 2004. A comparison of deterministic and probabilistic optimization algorithms for non-smooth, simulation-based optimization. *Building and Environment*, Volume 39, pp. 989-99.
- Zadeh L.A. 1963. Optimality and Nonscalar-Valued Performance Criteria. *IEEE Trans. Automat. Contr.*, Vol. AC-8, p. 1.
- Znouda E, Ghrab-Morcos N, Hadj-Alouane A. 2007. Optimization of Mediterranean buildings design using genetic algorithms, *Energy and Buildings*, Volume 39, pp. 148-53.

Use of PCM materials for the reduction of thermal energy requirements in buildings

Francesco Reda – University of Calabria, Arcavacata di Rende, Italy

Domenico Mazzeo – University of Calabria, Arcavacata di Rende, Italy

Natale Arcuri – University of Calabria, Arcavacata di Rende, Italy

Roberto Bruno – University of Calabria, Arcavacata di Rende, Italy

Abstract

The well-known insulation techniques of the building shell, if on the one hand ensure a reduction of energy requirements for winter heating, do not always allow a decrease in energy demand for the cooling of indoor environments and, in some cases, they cause an increase in thermal cooling requirements. For this reason it is necessary to use innovative passive techniques, which in summer are able to mitigate the indoor air temperature, thus limiting the use of air-conditioning plants, while in winter they contribute to achieving energy savings. Among the solutions recently introduced to reduce the buildings' energy requirements are the phase-change materials or PCMs. These are thermal storage materials with low melting/solidification temperature, able to store and release heat during the phenomena of phase transition, limiting the indoor air temperature variations within a building. The PCM, placed in the walls, floors or ceilings, limiting thermal fluctuations also allows a more rational use of the heat gains. Use of PMCs in summer, especially in locations characterized by a Mediterranean climate where the thermal energy requirement for cooling are comparable to those for heating is suggested.

In this work, through the use of the simulation code TRNSYS vs. 17, the efficacy of current insulation techniques combined with the benefits obtained with the use of PCMs is evaluated, through analysis conducted on an existing building sample.

The effects of a layer of PCM mounted on the internal vertical and horizontal opaque walls are investigated. A preliminary phase in order to achieve the best PCM melting temperature as a function of the conditioning season was conducted.

The influence of the thickness of PMC on reducing energy requirement in winter and summer has also been investigated.

The study, quantifying the reduction of building sample energy requirement respect to the case of the same building without PMC, has unequivocally confirmed that the PCMs represent an innovative technological solution to be used both in the existing building and on new buildings. In Mediterranean-type climate contexts, the most obvious benefits are found in the summer, and their use contributes substantially to the reduction of pollution produced by the residential sector.

1. Introduction

The building sector has become (together with the industrial sector) the world dominant energy consumer with 28% of worldwide energy consumption (Sarlos et al., 2003). As a consequence of the thermal comfort rise, the energy consumption is increasing. Housing and tertiary buildings consume about 46% of all energies and they are responsible for about 19% of the total CO₂ emissions (Climate plan, 2004). Referring to the building stock, buildings built before the emanation of restraining energy laws make up the largest part. An easy and economical solution in order to achieve energy savings consists of utilizing thermal storage. Thermal energy storage for space heating and cooling of buildings is becoming increasingly important due to the rising cost of fossil fuels and to environmental concerns. Conventional walls can be seen as sensible heat storages and they have been used for centuries by builders to store/release passively thermal energy, but a much larger volume of material is required to store the same amount of energy in comparison to latent heat storages. Storage of latent heat is

achievable by materials having low fusion/solidification points named Phase Change Materials (PCM). In particular, the thermal storage is obtainable by their fusion while the energy recovery by their freezing. Several studies have analyzed the use of PCM for building retrofitting to obtain an effective way to improve indoor thermal comfort, to reduce energy consumption and to alleviate the negative effect in the atmospheric environment (Athienitis et al., 1997; Banu et al., 1998; Rudd, 1993; Sary et al., 2001; Feldman et al., 1991; Dimaano et al., 1998; Feldman et al., 1995; Feldman et al., 1989; Ahmet et al., 2003). The utilization of latent heat storage, over a comfortable indoor temperature range in buildings, can result in an increase of the thermal storage capacity in the range of 100-130 % (Feldman et al., 1991; Feldman et al., 1989; Feldman et al., 1989; Hawes, 1991). The main disadvantage of light weight buildings is their low thermal mass. Obviously, they tend to large temperature fluctuations due to external conditions, solar gains and internal loads. Using PCM material in such buildings' walls can decrease the indoor air temperature fluctuations, particularly in cases of high solar radiations loads. Consequently it is a potential method for reducing energy consumption in passively designed buildings. This tendency is confirmed by numerous papers available in the literature during the last 20 years concerning the use of PCM in external walls (Tyagi et al., 2007; Khudhair et al., 2004; Zhang et al., 2007; Kuznik et al., Kuznik et al., 2009).

There are few studies on the PCM mounted on internal partitions (ceilings and vertical walls). Kuznik et al. in 2011 tested two identical rooms of a renovated tertiary building: one equipped with PCM wallboard and the other conventionally renovated, showing a real enhancement of occupant thermal comfort. This improvement can be very efficient if the building before renovation is a low thermal inertia building and if the internal air temperature fluctuation are around the PCM melting temperature (PMT).

The purpose of this paper is to study the thermal performance of one building with PCM mounted in the internal ceiling or in internal vertical walls, considering two Italian locations corresponding to

two different climates, varying the PCM thickness and comparing them with the cases without PCM taken as a reference. A specific PMT in order to decrease the building cooling energy need was chosen. The first part of this paper deals with the methodology used in order to carry out the energy saving analysis. The case study's procedures in terms of building and PCM features and the simulation configurations descriptions are shown in the second part. In the third part results and a comparison of the considered solutions are exposed. The last part concerns the main conclusions of this research.

2. Methodology

In order to examine the energy saving potential benefits integrating PCMs into building internal walls, the building thermal behaviour was simulated by using TRNSYS software (Solar Energy Laboratory University of Wisconsin-Madison, 2012). To model the building without PCM just the Type 56 has been used. The results of this analysis, in terms of energy needs, were taken as a reference for the comparison with the other considered solutions. As regards the building with PCM, in addition to Type 56, Type 1270 supplied by TESS must be used as well (Thermal Energy System Specialists, 2012). This component models a layer of a PCM that is entirely contained within a wall; in other words, the PCM is not directly adjacent to the zone air (figure 1). Type1270 is designed to interact with Type56 and can model a PCM located anywhere in the Type56 wall (figure 1). The user is able to specify the physical properties of the PCM: density, specific heat, PMT, solidification temperature and latent heat of fusion. The user has to split the wall containing the PCM into two parts (figure 1); each part containing the standard wall layers are located on one side of the PCM layer and they are set into the Type 56 as a BOUNDARY wall.

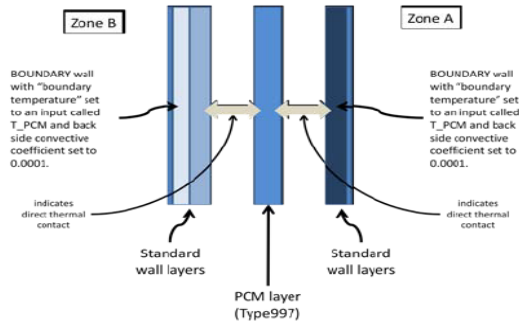


Fig. 1 – PCM layer model on TRNSYS.

This means that the building zone containing the wall with PCM sees the wall as a temperature node; therefore in this case, the node temperature is the temperature calculated by Type 1270. It makes the following assumptions:

1. The specific heat of the PCM is constant (it does not change with temperature) when fully solid. The user defines the solid-phase specific heat.
2. The specific heat of the PCM is constant (it does not change with temperature) when fully liquid. The user defines the liquid-phase specific heat.
3. The thermal contact resistance to energy flow between the PCM layer and the standard material layers adjacent to it is negligible.
4. The solidifying/melting process occurs at a constant temperature.

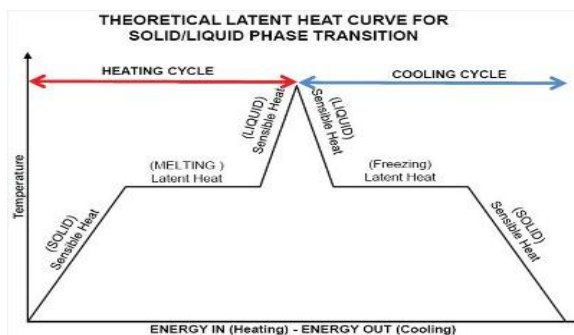


Fig. 2 – Simple PCM working chart

Indicating with \dot{q}_1 and \dot{q}_2 the quantities of energy entering the PCM from the adjacent wall layers, two circumstances are distinguished [24]:

- when the PCM material is fully solidified, the node temperature at the end of a timestep is given by:

$$T_f = T_i + \frac{(\dot{q}_1 + \dot{q}_2)}{m_{PCM}c_{ps}} \quad (1)$$

- when the PCM material is fully melted, the node temperature at the end of a timestep is given by:

$$T_f = T_i + \frac{(\dot{q}_1 + \dot{q}_2)}{m_{PCM}c_{pl}} \quad (2)$$

When the PCM material is in the melting/freezing phase (figure 2) the final temperature and initial temperature are equal (provided that the PCM does not become fully solid or fully liquid during the time step) and Type1270 simply keeps track of how much energy the PCM has absorbed or given off. If the energy absorbed by the PCM during a particular time step exceeds the PCM's latent storage capacity then Type1270 computes how much of the energy was needed to fully melt the PCM, then applies the remaining energy to a temperature change in the liquid phase using Equation 2. Likewise, if the PCM is giving off energy to the surrounding wall layers, and it gives off more energy than has been stored in a particular time step, then Type1270 computes how much energy was required to fully solidify the PCM and applies the remaining energy to a temperature change in the solid phase using Equation 1 (figure 2). Furthermore the quantities \dot{q}_1 and \dot{q}_2 are supplied by Type 56. The PCM was added first in the ceiling and then in internal vertical walls. In the first case, just a single Type 1270 was used. Instead, in the other case, for each internal vertical wall containing PCM one Type 1270 has to be used. In the preliminary phase an optimization analysis regarding the effect of the variation of PMTs, fixing an average PCM thickness regarding the considered range and considering two Italian cities, Milan (Latitude 45.45°) and Cosenza (Latitude 39.29°), was evaluated, leaving unchanged the PCM thermo-physical properties. This analysis was done in order to find the best PMT for cooling energy saving purpose. Once the best PMT was chosen, the energy saving analysis regarding different PCM thickness relating to the two localities were

carried out. Concerning the climate data of the abovementioned cities, they refer to Italian Standard UNI 10349 (Ente Nazionale di Unificazione, 1994). All the analysis refer to yearly simulations based on hourly timesteps. The last part of the research is the comparison between the energy performance of the building with PCM and the reference cases.

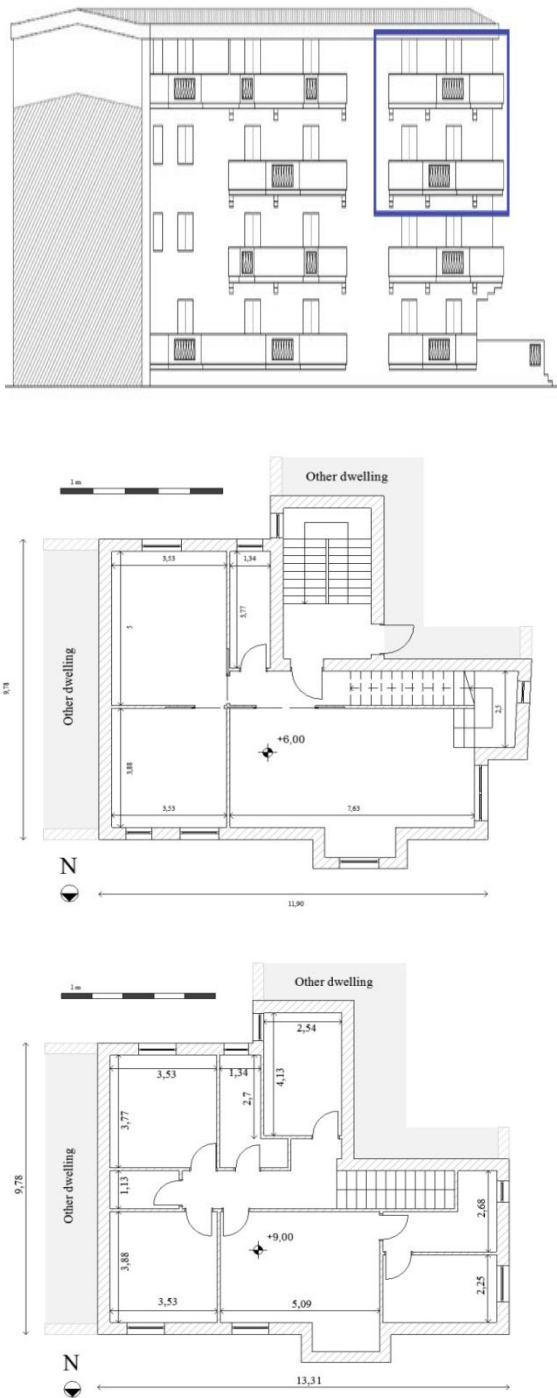


Fig. 3 – Location and orientation of the considered dwelling.

3. Case study

3.1 Building features

The considered building is a two-storey house, which is built on two floors, and it refers to a real building. The dwelling typology is an apartment and it is in a typical four-storey residential apartment building (figure 3). It is oriented and located within the whole building as the next figure shows.

The analyzed house is adjacent to other conditioned apartments on the east and bottom sides as the previous figure illustrates. Therefore the boundary wall with the other apartments and the internal ceiling were set with adiabatic conditions in the TRNSYS environment. The mean thermal properties of the opaque structural elements are reported in the table below.


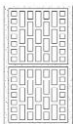
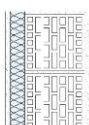

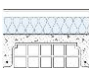
Partition					
	Material	Thickness [m]	Conductivity [W/mK]	Heat Capacity [J/kgK]	Density [kg/m³]
	Plaster	0,02	0,7	1000	1400
	Cored Brick	0,06	0,46	840	666,7
	Plaster	0,02	0,7	1000	1400
External Wall, type1					
	Material	Thickness [m]	Conductivity [W/mK]	Heat Capacity [J/kgK]	Density [kg/m³]
	Plaster	0,02	0,7	1000	1400
	Brick	0,30	0,35	840	686,7
	Plaster	0,02	0,7	1000	1400
External Wall, type2					
	Material	Thickness [m]	Conductivity [W/mK]	Heat Capacity [J/kgK]	Density [kg/m³]
	Plaster	0,02	0,7	1000	1400
	Insulation	0,06	0,036	1200	20
	Brick	0,30	0,35	840	686,7
	Plaster	0,02	0,7	1000	1400
Ceiling					
	Material	Thickness [m]	Conductivity [W/mK]	Heat Capacity [J/kgK]	Density [kg/m³]
	Ceramic tile	0,01	1	840	2300
	Mortar	0,05	1,4	1000	2000
	Concrete	0,22	0,46	840	666,7
	Plaster	0,02	0,7	1000	1400
Ceiling Roof					
	Material	Thickness [m]	Conductivity [W/mK]	Heat Capacity [J/kgK]	Density [kg/m³]
	Plaster	0,02	0,7	1000	1400
	Concrete	0,22	0,46	840	666,7
	Bitumen	0,004	0,7	1000	1200
	Insulation	0,12	0,036	1200	20
	Air	0,04	0,31	1008	1,3
	Tile	0,01	0,13	840	600

Table 1 – Opaque structural elements stratigraphy and thermal properties.

Furthermore the configuration and the mean thermal properties of the window systems are reported in the table 2.


Window System (WS)							
	Material	Thickness [mm]	Conductivity [W/mK]	Frame	R_{frame} [m ² K/W]	Solar factor	U_{window} [W/m ² K]
	Glass	5,7	1	40% of A_w	0,33	0,703	2,01
	Argon	6,4	0,017				
	Glass	5,7	1				

Table 2 – Window system stratigraphy and thermal properties.

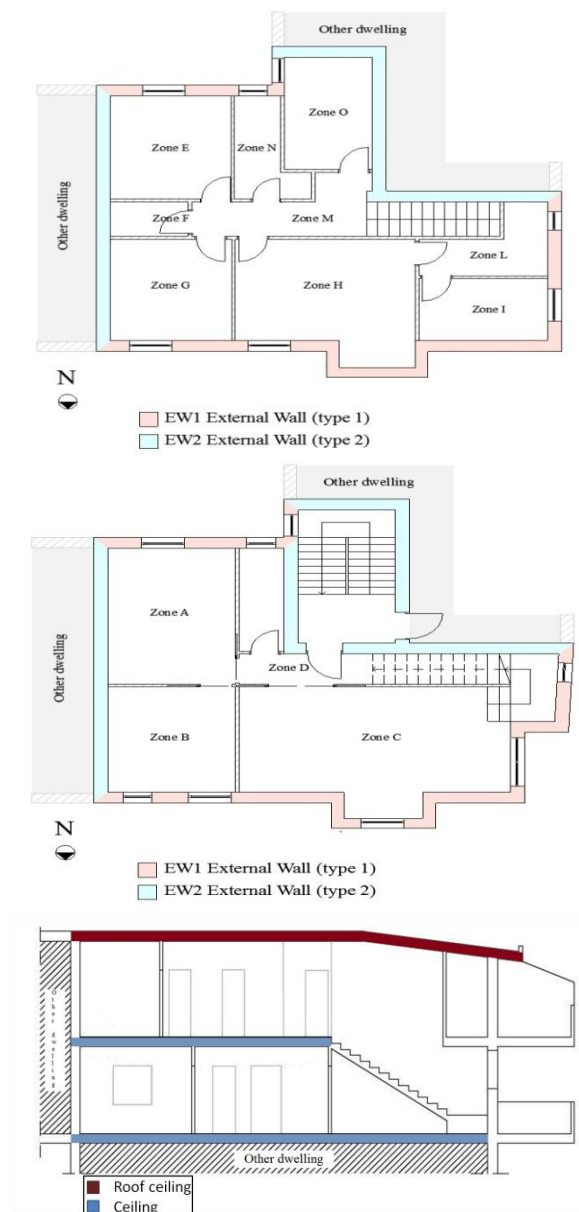


Fig. 4 – Location of the external wall types, house zone map and ceilings location.

Concerning the radiative coefficients, the long wave emissivity (ϵ), assumed equal to the long wave absorption coefficient, of the window frame and of the walls is 0.9, while it is 0.837 for the glass. Instead, regarding the short wave absorption coefficient (α), the window frame has a value of 0.4, the wall 0.35 and the glass 0.04. The figure 4 shows the location within the indoor environment of the different wall and ceiling typologies and the window systems.

The values of the internal and external superficial thermal resistances are respectively 0.2 and 0.05 m² K/W and the infiltration rate is 0.3 ac/h as the Italian standard suggests (Ente Nazionale di Unificazione, 2007). Moreover, the cooling and heating set point temperatures are respectively 26°C and 21°C.

3.2 PCM features

The PCM used in this research consists of hydrate salts; it is the SP25 PCM produced by Eps ltd. The related thermal properties are shown in table 3. The parametric analysis related to the PCM thickness refers to a range of 5 - 15 cm considering a 2.5 cm pitch for both configurations, mounted into the ceiling and into the internal vertical partitions. The PMT related to this PCM is 25°C, but, concerning the melting temperature optimization analysis, a range of temperature (table 2) was taken into account leaving the PCM thermal properties unchanged.

PCM (SP25)	Melting Temperature [°C]	19 - 27
	Density [kg/m ³]	1530
	Heat Capacity (cp _s and cp _l) [kJ/kgK]	2,2
	Latent heat [kJ/kg]	180
	Conductibility [W/mK]	0,54

Table 3 – PCM thermal properties.

3.3 PCM mounted into the ceilings and into internal vertical walls

The figure below shows the ceiling configuration with PCM. The PCM is mounted exactly in the middle of the ceiling between the storey of the considered dwellings.

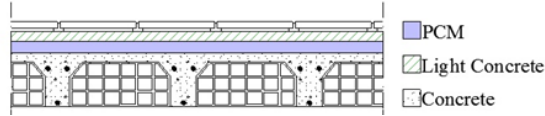


Fig. 5 – PCM ceiling stratigraphy.

Instead, the configuration of the cases with the PCM mounted in the internal vertical walls are shown in the figure below. The PCM is located on one side of the cored brick of the partition as shown in Figure 6.

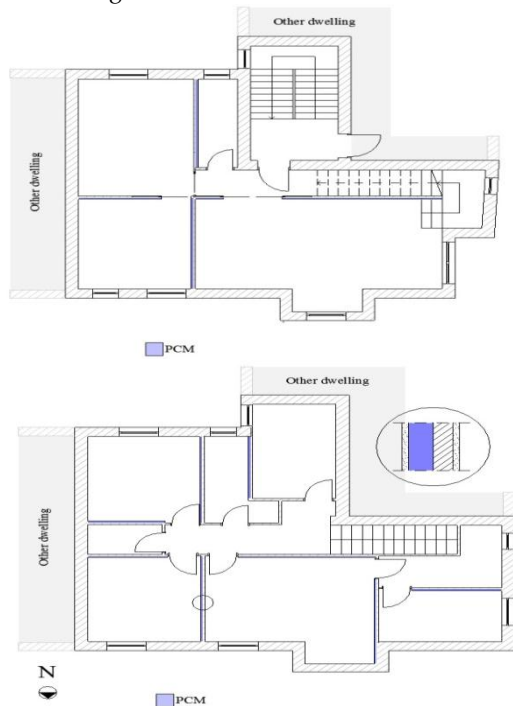


Fig. 6 – PCM internal vertical partition configuration.

4. Discussion and result analysis

4.1 Reference case

The reference cases' results, in terms of monthly and seasonal thermal energy requirements, both for cooling and heating related to the two considered cities are shown in the table 4.

It is important to notice that the cooling loads are greater in the city of Cosenza than in Milan, while

as regards the heating loads, the situation is the opposite.

	COSENZA	MILAN
MONTH	ENERGY NEED [kWh]	ENERGY NEED [kWh]
JANUARY	-1306.79	-2314.89
FEBRUARY	-1037.87	-1754.13
MARCH	-670.37	-1091.23
APRIL	-259.99	-372.28
MAY	10.35	-50.57
JUNE	432.73	281.77
JULY	820.14	613.60
AUGUST	732.76	419.43
SEPTEMBER	285.21	48.01
OCTOBER	-53.16	-455.86
NOVEMBER	-523.18	-1430.14
DECEMBER	-1145.39	-2180.81
HEATING ENERGY NEED [kWh]	-4996.76	-9649.92
COOLING ENERGY NEED [kWh]	2281.20	1362.81

Table 4 – Reference cases energy needs.

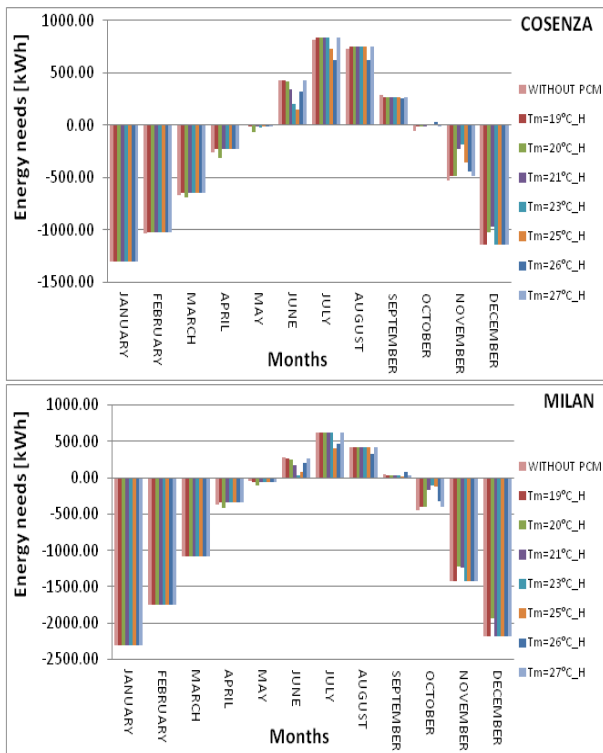
4.2 Melting temperature optimization analysis

The figures below show the monthly thermal energy needs considering a PMT range of 19 - 27 °C, fixing a PCM thickness of 7.5 centimetres, related to each considered cities for both mounting solutions, PCM mounted into the ceiling and into the vertical internal walls. The first two figures refer to the ceiling PCM configuration, while the others to the vertical internal walls PCM configuration.

The best value of the PMT varies over the year (figure 7). Moreover that value for a certain month changes as a function of the climate conditions and it depends on the considered mounting solution as well. It follows that, in order to achieve the optimized PMT related to a conditioning season, a seasonal energy need analysis is necessary (figure 7). The percentage reduction between the winter and summer overall energy needs achieved by different PMTs and the reference cases energy needs are shown in the next figures. In addition, the light coloured bars refer to the horizontal wall (ceiling) solutions, while the dark bars to the vertical wall solutions.

It is easy to understand that there is one optimized PMT for each conditioning season. In particular, concerning the winter it is in all cases 21°C. Instead, there are two optimized PMTs for the summer: 26°C for the ceiling solution located in Cosenza, while 25°C for the other cases. Whereas the aim of this research is to compare different internal mounting solutions to decrease the building cooling loads an unique value of PMT has to be chosen. Therefore, a value of 25°C as PMT is considered.

CEILING



INTERNAL VERTICAL WALLS

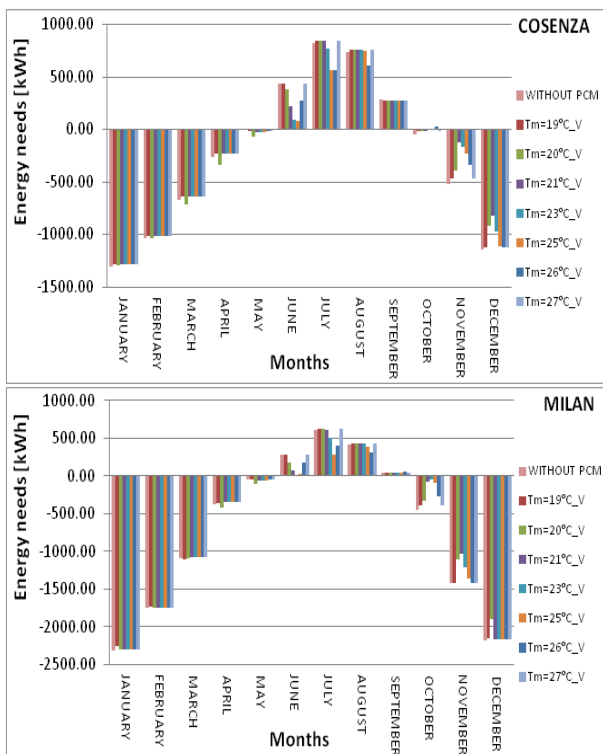


Fig. 7 – Monthly thermal energy needs considering a PMT range of 19 - 27 °C related to both mounting solutions for the two cities.

4.3 PCM mounted into the ceilings and into the vertical internal walls

Figure 8 shows the energy needs as a function of the PCM thickness, mounted into the ceiling for the two different considered cities.

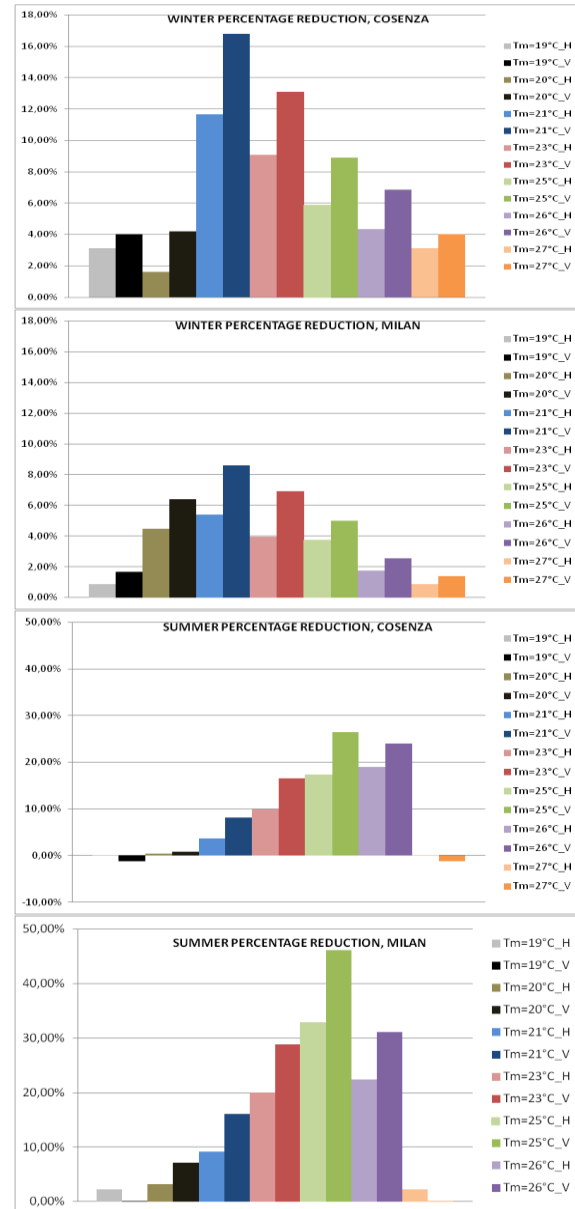


Fig. 8 – Percentage reduction between the winter and summer overall energy needs for different PMT value solutions and the reference cases energy needs.

As was to be expected, the chosen optimized PMT reduces much more the thermal cooling requirement than the heating loads (figure 9), because the latent effect of PCM during the heating season does not occur.

Over the year, it is possible to identify four

different periods: the charge period, characterized by indoor superficial PCM wall temperature fluctuations that go over the PMT with an average value less than the PMT and a temperature increasing trend, the charged period, where the average indoor superficial PCM wall temperature is greater than the PMT, the discharge period, characterized in the same way of the charged period but with a temperature decreasing trend and the uncharged period, where the indoor superficial PCM wall temperature is below the PMT.

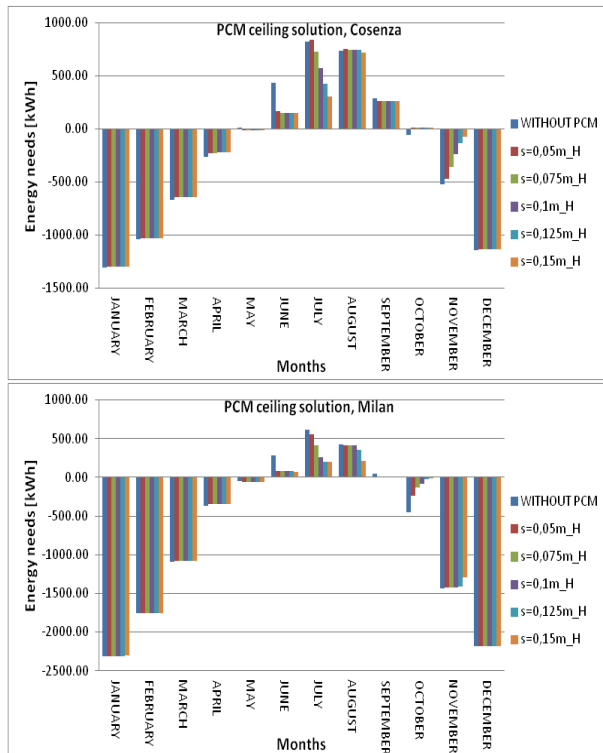


Fig. 9 – Ceiling solutions energy needs as a function of the PCM thickness for the two different considered cities.

Regarding the latent contribution it occurs only in the charge and in the discharge periods. All the above mentioned concepts deal with the set point temperatures. Specifically, the superficial temperatures of the internal structural element with PCM remain constant, equal to PMT. When the latent contribution occurs, on the contrary they always vary if the element does not contain PCM. This leads to an energy need variation as a function of the periods defined before. Therefore, benefits in terms of energy needs occur only during the charge and the discharge periods. Figure 9 shows that the charge period in both cities occurs in June and July,

the charged period in August and September, the discharge period in October and November regarding Cosenza, while in Milan it occurs only in October and the uncharged period in the other months. In particular, in June a small PCM thickness is sufficient to reduce the cooling energy need and if it is incremented, no additional benefits are obtained. In July the positive effects of the charge period are much marked as much the amount of PCM is greater. In July, during the so called charged period, benefits regarding the latent effect increase as the PCM quantity increases. Figure 10 shows this behaviour, in terms of superficial trend temperatures with different PCM thicknesses, without PCM and the external air temperature, for the external wall of the zone C (figure 4), in which there is the maximum advantage using PCM. Principally the internal superficial temperature decreases by increasing the PCM amount into the ceiling.

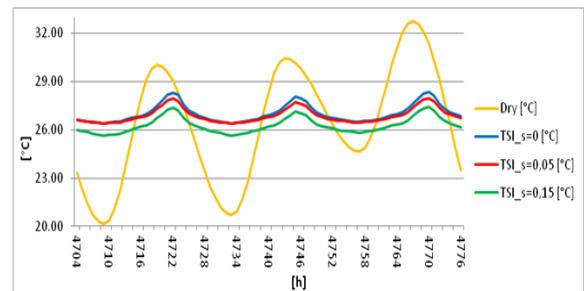


Fig. 10 – External wall indoor superficial trend temperature of the C zone and external dry temperature, location: Milan, month: July.

It is interesting to observe that in Milan a PCM thickness of 12.5 cm leads to the maximum benefit (figure 9) in July. In the charged period the PCM is in the overheating phase and the benefits that happen in Milan in August with a high PCM thickness are not due to the latent contribution, but to the largest PCM wall sensible heat capacity. In the discharge period the heat energy needs decrease by increasing the PCM thickness. Finally, in the uncharged period there are not advantages using PCM except in November in Milan, but this benefit is due to the increased PCM wall sensible heat capacity. The next figures show the energy needs as a function of the PCM thickness, mounted into the internal vertical walls for the two different considered cities.

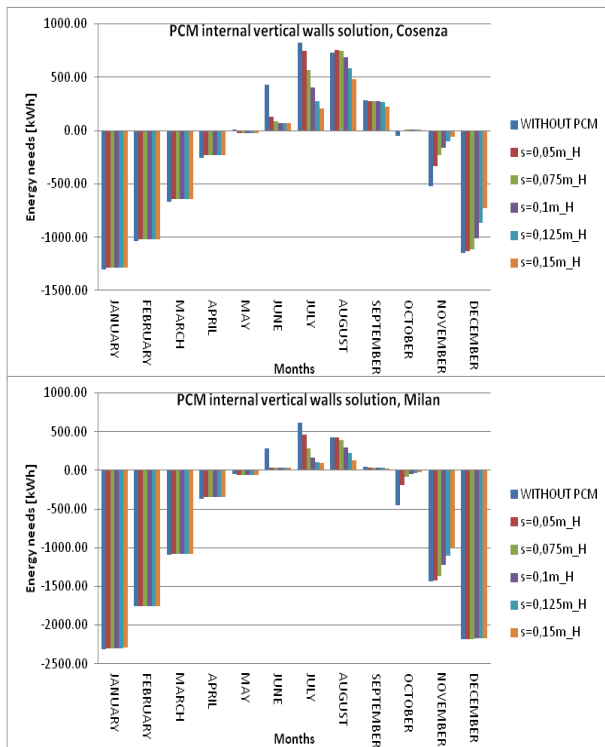


Fig. 11 – Internal vertical PCM wall solutions energy needs as a function of the PCM thickness for the two different considered cities.

In this case is possible to identify only the uncharged period: in Cosenza it goes from January to May while in Milan it goes from December to May. It is not possible to classify the remaining periods because there are at the same time zones characterized by a different PCM phases.

4.4 Comparison

In order to compare the proposed solutions, winter and summer energy needs' percentage reduction with respect to the reference cases for different PCM thickness are reported in figure 12. The best solution, in terms of energy needs, is PCM mounted into the internal vertical partitions, though the PCM quantity of the best solution is much higher than the PCM ceiling solution, because the internal vertical partition surface is more than the internal horizontal partition surface. Furthermore, it is important to notice that the winter energy savings in Cosenza are greater than in Milan for all cases, the opposite situation happens during summer. This is due to the fact that PCM benefits are much more significant during the conditioning system intermittence

periods that happen during the charge and discharge periods.

5. Conclusion and next steps

In this research the thermal performance of one building with PCM mounted in the internal ceiling and in internal vertical walls varying the PCM thickness and comparing them with the cases without PCM taken as a reference, considering two Italian locations corresponding to two different climates, was studied. Furthermore a PMT optimization analysis was carried out in order to decrease the building's cooling energy need. The results of the optimization analysis have showed that a deeper thermal analysis considering a zone level should be made in order to exploit the potential of PCM because its performance strongly depends on the thermal internal specific loads and especially on the zone orientation. A optimized PMT of about 25°C was evaluated. The best solution, in terms of energy needs, is PCM mounted into the internal vertical partitions. As regards the cooling season, an energy need reduction between 18% and 58% concerning Cosenza and between 30% and 80% for Milan related to a PCM thickness range from 5 to 15 cm was achieved. Instead, concerning the heating season there are fewer benefits, showing a reduction of about 20% in Cosenza and 9.2% in Milan related to the maximum PCM thickness of 15 cm. Furthermore, it is important to notice that the winter energy savings in Cosenza are greater than in Milan for all cases, whereas the opposite situation occurs in the summer. The same analysis should be made at level zone, and an energy saving analysis considering a PCM mounted on the external vertical wall solution should be studied in order to have a clear and more understandable pictures of the PCM building application.

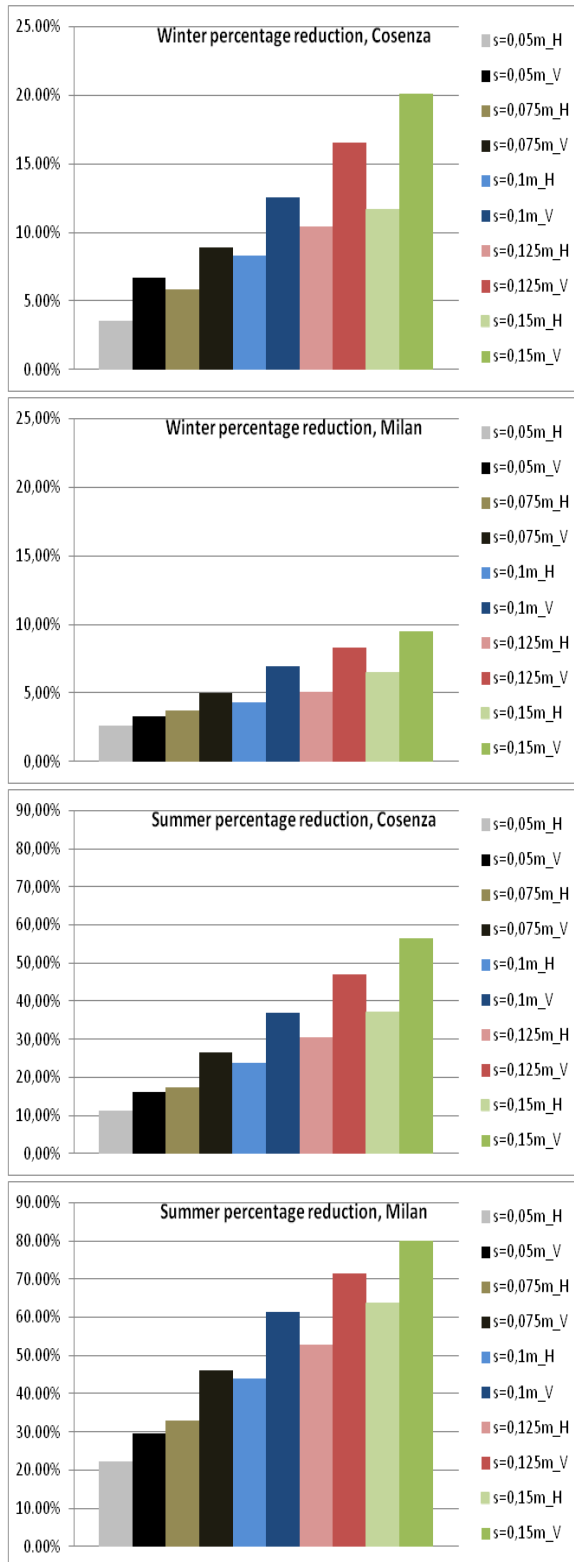


Fig.12 – Percentage reduction between the winter and summer energy needs for different PCM solutions and the reference cases energy needs.

6. Nomenclature

Symbols

T_f : temperature at the end of a timestep ($^{\circ}\text{C}$).

T_i : temperature at the start of a timestep ($^{\circ}\text{C}$).

\dot{q}_1, \dot{q}_2 : quantities of energy entering the PCM from the adjacent wall layers ($\text{kJ}/(\text{h}\cdot\text{m}^2)$).

m_{PCM} : mass of the PCM (kg).

c_{ps} : specific heat of the PCM when it is fully solid ($\text{kJ}/(\text{kg}\cdot\text{K})$).

c_{pl} : specific heat of the PCM when it is fully liquid ($\text{kJ}/(\text{kg}\cdot\text{K})$).

References

- G. Sarlos, A. Dauriat, Energy, a challenge for humanity in the 21st century, in: Proceedings of the International Conference on Energy and the Environment, Shanghai, China, December 11–23, 2003), pp. 1–5.
- Climate plan 2004: let's act together to challenge of climate change, Tech. rep., French Ministry of Ecology and Sustainable Development; 2004.
- A.K. Athienitis, C. Liu, D. Hawes, D. Banu, D. Feldman, Investigation of the thermal performance of a passive solar test-room with wall latent heat storage, Building and Environment 32 (1997) 405–410.
- D. Banu, D. Feldman, D.W. Hawes, Evaluation of thermal storage as latent heat in phase change material wallboard by differential scanning calorimetry and large scale thermal testing, Thermochimica Acta 317 (1998) 39–45.
- A.F. Rudd, Phase-change material wallboard for distributed thermal storage in buildings, ASHRAE Transactions 99 (2) (1993) 339–346.
- A. Sary, K. Kaygusuz, Thermal energy storage system using some fatty acids as latent heat storage materials, Energy Sources 23 (2) (2001) 75–85.
- D. Feldman, D. Banu, D. Hawes, E. Ghanbari, Obtaining an energy storing building material by direct incorporation of an organic phase change material in gypsum wallboard, Solar Energy Materials 22 (1991) 231–242.
- M.N.R. Dimaano, A. Escoto, Preliminary assessment of a mixture of capric acid and lauric acid for

- low-temperature thermal energy storage, *Energy* 23 (1998) 421–427.
- D. Feldman, D. Band, D.W. Hawes, Development and application of organic phase change mixtures in thermal storage gypsum wallboard, *Solar Energy Materials and Solar Cells* 36 (1995) 147–157.
- D. Feldman, M.M. Shapiro, D. Banu, C.J. Fuks, Fatty acids and their mixtures as phase change materials for thermal energy storage, *Solar Energy Materials* 18 (1989) 201–216.
- S. Ahmet, Thermal characteristics of a eutectic mixture of myristic and palmitic acids as phase change material for heating applications, *Applied Thermal Engineering* 23 (2003) 1005–1017.
- Feldman, D., Banu, D. and Ghanbari, E., Obtaining an energy storing building material by direct incorporation of an organic phase change material in gypsum wallboard. *Solar Energy Materials*, 1991, 22, 231–242.
- Feldman, D., Khan, M. A. and Banu, D., D., Energy storage composite with an organic phase change material, *Solar Energy materials*, 1989, 18, 333–341.
- Feldman, D., Shapiro, M., Banu, D. and Fuks, C. J., Fatty acids and their mixtures as phase change materials for thermal energy storage. *Solar Energy Materials*, 1989, 18, 201–216.
- Hawes D. W., Latent heat storage in concrete. Ph. D. thesis, Concordia University, Montreal, 1991.
- Tyagi VV, Buddhi D. Pcm thermal storage in buildings: a state of art. *Renewable and Sustainable Energy Reviews* 2007;11(6):1146–66.
- Khudhair AM, Farid MM. A review on energy conservation in building applications with thermal storage by latent heat using phase change materials. *Energy Conversion and Management* 2004;45(2):263–75.
- Zhang Y, Zhou G, Lin K, Zhang Q, Di H. Application of latent heat thermal energy storage in buildings: state-of-the-art and outlook. *Building and Environment* 2007;42(6):2197–209.
- Kuznik F, Virgone J, Roux J-J. Energetic efficiency of room wall containing pcm wallboard: a full-scale experimental investigation. *Energy and Buildings* 2008;40(2):148–56.
- Kuznik F, Virgone J. Experimental investigation of wallboard containing phase change material: data for validation of numerical modeling. *Energy and Buildings* 2009;41(5):561–70.
- Kuznik F, Virgone J. Experimental assessment of a phase change material for wall building use. *Applied Energy* 2009;86(10):2038–46.
- Kuznik F, Virgone J., Johannes K. In situ of thermal comfort enhancement in a renovated building equipped with phase change material wallboard. *Renewable Energy* 2011; 36(5):1458–1462.
- Solar Energy Laboratory University of Wisconsin-Madison, TRNSYS, Version 17, 2012.
- TESS – Thermal Energy System Specialists, LLC, TessLibs 3 – Mathematical Reference, 2012.
- UNI 10349 , Riscaldamento e raffrescamento degli edifici - Dati climatici", 1994. UNI — Ente Nazionale di Unificazione, Milano.
- Norma UNI EN ISO 6946, Resistenza termica e trasmittanza termica. Metodo di calcolo, 2007. UNI — Ente Nazionale di Unificazione, Milano.

Energy and daylighting interaction in offices with shading devices

Francesca Mazzichi – University of Trieste, Trieste, Italy

Marco Manzan – University of Trieste, Trieste, Italy

Abstract

Office buildings represent a challenge for reducing energy consumptions due to climatization, since they are characterized by high internal loads due to electronic equipment and illumination. Furthermore they are also characterized by large transparent surface areas in order to guarantee sufficient daylighting. The combination of these factors leads to high energy costs due to both internal and high solar loads. Furthermore, to guarantee healthy work places, glare problems should also be taken into account. To avoid glare and solar radiation, fixed or movable shading devices are usually provided. Nevertheless the interaction of these devices with the heating, cooling and lighting plant is not simple, since they affect both the loads and the illumination distribution, and their impact on global energy consumption should be analysed for a real energy efficient design.

In the present paper different types of shading devices, fixed, movable and combined are analysed by means of computer codes and a comparison of the energy performance of each system has been carried.

ESP-r has been used in order to study the energy behaviour of the building, while the lighting simulation package DAYSIM has been used to predict the consumption of the artificial illumination system.

DAYSIM can provide the energy code ESP-r with internal loads due to illumination for an energy simulation. Since the deployment of movable devices is automatically controlled by DAYSIM, in order to couple the two codes, the ESP-r source code has been modified introducing a controller to activate the movable shading devices in synchronous with the daylighting analysis. The results obtained with different shading devices are

compared in terms of energy required for heating, cooling and lighting and also in terms of daylight distribution using distributions of useful daylight illuminance.

1. Introduction

The energy consumption due to building climatization is becoming a major concern for industrialized countries. Therefore energy saving strategies must be sought in order to guarantee both healthy conditions and a low environmental impact. This is true especially for buildings in the Mediterranean area with extensive glazed areas and high cooling loads because of solar irradiance. In Italy, national codes require the compulsory installation of external shading devices or glazing systems with low solar gain coatings. The choice of the external shading devices is left to the designer and no guidelines are available.

The size and positioning of shading devices depend on the orientation of the building's façade, the size of the windows and the relative importance of heating and cooling loads. Furthermore external shading devices have an impact on the internal daylight distribution. The architectural impact must also be taken into account by inserting shading surfaces as little as possible without jeopardizing energy savings.

In designing an external shading device all the energetic, daylighting and architectural problems must be taken into account at the same time.

In this paper the multiple aspects of the problem have been tackled using the software tool ESP-r (Clarke, 2001), and DAYSIM for computing illuminance levels.

In the literature a number of papers which deal with the problem of the impact of shading devices

on energy consumption can be found, but only in recent years have climatization and daylight analysis problems been considered together.

A detailed comparison of solar gain models with external and internal shading screens were presented in Loutzenhiser et al. 2007. Different codes have been compared, among them the ESP-r tool used in this paper, the authors found that accurate results can be achieved when predicting the energy consumption for long periods of time for highly glazed buildings.

An insight into the coupling between daylight and thermal loads was conducted in Franzetti 2004, fourteen parameters were identified and the computations were performed using “the experience plan” method with the aim of reducing the number of simulations. Different relations linking the most important parameters with lighting energy consumption and annual energy needs were elaborated. It was found that an efficient lighting control device has a favourable impact on global energy needs emphasizing the importance of taking into account the interaction between lighting and HVAC system.

Ho et al. 2008 analysed the daylight illumination of a subtropical classroom seeking an optimal geometry for shading devices. They also evaluated the lighting power required to improve the illuminance conditions within the classroom. Gugliermetti et al. 2006 used the solar system luminous efficacies method to compute indoor natural illuminance. They introduced three simplified approaches for dealing with the effect of horizontal and vertical shading devices, comparing the obtained results with experimental data. They also included the developed methods in a building energy simulation code to compare the impact of the different methods on the heating, cooling and lighting requirements of an office building.

The interaction of shading control strategies on the whole building energy consumption were analysed by Carbonari et al. 2002 for different locations and expositions and they found that the benefit of the control is dependent on the location and orientation of the building, with in general a better solution for the case of automatic controlled shading devices. Furthermore the presence of louvers made the effect of orientation on the

energy requirement inappreciable. A controlled roller shade combined with an automatic controllable lighting system was analysed by Tzempelikos and al. (2007). They found that substantial energy savings can be obtained in perimeter spaces, and they changed the window to wall ratio obtaining an optimal 30% value for ensuring a good illumination of the room for a south facing window in Montreal.

In a previous work (Manzan, 2009), one author applied Genetic Optimization to the same problem, but the daylighting calculations used daylight factors obtained with RADIANCE, thus limiting the analysis to overcast skies.

The importance of automatic light dimming sensors for an energy efficient building in Abu Dhabi was highlighted by Fawwaz et al. 2010, who tested also vertical and horizontal external louvers slats at different angles and expositions. They found that the use of static louvers is more effective when applied to glazings with high shading coefficients.

The comparison of different shading devices was performed by Nielsen et al., 2011. They performed a concurrent energy and lighting simulation in order to quantify the potential of dynamic solar shading. They also emphasized the importance of introducing design alternatives from the beginning of the design of the façades.

In the present work different shading devices, both fixed and moveable, are taken into account. An integrated thermal and daylighting simulation has been performed for a south-facing window in an office building, the different behaviour of the façade system with different shading devices has been highlighted taking into account both energy and daylighting metrics. The solutions have been obtained by using two well-known freely available codes, DAYSIM and ESP-r.

2. Problem description

In the present study an office space has been used. The room is $2.87 \times 4.5 \times 2.96$ m (width \times height \times depth) with a south-facing window with a surface area of 3 m^2 . The south-facing wall has a heat transfer coefficient of $0.31 \text{ W}/(\text{m}^2 \text{ K})$, the heat

transfer coefficient of the glazing is $1.4 \text{ W}/(\text{m}^2 \text{ K})$, while the light transmittance is 0.6.

The dimensions of the office with the south exposed window are shown in Figure 1

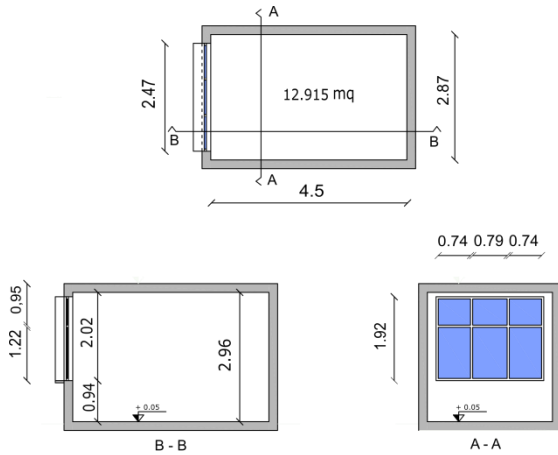


Fig. 1 – Room geometry

The office is considered occupied during workdays between 8:00 and 17:00, and the internal load due to occupancy and equipment is reported in Table 1. A maximum artificial lighting density of $12 \text{ W}/\text{m}^2$ has been considered, although the real lighting gain is controlled by a dimming sensor which varies continuously the output lighting power. For daylight simulation the reflectances of walls, floor and ceiling have been taken as 0.4, 0.13 and 0.86 respectively.

	Equipment	Occupancy
0-8	60 W	0 W
8-17	300 W	150 W
17-24	60 W	0 W

Table 1 – Weekday distribution of thermal gains

Five cases have been analysed as reported in Table 2, while the geometry of shading devices is presented in Figure 2. Case 1, which is the window without a shading device is unrealistic, but has been reported here for comparison with the other solutions and therefore to evaluate the improving effect on energy and internal illumination patterns due to shading devices. Case 2 is a simple fixed overhang which shades the office room from direct lighting. Case 3 is an external Venetian blind system with slats at an inclination angle of 45° , which can be retracted in an upper case. Case 4

represents a similar external Venetian system, but in this case the horizontal louvers can be inclined at 0° and 45° from the horizontal. The last case is the union of cases 2 and 3.

Case	description
1	No shading device
2	Fixed overhang
3	Retractable external venetian blind
4	Controlled angle of venetian blind
5	overhang + external venetian blind

Table 2 - Cases analysed

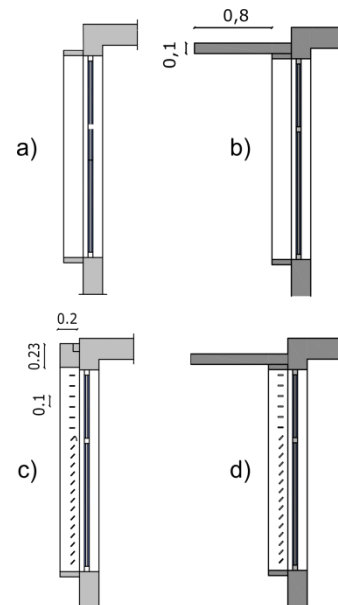


Fig. 2 – a) bare window b) overhang c) external blinds d) overhang with moveable blinds

3. Calculation procedure

Analyses were carried out using two simulation codes, ESP-r for energy simulation and DAYSIM for daylighting analysis.

The ESP-r code can cope with daylighting simulations, for instance it incorporates different coupling methods. It is possible to compute horizontal work plane daylight factors by combining analytical formula for sky component and split flux method for interreflected components, alternatively a user defined daylight

factor can be defined. More demanding computing methods are present as well: a full coupling method in which the lighting simulations are performed with Radiance at each time step and a daylight coefficient method where a set of daylight coefficients are pre-computed using Radiance.

A different approach has been adopted in this work, since the DAYSIM code has been used for daylighting analysis. In the proposed scheme the internal loads due to lighting are computed directly during daylighting simulations and then transferred to the energy computation code ESP-r by means of the ESP-r temporal data file facility. Since moveable shading devices are controlled by the lighting distribution into the room, their state has to be fed to the energy simulation code as well.

3.1 DAYSIM Simulation

DAYSIM is an analysis tool capable of calculating annual illuminance profiles. To efficiently obtain this result, it uses RADIANCE coupled with a daylight coefficient approach. For each geometrical configuration a set of daylight coefficients are computed then used to calculate internal illuminances at each simulation step with a variable sky luminance distribution. DAYSIM incorporates a user behaviour control model, called Lightswitch (Reinhart, 2002) which takes into account how occupants interact with light switches, and possible movable blinds. DAYSIM therefore is capable of computing the electric loads due to artificial illumination when no daylight is available or insufficient. The computed electrical consumption can be transferred to the simulation code ESP-r as an internal gain.

DAYSIM incorporates different methods to control the internal luminaries, in this work an efficient photo sensor-controlled dimmed lighting system with an energy-efficient occupancy sensor has been used. The photocell dims the activated lighting until the total work plane illuminance reaches the threshold of 500 lux.

Shading devices can be analysed with DAYSIM as fixed or moveable, in the latter case different sets of geometries are fed to the simulator with different positions of the devices. The code

computes different sets of daylight coefficients and illuminance values.

In this work an automated blind control based system has been adopted, the blinds are fully lowered to avoid glare as soon as direct sunlight above 50 W/m² is reached in the work place, and reopened when this value is no longer met.

A set of illuminance sensors are positioned at mid room as described in Figure 3 a) in the figure two possible locations of work places have been represented, the one placed in front of the window exploits the daylighting and is intended for paperwork; the illuminance levels can be retrieved from sensors S2 and S3. Instead the other, positioned far from the window, identified by sensors S5 and S6, is intended for computer work.

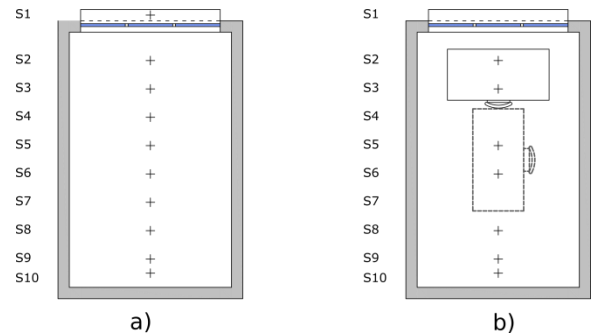


Fig. 3 – Sensors and work place positioning

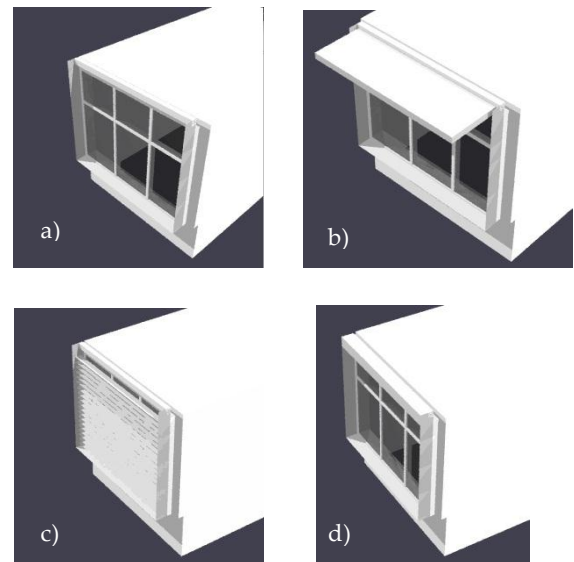


Fig. 4 – DAYSIM geometry, a) office room b) overhang c) deployed external blinds, d) retracted external blinds

The lighting simulation has been performed paying special attention to the geometric representation of

the office room. For instance the authors modelled the walls' thickness, windows sills and a case container for the retracted louvers in Case 3. In Figure 4 the developed models are presented.

3.2 Simulation in ESP-r

External shading devices can be modelled in ESP-r in different ways. Fixed shading devices, such as the overhang used in this work, can be treated as an obstruction, which is a prismatic block which projects a shadow on opaque and transparent external surfaces. Shading from other buildings, horizontal overhangs, vertical fins, windows sills and reveals are examples of the obstructions that can be represented with such a model. Instead the complex interaction occurring between an external or internal blind with a glazing system can be defined in ESP-r with the complex fenestration construction (CFC). Only Venetian blinds can be modelled at the moment, controlling strategies allow us also to drive the deployment of the device or the modification of slat inclination angle. The control algorithms can be set in ESP-r and react to a number of sensors such as internal temperature or climatic data.

Unfortunately the available control methods hinder the possibility to use the control strategies implemented into DAYSIM, so for this reason the code of ESP-r has been modified.

3.3 Modification to ESP-r routines

The data exchange between DAYSIM and ESP-r has been implemented by means of a temporal file which reports for each simulation time the loads due to illumination and occupancy. This file is generated using the results obtained by the DAYSIM run. The temporal definition file is read by ESP-r and used during the simulation in order to account for the correct loads. Internal loads can be read in using the temporal definition file, but additional information is required to operate the moveable shading devices as derived from the DAYSIM run.

To achieve these results the structure of the temporal definition file has been changed by adding new parameters which represent the position of the shading device, retracted and

deployed, or, if the slat angle changes, this control interacts with the CFC facility in order to synchronize the DAYSIM geometry with the ESP-r CFC model.

4. Results

Comparative data of energy demand and daylighting distribution are presented for the shading devices considered.

4.1 Energy demand

The results of the energy simulations are reported in Table 4, which represents the building's demand for heating, cooling required to maintain the internal temperature at 20 °C during heating season and 26 °C in summer conditions, and lighting. The energy carrier for heating, usually gas, is different for the one used for cooling and artificial lighting, usually electricity, therefore a primary energy consumption has been considered introducing plant efficiencies. Therefore the primary energy is computed as:

$$Q_p = \frac{Q_h}{\eta_h} + \frac{Q_c}{\eta_c} + \frac{Q_{el}}{\eta_{el}} Q_p = \frac{Q_h}{\eta_h} + \frac{Q_c}{\eta_c} + \frac{Q_{el}}{\eta_{el}} \quad (1)$$

where the efficiencies are set as $\eta_h = 0.8$, $\eta_c = 0.8$ and $\eta_{el} = 0.4$, while Q_h is the heating demand, Q_c the cooling demand and Q_{el} is the energy required by luminaries.

Figure 5 shows the annual energy demand for the simulated models, while Figure 6 shows the primary energy required calculated with Equation 1.

As expected, the maximum consumption is obtained in case 1, which is the office without shading devices. For this solution the heating required is minimum, but the energy required for cooling is the highest. Since the window is unobstructed, the energy required for lighting attains a minimum. A good energy behaviour is obtained by adding a simple overhang to the window, as in case 2. In this case the energy required for cooling is substantially reduced, while the one for heating and lighting increases somewhat. This behaviour is easily explained due

to the south exposure of the window and the different sun positions. In summer, when the solar elevation angle is high, the overhang is efficient in blocking solar radiation. In winter, due to the lower sun inclination angle, solar radiation is not intercepted by the shading device. However for this solution glare problems should be present, since the shading device is ineffective in blocking direct solar radiation especially during the winter months.

Case 3 is a moveable external venetian blind system. In this case the energy required for heating increases with respect to the other two cases, but unexpectedly the cooling load is higher than case 2. This behaviour can be easily explained: the blinds are activated when the direct sunlight above 50 W/m² is reached in the work place, in this case represented by sensors S3 and S6 in Figure 3. Since sensor S3 is positioned near the window, it drives the shading deployment, while sensor S6 positioned deeper inside the office drives the lighting dimming control. In this case the blinds are deployed more in winter as reported in Figure 8, so solar radiation entering the room is not blocked during the summer period, as reported in Figure 7. Case 4 represents the case with the blinds system always deployed, the control associated with sensor S3 alters only slat inclination, from 0° to 45° therefore the shading effect is always present as can be seen in Figure 7, leading to the lowest cooling load while the heating load is slightly higher than the one in Case 3. The number of hours of deployment is minimum, but it must be pointed out that the slats are always deployed and therefore only the inclination is altered.

Case 5 represents the combination of case 2 and case 3 and represents an attempt to obtain an efficient shading system reducing the hours of deployment allowing for a better unobstructed view outside the room. This effect can be confirmed by inspecting Table 3 and Figure 8. However the primary energy required is slightly higher if compared with case 2 with an increase in heating demand while the cooling load is only slightly affected. Again this behaviour can be explained by inspecting figures 7 and 8, the blinds are deployed mainly during the winter season, reducing the solar radiation with an increase of the

heating load, for the same reason the lighting energy consumption shows a slight increase.

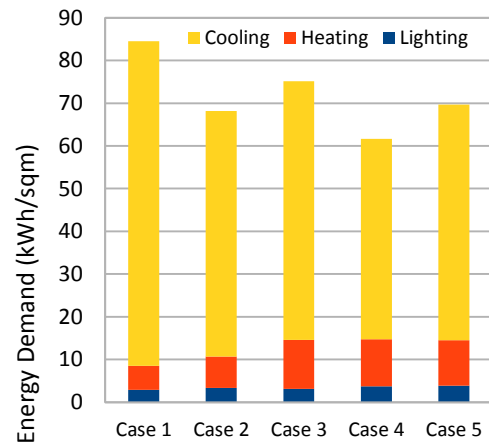


Fig. 5 – Annual energy demand

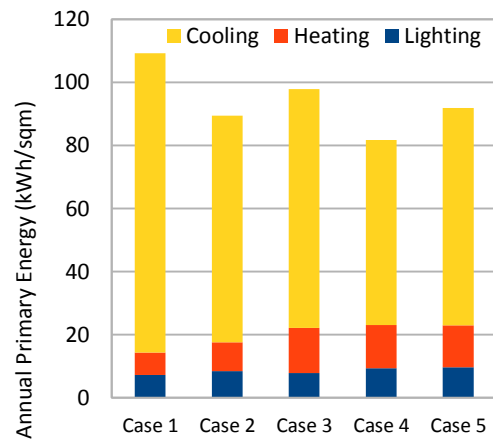


Fig. 6 – Annual primary energy required

Case	Q_h	Q_c	Q_{el}	Q_p	t_{on}
	Kwh/m ²				hours
1	5.66	75.95	2.90	109.3	-
2	7.30	57.48	3.38	89.4	-
3	11.51	60.54	3.12	97.8	317
4	10.99	46.92	3.74	81.7	209
5	10.65	55.12	3.87	91.9	276

Table 3 – Energy required and blinds time of activation

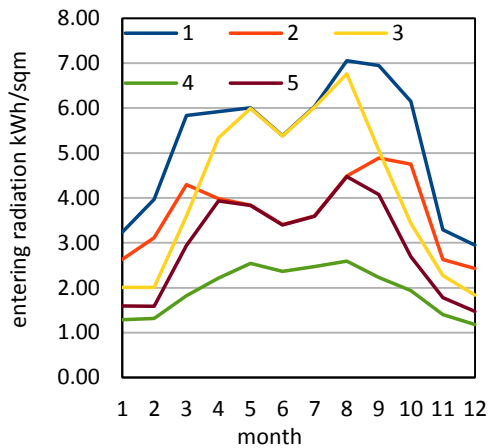


Fig. 7 – Entering solar radiation for different cases and months

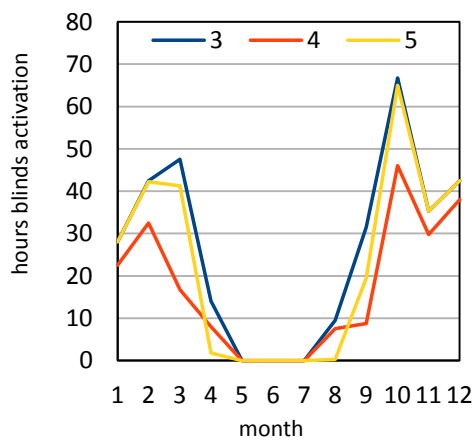


Fig. 8 – Number of hours of shading device activation per month

4.2 Daylight analysis

The amount of daylighting for the different cases is presented in terms of Useful Daylight Illuminance which is a parameter which indicates the percentage of working hours in which, in the work plane, a prescribed level of illumination is attained. This parameter is presented as a percentage of hours that attain three illumination ranges, 0-100 lux, 100-2000 lux, and over 2000 lux. In this work only data referring to the last two ranges are presented, since the percentages below 100 lux are always below 10% also for positions far from the window.

Figure 8 shows the distribution of UDI 100-2000 for the sensors presented in Figure 3, while Figure 9 presents the distribution of UDI 2000.

The daylighting maximum performance is obtained by case 4 which shows the highest values of UDI 100-2000. Similar results are obtained by

cases 3 and 5 until a depth of about 2 m, from this point onward the overhang increases the performance of case 5. As expected, case 1 shows a daylight illumination too strong, while case 2 although demonstrating an improvement respect case 1, results always underperforming if compared with the other cases.

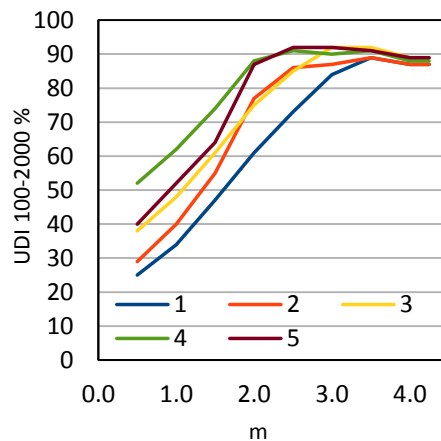


Fig. 9 – UDI 100-2000 distribution

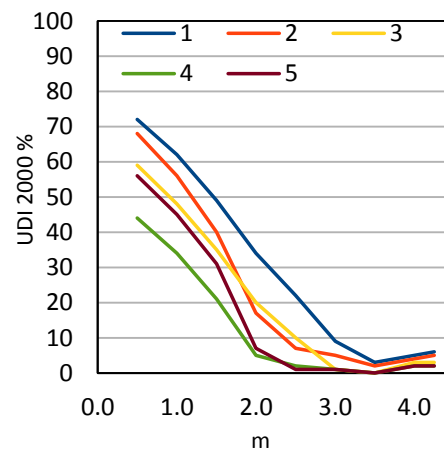


Fig. 10 – UDI 2000 distribution

Figures from 11 to 15 show the distribution of UDI 100-2000 in the work plane at a height of 0.85 m from the floor, and again the daylight distribution can be appreciated. The room always receives a sufficient quantity of daylighting as also shown in Figure 9. The low values of UDI 100-2000 near the window are due to higher values of UDI 2000. Again Cases 1 and 2 show high illuminance levels in proximity to the window. Using movable shading devices this effect is mitigated obtaining

acceptable values. Case 4 gives the better light uniformity with values nearly always higher than 50%. Case 5 gives the same results from a depth of 1 m onwards, which represents a good result since the window is for most of the time unobstructed as opposed to case 4, giving a free visual outside the room.

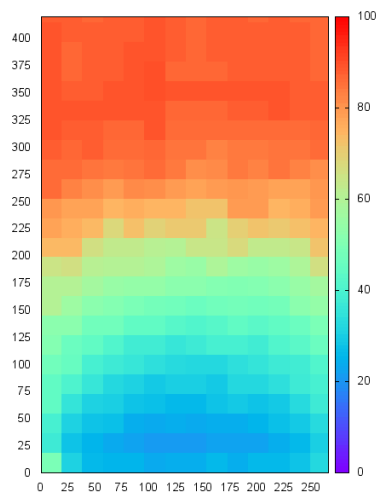


Fig. 11 – UDI 100-2000 distribution for case 1

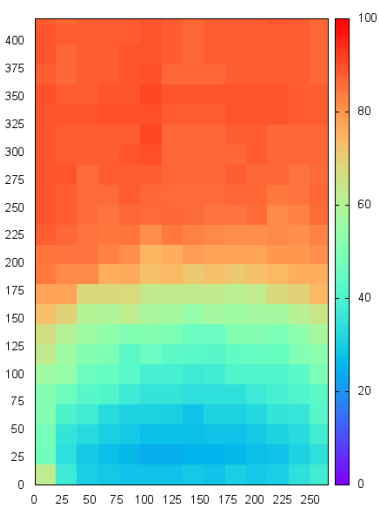


Fig. 12 – UDI 100-2000 distribution for case 2

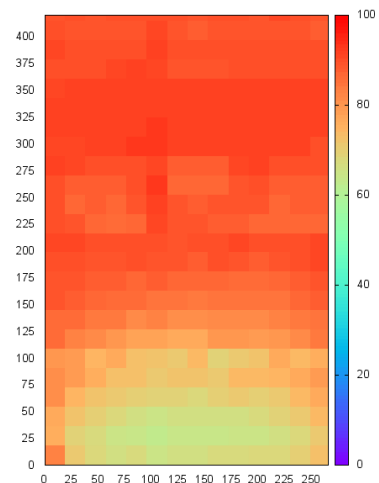


Fig. 13 – UDI 100-2000 distribution for case 3

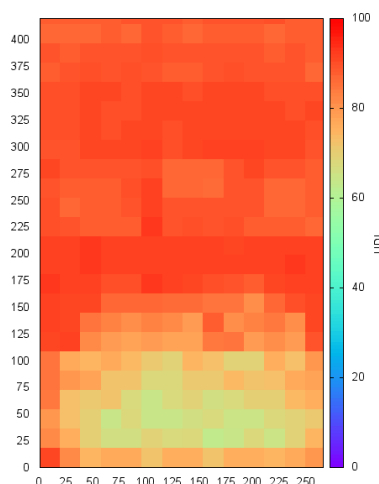


Fig. 14 – UDI 100-2000 distribution for case 4

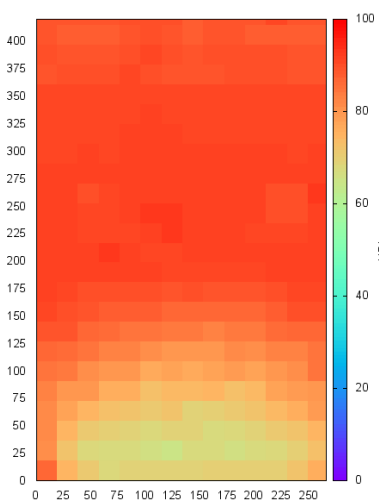


Fig. 15 – UDI 100-2000 distribution for case 5

5. Conclusions

Energy and daylight analysis have been performed for an office building with different shading devices. To obtain a dynamic simulation two codes have been used: DAYSIM for daylight analysis and ESP-r for energy analysis. The lighting analysis drives the movable external shading devices to avoid glare problems for two possible work places inside the room and computes the energy required for lighting. A new control variable has been added to the ESP-r code in order to synchronize the deployment of the shading devices with the results obtained with the daylighting analysis.

The obtained results show a good daylighting distribution and low energy consumption for the case with fixed venetian blinds with angle inclination control. Good results have also been obtained for the case with overhang and deployable devices. The fixed shading device showed good energy performance, but poor daylighting distribution with high illuminance levels near the window, this suggests that an additional analysis should be performed coupling fixed overhang with internal blinds.

The work presented demonstrates the usefulness of dynamic simulation for obtaining design scenarios which take into account different but strongly interconnected parameters such as energy performance and daylighting availability.

References

- Carbonari, A., Rossi G., Romagnoni, P., 2002, Optimal orientation and automatic control of external shading devices in office buildings, *Environmental Management and Health*, 13, 392-404
- Clarke J. A., *Energy Simulation in Building Design*, Butterworth Heinmann, Oxford, GB, 2001
- DAYSIM, version 3.1b, available at <http://www.DAYSIM.com>
- Fawwaz H., Bassam A., 2010, The energy savings potential of using dynamic external louvers in an office building, *Energy and Buildings*, 42, pp 1888-1895.
- Franzetti C., Fraisse G., Achard G., 2004, Influence of the coupling between daylight and artificial lighting on thermal loads in office buildings, *Energy and Buildings*, 36, 117-126
- Gugliermetti F., Bisegna F., 2006, Daylighting with external shading devices: design and simulation algorithms, *Building and Environment*, 41, 136-149.
- Ho M.C., Chiang C.M., Chou P.C., Chang K.F., Lee C.Y., 2008, Optimal sun-shading design for enhanced daylight illumination of subtropical classrooms, *Energy and Buildings* 40, 1844-1855
- Janak, M., 2003, Whole Building Energy Simulation With Complex External Shading Devices, *Building Simulation Conference*, Eindhoven, The Netherlands, August 11-14
- Loutzenhiser P.G., Manz H., Felsmann C., 2007, Strachan P.A., Maxwell G.M., An empirical validation of modeling solar gain through a glazing unit with external and internal shading screens, *Applied Thermal Engineering*, 27, 528-538
- Manzan M., Pinto. F., Genetic optimization of External Shading Devices., 2009, *Proc of Building Simulation 2009*, Glasgow (UK).
- Nielsen, M. V., Svendsen, S., Jensen, L. B., 2011, Quantifying the potential of automated dynamic solar shading in office buildings through integrated simulations of energy and daylight, *Solar Energy*, 85, pp 757-768
- Reinhart, C.F., 2002: Lightswitch a model for manual and automated control of electric lighting and blinds, *Solar Energy* 77, 15-28, 200
- Reinhart, C. F., Wienold, J., 2011. The Daylighting Dashboard - A Simulation-Based Design Analysis for Daylit Spaces, *Building and Environment*, 46:2, pp. 386-396,
- Tzempelikos, A., Athienitis, A.K., 2007, The Impact of Shading design and Control on Building Cooling and Lighting Demand, *Solar Energy*, 81, pp. 369-382.

Evaluating the nature and significance of ambient wind regimes on solar photovoltaic system performance

Abhishek Rao – Indian Institute of Science, Bangalore, India

Monto Mani – Indian Institute of Science, Bangalore, India

Abstract

Commercially available photovoltaic (PV) systems are predominantly silicon-based and their performances vary depending on inherent material properties, installation geometry and environmental factors. Ambient parameters vary from location to location, and can include the insolation level, ambient temperature, precipitation levels, dust regimes and local wind conditions. While the noticeable impact of the ambient temperature and dust settlement on PV efficiency has been recognized, the extent of influence attributed to wind patterns remains unclear. High wind speeds have the potential to enhance cell efficiencies by lowering the cell operating temperatures. Numerous correlations appear in literature that relate the cell temperature to the local wind speed, with a quoted efficiency gain of 0.7% for a 1 km hour⁻¹ rise in wind speed. Such a gain is significant considering the relatively low maximum efficiencies possible with present material technology and the large scale of PV installations. The applicability of the empirical correlations for wind flow over PV surfaces has been validated by wind tunnel experiments, particularly for wind movements parallel to the PV panels. However, wind speed and its direction rarely remain constant over time and terrain, and traditional heat transfer models inadequately account for these variations. The current study adopts a comprehensive approach to structure the nature of wind patterns for their direct or indirect influence on PV system performance.

This paper investigates the effect of wind related heat transfer on the performance of roof-mounted photovoltaic panels in tropical regions, where operating temperatures tend to be higher. The investigations are based on real-time monitoring of a Building-Integrated Photovoltaic roof combined with the development of simulation models. This paper reviews the current status of research in this domain. Further, attempts are made to

provide guidelines for the appropriate geometry for installation of roof-mounted PV panels taking into account prevalent wind regimes at the site.

1. Introduction

The use of building-integrated photovoltaic (BIPV) surfaces as building envelopes is on the rise. Silicon photovoltaic cells that are generally deployed in BIPVs have been reported to achieve a maximum solar energy conversion efficiency of 25% in laboratory testing (Green et al., 2011). Continuous exposure to intense solar radiation and an increase in the ambient temperature lead to a rise in the cell temperature. The direct effect of the cell temperature on the electrical conversion efficiency of the cell can be seen from the traditional linear expression for PV efficiency, Eq. (1) (Evans and Florschuetz, 1977)

$$\eta_c = \eta_{ref} [1 - \beta_{ref} (T_c - T_{ref})] \quad (1)$$

where η_{ref} is the electrical efficiency of the cell at the reference temperature, $T_{ref} = 25^\circ\text{C}$ and at an insolation of 1000 Wm⁻², and η_c is the cell efficiency at the cell operating temperature T_c . The temperature coefficient β_{ref} is a material property having a value of 0.0045 K⁻¹ for monocrystalline silicon (Notton et al., 2005). A single degree Celsius rise in cell temperature above 25°C would therefore result in a percentage efficiency loss equal in magnitude to β_{ref} , which is 0.45% in this case. This may seem small, but considering that most commercially available modules today have operating efficiencies between 12-18% and cell operating temperatures can rise by as much as 42°C above the ambient during operation (Radziemska and Klugmann, 2006) characteristic of

PV installations in tropical regions, the associated drop in efficiency becomes significant. It is evident then that the PV cell operating temperature plays a central role in the photovoltaic conversion process. As described by Mani and Pillai (2010), natural wind movements affect PV performance and installation geometries by effecting the accumulation or clearing of dust from PV surfaces. Natural wind movements may have the beneficial effect of lowering the PV cell temperature by carrying away some part of the surface heat through forced convective heat transfer. It is of interest, hence, to understand the nature and significance of the interactions of ambient wind regimes on solar photovoltaic system performance. The value of the reference efficiency η_{ref} of a cell varies with the material used for fabrication and is generally furnished by the respective manufacturers. Considering a typical value of 15%, and substituting the values of the reference temperature and the reference efficiency, Eq. (1) can be written as

$$\eta_c = 0.15[1 - 0.0045(T_c - 25)] \quad (2)$$

2. Effect of wind speed on photovoltaic performance

As previously stated, high wind speeds have the effect of lowering the cell operating temperature, thereby resulting in a potential gain in efficiency. It is possible to predict this gain in operating efficiency for a given set of weather conditions by estimating the corresponding operating temperature of the PV cell under those conditions. Applying the principle of energy conservation for a PV cell, its operating temperature can be derived, *ab initio* either as, an implicit function of the insolation level, the ambient temperature and the wind speed, or as an explicit function of the wind speed alone.

Consider the generic case of an unglazed PV cell (Figure 1) of unit area tilted at an angle θ (here 0°) to the horizontal, over which wind flows parallel to its surface and with a uniform speed V_w . A part of the insolation, G incident on the cell surface is converted into electric power W_p depending on the instantaneous efficiency η_c of the cell. The

remaining energy is converted into heat and is either accumulated within the cell, raising the cell temperature, or is dissipated to the environment through convective and radiative heat losses. The energy balance for the system can be written as

$$\alpha G = W_p + Q_{free\ conv} + Q_{wind} + Q_{rad} + \rho \delta C \frac{dT}{dt} \quad (3)$$

To compute the instantaneous cell temperature at known values of weather variables that include the insolation, the ambient temperature and the wind speed, we shall analyse the heat exchange at steady state where the rate of change of thermal energy contained within the cell is zero, and the cell is at an equilibrium temperature T_c .

The cell temperature can be estimated by solving Eq. (3), using appropriate relations for the convective and radiative heat transfer components. This comprises the implicit methodology for the estimation of T_c ,

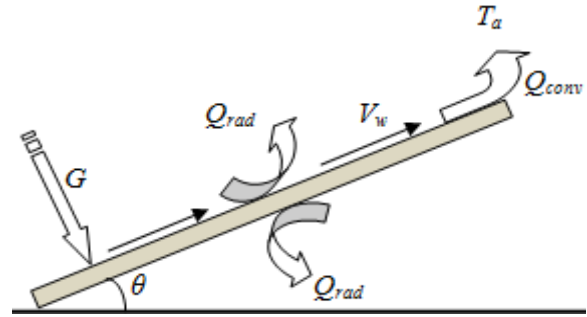


Fig. 1 – Heat exchanges in an unglazed PV cell

2.1 Implicit method for cell temperature estimation

The free and wind-induced convection components and the radiation heat transfer in Eq. (3) can be evaluated from the basic theory of heat transfer and from equations derived in previous studies.

The free convective heat transfer from the cell surfaces can be calculated as

$$Q_{free\ conv} = (h_f + h_b)(T_c - T_a) \quad (4)$$

where h_f and h_b are the coefficients of heat transfer for the front and back surfaces of the PV cell, and T_a is the ambient temperature. Approximations for the turbulent free-convective heat-transfer coefficients for the front and back surfaces tilted upward at an angle θ from the horizontal are shown in Eqs. (5) and (6) respectively (Raithby and Hollands, 1975).

$$h_f = 1.52[(T_c - T_a) \cos \theta]^{1/3} \quad (5)$$

$$h_b = 1.31[(T_c - T_a) \sin \theta]^{1/3} \quad (6)$$

The radiative heat loss per unit area of the PV surface can be approximated by Eq. (7)

$$Q_{\text{rad}} = F\varepsilon_f\sigma(T_c^4 - T_{\text{sky}}^4) + F\varepsilon_b\sigma(T_c^4 - T_a^4) \quad (7)$$

where ε_f and ε_b are the front and back surface emittances and can be taken as 0.9. The ground temperature can be assumed to be equal to the ambient temperature. The view factor F is unity for both surfaces (Armstrong and Hurley, 2010).

The sky temperature T_{sky} (Ware, 1974) is given as

$$T_{\text{sky}} = 0.914T_a \quad (\text{in K}) \quad (8)$$

The forced convective heat transfer induced by wind flowing over the PV cell surface can be calculated by

$$Q_{\text{wind}} = H(T_c - T_a) \quad (9)$$

where H is the forced-convective heat transfer coefficient, $\text{Wm}^{-2}\text{K}^{-1}$

Using these relations, Eq. (3) can be rewritten as

$$\alpha G = G \times 0.15[1 - 0.0045(T_c - 25)] + \{1.52[(T_c - T_a) \cos \theta]^{1/3} + 1.31[(T_c - T_a) \sin \theta]^{1/3}\} \cdot (T_c - T_a) + H(T_c - T_a) + \varepsilon_f\sigma(T_c^4 - T_{\text{sky}}^4) + \varepsilon_b\sigma(T_c^4 - T_a^4) \quad (10)$$

For a known set of values of the insolation, ambient temperature and wind speed, the calculation of the cell efficiency at a particular wind speed, can hence be determined by estimating the wind-induced convective heat transfer coefficient.

Numerous empirical formulae are available from heat transfer theory that correlate the convective heat transfer with the wind speed for the simple case of parallel flow over a surface. The earliest equation for wind-driven heat transfer was developed by Nusselt and Jürges (1922). In its traditional form, the Nusselt-Jürges correlation is expressed as

$$H = 5.678\{a + b[(\frac{29426}{T_a})V_w / 0.3048]^n\} \quad (11)$$

where a , b and n are empirical constants that depend on the surface texture and the wind speed. T_a is in K.

The Nusselt-Jürges correlation in SI units takes the simplified form

$$H = 5.8 + 3.95V_w \quad (12)$$

This equation is still popular and is widely used

for calculations and simulations. Palyvos (2008) points out that this dimensional equation includes radiation loss in addition to the convective heat loss and further, that the conditions in which the equation was derived differ widely from real life situations.

Over the years, several researchers have carried out experiments to correlate the wind heat transfer coefficient with the wind speed. It was found that linear regression equations of the form $H = a + bV_w$ were effective in fitting the test results obtained. Prominent among these are the equations published by McAdams (1954) and Lunde (1980) in their respective texts on convective heat transfer. Watmuff et al. (1977) developed a linear equation based on wind tunnel tests. A few other linear equations have been developed by Ito et al. (1972), Test et al. (1980), Cole and Sturrock (1977), and Sharples and Charlesworth (1998) based on field measurements. It should be noted that these equations include the effect of natural convection, thereby giving non-zero convection coefficients even for null wind speeds. An appraisal of these equations is given in Table 1.

As fundamental heat transfer theory supports a power relation between convective heat transfer coefficients and wind speed, many researchers such as McAdams (1954) and Loveday and Taki (1996) developed relations that were of the form $H = a + bV^n$. For steady-state parallel airflow over a plate, relations (13) and (14) for the wind heat transfer are found to be consistent with experimental measurements (McAdams, 1954), (Stultz and Wen, 1981)

$$H = 3.8V_w; \quad V_w \leq 5\text{ms}^{-1} \quad (13)$$

$$H = 7.13V_w^{0.78}; \quad V_w > 5\text{ms}^{-1} \quad (14)$$

These formulae were developed through laboratory tests with air blowing over the front surfaces of PV modules by means of a fan. The coefficients so derived include the free convection heat transfer component. However, natural wind movement being more complicated than fan-induced flows, these formulae may not be directly used for natural wind impinging on PV cell surfaces since wind is transient.

Kimura et al. (1975) derived the power-law equation

$$H = 18.63V_w^{0.605} \quad (15)$$

authors	correlations	comments
Nusselt, Jürges (1922)	$H = 5.8 + 3.95V_w$ $H = 7.13V_w^{0.78}$	Includes the radiation loss
McAdams (1954)	$H = 5.7 + 3.8V_w$	May include free convection and radiation losses
Kimura et al. (1975)	$H = 18.63V_w^{0.605}$	From field measurements
Cole, Sturrock (1977)	$H = 11.4 + 5.7V_w$	Applies to windward flow
Watmuff et al. (1977)	$H = 2.8 + 3.0V_w$	Exclusive of free convection and radiation losses
Lunde (1980)	$H = 4.5 + 2.9V_w$	Applies to smooth surfaces
Test et al. (1980)	$H = 8.55 + 2.56V_w$	V_w measured 1m above surface
Sparrow, Lau (1981)	$Nu = 0.86Re^{1/2}Pr^{1/3}$	From wind-tunnel testing
Schott (1985)	$H = 7.0 + 2.1V_w$ $H = 5.79V_w^{4/5}L^{-1/5}$	$\forall 1.0 \leq V_w \leq 1.5ms^{-1}$ $\forall V_w \geq 0.3ms^{-1}$
Loveday, Taki (1996)	$H = 8.91 + 2.0V_F$ $H = 4.93 + 1.77V_F$	Windward flow Leeward flow
ASHRAE (1997)	$H = 5.62 + 3.9V_w$	Proposed by ASHRAE
Sharples, Charlesworth (1998)	$H = 6.5 + 3.3V_w$ $H = 8.3 + 2.2V_w$	Windward flow Leeward flow
Furushima et al. (2006)	$H = 5.5 + 2.2V_w$	Measurements on PV modules
Sartori (2006)	$H = 5.74V_w^{4/5}L^{-1/5}$	Applies to fully turbulent flow
Palyvos (2008)	$H = 7.4 + 4.0V_F$	Averaged over 30 correlations

Table 1 – Wind heat transfer coefficient correlations

Davies (2004) has more recently found that linear equations are as effective as power-law equations

in predicting the heat transfer coefficient from the wind speed. ASHRAE has accepted one such linear correlation, with the values of the constants a and b as $a = 5.62$ and $b = 3.9$ (ASHRAE, 1997).

It is cumbersome to measure the component of wind velocity parallel to the PV surface. With a view to resolve this difficulty, Ito et al. (1972) correlated this component with the free stream velocity, V_F at a height 10 metres above the surface as:

$$V_w = 0.25V_F; \quad V_F > 2ms^{-1} \quad (16)$$

$$V_w = 0.5ms^{-1}; \quad V_F \leq 2ms^{-1} \quad (17)$$

The above listed correlations estimate the wind-induced heat transfer for only the front side of PV modules which is the case relevant for BIPVs in the windward direction. Through field measurements of the free stream wind speed Loveday and Taki (1996) developed relations for heat transfer from windward and leeward surfaces separately (see Table 1).

On the basis of data generated by thirty such linear correlations, Palyvos has derived purely empirical 'average' correlations for windward surfaces of the form of Eq. (18) and for leeward surfaces as Eq. (19):

$$H = 7.4 + 4.0V_F \quad (18)$$

$$H = 4.2 + 3.5V_F \quad (19)$$

A number of correlations have been developed that take into account the decrease of the wind convection coefficient in the direction of wind flow along the surface. They have the general form $H = aV^bL^c$. For instance, for fully turbulent airflows over flat surfaces, the equation is (Sartori, 2006)

$$H = 5.74V_w^{4/5}L^{-1/5} \quad (20)$$

The theory of thermal boundary layers has led to the development of correlations for the Nusselt number Nu in terms of the Reynolds number Re which depends on the wind speed, and the Prandtl number Pr . Through their findings on heat transfer from wind tunnel experiments on naphthalene plates, Sparrow et al. (1979) proposed a global correlation for angles of wind incidence between 90° and 25° from the horizontal with a maximum error of $\pm 10\%$ leading to

$$Nu = 0.86 Re^{1/2} Pr^{1/3}; \quad 20,000 < Re < 90,000 \quad (21)$$

The aforementioned correlations have been collated in Table 1. Using an iterative procedure, the cell efficiency at the cell operating temperature has been plotted over a range of wind speed for a few of these correlations for quantitative comparison, in Figure 2.

2.2 Explicit method for cell temperature estimation

The cell operating temperature can be arrived at by employing any of several equations expressing the cell temperature as an explicit function of the wind speed and the ambient temperature. Ross (1976) gave the earliest explicit equation for the PV cell operating temperature, in terms of the G and T_c as

$$T_c = T_a + kG \quad (22)$$

where k is known as the Ross coefficient. However, this equation only holds under zero wind conditions.

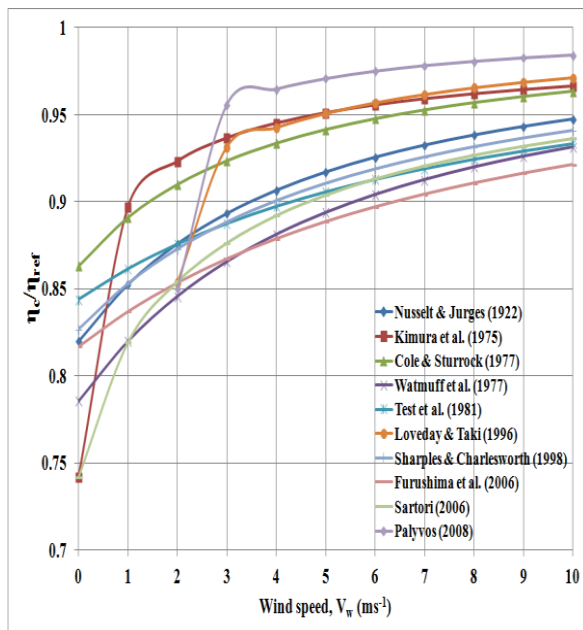


Fig. 2 – Comparison of η_c/η_{ref} as a function of wind speed as predicted by implicit correlations in Table 1 ($G = 800 \text{ Wm}^{-2}$, $T_a = 25^\circ\text{C}$, $\alpha = 0.9$, $\eta_{ref} = 15\%$)

An explicit methodology to estimate the effect of wind speed on the cell temperature T_c involves the use of the Nominal Operating Cell Temperature (NOCT). This quantity is specified by the module manufacturer, and is defined as the mean PV cell junction temperature in an open-rack mounted open-circuited module, tilted normal to the solar noon Sun in the so called Nominal Terrestrial

Environment (NTE) conditions: insolation level of 800 Wm^{-2} , ambient temperature of 20°C and an average wind speed of 1 ms^{-1} (Stultz and Wen, 1981).

With the NOCT, the Ross approximation can be used to estimate T_c as (Ross, 1980)

$$T_c = T_a + \frac{G}{G_{NOCT}} (T_{NOCT} - T_{a,NOCT}) \quad (23)$$

This approximation assumes that the overall heat transfer coefficient for the module remains constant. Skoplaki et al. (2008) have derived semi-empirical relations for PV cells, substituting typical values for NOCT and reference variables, and making use of the linear correlations for the wind heat transfer coefficient proposed by Loveday-Taki and Nusselt-Jürges, as Eqs. (24) and (25) respectively:

$$T_c = T_a + \left(\frac{0.32}{8.91 + 2.0V_F} \right) G \quad (24)$$

$$T_c = T_a + \left(\frac{0.25}{5.70 + 3.8V_w} \right) G \quad (25)$$

These equations are limited to use for free-standing PV modules, but can be extended to other mounting geometries using the mounting coefficient ω (see Table 2) (Ross, 1976) which is the ratio of the value of the Ross parameter for the mounting geometry in question to the Ross parameter for free-standing modules. T_c is expressed in terms of ω as

$$T_c = T_a + \omega \left(\frac{0.32}{8.91 + 2.0V_F} \right) G \quad (26)$$

Mounting situation	Ω
Free standing	1.000
Flat roof	1.238
Sloped roof (well cooled)	0.952
Façade integrated	2.667

Table 2 – Values of the mounting coefficient, ω employed in Eq. (26)

The NOCT methodology should be avoided for use in BIPV applications, since the under side of a building-integrated PV module experiences different ambient temperatures and wind conditions than the upper side. Moreover, the NOCT approach assumes that the overall heat transfer coefficient for the module remains constant over time, which is not valid under variable wind conditions. Davis et al. (2001) state

that the NOCT method can under-estimate PV cell operating temperatures by as much as 20°C below the actual temperatures.

In order to circumvent the limitations of the NOCT model, King et al. (2004) propose an empirical relation that incorporates the effect of the wind speed as well as the configuration of the installation as

$$T_c = T_a + Ge^{\{a+bV_w\}} \quad (27)$$

authors	correlations	comments
Ross (1980)	$T_c = T_a + \frac{G}{800}(T_{NOCT} - 20)$	Independent of the wind speed
Risser, Fuentes (1983)	$T_c = 3.12 + 0.025G + 0.899T_a - 1.3V_w$ $T_c = 3.81 + 0.0282G + 1.31T_a - 1.65V_w$	18 kW DC output to UPS 104 kW array with MPPT
King (1997)	$T_c = T_a + \frac{G}{800}[0.0712V_w^2 - 2.41V_w + 32.96]$	c-Si in open rack mount, $V_w < 18 \text{ ms}^{-1}$
King et al. (2004)	$T_c = T_a + Ge^{\{a+bV_w\}}$	Wind speed measured at a height of 10 m
Chenni et al. (2007)	$T_c = 0.943T_a + 0.028G - 1.528V_w + 4.3$	T is in °C
Skoplaki et al. (2008)	$T_c = T_a + \omega(\frac{0.25}{5.70 + 3.8V_w})G$	Using the Nusselt - Jürges relation in SI units

Table 3 - Correlations for T_c explicit in the wind speed

It should be noted that in Eq. (27) the index $a+bV_w$ is constant for a given wind speed. This model can estimate the cell temperature under more diverse conditions than the NOCT model.

A few other explicit correlations have been proposed by Risser and Fuentes (1983), King (1997), King et al. (2004) and Chenni et al. (2007) as illustrated in Table 3. The PV cell efficiency at the

operating temperature predicted by these correlations are plotted over a range of wind speed in Figure 3.

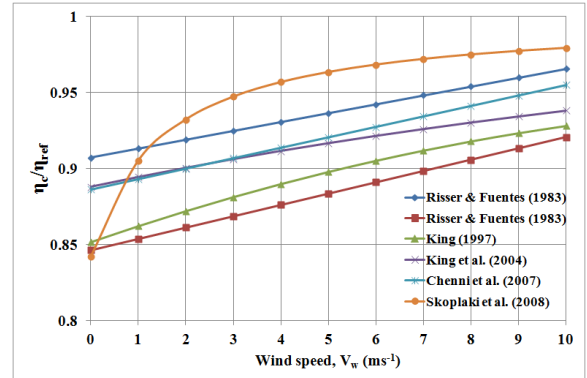


Fig. 3 – Comparison of η_c/η_{ref} as a function of wind speed as predicted by explicit correlations in Table 3. ($G = 800 \text{ Wm}^{-2}$, $T_a = 25^\circ\text{C}$, $\alpha = 0.9$, $\eta_{ref} = 15\%$)

The plots in Figures 2 and 3 indicate that the PV cell efficiency η_c increases by amounts of 5 to 14% of the reference cell efficiency η_{ref} as incident wind speed increases from a standstill 0 ms^{-1} to a speed of 10 ms^{-1} . This corresponds to an absolute increase in cell efficiency η_c of up to 2% which is significant for silicon-based PV systems. Also, it is seen that power-law relations predict higher cell efficiencies than other implicit correlations and thus may not precisely model the effect of wind on PV cell temperatures.

3. Effect of wind flow direction on photovoltaic performance

From the previous discussion, it is evident that the wind speed has a significant influence on the PV cell efficiency. The results were based on the simple case of parallel wind flow over flat surfaces. It is of interest to appreciate the effect of variation in wind flow direction on PV efficiency, which is closer to real world mounting geometries of BIPV arrays on different roof slopes. Conventionally, PV arrays are tilted to the horizontal at an inclination equal to the geographic latitude of the site and oriented facing due South (in the Northern hemisphere).

Most literature suggests that altering the tilt angles of PV arrays to accommodate for prevalent wind flow direction may not result in significant gains in

cell efficiencies. Through studies conducted on wind flow over inclined plates, Rowley and Eckley (1932) have found that the wind heat transfer coefficient for convection from an inclined plate reduced only slightly as the angle between the plate and the air stream is increased from 15° to 90°. They concluded that this reduction is insignificant and that the results obtained in the case of parallel air flow should be satisfactory for all design considerations.

Sparrow and Tien (1977) carried out tests to determine the average heat transfer coefficients for forced convection due to air flow over inclined plates. They employed the so-called *j*-factor to estimate heat transfer coefficient where *j* is given as

$$j = Nu / Re \cdot Pr^{1/3} \quad (28)$$

It is seen from their findings that the *j*-factor is insensitive to the angle of incidence, for the flow Reynolds numbers between 20,000 and 100,000. They report that the *j*-factor decreases by only 5% as the angle of incidence varies from 90° to 25°, which does not produce a significant change in wind heat transfer coefficient over the range of wind incidence.

The insensitivity of the wind heat transfer coefficient to the wind flow direction was validated by Karava et al. (2012) through two-dimensional steady Reynolds Averaged Navier Stokes (RANS) simulations of forced convective heat transfer from inclined roofs. Their results indicate that the slope of the roof has a less than 5% effect on Nusselt number, for Reynolds numbers up to 6.7×10^5 . The array tilt angle hence, has little role to play in enhancing PV cell efficiency.

As reported by Wen (1982) using results of field testing conducted at the Jet Propulsion Laboratory, the value of the coefficient of heat transfer is affected by wind direction. Incidence directions of 90 to 120° correspond to the highest values of wind heat transfer coefficient (see Figure 4) with a gain in the coefficient value of close to 25% with a 90° wind direction at a speed of 2 ms^{-1} , over a 150° directional flow. This value shows a dramatic 40% increase at a wind speed of 3 ms^{-1} . This implies that convective heat transfer is maximized when wind impinges on the PV cells in a plane perpendicular to the array.

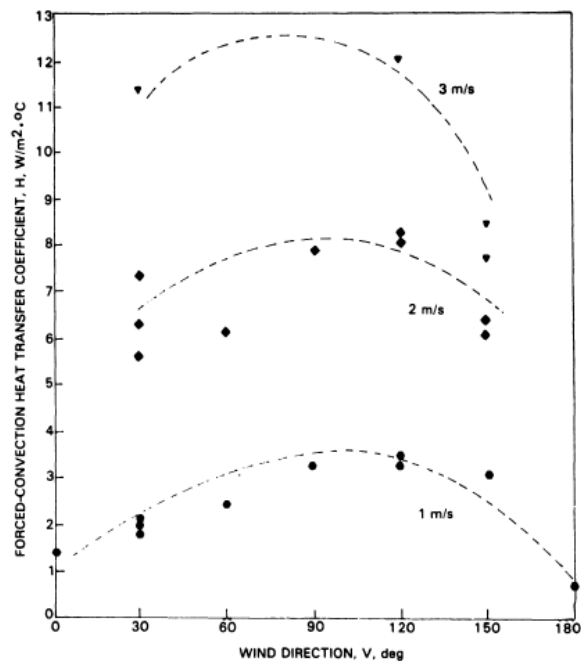


Fig. 4 – Convection heat transfer coefficient versus wind direction (Wen, 1982)

A study by Mondol et al. (2007) reveals that the variation of annual PV efficiency with respect to the orientation is insignificant for lower tilt angles. For tilt angles of 15-30°, the cell efficiency remains fairly constant for inclinations up to 45° east or west of due south. These findings can be used to optimize the orientation of PV panels taking into account the seasonal prevalent wind regimes, to allow for a more normal incidence of wind on the PV installation.

The city of Bangalore lies in a tropical region. In order to study the effect of ambient wind regimes on the performance of building envelope integrated PVs, instantaneous wind regimes were measured on the BIPV roof of the Centre for Sustainable Technologies at the Indian Institute of Science (IISc), Bangalore at five minute intervals throughout 2011. The BIPVs were installed as a joint collaboration between the Bharat Heavy Electricals Limited Electronics Division (BHEL EDN) and the Indian Institute of Science. It was observed that the wind speed striking the BIPV panels is under 1 ms^{-1} in all seasons. Also, the wind direction varies between 157.5° (SSE) and 225° (SW) (see Figure 5).

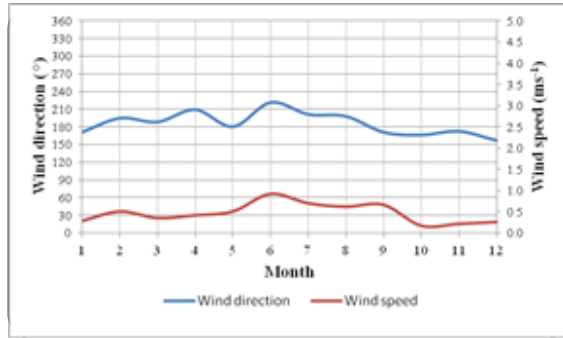


Fig. 5 – Prevalent wind regimes in different months at the IISc campus in Bangalore

Since the BIPV roof is tilted by 15° facing south i.e. 180° , the southerly wind regime on the roof rarely impinges on the surface of the PV panels. It is clear then that altering the orientation of the panels to accommodate a normal impinging of wind is not recommended for the roof as this would result in a significant drop in PV cell efficiency. However, the measured wind regime on the roof may be due to a local channel effect induced by trees around our Centre, as this differs from weather data published by the Indian Meteorological Department (IMD). Here, we demonstrate our results for the two extreme weather conditions experienced in Bangalore i.e. in May (summer) and December (winter). The average ambient temperature in May and December are 27°C and 21.1°C while the global insulations received are 900 Wm^{-2} and 650 Wm^{-2} respectively. The monthly average wind speed is 2.5 ms^{-1} in both months.

Considering these values, the BIPV cell temperature is estimated using Chenni et al.'s relation (ref. Table 3). The BIPV cell efficiency for the corresponding cell temperatures is computed based on Eq. (2). The cell operating efficiencies obtained for the summer and winter seasons under three different wind regimes are listed in Table 4. It may be seen that the PV cell efficiency under the free stream wind regime, recorded by the IMD, increases by an absolute 0.26% over the case of zero wind and by an absolute 0.21% to 0.23% over the lower wind speeds measured on our roof in both months. These are significant gains in cell efficiencies achieved by the impingement of natural wind on the PV surfaces. BIPV envelopes are thus seen to operate at their most efficient

when local wind regimes impinge the panels without obstruction.

wind regime	may	dec
Zero wind movement	12.98%	13.83%
Wind regimes measured on our BIPV roof	13.03%	13.86%
Meteorological wind records	13.24%	14.09%

Table 4 – BIPV cell efficiencies in two seasons under three different wind regimes (G – May: 900 Wm^{-2} , Dec: 650 Wm^{-2} ; Ta – May: 27°C , Dec: 21.1°C)

4. Conclusion

The current status of research in wind convective heat transfer from building envelopes and its effect on building-integrated PV systems indicates that BIPV performance is markedly affected by ambient wind regimes. A graphical representation of PV cell efficiencies predicted by several empirical relations appearing in literature reveals that a wind of 5 ms^{-1} striking a PV array can lead to a 1% gain in cell efficiency. This translates to a higher electrical output for a given insolation received at a site. Also, the percentage gain in PV cell efficiency is higher as the wind speed increases from a standstill to 5 ms^{-1} , than with increases in the wind speed beyond 5 ms^{-1} .

The cell efficiency is largely insensitive to the angle of incidence of wind on the PV surface. However, the orientation of the array, with respect to the prevalent wind direction at the site, has a significant effect on the performance of the array, with maximum cooling effect obtained when wind is incident normally on the PV surface. An installation geometry for normal wind incidence is especially beneficial for BIPVs in the tropics where cell temperatures tend to be higher.

Ambient wind regimes are therefore an important factor that must be considered for the performance of PV surfaces and of BIPV envelopes in particular.

5. Nomenclature

Symbols

a, b, c, n	constants in empirical relations
C	specific heat capacity ($\text{Jkg}^{-1}\text{K}^{-1}$)
G	solar insolation (Wm^{-2})
h	free convection coefficient ($\text{Wm}^{-2}\text{K}^{-1}$)
H	wind convection coefficient ($\text{Wm}^{-2}\text{K}^{-1}$)
k	Ross coefficient
L	surface length in wind direction (m)
NOCT	nominal operating cell temperature
Nu	($^{\circ}\text{C}$)
Pr	Nusselt number
$Q_{\text{free conv.}}$	Prandtl number
$Q_{\text{rad.}}$	free convective heat transfer (Wm^{-2})
Q_{wind}	radiative heat transfer (Wm^{-2})
Re	wind convective heat transfer (Wm^{-2})
t	Reynolds number
T	time (s)
T_a	temperature (K)
T_c	ambient temperature ($^{\circ}\text{C}$)
V, V_w	cell operating temperature ($^{\circ}\text{C}$)
V_f	wind velocity (ms^{-1})
W_p	free stream velocity (ms^{-1})
α	power output (Wm^{-2})
β_{ref}	solar absorptance
δ	temperature coefficient (K^{-1})
ε	thickness of PV cell (m)
η	emissivity
θ	efficiency
ϱ	tilt angle
σ	density (kgm^{-3})
ω	Stefan-Boltzmann constant ($\text{Wm}^{-2}\text{K}^{-4}$)
	mounting coefficient

Subscripts

a	ambient
b	back side
c	of the cell
f	front side
F	free stream
NOCT	at NOCT conditions
ref	at reference conditions
sky	of the sky
w	of the wind

References

- Armstrong, S., Hurley, W.G. 2010. A thermal model for photovoltaic panels under varying atmospheric conditions. *Applied Thermal Engineering*; 30: pp. 1488-1495.
- ASHRAE 1997. *Handbook of Fundamentals*, SI edition, Atlanta, Georgia.
- Chenni, R., Makhlouf, M., Kerbache, T., Bouzid, A.A. 2007. Detailed modelling method for photovoltaic cells. *Energy*; 32: pp. 1724-1730.
- Cole, R.J., Sturrock, N.S. 1977. The convective heat exchange at the external surface of buildings. *Building and Environment*; 12: pp. 207-214.
- Davies, M.G. 2004. *Building Heat Transfer*, John Wiley & Sons, Chichester, England, Ch. 5.7.
- Davis, M.W., Dougherty, B.P., Fanney, A.H. 2001. Prediction of Building Integrated Photovoltaic Cell Temperatures. *Transactions of the ASME Journal of Solar Energy Engineering*; 123(2); 200-210.
- Evans, D.L., Florschuetz, L.W. 1977. Cost studies on terrestrial photovoltaic power systems with sunlight concentration, *Solar Energy*; 19(3): pp. 255-262.
- Furushima, K., Nawata, Y., Sadatomi, M. 2006. Prediction of photovoltaic (PV) power output considering weather effects, *Proceedings of the SOLAR 2006 – Renewable Energy, Key to Climate Recovery*, July 7-13 2006, Denver, Colorado.
- Green, M.A., Emery, K., Hishikawa, Y., Warta, W. 2011. Solar cell efficiency tables (version 37), *Progress in Photovoltaics: Research and Applications*; 19: pp. 84-92.
- Ito, N., Kimura, K., Oka, J. 1972. A field experiment study on the convective heat transfer coefficient on exterior surface of a building, *ASHRAE Transactions* 78: pp. 184-191.
- Karava, P., Jubayer, C.M., Savory, E., Li, S. 2012. Effect of incident flow conditions on convective heat transfer from the inclined windward roof of a low-rise building with application to photovoltaic-thermal systems. *Journal of Wind Engineering and Industrial Aerodynamics*; 104-106, 428-438.

- Kimura et al. 1975. Procedure for determining heating and cooling loads for computerizing energy calculations, Algorithms for building heat transfer subroutines, ASHRAE, NY; pp. 76-78.
- King, D.L., 1997. Photovoltaic module and array performance characterization methods for all system operating conditions. Proceedings of the NREL/SNL photovoltaic program review meeting, Lakewood, Colorado, November 18–22 1997; pp. 1–22.
- King, D.L., Boyson, W.E., Kratochvil, J.A. 2004. Photovoltaic array performance model, SAND2004-3535, Sandia National Laboratories.
- Loveday, D.L., Taki, A.H. 1996. Convective heat transfer coefficients at a plane surface on a full-scale building façade, International Journal of Heat and Mass Transfer; 39(8): pp. 1729–1742.
- Lunde, P.J., 1980. Solar Thermal Engineering, John Wiley & Sons.
- Mani, M., Pillai, R., 2010. Impact of dust on solar photovoltaic (PV) performance: Research status, challenges and recommendations, Renewable and Sustainable Energy Reviews; 14: pp. 3124–31.
- McAdams, W.H. 1954. Heat Transmission, Third ed. McGraw-Hill, New York; p. 249.
- Mondol, J.B., Yohanis Y.G., Norton, B. 2007. The impact of array inclination and orientation on the performance of a grid-connected photovoltaic system. Renewable Energy; 32: pp. 118–140.
- Notton, G., Cristofari, C. Mattei, M., Poggi, P. 2005. Applied Thermal Engineering; 25: pp. 2854–77.
- Nusselt, W., Jürges, W. 1922. Die Kühlung einer ebenen Wand durch einen Luftstrom, Gesundheits Ingenieur 52. Heft, 45. Jahrgang: pp. 641–642.
- Palyvos, J.A. 2008. A survey of wind convection coefficient correlations for building envelope energy systems' modeling, Applied Thermal Engineering; 28: pp. 801–808.
- Radziemska, E., Klugmann, E. 2006. Photovoltaic maximum power point with illumination and temperature, Journal of Solar Energy Engineering; 128: pp. 34–39.
- Raithby, G.D., Hollands, H.G.T. 1975. A general method of obtaining approximate solutions to laminar and turbulent free convection problems, Advances in Heat Transfer; 11: pp. 265–315.
- Risser, V.V., Fuentes, M.K., 1983. Linear regression analysis of flat-plate photovoltaic system performance data. Proceedings of the 5th EC Photovoltaic Solar Energy Conference, October 12–16, Athens, Greece; pp. 623–627.
- Ross, R.G. 1976. Interface design considerations for terrestrial solar cell modules. Proceedings of the 12th IEEE Photovoltaic Specialists Conference, Baton Rouge, LA, December 1976. pp. 801–806.
- Ross, R.G. 1980. Flat-plate photovoltaic array design optimization. Conference Record, 14th IEEE Photovoltaic Specialists Conference, San Diego, California; pp. 1126–1132.
- Rowley, F.P., Eckley, W.A. 1932. Surface coefficients as affected by wind direction. Trans. ASHRAE; 38: pp. 33–46.
- Sartori, E. 2006. Convection coefficient equations for forced air flow over flat surfaces, Solar Energy; 80: pp. 1063–1071.
- Schott, T. 1985. Operation temperatures of PV modules, Proceedings of the 6th E.C. PV Solar Energy Conference, London, April 15–19 1985, D. Reidel Publ. Co.; pp. 392–396.
- Sharples, S., Charlesworth, P.S. 1998. Full-scale measurements of wind-induced convective heat transfer from a roof-mounted flat plate solar collector. Solar Energy; 62(2): pp. 69–77.
- Skoplaki, E., Boudouvis, A.G., Palyvos, J.A. 2008. A simple correlation for the operating temperature of photovoltaic modules of arbitrary mounting. Solar Energy Materials and Solar Cells; 92: pp. 1393–1402.
- Sparrow, E.M., Lau, S.C. 1981. Effect of adiabatic coplanar extension surfaces on wind-related solar-collector heat transfer coefficients, Trans. ASME J. of Heat Transfer; 103: pp. 268–271.
- Sparrow, E.M., Ramsey, J.W., Mass, E.A. 1979. Effect of finite width on heat transfer and fluid flow about an inclined rectangular plate, Trans. ASME J. of Heat Transfer; 101: pp. 199–204.

- Sparrow, E.M., Tien, K.K. 1977. Forced Convection Heat Transfer at an Inclined and Yawed Square Plate – Application to Solar Collectors, Trans. ASME J. of Heat Transfer; 99: pp. 507-512.
- Stultz, J.W., Wen, L. 1981. Thermal Performance Testing and Analysis of Photovoltaic Modules in Natural Sunlight, LSSA Project Task Report 5101-31, JPL, Pasadena, California.
- Test, F.L., Lessmann, R.C., Johary, A 1980. Heat transfer during wind flow over rectangular bodies in the natural environment, Journal of Heat Transfer; 103(2): pp. 262-267.
- Ware, J.C. 1974. Clear Sky Temperature, presented at ISES Meeting, Fort Collins, CO, August 1974.
- Watmuff, J.H., Charters, W.W.S., Proctor, D. 1977. Solar and Wind Induced External Coefficients Solar Collectors 2nd Quarter, Revue Internationale d’Helio- technique; p. 56.
- Wen, L. 1982. An Investigation of the Effect of Wind Cooling on Photovoltaic Arrays, Report DOE/JPL 1012-69, JPL, Pasadena, California.

Thermo-fluid dynamics of woody biomass flue gas in the heat accumulation stoves

Paolo Scotton – University of Padova, Padova, Italy

Daniele Rossi – University of Padova, Padova, Italy

Mauro Barberi – Barberi Stufe LTD, Trento Italy

Stefano De Toni – Barberi Stufe LTD, Trento Italy

Abstract

The research aims to clarify some aspects of the thermo-fluid dynamics of woody biomass flue gas within the refractory twisted conduit inside heat accumulation stoves. These are traditional heating elements in the European Alpine regions, whose history began in the fifteenth century. The high temperature flue gas flows in a twisted conduit, releasing heat along its path to the refractory. The heat stored in the refractory is then released slowly into the environment mainly as a radiant component. The physical phenomena that occur in an accumulation stove, once the activation energy in the combustion chamber has been provided, continues, initially increasing temperature and velocity of flue gases and then decreasing the two variables until the end of the reaction. The decreasing temperatures of flue gases, flowing from the combustion chamber in the twisted conduit, tends to cause the transition of the flow regime from laminar to turbulent conditions [1] [2]. Moreover the continuous changes of direction imposed by the curves cause local contractions and expansions of the flux and, consequently, energy losses which are difficult to evaluate. The way the heat transfer occurs appears to depend mainly on gas flow conditions (laminar or turbulent) and on the radiative properties of the hot particle cloud inside the flue gas. The physical properties of the conduit (roughness of the internal surface), as well as the thermodynamic properties of the refractory material (its mass and its geometric arrangement), play a fundamental role in the functionality of the stove. This paper describes some analysis performed on heat transport and exchange processes inside the flue gases and between them and the refractory. The importance of the radiation properties of the flue gasses has been highlighted. The numerical results, obtained with

COMSOL® Non Isothermal Flow ($k-\epsilon$ turbulent model), have been compared with laboratory measures.

1. Introduction

The research regards some thermo-fluid dynamic aspects of the biomass flue gas of a particular kind of heat accumulation stove made of ceramic and refractory. They consist of a combustion chamber,



Fig. 1 – View of a project design of a modern stove, where the combustion chamber and twisted conduit are visible and a phase of its construction (Barberi Ltd).

where woody material is burned, followed by a twisted conduit where the flue gases transfer heat to the refractory.

Due to the heat transfer along the pipe, the kinematic viscosity of the flue gas decreases, the density increases and the Reynolds number increases causing transition from laminar to turbulent motion. Moreover the continuous changes of direction imposed by the curves cause local contractions and expansions of the flux and, consequently, energy losses that are difficult to evaluate. The stored heat is released slowly in the rooms of the house mainly in the form of radiant heat from the ceramic tiles of the external surface.

The way the heat transfer happens depends mainly on gas flow conditions (laminar or turbulent) and on the radiative properties of the hot particle cloud inside the flue gas. From this point of view, the composition of flue gas plays a fundamental role in the global behaviour of the heat transfer. The physical properties of the conduit (shape, roughness of the internal surface), as well as the thermodynamic properties of the refractory material, its mass and its geometric arrangement, are other main aspects of the stove's functionality. The representation of the phenomena described above is the goal of the present research, in order to provide increased awareness in the design process of these technological elements, which is strongly affected by the uncertainties described above.

Working in that direction, some physical models have been realized by the laboratory of Barberi Ltd, on which several measures of temperature, pressure and velocity have been taken, both inside the gases and on the outer surface of the conduit. In the present paper we show the numerical results obtained reproducing one geometrically simplified physical model, under unsteady flow regime. All the numerical applications have been performed on the basis of previous experiences reported in [1], [2] and [4].

2. Physical Model

For a simplified analysis of the behaviour of the heat accumulation stove a physical model has been

built. It was realized in blocks of refractory material (normally used for the construction of the stoves) and it is described below.

2.1 Geometry and materials

The physical model is composed by a combustion chamber (height 0.89 m, width 0.81 m, depth 0.70 m), a straight refractory conduit (length 6.0 m, inner diameter 180.0 mm) and a chimney (Fig. 2). The combustion chamber has been connected to the refractory conduit by means of a black steel pipe.

The conduit lies on a continuous support made of calcespan. The air, necessary for the combustion reactions, was supplied by a natural draught. It was introduced into the combustion chamber through an instrumented stainless steel pipe where a valve, a diaphragm and a thermocouple were installed. The mass flow of the flue gas was deduced from the mass flow of the air supply, according to EN 15544 [5].

In Table the thermo-technical characteristics of the materials are reported.

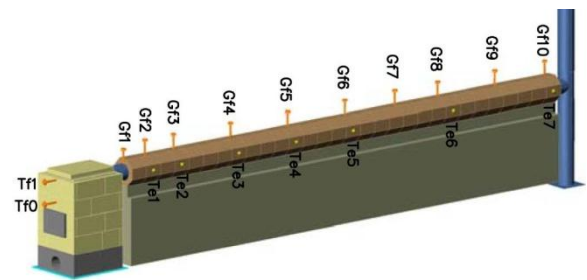


Fig. 2 – The simplified configuration of a heat accumulation stove built for the study of its behaviour (Barberi Ltd).

	refract.	calcespan	steel
ρ	2550 [kg/m ³]	600 [kg/m ³]	7990 [kg/m ³]
C_p	859 [J/kg K]	1000 [J/kg K]	500 [J/kg K]
k	3.16 [W/m K]	0.15 [W/m K]	50 [W/m K]
ε	0.95 [-]	0.70 [-]	0.95 [-]

Table 1: Thermo-technical properties of the materials (Barberi Ltd).

2.2 Experimental measures

The measurements of temperature inside the flue gas have been taken at the middle point of ten sections of the pipe (G_f) by K – thermocouples. The temperatures at the outer surface are taken at 7 positions as indicated in Fig. 2 (T_e). Three

temperature measurements of the surrounding atmosphere have been taken: one above and two on the lateral side of the refractory conduit. The radiant heat of one side of the conduit was caught by means of an infrared camera, in order to obtain another temperature estimation.

The physical phenomena that occur in an accumulation stove, once the activation energy in the combustion chamber has been provided, continue, initially increasing temperature and velocity of flue gases and then decreasing the two variables until the end of the reaction. This causes a continuous variation in the motion conditions at the inlet of refractory conduit (Table 2). In addition, due to the heat transfer along the pipe, the gas kinematic viscosity decreases whereas the density increases, causing the increase of the Reynolds number.

The variability in time of some parameters, estimated at the *Gf1* thermocouple (Fig. 2), are shown in Fig. 3 and Table 2.

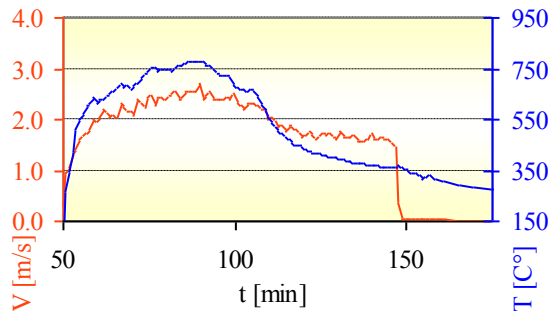


Fig. 3 – Measured temperature and calculated velocity at the inlet of refractory conduit.

3. Mathematical model

The set of physical and chemical processes taking place inside the combustion chamber and inside the flue gas conduit are very complex and, currently, not yet completely understood.

t [min.]	T _{Gf1} [°C]	ρ [kg/m ³]	V [m/s]	Re [-]	h _{PL} [mm]
50.0	14.95	1.186	0.30	4079	12.5
51.4	347.02	0.551	1.04	3578	14.2
53.8	510.13	0.436	1.42	3301	15.1
55.8	570.66	0.405	1.70	3509	14.3
60.7	628.91	0.379	2.04	3795	13.3
67.7	671.90	0.361	2.28	3951	12.9
75.8	755.86	0.332	2.46	3760	13.4
82.8	751.50	0.333	2.53	3891	13.0
88.7	776.83	0.325	2.55	3787	13.4
92.7	759.41	0.331	2.55	3878	13.1
99.7	686.94	0.356	2.46	4163	12.3
108.7	584.74	0.398	2.18	4384	11.7
117.7	449.48	0.473	1.82	4827	10.7
126.8	408.22	0.501	1.68	4914	10.5
139.8	366.65	0.534	1.67	5433	9.6
146.8	362.53	0.537	1.44	4737	10.9
147.8	366.74	0.534	0.36	1171	41.1
147.9	360.75	0.539	0.04	132	—

Table 2 – Temperatures surveyed from *Gf1* thermocouple, calculated density [5], velocity and Reynolds number of flue gas and, in the last column, the thickness required (by the software Consol [7]) for the first cells of the boundary layer.

In the present work we have focused our attention on fluid dynamics and thermal processes inside the flue gas conduit.

3.1 Governing equations

The Navier – Stokes equations describe the motion of viscous fluids. For a single-phase flow they are composed by the continuity equation:

$$\frac{\partial \rho}{\partial t} + \nabla \cdot (\rho \vec{u}) = 0, \quad (1)$$

and by the momentum equation:

$$\rho \frac{\partial \vec{u}}{\partial t} + \rho \vec{u} \cdot \nabla \vec{u} = -\nabla p + \nabla \cdot \tau + F, \quad (2)$$

where the viscous stress tensor is given by

$$\tau = \mu \left(\nabla \vec{u} + \nabla \vec{u}^T \right) - \frac{2}{3} \mu \left(\nabla \cdot \vec{u} \right) \vec{I}.$$

For turbulent flows the Navier – Stokes equations are simplified, through the average over the time, in the Reynolds – Averaged Navier Stokes (RANS) equations [6] [7].

In the term F , to the right hand of (2), are present also the buoyancy forces $F = -\rho g$, responsible for

the flow stratification and for the natural draught of the stove. The density ρ is, however, a variable of the problem and depends on the temperature. Therefore, the buoyancy forces can be introduced in the momentum equations through the first Boussinesq approximation:

$$F = -(\rho - \rho_R)g \quad (3)$$

or with the second order of approximation:

$$F = -\rho_R \beta (T - T_R)g \quad (4)$$

For both Boussinesq approximations the associated boundary condition is $dp/dy = 0$.

The heat transfer in one physic system is provided by conduction, convection and radiation. For conduction in a multidimensional isotropic system, the Fourier law can be rewritten in the form ([8] [10]):

$$q = -k \nabla T \quad (5)$$

The convection heat transfer, which occurs between a wall at temperature T_w and the surrounding atmosphere at undisturbed temperature T_∞ ([8] [10]), can be represented by

the equation:

$$q = h(T_w - T_\infty). \quad (6)$$

where $h = Nu \cdot k / d$.

In the study of the heat transfer by radiation, in the cases where heat is supplied to the physical system by combustion of any fuel type, the flue gas has to be considered as a participant medium. It is composed of a fraction of molecular gas and a part of particulate matter. Its interaction with the radiative intensity travelling in a given direction ($I(\Omega_i)$) occurs through absorption, emission and scattering [10].

The radiation absorption of the particulate matter has been observed to be proportional to the magnitude of the incident energy as well as the distance the beam travels (s) through the medium:

$$\frac{dI_{abs}}{ds} = -\kappa I(\Omega; s). \quad (7)$$

At the given temperature T , the rate of emission from a volume element will be equivalent to a fraction of emission intensity of the black body:

$$\frac{dI_{em}}{ds} = \kappa I_b(T). \quad (8)$$

The scattering can be distinguished in out-scattering and in-scattering. The out-scattering

considers the part of incoming intensity that is deviated from the considered direction of propagation (9). The out-scattering intensity appears, therefore, as augmentation energy (in-scattering) along another direction.

$$\frac{dI_{out-sc}}{ds} = -\sigma_s I(\Omega; s) \quad (9)$$

The in-scattering has contributions from all directions and, therefore, must be calculated by integration over all solid angles Ω_i :

$$\frac{dI_{in-sc}}{ds} = -\sigma_s / (4\pi) \int_{4\pi} I(\Omega_i) \phi(\Omega_i; \Omega) d\Omega_i \quad (10)$$

Considering the two terms of attenuation, absorption and out-scattering, leads to define the extinction coefficient through the path s :

$$\frac{dI_{extinction}}{ds} = -\beta I(\Omega; s), \quad (11)$$

where $\beta = \kappa + \sigma_s$ is the extinction coefficient.

The equation of heat transfer by radiation (Radiation Transfer Equation - RTE), in the direction of solid angle ($\Omega \cdot \nabla I(\Omega)$) reads [9] [10]:

$$\kappa I_b(T) - \beta I(\Omega; s) - \frac{\sigma_s}{4\pi} \int_{4\pi} I(\Omega_i) \phi(\Omega_i; \Omega) d\Omega_i. \quad (12)$$

Another component of heat transfer by radiation occurs between the outer surface, at temperature T_w , and the surrounding ambient at undisturbed temperature T_∞ . This component of heat exchange can be written as:

$$q = \varepsilon \sigma (T_\infty^4 - T_w^4) \quad (13)$$

3.2 Model settings

The first set of simulations was carried out on the part of experimental apparatus that goes from the steel conduit, required to connect the heater to the refractory conduit, to the control section located in the chimney, 2.7 m above the floor. The flue gas was considered radiatively a transparent medium. The boundary conditions for the unsteady problem are the pressure at the final section and mass discharge (calculated using the literature equations reported in EN 15544 [5]) at the initial section. In these numerical models the buoyancy forces have been considered using the first Boussinesq approximation (3).

On the outer surface, a boundary condition of convective cooling (6) was used together with a

boundary condition for the radiation from surface to the ambient (13).

	Complete model (M1) no radiation	partial model (M2) yes radiation
h_{FL}	0.36 [mm]	—
h_{Tr}	2.9 [mm]	14.4 [mm]
h_{Te}	29.1 [mm]	480.0 [mm]
N° El.	$139.1 \cdot 10^3$	$9.8 \cdot 10^3$
D.O.F.	$175.5 \cdot 10^3$	$114.5 \cdot 10^3$

Table 3 – Thickness of the first layer of boundary layer h_{FL} ; minimum height of triangular cells h_{Tr} and tetrahedral cells h_{Te} , total number of mesh elements N° El.; degrees of freedom of the system for the two configurations.

The numerical results of temperature were significantly different from the measured ones. So, it was supposed that the heat transfer by radiation of the flue gas could not be neglected.

In order to investigate the effects of the radiation with participant media, a second set of simulations were made.

Because of the slowness of the numerical research of the solution of these problems, a reduced geometry, first four meters, with a coarse mesh was considered.

The Radiation Transfer Equation – RTE (12), introduced into the numerical model, was solved using the method of Discrete – Ordinate Approximation with the S_2 discretization [9] [10]. The values of absorption and scattering used are respectively equal to 0.8307 [1/m] and 0.0 [1/m].

It was decided to use the k- ϵ model [6]. The characteristics of the meshes are shown in Table 3.

The characteristics of the workstation are two Intel® Xeon® CPU X5550, 2.67 GHz (eight processors) and 24GB ram with a 64 bit software.

3.3 Results and discussion

The average cross-sectional values of velocity, pressure and temperature along the conduit were evaluated (Fig. 4). The data were calculated at the 88th minute, corresponding to the peak time of the temperature (Fig. 3). The average velocity of the flue gas is well approximated by a segment of straight line with a mean-square deviation (R2) equal to 0.95.

The average temperature distribution can be well represented by an exponential function. The mean-square deviation, in this case, was equal to 0.99.

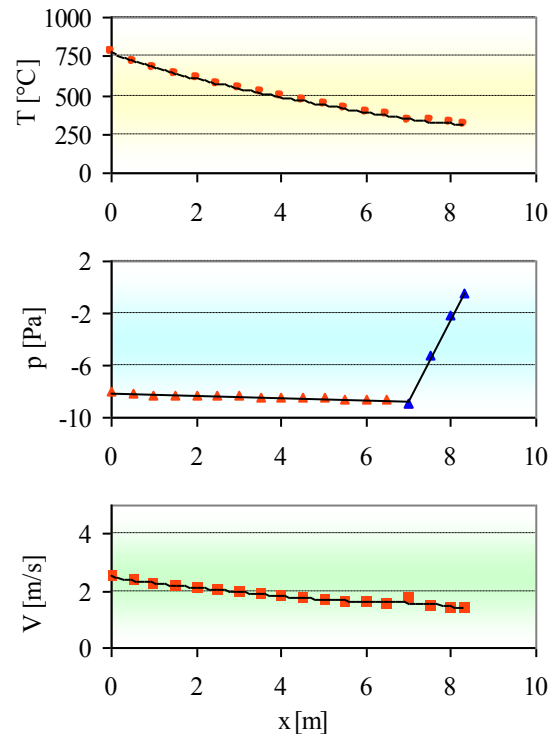


Fig. 4 – Longitudinal evolution of the mean cross-sectional values (temperature, pressure, velocity) at the 88th minute.

As far as the pressure is concerned, a more complex reasoning should be made. In the horizontal refractory pipe, the pressure values decrease gradually until the sharp curve, used as a connection between the horizontal section and the chimney. Then the trend starts to grow again to reach the undisturbed pressure value of the outlet cross section.

This pressure trend is caused by buoyancy forces (3). Previous results of numerical simulations showed that if those forces were neglected, it was not possible to obtain this behaviour [3]. In general, the average pressure pattern can be well approximated by a segment of straight line, both for the first horizontal section (mean-square deviation equal to 0.89) and for the vertical chimney section (mean-square deviation equal to 1.00).

In Fig. 5 the temperature values, measured and calculated, obtained from the first numerical model (M1), considering the flue gas as a transparent

medium are compared at three cross-sections. At the first section, the temperature of the flue gas measured and calculated in the middle of the conduit are in quite good agreement (Gf3), especially after the instant of the maximum temperature. This is not the same, however, for the outer surface (Te2). At the other two sections the behaviour tends to be the opposite. The interruption of the combustion air supply, after 150 minutes, produces numerical results quite different from the measured ones, mainly at the first section. An explanation for that has not yet been reached by the authors. The point could be investigated by analysing the effect of the mesh discretization, of the heat transfer coefficients and also of the system's thermal capacity, including the thermal capacity of the flue gas.

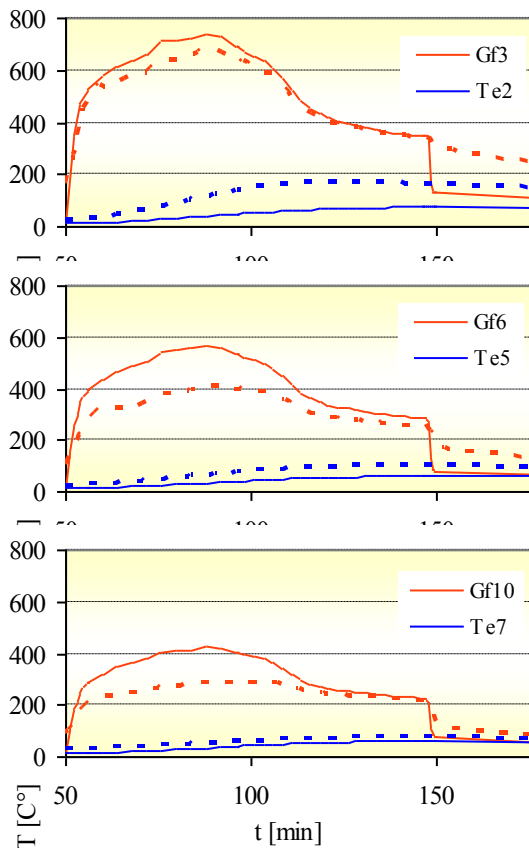


Fig. 5 – Temperatures measured on a physical model (dotted line) and calculated from a numerical model (solid line) at three cross-sections.

Due to the high temperatures of the phenomenon, it is reasonable to give radiation an important role. So, we introduced the radiative transfer equation into the model.

The length of the numerical apparatus has been limited to four meters because of the large increase of equations to solve. The value 0.831 has been given to the absorption coefficient κ , and the value 1.073 has been given to the scattering coefficient σ_s , ([9]).

The agreement between the calculated and measured temperature was significantly improved, especially in the first meters of the model, in the time period during which the model kept the numerical stability.

At the Gf3 thermocouple, the numerical results are superimposed on those measured. At the Gf6 thermocouple the numerical results are closer to the physical data but not yet satisfactory (Fig. 6). The behaviour of the temperatures calculated on the outer surface of the pipe (not shown in Fig. 6) does not differ significantly from the one calculated with the first numerical model (Fig. 5).

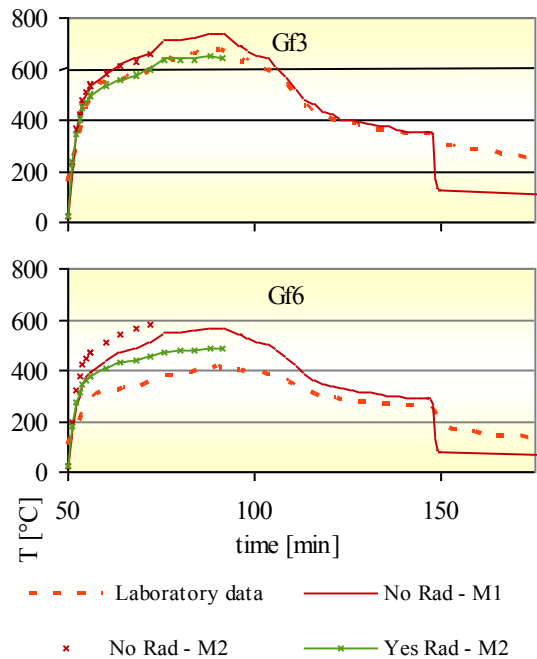


Fig. 6 – Temperatures experimentally measured and numerically calculated with the first (M1, Table 2) and the second (M2, Table 2) numerical model at the Gf3 and Gf6 thermocouples (Fig. 2).

In order to cover the gap between physical and numerical data, we are working on a better definition of the radiative parameters of the flue gas, on the thermal characteristics of the refractory material, which have been considered, until now, independent of temperature, and on the boundary conditions posed on the outer surface of the conduit.

4. Conclusions

Even if the numerical applications show significant differences from the laboratory data, we think we are going in the right direction to simulate this challenging thermo-fluid-dynamic process.

There should be at least three main reasons for the differences.

The first one is related to the reliability of the experimental measurements. The very difficult experimental conditions (very high temperatures, very low pressures) induce to accept high errors of the order of 15%-20%.

The second one is of a numerical type. The choice of the mesh significantly influences the numerical solution [4]. In particular, near a wall, the choice of the mesh could have great influence on the heat transfer through the wall. Some calculations based on the numerical results of the liminar coefficients have produced values that seem to be three or four times lower than the physical ones.

The third reason is the capability of taking account of all the physical processes which are present in the real phenomenon. Problems arise both from the physical interpretation of the phenomena and from the capability of the software to positively complete the numerical simulation. In the present simulations, for instance, we have seen the importance of the radiation absorption and emission phenomena of particle fraction of the flue gas [9]. At the same time we needed to limit the numerical integration in time because of numerical instabilities.

The research is currently devoted to a deeper understanding of the role of the different radiative terms of the flue gas and to their appropriate definition in our case.

5. Acknowledgement

The research has been financed by the Trentino (Italy) Provincial law n. 6, 1999, call 2008 - project: "La stufa ad accumulo-Innovazione nella tradizione" of the Barberi Ltd.

6. Nomenclature

Symbols

d	diameter	[m]
h	convective coefficient	[W/(m ² K)]
h_{FL}	thickness of the first layer of boundary layer	[mm]
h_{Tr}	minimum height of triangular cells	[mm]
h_{Te}	minimum height of tetrahedral cells	[mm]
k	thermal conductivity	[W/(m K)]
κ	absorption coefficient	[1/m]
\mathbf{I}	identity matrix	[-]
I	radiative intensity	[-]
I_b	black body radiative intensity	[-]
μ	dynamic viscosity	[Pa]
Nu	Nusselt number	[-]
Ω_i	solid angle in i direction	[sr]
p	Pressure	[Pa]
q	heat flux	[W/m ²]
ρ	density	[kg/m ³]
ρ_R	reference density	[kg/m ³]
s	beam travel distance	[m]
σ_s	scattering coefficient	[1/m]
t	time	[s]
T	temperature	[°C]
T_w	wall temperature	[°C]
T_∞	undisturbed temperature	[°C]
T_R	reference temperature	[°C]
τ	viscous stress tensor	[Pa]
\vec{u}	velocity vector	[m/s]

References

- [1] Scotton P., Rossi D. 2011, Studio della dinamica del moto dei fumi nelle stufe ad accumulo – Relazione 1° anno, (2011), prot. n. 442 (2010), Department of Geosciences, Univ. of Padova;
- [2] Scotton P., Rossi D. 2011, Study of Gas Dynamics in the Heat-accumulation Stoves, Comsol Conference 2011 Stuttgart Proceedings, ISBN 978-0-9839688-0-1;
- [3] Scotton P., Rossi D. 2012, Studio della dinamica del moto dei fumi nelle stufe ad accumulo – Relazione 2° anno, (2012), prot. n. 442 (2010), Department of Geosciences, Univ. of Padova;
- [4] Scotton P. Rossi D., Barberi M., De Toni S. 2012, Thermo-Fluid Dynamics of Flue Gas in Heat Accumulation Stoves: Study Cases, Comsol Conference 2012 Boston Proceedings, ISBN 978-0-9839688-8-7;
- [5] EN-15544, One of kachelgrundöfen putzgrundöfen (tiled mortared stoves) – calculation method;
- [6] Garde R. J. 2010, Turbulent Flow, New Age International, 2010.
- [7] Comsol Multiphysics, CFD Module User's Guid;
- [8] Faghri A., Zhang Y., Howel J. 2010, Advanced Heat and Mass Transfer, Global Digital Press, Columbia, USA;
- [9] Modest M. F. 1993, Radiative Heat Transfer, McGraw Hill;
- [10] Comsol Multiphysics, Heat Transfer Module User's Guid;

List of authors

Aghemo, Chiara	chiara.aghemo@polito.it	Politecnico di Torino, Turin, Italy
Albatici, Rossano	rossano.albatici@unitn.it	University of Trento, Trento, Italy
Ansuini, Roberta	r.ansuini@univpm.it	Università Politecnica delle Marche, Ancona, Italy
Antonacci, Gianluca	gianluca.antonacci@cisma.bz.it	CISMA Srl, Bolzano, Italy
Arcuri, Natale	natale.arcuri@unical.it	University of Calabria, Arcavacata di Rende (CS), Italy
Atzeri, Anna Maria	annamaria.atzeri@natec.unibz.it	Free University of Bozen-Bolzano, Bolzano, Italy
Avesani, Stefano	stefano.avesani@eurac.edu	Eurac Research, Bolzano, Italy
Baggio, Paolo	paolo.baggio@unitn.it	University of Trento, Trento, Italy
Balaji, Nallaval Chinnaswamy	balajinallaval@gmail.com	Indian Institute of Science, Bangalore, India
Baldracchi, Paolo	paolo.baldracchi@eurac.edu	Eurac Research, Bolzano, Italy
Ballarini, Ilaria	ilaria.ballarini@polito.it	Politecnico di Torino, Turin, Italy
Baratieri, Marco	marco.baratieri@unibz.it	Free University of Bozen-Bolzano, Bolzano, Italy
Barberi, Mauro	info@barberistufe.com	Barberi Stufe LTD, Trento, Italy
Bettoni, Davide	davide.bettoni@eurac.edu	Eurac Research Centre, Bolzano, Italy
Blaso, Laura	laura.blaso@polito.it	Politecnico di Torino, Turin, Italy
Bogar, Debora	debora.bogar@uniud.it	Università degli Studi di Udine, Udine, Italy
Bruno, Roberto	roberto.bruno@unical.it	University of Calabria, Arcavacata di Rende (CS), Italy
Cappelletti, Francesca	francesca.cappelletti@iuav.it	University IUAV of Venezia, Venezia, Italy
Chiogna, Michela	michela.chiogna@ing.unitn.it	University of Trento, Trento, Italy
Corrado, Vincenzo	vincenzo.corrado@polito.it	Politecnico di Torino, Turin, Italy
Dalmasso, Daniele	daniele.dalmasso@polito.it	Politecnico, di Torino, Turin, Italy
D'Antoni, Matteo	matteo.dantoni@eurac.edu	Eurac Research Centre, Bolzano, Italy
De Toni, Stefano	info@barberistufe.com	Barberi Stufe LTD, Trento, Italy
Del Giudice, Matteo	matteo.delgiudice@polito.it	Politecnico di Torino, Turin, Italy
Demattè, Silvia	s.dematte@enginsoft.it	EnginSoft, Trento, Italy
Di Perna, Costanzo	c.diperna@univpm.it	Università Politecnica delle Marche, Ancona, Italy
Dias, Diana	deq08016@fe.up.pt	Universidade do Porto, Porto, Portugal
Dipasquale, Chiara	chiara.dipasquale@eurac.edu	University of Catania, Catania, Italy
Doust, Narghes	narghes.doust@gmail.com	Politecnico di Milano, Milano, Italy
Erba, David	david.erba@polito.it	Politecnico di Torino, Turin, Italy
Evola, Gianpiero	gevola@unict.it	University of Catania, Catania, Italy
Fedrizzi, Roberto	roberto.fedrizzi@eurac.edu	Eurac Research Centre, Bolzano, Italy
Filippi Oberegger, Ulrich	ulrich.filippi@eurac.edu	Eurac Research Centre, Bolzano, Italy
Fortuna, Stefano	stefogeom@libero.it	University IUAV of Venice, Venice, Italy
Fracastoro, Giovanni	giovanni.fracastoro@polito.it	Politecnico di Torino, Turin, Italy
Frattari, Antonio	antonio.frattari@unitn.it	University of Trento, Trento, Italy

List of authors

Frontini, Francesco	francesco.frontini@supsi.ch	University of applied Science and Arts, Canobbio, Switzerland
Gasparella, Andrea	andrea.gasparella@unibz.it	Free University of Bozen-Bolzano, Bolzano, Italy
Gayathri, Aaditya	gayathriaaditya@gmail.com	Indian Institute of Science, Bangalore, India
Gigli, Davide S.	davidesilvio.gigli2@unibz.it	Free University of Bozen-Bolzano, Bolzano, Italy
Giretti, Alberto	a.giretti@univpm.it	Università Politecnica delle Marche, Ancona, Italy
Giuga, Maria		University of Catania, Catania, Italy
Gober, Alessandro	alessandro.gober@unibo.it	University of Bologna, Bologna, Italy
Gorrino, Alice	alice.gorrino@polito.it	Politecnico di Torino, Turin, Italy
Grassi, Walter	w.grassi@ing.unipi.it	University of Pisa, Pisa, Italy
Grillo, Maria Cristina	maria.grillo@ing.unitn.it	University of Trento, Trento, Italy
Hensen, Jan	j.hensen@tue.nl	Eindhoven University of Technology, Eindhoven, The Netherlands
Hirsch, Elian	Elian.Hirsch@kadm.dk	Royal Danish Academy of Fine Arts, School of Architecture, Copenhagen, Denmark
Kummert, Michaël	michael.kummert@polymtl.ca	École Polytechnique, Montréal, Canada
Larghetti, Roberto	r.larghetti@univpm.it	Università Politecnica delle Marche, Ancona, Italy
Leal, Vítor	vleal@fe.up.pt	Universidade do Porto, Porto, Portugal
Lezzi, Daniele	daniele.lezzi@bsc.es	Barcelona Supercomputer Center, Barcelona, Spain
Lollini, Roberto	roberto.lollini@eurac.edu	Eurac Research Centre, Bolzano, Italy
Maccarini, Alessandro	amac@kadm.dk	Royal Danish Academy of Fine Arts, School of Architecture, Copenhagen, Denmark
Machado, João	jmachado@cin.pt	Corporação Industrial do Norte, Maia, Portugal
Mahdavi, Ardeshtir	amahdavi@tuwien.ac.at	Vienna University of Technology, Vienna, Austria
Mani, Monto	monto.mani@gmail.com	Indian Institute of Science, Bangalore, India
Manzan, Marco	manzan@units.it	University of Trieste, Trieste, Italy
Marengo, Marco	marco.marengo@unibg.it	University of Bergamo, Dalmine (BG), Italy
Marinosci, Cosimo	cosimo.marinosci@unibo.it	Università di Bologna, Bologna, Italy
Marletta, Luigi	luigi.marletta@dii.unict.it	University of Catania, Catania, Italy
Marzoli, Matteo	matteo.marzoli@supsi.ch	University of applied Science and Arts, Canobbio, Switzerland
Mazzarella, Livio	livio.mazzarella@polimi.it	Politecnico di Milano, Milan, Italy
Mazzeo, Domenico		University of Calabria, Arcavacata di Rende (CS), Italy
Mazzichi, Francesca	mazzichi@units.it	University of Trieste, Trieste, Italy
Menchetti, Elena	e.menchetti@adm.unipi.it	University of Pisa, Pisa, Italy
Mendes, Adélio	mendes@fe.up.pt	Universidade do Porto, Porto, Portugal
Messina, Angelo	a.messina@enginsoft.it	EnginSoft, Trento, Italy
Moret, Stefano	moret.stefano@gmail.com	Università degli Studi di Padova, Vicenza, Italy
Moro, Lorenzo	lorenzo.moro@unipd.it	Università degli Studi di Padova, Padova, Italy
Naboni, Emanuele	Emanuele.Naboni@kadm.dk	Royal Danish Academy of Fine Arts, School of Architecture, Copenhagen, Denmark
Neri, Paolo	paolo.neri@enea.it	LCA-lab, Bologna, Italy
Neyer, Daniel	daniel.neyer@uibk.ac.at	University of Innsbruck, Innsbruck, Austria
Noro, Marco	marco.noro@unipd.it	Università degli Studi di Padova, Vicenza, Italy
Osello, Anna	anna.osello@polito.it	Politecnico di Torino, Turin, Italy
Paduos, Simona	simona.paduos@polito.it	Politecnico di Torino, Turin, Italy

Papamichael, Konstantinos	kpapamichael@ucdavis.edu	University of California Davis, Davis (CA), USA
Passerini, Francesco	francesco.passerini@ing.unitn.it	University of Trento, Trento, Italy
Patuzzi, Francesco	francesco.patuzzi@natec.unibz.it	Free University of Bozen-Bolzano, Bolzano, Italy
Pedretti, Laura	laura.pedretti@unibo.it	Università di Bologna, Bologna, Italy
Pellegrino, Anna	anna.pellegrino@polito.it	Politecnico di Torino, Turin, Italy
Penna, Paola	paola.penna@natec.unibz.it	Free University of Bozen-Bolzano, Bolzano, Italy
Pernetti, Roberta	roberta.pernetti@unipv.it	University of Pavia, Pavia, Italy
Pernigotto, Giovanni	pernigotto@gest.unipd.it	University of Padova, Vicenza, Italy
Peron, Fabio	fperon@iuav.it	University IUAV of Venice, Venice, Italy
Picco, Marco	marco.picco@unibg.it	University of Bergamo, Dalmine (BG), Italy
Prada, Alessandro	alessandro.prada@unibz.it	Free University of Bozen-Bolzano, Bolzano, Italy
Prando, Dario	dario.prando@natec.unibz.it	Free University of Bozen-Bolzano, Bolzano, Italy
Rao, Abhishek	abhishek.rao247@gmail.com	Indian Institute of Science, Bangalore, India
Rapone, Gianluca	gianluca.rapone@arup.com	Ove Arup & Partners Ltd, London, UK
Reda, Francesco	francesco.reda@unical.it	University of Calabria, Arcavacata di Rende (CS), Italy
Rohitkumar, Pillai	rohitkumar.pillai@gmail.com	Indian Institute of Science, Bangalore, India
Romagnoni, Piercarlo	piercarlo.romagnoni@iuav.it	University IUAV of Venezia, Venezia, Italy
Rossi, Daniele	daniele.rossi@unipd.it	University of Padova, Padova, Italy
Ruffino, Pablo	pablroruffino87@gmail.com	Politecnico, di Torino, Turin, Italy
Saro, Onorio	onorio.saro@uniud.it	University of Udine, Udine, Italy
Schito, Eva	e.schito@ing.unipi.it	University of Pisa, Pisa, Italy
Scotton, Paolo	paolo.scotton@unipd.it	University of Padova, Padova, Italy
Semprini, Giovanni	giovanni.semprini@unibo.it	University of Bologna, Bologna, Italy
Sicurella, Fabio	fabio.sicurella@gmail.com	Professional Engineer, Catania, Italy
Testi, Daniele	d.testi@ing.unipi.it	University of Pisa, Pisa, Italy
Todeschini, Ilaria	ilaria.todeschini@cisma.bz.it	CISMA Srl, Bolzano, Italy
Tzempelikos, Athanasios	ttzempel@purdue.edu	Purdue University, West Lafayette, Indiana (USA)
Valdiserri, Paolo	paolo.valdiserri@unibo.it	Università di Bologna, Bologna, Italy
Venkatarama, Reddy B.V.	venkat@civil.iisc.ernet.in	Indian Institute of Science, Bangalore, India
Zemella, Giovanni	giovanni.zemella@arup.com	Ove Arup & Partners Ltd, London, United Kingdom
Zhang, Yi	YiZhang@dmu.ac.uk	De Montfort University, Leicester, United Kingdom